UNIVERSIDADE D
COIMBRA

Gianluca Utzeri

SUSTAINABLE STRATEGY AND BIO-BASED SORBENTS FOR PESTICIDES REMOVAL

PhD thesis in Chemistry, Specialization in Macromolecular Chemistry supervised by Professor Doctor Artur José Monteiro Valente and submitted to the Department of Chemistry of the Faculty of Sciences and Technology of University of Coimbra.

November of 2023

SERVIÇOS DE AÇÃO SOCIAL
UNIVERSIDADE D
COIMBRA

Gianluca Utzeri

SUSTAINABLE STRATEGY AND BIO-BASED SORBENTS FOR PESTICIDES REMOVAL

PhD thesis in Chemistry, Specialization in Macromolecular Chemistry supervised by Professor Doctor Artur José Monteiro Valente and submitted to the Department of Chemistry of the Faculty of Sciences and Technology of University of Coimbra.

November of 2023

Fundings

The thesis was developed under the PhD fellowship SFRH/BD/146358/2019 (2020-2024) with the title *Novel adsorbents for pesticide removal and their reusability* granted by *Fundação para a Ciência e Tecnologia* (FCT) funded by national funds and European Commision through the European Social Fund.

The research initiated with the grant WaterJPI/0006/2016 and UID/QUI/00313/2019.

Acknowledgments

Many people deserve my thanks, so first of all I want to make it clear that order is not synonymous with importance, because everyone has contributed in a different way to this academic journey that marks an important and great period of my life.

Definitely, as importance, my son Noah who supported me, in his own way, by patiently waiting for his father to finish work. For all the fantastic and unforgettable moments, he gave me during my PhD, almost equal to his life.

For my parents who, despite being far away, always supported me in every possible way. There are no words to adequately express the recognition they deserve.

To my supervisor Prof. Artur Monterio José Valente for welcoming me into his laboratory seven years ago. For being not only my professor and supervisor during my academic career, for always being available for teaching and explanations, but also a patient mentor during a difficult time in my life and a 'friend'.

To Prof. Dina Murtinho for her kindness and availability along the way.

My colleagues and friends Pedro Matias, Eva Bernardino, Tiago Machado, João Batista for the moments of fun, stress and coffee breaks.

Of course, the Moon Team, too numerous to mention (Estefania, Sara, Roberto, Daniel, Ulisses, Aingeru, Emilio, Saul, Carlos and so on). They were and are a second family, a family of friends, always together.

Maria for coming into my life, helping me and deciding to walk together.

Abstract

Environmental pollution is recognized serious concern that causes continuous environmental changes such as desertification, loss of biodiversity, ozone depletion and drought. The application of pesticide is a major anthropogenic source of contamination, considering that 400 tones were sold in Europe, only in 2021. The pathways of pesticides in the environment are strongly influenced by their physico-chemical properties such as hydrophilicity, ionization constant and solubility. Their spreading in the environment can cause the accumulation in soil, water streams and air, striking target and non-target organisms with consequent bio-accumulation and bio-magnification. Thus, it is of utmost importance the development of efficient strategies for the preservation of the environment, minimizing pesticide concentrations in soil or water, because only 1% of the pesticides reach the target whereas 99% is dispersed in the environment.

Along the thesis have been tested the widely applied: ammonium glufosinate, cymoxanil, (2,4-dichlorophenoxy)acetic acid, bentazon and mecoprop as broad or selective herbicides, highly soluble in water from moderately toxic to mammals to genotoxic, reprotoxic or neurotoxic; cymoxanil, as highly soluble foliar fungicide with probable genotoxicity; and imidacloprid as highly soluble neonicotinoid insecticide and veterinary substance, persistent in soil and toxic to birds, honey-bees and mammals with probable genotoxicity and reprotoxicity. The aim was to develop a deeply understanding of the physical or chemical interactions involved at the liquid-liquid and solid-liquid interfaces.

The mass transport phenomena at the liquid-liquid interface have been studied for ammonium glufosinate, cymoxanil and imidacloprid in water media by Taylor dispersion technique. The mutual diffusion coefficients of 1.1×10^{-9} m^2 s^{-1} for ammonium glufosinate, 0.8×10^{-9} m^2 s^{-1} for cymoxanil and 0.7×10^{-9} m^2 s^{-1} for imidacloprid were determined as measure of their behaviour in water. These values indicate that the electrolyte ammonium glufosinate diffuses faster than the non-electrolyte cymoxanil and imidacloprid, in water.

Sorption was chosen as valid water treatment strategy for the removal of pesticides at the solid-liquid interface. Cyclodextrin-based nanosponges were employed to study the sorption mechanisms in aqueous media. Carbamate and amine nanosponge, as function of the resulting functional groups, were the two families of nanosponges used along the thesis in form of xerogel and powder materials, respectively. The carbamate β-cyclodextrin nanosponges (poly-βcyclodextrin - PCD) were synthesized via one-pot catalyzed polymerization reaction; whereas the amine nanosponges were performed via multi-step functionalization of α- and β-cyclodextrin

with three different amine (-NH_2, hexane-1,6-diamine and dodecane-1,12-diamine) via microwave-assisted procedures and subsequent polymerization via nucleophilic substitution or click-condensation. The aim was to ameliorate the route of synthesis reducing the time-consuming of the reaction, the amount of solvent used, increasing the yield of reaction in terms of amount of product obtained, as exhibit in Chapter 3.

Nanosponges were characterized by physical, chemical and thermal analysis, whose fundamentals and the comparison of the properties of the different materials are described in Chapter 4. Comparing the poly-βcyclodextrin with the first class of amine nanosponges (αCDAM$_6$, αCDAM$_{12}$, βCDAM$_6$ and βCDAM$_{12}$) in terms of sorption capability towards imidacloprid at the optima experimental conditions, PCD reached ≈ 27% of removal and a maximum sorbed amount of 31 mg per gram of material; while βCDAM$_6$ and βCDAM$_{12}$ attained efficiencies of ≈ 96% and 90% and maximum sorption capacities of 68 mg g^{-1} and 52 mg g^{-1}, respectively. The superior performance of βCDAM$_6$ can be explained by: its higher surface area and porosity (S_{BET} = 22 m^2 g^{-1} and P_d = 27 nm) than PCD (S_{BET} = 11 m^2 g^{-1} and P_d = 11 nm); the presence of electron acceptor and donor atoms of the primary and secondary amine groups in the βCDAM$_6$ surface able to establish hydrogen bonding; and the -CH_2- groups in the aliphatic chain which can establish CH-π interactions with the aromatic rings in IMD molecular structure. The advantage of PCD-xerogel was the easier recovery and reusability of the material due to the microparticles, compared to the submicron particles of βCDAM$_6$ (254 < *Z-average* (nm) < 480). However, βCDAM$_6$ exhibited a superior sorption capability also if compared to αCDAM$_6$, αCDAM$_{12}$ and βCDAM$_{12}$ for removal of imidacloprid from its commercial formulation (Confidor O-TEQ®), namely a removal efficiency ≈ 95% and a maximum sorption uptake of 288 mg g^{-1} (constant after 5 cycles of reuse). The result can be justified considering its high S_{BET}, moles of free-CD per gram of NS (molCD_{free} $g^{-1}{}_{NS}$) and ratio between moles of free-*N* and total-*N* per gram of NS (molN_f $g^{-1}{}_{NS}$/molN_t $g^{-1}{}_{NS}$). βCDAM$_6$ and βCDAM$_{12}$ were also employed for the sorption of (2,4-dichlorophenoxy)acetic acid and the optimum performance were obtained at pH = 4 and 3, respectively. At this pH values, the carboxylic group of the pesticide is negatively charged whereas the amine groups of the nanosponges are positively charged, favouring the electrostatic interaction sorbent-sorbate. βCDAM$_{12}$ shown a maximum of sorption 4-times higher than βCDAM$_6$, which remained constant after 3 cycles of reuse, where the regeneration of the nanosponge was obtained by using a NaOH aqueous solution.

For the second class of amine nanosponges, αCDGNH$_2$, αCDGAM$_6$, αCDGAM$_{12}$, βCDGNH$_2$, βCDGAM$_6$ and βCDGAM$_{12}$, at first it must be stressed that via click-condensation reaction was possible to drastically reduce the time of the reaction and increase the amount of nanosponge obtained. Compared to the first class amine-nanosponges, they shown an average size between

489 nm and 663 nm, higher average pore size diameters, cyclodextrin content ad thermal stability. The nanosponges have been tested for the removal of the highly soluble herbicide bentazon and mecoprop with acidic behaviour. At the current state of the study, αCDGNH$_2$, βCDGNH$_2$ and αCDGAM$_6$ have been applied for bentazon and mecoprop sorption in one ingredient and mixture batches. They have shown a complete removal ($\geq$ 99%) of mecoprop either in individual and mixture batches in water. The high efficiency can be due to electrostatic interactions between the deprotonated acid group of mecoprop (K_a = 3.11) and the primary and secondary amine groups on the surface of the nanosponges. Differently, the bentazon sorption process is based on homogeneous systems with cooperative interactions whose contribute increases with the concentration, attaining a maximum removal of $\approx$ 97% in single batch, probably due to the delocalized negative charge in its molecular structure. Moreover, in presence of mecoprop the maximum sorption capability of αCDGNH$_2$ and βCDGNH$_2$ toward bentazon doubled from $\approx$ 70 mg g^{-1} to $\approx$ 134 mg g^{-1}, indicating that mecoprop favours the cooperative process by electrostatic interactions, hydrogen bonding or π-π stacking between the aromatic rings. Finally, αCDGAM$_6$ reached a RE of bentazon $\geq$ 99%, in binary system with mecoprop.

Molecular dynamic simulations were also performed to understand the sorbent-sorbate interactions acting into the sorption processes, at molecular level. The analysis permitted to determine the effect of the cyclodextrins, their amine-functionalization and their dimeric form (as representative of the nanosponge structure) on the sorption process of Confidor O-TEQ® into αCDAM$_6$, αCDAM$_{12}$, βCDAM$_6$ and βCDAM$_{12}$. A reduction of host-guest supramolecular structure formation between imidacloprid and cyclodextrin is observed, with a growing interaction at level of the aliphatic chain of the crosslinker, probably due to the hydrophobic effect of the aliphatic chain length.

Resumo

A poluição ambiental é amplamente reconhecida como uma séria preocupação que causa alterações ambientais contínuas, como a desertificação, a perda de biodiversidade, a destruição da camada de ozono e a seca. A aplicação de pesticidas constitui uma fonte antropogénica de contaminação importante, considerando que 400 toneladas foram vendidas na Europa, apenas em 2021. A disseminação dos pesticidas no ambiente é fortemente influenciada pelas suas propriedades físico-químicas, como a hidrofilicidade, a constante de ionização e a solubilidade. A sua consequente acumulação nos solos, nos cursos de água e no ar pode afetar tanto organismos-alvo como não-alvo, resultando em bioacumulação e biomagnificação. Assim, é de extrema importância o desenvolvimento de estratégias eficientes para a preservação do meio ambiente, que visem a minimização das concentrações de pesticidas nos solos ou nas águas, uma vez que apenas 1% dos pesticidas atinge o alvo e os restantes 99% se dispersa no ambiente.

Ao longo do trabalho desenvolvido no âmbito do projeto de tese, foram testados: o glufosinato de amónio, o ácido (2,4-diclorofenoxi)acético, a bentazona e o mecoprop, que são amplamente aplicados como herbicidas de largo espetro ou seletivos, altamente solúveis em água, apresentando-se desde moderadamente tóxicos para os mamíferos até genotóxicos, reprotóxicos ou neurotóxicos; o cimoxanil, como um fungicida foliar altamente solúvel com provável genotoxicidade; e a imidacloprida, como um inseticida e substância veterinária neonicotinóide altamente solúvel, persistente no solo e tóxica para as aves, as abelhas e os mamíferos, e com provável genotoxicidade e reprotoxicidade. O objetivo foi desenvolver uma compreensão profunda das interações físicas ou químicas envolvidas nas interfaces líquido-líquido e sólido-líquido.

Ao nível da interface líquido-líquido, foram estudados os fenómenos de transporte de massa para o glufosinato de amónio, o cimoxanil e a imidacloprida em meio aquoso através da técnica de dispersão de Taylor. Como medida do seu comportamento em água, foram determinados coeficientes de difusão mútua de $1{,}1 \times 10^{-9}$ m^2 s^{-1} para o glufosinato de amónio, de $0{,}8 \times 10^{-9}$ m^2 s^{-1} para o cimoxanil e de $0{,}7 \times 10^{-9}$ m^2 s^{-1} para a imidacloprida. Estes valores indicam que o eletrólito glufosinato de amónio se difunde mais rapidamente em água do que os não electrólitos cimoxanil e imidacloprida.

A sorção foi escolhida como uma estratégia válida de tratamento de águas para a remoção de pesticidas numa interface sólido-líquido. Foram utilizadas nanoesponjas à base de ciclodextrina para estudar os mecanismos de sorção em meios aquosos. Duas famílias de nanoesponjas,

nomeadamente de carbamato e de amina, em função dos grupos funcionais resultantes, foram utilizadas ao longo da tese, sob a forma de xerogel e de materiais em pó, respetivamente. As nanoesponjas de β-ciclodextrina do tipo carbamato (poli-βciclodextrina - PCD) foram sintetizadas através de uma reação de polimerização catalisada *one-pot*; enquanto as nanoesponjas do tipo amina foram sintetizadas através de uma funcionalização multi-etapas de α- e β-ciclodextrina com três aminas diferentes (-NH_2, hexano-1,6-diamina e dodecano-1,12-diamina), através de procedimentos assistidos por micro-ondas e subsequente polimerização via substituição nucleofílica ou condensação do tipo *click*. O objetivo foi melhorar a via sintética, reduzindo o tempo de reação, a quantidade de solvente utilizado e aumentando o rendimento da reação em termos da quantidade de produto obtido, como se expõe no Capítulo 3.

As nanoesponjas foram caracterizadas por análises físicas, químicas e térmicas, cujos fundamentos e a comparação das propriedades dos diferentes materiais se encontram descritos no Capítulo 4. Comparando a poli-βciclodextrina com a primeira classe de nanoesponjas do tipo amina (αCDAM$_6$, αCDAM$_{12}$, βCDAM$_6$ e βCDAM$_{12}$) em termos da capacidade de sorção da imidacloprida nas condições experimentais ótimas, observou-se que a PCD atinge ≈ 27% de remoção e uma quantidade máxima de sorção de 31 mg por grama de material, enquanto a βCDAM$_6$ e a βCDAM$_{12}$ atingem eficiências de ≈ 96% e 90% e capacidades máximas de sorção de 68 mg g^{-1} e 52 mg g^{-1}, respetivamente. O desempenho superior da βCDAM$_6$ pode ser explicado: pela sua área de superfície e porosidade mais elevadas (S_{BET} = 22 m^2 g^{-1} e P_d = 27 nm) em relação à PCD (S_{BET} = 11 m^2 g^{-1} e P_d = 11 nm); pela presença de átomos aceitadores e dadores de eletrões dos grupos amina primários e secundários na superfície da βCDAM$_6$, capazes de estabelecer ligações de hidrogénio; e pelos grupos -CH_2- das cadeias alifáticas que podem estabelecer interações CH-π com os anéis aromáticos na estrutura molecular do IMD. A vantagem do xerogel PCD é ser mais facilmente recuperável e reutilizável, devido ao tamanho micrométrico das partículas, quando comparado com o tamanho sub-micrométrico das partículas de βCDAM$_6$ (254 < *Z-average* (nm) < 480). No entanto, a βCDAM$_6$ mostrou um melhor desempenho em relação às αCDAM$_6$, αCDAM$_{12}$ e βCDAM$_{12}$ para a remoção da imidacloprida da sua formulação comercial (Confidor O-TEQ®), nomeadamente uma eficiência de remoção de ≈ 95% e uma capacidade máxima de sorção de 288 mg g^{-1} (constante após 5 ciclos de reutilização). Este resultado pode ser explicado considerando a maior S_{BET}, moles de CD livre por grama de NS (molCD_{free} g^{-1}_{NS}) e razão entre moles de N livre e N total por grama de NS (molN_f g^{-1}_{NS}/molN_t g^{-1}_{NS}) da βCDAM$_6$. A βCDAM$_6$ e a βCDAM$_{12}$ foram também utilizadas para a sorção do ácido (2,4-diclorofenoxi)acético, tendo os valores ótimos sido obtidos a pH = 4 e 3, respetivamente. A estes valores de pH, o grupo carboxilo do pesticida encontra-se carregado negativamente, enquanto os grupos amina das nanoesponjas possuem carga positiva, favorecendo a interação eletrostática sorvente-sorvato. A βCDAM$_{12}$ apresentou uma capacidade máxima de sorção

4 vezes superior à da βCDAM$_6$ que se manteve constante após 3 ciclos de reutilização, ao longo dos quais a regeneração da nanoesponja foi conseguida com uma solução aquosa de NaOH.

Relativamente à segunda classe de nanoesponjas do tipo amina, αCDGNH$_2$, αCDGAM$_6$, αCDGAM$_{12}$, βCDGNH$_2$, βCDGAM$_6$ e βCDGAM$_{12}$, deve salientar-se, em primeiro lugar, que através da reação de condensação *click* foi possível reduzir drasticamente o tempo da reação e aumentar a quantidade de nanoesponja obtida. Em comparação com as nanoesponjas do tipo amina de primeira classe, estas apresentaram um tamanho médio entre 489 nm e 663 nm, diâmetros médios de poros mais elevados, maior teor de ciclodextrina e estabilidade térmica. As nanoesponjas foram testadas para a remoção do herbicida altamente solúvel bentazona e mecoprop com comportamento ácido. No estado atual do estudo, αCDGNH$_2$, βCDGNH$_2$ e αCDGAM$_6$ foram aplicadas para a sorção de bentazona e mecoprop separadamente e em mistura. Estes mostraram uma remoção completa ($\geq$ 99%) para o mecoprop, tanto na ausência quanto na presença de bentazona. A elevada eficiência pode ser devida às interações eletrostáticas entre o grupo ácido desprotonado do mecoprop (K_a = 3.11) e os grupos amina primários e secundários na superfície das nanoesponjas. Por outro lado, o processo de sorção da bentazona baseia-se em sistemas homogéneos com interações cooperativas cujo contributo aumenta com o aumento da concentração, atingindo uma remoção máxima de $\approx$ 97% em sistema mono-componente, provavelmente devido à carga negativa deslocalizada na sua estrutura molecular. Além disso, na presença de mecoprop, a capacidade máxima de sorção da bentazona por parte das nanoesponjas αCDGNH$_2$ e βCDGNH$_2$ aumentou de 63 mg g^{-1} para 92 mg g^{-1} e de 66 mg g^{-1} para 109 mg g^{-1}, respetivamente, indicando que a presença do mecoprop favorece a cooperatividade através de interações eletrostáticas, ligações de hidrogénio ou empilhamento π-π entre os anéis aromáticos. Por fim, αCDGAM$_6$ alcançou uma eficiência de remoção da bentazona $\geq$ 99%, no sistema bi-componente com mecoprop.

Foram também realizadas simulações de dinâmica molecular para compreender as interações sorvente-sorvato que actuam nos processos de sorção, a nível molecular. A análise permitiu determinar o efeito das ciclodextrinas, da sua funcionalização com grupos amina e da sua forma dimérica (como estrutura representativa das nanoesponjas) no processo de sorção do Confidor O-TEQ® em αCDAM$_6$, αCDAM$_{12}$, βCDAM$_6$ e βCDAM$_{12}$. Observou-se uma redução da formação da estrutura supramolecular *host-guest* entre a imidacloprida e a ciclodextrina, com uma interação crescente ao nível da cadeia alifática do reticulante, provavelmente devido ao efeito hidrofóbico do comprimento da cadeia alifática.

Table of Contents

List of figures

(pag.)

Chapter 1.

Chapter 3.

Chapter 4.

Chapter 5.

List of tables

Chapter 5.

List of papers

(pag.)

I. **Introduction to cyclodextrin-based nanosponges**

Gianluca Utzeri, Dina Murtinho, Artur J.M. Valente. In: Gulati, S. (eds) *Nanosponges for Environmental Remediation*, chapter 5, 87-115, 2023. (49)

II. **Cyclodextrin-based nanosponges: overview and opportunities**

Gianluca Utzeri, Pedro M.C. Matias, Dina Murtinho, Artur J.M. Valente. *Front. Chem.* 10, 859406, 2022. (50)

III. **Limiting diffusion coeffiecients of glufosinate ammonium, cymoxanil and imidacloprid in aqueous solutions**

Luis M.P. Verissimo, Gianluca Utzeri, M. Luísa Ramos, Ana C.F. Ribeiro, Artur J.M. Valente. *J. Mol. Liq.* 293, 111459, 2019. (104)

IV. **Poly(*β*-cyclodextrin)-activated carbon gel composites for removal of pesticides from water**

Gianluca Utzeri, Luis Verissimo, Dina Murtinho, Alberto A.C.C. Pais, F. Xavier Perrin, Fabio Ziarelli, Tanta-Verona Iordache, Andrei Sarbu, Artur J.M. Valente. *Molecules.* 26 (2021) 1426. (105)

V. **Amine-*β*-cyclodextrin-based nanosponges. The role of cyclodextrin amphiphilicity in the imidacloprid uptake**

Gianluca Utzeri, Dina Murtinho, Teresa M.R. Maria, Alberto A.C.C. Pais, Filomena Sannino, Artur J.M. Valente. *J. Coll.Surf. A*. 635 (2022) 128044. (106)

VI. **Synthesis of *β*-cyclodextrin-based nanosponges for remediation of 2,4-D polluted waters**

Artur J.M. Valente, Domenico Pirozzi, Alessia Cinquegrana, Gianluca Utzeri, Dina Murtinho, Filomena Sannino. *J. Env. Res.* 215 (2022) 114214. (107)

VII. **Insights on macro- and microscopic interactions between Confidor and cyclodextrin-based nanosponge**

Gianluca Utzeri, Tânia F. Cova, Dina Murtinho, Alberto A.C.C. Pais, Artur J.M. Valente. *Chem. Eng. J.* 455 (2023) 140882. (108)

The papers are labelled in the thesis by roman numbers, the pages indicated in “List of papers” facilitate the index.

VIII. **Click strategy for mesoporous cyclodextrin nanosponge synthesis for complete removal of bentazon and mecoprop**

Gianluca Utzeri, Tânia F. Cova, Dina Murtinho, Alberto A.C.C. Pais, Artur J.M. Valente. *In preparation* (109)

Paper not included in this thesis

Revolutionizing pesticide extraction: the role of reusable polyacrylic membranes in mecoprop and bentazon removal

Gianluca Utzeri, José Carlos Guirado-Moreno, Tânia F.G.G. Cova, Alberto A.C.C. Pais, Luis A.E. Batista de Carvalho, Saturnino Ibeas, José M. Garcia, Artur J.M. Valente, Saul Vallejos. *Npj Clean Water* (peer-review)

The papers are labelled in the thesis by roman numbers, the pages indicated in "List of papers" facilitate the index.

Abbreviations

μ:	Chemical potential
μ_e:	Electrophoretic mobility
ρ:	electronic density
ζ:	Zeta-potential
2,4-D:	(2-(2,4-dichlorophenoxy)acetic acid)
AC:	Activated carbon
AFM:	Atomic force microscopy
AGF:	Ammonium glufosinate
AIC:	Akaike's Information Criterion
AM_{12}:	Dodecane-1,12-diamine
$_{AM12}$CD:	*Heptakis*-[6-(12-amino-1-dodecylamine)]-(6-deoxy)-cyclodextrin
AM_6:	Hexane-1,6-diamine
$_{AM6}$CD:	*Heptakis*-[6-(6-amino-1-hexylamine)]-(6-deoxy)-cyclodextrin
AOP:	Advanced oxidation processes
ATM:	Atomic force microscopy
BET:	Brunauer, Emmett and Teller model
BJH:	Barrett, Joyner and Halenda model
BTL:	Dibutylin dilaurate
CB:	Carbamates
CDAM-NS:	Amine-cyclodextrin-based nanosponges
CD-I:	*Heptakis*-(6-iodo)-(6-deoxy)-cyclodextrin
CDNS:	Cyclodextrin-based nanosponges
CLP:	Chlorpyrifos

CRT: Cathode-ray tube

CSF: Coagulation-sedimentation-filtration

CYM: Cymoxanil

D: Diffusion coefficient

DDT: 1,1,1-trichloro-2,2-bis(4-chlorophenyl)ethane

DETA: Dielectric thermal analysis

DLS: Dynamic Light scattering

DOC: Dissolved organic carbon

DSC: Differential scanning calorimetry

D_T: Tracer diffusion coefficient

DT_{50}: Half-life time

DTA: Differential thermal analysis

dTG: Derivative TG curve

DWD: Drinking water Directive EU 2020/2184

E^0: Oxidation potential

EDS: Energy-dispersive spectrometer

EFD: European Framework Directive 2009/128/EC

FTIR: Fourier transform infrared spectrometer

GD: Groundwater Directive 2006/118/EC

GLT: Glutaraldehyde

GWL: Groundwater Watch List

HAA: Haloacetic acids

HDI: 1,6-hexamethylene diisocyanate

IGM: Independent Gradient Model

IMD: Imidacloprid

IPM: Integrated Pest Management

IUPAC: International Union of Pure and Applied Chemistry

J: Rate of transport

K_{11}: Binding constant

K_a: Acid ionisation constant

K_{oc}: Sorption coefficient

K_{ow}: Octanol-water partition coefficient

L-L: Liquid-liquid interface

MD: Molecular dynamic

M_L: Rate of mass loss

MRL: Maximum residual levels

MW: Microwave-assisted procedure

NCI: Non-covalent interactions

$_{NH2}$CD: *Heptakis*-(6-amine)-(6-deoxy)-cyclodextrin

NP: Nanoparticles

OC: Organochlorines

OP: Organophosphates

PCD: Poly-*β*cyclodextrin

PCS: Photon correlation spectroscopy

PDI: Polydispersity index

PFO: Pseudo first-order

POP: Persistent organic pollutants

PP: Phenolphthalein

PRT: Parathion

PSO: Pseudo second-order

PT: Pyrethroids

PURE: Pesticide use-and-risk reduction in Europe

PVA: Poly(vinyl alcohol)

PVP: Poly(vinylpyrrolidone)

q_e: Amount of sorbed analyte per gram of sorbent

RE%: Removal efficiency

R_h: Hydrodynamic radius

RI: Refractive index

S-L: Solid-liquid interface

SANS: Small angle neutron scattering

S_{BET}: Specific surface area

SEM: Scanning electron microscopy

SMP: Submicron particles

SSA: Specific surface area

STM: Scanning tunneling microscopy

TEM: Transmission electron microscopy

TGA: Thermogravimetric analysis

THM: Trihalomethanes

T_{max}: Maximum temperature of a thermal event

TOC: Total organic content

UNEP: United Nations Environment Programme

USANS: Ultra small angle neutron scattering

UV: Ultraviolet light

WDS: Wavelength-dispersive spectromete

Chapter 1.

1. Introduction to the environmental pollution statement

Environmental degradation is a recognized global concern and source of complicated debates [1], which can be associated with a miscellaneous of geogenic and anthropogenic factors. The production and consumption of chemicals in every aspect of daily life and industrial activities, as a function of the ever-increasing global population (9.8 billion by 2050 [2]), and consequent growing demand for goods, play a significant role in the environmental. The controlled and safe use, storage and disposal of chemicals are extremely important and must be strictly controlled to mitigate or avoid their impact on the ecosystem [3]. The movement of chemicals in the environment depends on physical routes of transport, namely advection, dispersion, volatilization and evaporation; or chemical processes such as solubilization, complexation or precipitation [4–6]; which influence the persistence of chemicals in nature and their modes of action and effects. Mobility is also biased by their physico-chemical-biologic properties, such as: the octanol-water partition coefficient (K_{ow}), which is related to the lipophilicity of the pesticide; the acid ionisation constant (K_a), which determines the pH-responsiveness of soil and water; the sorption coefficient (K_{oc}) which describes the interaction of the pesticide with the soil particles depending on its composition; degradability; bio-accumulation and bio-magnification; and toxicity [7]. As a result, chemicals can spread through soil and air, possibly attaining water-streams, increasing the level of exposure of target and non-target organisms with harmful effects [8]. Hence, the 17 global goals were established (*e.g.* zero hunger (2), good health and well-being (3), clean water and sanitation (6), industry, innovation and infrastructure (9), sustainable cities and communities (11), responsible consumption and production (12), climate action (13), life below water (14), life on land (15) and partnerships for the goals (17)). In addition, the water demand is expected to increase by 1000% by 2050 [9]. These requirements led United Nations to develop the United Nations Environment Programme (UNEP) for chemicals and waste management (*e.g.* chemicals in products, endocrine disrupting chemicals, persistent pollutants, hazardous compounds in electronic products, heavy metals, nanotechnology and nanomaterials, and polyfluoroalkyl substances) [10–12] (https://www.unep.org/explore-topics/chemicals-waste/what-we-do/emerging-issues). Persistent, toxic, mobile and bio-cumulative compounds have the highest priority and are classified as persistent organic pollutants (POP); their use is regulated by Stockholm Convention in 2001 [13]

Considering the importance of the issue, the PhD project focuses on the development of new high-performance polymeric materials for the removal of pesticides/phytopharmaceuticals, which fall into 4 of the 7 previously mentioned classes, from aqueous media [14].

However, before getting into the core of the project, the importance of pesticide usage and its implications are introduced.

1.1.Introduction to the pesticide landscape

According to the International Union of Pure and Applied Chemistry (IUPAC), the term pesticide means: "*Strictly, a substance intended to kill pests: in common usage, any substance used for controlling, preventing, or destroying animal, microbiological, or plant pests."* [15]. The term usually refers to commercial formulations consisting of one or more active ingredients between 2% and 80% and, adjuvants or inert ingredients to improve dispersibility, solubility, wettability and sorption. The active ingredients can be classified as natural or synthetic compounds, respectively, based on their origin [16]. Natural pesticides are derived from plants or microbes and are characterized by low or null mammalian toxicity and high degradability in nature. Synthetic compounds are appropriately designed as stable inorganic or organic molecules, characterized by high persistence/mobility, bio-accumulation, bio-magnification and toxicity. Different classes can be also identified according to the target. The most known classes are: herbicides, synthetic substances in form of granules or fumigant liquid that act as inhibitors of photosynthesis, amino-acids' formation, cell division and/or plant growth; fungicides, in form of powder or liquid, employed by foliar or dressing application and acting as protective, therapeutic, or eradicant [17]; insecticides; rodenticides; bactericides; repellents and growth regulators [18,19]. The 2021 Eurostat data (Figure 1.1) highlights that fungicides and herbicides are the most widely marketed, accounting for approximately 46% worldwide in 2019 and 75% of all crop protection chemicals sold in Europe in 2021 [16,17,20]; 79% of these are sold in Spain, Italy, Germany and France. Currently, 452 substances are approved in Europe, including active ingredients, synergists and safeners (according to the EU pesticides database), with the strictest regulation in the world of the maximum residual levels (MRL) permitted in drinking water, Drinking water Directive EU 2020/2184 (DWD).

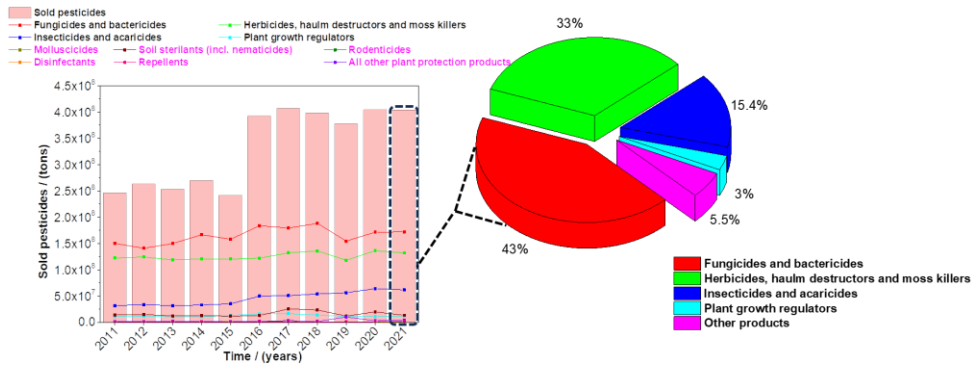

Figure 1.1. Representation of the tons of pesticides sold from 2011 to 2021 based on European data (Eurostat - 15-05.2023 23:00H).

Due to their superior efficacy, synthetic active ingredients are most widely employed and can be divided into four main classes [21]: *i)* organochlorines (OC) are characterized by low aqueous solubility, low polarity and high persistence in soil, which enable them to reach non-target organisms, favouring their bio-magnification and accumulation, causing reprotoxic effects, and acting at level of the central nervous system by inhibiting the ion channels and hepatic systems [17], therefore, they were banned or restricted in the 1960s and replaced by fluorinated pesticides due to their advantageous properties, such as high selectivity and specificity [22]; *ii)* the same year was marked by organophosphates (OP) entry into the market, which are esters of phosphoric acid that can accumulate in soils and waterways, which adverse effects depend on the amount of sulphur atoms and the valence of the phosphorus, ranging from low to high toxicity [23,24], mainly acting as inhibitors of acetylcholine-esterase involved in the nervous impulse cascades (in 2015, residues of 9 OPs were found in the Sarno river in Italy, with values ranging from 5.6 - 39.3 ng L^{-1} [25]); *iii)* the carbamates (CB) were introduced in the 1970s with an annual consumption growth of *ca.* 6% - they mainly present amide-ester bonds and are adsorbed by coordination/protonation with a mode of action analogous to that of OP, incrementing the risk of lung cancer [26]; *iv)* pyrethroids (PT) entered onto the market in 1980s as synthetic form of the natural pyrethrins, characterized by the high biodegradability and low toxicity to mammals, which produce reactive oxygen species that lead to the disruption of the cellular homeostasis and have 12 - 96 days half-life time (DT_{50}). Particularly, CP and PT can cause reversible or irreversible side effects in humans. Cypermethrin, fenvalerate, deltamethrin and permethrin are the most frequently detected pyrethroids in agricultural and non-agricultural use [27].

Despite their low bioaccumulation capacity, OP and CB have been replaced due to increasing socio-economic and environmental pressures, which brought to the development of high-performance compounds called neonicotinoids. In Europe, 20% of neonicotinoids sold were applied for seed treatment, later banned due to their side effects on the central nervous system of

mammals and honeybees [28]. Today, the focus is on more efficient and safer strategies to reduce the amount and application rate of pesticides [29,30], and the environmental contamination [31] with a narrower spectrum of action (Figure 1.2) (Table 1.1).

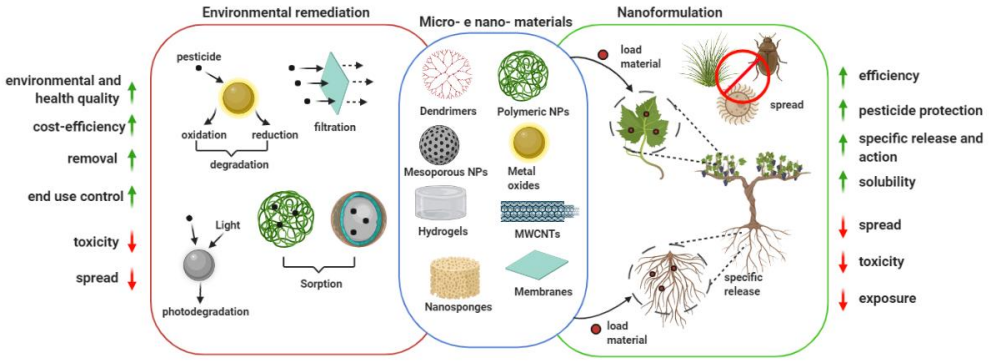

Figure 1.2. Examples of organic and inorganic materials applied in remediation processes and as sustainable agricultural strategies.

So, why do we need pesticides? In 1960, the usage of pesticides was called the *Green Revolution* because it catered to the growing demand for goods, including food. This demand is expected to boost even more, up to +60% by 2050 [14], as a function of the expanding global population that would reach *ca.* 10 billion by 2030. It is therefore essential to mention the often-forgotten upsides [20], of pesticide usage. It maximizes agricultural yields by controlling plagues and disease vectors of plants in crop production processes, ensuring food supply and higher financial incomes. Non-agricultural applications represent about 13% and include the control of disease vectors of livestock and human, turf and sport fields' maintenance, among others [40]. This lead to an increase in habitable areas, with a reduction in invasive species and a decrease in the spread of diseases [41]. One example is the reduction in the incidence of malaria worldwide [42]. The benefits of pesticides employment would be even more evident if they were applied following the principles of Integrated Pest Management (IPM) [43], labelling and technical information [44]. These have been developed to face the indiscriminate application of pesticide and ensure a sustainable agriculture, food safety and quality of life, in conformity with European Framework Directive 2009/128/EC (EFD), European Regulation N. 1107/2009 (consolidated in March 2021), REACH Regulation 1907/2006, Regulation 1223/2009, Regulation 528/2012 (updated and consolidated in June 2021) and Regulation (EC) N. 396/2005 [45–47]. The PURE (Pesticide Use-and-Risk Reduction in Europe) project, the DEXiPM model, the SYNOPS-WEB or VULPES software tools are among other examples of efforts aimed to address the need for more innovative and sustainable strategies [48] and to predict or identify vulnerable areas. [49–51].

Table 1.1. Micro- and nano-materials as sustainable strategy in agriculture.

Nanopesticide compositions	Form	Name of products	Results	Ref.
$Cu(OH)_2$	NPs (50-1000 nm)	**Kocide 3000**: pK_{ow}[a] = 0.44; sol.[b] (mg L^{-1}) = 0.506;	-Enhancing foliar uptake to 97-99%;	[32]
Silica	NPs (423 nm)	**2,4-dichlorophenoxy acetic acid (2,4-D)**: pK_{ow}[a] = 0.82; sol.[b] (mg L^{-1})= 24300;	-Release up to 96% (0.1 mol L^{-1} NaCl, 40 °C);	[33]
Chitosan/pectin	NPs (70-90 nm)	**Carbendazim**: pK_{ow}[a] = 1.48; sol.[b] (mg L^{-1}) = 8.0;	-100% growth fungi inhibition and slower release;	[34]
Chitosan/TPP	NPs (282 nm)	**Paraquat dichloride**: pK_{ow}[a] = 4.5; sol.[b] (mg L^{-1}) = 620000;	-*EE%* = 62; -slow release, lower toxicity, higher effectiveness;	[35]
Bentonite modified with DMTA and HTMA	Composite	**Pretilachlor**: pK_{ow}[a] = 4.08; sol.[b] (mg L^{-1}) = 500;	-*LE* (mg g^{-1}) = 138.1-153.8; -T_{50} (days) = 4.75 (DMTA); -T_{50} (days) = 4.16 (HTMA);	[36]
Diatomite/Fe_3O_4/chitosan	Films	**Glyphosate**: pK_{ow}[a].= 3.2; sol.[b] (mg L^{-1}) = 10500; **Cypermethrin**: pK_{ow}[a] = 5.55; sol.[b] (mg L^{-1}) = 0.009;	-Release up to ≈ 90% at pH5.0; -highest effectiveness at pH5.0;	[37]
PDI cationic dendrimer (G1,G2,G3)	Dendrimer (1.1, 1.8, 3.2 nm)	**Thiamethoxan**: pK_{ow}[a] = 0.13; sol.[b] (mg L^{-1}) = 4100;	-cell viability >92%, higher cytotoxicity; -90% died larvae G2;	[38]
glycerol tripalmitate/PVA	NPs (178 nm)	**Atrazine** (ATZ) pK_{ow}[a] = 2.7; sol.[b] (mg L^{-1}) = 35.0; **Simazine** (SMZ) pK_{ow}[a] = 2.3; sol.[b] (mg L^{-1}) = 5.0;	-*EE%* = 89.7; -*EE%* = 97.3; -high stability (over 120 days); -T_{50} (h) = 52.9 (ATR); -T_{50} (h) = 51.1 (SMZ); -higher cytotoxicity;	[39]

[a]:pK_{ow} at pH=7 and 20°C; [b]:water solubility at 20°C (data source: www.herts.ac.uk/aeru)
Notes: DMTA: dodecyltrimethyl ammonium chloride; *EE%*: encapsulation efficiency; HTMA: hexadecyltrimethyl ammonium chloride; *LE*=loading efficiency; NPs: nanoparticles; PDI: perylene-3,4,9,10-tetracarboxydiimide; PVA: poly(vinyl alcohol); T_{50}: time taken to release 50% of the active ingredient; TPP: sodium tripolyphosphate;

Hence, the controversy and long-lasting debates come from the indiscriminate abuse and misapplication (misuse or unintentional use) of pesticides and the resulting contamination of the ecosystem (*e.g.* desertification, loss of biodiversity, ozone depletion, drought) [52,53]. A famous study, Pimentel [54], states that only 0.1% of pesticides reach their target. Once in the environment, inter– and intra–transfer processes of pesticides occur between organisms resulting in bio-accumulation and bio-magnification, with possible development of resistant specimens as an adaptation to stressor elements [55–59]. Therefore, higher application quantities and times and the development of deadlier formulations are required. The Groundwater Watch List (GWL) was introduced to minimize the bio-accumulation and bio-magnification, ameliorate the data monitoring and simplify the recognition of compounds. The first factors influencing the pathway of pesticides in nature are their formulation (*i.e.* aqueous solution, emulsifiable in petroleum-based solvent, power dusts, wettable powder or granules), and the method of application. For instance, wettable powder applied by spraying is one of the most common combinations, due to the generally low solubility of the active compounds and the ability to cover wide areas. Poorly soluble pesticides often show low mobility and high persistence in soil, favouring the transport to surrounding lands via the wind. In contrast, soluble compounds can move faster through the soil by leaching (depending on soil composition), potentially reaching surface and groundwater [41,60]. Approximately 10% of pesticides applied in agriculture spread into non-target areas [61]. K_{ow}, K_a, and K_{oc} are key parameters of pesticides mobility [7]. A field study demonstrated that banding application is a more effective practice than the broadcast application for atrazine and diuron (two banded active ingredients) with over 90% reduction in average total load mobility in drainage water [62]. In 2017, a study conducted in Rochefort-sur-Loire (France) revealed the presence and the influence of rainfall events on the mobility of 7 pesticides, which always exceeded the European legal limit for at least one active ingredient; the relative toxicity is cause for social concern [63]. Furthermore, after the application of fumigants, such as methyl isothiocyanate, under partially anaerobic conditions, an increase of N_2O emissions from agriculture soils was registered [64]. A vulnerable area has also been identified in Martinique (French west Indies), where horticultural practices are still a source of water pollution [65]. Herein, the contamination of groundwater is a major problem, especially in countries where it represents the main source of drinking water. In Europe, groundwater produces 65% of drinking water, culminating in the Groundwater Directive 2006/118/EC (GD) [47] and DWD. They set the general MRL of pesticides in the drinking water to 0.1 µg L^{-1} and 0.5 µg L^{-1} for mono- and multi-residues, respectively, where non-specification are declared. A recent study in France, Denmark, England and Switzerland demonstrated the importance of having harmonized protocols to ensure comparable reporting to the European Environment Agency every three years [47].

It should be emphasized that each active ingredient and/or pesticide is characterized by one or more DT_{50} values, which represent the time needed to break down half of the amount of pesticide, depending on the environmental conditions (pH, temperature, sun-light, organic matter and microorganisms, among others) [66]. Active ingredients with low DT_{50} values are considered non-persistent, as opposite to those with higher DT_{50} values [67]. Thus, the formation of by-products along the transport of pesticides must also be considered [68], even more with a steady increase in the residual amount of pesticide in the ecosystem [19,69]. Indeed, a study showed that more than 80% of surface soils in European Union present one or more residues, with the highest amount in Southern Europe. Glyphosate, AMPA and phthalimide are the most commonly detected compounds [70]. Glyphosate (DT_{50} = 1 - 197 days) and its metabolite AMPA (DT_{50} = 23 - 958 days) [71] have been determined in the Meuse river (Netherlands) and in the Têt river (France) which concentrations are dependent on the season [72,73]. Furthermore, glyphosate poses a high risk in surface water in urbanized areas in the Lombardia region (Italy) due to non-agricultural applications [74]. A complex study assessed the presence of pesticides mixture in the watercourses in Germany, France, Netherlands, and USA. Herbicides were mainly detected as mixture of 2 and 5 active ingredients, followed by fungicides and insecticides [75]. Herbicide residues are also predominant in Louro river (Greece) yet followed by insecticides and fungicides in concentrations often exceeding European limits [76]. In the Mondego Estuary (Portugal), residues of atrazine (sediment), azoxystrobin (water, sediment and, bivalve), bentazon (water and bivalve), λ–cyhalothrin (bivalve), penoxsulam (bivalve) and terbuthylazine (microalgae and bivalve) were detected [77]. In a global study, thousands of active ingredients of hundreds of pesticides were found in the surface water of 53 countries with different quality standards [78]. This increases the probable exposure of non-target organisms, starting with plants, bees, earthworms, birds, farmers (occupational exposure), and citizens (non-occupational exposure), along the evolutionary scale and food chain [21,79–83]. Some studies have associated disturbs/diseases/disorders with acute (*e.g.* blindness, rashes, diarrhoea, vomiting) or chronic (*e.g.* cancer development, birth defects, Parkinson, diabetes, asthma, cardiovascular or central nervous disorders, immune suppression) exposure to pesticides [23,42,45,84–87]. In Greece, approximately 97% of the sampled milks contained residues of 1,1,1-trichloro-2,2-bis(4-chlorophenyl)ethane (DDT) and its metabolite, below the legislative level but still representing high risk values for children aged 1–3 years [88]. In Canada, the effects of the insecticides OP and PT on the respiratory health of the non-occupational citizens have been evaluated [89]. Recent research has determined the effect of 20 commercial pesticide formulations (such flutriafol, imidacloprid and azoxystrobin) on *N*–acetylglucosamine enzymatic activity, nitrogen mineralization/fixation and γ–aminobutiric acid receptors of prokaryotes, fungi and eukaryotes, and soil composition in south Australia [90]. Among the population, farmers and farm workers are the most susceptible to neurological disorders, cancer, eye and skin irritation, fever, nausea, vomiting or respiratory disorders [91]. In

a study of 2019, the presence of at least one neonicotinoid was determined in the fruits and vegetables in the daily diet of 103 children. The first to be placed on the market in 1991 was the imidacloprid [92], with an average DT_{50} = 2 - 3 years in soil [28]. Since this time, the number of reports on neonicotinoid-resistant species has also increased; for example, those on *Bemisia tabaci, Myzus persicae* or *Nilaparvata lugens*, among others, which are known to be economically significant pests [92]. Furthermore, in a study performed on pesticide sprayers in Tesshaly (Greece), neonicotinoids were shown to be correlated to oxidative DNA damage [93]. Due to their hazardous effects on the ecosystem, the use of neonicotinoids in Europe has been restricted or banned [94], evaluation studies are still ongoing. Interesting research demonstrates the ability of the *Anguilla Anguilla* species to recover from non-specific DNA damage after a short-term exposure to Roundup® and Garlon®. Roundup® has been shown to cause long-term damages [95].

As Rachel Carson wrote in her famous book *Silent Spring*: "*…the central problem of our age has therefore become the contamination of man's total environment with such substances of incredible potential for harm – substances that accumulate in the tissues of plants and animals and even penetrate the germ cells to shatter or alter the very material of heredity upon which the shape of future depends.*"

1.2.Objectives and structure of the work

As discussed in section 1.1., the contamination of our environment by pesticides stands as a prominent and concerning issue, playing a pivotal role in the ongoing degradation of our natural surroundings. The widespread contamination not only poses a significant threat to the delicate balance of our ecosystems but also carries dire consequences for both animal and human well-being. Thus, in order to understand the behaviour of the pesticides in water-streams, the transport phenomena parameters of imidacloprid ((NE)-*N*-[1-[(6-chloropyridin-3-yl)methyl]imidazolidin-2-ylidene]nitramide) (IMD), cymoxanil ((1E)-2-(ethylcarbamoylamino)-*N*-methoxy-2-oxoethanimidoyl cyanide) (CYM) and ammonium glufosinate (azanium;2-amino-4-[hydroxy(methyl)phosphoryl]butanoate) (GLF) have been studied by Taylor dispersion technique (Chapter 6-III). Then, sorption as effective water treatment methodology for pesticides removal with potential reusability of the sorbent materials was employed. The attention was focused on active ingredients or commercial formulations whose usage is approved in Europe, namely imidacloprid and its commercial formulation Confidor O-TEQ®, cymoxanil, 2,4-D (2-(2,4-dichlorophenoxy)acetic acid), bentazon (2,2-dioxo-3-propan-2-yl-1H-2l6,1,3-benzothiadiazin-4-one) (BTZ), and mecoprop (2-(4-chloro-2-methylphenoxy)propanoic acid) (MCP). The approval of imidacloprid expired in 2021 based in the information reported in the European database of

active ingredients. The main aim of the thesis encompasses the development of novel polymeric materials highly efficient as sorbents for pesticides uptake from aqueous media, namely cyclodextrin-based nanosponges (CDNS) (Chapter 3.). Their application in the environmental remediation processes [96] is a field in its early years of development, particularly regarding pesticides removal [97,98]. Based on the class of the monomer used as crosslinker along the project, two families of CDNS can be identified, namely carbamate-CDNS and amine-CDNS. In particular, the focus is centred on how the physico-chemical properties of the crosslinkers and cyclodextrins can influence the physico-chemical characteristics of the material, and consequently the sorbent-sorbate interactions. The synthesized CDNS were deeply characterized (Chapter 4.), the uptake capability of pesticides was assessed via equilibria and kinetic sorption methodologies. The sorbent-sorbate interaction was also molecularly studied via molecular dynamic simulations (Chapter 5.). The scientific results are presented in Chapter 6 from III to VIII.

1.3. Thesis structure

For the sake of clarity and to guide the reader along the thesis, this is divided as briefly described below:

Chapter 1 introduces the reader to the issue of environmental pollution, surveying on the upsides and down sides of the pesticide's application. The objective of the PhD project is described based on the scientific outcomes.

Chapter 2 features the state of art of the commonly water treatment technologies applied for pesticides removal.

Chapter 3 presents the main component of the thesis, namely the cyclodextrin and the cyclodextrin-based nanosponges. The state-of-art, route of synthesis, physico-chemical properties and the areas of application are described in detail in the reported book chapter (I) and review paper (II).

Chapter 4 presents the main methods utilized to fully characterize the sorbent systems, the physico-chemical properties of the cyclodextrin-based nanosponges are compared in order to give a deep understanding of the systems used for pesticides removal.

Chapter 5 introduces the theoretical background of the main methodologies that have been used to understand the transport phenomena in the two main liquid-liquid and solid-liquid interface systems.

Chapter 6 reports the scientific outcomes that have been published along the PhD project.

References of chapter 1.

[1] M.L. Brusseau, I.L. Pepper, C.P. Gerba, The Extent of Global Pollution, in: M.L. Brusseau, I.L. Pepper, C.P. Gerba (Eds.), Environ. Pollut. Sci., 3rd ed., Elsevier, 2019: pp. 3–8. https://doi.org/10.1016/B978-0-12-814719-1.00001-X.

[2] U. Nations, World Population Prospects 2022, 2022. www.un.org/development/ desa/pd/.

[3] V. Srivastava, E.N. Zare, P. Makvandi, X. Zheng, S. Iftekhar, A. Wu, V.V.T. Padil, B. Mokhtari, R.S. Varma, F.R. Tay, M. Sillanpaa, Cytotoxic aquatic pollutants and their removal by nanocomposite-based sorbents, Chemosphere. 258 (2020) 127324. https://doi.org/10.1016/j.chemosphere.2020.127324.

[4] M.L. Brusseau, Physical Processes Affecting Contaminant Transport and Fate, in: M.L. Brusseau, I.L. Pepper, C.P. Gerba (Eds.), Environ. Pollut. Sci., 3rd ed., Elsevier, 2019: pp. 103–112. https://doi.org/10.1016/B978-0-12-814719-1.00007-0.

[5] J. Maximillian, M.L. Brusseau, E.P. Glenn, A.D. Matthias, Pollution and Environmental Perturbations in the Global System, in: M.L. Brusseau, I.L. Pepper, C.P. Gerba (Eds.), Environ. Pollut. Sci., 3rd ed., Elsevier, 2019: pp. 457–476. https://doi.org/10.1016/B978-0-12-814719-1.00025-2.

[6] M.L. Brusseau, J. Chorover, Chemical Processes Affecting Contaminant Transport and Fate, in: M.L. Brusseau, I.L. Pepper, C.P. Gerba (Eds.), Environ. Pollut. Sci., 3rd ed., Elsevier, 2019: pp. 113–130. https://doi.org/10.1016/B978-0-12-814719-1.00008-2.

[7] S. Rasool, T. Rasool, K.M. Gani, A review of interactions of pesticides within various interfaces of intrinsic and organic residue amended soil environment, Chem. Eng. J. Adv. 11 (2022) 100301. https://doi.org/10.1016/j.ceja.2022.100301.

[8] C.P. Gerba, Environmental Toxicology, in: M.L. Brusseau, I.L. Pepper, C.P. Gerba (Eds.), Environ. Pollut. Sci., 3rd ed., Elsevier, 2019: pp. 511–540. https://doi.org/10.1016/B978-0-12-814719-1.00028-8.

[9] M.W. Shahzad, M. Burhan, L. Ang, K.C. Ng, Energy-water-environment nexus underpinning future desalination sustainability, Desalination. 413 (2017) 52–64. https://doi.org/10.1016/j.desal.2017.03.009.

[10] S. Gligorovski, R. Strekowski, S. Barbati, D. Vione, Environmental Implications of Hydroxyl Radicals (• OH), Chem. Rev. 115 (2015) 13051–13092. https://doi.org/10.1021/cr500310b.

[11] L. Wang, W.-M. Wu, N.S. Bolan, D.C.W. Tsang, Y. Li, M. Qin, D. Hou, Environmental fate, toxicity and risk management strategies of nanoplastics in the environment: Current status and future perspectives, J. Hazard. Mater. 401 (2021) 123415. https://doi.org/10.1016/j.jhazmat.2020.123415.

[12] V. Tornero, M. Ribera d'Alcalà, Contamination by hazardous substances in the Gulf of

Naples and nearby coastal areas: A review of sources, environmental levels and potential impacts in the MSFD perspective, Sci. Total Environ. 466–467 (2014) 820–840. https://doi.org/10.1016/j.scitotenv.2013.06.106.

[13] UNEP, Stockholm Convention on persistent organic pollutants (POPS) - Texts and Annexes, Stockholm, 2019.

[14] W. and U. FAO, Synthesis Report on the Environmental and Health Impacts of Pesticides and Fertilizers and Ways to Minimize Them, 2022. https://wedocs.unep.org/xmlui/bitstream/handle/20.500.11822/38409/pesticides.pdf.

[15] D. McNaught, A. Wilkinson, pesticide, in: IUPAC Compend. Chem. Terminol., 2nd ed., IUPAC, Research Triagle Park, NC, 1997: p. 4519. https://doi.org/10.1351/goldbook.P04519.

[16] A. Sharma, A. Shukla, K. Attri, M. Kumar, P. Kumar, A. Suttee, G. Singh, R.P. Barnwal, N. Singla, Global trends in pesticides: A looming threat and viable alternatives, Ecotoxicol. Environ. Saf. 201 (2020) 110812. https://doi.org/10.1016/j.ecoenv.2020.110812.

[17] A. Mojiri, J.L. Zhou, B. Robinson, A. Ohashi, N. Ozaki, T. Kindaichi, H. Farraji, M. Vakili, Pesticides in aquatic environments and their removal by adsorption methods, Chemosphere. 253 (2020) 126646. https://doi.org/10.1016/j.chemosphere.2020.126646.

[18] G.R. Stephenson, I.G. Ferris, P.T. Holland, M. Nordberg, Glossary of terms relating to pesticides (IUPAC Recommendations 2006), Pure Appl. Chem. 78 (2006) 2075–2154. https://doi.org/10.1351/pac200678112075.

[19] R.M. de Souza, D. Seibert, H.B. Quesada, F. de Jesus Bassetti, M.R. Fagundes-Klen, R. Bergamasco, Occurrence, impacts and general aspects of pesticides in surface water: A review, Process Saf. Environ. Prot. 135 (2020) 22–37. https://doi.org/10.1016/j.psep.2019.12.035.

[20] J. Cooper, H. Dobson, The benefits of pesticides to mankind and the environment, Crop Prot. 26 (2007) 1337–1348. https://doi.org/10.1016/j.cropro.2007.03.022.

[21] L. Parra-Arroyo, R.B. González-González, C. Castillo-Zacarías, E.M. Melchor Martínez, J.E. Sosa-Hernández, M. Bilal, H.M.N. Iqbal, D. Barceló, R. Parra-Saldívar, Highly hazardous pesticides and related pollutants: Toxicological, regulatory, and analytical aspects, Sci. Total Environ. 807 (2022) 18–26. https://doi.org/10.1016/j.scitotenv.2021.151879.

[22] D.A.M. Alexandrino, C.M.R. Almeida, A.P. Mucha, M.F. Carvalho, Revisiting pesticide pollution: The case of fluorinated pesticides, Environ. Pollut. 292 (2022) 118315. https://doi.org/10.1016/j.envpol.2021.118315.

[23] T.O. Ajiboye, P.O. Oladoye, C.A. Olanrewaju, G.O. Akinsola, Organophosphorus pesticides: Impacts, detection and removal strategies, Environ. Nanotechnology, Monit.

Manag. 17 (2022) 100655. https://doi.org/10.1016/j.enmm.2022.100655.

[24] H. Fu, P. Tan, R. Wang, S. Li, H. Liu, Y. Yang, Z. Wu, Advances in organophosphorus pesticides pollution: Current status and challenges in ecotoxicological, sustainable agriculture, and degradation strategies, J. Hazard. Mater. 424 (2022) 127494. https://doi.org/10.1016/j.jhazmat.2021.127494.

[25] P. Montuori, S. Aurino, A. Nardone, T. Cirillo, M. Triassi, Spatial distribution and partitioning of organophosphates pesticide in water and sediment from Sarno River and Estuary, Southern Italy, Environ. Sci. Pollut. Res. 22 (2015) 8629–8642. https://doi.org/10.1007/s11356-014-4016-z.

[26] R.C. Gupta, Carbamate Pesticides, Encycl. Toxicol. 1 (2014) 661–664. https://doi.org/10.1016/B978-0-12-386454-3.00106-8.

[27] W. Tang, D. Wang, J. Wang, Z. Wu, L. Li, M. Huang, S. Xu, D. Yan, Pyrethroid pesticide residues in the global environment: An overview, Chemosphere. 191 (2018) 990–1007. https://doi.org/10.1016/j.chemosphere.2017.10.115.

[28] Q. Zhang, Z. Li, C.H. Chang, J.L. Lou, M.R. Zhao, C. Lu, Potential human exposures to neonicotinoid insecticides: A review, Environ. Pollut. 236 (2018) 71–81. https://doi.org/10.1016/j.envpol.2017.12.101.

[29] A. Knowles, Recent developments of safer formulations of agrochemicals, Environmentalist. 28 (2008) 35–44. https://doi.org/10.1007/s10669-007-9045-4.

[30] M. Wypij, J. Trzcińska-Wencel, P. Golińska, G.D. Avila-Quezada, A.P. Ingle, M. Rai, The strategic applications of natural polymer nanocomposites in food packaging and agriculture: Chances, challenges, and consumers' perception, Front. Chem. 10 (2023) 1–18. https://doi.org/10.3389/fchem.2022.1106230.

[31] P. Fincheira, N. Hoffmann, G. Tortella, A. Ruiz, P. Cornejo, M.C. Diez, A.B. Seabra, A. Benavides-Mendoza, O. Rubilar, Eco-Efficient Systems Based on Nanocarriers for the Controlled Release of Fertilizers and Pesticides: Toward Smart Agriculture, Nanomaterials. 13 (2023) 1978. https://doi.org/10.3390/nano13131978.

[32] L. Zhao, C. Ortiz, A.S. Adeleye, Q. Hu, H. Zhou, Y. Huang, A.A. Keller, Metabolomics to Detect Response of Lettuce (Lactuca sativa) to Cu(OH) 2 Nanopesticides: Oxidative Stress Response and Detoxification Mechanisms, Environ. Sci. Technol. 50 (2016) 9697–9707. https://doi.org/10.1021/acs.est.6b02763.

[33] L. Cao, Z. Zhou, S. Niu, C. Cao, X. Li, Y. Shan, Q. Huang, Positive-Charge Functionalized Mesoporous Silica Nanoparticles as Nanocarriers for Controlled 2,4-Dichlorophenoxy Acetic Acid Sodium Salt Release, J. Agric. Food Chem. 66 (2018) 6594–6603. https://doi.org/10.1021/acs.jafc.7b01957.

[34] Sandhya, S. Kumar, D. Kumar, N. Dilbaghi, Preparation, characterization, and bio-efficacy evaluation of controlled release carbendazim-loaded polymeric nanoparticles,

Environ. Sci. Pollut. Res. 24 (2017) 926–937. https://doi.org/10.1007/s11356-016-7774-y.

[35] R. Grillo, Z. Clemente, J.L. de Oliveira, E.V.R. Campos, V.C. Chalupe, C.M. Jonsson, R. de Lima, G. Sanches, C.S. Nishisaka, A.H. Rosa, K. Oehlke, R. Greiner, L.F. Fraceto, Chitosan nanoparticles loaded the herbicide paraquat: The influence of the aquatic humic substances on the colloidal stability and toxicity, J. Hazard. Mater. 286 (2015) 562–572. https://doi.org/10.1016/j.jhazmat.2014.12.021.

[36] J. Mo, L. Dai, L. Chen, Y. Wang, A. Huang, L. Wang, L. Ma, Structural effects of organobentonites on controlled release of pretilachlor, Appl. Clay Sci. 115 (2015) 150–156. https://doi.org/10.1016/j.clay.2015.07.036.

[37] Y. Xiang, G. Zhang, Y. Chi, D. Cai, Z. Wu, Fabrication of a controllable nanopesticide system with magnetic collectability, Chem. Eng. J. 328 (2017) 320–330. https://doi.org/10.1016/j.cej.2017.07.046.

[38] X. Liu, B. He, Z. Xu, M. Yin, W. Yang, H. Zhang, J. Cao, J. Shen, A functionalized fluorescent dendrimer as a pesticide nanocarrier: application in pest control, Nanoscale. 7 (2015) 445–449. https://doi.org/10.1039/C4NR05733C.

[39] J.L. de Oliveira, E.V.R. Campos, C.M. Gonçalves da Silva, T. Pasquoto, R. Lima, L.F. Fraceto, Solid Lipid Nanoparticles Co-loaded with Simazine and Atrazine: Preparation, Characterization, and Evaluation of Herbicidal Activity, J. Agric. Food Chem. 63 (2015) 422–432. https://doi.org/10.1021/jf5059045.

[40] M.F.B. Mfarrej, F.M. Rara, Competitive, Sustainable Natural Pesticides, Acta Ecol. Sin. 39 (2019) 145–151. https://doi.org/10.1016/j.chnaes.2018.08.005.

[41] I. Md Meftaul, K. Venkateswarlu, R. Dharmarajan, P. Annamalai, M. Megharaj, Pesticides in the urban environment: A potential threat that knocks at the door, Sci. Total Environ. 711 (2020) 134612. https://doi.org/10.1016/j.scitotenv.2019.134612.

[42] W. Aktar, D. Sengupta, A. Chowdhury, Impact of pesticides use in agriculture: their benefits and hazards, Interdiscip. Toxicol. 2 (2009) 1–12. https://doi.org/10.2478/v10102-009-0001-7.

[43] M. Barzman, P. Bàrberi, A.N.E. Birch, P. Boonekamp, S. Dachbrodt-Saaydeh, B. Graf, B. Hommel, J.E. Jensen, J. Kiss, P. Kudsk, J.R. Lamichhane, A. Messéan, A.-C. Moonen, A. Ratnadass, P. Ricci, J.-L. Sarah, M. Sattin, Eight principles of integrated pest management, Agron. Sustain. Dev. 35 (2015) 1199–1215. https://doi.org/10.1007/s13593-015-0327-9.

[44] A. Dugger-Webster, C.E. LePrevost, Following pesticide labels: A continued journey toward user comprehension and safe use, Curr. Opin. Environ. Sci. Heal. 4 (2018) 19–26. https://doi.org/10.1016/j.coesh.2018.03.004.

[45] P. Kalofiri, G. Balias, F. Tekos, The EU endocrine disruptors' regulation and the glyphosate controversy, Toxicol. Reports. 8 (2021) 1193–1199.

https://doi.org/10.1016/j.toxrep.2021.05.013.

[46] M. Lykogianni, E. Bempelou, F. Karamaouna, K.A. Aliferis, Do pesticides promote or hinder sustainability in agriculture? The challenge of sustainable use of pesticides in modern agriculture, Sci. Total Environ. 795 (2021) 148625. https://doi.org/10.1016/j.scitotenv.2021.148625.

[47] N. Baran, A.E. Rosenbom, R. Kozel, D. Lapworth, Pesticides and their metabolites in European groundwater: Comparing regulations and approaches to monitoring in France, Denmark, England and Switzerland, Sci. Total Environ. 842 (2022) 156696. https://doi.org/10.1016/j.scitotenv.2022.156696.

[48] I. Iavicoli, V. Leso, D.H. Beezhold, A.A. Shvedova, Nanotechnology in agriculture: Opportunities, toxicological implications, and occupational risks, Toxicol. Appl. Pharmacol. 329 (2017) 96–111. https://doi.org/10.1016/j.taap.2017.05.025.

[49] J.R. Lamichhane, Pesticide use and risk reduction in European farming systems with IPM: An introduction to the special issue, Crop Prot. 97 (2017) 1–6. https://doi.org/10.1016/j.cropro.2017.01.017.

[50] D.S. Gamble, The chemistry component of agricultural pesticide regulatory technology, Curr. Opin. Environ. Sci. Heal. 4 (2018) 16–18. https://doi.org/10.1016/j.coesh.2018.03.003.

[51] A. Di Guardo, A. Finizio, A moni-modelling approach to manage groundwater risk to pesticide leaching at regional scale, Sci. Total Environ. 545–546 (2016) 200–209. https://doi.org/10.1016/j.scitotenv.2015.12.056.

[52] C.A. Damalas, Pesticides in agriculture: Environmental and health risks, Curr. Opin. Environ. Sci. Heal. 4 (2018) 4–5. https://doi.org/10.1016/j.coesh.2018.08.001.

[53] H.A. Rother, Pesticide labels: Protecting liability or health? – Unpacking “misuse” of pesticides, Curr. Opin. Environ. Sci. Heal. 4 (2018) 10–15. https://doi.org/10.1016/j.coesh.2018.02.004.

[54] D. Pimentel, Amounts of pesticides reaching target pests: Environmental impacts and ethics, J. Agric. Environ. Ethics. 8 (1995) 17–29. https://doi.org/10.1007/BF02286399.

[55] J.S. Brown, K. Staňková, Game theory as a conceptual framework for managing insect pests, Curr. Opin. Insect Sci. 21 (2017) 26–32. https://doi.org/10.1016/j.cois.2017.05.007.

[56] T.W. Sappington, N.J. Miller, Editorial overview: Pests and resistance: Shedding the albatross of resistance starts by embracing the ecological complexities of its evolution, Curr. Opin. Insect Sci. 21 (2017) v–viii. https://doi.org/10.1016/j.cois.2017.07.003.

[57] T. Perry, P. Batterham, Harnessing model organisms to study insecticide resistance, Curr. Opin. Insect Sci. 27 (2018) 61–67. https://doi.org/10.1016/j.cois.2018.03.005.

[58] M. Zalucki, M. Furlong, Behavior as a mechanism of insecticide resistance: evaluation of the evidence, Curr. Opin. Insect Sci. 21 (2017) 19–25.

https://doi.org/10.1016/j.cois.2017.05.006.

[59] A. Alyokhin, Y.H. Chen, Adaptation to toxic hosts as a factor in the evolution of insecticide resistance, Curr. Opin. Insect Sci. 21 (2017) 33–38. https://doi.org/10.1016/j.cois.2017.04.006.

[60] P. Segurado, N. Caiola, D. Pont, J.M. Oliveira, O. Delaigue, M.T. Ferreira, Comparability of fish-based ecological quality assessments for geographically distinct Iberian regions, Sci. Total Environ. 476–477 (2014) 785–794. https://doi.org/10.1016/j.scitotenv.2013.09.004.

[61] R. Schulz, Field Studies on Exposure, Effects, and Risk Mitigation of Aquatic Nonpoint-Source Insecticide Pollution: A Review, J. Environ. Qual. 33 (2004) 419–448. https://doi.org/10.2134/jeq2004.4190.

[62] D.P. Oliver, J.S. Anderson, A. Davis, S. Lewis, J. Brodie, R. Kookana, Banded applications are highly effective in minimising herbicide migration from furrow-irrigated sugar cane, Sci. Total Environ. 466–467 (2014) 841–848. https://doi.org/10.1016/j.scitotenv.2013.07.117.

[63] M. Lefrancq, A. Jadas-Hécart, I. La Jeunesse, D. Landry, S. Payraudeau, High frequency monitoring of pesticides in runoff water to improve understanding of their transport and environmental impacts, Sci. Total Environ. 587–588 (2017) 75–86. https://doi.org/10.1016/j.scitotenv.2017.02.022.

[64] S. Das, W. Wang, S. Reeves, R.C. Dalal, Y.P. Dang, A. Gonzalez, P.M. Kopittke, Non-target impacts of pesticides on soil N transformations, abundances of nitrifying and denitrifying genes, and nitrous oxide emissions, Sci. Total Environ. 844 (2022) 157043. https://doi.org/10.1016/j.scitotenv.2022.157043.

[65] C. Mottes, M. Lesueur Jannoyer, M. Le Bail, M. Guéné, C. Carles, E. Malézieux, Relationships between past and present pesticide applications and pollution at a watershed outlet: The case of a horticultural catchment in Martinique, French West Indies, Chemosphere. 184 (2017) 762–773. https://doi.org/10.1016/j.chemosphere.2017.06.061.

[66] E. Borrás, M. Ródenas, T. Vera, T. Gómez, A. Muñoz, Atmospheric degradation of the organothiophosphate insecticide – Pirimiphos-methyl, Sci. Total Environ. 579 (2017) 1–9. https://doi.org/10.1016/j.scitotenv.2016.11.009.

[67] Z. Vryzas, Pesticide fate in soil-sediment-water environment in relation to contamination preventing actions, Curr. Opin. Environ. Sci. Heal. 4 (2018) 5–9. https://doi.org/10.1016/j.coesh.2018.03.001.

[68] K. Anagnostopoulou, C. Nannou, E. Evgenidou, D. Lambropoulou, Overarching issues on relevant pesticide transformation products in the aquatic environment: A review, Sci. Total Environ. 815 (2022) 152863. https://doi.org/10.1016/j.scitotenv.2021.152863.

[69] S. Sabzevari, J. Hofman, A worldwide review of currently used pesticides' monitoring in

agricultural soils, Sci. Total Environ. 812 (2022) 152344. https://doi.org/10.1016/j.scitotenv.2021.152344.

[70] V. Silva, H.G.J. Mol, P. Zomer, M. Tienstra, C.J. Ritsema, V. Geissen, Pesticide residues in European agricultural soils – A hidden reality unfolded, Sci. Total Environ. 653 (2019) 1532–1545. https://doi.org/10.1016/j.scitotenv.2018.10.441.

[71] C.P.M. Bento, D. Goossens, M. Rezaei, M. Riksen, H.G.J. Mol, C.J. Ritsema, V. Geissen, Glyphosate and AMPA distribution in wind-eroded sediment derived from loess soil, Environ. Pollut. 220 (2017) 1079–1089. https://doi.org/10.1016/j.envpol.2016.11.033.

[72] N. Desmet, K. Touchant, P. Seuntjens, T. Tang, J. Bronders, A hybrid monitoring and modelling approach to assess the contribution of sources of glyphosate and AMPA in large river catchments, Sci. Total Environ. 573 (2016) 1580–1588. https://doi.org/10.1016/j.scitotenv.2016.09.100.

[73] B. Reoyo-Prats, D. Aubert, C. Menniti, W. Ludwig, J. Sola, M. Pujo-Pay, P. Conan, O. Verneau, C. Palacios, Multicontamination phenomena occur more often than expected in Mediterranean coastal watercourses: Study case of the Têt River (France), Sci. Total Environ. 579 (2017) 10–21. https://doi.org/10.1016/j.scitotenv.2016.11.019.

[74] A. Di Guardo, A. Finizio, A new methodology to identify surface water bodies at risk by using pesticide monitoring data: The glyphosate case study in Lombardy Region (Italy), Sci. Total Environ. 610–611 (2018) 421–429. https://doi.org/10.1016/j.scitotenv.2017.08.049.

[75] V.C. Schreiner, E. Szöcs, A.K. Bhowmik, M.G. Vijver, R.B. Schäfer, Pesticide mixtures in streams of several European countries and the USA, Sci. Total Environ. 573 (2016) 680–689. https://doi.org/10.1016/j.scitotenv.2016.08.163.

[76] M. Kapsi, C. Tsoutsi, A. Paschalidou, T. Albanis, Environmental monitoring and risk assessment of pesticide residues in surface waters of the Louros River (N.W. Greece), Sci. Total Environ. 650 (2019) 2188–2198. https://doi.org/10.1016/j.scitotenv.2018.09.185.

[77] E.T. Rodrigues, M.F. Alpendurada, F. Ramos, M.Â. Pardal, Environmental and human health risk indicators for agricultural pesticides in estuaries, Ecotoxicol. Environ. Saf. 150 (2018) 224–231. https://doi.org/10.1016/J.ECOENV.2017.12.047.

[78] Z. Li, P. Fantke, Toward harmonizing global pesticide regulations for surface freshwaters in support of protecting human health, J. Environ. Manage. 301 (2022) 113909. https://doi.org/10.1016/j.jenvman.2021.113909.

[79] A. Pérez-Parada, G. Goyenola, F. Teixeira de Mello, H. Heinzen, Recent advances and open questions around pesticide dynamics and effects on freshwater fishes, Curr. Opin. Environ. Sci. Heal. 4 (2018) 38–44. https://doi.org/10.1016/j.coesh.2018.08.004.

[80] P.C. Jepson, K. Murray, O. Bach, M.A. Bonilla, L. Neumeister, Selection of pesticides to reduce human and environmental health risks: a global guideline and minimum pesticides

list, Lancet Planet. Heal. 4 (2020) e56–e63. https://doi.org/10.1016/S2542-5196(19)30266-9.

[81] I.M. Meftaul, K. Venkateswarlu, P. Annamalai, A. Parven, M. Megharaj, Glyphosate use in urban landscape soils: Fate, distribution, and potential human and environmental health risks, J. Environ. Manage. 292 (2021) 112786. https://doi.org/10.1016/j.jenvman.2021.112786.

[82] V.P. Kalyabina, E.N. Esimbekova, K. V. Kopylova, V.A. Kratasyuk, Pesticides: formulants, distribution pathways and effects on human health – a review, Toxicol. Reports. 8 (2021) 1179–1192. https://doi.org/10.1016/j.toxrep.2021.06.004.

[83] A. Intisar, A. Ramzan, T. Sawaira, A.T. Kareem, N. Hussain, M.I. Din, M. Bilal, H.M.N. Iqbal, Occurrence, toxic effects, and mitigation of pesticides as emerging environmental pollutants using robust nanomaterials – A review, Chemosphere. 293 (2022) 133538. https://doi.org/10.1016/j.chemosphere.2022.133538.

[84] M. Eddleston, Poisoning by pesticides, Medicine (Baltimore). 48 (2020) 214–217. https://doi.org/10.1016/j.mpmed.2019.12.019.

[85] G. Wang, J. Li, N. Xue, A. Abdulkreem AL-Huqail, H.S. Majdi, E. Darvishmoghaddam, H. Assilzadeh, M.A. Khadimallah, H.E. Ali, Risk assessment of organophosphorus pesticide residues in drinking water resources: Statistical and Monte-Carlo approach, Chemosphere. 307 (2022) 135632. https://doi.org/10.1016/j.chemosphere.2022.135632.

[86] I.R.G. Prudente, C.L. Cruz, L. de C. Nascimento, C.C. Kaiser, A.G. Guimarães, Evidence of risks of renal function reduction due to occupational exposure to agrochemicals: A systematic review, Environ. Toxicol. Pharmacol. 63 (2018) 21–28. https://doi.org/10.1016/j.etap.2018.08.006.

[87] Z. Fallah, E.N. Zare, M. Ghomi, F. Ahmadijokani, M. Amini, M. Tajbakhsh, M. Arjmand, G. Sharma, H. Ali, A. Ahmad, P. Makvandi, E. Lichtfouse, M. Sillanpää, R.S. Varma, Toxicity and remediation of pharmaceuticals and pesticides using metal oxides and carbon nanomaterials, Chemosphere. 275 (2021) 130055. https://doi.org/10.1016/j.chemosphere.2021.130055.

[88] I.N. Tsakiris, M. Goumenou, M.N. Tzatzarakis, A.K. Alegakis, C. Tsitsimpikou, E. Ozcagli, D. Vynias, A.M. Tsatsakis, Risk assessment for children exposed to DDT residues in various milk types from the Greek market, Food Chem. Toxicol. 75 (2015) 156–165. https://doi.org/10.1016/j.fct.2014.11.012.

[89] M. Ye, J. Beach, J.W. Martin, A. Senthilselvan, Pesticide exposures and respiratory health in general populations, J. Environ. Sci. 51 (2017) 361–370. https://doi.org/10.1016/j.jes.2016.11.012.

[90] J.X.F. Sim, C.L. Doolette, S. Vasileiadis, B. Drigo, E.R. Wyrsch, S.P. Djordjevic, E. Donner, D.G. Karpouzas, E. Lombi, Pesticide effects on nitrogen cycle related microbial

functions and community composition, Sci. Total Environ. 807 (2022) 150734. https://doi.org/10.1016/j.scitotenv.2021.150734.

[91] V. Dhananjayan, B. Ravichandran, Occupational health risk of farmers exposed to pesticides in agricultural activities, Curr. Opin. Environ. Sci. Heal. 4 (2018) 31–37. https://doi.org/10.1016/j.coesh.2018.07.005.

[92] C. Bass, I. Denholm, M.S. Williamson, R. Nauen, The global status of insect resistance to neonicotinoid insecticides, Pestic. Biochem. Physiol. 121 (2015) 78–87. https://doi.org/10.1016/j.pestbp.2015.04.004.

[93] M. Koureas, A. Tsezou, A. Tsakalof, T. Orfanidou, C. Hadjichristodoulou, Increased levels of oxidxative DNA damage in pesticide sprayers in Thessaly Region (Greece). Implications of pesticide exposure, Sci. Total Environ. 496 (2014) 358–364. https://doi.org/10.1016/j.scitotenv.2014.07.062.

[94] Q. Zhang, Z. Lu, C.-H. Chang, C. Yu, X. Wang, C. Lu, Dietary risk of neonicotinoid insecticides through fruit and vegetable consumption in school-age children, Environ. Int. 126 (2019) 672–681. https://doi.org/10.1016/j.envint.2019.02.051.

[95] S. Guilherme, M.A. Santos, I. Gaivão, M. Pacheco, Are DNA-damaging effects induced by herbicide formulations (Roundup® and Garlon®) in fish transient and reversible upon cessation of exposure?, Aquat. Toxicol. 155 (2014) 213–221. https://doi.org/10.1016/j.aquatox.2014.06.007.

[96] K. Köse, M. Tüysüz, D. Aksüt, L. Uzun, Modification of cyclodextrin and use in environmental applications, Environ. Sci. Pollut. Res. 29 (2022) 182–209. https://doi.org/10.1007/s11356-021-15005-y.

[97] A. Marican, E.F. Durán-Lara, A review on pesticide removal through different processes, Environ. Sci. Pollut. Res. 25 (2018) 2051–2064. https://doi.org/10.1007/s11356-017-0796-2.

[98] G. Utzeri, P.M.C. Matias, D. Murtinho, A.J.M. Valente, Cyclodextrin-Based Nanosponges: Overview and Opportunities, Front. Chem. 10 (2022) 1–25. https://doi.org/10.3389/fchem.2022.859406.

Chapter 2.

2. Pesticides cleaning techniques

The application of the right technologies for the remediation of water-stream is of immeasurable importance. These enable the profitable use of surface and groundwater, to provide drinking water in urban areas and uncontaminated water for agriculture and fosterage. The treatment of water usually foresees the combination of physical (filtration, distillation, sedimentation, and reverse osmosis), chemical (photodegradation, electrochemical oxidation, advanced oxidation processes (AOP)), biological (bioremediation, phytoremediation), and physico-chemical methods (sorption) [1–9]. Following, the strategies commonly used for pesticide removal are discussed [10]. The Table 2.1 highlights the advantages and disadvantages of the main methods' classes.

2.1.Biological treatments

Bioremediation can be divided into three different processes such the activated sludge with usage of microorganisms, the constructed wetland with application of plants (also called phytoremediation), and different types of bioreactors (*e.g.* membrane bioreactor, aerobic or anaerobic, microalgae bioreactor, and fungal bioreactor, among others). The aim is the conversion of pollutant molecules into less harmful by-products and/or mineralization in CO_2 and H_2O. Several factors such as soil type, moisture, pH, organic matter, temperature, pesticides concentration and their properties can influence the process [11]. The main advantages of the biological methods are the lower operational and management costs than chemical treatment as AOP or physical treatment as reverse osmosis or nanofiltration; and the production of less toxic by-products compared to chlorination or electrochemical approaches discussed below. However, it involves a massive production of sludge wastes, long-time consumption and installation processes [12]. The activated sludge is one of the most conventional and applied wastewater treatment methods [13]. It is based on the microorganisms growing via aerobic, anaerobic or anoxic routes depending on the concentration of dissolved oxygen. The process could be performed by natural attenuation (exploitation of the natural capacities of the matrix), bioaugmentation (introduction of endogenous, exogenous, or modified microorganisms) [14] and bio-stimulation (addition of nutrients). Matrixes are usually composed of humic-rich substances which collect and increase soil, microorganisms, and pesticides concentration.

Table 2.1. Advantages and disadvantages of water treatment methods.

Treatment	Advantages	Disadvantages
Chemical methods		
Oxidation processes	- disinfection properties; - low costs; -easily applicable; - reduction of odors; - faster precipitation processes; - precipitation of colloidal particles.	- high operational costs; - separation step needed; - catalysts; - hazardous by-products; - large amount of wastes; - harmful wastes; - high time consumption for optimization
Advanced oxidation processes	- low sludges production; - high reaction rate; - disinfection properties; - Low cost of reagents.	- high operational costs; - high maintenance costs; - not available in turbid batches.
Photocatalysis	- wide range of pollutants; - high degradation rate.	- operational costs; - large volume of wastewater.
Physical methods		
Nanofiltration	- high rejection yield; - pore size dependency.	- high operational costs; - high maintenance costs; - pores size dependence: - disposal; - fouling.
Reverse osmosis	- high rejection yield; - pore size dependency; - efficient for ions and organic pollutants.	- high operational costs; - high maintenance costs; - fouling; - water wastes.
Biological methods		
Activated sludge	- low installation costs; - environmentally friendly; - reduction of odours.	- high amount of wastes; - high maintenance demand; - suitable for COD < 4000 mg L^{-1}. - required disposal methods.
Phytoremediation	- environmentally friendly; - low sludge production; -low management costs.	- high procedural costs; - high time consuming; - seasonal dependency.
Microalgae	- reusability; - environmentally friendly; - low toxicity risk; - source of biomass and fertilizer.	- high controlling parameters; - narrow range of contaminants; - seasonal dependency.

Notes: COD: chemical oxygen demand

Different types of microorganisms can be adopted such as bacteria [15], protozoa, fungi, enzymes, and algae. An active bacteria from Alkali Lake degrades 3.0 g L^{-1} of 2,4-D in 3 days [16]. *Bacillus thuringiensis* has demonstrated high capacity to mineralize a wide range of pollutants such imidacloprid (71% in 11 days) [17]. *Stenotrophomonas maltophilia* CGMCC 1.1788 hydroxylases thiacloprid and imidacloprid which hydroxylated form presents lower and higher insecticidal activity, respectively [18,19]. On the other hand, the same bacterial strain is able to demethylate the acetamiprid that in presence of 5% sucrose led to an enhancement of 59% of pesticide degradation with 17% of its reduction [20]. The white-rot fungus, *Trametes versicolor* was employed in bioaugmentation process for mineralization of carbendazim, edifenphos and metalaxyl [21]. It was also tested to degrade three insecticides with the follow decreasing efficiency: imiprothrin > cypermethrin > carbofuran [22].

Phytoremediation is an *ex-situ* or *in-situ* strategy used to degrade, stabilize and/or remove soil contaminants. Within phytoremediation, rhizoremediation is a specific approach based on the employment of the microbes developed at the level of the rhizosphere [23,24]. These are environmentally friendly methods, but prior excavation and large areas of installation are needed. Moreover, several years are required so that plants and roots attain an efficient removal rate, in which several factors such as selected species, soil, pH, moisture content and microbial activity play a crucial role [25]. A review reports that the removal efficiency of the constructed wetlands generally increases with the K_{oc} of the pesticides reaching the highest capability for organochlorine [26], organophosphate [27,28] and pyrethroid [29] classes of pesticides [30]. The design of vegetative filter strips near to agricultural fields permits the reduction of pesticide run-off as function of the vegetation species and width [31]. The reduction of atrazine, diazinon and permethrin concentration in simulated agricultural water was studied using *Leersia oryzoides, Typha latifolia* and *Sparganium Americanum*. The first one was the most effective in the atrazine and permethrin concentration reduction [32]. Algae, such *Pseudokirchneriella subcapitata* and *Chlorococcum sp.* were used to assess the toxicity and degradative ability for fenamiphos and its metabolites. Active ingredient and its metabolites are accumulated into *Chlorococcum sp.*, whereas only the metabolites are absorbed into *Pseudokirchneriella subcapitata* [33]. This study gives an idea about the role played by the chosen vegetative species and their possible selective interaction with the pollutant. Recently, genetically modified plants have been considered as a promising strategy to increase the tolerance and the metabolism of pesticides. Transgenic rice plants modified with the human cytochrome P450 CYP1A1 gene have demonstrated higher tolerance and metabolism rate for quizalofop-ethyl, norflurazon, mefenacet and chlortoluron [34]. The introduction of the genes P450 CYP1A1, CYP2B6 and CYP2C19 have conducted to larger tolerance for the herbicides atrazine, metolachlor and norflurazon, and their mixture [35]. The cytochrome P450 activity, in maize, is expressed at the level of the shoots and can be inhibited by CO or O_2 presence. On the other hand, the activity can be also stimulated to two-fold of the

hydroxylation rate of the pyrimidine ring of primisulfuron [36]. In wheat plants, the NADPH-cytochrome P450 reductase degrades the chlortoluron by hydroxylation and *N*-demethylation reactions [37].

Even if biological treatments are the greenest methods simulating the natural ecosystem ability to respond against the water and soil pollution, many environmental and operating parameters must be controlled. In order to obtain faster degradation rates, higher efficiency and expand the range of treated pollutants, they are usually coupled with other treatments methods. An enhancement of atrazine degradation by 61% was achieved by immobilization of laccase in microporous starch [38]. Iron nanoparticles loaded with laccase have shown a higher removal efficiency for chlorpyrifos, where the presence of copper in the laccase play a key role in the sorption process [39]. Nanocellulose fibers were also used to immobilise and protect the laccase maintaining 75% of activity after 45 days, obtaining a complete degradation of trifluralin in 24 hours [40]. The grafting of the laccase to poly(glycidyl methacrylate) microsphere increases the temperature and pH stability of the enzyme with higher removal capability towards diazinon [41].

2.2.Chemical treatments

The chemical water treatments are based on chemical reactions which by-products are generally safer compounds. The most common are the oxidative, AOP and photochemical degradation.

Chlorination is a low expensive oxidative method easily implemented in water-treatment plants as pre- and/or post-treatment strategy. The process is based in the pH dependent hydrolysis of chlorine [42], therefore in the species present at equilibrium in water:

$$\underset{2.5 < pH < 5}{Cl_2 + 2H_2O \rightleftharpoons HOCl + H_3O^+ + Cl^-} \qquad \underset{5 < pH < 10}{HOCl + H_2O \rightleftharpoons OCl^- + H_3O^+}$$

The oxidative strength of the species Cl_2, HOCl and ClO^- permits them to unselectively react with a wide range of molecules, justifying its application as pre- and post-treatment of water. It is mainly used to limit the bacterial, algae and virus growth which can cause unpleasant odours, taste and act as vector disease. In particular, the main biocide ability is obtained when the HOCl and ClO^- are in equilibrium forming the "free chlorine" able to disrupt the lipidic membranes of pathogens. Moreover, some secondary reactions can occur, such as the oxidation of metal ions that precipitate, being removed by filtration. On the other hand, the high reactivity is at the same time the major drawback of the chlorination process because of the by-products with high toxicity such as the halogenated compounds: trihalomethanes (THM) and haloacetic acids (HAA). The THM are considered carcinogenic, and chronic exposure can damage liver and kidneys; the HAA are applied as harmful herbicides with side effects for the respiratory system. Chlorination can be successfully used to degrade OP pesticides (as described in Chapter 1-section 1.1, OP toxicity

depends on the amount of sulphur and valence of the phosphorus atoms). The presence of sulphur atoms represents a key factor in the degradation rate of OP pesticides. A study demonstrated that pH = 7 is optimum for degradation of three OP, which rate decreases in order diazinon > chlorpyrifos >> chlorfenvinfos. The presence of phosphorotioate groups in chlorpyrifos and diazinon speeds-up the oxidative reaction by HOCl into the oxon groups. THMs have been detected as by-products [43]. Oxidative reaction was performed for isoxathion, malathion and tolclofos-methyl adsorbed on powdered activated carbon. Thus, oxidation approaches were combined with sorption process [44]. The higher solubility and hydrophilicity of the oxon derivatives of diazinon chlorpyrifos, malathion and tolclofos-methyl make their removal more difficult by powdered activated carbon (AC) coupling coagulation-sedimentation-filtration (CSF). Additionally, they are more toxic and resistant to post-chlorination process with consequent accumulation [45]. The kinetic rate was also studied for phosphorothioate and phosphorodithioate pesticides, such chloroehoxyfos, chlorpyrifos, diazinon, parathion, tebupirimfos and malathion, methidathion, phosmet, respectively. In agreement with the other studies, higher kinetic constant values are obtained around pH = 7, with formation of the oxon derivatives [46]. Other important scientific outcomes involve the oxidation study of 10 organophosphate reporting the oxon formation from 7 of them [47]; the treatment of 44 pesticides in Ebro river Basin water via different methods, reaching 60% and 70% by chlorination and ozonation, respectively, and 90% combining the ozonation with adsorption into activated carbon [48].

Advanced oxidation processes encompass the usage of strong oxidative agents as hydroxyl (•OH) and sulphate ($\bullet SO_4^-$) radicals, with oxidation potential (E^0) of 2.72 V and 2.6 V and DT_{50} of 1 μs and *ca.* 35 μs, respectively. Ozone, ultraviolet light (UV), electrochemical-, catalytic- and photo-AOP can also be used [49–51]. AOP are environmentally friendly methods with a high degradation rate of a wide range of organic contaminant molecules and production of low amounts of wastes. However, the system design of AOP is complex and the application requires high operational and maintenance costs. $Na_2S_2O_8$ is used as strong oxidative agent, which can produce $\bullet SO_4^-$ radicals by heat, transition metals and ultraviolet or sunlight irradiation, Fe^{3+}-EDTA and pH; at the expense of the costs [52,53]:

$$S_2O_8^{2-} + hv/\Delta/UV \longrightarrow 2\ SO_4^{-}\bullet$$

Sulphate radicals react by oxidative process, electron transfer [54]. However, $\bullet SO_4^-$ radicals are the predominant species only at pH < 7, alkaline pH favours the formation of hydroxyl radical [55]. Sulphate radicals have been applied to degrade 17 pesticides with yield > 97% [56]. Atrazine was fully degraded after 2 h, using heat as an activation system [57]. Degradation of 90% of atrazine was obtained by iron-catalized photo-activation of $Na_2S_2O_8$, at acidic pH [58]. $\bullet SO_4^-$ also

ameliorates the degradative efficiency of UV photolysis rising the kinetic rate. However, the pH is a key parameter [59].

Ultraviolet light can be divided into UV-A (315-400 nm), UV-B (280-315 nm), UV-C (280-315 nm) and vacuum UV (10-180 nm). As electromagnetic radiation, lower wavelength means higher energy that can be employed as water treatment technology. Absorbing the energy light, pollutant molecules can be excited higher than activation energy permitting their transformation or reaction with other species. However, the photodegradation method requires high operational costs and is usually combined with other treatments, such H_2O_2 and O_3. Albeit UV-H_2O_2 and UV-O_3 are environmentally friendly and effective for a broad range of organic pollutant molecules, they cannot be employed in turbid media. The addition of H_2O_2 limits the range of efficient wavelengths; whereas concerning gas emissions must be considered with O_3. UV was applied for photo-degradation of parathion and chlorpyrifos in presence of $\bullet OH$ and $\bullet CO_3^-$ (E^0 = 1.78 V) with an enhancement of the degradation rate of both pesticides [60]. Malathion degradation by UV-H_2O_2 method is reported to be affected by pH and temperature [61]. In a study UV-H_2O_2 and UV-C processes were employed to degrade up to 97% of chlorpyrifos. However, UV-H_2O_2 leads to by-products formation [62].

Ozonation efficiency is based on direct reaction with O_3 (E^0 = 2.07 V) or indirectly reacting with the formed oxidative radicals. Due to the short lifetime of O_3, it must be generated *in-situ* with consequent increases of the operational costs. However, the high rate of reaction permits to treat large amount of water. In a study upon 23 pesticides, ozonation reaches around 85% of degradation for 6 pesticides [63]. The pH can play a crucial role as observed for the removal of endosulfan (89%) and lindane (43%) [64]. However, the efficiency can be increased if combined with hydrogen peroxide, H_2O_2/O_3 [65]. Combining ozonation with sorption into activated carbon, yield $\geq$ 50% was obtained for three pesticides within the 40 analysed [48]. Again, improved performances were obtained combining O_3 with activated carbon in a study performed in a water-treatment plant in Spain, reaching 70% of degradation for 44 pesticides [48]. Similar approach, which consists in combining O_3 and ZnO led to ca. 99% of removal for atrazine [66]. A complete degradation of triazophos was obtained combining ozonation and hydrodynamic cavitation treatment with removal of 96% of total organic content (TOC) [67]. Cavitation treatment exploits the transition phase from liquid to vapour phase with release of large amount of energy and formation of radical species. Different types of cavitation can be used (optic, particle, acoustic and hydrodynamic cavitation). The latter one is based on flow and pressure changes. The main disadvantages are the noise, the vibration, high pressure and temperature, and corrosion phenomena which can be solved/reduced by a proper design at expense of higher installation costs [68].

Fenton process is one of the most used oxidative pre- or post-treatment methods for organic contaminants, involving the reaction between H_2O_2 and Fe^{2+} ions that act as initiator and catalyst.

$$Fe^{2+} + H_2O_2 + H^+ \longrightarrow Fe^{3+} + OH\cdot + H_2O$$
$$Fe^{3+} + H_2O_2 \longrightarrow Fe^{2+} + \cdot HO_2 + H^+$$

It is an environmentally friendly process, employing abundant and non-expensive reagents, with short reaction time. The molar ratio of Fe^{2+}/Fe^{3+} and Fe^{2+}/H_2O_2 is a key factor and the equilibrium of speciation for Fe^{2+} and H_2O_2 is strongly dependent on pH. The reaction occurs at acidic pH, otherwise, the regeneration of ferrous ions is slow and the Fe^{3+} ions accumulate precipitating in the form of $Fe(OH)_3$(s) as by-products. Other drawback is represented by side-reaction of •OH with H_2O_2 and Fe^{2+}, and its consequent consumption. These technical specifications lead to higher amounts of reagents' consumption and operational costs. Studies reported the application of Fenton process for malathion removal coupled with other water-treatment methods such nanofiltration [69], hydrodynamic cavitation for methyl parathion [70] and triazophos [67], UV-light irradiation for chlorpyrifos, cypermethrin and chlorothalonil [71]. UV-Vis irradiation catalyses the photolysis of Fe^{3+}-complexes favouring Fe^{2+} ions formation; a combination called photo-assisted Fenton process. This method was applied in Murcia (Spain) with 90% of removal efficiency in a few minutes for 10 pesticides [72].

Photocatalysis method can overcome the needed of UV-Vis catalytic irradiation, utilizing the solar irradiation as activation system of the photo-catalytic properties of semiconductors such TiO_2, ZnO, ZnS, CdS, Fe_2O_3, WO_3, among others [73–75]. Once excited the electrons to the conduction band, a cascade of reactions starts with formation of •OH radicals [3]. Atrazine and diuron have been completely degraded using TiO_2/solar light in polluted soils [76,77]. Molecular imprinting TiO_2 sol-gel synthesis was performed in order to improve the specificity and degradation yield of *ca.* 35% for IMD or 2,4-D [78]. Around 95% of imidacloprid removal was achieved using photocatalysts composite of carbon nanotubes and H_2O_2 [79]. Abamectin was degraded at 99% using $Cu_2(OH)PO_4$-MOF activated by blue light irradiation and coupled to ultrasonic cavitation using a continuous flow-loop reactor [80]. The usage of composites usually led to complex and non-scalable synthesis processes; in the meanwhile the combination of different removal strategies led to higher costs [81]. More details about the state of art and future perspective of photocatalytic processes and its coupling with biological technologies has been described by K. Liu et al. [82].

Electrochemical methods are based on surface and bulk oxidative processes such as electrochemical, sono-, photo-, Fenton-electrochemical methods. These have been observed to be efficient on the mineralization of a wide range of classes of compounds including pesticides with a TOC reduction > 50%, either for water or soil treatment. For pesticides removal electro-Fenton and electrooxidation are the most used. The electrooxidation can be performed exploiting the physical-chemical properties of the material constituting the electrodes as platinum, boron-doped diamond [83], doped-SnO_2, PbO_2, carbonaceous materials and stainless steel, among others. The

hydroxyl radicals are formed on the anode surface by water oxidation through inactive or active electrode.

$$H_2O \longrightarrow OH\cdot + H^+ + e^-$$

A first drawback of this technique is the oxidation rate limited by chemical and mass transport phenomena in traditional-parallel reactors. Thus, research shifts the attention to porous membrane-electrodes with high surface areas which avoid diffusional limits. However, pressure is needed for water/wastewater passes into the electrode, increasing the costs. This technique is also dependent on the matrix composition given that the presence of inorganic species reduces the degradation rate. Moreover, the formation of halogenated by-product such as chlorine and perchlorate species was observed [84]. The *in-situ* application led to a mineralization degree of about 80% of TOC for lindane [85]. 2,4-D mineralization of 80% was achieved using N-doped graphene felt cathode [86]. Many other examples of different electrochemical processes applied for pesticides removal can be found in the following review [87].

2.3.Physical treatments

Generally, for physical treatment the separation process of solids is intended, which is usually applied as pre-treatment but not only. If pesticides are considered, the main applied physical treatments are reverse osmosis [88] and nanofiltration [89–92]. Both are membrane-based methods. The analyte-membrane interactions are dependent on the transport phenomena such as the diffusion of the analyte into the membrane, influenced by the solubility, hydrophilicity, charges and functional groups, both of analyte and membrane [93]. In order to ameliorate the rejection efficiency, the employed material, synthesis and surface modification routes are critical steps of the process [94,95]. Both reverse osmosis and nanofiltration systems work under pressure. The reverse osmosis exploits semipermeable membranes (*e.g.* cellulose acetate or triacetate, aromatic polyamides). The principle is based on the chemical affinity for the water, reaching *ca.* 99% of rejection of organic and inorganic solute [96,97]. Nanofiltration membranes have a pore size range of 1-10 nm. It works at lower pressure than reverse osmosis, still enabling the removal of ions and organic pollutants. Herein, porosity, pore size distribution and charges on the surface of the membranes play a crucial role in the rejection efficiency [98]. The application of pressure is considered a drawback due to the increase of the energetic costs. Moreover, the fouling phenomenon represents another critical point which led to high maintenance of the systems. Reverse osmosis tests have been performed using three commercial membranes at two different pressures with rejection > 95%, for four pesticides [99]. Similarly, seven membranes were tested for the rejection of three uncharged pesticides, namely terbutylazine, mecoprop and atrazine. Only two membranes have reached *ca.* 90% of rejection for all pesticides [100]. The

presence of dissolved organic carbon can limit the rejection. That was the case of atrazine, where the presence of dissolved organic carbon (DOC) decreases the efficiency from 99% to 50%, due to complexation and electrostatic repulsion with the analyte [101].

2.4.Physico-chemical treatment

A physico-chemical process extensively studied in the last decades is the sorption process. The easy application of the sorption method with high efficiency/cost ratio, makes it one of the most affordable techniques for pesticides removal [102]. Sorption results to be faster than biological methods such as bioremediation or phytoremediation [103]. It is also less expensive than chemical or physical treatments, like AOP or reverse osmosis. The classification as physico-chemical method is based on considering that chemical or physical interactions of sorbent-sorbate can take place as function of the structural design of the material. Among the more conventional materials used are clay [104], activated carbon or biochar, graphite and carbon nanotubes, and zeolites. These materials usually exhibit an amorphous or crystalline structure, negative charges, macro- (> 50 nm) to meso-porous (< 50 nm) and high surface area. However, the disadvantages are the high production and regeneration costs which do not permit an easy industrial scale-up [105,106]. In the past decades, great efforts have been made to design novel high-performant micro- or nano-materials, inorganic [107,108] or organic, and their composites [4,98,109,110] (Table 2.2. and Table 2.3.). The use of micro- and nano-particles of metal-oxides is favoured by their electrical, optical and magnetic properties, as well as their catalytic and antibacterial activities [111]. These properties of metal-oxide particles represent an advantage in the sorption process because chemical and physical interactions can occur simultaneously, favouring the removal efficiency. Yet, the application of inorganic nanoparticles is limited by aggregation phenomena, and nowadays deeply discussed because of various phytotoxic effects [112]. Polymeric materials have been the focus of extensive research, in the form of micro-/nano-spheres, powder, membranes [113], and hydrogels [114], among others [115]. Their abundance and/or low cost represent two significant upsides associated with fast kinetics and high removal efficiencies. Moreover, polymers can be chemically modified which pave the way to perform specific material design optimizing the physico-chemical properties and the performance of the so-called ‘biosorbents’ [116,117]. Examples of biosorbents include chitosan, poly(vinyl chloride), poly(vinyl alcohol) (PVA), poly(vinyl pyrrolidone) (PVP), cellulose [118,119], alginate, cucurbiturils, starch [120] and cyclodextrins, among others.

The focus of this thesis is centered in the application of cyclodextrins as substrate for the development of polymeric sorbents, named nanosponges. The state of art of the cyclodextrins, the method of modification and in particular the synthesis routes of the cyclodextrin-based

nanosponges with their application areas are extensively discussed in Chapter 3. Their physico-chemical properties will be discussed and compared in Chapter 4, along the exposition of the fundamentals of the methods of characterization.

Table 2.2. Advantages and disadvantages of common sorbent materials.

Materials	**Advantages**	**Challenges**
Zeolites	- Low cost; - High surface area; - suitable for different contaminants.	- Low capacity; - Low permeability; - Not suitable for organic contaminants.
Clays	- Low cost; - High surface area; - suitable for inorganic/organic contaminants; - high abundance.	- Low capacity; - pH sensitivity.
Carbonaceous-based	- Good capacity; - High efficiency in water; - Suitable for inorganic/organic contaminants.	- High cost; - Low selectivity; - Poor regeneration.
Silica-based	- Low cost; - High abundance.	- Degradation at alkaline pH.
Metal-oxide-based	- Low to high cost; - High surface area; - Tunable property structure; - High sensitivity.	- Low to high cost; - Safety assessment; - Aggregation; - Scale-up.
Polymer-based	- Low cost; - Tunable property structure; - Good biocompatibility; - Environmentally friendly.	- Degradation; - Safety assessment; - Scale-up.

Table 2.3. Examples of sorbent materials used in pesticide uptake.

Adsorbent materials	Form	Name of products	Results	Ref.
ZnO modified with BMTF-IL	NPs (4.25 nm)	**Naphthalene**: -pK_{ow}[a] = 3.29; -sol.[b] (mg L^{-1}) = 31.0.	-q_{max} (mg g^{-1}) = 148.3; -*RE%* = 98.8%.	[121]
Palygorskite modified with Fe_2O_3	NPs	**Fenarimol**: -pK_{ow}[a] = 3.69; -sol.[b] (mg L^{-1}) = 13.7.	-*RE%* = 70%; -ΔH (kJ mol^{-1}) = -128.41.	[122]
Fe_3O_4/SiO_2/GO -PEA	NSs	**Chlorpyrifos**: -pK_{ow}[a] = 4.7; -sol.[b] (mg L^{-1}) = 1.05. **Parathion** : -pK_{ow}[a] = 3.83; -sol.[b] (mg L^{-1}) = 12.4. **Malathion** (MLT): -pK_{ow}[a] = 2.75; -sol.[b] (mg L^{-1}) = 148.	-q_{max} (mg g^{-1}) = 11.1. -q_{max} (mg g^{-1}) = 10.6 (PRT). -q_{max} (mg g^{-1}) = 10.9 (MLT)..	[123]
NH_2-Fe/SBA-15	NPs (10-20nm)	**Glyphosate**: -pK_{ow}[a] = 3.2; -sol.[b] (mg L^{-1})= 10500.	-< *LOD*: 100 µg L^{-1} (pH = 2.1); -*DE%* = 100% (pH = 12.5).	[124]
MWCNTs	NTs (outer d.: 10-30nm; inner d.: 5-10nm)	**Malathion**: -pK_{ow}[a] = 2.75; -sol.[b] (mg L^{-1}) = 148.	-*RE%* = 100%.	[125]
HPVPcoS/MMT	NCs	**Diazinon**: -pK_{ow}[a] = 1.75; -sol.[b] (mg L^{-1}) = 10700.	-q_{max} (mol g^{-1}) = $5.4\times10^{-4;}$ -*RE%* = 80%; -*DE%* = 64%.	[126]
CMCD/SiO_2/Fe_3O_4	NPs	**Paraquat**: -pK_{ow}[a] = 3.83; -sol.[b] (mg L^{-1}) = 12.4. **Diquat**: -pK_{ow}[a] = 4.6; -sol.[b] (mg L^{-1}) = 718000.	-RE% = 70.2% paraquat; -RE% = 99% diquat (environmental water sample).	[127]

[a]:pK_{ow} at pH=7 and 20°C; [b]:water solubility at 20°C (data source: www.herts.ac.uk/aeru)
Notes: BMTF-IL: 1-butyl-3-methylimidazolium tetrafluoroborate; CMCD: carboxymethyl β-cyclodextrin; d.: diameter; *DE%* = desorption efficiency; GO: graphene oxide; HPVPcoS: protonated poly(4-vinyl-pyridine-co-styrene); LOD: limit of detection; MMT: montmorillonite; MSGB: magnetic switchgrass biochar; MWCNTs: multi-walled carbon nanotubes; NCs: nanocomposites; NSs: nanosheets; NTs: nanotubes; PEA: 2-phenylethylamine; q_{max}: adsorbed amount (mg or mol) per gram of adsorbent; *RE%*: removal efficiency; SBA-15: ordered mesoporous silica;

References of chapter 2.

[1] S. Esplugas, D.M. Bila, L.G.T. Krause, M. Dezotti, Ozonation and advanced oxidation technologies to remove endocrine disrupting chemicals (EDCs) and pharmaceuticals and personal care products (PPCPs) in water effluents, J. Hazard. Mater. 149 (2007) 631–642. https://doi.org/10.1016/j.jhazmat.2007.07.073.

[2] A. Marican, E.F. Durán-Lara, A review on pesticide removal through different processes, Environ. Sci. Pollut. Res. 25 (2018) 2051–2064. https://doi.org/10.1007/s11356-017-0796-2.

[3] A. Saravanan, P.S. Kumar, S. Jeevanantham, M. Anubha, S. Jayashree, Degradation of toxic agrochemicals and pharmaceutical pollutants: Effective and alternative approaches toward photocatalysis, Environ. Pollut. 298 (2022) 118844. https://doi.org/10.1016/j.envpol.2022.118844.

[4] A. Mojiri, J.L. Zhou, B. Robinson, A. Ohashi, N. Ozaki, T. Kindaichi, H. Farraji, M. Vakili, Pesticides in aquatic environments and their removal by adsorption methods, Chemosphere. 253 (2020) 126646. https://doi.org/10.1016/j.chemosphere.2020.126646.

[5] S. Gangola, P. Bhatt, A.J. Kumar, G. Bhandari, S. Joshi, A. Punetha, K. Bhatt, E.R. Rene, Biotechnological tools to elucidate the mechanism of pesticide degradation in the environment, Chemosphere. 296 (2022) 133916. https://doi.org/10.1016/j.chemosphere.2022.133916.

[6] O.M. Rodriguez-Narvaez, J.M. Peralta-Hernandez, A. Goonetilleke, E.R. Bandala, Treatment technologies for emerging contaminants in water: A review, Chem. Eng. J. 323 (2017) 361–380. https://doi.org/10.1016/j.cej.2017.04.106.

[7] M. Varsha, P. Senthil Kumar, B. Senthil Rathi, A review on recent trends in the removal of emerging contaminants from aquatic environment using low-cost adsorbents, Chemosphere. 287 (2022) 132270. https://doi.org/10.1016/j.chemosphere.2021.132270.

[8] C. Teodosiu, A.-F. Gilca, G. Barjoveanu, S. Fiore, Emerging pollutants removal through advanced drinking water treatment: A review on processes and environmental performances assessment, J. Clean. Prod. 197 (2018) 1210–1221. https://doi.org/10.1016/j.jclepro.2018.06.247.

[9] Z. Maqbool, S. Hussain, M. Imran, F. Mahmood, T. Shahzad, Z. Ahmed, F. Azeem, S. Muzammil, Perspectives of using fungi as bioresource for bioremediation of pesticides in the environment: a critical review, Environ. Sci. Pollut. Res. 23 (2016) 16904–16925. https://doi.org/10.1007/s11356-016-7003-8.

[10] G. L, C. I, C. P, S. A, Treatment Options for Reclaiming Wastewater Produced by the Pesticide Industry, Int. J. Water Wastewater Treat. 4 (2018). https://doi.org/10.16966/2381-5299.149.

[11] C. Niti, S. Sunita, K. Kamlesh, K. Rakesh, Bioremediation: An emerging technology for remediation of pesticides, Res. J. Chem. Environ. 17 (2013) 88–105.

[12] M. Vidali, Bioremediation. An overview, Pure Appl. Chem. 73 (2001) 1163–1172. https://doi.org/10.1351/pac200173071163.

[13] M. Scholz, Activated Sludge Processes, in: Wetl. Water Pollut. Control, 2nd ed., Elsevier, 2016: pp. 91–105. https://doi.org/10.1016/B978-0-444-63607-2.00015-0.

[14] M. Herrero, D.C. Stuckey, Bioaugmentation and its application in wastewater treatment: A review, Chemosphere. 140 (2015) 119–128. https://doi.org/10.1016/j.chemosphere.2014.10.033.

[15] S.K. Nayak, B. Dash, B. Baliyarsingh, Microbial Remediation of Persistent Agro-chemicals by Soil Bacteria: An Overview, in: J. Patra, G. Das, H. Shin (Eds.), Microb. Biotechnol., 1st ed., Springer Singapore, Singapore, 2018: pp. 275–301. https://doi.org/10.1007/978-981-10-7140-9_13.

[16] O. Maltseva, C. McGowan, R. Fulthorpe, P. Oriel, Degradation of 2,4-dichlorophenoxyacetic acid by haloalkaliphilic bacteria, Microbiology. 142 (1996) 1115–1122. https://doi.org/10.1099/13500872-142-5-1115.

[17] L. Ferreira, E. Rosales, A.S. Danko, M.A. Sanromán, M.M. Pazos, Bacillus thuringiensis a promising bacterium for degrading emerging pollutants, Process Saf. Environ. Prot. 101 (2016) 19–26. https://doi.org/10.1016/j.psep.2015.05.003.

[18] Y.-J. Zhao, Y.-J. Dai, C.-G. Yu, J. Luo, W.-P. Xu, J.-P. Ni, S. Yuan, Hydroxylation of thiacloprid by bacterium Stenotrophomonas maltophilia CGMCC1.1788, Biodegradation. 20 (2009) 761–768. https://doi.org/10.1007/s10532-009-9264-0.

[19] Y. Dai, S. Yuan, F. Ge, T. Chen, S. Xu, J. Ni, Microbial hydroxylation of imidacloprid for the synthesis of highly insecticidal olefin imidacloprid, Appl. Microbiol. Biotechnol. 71 (2006) 927–934. https://doi.org/10.1007/s00253-005-0223-3.

[20] T. Chen, Y.-J. Dai, J.-F. Ding, S. Yuan, J.-P. Ni, N-demethylation of neonicotinoid insecticide acetamiprid by bacterium Stenotrophomonas maltophilia CGMCC 1.1788, Biodegradation. 19 (2008) 651–658. https://doi.org/10.1007/s10532-007-9170-2.

[21] S. Murillo-Zamora, V. Castro-Gutiérrez, M. Masís-Mora, V. Lizano-Fallas, C.E.

Rodríguez-Rodríguez, Elimination of fungicides in biopurification systems: Effect of fungal bioaugmentation on removal performance and microbial community structure, Chemosphere. 186 (2017) 625–634. https://doi.org/10.1016/j.chemosphere.2017.07.162.

[22] J.A. Mir-Tutusaus, M. Masís-Mora, C. Corcellas, E. Eljarrat, D. Barceló, M. Sarrà, G. Caminal, T. Vicent, C.E. Rodríguez-Rodríguez, Degradation of selected agrochemicals by the white rot fungus Trametes versicolor, Sci. Total Environ. 500–501 (2014) 235–242. https://doi.org/10.1016/j.scitotenv.2014.08.116.

[23] E. Pilon-Smits, PHYTOREMEDIATION, Annu. Rev. Plant Biol. 56 (2005) 15–39. https://doi.org/10.1146/annurev.arplant.56.032604.144214.

[24] S. Susarla, V.F. Medina, S.C. McCutcheon, Phytoremediation: An ecological solution to organic chemical contamination, Ecol. Eng. 18 (2002) 647–658. https://doi.org/10.1016/S0925-8574(02)00026-5.

[25] K.E. Gerhardt, X.D. Huang, B.R. Glick, B.M. Greenberg, Phytoremediation and rhizoremediation of organic soil contaminants: Potential and challenges, Plant Sci. 176 (2009) 20–30. https://doi.org/10.1016/j.plantsci.2008.09.014.

[26] M.K. Javaid, M. Ashiq, M. Tahir, Potential of Biological Agents in Decontamination of Agricultural Soil, Scientifica (Cairo). 2016 (2016) 1–9. https://doi.org/10.1155/2016/1598325.

[27] M.T. Moore, C.M. Cooper, S. Smith, R.F. Cullum, S.S. Knight, M.A. Locke, E.R. Bennett, Diazinon Mitigation in Constructed Wetlands: Influence of Vegetation, Water. Air. Soil Pollut. 184 (2007) 313–321. https://doi.org/10.1007/s11270-007-9418-9.

[28] T. Liu, S. Xu, S. Lu, P. Qin, B. Bi, H. Ding, Y. Liu, X. Guo, X. Liu, A review on removal of organophosphorus pesticides in constructed wetland: Performance, mechanism and influencing factors, Sci. Total Environ. 651 (2019) 2247–2268. https://doi.org/10.1016/j.scitotenv.2018.10.087.

[29] M.T. Moore, C.M. Cooper, S. Smith, R.F. Cullum, S.S. Knight, M.A. Locke, E.R. Bennett, Mitigation of two pyrethroid insecticides in a Mississippi Delta constructed wetland, Environ. Pollut. 157 (2009) 250–256. https://doi.org/10.1016/j.envpol.2008.07.025.

[30] J. Vymazal, T. Březinová, The use of constructed wetlands for removal of pesticides from agricultural runoff and drainage: A review, Environ. Int. 75 (2015) 11–20. https://doi.org/10.1016/j.envint.2014.10.026.

[31] S. Otto, M. Vianello, A. Infantino, G. Zanin, A. Di Guardo, Effect of a full-grown vegetative filter strip on herbicide runoff: Maintaining of filter capacity over time,

Chemosphere. 71 (2008) 74–82. https://doi.org/10.1016/j.chemosphere.2007.10.029.

[32] M.T. Moore, H.L. Tyler, M.A. Locke, Aqueous pesticide mitigation efficiency of Typha latifolia (L.), Leersia oryzoides (L.) Sw., and Sparganium americanum Nutt., Chemosphere. 92 (2013) 1307–1313. https://doi.org/10.1016/j.chemosphere.2013.04.099.

[33] T. Cáceres, M. Megharaj, R. Naidu, Toxicity and transformation of fenamiphos and its metabolites by two micro algae Pseudokirchneriella subcapitata and Chlorococcum sp., Sci. Total Environ. 398 (2008) 53–59. https://doi.org/10.1016/j.scitotenv.2008.03.022.

[34] H. Kawahigashi, S. Hirose, H. Ohkawa, Y. Ohkawa, Transgenic rice plants expressing human CYP1A1 exude herbicide metabolites from their roots, Plant Sci. 165 (2003) 373–381. https://doi.org/10.1016/S0168-9452(03)00197-3.

[35] H. Kawahigashi, S. Hirose, H. Ohkawa, Y. Ohkawa, Phytoremediation of the Herbicides Atrazine and Metolachlor by Transgenic Rice Plants Expressing Human CYP1A1 , CYP2B6 , and CYP2C19, J. Agric. Food Chem. 54 (2006) 2985–2991. https://doi.org/10.1021/jf052610u.

[36] R. Fonné-Pfister, J. Gaudin, K. Kreuz, K. Ramsteiner, E. Ebert, Hydroxylation of primisulfuron by an inducible cytochrome P450-dependent monooxygenase system from maize, Pestic. Biochem. Physiol. 37 (1990) 165–173. https://doi.org/10.1016/0048-3575(90)90122-I.

[37] C. Mougin, F. Cabanne, M.-C. Canivenc, R. Scalla, Hydroxylation and N-demethylation of chlorotoluron by wheat microsomal enzymes, Plant Sci. 66 (1990) 195–203. https://doi.org/10.1016/0168-9452(90)90204-2.

[38] X. Chen, Q. Zhou, F. Liu, Q. Peng, Y. Bian, Performance and kinetic of pesticide residues removal by microporous starch immobilized laccase in a combined adsorption and biotransformation process, Environ. Technol. Innov. 21 (2021) 101235. https://doi.org/10.1016/j.eti.2020.101235.

[39] A. Das, V. Jaswal, K.N. Yogalakshmi, Degradation of chlorpyrifos in soil using laccase immobilized iron oxide nanoparticles and their competent role in deterring the mobility of chlorpyrifos, Chemosphere. 246 (2020) 125676. https://doi.org/10.1016/j.chemosphere.2019.125676.

[40] M. Bansal, D. Kumar, G.S. Chauhan, A. Kaushik, Preparation, characterization and trifluralin degradation of laccase-modified cellulose nanofibers, Mater. Sci. Energy Technol. 1 (2018) 29–37. https://doi.org/10.1016/j.mset.2018.04.002.

[41] M. Vera, G.S. Nyanhongo, G.M. Guebitz, B.L. Rivas, Polymeric microspheres as support

to co-immobilized Agaricus bisporus and Trametes versicolor laccases and their application in diazinon degradation, Arab. J. Chem. 13 (2020) 4218–4227. https://doi.org/10.1016/j.arabjc.2019.07.003.

[42] D.P. Cherney, S.E. Duirk, J.C. Tarr, T.W. Collette, Monitoring the Speciation of Aqueous Free Chlorine from pH 1 to 12 with Raman Spectroscopy to Determine the Identity of the Potent Low-pH Oxidant, Appl. Spectrosc. 60 (2006) 764–772. https://doi.org/10.1366/000370206777887062.

[43] L.J. Acero, F.J. Benítez, J.F. Real, M. González, Chlorination of organophosphorus pesticides in natural waters, J. Hazard. Mater. 153 (2008) 320–328. https://doi.org/10.1016/j.hazmat.2007.08.051.

[44] K. Ohno, T. Minami, Y. Matsui, Y. Magara, Effects of chlorine on organophosphorus pesticides adsorbed on activated carbon: Desorption and oxon formation, Water Res. 42 (2008) 1753–1759. https://doi.org/10.1016/j.watres.2007.10.040.

[45] W. Li, R. Wu, J. Duan, C.P. Saint, J. van Leeuwen, Impact of prechlorination on organophosphorus pesticides during drinking water treatment: Removal and transformation to toxic oxon byproducts, Water Res. 105 (2016) 1–10. https://doi.org/10.1016/j.watres.2016.08.052.

[46] S.E. Duirk, L.M. Desetto, G.M. Davis, Transformation of Organophosphorus Pesticides in the Presence of Aqueous Chlorine: Kinetics, Pathways, and Structure−Activity Relationships, Environ. Sci. Technol. 43 (2009) 2335–2340. https://doi.org/10.1021/es802868y.

[47] A. Kamel, C. Byrne, C. Vigo, J. Ferrario, C. Stafford, G. Verdin, F. Siegelman, S. Knizner, J. Hetrick, Oxidation of selected organophosphate pesticides during chlorination of simulated drinking water, Water Res. 43 (2009) 522–534. https://doi.org/10.1016/j.watres.2008.10.038.

[48] M.P. Ormad, N. Miguel, A. Claver, J.M. Matesanz, J.L. Ovelleiro, Pesticides removal in the process of drinking water production, Chemosphere. 71 (2008) 97–106. https://doi.org/10.1016/j.chemosphere.2007.10.006.

[49] H. Suty, C. De Traversay, M. Cost, Applications of advanced oxidation processes: present and future, Water Sci. Technol. 49 (2004) 227–233. https://doi.org/10.2166/wst.2004.0270.

[50] R. Andreozzi, V. Caprio, A. Insola, R. Marotta, Advanced oxidation processes (AOP) for water purification and recovery, Catal. Today. 53 (1999) 51–59.

https://doi.org/10.1016/S0920-5861(99)00102-9.

[51] M.A. Oturan, J.-J. Aaron, Advanced Oxidation Processes in Water/Wastewater Treatment: Principles and Applications. A Review, Crit. Rev. Environ. Sci. Technol. 44 (2014) 2577–2641. https://doi.org/10.1080/10643389.2013.829765.

[52] L.W. Matzek, K.E. Carter, Activated persulfate for organic chemical degradation: A review, Chemosphere. 151 (2016) 178–188. https://doi.org/10.1016/J.CHEMOSPHERE.2016.02.055.

[53] O.S. Furman, A.L. Teel, R.J. Watts, Mechanism of Base Activation of Persulfate, Environ. Sci. Technol. 44 (2010) 6423–6428. https://doi.org/10.1021/es1013714.

[54] P. Neta, V. Madhavan, H. Zemel, R.W. Fessenden, Rate constants and mechanism of reaction of sulfate radical anion with aromatic compounds, J. Am. Chem. Soc. 99 (1977) 163–164. https://doi.org/10.1021/ja00443a030.

[55] C. Liang, H.-W. Su, Identification of Sulfate and Hydroxyl Radicals in Thermally Activated Persulfate, Ind. Eng. Chem. Res. 48 (2009) 5558–5562. https://doi.org/10.1021/ie9002848.

[56] N. Vela, J. Fenoll, I. Garrido, G. Pérez-Lucas, P. Flores, P. Hellín, S. Navarro, Reclamation of agro-wastewater polluted with pesticide residues using sunlight activated persulfate for agricultural reuse, Sci. Total Environ. 660 (2019) 923–930. https://doi.org/10.1016/j.scitotenv.2019.01.060.

[57] Y. Ji, C. Dong, D. Kong, J. Lu, Q. Zhou, Heat-activated persulfate oxidation of atrazine: Implications for remediation of groundwater contaminated by herbicides, Chem. Eng. J. 263 (2015) 45–54. https://doi.org/10.1016/j.cej.2014.10.097.

[58] S. Popova, G. Matafonova, V. Batoev, Simultaneous atrazine degradation and E. coli inactivation by UV/S2O82-/Fe2+ process under KrCl excilamp (222 nm) irradiation, Ecotoxicol. Environ. Saf. 169 (2019) 169–177. https://doi.org/10.1016/j.ecoenv.2018.11.014.

[59] J.A. Khan, X. He, N.S. Shah, H.M. Khan, E. Hapeshi, D. Fatta-Kassinos, D.D. Dionysiou, Kinetic and mechanism investigation on the photochemical degradation of atrazine with activated H2O2, S2O82− and HSO5−, Chem. Eng. J. 252 (2014) 393–403. https://doi.org/10.1016/j.cej.2014.04.104.

[60] C. Wu, K.G. Linden, Phototransformation of selected organophosphorus pesticides: Roles of hydroxyl and carbonate radicals, Water Res. 44 (2010) 3585–3594. https://doi.org/10.1016/j.watres.2010.04.011.

[61] M. Chenna, K. Messaoudi, N. Drouiche, H. Lounici, Study and modeling of the organophosphorus compound degradation by photolysis of hydrogen peroxide in aqueous media by using experimental response surface design, J. Ind. Eng. Chem. 33 (2016) 307–315. https://doi.org/10.1016/j.jiec.2015.10.016.

[62] L.M. Utzig, R.M. Lima, M.F. Gomes, W.A. Ramsdorf, L.R.R. Martins, M. V. Liz, A.M. Freitas, Ecotoxicity response of chlorpyrifos in Aedes aegypti larvae and Lactuca sativa seeds after UV/H2O2 and UVC oxidation, Ecotoxicol. Environ. Saf. 169 (2019) 449–456. https://doi.org/10.1016/j.ecoenv.2018.11.003.

[63] R.T. Meijers, E. Oderwald-Muller, P.A.N.M. Nuhn, J.C. Kruithof, Degradation of Pesticides by Ozonation and Advanced Oxidation, Ozone Sci. Eng. 17 (1995) 673–686. https://doi.org/10.1080/01919512.1995.10555778.

[64] A. Begum, S.K. Gautam, Endosulfan and lindane degradation using ozonation, Environ. Technol. 33 (2012) 943–949. https://doi.org/10.1080/09593330.2011.603752.

[65] G.F. Upelaar, R.T. Meijers, R. Hopman, J.C. Kruithof, Oxidation of Herbicides in Groundwater by the Fenton Process: A Realistic Alternative for O3/H2O2 Treatment?, Ozone Sci. Eng. 22 (2000) 607–616. https://doi.org/10.1080/01919510009408802.

[66] M.I. Maldonado, S. Malato, L.A. Pérez-Estrada, W. Gernjak, I. Oller, X. Doménech, J. Peral, Partial degradation of five pesticides and an industrial pollutant by ozonation in a pilot-plant scale reactor, J. Hazard. Mater. 138 (2006) 363–369. https://doi.org/10.1016/j.jhazmat.2006.05.058.

[67] P.R. Gogate, P.N. Patil, Combined treatment technology based on synergism between hydrodynamic cavitation and advanced oxidation processes, Ultrason. Sonochem. 25 (2015) 60–69. https://doi.org/10.1016/j.ultsonch.2014.08.016.

[68] B. Wang, H. Su, B. Zhang, Hydrodynamic cavitation as a promising route for wastewater treatment – A review, Chem. Eng. J. 412 (2021) 128685. https://doi.org/10.1016/j.cej.2021.128685.

[69] Y. Zhang, K. Pagilla, Treatment of malathion pesticide wastewater with nanofiltration and photo-Fenton oxidation, Desalination. 263 (2010) 36–44. https://doi.org/10.1016/j.desal.2010.06.031.

[70] P.N. Patil, P.R. Gogate, Degradation of methyl parathion using hydrodynamic cavitation: Effect of operating parameters and intensification using additives, Sep. Purif. Technol. 95 (2012) 172–179. https://doi.org/10.1016/j.seppur.2012.04.019.

[71] A.C. Affam, M. Chaudhuri, S.R.M. Kutty, K. Muda, UV Fenton and sequencing batch

reactor treatment of chlorpyrifos, cypermethrin and chlorothalonil pesticide wastewater, Int. Biodeterior. Biodegradation. 93 (2014) 195–201. https://doi.org/10.1016/j.ibiod.2014.06.002.

[72] S. Navarro, J. Fenoll, N. Vela, E. Ruiz, G. Navarro, Removal of ten pesticides from leaching water at pilot plant scale by photo-Fenton treatment, Chem. Eng. J. 167 (2011) 42–49. https://doi.org/10.1016/j.cej.2010.11.105.

[73] H. Karimi-Maleh, B.G. Kumar, S. Rajendran, J. Qin, S. Vadivel, D. Durgalakshmi, F. Gracia, M. Soto-Moscoso, Y. Orooji, F. Karimi, Tuning of metal oxides photocatalytic performance using Ag nanoparticles integration, J. Mol. Liq. 314 (2020) 113588. https://doi.org/10.1016/j.molliq.2020.113588.

[74] S.N. Ahmed, W. Haider, Heterogeneous photocatalysis and its potential applications in water and wastewater treatment: a review, Nanotechnology. 29 (2018) 342001. https://doi.org/10.1088/1361-6528/aac6ea.

[75] A. Fujishima, T.N. Rao, D.A. Tryk, Titanium dioxide photocatalysis, J. Photochem. Photobiol. C Photochem. Rev. 1 (2000) 1–21. https://doi.org/10.1016/S1389-5567(00)00002-2.

[76] E. Pelizzetti, C. Minero, V. Carlin, E. Borgarello, Photocatalytic soil decontamination, Chemosphere. 25 (1992) 343–351. https://doi.org/10.1016/0045-6535(92)90551-2.

[77] M.M. Higarashi, W.F. Jardim, Remediation of pesticide contaminated soil using TiO2 mediated by solar light, Catal. Today. 76 (2002) 201–207. https://doi.org/10.1016/S0920-5861(02)00219-5.

[78] R. Fiorenza, A. Di Mauro, M. Cantarella, C. Iaria, E.M. Scalisi, M.V. Brundo, A. Gulino, L. Spitaleri, G. Nicotra, S. Dattilo, S.C. Carroccio, V. Privitera, G. Impellizzeri, Preferential removal of pesticides from water by molecular imprinting on TiO2 photocatalysts, Chem. Eng. J. 379 (2020) 122309. https://doi.org/10.1016/j.cej.2019.122309.

[79] A. Sudhaik, P. Raizada, S. Thakur, R. V. Saini, A.K. Saini, P. Singh, V. Kumar Thakur, V.-H. Nguyen, A.A.P. Khan, A.M. Asiri, Synergistic photocatalytic mitigation of imidacloprid pesticide and antibacterial activity using carbon nanotube decorated phosphorus doped graphitic carbon nitride photocatalyst, J. Taiwan Inst. Chem. Eng. 113 (2020) 142–154. https://doi.org/10.1016/j.jtice.2020.08.003.

[80] S. Mosleh, M.R. Rahimi, Intensification of abamectin pesticide degradation using the combination of ultrasonic cavitation and visible-light driven photocatalytic process:

Synergistic effect and optimization study, Ultrason. Sonochem. 35 (2017) 449–457. https://doi.org/10.1016/j.ultsonch.2016.10.025.

[81] K. Yari, A. Seidmohammadi, M. Khazaei, A. Bhatnagar, M. Leili, A comparative study for the removal of imidacloprid insecticide from water by chemical-less UVC, UVC/TiO2 and UVC/ZnO processes, J. Environ. Heal. Sci. Eng. 17 (2019) 337–351. https://doi.org/10.1007/s40201-019-00352-3.

[82] K. Liu, J. Chen, F. Sun, Y. Liu, M. Tang, Y. Yang, Historical development and prospect of intimately coupling photocatalysis and biological technology for pollutant treatment in sewage: A review, Sci. Total Environ. 835 (2022) 155482. https://doi.org/10.1016/j.scitotenv.2022.155482.

[83] P. V. Nidheesh, G. Divyapriya, N. Oturan, C. Trellu, M.A. Oturan, Environmental Applications of Boron-Doped Diamond Electrodes: 1. Applications in Water and Wastewater Treatment, ChemElectroChem. 6 (2019) 2124–2142. https://doi.org/10.1002/celc.201801876.

[84] B.P. Chaplin, Critical review of electrochemical advanced oxidation processes for water treatment applications, Environ. Sci. Process. Impacts. 16 (2014) 1182–1203. https://doi.org/10.1039/c3em00679d.

[85] C.M. Dominguez, N. Oturan, A. Romero, A. Santos, M.A. Oturan, Lindane degradation by electrooxidation process: Effect of electrode materials on oxidation and mineralization kinetics, Water Res. 135 (2018) 220–230. https://doi.org/10.1016/j.watres.2018.02.037.

[86] W. Yang, M. Zhou, N. Oturan, Y. Li, P. Su, M.A. Oturan, Enhanced activation of hydrogen peroxide using nitrogen doped graphene for effective removal of herbicide 2,4-D from water by iron-free electrochemical advanced oxidation, Electrochim. Acta. 297 (2019) 582–592. https://doi.org/10.1016/j.electacta.2018.11.196.

[87] C. Trellu, H. Olvera Vargas, E. Mousset, N. Oturan, M.A. Oturan, Electrochemical technologies for the treatment of pesticides, Curr. Opin. Electrochem. 26 (2021) 100677. https://doi.org/10.1016/j.coelec.2020.100677.

[88] L. Malaeb, G.M. Ayoub, Reverse osmosis technology for water treatment: State of the art review, Desalination. 267 (2011) 1–8. https://doi.org/10.1016/j.desal.2010.09.001.

[89] B. Van der Bruggen, C. Vandecasteele, Removal of pollutants from surface water and groundwater by nanofiltration: overview of possible applications in the drinking water industry, Environ. Pollut. 122 (2003) 435–445. https://doi.org/10.1016/S0269-7491(02)00308-1.

[90] O. Labban, C. Liu, T.H. Chong, J.H. Lienhard V, Fundamentals of low-pressure nanofiltration: Membrane characterization, modeling, and understanding the multi-ionic interactions in water softening, J. Memb. Sci. 521 (2017) 18–32. https://doi.org/10.1016/j.memsci.2016.08.062.

[91] A.W. Mohammad, Y.H. Teow, W.L. Ang, Y.T. Chung, D.L. Oatley-Radcliffe, N. Hilal, Nanofiltration membranes review: Recent advances and future prospects, Desalination. 356 (2015) 226–254. https://doi.org/10.1016/j.desal.2014.10.043.

[92] K. V. Plakas, A.J. Karabelas, Removal of pesticides from water by NF and RO membranes — A review, Desalination. 287 (2012) 255–265. https://doi.org/10.1016/j.desal.2011.08.003.

[93] B. Van der Bruggen, J. Schaep, D. Wilms, C. Vandecasteele, Influence of molecular size, polarity and charge on the retention of organic molecules by nanofiltration, J. Memb. Sci. 156 (1999) 29–41. https://doi.org/10.1016/S0376-7388(98)00326-3.

[94] Y. Mansourpanah, MXenes and other 2D nanosheets for modification of polyamide thin film nanocomposite membranes for desalination, Sep. Purif. Technol. 289 (2022) 120777. https://doi.org/10.1016/j.seppur.2022.120777.

[95] D. Suresh, P.S. Goh, A.F. Ismail, N. Hilal, Surface Design of Liquid Separation Membrane through Graft Polymerization: A State of the Art Review, Membranes (Basel). 11 (2021) 832. https://doi.org/10.3390/membranes11110832.

[96] M.H. Abd El-Salam, MEMBRANE TECHNIQUES | Applications of Reverse Osmosis, Encycl. Food Sci. Nutr. 49 (2003) 3833–3837. https://doi.org/10.1016/B0-12-227055-X/00762-8.

[97] H.N. Lazarides, E. Katsanidis, MEMBRANE TECHNIQUES | Principles of Reverse Osmosis, Encycl. Food Sci. Nutr. (2003) 3827–3833. https://doi.org/10.1016/B0-12-227055-X/00761-6.

[98] V. Srivastava, E.N. Zare, P. Makvandi, X. Zheng, S. Iftekhar, A. Wu, V.V.T. Padil, B. Mokhtari, R.S. Varma, F.R. Tay, M. Sillanpaa, Cytotoxic aquatic pollutants and their removal by nanocomposite-based sorbents, Chemosphere. 258 (2020) 127324. https://doi.org/10.1016/j.chemosphere.2020.127324.

[99] N. Ates, N. Uzal, U. Yetis, F.B. Dilek, Removal of pesticides from secondary treated urban wastewater by reverse osmosis, Environ. Sci. Pollut. Res. 30 (2022) 8732–8745. https://doi.org/10.1007/s11356-022-20077-5.

[100] P. Berg, G. Hagmeyer, R. Gimbel, Removal of pesticides and other micropollutants by

nanofiltration, Desalination. 113 (1997) 205–208. https://doi.org/10.1016/S0011-9164(97)00130-6.

[101] K.M. Agbekodo, B. Legube, S. Dard, Atrazine and simazine removal mechanisms by nanofiltration: Influence of natural organic matter concentration, Water Res. 30 (1996) 2535–2542. https://doi.org/10.1016/S0043-1354(96)00128-5.

[102] A. Mojiri, J.L. Zhou, B. Robinson, A. Ohashi, N. Ozaki, T. Kindaichi, H. Farraji, M. Vakili, Pesticides in aquatic environments and their removal by adsorption methods, Chemosphere. 253 (2020) 126646. https://doi.org/10.1016/j.chemosphere.2020.126646.

[103] I.A. Saleh, N. Zouari, M.A. Al-Ghouti, Removal of pesticides from water and wastewater: Chemical, physical and biological treatment approaches, Environ. Technol. Innov. 19 (2020) 101026. https://doi.org/10.1016/j.eti.2020.101026.

[104] A. Amari, F.M. Alzahrani, K.M. Katubi, N.S. Alsaiari, M.A. Tahoon, F. Ben Rebah, Clay-polymer nanocomposites: Preparations and utilization for pollutants removal, Materials (Basel). 14 (2021) 1–21. https://doi.org/10.3390/ma14061365.

[105] D. Debnath, A.K. Gupta, P.S. Ghosal, Recent advances in the development of tailored functional materials for the treatment of pesticides in aqueous media: A review, J. Ind. Eng. Chem. 70 (2019) 51–69. https://doi.org/10.1016/j.jiec.2018.10.014.

[106] M.P. Ajith, M. Aswathi, E. Priyadarshini, P. Rajamani, Recent innovations of nanotechnology in water treatment: A comprehensive review, Bioresour. Technol. 342 (2021) 126000. https://doi.org/10.1016/j.biortech.2021.126000.

[107] S. Akash, B. Sivaprakash, N. Rajamohan, C.M. Pandiyan, D.-V.N. Vo, Pesticide pollutants in the environment – A critical review on remediation techniques, mechanism and toxicological impact, Chemosphere. 301 (2022) 134754. https://doi.org/10.1016/j.chemosphere.2022.134754.

[108] S.H. Gebre, Nanoscale zero-valent iron for remediation of toxicants and wastewater treatment, Environ. Technol. Rev. 12 (2023) 390–419. https://doi.org/10.1080/21622515.2023.2220090.

[109] H. Srichandan, P.K. Singh, P.K. Parhi, P. Mohanty, T.K. Adhya, R. Pattnaik, S. Mishra, P.K. Hota, Environmental remediation using metals and inorganic and organic materials: a review, J. Environ. Sci. Heal. Part C. 40 (2022) 197–226. https://doi.org/10.1080/26896583.2022.2065871.

[110] I. Borišev, M. Borišev, D. Jović, M. Župunski, D. Arsenov, S. Pajević, A. Djordjevic, Nanotechnology and remediation of agrochemicals, in: M. Narashimha, V. Prasad (Eds.),

Agrochem. Detect. Treat. Remediat., Elsevier, 2020: pp. 487–533. https://doi.org/10.1016/B978-0-08-103017-2.00019-2.

[111] A. Ali, H. Zafar, M. Zia, I. ul Haq, A.R. Phull, J.S. Ali, A. Hussain, Synthesis, characterization, applications, and challenges of iron oxide nanoparticles, Nanotechnol. Sci. Appl. 9 (2016) 49–67. https://doi.org/10.2147/NSA.S99986.

[112] S. Jogaiah, M.K. Paidi, K. Venugopal, N. Geetha, M. Mujtaba, S.S. Udikeri, M. Govarthanan, Phytotoxicological effects of engineered nanoparticles: An emerging nanotoxicology, Sci. Total Environ. 801 (2021) 149809. https://doi.org/10.1016/j.scitotenv.2021.149809.

[113] R. Selvasembian, W. Gwenzi, N. Chaukura, S. Mthembu, Recent advances in the polyurethane-based adsorbents for the decontamination of hazardous wastewater pollutants, J. Hazard. Mater. 417 (2021) 125960. https://doi.org/10.1016/j.jhazmat.2021.125960.

[114] E. Baigorria, J.A. Galhardi, L.F. Fraceto, Trends in polymers networks applied to the removal of aqueous pollutants: A review, J. Clean. Prod. 295 (2021) 126451. https://doi.org/10.1016/j.jclepro.2021.126451.

[115] S. Bhogal, K. Kaur, I. Mohiuddin, S. Kumar, J. Lee, R.J.C. Brown, K.-H. Kim, A.K. Malik, Hollow porous molecularly imprinted polymers as emerging adsorbents, Environ. Pollut. 288 (2021) 117775. https://doi.org/10.1016/j.envpol.2021.117775.

[116] G. Crini, E. Lichtfouse, L.D. Wilson, N. Morin-Crini, Conventional and non-conventional adsorbents for wastewater treatment, Environ. Chem. Lett. 17 (2019) 195–213. https://doi.org/10.1007/s10311-018-0786-8.

[117] M.A. Kaczorowska, D. Bożejewicz, K. Witt, The Application of Polymer Inclusion Membranes for the Removal of Emerging Contaminants and Synthetic Dyes from Aqueous Solutions—A Mini Review, Membranes (Basel). 13 (2023) 132. https://doi.org/10.3390/membranes13020132.

[118] B. Aoudi, Y. Boluk, M. Gamal El-Din, Recent advances and future perspective on nanocellulose-based materials in diverse water treatment applications, Sci. Total Environ. 843 (2022) 156903. https://doi.org/10.1016/j.scitotenv.2022.156903.

[119] R. Das, T. Lindström, P.R. Sharma, K. Chi, B.S. Hsiao, Nanocellulose for Sustainable Water Purification, Chem. Rev. 122 (2022) 8936–9031. https://doi.org/10.1021/acs.chemrev.1c00683.

[120] P.S. Khoo, R.A. Ilyas, M.N.A. Uda, S.A. Hassan, A.H. Nordin, A.S. Norfarhana, N.H. Ab

Hamid, M.S.A. Rani, H. Abral, M.N.F. Norrrahim, V.F. Knight, C.L. Lee, S.A. Rafiqah, Starch-Based Polymer Materials as Advanced Adsorbents for Sustainable Water Treatment: Current Status, Challenges, and Future Perspectives, Polymers (Basel). 15 (2023) 3114. https://doi.org/10.3390/polym15143114.

[121] Y. Kaur, Y. Bhatia, S. Chaudhary, G.R. Chaudhary, Comparative performance of bare and functionalize ZnO nanoadsorbents for pesticide removal from aqueous solution, J. Mol. Liq. 234 (2017) 94–103. https://doi.org/10.1016/j.molliq.2017.03.069.

[122] A. Ouali, L.S. Belaroui, A. Bengueddach, A.L. Galindo, A. Peña, Fe2O3–palygorskite nanoparticles, efficient adsorbates for pesticide removal, Appl. Clay Sci. 115 (2015) 67–75. https://doi.org/10.1016/j.clay.2015.07.026.

[123] V.W.O. Wanjeri, C.J. Sheppard, A.R.E. Prinsloo, J.C. Ngila, P.G. Ndungu, Isotherm and kinetic investigations on the adsorption of organophosphorus pesticides on graphene oxide based silica coated magnetic nanoparticles functionalized with 2-phenylethylamine, J. Environ. Chem. Eng. 6 (2018) 1333–1346. https://doi.org/10.1016/j.jece.2018.01.064.

[124] S. Fiorilli, L. Rivoira, G. Calì, M. Appendini, M.C. Bruzzoniti, M. Coïsson, B. Onida, Iron oxide inside SBA-15 modified with amino groups as reusable adsorbent for highly efficient removal of glyphosate from water, Appl. Surf. Sci. 411 (2017) 457–465. https://doi.org/10.1016/j.apsusc.2017.03.206.

[125] M.H. Dehghani, Z.S. Niasar, M.R. Mehrnia, M. Shayeghi, M.A. Al-Ghouti, B. Heibati, G. McKay, K. Yetilmezsoy, Optimizing the removal of organophosphorus pesticide malathion from water using multi-walled carbon nanotubes, Chem. Eng. J. 310 (2017) 22–32. https://doi.org/10.1016/j.cej.2016.10.057.

[126] I.A. Shabtai, Y.G. Mishael, Catalytic polymer-clay composite for enhanced removal and degradation of diazinon, J. Hazard. Mater. 335 (2017) 135–142. https://doi.org/10.1016/j.jhazmat.2017.04.017.

[127] C. Liu, P. Wang, Z. Shen, X. Liu, Z. Zhou, D. Liu, pH-controlled quaternary ammonium herbicides capture/release by carboxymethyl-β-cyclodextrin functionalized magnetic adsorbents: Mechanisms and application, Anal. Chim. Acta. 901 (2015) 51–58. https://doi.org/10.1016/j.aca.2015.10.027.

Chapter 3.

3. Cyclodextrin

Cyclodextrins and their derivatives have been extensively studied due to the advantageous properties of their structure, such as amphiphilicity, non-toxicity, biodegradability, and the easy chemical modification [1,2] to design soluble [3] or insoluble 3D-structures, or molecularly imprinted polymers [4,5]. Cyclodextrins have long been employed in the pharmaceutical, food and cosmetic fields [6]. That is because most of the active pharmaceutical ingredient's molecules have low aqueous solubility, which represents a disadvantage in preparing commercial formulations of pharmaceuticals due to the need of excipients, organic solvents or co-formulants. Therefore, cyclodextrins continue to be studied thanks to their amphiphilic behaviour, which permits to increase the solubility, availability and water stability of the pharmaceutical molecules [7–9]. Similarly, most of the active substances of pesticides have low solubility. The unique hydrophilic/hydrophobic duality of the pristine cyclodextrins and their derivatives can be used to design novel and greener phytopharmaceutical formulations [3,9,10]. From another point of view, the cyclodextrin-analyte interaction via host-guest complexes formation can be advantageously used in environmental processes to remove hydrophobic molecules either pharmaceutical [11,12] or phyto-pharmaceutical [13–15]. However, hydrophilic active ingredients of phytopharmaceuticals must be also considered. Thus, cyclodextrin-based polymers, such nanosponges, are considered promising sorbent materials encompassing the hydrophobic cavity of the cyclodextrins and the hydrophilic 3D-structure which properties can be modulated by proper design [16–18].

Hence, the interest focused in the development of novel cyclodextrin-based sorbent materials and their application in environmental remediation processes through the sorption of pesticides from aqueous media [15,18,19].

3.1. Cyclodextrin-based nanosponges of interest

Based on the class of monomer used as crosslinkers and the functional group resulting from the polymerization reaction two families of CDNS can be identified, namely carbamate-CDNS and amine-CDNS (in the latter one, two classes can be identified). The focus is centred on how the physico-chemical properties of the crosslinkers can influence the characteristics of the polymers, and therefore the sorbent-sorbate interactions, thereby, their sorption capability and removal efficiency. The cyclodextrin-based sorbent materials were deeply characterized by different techniques and the fundamentals of the main methods are discussed in Chapter 4. The methodologies used to understand the mechanism of interaction in aqueous media are discussed in Chapter 5, such as equilibria and kinetic sorption models, and molecular dynamic simulations for an atomistic understanding.

3.1.1. Diisocyanate crosslinker

The first family of *β*CDNS was synthesized using as a monomer 1,6-hexamethylene diisocyanate (HDI), via wet-chemistry. The reaction between the -OH group at C(6) position of CD and the highly reactive -N=C=O group of HDI, is coordinated by the catalyst dibutylin dilaurate (BTL). The reaction led to a crosslinked 3D-structure with yield ≥ 90%, (w/w) (Figure 3.1.). The formed carbamate linkages are chemically stable, in acidic and alkaline pH, which can represent an advantageous for industrial application. *β*CD-HDI is one of the most common nanosponges employed in the pharmaceutical field, but only few studies on environmental application have been reported [12,20].

In a preliminary study, the effect of the molar ratio (mol:mol) between CD:crosslinker was assessed. An increase of the stiffness of the product with the molar ratio CD:crosslinker was macroscopically observed (1:2, 1:4 and 1:8); shifting from a yellowish material with weak-mechanical properties, *β*CD-HDI 1:2 (mol:mol), to a white rigid and non-elastic polymer *β*CD-HDI 1:8 (mol:mol) (Figure 3.2.). Moreover, at 1:4 mol:mol and 1:8 mol:mol the polymer has hydrogel features. The three *β*CD-HDI were tested for removal of IMD and CYM, observing that the poly-*β*cyclodextrin (PCD) at molar ratio 1:4 mol:mol had the higher sorption performance (Table 3.1.). PCD 1:4 (mol:mol) was chosen for further analysis with both active ingredients, which optima experimental conditions were determined by full 2^k factorial experimental design (Chapter 5.). Moreover, the 3D-structure of PCD was employed as polymeric scaffold for powdered activated carbon. The results are shown in chapter 6-IV.

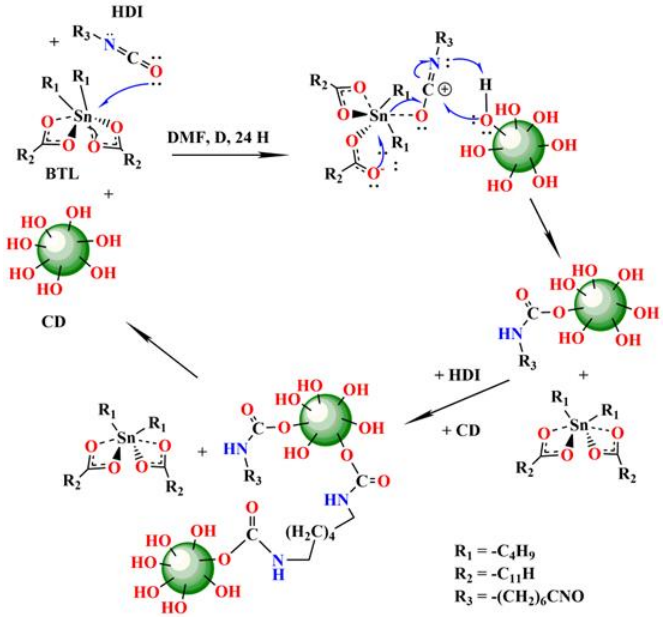

Figure 3.1. Scheme of the synthesis route of poly-*β*cyclodextrin.

Figure 3.2. Images of CD-HDI at different molar ratio (a) 1:2 (mol:mol); (b) 1:4 (mol:mol); (c) 1:8 (mol:mol).

Table 3.1. Results of the preliminary testes of pesticides uptake into poly-*β*cyclodextrins.

Molar ratio	**IMD**		**CYM**	
	q_e (mg g^{-1})	**Q%**	**q_e (mg g^{-1})**	**Q%**
PCD 1:2 (50 mg)	1.38 (± 0.03) (25 mg L^{-1})	40.00 (± 0.82) (25 mg L^{-1})	0.11 (± 0.04) (25 mg L^{-1})	5.00 (± 1.79) (25 mg L^{-1})
	0.70 (± 0.04) (50 mg L^{-1})	15.26 (± 0.85) (50 mg L^{-1})	0.20 (± 0.08) (50 mg L^{-1})	4.43 (± 1.79) (50 mg L^{-1})
PCD 1:4 (50 mg)	1.60 (± 0.03) (25 mg L^{-1})	46.15 (± 0.82) (25 mg L^{-1})	0.14 (± 0.04) (25 mg L^{-1})	5.93 (± 1.78) (25 mg L^{-1})
	1.32 (± 0.04) (50 mg L^{-1})	22.18 (± 0.82) (50 mg L^{-1})	0.32 (± 0.08) (50 mg L^{-1})	6.91 (± 1.77) (50 mg L^{-1})
PCD 1:8 (50 mg)	0.45 (± 0.03) (25 mg L^{-1})	13.18 (± 0.90) (25 mg L^{-1})	0.17 (± 0.06) (25 mg L^{-1})	4.97 (± 1.79) (25 mg L^{-1})
	0.56 (± 0.04) (50 mg L^{-1})	9.91 (± 0.80) (50 mg L^{-1})	0.37 (± 0.12) (50 mg L^{-1})	5.36 (± 1.78) (50 mg L^{-1})

3.1.2. Diamine crosslinker

The second family of CDNS are the amine-cyclodextrin-based nanosponges (CDAM-NS). Differently to the carbamate-NSs, the synthesis of CDAM-NS provides the previous functionalization of the CDs. Amine-terminal groups pave the way for a broad range of following modifications (*e.g.* alkylation, acylation, carbylamine reaction of Hoffmann isocyanide synthesis, diazotization and sulfonylation). In this way, it is possible to obtain materials responsive to external stimuli. First of all, the pH is an example of how it is possible to alter the charge of the polymer, obtaining controlled sorption and release processes. The amine reactivity is influenced by their nucleophilicity, which generally decreases from tertiary to primary amine groups; but steric hindrance must be considered as an influent factor. The synthetic routes of CDAM-NS reported in literature are based on three steps, such as *i)* halogenation; *ii)* amination and *iii*) polymerization. The *per*-halogenation can be performed with iodine or bromide, obtaining the *heptakis*-halide-cyclodextrins [21]. Then, the amine-modified cyclodextrin and the CDAM-NS with application for drug delivery or as sequestrant systems were synthesized [22,23]; to the best of our knowledge, these are the only papers related with CDAM-NS.

Along the PhD project, only iodine was used in the *per*-halogenation because of its superior behaviour as leaving group even with lower reactivity than bromine. Bromine was excluded due to the potential bioaccumulation at the level of liver, kidneys, brain, blood, heart and thyroid gland, resulting in, for example, hypertrophy and hyperplasia [24]; on the other hand, iodine has no side effects or, at least, so serious effects. Hence, with the *heptakis*-(6-iodo)-(6-deoxy)-cyclodextrin (CD-I) as substrate, amine-derivatives of both α- or β-cyclodextrins have been synthesized using sodium azide(NH_2), hexane-1,6-diamine (AM_6) and dodecane-1,12-diamine (AM_{12}), obtaining *heptakis*-(6-amine)-(6-deoxy)-cyclodextrin, ($_{NH2}$CD), *heptakis*-[6-(6-amino-1-hexylamine)]-(6-deoxy)-cyclodextrin ($_{AM6}$CD), and *heptakis*-[6-(12-amino-1-dodecylamine)]-(6-deoxy)-cyclodextrin ($_{AM12}$CD), respectively. Then, the nanosponges were obtained by polymerization (Figure 3.3.).

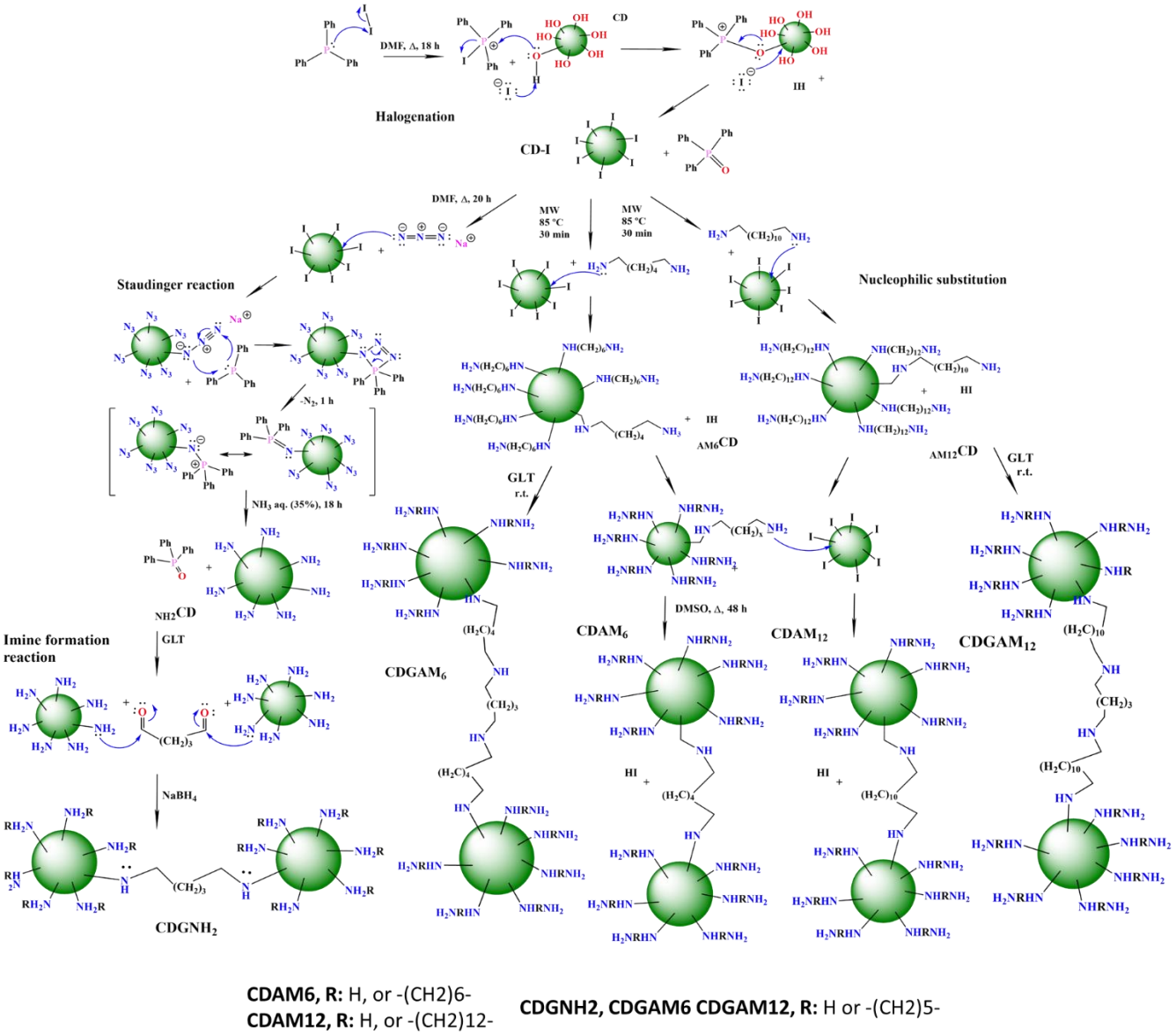

Figure 3.3. Synthetical routes of the novel cyclodextrin-based nanosponges employed as sorbent.

In the first research paper published in 2022 in *Col. Surf. A* [25] and reprinted in Chapter 6-V, *β*-CDs were used to synthesize two nanosponges, namely *β*CDAM$_6$ and the novel *β*CDAM$_{12}$. The main disadvantage of the synthesis route reported in literature was the high time-consumption in the amination and polymerization steps (48 hours), at expense of prolonged energy consumption in terms of electricity (0.20 euro per kW h^{-1}, Portugal cost), and water (2.4 € per m^3 for consumption over 25 m^3/30 days, Portugal cost). In this sense, the amination reaction was altered from wet-chemistry to the greener microwave-assisted procedure (MW), which drastically reduce the reaction time to 45 min, with analogous molar yields, > 90% and ≈ 80%, for AM$_6$ and AM$_{12}$, respectively. The influence of the chain length of the crosslinkers and sorbent capabilities of *β*CDAM$_6$ and *β*CDAM$_{12}$ were assessed for imidacloprid uptake.

*β*CDAM$_6$ and *β*CDAM$_{12}$ were also tested for the removal of 2,4-D. The study, published in 2022 in *Env. Res. Journal* (Chapter 6-VI) was developed in collaboration with the research group of Prof. Sannino Filomena in the University of Naples.

Subsequently beyond *β*-cyclodextrin, *α*-CD was used in the synthesis of CDNS. In this study, over the effect of the chain-length of the crosslinkers, the role of the two cyclodextrins was evaluated. The wet-chemistry and the MW procedures were compared for the synthesis of $_{AM6}$*α*CD and $_{AM12}$*α*CD. Albeit the wet-chemistry protocol can be applied for the *per*-amination of $_{AM6}$*α*CD, that is not possible for $_{AM12}$*α*CD. On the contrary, the MW procedure permits the amination of *α*CD-I with both AM$_6$ and AM$_{12}$, with molar yield ≥ 80%. The resulting nanosponges, *α*CDAM$_6$, *α*CDAM$_{12}$, *β*CDAM$_6$ and *β*CDAM$_{12}$ were tested for the uptake of a commercial formulation of IMD, Confidor O-TEQ®. The research paper was published in 2023 in *Chem. Eng. J.* (chapter 6-VII).

In the last work, further $_{AM6}$CD and $_{AM12}$CD, $_{NH2}$CD was synthesized [21] with *α*- and *β*-CD, respectively. The second novelty, in the synthesis of the second class of CDAM-NS, is represented by the polymerization step. In the previous studies the polymerization was performed by a nucelophilic substitution between CD-I and $_{AM}$CD at molar ratio 1:1 mol:mol. Herein, the NS have been synthesized via *click*-condensation between the amine groups of $_{NH2}$CD, $_{AM6}$CD and $_{AM12}$CD and the highly reactive aldehyde groups of the pentanedial (commonly named glutaraldehyde) (GLT), at molar ratio 1:7 mol:mol. The instantaneous reaction led to the products labelled as CDGNH$_2$, CDGAM$_6$ and CDGAM$_{12}$. In this way, the time-reaction of the polymerization step was drastically reduced to some minutes and the amount of NS produced were highly increased. However, the formed imine linkages are chemically unstable at acidic pH, so, they are reduced to the more stable amine groups, before the application. GLT is usually employed as crosslinker in materials for biomedical application, and for the fast action as bactericidal with broad spectrum and low cytotoxicity, high accessibility, low cost and high-water solubility. The preliminary results of the study are reported in Chapter 6-VIII.

In order to provide to the reader a deeper understanding about the cyclodextrin-based materials developed along the thesis, two scientific outcomes are reported below.

The role played by cyclodextrins over 130 years due to their peculiar physical-chemical properties and an introduction to the CDNS classified in terms of monomers used as crosslinker, are discussed in *Introduction to cyclodextrin-Based Nanosponges*, as Chapter 5 in *Nanosponges for Environmental Remediation* [26].

In addition, a detailed discussion about the routes of synthesis of CDNS, their physico-chemical properties and the main application areas are reported in the scientific review published in *Front. Chem.* in 2022 [18].

Introduction to cyclodextrin-based nanosponges

I

G. Utzeri, D. Murtinho, A.J.M Valente

On-publishing in, Gulati, S. (eds) *Nanosponges for Environmental Remediation*

Springer, Cham. https://doi.org/10.1007/978-3-031-41077-2_5

Introduction to Cyclodextrin-Based Nanosponges

Gianluca Utzeri, Dina Murtinho, and Artur J. M. Valente

Abbreviations

1,4AP	1,4-Disacryloylpiperazine
2,2AAA	2,2-Bisacryloamidoacetic acid
AIBN	Azobisisobutyronitrile
APM	Pyromellitic anhydride
BET	Brunauer-Emmett-Teller analysis
CD	Cyclodextrin
CDI	Carbonyldiimidazole
CDNS	Cyclodextrin-based nanosponge
CGTase	Cyclodextrin glucosyl transferase
CTA	Citric acid
CuAAC	Cu(I)-catalyzed azide-alkyne cycloaddition
DEET	*N,N*-Diethyl-3-toluamide
DMC	Dimethylcarbonate
DMF	Dimethylformamide
DMSO	Dimethyl sulfoxide
DPC	Diphenylcarbonate
DSC	Differential scanning calorimetry
EDTA	Ethylenediaminetetraacetic acid
EPB	Epiclon B-440
EPI	Epichlorohydrin

G. Utzeri (✉) · D. Murtinho · A. J. M. Valente
CQC—IMS, Department of Chemistry, University of Coimbra, 3004-535 Coimbra, Portugal
e-mail: gianlucautz@gmail.com

D. Murtinho
e-mail: dmurtinho@ci.uc.pt

A. J. M. Valente
e-mail: avalente@ci.uc.pt

S. Gulati (ed.), *Nanosponges for Environmental Remediation*,
https://doi.org/10.1007/978-3-031-41077-2_5

FTIR	Fourier-transform infrared spectroscopy
HβCD	Hydroxypropyl-β-CD
HDI	1,6-Hexamethylenediisocyanate
MDI	4,4-Methylenediphenyl diisocyanate
NMR	Nuclear magnetic resonance
NS	Nanosponge
PCBs	Polychlorinated biphenyls
SEM	Scanning electron microscopy
TDI	Toluene diisocyanate
TEM	Transmission electron microscopy
TFTPN	2,3,5,6-Tetrafluoroterephthalonitrile
TGA	Thermogravimetric analysis

1 Cyclodextrin

The development of cyclodextrins has, in the opinion of these authors, three important milestones. The first data, from the late 19th century, are due to the Frenchman Antoine Villiers and his studies on the effect of microorganisms, in particular *Bacillus amylobacter* (*Clostridium butyricum*), on potato starch, having observed the respective fermentation in the presence of these microorganisms. The main reaction products, which Villiers observed in the form of crystals, were made up of dextrins (a term *in illo tempore* a degradation product of starch [1, 2]) and later were referred as "cellulosines" [3, 4]; being the first references to the molecules that would later be known as cyclodextrins.

Around 15 years after the first references to *cellulosines*, Franz Schardinger—an Austrian chemist and bacteriologist—isolated *Bacillus macerans* (*Aerobacillus macerans*) and found that its action on potato starch produces crystalline dextrins similar to those described by Villiers [5, 6]. Schardinger developed protocols that allowed the synthesis and purification of 2 different dextrins, labelled as α- and β-dextrins [7]. The importance of Schardinger's work lies in the isolation of the microorganism capable of generating the extracellular enzyme CGTase (cyclodextrin glucosyl transferase) that hydrolyzes starch-forming dextrins [8], as well as being the first to hypothesize that dextrins are cyclic polysaccharides. The relevance of Schardinger's work was recognized and for more than a century dextrins were described as "Schardinger dextrins" [9, 10].

Although Schardinger dextrins, afterward also named cycloamylases [11], have always received attention from researchers [12, 13], the awakening to the unique properties and multiple applications only occurred in the last quarter of the twentieth century with the crucial contributions of Wolfram Saenger and József Szejtli. Among other things, the decisive contribution of these researchers has been to unveil the crystal structure of cyclodextrins [14] and to understand the mechanisms of inclusion complex formation [15, 16] (originally described by Cramer et al. [17]). Szejtli also

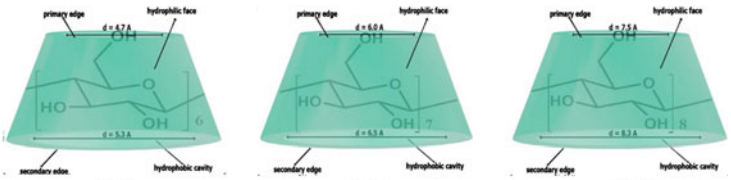

	α-CD	β-CD	γ-CD
Molecular weight (g mol^{-1})	973	1134	1297
Water solubility at 25 °C (g L^{-1})	145	18.5	232
Cavity volume (A^3)	174	262	427

Fig. 1 Pictoral representation of the most common native cyclodextrins and their physical properties

had an outstanding role in the large-scale use of cyclodextrins, which continues to this day.

In structural terms, cyclodextrins are macrocyclic oligosaccharides with a hollow truncated cone shape following the rigid $^4C_1$ chair conformation of the glucopyranose units linked by α(1-4) ether bonds. The well known native cyclodextrins, called α-, β- and γ-cyclodextrins, consist of 6, 7 e 8 monomeric units, and have outer diameters of 13.7, 15.3 e 16.9 Å, and cavity volumes equal to 174, 262, e 427 Å^3, respectively [18, 19] (Fig. 1).

Nevertheless, in aqueous solution, the structure of cyclodextrins undergoes significant distortion or, although less frequently, exhibits a collapsing conformation [20]. The number of water molecules that can be located in the cavity of cyclodextrins depends on their volume; thus, considering the volume of one water molecule equal to 30 Å^3 [21] 5, 8, and 14 water molecules can be expected to be present in α-, β- and γ-cyclodextrins, respectively. However, whereas water molecules in the presence of β- and γ-cyclodextrins exhibit similar behavior to that in liquid water, the water molecules in α-cyclodextrin are less hydrogen bridge bonded, as can be inferred from heat capacity measurements carried out by Brignner and Wadsö [22]. Another crucial aspect to consider is the solubility of the cyclodextrins. This property does not follow a particular trend, with higher solubility of α- and γ-CD and relatively low solubility of β-CD [18]. The solubility of CDs is justified by the presence of hydroxyl groups on both rims of the structure, either on the larger rim (wider rim) (secondary hydroxyls) or on the smaller rim (narrow rim or edge). The occurrence of intramolecular hydrogen bonds between the secondary hydroxyls of β-CD is pointed out as a possible justification for the low solubility of this cyclodextrin [23, 24]. In fact, such drawback is overcome when using, for example, hydroxypropyl-β-cyclodextrin. Nonetheless, unlike the outside, the inside of cyclodextrins exhibits hydrophobic characteristics, since it is lined with hydrogen atoms and oxygen glycosidic bridges, giving it a Lewis base character.

The amphiphilicity associated with the donut-like structure and water solubility of cyclodextrins allows the formation of highly stable supramolecular adducts, essentially of host-guest type, with a wide range of hydrophobic or moderately

hydrophobic compounds [25–27]. In thermodynamic terms, host-guest supramolecular adducts are highly stable due to the gain in enthalpy and entropy upon complexation. The former occurs mainly due to hydrophobic interactions, whilst the latter occurs as a consequence of dehydration of the guest as well as the cyclodextrin cavity leading to a positive entropic variation [28]. This capacity of cyclodextrins to react and produce supramolecular host-guest adducts had (and still has) a significant impact on the development of methodologies and formulations in a wide variety of areas [27, 29, 30], such as pharmaceuticals [31, 32] and food and beverages [33–35]. Such a success is justified due to the possibility of cyclodextrins being used to modify, improve or control the properties of guest compounds as, for example, to increase solubility and bioavailability [36–38], enantiomeric differentiation [39, 40], to control the volatility and antioxidant properties [41–44], to modify surfactant micellization properties [25], permeation and preservation properties in food packaging [45] and catalysis [46, 47]. The versatility of cyclodextrins and the ease in forming supramolecular compounds in solution, led to the synthesis of polymeric materials containing cyclodextrins, either as building blocks or as pending groups, by grafting CD in polymers [21, 48–50]. Major applications of these materials include environmental remediation and biomedical and pharmaceutical areas [51–54].

2 Cyclodextrin-Based Nanosponges

Cyclodextrin-based polymers emerged with the need to develop materials that combine the advantages of cyclodextrins, namely the possibility of establishing inclusion complexes with numerous molecules, with the facility of removal and recycling after use, since the inclusion process can be reversible. The obtainment of crosslinked and water-insoluble materials, in addition to the possibility to introduce new functionalities in CDs, specifically through the use of different crosslinkers, has allowed the development of a smorgasbord of new materials with applications ranging from pharmaceuticals to environmental remediation. Hence, by a careful choice of the type of crosslinker, it is possible to prepare materials with different degrees of hydrophilicity, depending on the intended application.

Although the denomination cyclodextrin nanosponge was only introduced in 1999 by Li and Ma [55, 56] many other researchers have previously synthesized hyper reticulated materials that fall into this category. The first polymers using cyclodextrins as monomers were described in 1965 by Solms and Egli and resulted from the reaction of epichlorohydrin with native cyclodextrins with, giving rise to crosslinked materials with glyceryl groups linking the CDs [57]. Since this first work until today, many other crosslinked cyclodextrin-based polymers have been developed including hydrogels, foams, sponges, and particles, among others.

Defined as a 3D-supramolecular structure, nanosponges are highly reticulated, nanoporous, crystalline, or paracrystalline polymers, forming colloidal dispersions in aqueous media. As will be mentioned in this chapter, these can be synthesized in the form of powder or gels, as a function of the crosslinker class and the molar

ratio linker-substrate. The latter can be divided into two major categories: inorganic, such as magnetic-iron, titanium oxide, silver- or silica-based nanoparticles, and organic, such as polystyrene, cellulose, starch, or cyclodextrins. For the preparation of nanosponges, a great variety of synthetic strategies can be applied: from the most traditional wet chemistry via multi-steps or one-pot reactions usually with a higher solvent volume consumption, prolonged times, and high temperatures, that typically results in amorphous products; microwave or ultrasonic-assisted processes with reduced solvent volumes and times; mechanical synthesis processes (dry-chemistry) where the use of solvent is minimal or absent, with minimal reaction times, low temperatures and higher crystallinity of the products. Thus, the high degree of freedom in choice the of synthetic pathways allows to design of materials with specific physicochemical properties. However, it must be specified that the usage of inorganic substrates foresees higher costs both in reagents and energetic terms since the synthesis is usually based on multi-steps processes [58], besides the need for a support structure, mostly of polymeric nature [59]. Additionally, in the last years, the application of inorganic nanomaterials has been the subject of discussion due to their toxicity and persistence (their size allows them to enter animal and vegetal cells, where they can accumulate) [60]. These aspects are two considerable disadvantages in biomedical and environmental remediation fields, for example. Those drawbacks are significantly reduced when using polymeric substrates, especially natural polymers that present low toxicity [61] and high biodegradability; beyond being abundant in nature and, therefore, with a low cost/efficiency ratio. Excellent examples are the cyclodextrin-based nanosponges (CDNSs) obtained from α-, β-, γ-, hydroxypropyl-, their derivatives, or even their mixtures as substrate.

CDNSs demonstrate superior performance when compared to native cyclodextrins in increasing the availability and shelf life of active ingredients (e.g. pharmaceuticals or phytopharmaceuticals) and also ameliorating their sustained release. When used in pharmaceutical applications, CDNSs must comply with some specific requirements, mainly regarding biocompatibility and biodegradability. The non- formation of toxic degradation products under physiological conditions as well as the excretion mechanisms after use are aspects of special relevance. In this context, the shape and dimensions of the particles and the composition of the NSs are parameters that can affect their biocompatibility and biodegradability. Some cell viability studies have demonstrated that CDNSs are safe for clinical usage [62].

Cyclodextrin nanosponges are characterized by having a nanoporous and highly crosslinked structure capable of hosting smaller, hydrophobic molecules in the CD cavity and interacting with more hydrophilic or larger molecules in the pores formed by the crosslinking. They are usually prepared by polymerization methods, using solvents capable of dissolving the CDs, such as DMF or DMSO. References are also found about the use of bulk polymerization methods, in which the reaction is carried out only using the CDs and the crosslinkers, that the liquid can act as both solvents and reactants. In both methods, it is possible to perform the reactions using ultrasound or microwave irradiation which, in general, allows the use of lower temperatures and/or the reduction of reaction times [63]. Characteristics such as a synthetic process with some degree of randomness due to the existence of three reactive groups for

each glucose unit of the cyclodextrin, that allows a multitude of combinations, as well as the somewhat random nature of the crosslinking process, combined with the formation of insoluble materials, generally make difficult the structural characterization of CDNS. Nonetheless, it is possible to obtain structural information using spectroscopic methods (e.g. FTIR, Raman, UV-vis), solid-state NMR, thermal analysis (e.g. DSC, TG), X-ray diffraction, microscopy techniques (e.g. SEM, TEM), porosimetry methods (e.g. BET), zeta potential, etc. [64]. Moreover, the loading and release capacity are two essential properties where the amount of available CDs in the polymeric network is of great importance. Hence, direct and indirect techniques have been applied to determine the cyclodextrin content, i.e. its availability, such as elemental analysis or inclusion complexes analysis with model compounds that have high formation constant (e.g. phenolphthalein or methyl orange, among others).

The presence of domains with different degrees of hydrophilicity in polycyclodextrins overcomes the main limitations of pure cyclodextrins, enlarging their application to a wider range of lipophilic and hydrophilic compounds with higher molecular weights, as well as heavy metals [65]. Herein, their ability to interact with heavy metals makes them excellent substrates for the inclusion of metal nanoparticles [66], improving their performance in bioimaging, as sensors, and as catalysts. The range of applications is additionally enlarged if several manageable variables in the synthesis process are considered [67], such as the class of crosslinkers, the degree of crosslinking, the type of free functional groups acting as active sites [68], etc., on which the physicochemical properties of CDNSs depend (including amphiphilic behaviour, response to temperature or pH, mechanical properties, available surface area, porosity, and size distribution). Thus, if we consider the unique ability of the CDs to form host-guest compounds, it is quite logic that the main applications of the CDNSs are in the pharmaceutical/biomedical field, followed by environmental application, analytical chemistry [69], cosmetic, food, and catalysis.

In this chapter, for the sake of clarity, CDNSs will be divided according to the class of crosslinkers used to prepare the nanosponges (Fig. 2) and greater emphasis will be given to the prepared nanomaterials, to the detriment of applications. It should be stressed that the main focus of this chapter does not include applications.

2.1 Principal Classes of Crosslinking Agents

Epoxides

Epichlorohydrin is the most widely used crosslinking monomer for the preparation of CD-based polymers, even for historical reasons, and allows to obtain polymers with high cyclodextrin incorporation and considerably high molecular weights [70]. These polymers are obtained in a single step using basic catalysis and heating and, depending on the stoichiometry and reaction conditions, water-soluble, gels or highly crosslinked polymers, and therefore insoluble, can be prepared [71].

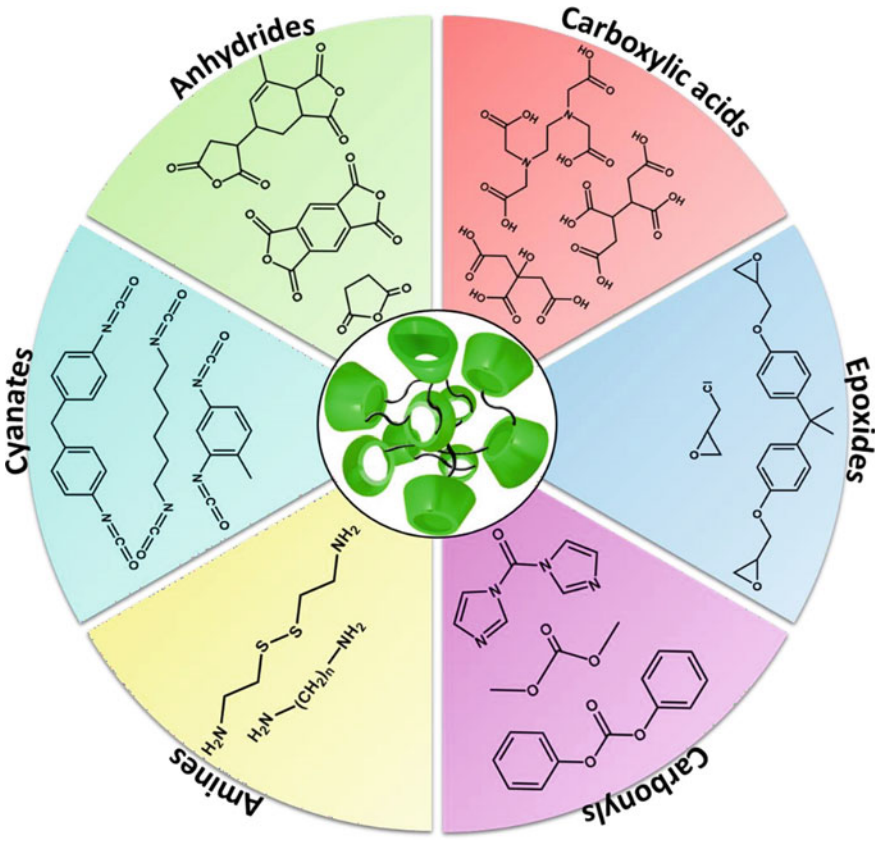

Fig. 2 Scheme of the classes of linkers commonly used in cyclodextrin-based nanosponges

Changing other reaction parameters such as base concentration (usually NaOH) and temperature also allows the modeling of the properties of the obtained polymers [48]. The crosslinking reaction is well studied and involves the first step the opening of the epoxide ring, by reaction with a deprotonated hydroxyl group of the cyclodextrin, and the formation of an alkoxide. The alkoxide, through an SN_2-type reaction, may give rise to a new terminal epoxide by elimination of the chloride ion, which can react with the alkoxy group of another CD (Fig. 3). The final hydrophilic, amorphous polymer contains ether and hydroxyl groups in its structure. Substitution can occur at any of the available hydroxyl groups of the CD glucopiranose ring.

The hyper-reticulated polymers are mostly used in chromatographic applications while gels have been widely explored for environmental remediation. Another important aspect that must be considered in this type of material that influences the final application is the porosity. Usually, CD-EPI polymers exhibit low porosity and low surface areas (typically 1 to 10 $m^2\ g^{-1}$) [72]. However, it is possible to prepare materials with higher porosity and larger surface areas by using organic solvents instead

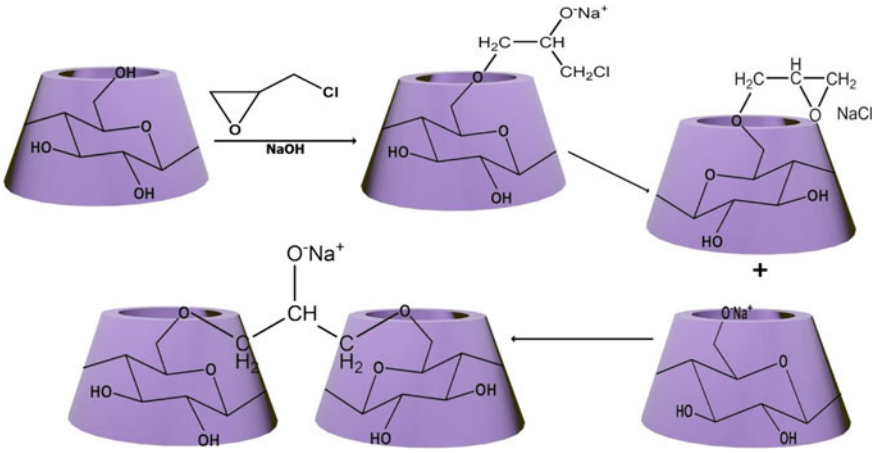

Fig. 3 Cyclodextrin-based nanosponges crosslinked with epichlorohydrin (EPI)

of water to undertake the reaction or by using co-crosslinkers with a more rigid structure (e.g. tetrafluoroterephthalonitrile) [73, 74]. There are other approaches that allow modeling the properties of the obtained polymers, for example through the addition of other reagents, besides EPI, during or after the polymerization reaction. The use of compounds such as glycidyl trimethylammonium chloride, which introduce ionic groups in the polymers, chloroacetic acid, chloroalkylamines, among others, confer more diversified properties and functionalities to the obtained materials [75].

Although the use of EPI crosslinked CDs is widely described in the literature, namely for the removal of environmental pollutants [71, 75] (e.g. dyes, metals, aromatic compounds), for biomedical applications [70] (e.g. increased bioavailability and controlled release of drugs), food science [52], among others, not all articles mention whether or not these are nanoporous materials.

Most of the CD-EPI nanosponges described in the literature were synthesized using CD:EPI molar ratios of 1:10 and NaOH as catalysts, with the reaction stopped near the gelation point. Some papers report that the obtained polymers present average pore size between 2 and 5 nm, pore volumes of 1.3–14 $\times$ 10^{-3} cm^3 g^{-1} and low surface areas (0.005–11 m^2 g^{-1}) [74, 76, 77]. With regard to particle size, the mentioned values can be quite different, ranging from just a few nanometers to values in the order of hundreds, depending on the synthetic method and also on the type of CDs used in the preparation of the polymers [78–80].

The percentages of CD incorporation in the final polymer can range from approximately 40 to 70% [76, 78, 79, 81].

As for applications, CD-EPI nanosponges have been employed in the increase the physiological availability of some drugs (e.g. ethionamide [78, 81], repaglinide [82], temoporfin [79]) and herbicides (e.g. nicosulfuron [80]), in pollutant removal [71, 74, 76, 83], in flame retardance [84] and also in catalysis [77].

Recently, a more complex and planned study envisages the synthesis of nanosponges crosslinked with epichlorohydrin as support for ferromagnetic nanoparticles with improved biocompatibility and excellent haemocompatibility, responsive to external magnetic fields (e.g. nuclear magnetic resonance) and decorate on the surface with pending folic groups, as tumor cell recognition sites [85].

The use of ethers other than epichlorohydrin (e.g. 1,4 butanediol diglycidyl ether) for the synthesis of nanosponges has also been referenced [86].

Carbonyls

The use of crosslinkers such as diphenyl and dimethylcarbonate, carbonyl diimidazole, or triphosgene allows the introduction of a carbonyl function linking the CD rings, through the formation of carbonates. Amorphous or semi-crystalline polymers can be obtained, depending on the conditions used in the reaction. In-mass and ultrasonic-assisted reactions allow to induce crystallinity and solution reactions lead to the formation of more amorphous structures [87]. These nanosponges can be prepared with different average particle diameters, from about 200 nm to values close to 1 μm [88].

Crosslinked CDs with carbonyl groups are hard polymers that exhibit some hydrophobicity and high thermal stability (up to about 300 °C). These materials show a characteristic band in FTIR, around 1700–1750 cm^{-1}, due to carbonyl groups [89, 90].

Generally, the crosslinking reaction occurs through a nucleophilic attack from the oxygen of a hydroxyl group of the CD to the carbonyl group of the different crosslinkers, with the formation of a tetrahedral intermediate, followed by elimination of phenol, methanol, or imidazole (depending on the crosslinking agent) and formation of the carbonyl group again. A second attack from another hydroxyl group of another CD to the carbonyl group leads to the formation of carbonate groups and thus to the crosslinking of the CDs (Fig. 4).

Carbonate nanosponges were developed by Trotta et al. and the first published papers refer to their use for the increase of drug solubilization efficiency (dexamethasone or flurbiprofen) and for the removal of chlorinated aromatic compounds from water. These materials were synthesized by reaction of β-cyclodextrin with carbonyldiimidazole (solution polymerization) or diphenylcarbonate (bulk polymerization) [90–92].

Subsequently, NS of α- β- and γ-cyclodextrins crosslinked with carbonyldiimidazole (CDI) were also synthesized and used for oxygen delivery. The NS had surface areas of 40–50 $m^2\ g^{-1}$, an average diameter of 400–550 nm, and a zeta potential of − 30 mV [93]. Since these pioneering works, many others have been published using CDs and derivatives crosslinked with carbonyl compounds and used mainly in pharmaceutical applications (increased bioavailability and controlled release of drugs, including cancer drugs) [62, 64, 67, 94, 95]. Biocompatibility studies have shown that these NSs are non-toxic and show no appreciable degradation during

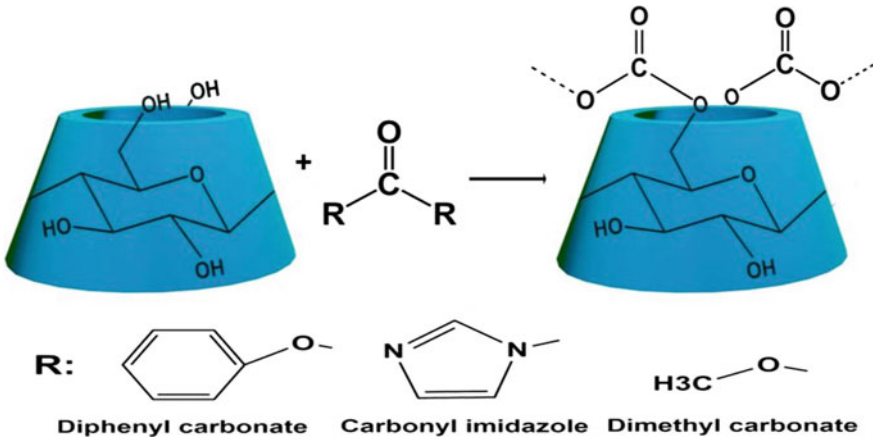

Fig. 4 Scheme of the synthesis of carbonyl-cyclodextrin-based nanosponges

gastrointestinal transit, so they are considered safe for concentrations up to 2 g kg^{-1} for drug delivery [96].

CDNSs using carbonyldiimidazole as crosslinker are usually synthesized using β-CD, DMF or DMSO as a solvent, and different ratios of β-CD: CDI, usually 1:2, 1:3, 1:4, 1:6, or 1:8. The reaction occurs at temperatures varying from 100 °C to DMSO reflux (189 °C) The particle sizes obtained are in the range 300–600 nm and the zeta potentials are negative (between −10 and −30 mV). The polymers show high thermal stability and no thermal degradation is observed up to 320 °C [97–99].

The preparation of CDNS-CDI using an interfacial polymerization method in which β-CD is dissolved in a basic aqueous solution and CDI in dichloromethane has also been described. The NSs obtained in this way present smaller average particle sizes (~100–250 nm) than those obtained by solution polymerization [100]. More recently the use of a ball-mill to prepare CDNS-CDI in the absence of solvents has also been described [101, 102].

CDNS-CDI were used to increase biological availability, solubility, and durability of drugs (piroxicam [97], resveratrol [103], atorvastatin calcium [99], sulfamethoxazole [104], econazole nitrate [105], among others), controlled-release of drugs, including for cancer treatment (e.g. tamoxifen [98], L-DOPA [106], erlotinib [107], paclitaxel [108], bortezomib [109]), antimicrobial activity [100], encapsulation of antioxidants (polyphenols [110], kynurenic acid [102]) and as a carrier for herbicides (ailanthone) [111]. As an alternative to carbonyldiimidazole, diphenylcarbonate (DPC) is widely used to obtain crosslinked CDNS with carbonyl groups. In this case, diphenylcarbonate and CD are usually fused in the absence of solvent by heating to about 100 °C. CD:DPC ratios of 1:2, 1:4, 1:6, 1:8, 1:10 are commonly used, obtaining polymers with average particle size between ~ 100-1000 nm and zeta potentials between − 10 and − 30 mV [112–115]. The use of solvents [116] or ultrasound (to promote the in-mass reaction) has also been described, obtaining in the latter case particles with an average diameter of approximately 650 nm and zeta potentials of

− 15 to − 24 mV [117]. Microwave irradiation was recently used for the synthesis of CDNS- DPC and particles with an average size close to 200 nm, using a CD:DPC ratio of 1:6, were obtained [118, 119].

The increase in bioavailability of drugs (nicosulfuron [80], dithranol [113], nifedipine [117], rilpivirine [118], domperidone [119], giseofulvin [120], anti-restenotic agent DB103 [121]), the transport of therapeutic agents (phenylethylamine and 2-amino-4-(4-chlorophenyl)-thiazole and gold nanoparticles [112]), cancer therapy (camptothecin [122, 123], diosmin [115], curcumin [124]) and the encapsulation of food additives [116], essentials oils [114], antioxidants (ferulic acid [125] and limonene [126]) have been referred as applications of these kind of NSs.

Dimethylcarbonate (DMC) can also be used for the preparation of crosslinked CDNS with a carbonate function. References to the use of this monomer are scarce in the literature, however, the preparation of these nanosponges is performed using dimethylformamide as solvent at reflux temperature. Particles with an average diameter of 487 nm were produced and these nanosponges were used for the release of curcumin [127].

The synthesis of CDNS-DMC through a hot-melt synthesis has also been reported. NSs were synthesized using different proportions of dimethyl carbonate and particles with an average diameter within approximately 200–280 nm were prepared and used for the encapsulation of paracetamol, aceclofenac, and caffeine in order to increase their solubility for application in combined therapy [128].

Anhydrides/carboxylic acids/acid chlorides

Poly-anhydrides/carboxylic acids and acid chlorides can be joined in the same group of crosslinkers due to the resulting ester functional group that is obtained. However, NSs with lower chemical stability are obtained if compared to those with urethane groups. These three classes of monomers, together with the class of epoxides, are the most widely used for the synthesis of soluble and insoluble cyclodextrin- based polymers due to the simplicity of the reaction, often without prior modification of the CDs. Herein, only insoluble polymers it will be discussed. Generally, the ester-CDNSs exhibit a high-water sorption capacity, due to the contribution of the ester groups to the formation of hydrogen bonding, which is inversely proportional to the degree of crosslinking. Within the anhydride class and in general, pyromellitic anhydride (APM) is one of the most common monomers used for cyclodextrins polymerization. Generally, increasing the molar ratio of CD-APM allows to preparation of hydrogels (1:3) to powders (1:4, 1:6, and 1:8), as expected, due to the higher crosslinking degree, although with a reduction in the surface area. However, minimum particle size and PDI (polydispersity index) were obtained for CD-APM 1:6 ratio with the largest pore size (242 nm—technically outside the definition of nanosponge) [129]. The hydrogel CD-APM presents a high-water absorption capacity (830%) [130]. CDNS-APM has been applied as a diclofenac-selective fluorescent sensor [131] and, for the first time, in 2014, as a transport and permeation system for diclofenac through the

skin [132]. CDNS-APM sensors have also been developed by multi-surface functionalization with anti-IgG and loaded with a peroxidase enzyme as a colorimetric and/or electrochemical detection probe [133]. Differently, CDNS- APM has been applied as a nanosystem for the transport of *N*,*N*-diethyl-3-toluamide (DEET—insecticide) [134]. CDNS-APM prepared with different molar ratios were compared as transport systems for rosuvastatin (hepatic sterol synthase inhibitor). Increasing molar content of APM implies a considerable increase in pore size, which does not fit in the definition of nanosponges, although the drug loading capacity is promising [129]. CDNS-APM achieves an encapsulation efficiency of curcumin of ≈98% [135]. Other examples of anhydride monomers are phthalic and nitrophthalic anhydride. It was observed that higher molar ratios and reaction temperatures led to polymers with higher molecular weight (> 100 kDa), higher crosslinking degree, and the number of active sites, which play a key role in the flocculation process of Cu^{2+} ions [136].

Considering carboxylic acids, the reactions are mainly carried out at high temperatures. The usage of naphthalene dicarboxylic acid as a crosslinker led to a polymer whose particle size increases with the variation of time and temperature. This NS was applied to increase the solubility/stability and hence the applicability of Salvia officinalis essential oil [137]. Phthalic acid and succinic acid were used in the acid or acyl chloride forms, overcoming the previous functionalization of cyclodextrin and, obtaining polymers with a certain degree of crystallinity. By increasing the molar content of the crosslinking agent, higher efficiency of the reaction and crosslinking degree are obtained, with a homogeneous distribution of particle size. The two NSs showed a superior complexation of curcumin (≥ 60%) when compared to pure cyclodextrin (≈30%) [138]. The effect of the molar ratio and temperature on the synthesis of CDNSs with succinic acid was investigated via thermal analysis of the polymers, both in dried and hydrated forms. An increase in thermal stability was obtained using higher molar content of NaH, to deprotonate the CD, and temperature [139]. Succinic acid and Epiclon B-4400 (EPB) were also used as polyacid monomers for the inclusion of magnetic iron nanoparticles via chelation between carboxylate groups. The polymers were successfully applied to remove rhodamine B and methylene blue from aqueous solutions and reused for up to 5 cycles [140]. The preparation of βCD-based polymers with increasing molar content of EPB showed a reduction in pore size with an increase in surface area, thermal stability, and water-uptake capacity. The most crosslinked polymer also shows the highest ability to solubilize curcumin [141]. A study of diffusion of ibuprofen was carried out using CDNS-EDTA in molar ratio 1:4 and 1:8 as a delivery system [142, 143]. The same group of research demonstrated that a complete structural characterization of CD-EDTA hydrogels can be obtained by FTIR and Raman analysis [144]. CDNS-EDTA shows a superior capacity for 5-fluorouracil solubilization when compared with pure β-CD and CDNS-DPC [145]. Another study compares hydroxypropyl-β-CD (HβCD) nanosponges synthesized using APM, DPC, and citric acid (CTA); the crosslinking with APM and CTA is achieved in the presence of a catalyst. The three polymers are used as transport systems for the anticancer drug naringenin [146]. CDNS-APM and CDNS-CTA exhibit good water-swelling ability as well as high interaction with Cu^{2+} and Zn^{2+} ions due to the presence of the carboxylate chelating group [147,

148]. Recently, a synthetic process was developed that considers the use of CTA as a crosslinking agent and choline chloride as a co-solvent for the formation of a natural deep eutectic solvent. Three molar ratios, temperatures, and reaction times were tested, observing that the molar ratio plays a key role in the polymer properties, controlling the number of active groups and, consequently the removal efficiency of caffeine, molybdenum blue, and methyl orange [149]. Maleic acid has also been used as a monomer and was observed an enhancement in the thermal stability of CDNSs by decreasing the molar content of the acid and increasing the reaction temperature [150]; the monomer has also been used in the anhydride form [151]. Less common is the usage of 2,2-bisacryloamidoacetic acid (2,2AAA) as a crosslinking agent, which was compared with 1,4-disacryloylpiperazine (1,4AP) for the synthesis of NSs with α-, β- and γ-cyclodextrins. α- and γ-CDs crosslinked with 2,2AAA and 1,4AP, respectively, result in soluble polymers. On the other hand, for the insoluble polymers, the water-swelling ability decreases in the order γCD-2,2AAA < βCD-2,2AAA < αCD-2,2AAA < βCD-1,4AP < αCD-1,4AP, probably due to greater structural flexibility of the aliphatic monomers when compared to the cyclic ones. [152]. Moreover, hydrogels of βCD-2,2AAA exhibit good thermal stability, with a water-swelling capacity of 1400% [153]. Terephthaloyl chloride was used as a crosslinking monomer in the preparation of nanosponges used as a polymeric support for tannic acid, which considerably increases Pb^{2+} uptake and presents high selectivity [154].

Isocyanates

The usage of isocyanides as crosslinking monomers led to the formation of urethane linkages, that present a high chemical stability. Moreover, the high reactivity of the isocyanide groups results in a high yield of the reaction with the –OH groups of the cyclodextrins, obtaining thickly crosslinked and rigid structures. It is even possible to obtain polymers with similar physicochemical properties through different synthesis routes, without or in the presence of catalysts, by wet route (using very variable temperature range and reaction time), or by mechanochemical route (in the presence or not of inorganic particles). Similarly to anhydrides, by changing the molar ratio of CD-monomer, a gel or a powder product can be synthesized. The firsts are usually responsive to temperature variations, although with low-water sorption capacity [155–158]. At a constant molar ratio CD-crosslinker, the effect that aliphatic or aromatic isocyanides and chain size have on the surface area, porosity, CD content, and availability [159–161] was evaluated. It was observed that they mainly depend on the degree of rotational freedom of the crosslinker, stiffness, and steric hindrance (Fig. 5). By increasing the molar content of the crosslinkers, a decrease in particle size [157] and thermal stability [162] was observed. For instance, isocyanate monomers, such as 1,6-hexamethylene diisocyanate (HDI), 4,4-methylenediphenyl diisocyanate (MDI) and toluene diisocyanate (TDI), among others, have been successfully used in the synthesis of nanosponges for the removal of azo dyes and aromatic amines [163], as well as nitrosamines from model and real water samples from South Africa [164]; and as solid-phase for extraction processes [165]. CDNS-HDI were applied to

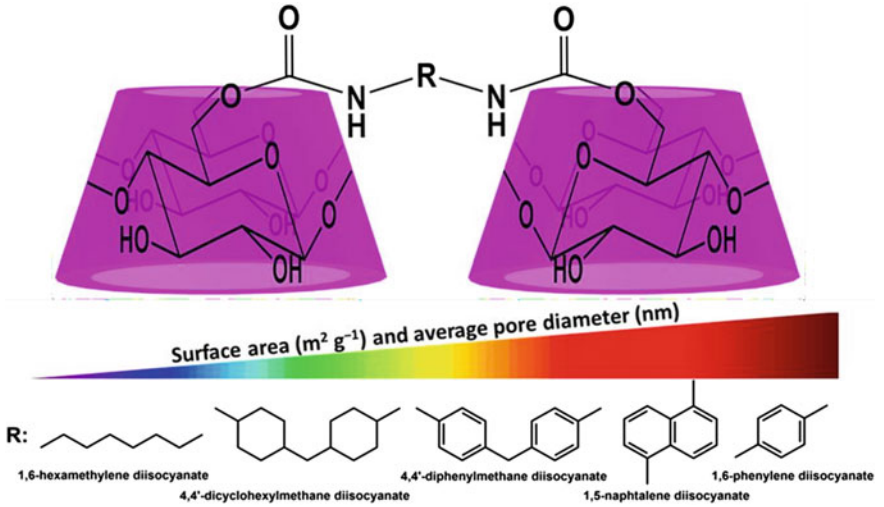

Fig. 5 Representation of isocyanate-cyclodextrin-based nanosponges and effect of the different linkers in some physical properties of the nanosponges

remove ibuprofen from water and sewage [166] and as polymeric support for different Au nanoparticle clusters to evaluate their catalytic properties for the 4-nitrophenol reduction [167]. Epichlorohydrin and HDI as crosslinkers were compared at different molar ratios, showing similar complexation abilities for beta-carotene. However, CDNS-EPI is more efficient to enhance the carotene solubility [168]. Cyclodextrin derivatives can also be used to advantageously modulate the amphiphilic character of the polymer; for example, the use of heptakis(2,6-di-*O*-methyl)-β-CD crosslinked with diisocyanates is highly performant for the polychlorinated biphenyls (PCBs) removal of [169].

Amines/amides

The usage of polyamines as crosslinkers in the synthesis of nanosponges needs the previous modification of cyclodextrins with better-leaving groups, such as tosylates or halogens, through mono-, di- or per- substitutions. Through correct synthetic planning, it has been possible to obtain doubly responsive materials, for example to pH or glutathione, using a mixture of monomers as crosslinkers, which were applied for the controlled release of doxorubicin [170]. Another interesting example is the use of aminated-CDNSs in their pure form or as a support structure for silver nanoparticles sensitive to pH variations, that were applied as sorbent for 11 compounds with different physicochemical properties [171] or as catalysts in the reduction of nitroarenes and the oxidation of anilines [172]. Recently, amino-CDNSs were successfully applied in the removal of a pure active ingredient and a commercial formulation of pesticide. The effect of the use of α- or β-cyclodextrin and the

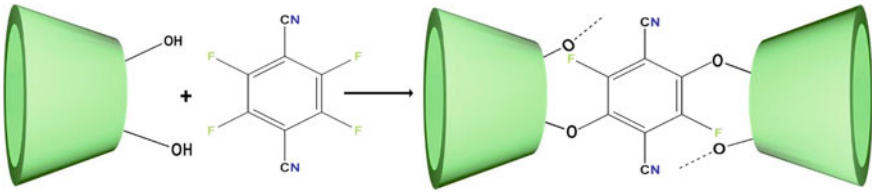

Fig. 6 Cyclodextrin-based nanosponges crosslinked with 2,3,5,6-tetrafluoroterephthalonitrile

aliphatic chain length of the diamines used as crosslinkers has been evaluated [173, 174]. Chain reaction polymerization is another technique used for the synthesis of nanosponges, with the use of highly reactive monomers, such as methylene bisacrylamide and acrylic acid. The nanosponges exhibit high chemical and thermal stability, high water-swelling capacity, ameliorate solubilization ability of dexibuprofen, and non-toxicity in ex-vivo studies [175].

Halogenated compounds

Halogenated compounds, such as cyanuric chloride or 2,3,5,6-tetrafluoroterephthalonitrile (TFTPN), can be used as crosslinkers for the preparation of CDNSs, through nucleophilic substitution reactions (Fig. 6).

The polymerization reaction of β-CD with 2,3,5,6-tetrafluoroterephthalonitrile, described by Alsbaiee et al., when carried out in a mixture of THF:DMF 9:1, at 80 °C in the presence of potassium carbonate, allows obtaining the respective polymers in 45% yield. The reaction was done using several β-CD:TFTN ratios and surface areas between 35 and 263 $m^2\ g^{-1}$ (the highest value is obtained for a β-CD:TFTN ratio of 1:3) and pore size ranging from 1.8 to 3.5 nm was obtained. If the reaction was carried out using NaOH at 60 °C, a non-porous polymer was obtained, with a smaller surface area (6 $m^2\ g^{-1}$) and a lower water absorption capacity (86% versus 265%). Changing some reaction parameters such as base addition rate or initial monomer concentration led to higher reaction yields (up to 67%) [176].

More recently, other authors report the preparation of a polymer of βCD-TFTN 1:3.3, synthesized under similar conditions to those previously mentioned, with yields close to 40%. Analysis of the polymer by FTIR shows a band at 2252 cm^{-1}, characteristic of CN bonds. The specific surface area obtained was 55.2 $m^2\ g^{-1}$, total pore volume of 0.108 $cm^3\ g^{-1}$, and average pore diameter of 7.88 nm. This material was used for the solid phase extraction of aromatic amines [177].

CDNS-TFTPN has shown good results in the removal of several organic pollutants [73], in the separation and concentration of trace quinolones from wastewater [178], in the removal of a wide variety of organic micropollutants [179], and as a binding agent for monitoring endocrine disrupting chemicals [180].

The reduction of nitrile groups to amine, using $BH_3S(CH_3)_2$, allowed the synthesis of another material, which has a high affinity for the removal of anionic micropollutants, in particular, anionic perfluorinated alkyl substances [181].

Reacting a mixture of β-CD and heptakis-(6-deoxy-6-azido)-β-cyclodextrin with TFTN, followed by reduction of the azide to amine and reaction with D-(+)-gluconic acid δ-lactone, allowed to prepare a NS that was used in the removal of boric acid and bisphenol A. The obtained NS presented a surface area of 9.11 $m^2\ g^{-1}$, and pore size < 8 nm before modification with D-(+)-gluconic acid δ-lactone [182].

The crosslinking reaction of β-CD with cyanuric chloride has also been described and a polymer containing triazine rings in its structure was prepared. The reaction was carried out using different percentages of β-CD-cyanuric chloride, in the presence of NaOH and benzyldimethylhexadecyl ammonium chloride, in an acetonitrile/water mixture. Under these conditions, the obtained polymers have a low surface area (4.5 $m^2\ g^{-1}$). FTIR bands at 1720, 842, and 790 cm^{-1} confirm the presence of C=N bonds (first one) and aryl chloride in the final polymer. TGA analysis proves that these polymers are stable up to at least 250 °C. These polymers were used in the removal of benzene, bisphenol A, 2-naphthol, 2-cholor-biphenyl, and dibutyl phthalate with good removal efficiencies [183].

3 Miscellaneous and Other Crosslinkers

A very interesting study on the application of CDNSs in-vitro and in-vivo, has evaluated the performance of 4 different polymers obtained with 4 different classes of monomers: toluene diisocyanate, carbonyldiimidazole, pyromellitic dianhydride, and citric acid. It was observed that the nanosponges showed decreasing thermal stability in the order: anhydride > epoxy > cyanate ≈ carbonate, similar size in water and tendency to aggregate in biological fluids, with exception of NS-urethane. The last one also shows a better sorption capacity of indole in water as well as in biological matrices, followed by NS-epoxy > NS-carbonate > NS-anhydride [184]. Another study used 1,6-hexamethylene diisocyanate, carbonyldiimidazole, and pyromellitic dianhydride in a molar ratio of 1:8 CD:crosslinkers. Two different synthetic processes were considered, namely bulk condensation and interfacial condensation. It was observed a pronounced effect of the synthetic process on particle size distribution 400–500 nm and 50–200 nm, respectively, and all polymer formulations did not exhibit toxicity at the limits studied [96].

In addition to the classes of crosslinkers mentioned above, it must be referred the synthesis of nanosponges via Click Chemistry methods, namely by reaction of azido-cyclodextrins with compounds containing terminal alkynes, in the presence of copper (CuAAC), originating triazoles. NSs of this type were synthesized by reacting heptakis-(6-deoxy)-(6-azido)-β-CD with tetrakis-(25,26,27,28-propargyloxy)-(5,11,17,23-tert-butyl)-calix[4]arene using different ratios of CD:calixarene. Materials with mass yields between 72 and 96%, average pore sizes between 1.9 and 3.9 nm (pore size decreases with the increase in the

percentage of crosslinker), surface areas between 3.2 and 8.1 $m^2\ g^{-1}$ and pore volumes between 0.009 and 0.026 $cm^3\ g^{-1}$ were prepared. The occurrence of vibrational modes at 1239 and 1015 cm^{-1}, confirm the formation of the triazine ring. This NSs were used for the sequestration of nitroarenes and for the release of bioactive molecules (quercetin and silibinin) [185, 186].

In addition to the aforementioned compounds, the usage of heptakis-(2,3-dimethoxy)-(6-deoxy)-(6- azido)-β-CD and tetrakis-propargyloxy-calix[4]arene for the synthesis of different NSs have also been described. Post-modification of NSs was also performed by reduction of the unreacted azide groups to amine or by modification of the triazine formed ring with sodium carboxylate groups. These materials were used for the removal of p-nitroaniline, Bromocresol Green and Pb^{2+} from water [187, 188].

Another crosslinking strategy mentioned in the literature consists of using CDs modified with vinylic monomers that can be crosslinked by reaction with thiols or by Michael polyadditions [152]. For example, heptakis-6-(tert-butyldimethylsilyl)-2-allyloxy-β-cyclodextrin was reacted with an inorganic halloysite clay modified with 3-mercaptopropyltrimethoxysilane, in the presence of AIBN, herein, obtaining an organic-inorganic hybrid nanosponge that was used in the absorption of cationic dyes [189].

4 Conclusion

Cyclodextrin-based nanosponges have unique characteristics mainly due to the amphiphilic properties of cyclodextrins, as well as their ability to form supramolecular adducts, associated with the high surface areas of nanosponges. These and other properties can be modeled either with the use of different cyclodextrins, or even mixtures of cyclodextrins or with an appropriate choice of crosslinkers. The latter can play an important role in increasing the functions and applications of nanosponges. Although five different generations of nanosponges have been developed, from nanosponges with tunable swelling properties to nanosponges that may be able to permeate the cellular membrane, there is a long way to go in the development of nanosponges by using green synthesis approaches and new crosslinkers, as well as in the development of nanosponges with dual or multifunctions. With regard to the applications of nanosponges, there is still much to explore in order to take full advantage of the properties of nanosponges, in areas such as food packaging and catalysis. For these reasons, cyclodextrins remain one of those molecules that, although old, still have a promising future in research laboratories and industry.

Acknowledgements The authors acknowledge Fundação para a Ciência e a Tecnologia (FCT), the Portuguese Agency for Scientific Research for the financial support through projects UIDP/00313/2020. Gianluca Utzeri thanks FCT for the PhD grant SFR/BD/146358/2019.

References

1. Villiers, A. (1891). Sur la transformation de la fécule en dextrine par le ferment butyrique. *Bulletin la Société Chim. Paris., 45*, 468–470.
2. Villiers, A. (1891). Sur la transformation de la fécule en dextrine par le ferment butyrique. *Compte Rendus Des Séances LAcadémie Des Sci.* (1891), 435–437.
3. Villiers, A. (1891). Sur la fermentation de la fécule par l'action du ferment butyrique. *Compte Rendus Des Séances LAcadémie Des Sci.* (1891), 536–538.
4. Villiers, A. (1891). Sur la fermentation de la fécule par l'action du ferment butyrique. *Bulletin la Société Chim Paris* (1891), 470–472.
5. Schardinger, F. (1903). Über thermophile Bakterien aus verschiedenen Speisen und Milch. *Zeitschrift Für Untersuchung der Nahrungs—und Genußm., 6*, 865–880. https://doi.org/10.1007/BF02067497
6. Schardinger, F. (1904). Bacillus macerans, ein aceton bildender Rottebacillus. *Wiener Klinische Wochenschrift, 17*, 468–474.
7. Schardinger, F. (1911). Bildung kristallisier polysaccharide (dextrine) aus starkekleister durch mikrobien. *Zentralblatt Für Bakteriol. Parasitenkunde, Infekt. Und Hyg. 2*(1911), 188–197.
8. Benavent-Gil, Y., Rosell, C. M., & Gilbert, E. P. (2021). Understanding CGTase action through the relationship between starch structure and cyclodextrin formation. *Food Hydrocolloids, 112*, 106316. https://doi.org/10.1016/j.foodhyd.2020.106316
9. French, D. (1957). The schardinger dextrins. *Advances in Carbohydrate Chemistry, 12*, 189–260. https://doi.org/10.1016/S0096-5332(08)60209-X
10. Crini, G. (2020). The contribution of Franz Schardinger to cyclodextrins: A tribute on the occasion of the centenary of his death. *Journal of Inclusion Phenomena and Macrocyclic Chemistry, 97*, 19–28. https://doi.org/10.1007/s10847-020-00990-3
11. Crini, G., French, A. D., Kainuma, K., Jane, J., & Szente, L. (2021). Contributions of Dexter French (1918–1981) to cycloamylose/cyclodextrin and starch science. *Carbohydrate Polymers, 257*, 117620. https://doi.org/10.1016/j.carbpol.2021.117620
12. Crini, G. (2014). Review: A history of cyclodextrins. *Chemical Reviews, 114*, 10940–10975. https://doi.org/10.1021/cr500081p
13. Morin-Crini, N., Fourmentin, S., Crini, G. (Eds). (2015). *Cyclodextrines, Presses universitaires de Franche-Comté*.
14. Saenger, W., Jacob, J., Gessler, K., Steiner, T., Hoffmann, D., Sanbe, H., Koizumi, K., Smith, S. M., & Takaha, T. (1998). Structures of the common cyclodextrins and their larger analogues beyond the doughnut. *Chemical Reviews, 98*, 1787–1802. https://doi.org/10.1021/cr9700181
15. Szejtli, J. (1998). Introduction and general overview of cyclodextrin chemistry. *Chemical Reviews, 98*, 1743–1754. https://doi.org/10.1021/cr970022c
16. Szejtli, J. (1988). *Cyclodextrin technology*. Springer Netherlands.https://doi.org/10.1007/978-94-015-7797-7
17. Cramer, F., & Hettler, H. (1967). Inclusion compounds of cyclodextrins. *Naturwissenschaften, 54*, 625–632. https://doi.org/10.1007/BF01142413
18. Sabadini, E., Cosgrove, T., & do C. Egídio, F. (2006). Solubility of cyclomaltooligosaccharides (cyclodextrins) in H_2O and D_2O: A comparative study. *Carbohydrate Research, 341*(2006), 270–274. https://doi.org/10.1016/j.carres.2005.11.004.
19. Messner, M., Kurkov, S. V., Jansook, P., & Loftsson, T. (2010). Self-assembled cyclodextrin aggregates and nanoparticles. *International Journal of Pharmaceutics, 387*, 199–208. https://doi.org/10.1016/j.ijpharm.2009.11.035
20. Figueiras, A., Sarraguça, J. M. G., Carvalho, R. A., Pais, A. A. C. C., & Veiga, F. J. B. (2007). Interaction of omeprazole with a methylated derivative of β-cyclodextrin: Phase solubility, NMR spectroscopy and molecular simulation. *Pharmaceutical Research, 24*, 377–389. https://doi.org/10.1007/s11095-006-9161-8
21. Cova, T. F., Murtinho, D., Pais, A. A. C. C., & Valente, A. J. M. (2018). Combining cellulose and cyclodextrins: Fascinating designs for materials and pharmaceutics. *Frontiers in Chemistry, 6*(2018). https://doi.org/10.3389/fchem.2018.00271

22. Briggner, L.-E., & Wadsö, I. (1990). Heat capacities of maltose, maltotriose, maltotetrose and α-, β-, and γ-cyclodextrin in the solid state and in dilute aqueous solution. *The Journal of Chemical Thermodynamics, 22*, 1067–1074. https://doi.org/10.1016/0021-9614(90)90156-K
23. Naidoo, K. J., Chen, J. Y.-J., Jansson, J. L. M., Widmalm, G., & Maliniak, A. (2004). Molecular properties related to the anomalous solubility of β-cyclodextrin. *The Journal of Physical Chemistry B, 108*, 4236–4238. https://doi.org/10.1021/jp037704q
24. Cai, W., Sun, T., Shao, X., & Chipot, C. (2008). Can the anomalous aqueous solubility of β-cyclodextrin be explained by its hydration free energy alone? *Physical Chemistry Chemical Physics: PCCP, 10*, 3236. https://doi.org/10.1039/b717509d
25. Valente, A. J. M., & Söderman, O. (2014). The formation of host–guest complexes between surfactants and cyclodextrins. *Advances in Colloid and Interface Science, 205*, 156–176. https://doi.org/10.1016/j.cis.2013.08.001
26. Wankar, J., Kotla, N. G., Gera, S., Rasala, S., Pandit, A., & Rochev, Y. A. (2020). Recent advances in host-guest self-assembled cyclodextrin carriers: Implications for responsive drug delivery and biomedical engineering. *Advanced Functional Materials, 30*, 1909049. https://doi.org/10.1002/adfm.201909049
27. Szente, L., & Szemán, J. (2013). Cyclodextrins in analytical chemistry: Host-guest type molecular recognition. *Analytical Chemistry, 85*, 8024–8030. https://doi.org/10.1021/ac400639y
28. Nilsson, M., Valente, A. J. M., Olofsson, G., Söderman, O., & Bonini, M. (2008). Thermodynamic and kinetic characterization of host−guest association between bolaform surfactants and α- and β-cyclodextrins. *The Journal of Physical Chemistry B, 112*, 11310–11316. https://doi.org/10.1021/jp802963x
29. Muankaew, C., & Loftsson, T. (2018). Cyclodextrin-based formulations: A non-invasive platform for targeted drug delivery. *Basic & Clinical Pharmacology & Toxicology, 122*, 46–55. https://doi.org/10.1111/bcpt.12917
30. Wang, Q. (2020). Industrial applications of cyclodextrins. In: *Handbook of macrocyclic supramolecular assembly* (pp. 1665–1697). Springer Singapore. https://doi.org/10.1007/978-981-15-2686-2_69
31. Loftsson, T., & Duchene, D. (2007). Cyclodextrins and their pharmaceutical applications. *International Journal of Pharmaceutics, 329*, 1–11. https://doi.org/10.1016/j.ijpharm.2006.10.044
32. Dhiman, P., & Bhatia, M. (2020). Pharmaceutical applications of cyclodextrins and their derivatives. *Journal of Inclusion Phenomena and Macrocyclic Chemistry, 98*, 171–186. https://doi.org/10.1007/s10847-020-01029-3
33. Liu, Y., Sameen, D. E., Ahmed, S., Wang, Y., Lu, R., Dai, J., Li, S., & Qin, W. (2022). Recent advances in cyclodextrin-based films for food packaging. *Food Chemistry, 370*, 131026. https://doi.org/10.1016/j.foodchem.2021.131026
34. Astray, G., Gonzalez-Barreiro, C., Mejuto, J. C., Rial-Otero, R., & Simal-Gándara, J. (2009). A review on the use of cyclodextrins in foods. *Food Hydrocolloids, 23*, 1631–1640. https://doi.org/10.1016/j.foodhyd.2009.01.001
35. Cid-Samamed, A., Rakmai, J., Mejuto, J. C., Simal-Gandara, J., & Astray, G. (2022). Cyclodextrins inclusion complex: Preparation methods, analytical techniques and food industry applications. *Food Chemistry, 384*, 132467. https://doi.org/10.1016/j.foodchem.2022.132467
36. Saokham, P., Muankaew, C., Jansook, P., & Loftsson, T. (2018). Solubility of cyclodextrins and drug/cyclodextrin complexes. *Molecules, 23*, 1161. https://doi.org/10.3390/molecules23051161
37. Kim, D.-H., Lee, S.-E., Pyo, Y.-C., Tran, P., & Park, J.-S. (2020). Solubility enhancement and application of cyclodextrins in local drug delivery. *Journal of Pharmaceutical Investigation, 50*, 17–27. https://doi.org/10.1007/s40005-019-00434-2
38. Loftsson, T., Moya-Ortega, M. D., Alvarez-Lorenzo, C., & Concheiro, A. (2016). Pharmacokinetics of cyclodextrins and drugs after oral and parenteral administration of drug/cyclodextrin complexes. *Journal of Pharmacy and Pharmacology, 68*, 544–555. https://doi.org/10.1111/jphp.12427

39. Nagy, G., Chouinard, C. D., Attah, I. K., Webb, I. K., Garimella, S. V. B., Ibrahim, Y. M., Baker, E. S., & Smith, R. D. (2018). Distinguishing enantiomeric amino acids with chiral cyclodextrin adducts and structures for lossless ion manipulations. *Electrophoresis, 39*, 3148–3155. https://doi.org/10.1002/elps.201800294
40. Hobbs, C., Řezanka, P., & Řezanka, M. (2020). Cyclodextrin-functionalised nanomaterials for enantiomeric recognition. *ChemPlusChem, 85*, 876–888. https://doi.org/10.1002/cplu.202000187
41. Paiva-Santos, A. C., Ferreira, L., Peixoto, D., Silva, F., Soares, M. J., Zeinali, M., Zafar, H., Mascarenhas-Melo, F., Raza, F., Mazzola, P. G., & Veiga, F. (2022). Cyclodextrins as an encapsulation molecular strategy for volatile organic compounds—Pharmaceutical applications. *Colloids Surfaces B Biointerfaces, 218*, 112758. https://doi.org/10.1016/j.colsurfb.2022.112758
42. Jo, Y.-J., Cho, H.-S., & Chun, J.-Y. (2021). Antioxidant activity of β-cyclodextrin inclusion complexes containing trans-cinnamaldehyde by DPPH, ABTS and FRAP. *Food Science and Biotechnology, 30*, 807–814. https://doi.org/10.1007/s10068-021-00914-y
43. López-Nicolás, J. M., Rodríguez-Bonilla, P., & García-Carmona, F. (2014). Cyclodextrins and antioxidants. *Critical Reviews in Food Science and Nutrition, 54*, 251–276. https://doi.org/10.1080/10408398.2011.582544
44. Medronho, B., Valente, A. J. M., Costa, P., & Romano, A. (2014). Inclusion complexes of rosmarinic acid and cyclodextrins: Stoichiometry, association constants, and antioxidant potential. *Colloid and Polymer Science, 292*, 885–894. https://doi.org/10.1007/s00396-013-3124-5
45. Arruda, T. R., Marques, C. S., & Soares, N. F. F. (2021). Native cyclodextrins and their derivatives as potential additives for food packaging: A review. *Polysaccharides, 2*, 825–842. https://doi.org/10.3390/polysaccharides2040050
46. Bai, C., Tian, B., Zhao, T., Huang, Q., & Wang, Z. (2017). Cyclodextrin-catalyzed organic synthesis: Reactions. *Mechanisms, and Applications, Molecules, 22*, 1475. https://doi.org/10.3390/molecules22091475
47. Dalal, D. S., Patil, D. R., & Tayade, Y. A. (2018). β-Cyclodextrin: A green and efficient supramolecular catalyst for organic transformations. *Chemical Record, 18*, 1560–1582. https://doi.org/10.1002/tcr.201800016
48. Seidi, F., Jin, Y., & Xiao, H. (2020). Polycyclodextrins: Synthesis, functionalization, and applications. *Carbohydrate Polymers, 242*, 116277. https://doi.org/10.1016/j.carbpol.2020.116277
49. Filho, C. M. C., Bueno, P. V. A., Matsushita, A. F. Y., Vilsinski, B. H., Rubira, A. F., Muniz, E. C., Murtinho, D. M. B., & Valente, A. J. M. (2020). Uncommon sorption mechanism of aromatic compounds onto poly(vinyl alcohol)/chitosan/maleic anhydride-β-cyclodextrin hydrogels. *Polymers (Basel)., 12*, 877. https://doi.org/10.3390/polym12040877
50. Cesteros, L. C., Ramírez, C. A., Peciña, A., & Katime, I. (2006). Poly(ethylene glycol-β-cyclodextrin) gels: Synthesis and properties. *Journal of Applied Polymer Science, 102*, 1162–1166. https://doi.org/10.1002/app.24390
51. Cova, T. F. G. G., Murtinho, D., Pais, A. A. C. C., & Valente, A. J. M. (2018). Cyclodextrin-based materials for removing micropollutants from wastewater. *Current Organic Chemistry, 22*, 2150–2181. https://doi.org/10.2174/1385272822666181019125315
52. Petitjean, M., García, I. X., José, Z., & Isasi, R. (2021). History of cyclodextrin-based polymers in food and pharmacy : A review. *Environmental Chemistry Letters, 19*, 3465–3476. https://doi.org/10.1007/s10311-021-01244-5
53. Concheiro, A., & Alvarez-Lorenzo, C. (2013). Chemically cross-linked and grafted cyclodextrin hydrogels: From nanostructures to drug-eluting medical devices. *Advanced Drug Delivery Reviews, 65*, 1188–1203. https://doi.org/10.1016/j.addr.2013.04.015
54. Cova, T. F., Murtinho, D., Aguado, R., Pais, A. A. C. C., & Valente, A. J. M. (2021). Cyclodextrin polymers and cyclodextrin-containing polysaccharides for water remediation. *Polysaccharides, 2*, 16–38. https://doi.org/10.3390/polysaccharides2010002

55. Li, D., & Ma, M. (1999). Nanoporous polymers: New nanosponge absorbent media. *Filtration & Separation, 36*, 26–28. https://doi.org/10.1016/S0015-1882(00)80050-6
56. Li, D., & Ma, M. (2000). Nanosponges for water purification. *Clean Products and Processes, 2*(2), 112–116.
57. Solms, J., & Egli, R. H. (1965). Harze mit einschlusshohlraumen von cyclodextrin-struktur. *Helvetica Chimica Acta, 48*, 1225–1228.
58. Lee, C.-L., Wu, C.-C., Chiou, H.-P., Syu, C.-M., Huang, C.-H., & Yang, C.-C. (2011). Mesoporous platinum nanosponges as electrocatalysts for the oxygen reduction reaction in an acidic electrolyte. *International Journal of Hydrogen Energy, 36*, 6433–6440. https://doi.org/10.1016/j.ijhydene.2011.03.034
59. Zhang, L., Guo, Y., Hao, R., Shi, Y., You, H., Nan, H., Dai, Y., Liu, D., Lei, D., & Fang, J. (2021). Ultra-rapid and highly efficient enrichment of organic pollutants via magnetic mesoporous nanosponge for ultrasensitive nanosensors. *Nature Communications, 12*, 6849. https://doi.org/10.1038/s41467-021-27100-2
60. Ray, P. C., Yu, H., & Fu, P. P. (2009). Toxicity and environmental risks of nanomaterials: Challenges and future needs. *Journal of Environmental Science and Health, Part C., 27*, 1–35. https://doi.org/10.1080/10590500802708267
61. Cavalli, R., Donalisio, M., Bisazza, A., Civra, A., Ranucci, E., Ferruti, P., & Lembo, D. (2012). Enhanced antiviral activity of acyclovir loaded into nanoparticles. In N. Düzgüneş (Ed.), *Methods Enzymol* (1st ed., pp. 1–19). Elsevier Inc. https://doi.org/10.1016/B978-0-12-391858-1.00001-0
62. Allahyari, S., Zahednezhad, F., Khatami, M., Hashemzadeh, N., Zakeri-Milani, P., & Trotta, F. (2022). Cyclodextrin nanosponges as potential anticancer drug delivery systems to be introduced into the market, compared with liposomes. *Journal of Drug Delivery Science and Technology, 67*, 102931. https://doi.org/10.1016/j.jddst.2021.102931
63. Sherje, A. P., Dravyakar, B. R., Kadam, D., & Jadhav, M. (2017). Cyclodextrin-based nanosponges: A critical review. *Carbohydrate Polymers, 173*, 37–49. https://doi.org/10.1016/j.carbpol.2017.05.086
64. Kumar, S., & Rao, R. (2019). Analytical tools for cyclodextrin nanosponges in pharmaceutical field: A review. *Journal of Inclusion Phenomena and Macrocyclic Chemistry, 94*, 11–30. https://doi.org/10.1007/s10847-019-00903-z
65. Seglie, L., Martina, K., Devecchi, M., Roggero, C., Trotta, F., & Scariot, V. (2011). The effects of 1-MCP in cyclodextrin-based nanosponges to improve the vase life of *Dianthus caryophyllus* cut flowers. *Postharvest Biology and Technology, 59*, 200–205. https://doi.org/10.1016/j.postharvbio.2010.08.012
66. Jicsinszky, L., Rossi, F., Solarino, R., & Cravotto, G. (2023). Comparison of the conventional and mechanochemical syntheses of cyclodextrin derivatives. *Molecules, 28*(2023). https://doi.org/10.3390/molecules28020467
67. Pushpalatha, R., Selvamuthukumar, S., & Kilimozhi, D. (2018). Hierarchy analysis of different cross-linkers used for the preparation of cross-linked cyclodextrin as drug nanocarriers. *Chemical Engineering Communications, 205*, 759–771. https://doi.org/10.1080/00986445.2017.1416354
68. Pawar, S., Shende, P., & Trotta, F. (2019). Diversity of β-cyclodextrin-based nanosponges for transformation of actives. *International Journal of Pharmaceutics, 565*, 333–350. https://doi.org/10.1016/j.ijpharm.2019.05.015
69. Gentili, A. (2020). Cyclodextrin-based sorbents for solid phase extraction. *Journal of Chromatography A, 1609*, 460654. https://doi.org/10.1016/j.chroma.2019.460654
70. Agnes, M., Pancani, E., Malanga, M., Fenyvesi, E., & Manet, I. (2022). Implementation of water-soluble cyclodextrin-based polymers in biomedical applications: How far are we? *Macromolecular Bioscience, 22*, 2200090. https://doi.org/10.1002/mabi.202200090
71. Crini, G. (2021). Cyclodextrin–epichlorohydrin polymers synthesis, characterization and applications to wastewater treatment: A review. *Environmental Chemistry Letters, 19*, 2383–2403.

72. Morin-Crini, N., & Crini, G. (2013). Environmental applications of water-insoluble β-cyclodextrin–Epichlorohydrin polymers. *Progress in Polymer Science, 38*, 344–368. https://doi.org/10.1016/j.progpolymsci.2012.06.005
73. Alsbaiee, A., Smith, B. J., Xiao, L., Ling, Y., Helbling, D. E., & Dichtel, W. R. (2016). Rapid removal of organic micropollutants from water by a porous β-cyclodextrin polymer. *Nature, 529*, 190–194. https://doi.org/10.1038/nature16185
74. Xu, G., Xie, X., Qin, L., Hu, X., Zhang, D., Xu, J., Li, D., Ji, X., Juang, L., Wei, D., Huang, Y., & Tu, Y. (2019). Simple synthesis of a swellable porous β-cyclodextrin-based polymer in the aqueous phase for the rapid removal of organic micro-pollutants from water. *Green Chemistry, 21* (2019), 6062–6072. https://doi.org/10.1039/c9gc02422k
75. Morin-Crini, N., Winterton, P., Fourmentin, S., Wilson, L. D., Fenyvesi, É., & Crini, G. (2018). Water-insoluble β-cyclodextrin–epichlorohydrin polymers for removal of pollutants from aqueous solutions by sorption processes using batch studies: A review of inclusion mechanisms. *Progress in Polymer Science, 78*, 1–23. https://doi.org/10.1016/j.progpolymsci.2017.07.004
76. Liu, H., Cai, X., Wang, Y., & Chen, J. (2011). Adsorption mechanism-based screening of cyclodextrin polymers for adsorption and separation of pesticides from water. *Water Research, 45*, 3499–3511. https://doi.org/10.1016/j.watres.2011.04.004
77. Nasab, M. J., Kiasat, A. R., & Zarasvandi, R. (2018). β-Cyclodextrin nanosponge polymer: A basic and eco- friendly heterogeneous catalyst for the one-pot four-component synthesis of pyranopyrazole derivatives under solvent-free conditions. *Reaction Kinetics, Mechanisms and Catalysis, 124*, 767–778. https://doi.org/10.1007/s11144-018-1373-5
78. Salzano, G., Wankar, J., Ottani, S., Villemagne, B., Baulard, A. R., Willand, N., Brodin, P., Manet, I., & Gref, R. (2017). Cyclodextrin-based nanocarriers containing a synergic drug combination: A potential formulation for pulmonary administration of antitubercular drugs. *International Journal of Pharmaceutics, 531*, 577–587. https://doi.org/10.1016/j.ijpharm.2017.05.030
79. Yakavets, I., Guereschi, C., Lamy, L., Kravchenko, I., Lassalle, H.-P., Zorin, V., Bezdetnaya, L., De Lorraine, U., & Nancy, F. (2020). Cyclodextrin nanosponge as a temoporfin nanocarrier: Balancing between accumulation and penetration in 3D tumor spheroids. *European Journal of Pharmaceutics and Biopharmaceutics, 154* (2020) 33–42. https://doi.org/10.1016/j.ejpb.2020.06.022
80. Liu, X., Li, W., & Xuan, G. (2020). Preparation and characterization of β-cyclodextrin nanosponges and study on enhancing the solubility of insoluble nicosulfuron. *IOP Conference Series Material Science Engineering, 774*, 012108. https://doi.org/10.1088/1757-899X/774/1/012108
81. Wankar, J., Salzano, G., Pancani, E., Benkovics, G., Malanga, M., Manoli, F., Gref, R., Fenyvesi, E., & Manet, I. (2017). Efficient loading of ethionamide in cyclodextrin-based carriers offers enhanced solubility and inhibition of drug crystallization. *International Journal of Pharmaceutics, 531*, 568–576. https://doi.org/10.1016/j.ijpharm.2017.05.041
82. Olteanu, A. A., Aramə, C. C., Radu, C., Mihəescu, C., & Monciu, C. M. (2014). Effect of β-cyclodextrins based nanosponges on the solubility of lipophilic pharmacological active substances (repaglinide). *Journal of Inclusion Phenomena and Macrocyclic Chemistry, 80*, 17–24. https://doi.org/10.1007/s10847-014-0406-6
83. Romita, R., Rizzi, V., Semeraro, P., Gubitosa, J., Gabaldón, J. A., Gorbe, M. I. F., López, V. M. G., Cosma, P., & Fini, P. (2019). Operational parameters affecting the atrazine removal from water by using cyclodextrin based polymers as efficient adsorbents for cleaner technologies. *Environmental Technology and Innovation, 16*, 100454. https://doi.org/10.1016/j.eti.2019.100454
84. Lai, X., Zeng, X., Li, H., Yin, C., Zhang, H., & Liao, F. (2012). Synergistic effect of phosphorus-containing nanosponges on intumescent flame-retardant polypropylene. *Journal of Applied Polymer Science, 125*, 1758–1765. https://doi.org/10.1002/app
85. Gholibegloo, E., Mortezazadeh, T., Salehian, F., Forootanfar, H., Firoozpour, L., Foroumadi, A., Ramazani, A., & Khoobi, M. (2019). Folic acid decorated magnetic nanosponge: An

efficient nanosystem for targeted curcumin delivery and magnetic resonance imaging. *Journal of Colloid and Interface Science, 556*, 128–139. https://doi.org/10.1016/j.jcis.2019.08.046
86. Rizzi, V., Gubitosa, J., Signorile, R., Fini, P., & Cecone, C. (2021). Cyclodextrin nanosponges as adsorbent material to remove hazardous pollutants from water: The case of ciprofloxacin. *Chemical Engineering Journal, 411*, 128514. https://doi.org/10.1016/j.cej.2021.128514
87. Tejashri, G., Amrita, B., & Darshana, J. (2013). Cyclodextrin based nanosponges for pharmaceutical use: A review. *Acta Pharmaceutica, 63*, 335–358.
88. Trotta, F., Zanetti, M., & Cavalli, R. (2012). Cyclodextrin-based nanosponges as drug carriers. *Beilstein Journal of Organic Chemistry, 8*, 2091–2099. https://doi.org/10.3762/bjoc.8.235
89. Ahmed, R. Z., Patil, G., & Zaheer, Z. (2012). Nanosponges—A completely new nano-horizon: Pharmaceutical applications and recent advances. *Drug Development and Industrial Pharmacy, 39*, 1263–1272. https://doi.org/10.3109/03639045.2012.694610
90. Trotta, F., Dianzani, C., Caldera, F., Mognetti, B., & Cavalli, R. (2014). The application of nanosponges to cancer drug delivery. *Expert Opinion on Drug Delivery, 11*, 931–941. https://doi.org/10.1517/17425247.2014.911729
91. Cavalli, R., Trotta, F., & Tumiatti, W. (2006). Cyclodextrin-based nanosponges for drug delivery. *Journal of Inclusion Phenomena and Macrocyclic Chemistry, 56*, 209–213. https://doi.org/10.1007/s10847-006-9085-2
92. Trotta, F., & Cavalli, R. (2009). Characterization and applications of new hyper-cross-linked cyclodextrins. *Composites Interfaces, 16*, 39–48. https://doi.org/10.1163/156855408X379388
93. Cavalli, R., Khalid, A., Bisazza, A., Giustetto, P., Trotta, F., & Vavia, P. (2010). Nanosponge formulations as oxygen delivery systems. *International Journal of Pharmaceutics, 402*, 254–257. https://doi.org/10.1016/j.ijpharm.2010.09.025
94. Allahyari, S., Trotta, F., Valizadeh, H., Jelvehgari, M., & Zakeri-Milani, P. (2019). Cyclodextrin-based nanosponges as promising carriers for active agents. *Expert Opinion on Drug Delivery, 16*, 467–479. https://doi.org/10.1080/17425247.2019.1591365
95. dos P. Menezes, P., de A. Andrade, T., Frank, L. A., de Souza, E. P. B. S. S., das G.G. Trindade, G., Trindade, I. A. S., Serafini, M. R., Guterres, S. S., & de S. Araújo, A. A. (2049). Advances of nanosystems containing cyclodextrins and their applications in pharmaceuticals. *International Journal of Pharmaceutics, 559* (2019) 312–328. https://doi.org/10.1016/J.IJPHARM.2019.01.041
96. Shende, P., Kulkarni, Y. A., Gaud, R. S., Deshmukh, K., Cavalli, R., Trotta, F., & Caldera, F. (2015). Acute and repeated dose toxicity studies of different β-cyclodextrin-based nanosponge formulations. *Journal of Pharmaceutical Sciences, 104*, 1856–1863. https://doi.org/10.1002/jps.24416
97. Gaber, D. A., Radwan, M. A., Alzughaibi, D. A., Alail, J. A., Aljumah, R. S., Aloqla, R. M., Alkhalifah, S. A., & Abdoun, S. A. (2023). Formulation and evaluation of Piroxicam nanosponge for improved internal solubility and analgesic activity. *Drug Delivery, 30*(2023). https://doi.org/10.1080/10717544.2023.2174208
98. Torne, S., Darandale, S., Vavia, P., Trotta, F., & Cavalli, R. (2013). Cyclodextrin-based nanosponges: Effective nanocarrier for tamoxifen delivery. *Pharmaceutical Development and Technology, 18*, 619–625. https://doi.org/10.3109/10837450.2011.649855
99. Zidan, M. F., Ibrahim, H. M., Afouna, M. I., & Ibrahim, E. A. (2018). In vitro and in vivo evaluation of cyclodextrin-based nanosponges for enhancing oral bioavailability of atorvastatin calcium. *Drug Development and Industrial Pharmacy, 44*, 1243–1253. https://doi.org/10.1080/03639045.2018.1442844
100. Desai, D., & Shende, P. (2021). Drug-free cyclodextrin-based nanosponges for antimicrobial activity. *Journal of Pharmaceutical Innovation, 16*(2021), 258–268. https://doi.org/10.1007/s12247-020-09442-4
101. Pedrazzo, A. R., Caldera, F., Zanetti, M., Appleton, S. L., Dhakar, N. K., & Trotta, F. (2020). Mechanochemical green synthesis of hyper-crosslinked cyclodextrin polymers. *Beilstein Journal of Organic Chemistry, 16*, 1554–1563. https://doi.org/10.3762/bjoc.16.127

102. Monfared, Y. K., Pedrazzo, A. R., Mahmoudian, M., Caldera, F., Zakeri-Milani, P., Valizadeh, H., Cavalli, R., Matencio, A., & Trotta, F. (2023). Oral supplementation of solvent-free kynurenic acid/cyclodextrin nanosponges complexes increased its bioavailability. *Colloids Surfaces B Biointerfaces, 222*(2023). https://doi.org/10.1016/j.colsurfb.2022.113101
103. Ansari, K. A., Vavia, P. R., Trotta, F., & Cavalli, R. (2011). Cyclodextrin-based nanosponges for delivery of resveratrol: In vitro characterisation, stability, cytotoxicity and permeation study. *An Official Journal of the American Association of Pharmaceutical Scientists, 12*, 279–286. https://doi.org/10.1208/s12249-011-9584-3
104. Yaşayan, G., Şatıroğlu Sert, B., Tatar, E., & Küçükgüzel, İ. (2020). Fabrication and characterisation studies of cyclodextrin-based nanosponges for sulfamethoxazole delivery. *Journal of Inclusion Phenomena and Macrocyclic Chemistry, 97*(2020), 175–186. https://doi.org/10.1007/s10847-020-01003-z
105. Srivastava, S., Mahor, A., Singh, G., Bansal, K., Singh, P. P., Gupta, R., Dutt, R., Alanazi, A. M., Khan, A. A., & Kesharwani, P. (2021). Formulation development, in vitro and in vivo evaluation of topical hydrogel formulation of econazole nitrate-loaded β-cyclodextrin nanosponges. *Journal of Pharmaceutical Sciences, 110*, 3702–3714. https://doi.org/10.1016/j.xphs.2021.07.008
106. Trotta, F., Caldera, F., Cavalli, R., Soster, M., Biasizzo, M., Barretta, G. U., & Balzano, F. (2017). Molecularly imprinted cyclodextrin nanosponges for the controlled delivery of L-DOPA: Perspectives for the treatment of Parkinson's disease. *Expert Opinion on Drug Delivery, 130*, 1671–1680. https://doi.org/10.1080/17425247.2017.1248398
107. Dora, C. P., Trotta, F., Kushwah, V., Devasari, N., Singh, C., Suresh, S., & Jain, S. (2016). Potential of erlotinib cyclodextrin nanosponge complex to enhance solubility, dissolution rate, in vitro cytotoxicity and oral bioavailability. *Carbohydrate Polymers, 137*, 339–349.
108. Mognetti, B., Barberis, A., Marino, S., Berta, G., De Francia, S., Trotta, F., & Cavalli, R. (2012). In vitro enhancement of anticancer activity of paclitaxel by a Cremophor free cyclodextrin-based nanosponge formulation. *Journal of Inclusion Phenomena and Macrocyclic Chemistry, 74*, 201–210. https://doi.org/10.1007/s10847-011-0101-9
109. Allahyari, S., Valizadeh, H., Roshangar, L., Mahmoudian, M., Trotta, F., Caldera, F., Jelvehgari, M., & Zakeri-Milani, P. (2020). Preparation and characterization of cyclodextrin nanosponges for bortezomib delivery. *Expert Opinion on Drug Delivery, 17*, 1807–1816. https://doi.org/10.1080/17425247.2020.1800637
110. Ramírez-Ambrosi, M., Caldera, F., Trotta, F., Berrueta, L. Á., & Gallo, B. (2014). Encapsulation of apple polyphenols in b-CD nanosponges. *Journal of Inclusion Phenomena and Macrocyclic Chemistry, 80*, 85–92. https://doi.org/10.1007/s10847-014-0393-7
111. Demasi, S., Caser, M., Caldera, F., Kumar, N., Vidotto, F., Trotta, F., & Scariot, V. (2021). Functionalized dextrin-based nanosponges as effective carriers for the herbicide ailanthone. *Industrial Crops and Products, 164*, 113346. https://doi.org/10.1016/j.indcrop.2021.113346
112. Asela, I., Donoso-González, O., Yutronic, N., & Sierpe, R. (2021). β-Cyclodextrin-based nanosponges functionalized with drugs and gold nanoparticles. *Pharmaceutics, 13*, 513. https://doi.org/10.3390/pharmaceutics13040513
113. Kadian, V., Dalal, P., Kumar, S., Kapoor, A., & Rao, R. (2023). Comparative evaluation of dithranol-loaded nanosponges fabricated by solvent evaporation technique and melt method. *Future Journal of Pharmaceutical Sciences, 9*, 13. https://doi.org/10.1186/s43094-023-00461-9
114. Kumar, S., Pooja, Trotta, F., & Rao, R. (2018). Encapsulation of Babchi oil in cyclodextrin-based nanosponges: Physicochemical characterization, photodegradation, and in vitro cytotoxicity studies. *Pharmaceutics, 10*(2018), 169. https://doi.org/10.3390/pharmaceutics10040169
115. Anwer, M. K., Ahmed, M. M., Aldawsari, M. F., Iqbal, M., & Kumar, V. (2023). Preparation and evaluation of diosmin-loaded diphenylcarbonate-cross-linked cyclodextrin nanosponges for breast cancer therapy. *Pharmaceuticals, 16*(2023). https://doi.org/10.3390/ph16010019
116. Garrido, B., González, S., Hermosilla, J., Millao, S., Quilaqueo, M., Guineo, J., Acevedo, F., & Pesenti, H. (2019). Carbonate-β-Cyclodextrin-based nanosponge as a nanoencapsulation

system for piperine: Physicochemical characterization. *Journal of Soil Science and Plant Nutrition, 19*, 620–630.
117. Shringirishi, M., Mahor, A., Gupta, R., Prajapati, S. K., Bansal, K., & Kesharwani, P. (2017). Fabrication and characterization of nifedipine loaded β-cyclodextrin nanosponges: An in vitro and in vivo evaluation. *Journal of Drug Delivery Science and Technology, 41*, 344–350. https://doi.org/10.1016/j.jddst.2017.08.005
118. Zainuddin, R., Zaheer, Z., Sangshetti, J. N., & Momin, M. (2017). Enhancement of oral bioavailability of anti-HIV drug Rilpivirine HCl through nanosponge formulation. *Drug Development and Industrial Pharmacy, 43*, 2076–2084. https://doi.org/10.1080/03639045.2017.1371732
119. Vij, M., Dand, N., Kumar, L., Wadhwa, P., Ud, S., Wani, D., & Mahdi, W. A. (2023). Optimisation of a greener-approach for the synthesis of cyclodextrin-based nanosponges for the solubility enhancement of domperidone, a BCS class II drug. *Pharmaceuticals, 16*, 567.
120. Omar, S. M., Ibrahim, F., & Ismail, A. (2020). Formulation and evaluation of cyclodextrin-based nanosponges of griseofulvin as pediatric oral liquid dosage form for enhancing bioavailability and masking bitter taste. *Saudi Pharmaceutical Journal, 28*, 349–361. https://doi.org/10.1016/j.jsps.2020.01.016
121. Coviello, V., Sartini, S., Quattrini, L., Baraldi, C., Cristina, M., & La, C. (2017). Cyclodextrin-based nanosponges for the targeted delivery of the anti-restenotic agent DB103: A novel opportunity for the local therapy of vessels wall subjected to percutaneous intervention. *European Journal of Pharmaceutics and Biopharmaceutics, 117*, 276–285. https://doi.org/10.1016/j.ejpb.2017.04.028
122. Swaminathan, S., Pastero, L., Serpe, L., Trotta, F., Vavia, P., Aquilano, D., Trotta, M., Zara, G. P., & Cavalli, R. (2010). Cyclodextrin-based nanosponges encapsulating camptothecin: Physicochemical characterization, stability and cytotoxicity. *European Journal of Pharmaceutics and Biopharmaceutics, 74*, 193–201. https://doi.org/10.1016/j.ejpb.2009.11.003
123. Minelli, R., Cavalli, R., Ellis, L., Pettazzoni, P., Trotta, F., Ciamporcero, E., Barrera, G., Fantozzi, R., Dianzani, C., & Pili, R. (2012). Nanosponge-encapsulated camptothecin exerts anti-tumor activity in human prostate cancer cells. *European Journal of Pharmaceutical Sciences, 47*, 686–694. https://doi.org/10.1016/j.ejps.2012.08.003
124. Pushpalatha, R., Selvamuthukumar, S., & Kilimozhi, D. (2018). Cross-linked, cyclodextrin-based nanosponges for curcumin delivery—Physicochemical characterization, drug release, stability and cytotoxicity. *Journal of Drug Delivery Science and Technology, 45*, 45–53.
125. Rezaei, A., Varshosaz, J., Fesharaki, M., Farhang, A., & Jafari, S. M. (2019). Improving the solubility and in vitro cytotoxicity (anticancer activity) of ferulic acid by loading it into cyclodextrin nanosponges. *International Journal of Nanomedicine, 14*, 4589–4599.
126. Salehi, O., Sami, M., & Rezaei, A. (2021). Limonene loaded cyclodextrin nanosponge: Preparation, characterization, antibacterial activity and controlled release. *Food Bioscience, 42*, 101193. https://doi.org/10.1016/j.fbio.2021.101193
127. Darandale, S. S., & Vavia, P. R. (2013). Cyclodextrin-based nanosponges of curcumin: Formulation and physicochemical characterization. *Journal of Inclusion Phenomena and Macrocyclic Chemistry, 75*, 315–322. https://doi.org/10.1007/s10847-012-0186-9
128. Moin, A., Roohi, N. K. F., Danish, M., & Ashraf, A. (2020). Design and formulation of polymeric nanosponge tablets with enhanced solubility for combination. *RSC Advances, 10*, 34869–34884. https://doi.org/10.1039/d0ra06611g
129. Gabr, M. M., Mortada, S. M., & Sallam, M. A. (2018). Carboxylate cross-linked cyclodextrin: A nanoporous scaffold for enhancement of rosuvastatin oral bioavailability. *European Journal of Pharmaceutical Sciences, 111*, 1–12. https://doi.org/10.1016/j.ejps.2017.09.026
130. Pivato, R. V., Rossi, F., Ferro, M., Castiglione, F., Trotta, F., & Mele, A. (2021). β-Cyclodextrin nanosponge hydrogels as drug delivery nanoarchitectonics for multistep drug release kinetics. *ACS Applied Polymer Materials, 3*, 6562–6571. https://doi.org/10.1021/acsapm.1c01262

131. Nazerdeylami, S., Ghasemi, J. B., Mohammadi Ziarani, G., Amiri, A., & Badiei, A. (2021). Direct monitoring of diclofenac using a supramolecular fluorescent approach based on β-cyclodextrin nanosponge. *Journal of Molecular Liquids, 336*(2021), 116104. https://doi.org/10.1016/j.molliq.2021.116104
132. Conte, C., Caldera, F., Catanzano, O., D'Angelo, I., Ungaro, F., Miro, A., Pellosi, D. S., Trotta, F., & Quaglia, F. (2014). β-Cyclodextrin nanosponges as multifunctional ingredient in water-containing semisolid formulations for skin delivery. *Journal of Pharmaceutical Sciences, 103*, 3941–3949. https://doi.org/10.1002/jps.24203
133. Wajs, E., Caldera, F., Trotta, F., & Fragoso, A. (2014). Peroxidase-encapsulated cyclodextrin nanosponge immunoconjugates as a signal enhancement tool in optical and electrochemical assays. *The Analyst, 139*, 375–380. https://doi.org/10.1039/C3AN01643A
134. Cecone, C., Caldera, F., Trotta, F., Bracco, P., & Zanetti, M. (2018). Controlled release of DEET loaded on fibrous mats from electrospun PMDA/cyclodextrin polymer. *Molecules, 23*, 1694. https://doi.org/10.3390/molecules23071694
135. Rafati, N., Zarrabi, A., Caldera, F., Trotta, F., & Ghias, N. (2019). Pyromellitic dianhydride crosslinked cyclodextrin nanosponges for curcumin controlled release; formulation, physicochemical characterization and cytotoxicity investigations. *Journal of Microencapsulation, 36*, 715–727. https://doi.org/10.1080/02652048.2019.1669728
136. Kozlowski, C. A., Girek, T., Walkowiak, W., & Kozlowska, J. (2006). The effect of β-CD polymers structure on the efficiency of copper(II) ion flotation. *Journal of Inclusion Phenomena and Macrocyclic Chemistry, 55*, 71–77. https://doi.org/10.1007/s10847-005-9020-y
137. Nait Bachir, Y., Nait Bachir, R., & Hadj-Ziane-Zafour, A. (2019). Nanodispersions stabilized by β- cyclodextrin nanosponges: Application for simultaneous enhancement of bioactivity and stability of sage essential oil. *Drug Development and Industrial Pharmacy, 45*(2019), 333–347. https://doi.org/10.1080/03639045.2018.1542705
138. Arya, P., Sharma, M. R., & Raghav, N. (2023). A biomimetic study of aliphatic and aromatic dicarboxylic acids engineered β-CD targeted for intestinal maladies. *Chemical Engineering Journal, 461*, 141929. https://doi.org/10.1016/j.cej.2023.141929
139. Girek, T., & Ciesielski, W. (2011). Polymerization of β-cyclodextrin with succinic anhydride and thermogravimetric study of the polymers. *Journal of Inclusion Phenomena and Macrocyclic Chemistry, 69*, 439–444. https://doi.org/10.1007/s10847-010-9777-5
140. Vahedi, S., Tavakoli, O., Khoobi, M., Ansari, A., & Ali Faramarzi, M. (2017). Application of novel magnetic β-cyclodextrin-anhydride polymer nano-adsorbent in cationic dye removal from aqueous solution. *Journal of the Taiwan Institute of Chemical Engineers, 80*(2017), 452–463. https://doi.org/10.1016/j.jtice.2017.07.039
141. Gholibegloo, E., Mortezazadeh, T., Salehian, F., Ramazani, A., Amanlou, M., & Khoobi, M. (2019). Improved curcumin loading, release, solubility and toxicity by tuning the molar ratio of cross- linker to β-cyclodextrin. *Carbohydrate Polymers, 213*(2019), 70–78. https://doi.org/10.1016/j.carbpol.2019.02.075
142. Ferro, M., Castiglione, F., Punta, C., Melone, L., Panzeri, W., Rossi, B., Trotta, F., & Mele, A. (2014). Anomalous diffusion of Ibuprofen in cyclodextrin nanosponge hydrogels: An HRMAS NMR study. *Beilstein Journal of Organic Chemistry, 10*, 2715–2723. https://doi.org/10.3762/bjoc.10.286
143. Ferro, M., Castiglione, F., Pastori, N., Punta, C., Melone, L., Panzeri, W., Rossi, B., Trotta, F., & Mele, A. (2017). Dynamics and interactions of ibuprofen in cyclodextrin nanosponges by solid-state NMR spectroscopy. *Beilstein Journal of Organic Chemistry, 13*, 182–194. https://doi.org/10.3762/bjoc.13.21
144. Venuti, V., Rossi, B., D'Amico, F., Mele, A., Castiglione, F., Punta, C., Melone, L., Crupi, V., Majolino, D., Trotta, F., Gessini, A., & Masciovecchio, C. (2015). Combining Raman and infrared spectroscopy as a powerful tool for the structural elucidation of cyclodextrin-based polymeric hydrogels. *Physical Chemistry Chemical Physics: PCCP, 17*, 10274–10282. https://doi.org/10.1039/C5CP00607D

145. Mashaqbeh, H., Obaidat, R., Al-Shari, N., El-Elimat, T., & Alnabulsi, S. (2022). Weak complexation of 5-fluorouracil with β-cyclodextrin, carbonate, and dianhydride crosslinked β-cyclodextrin: In vitro and in silico studies. *Research in Pharmaceutical Sciences, 17*, 334–349. https://doi.org/10.4103/1735-5362.350235
146. Peimanfard, S., Zarrabi, A., Trotta, F., Matencio, A., Cecone, C., & Caldera, F. (2022). Developing novel hydroxypropyl-β-cyclodextrin-based nanosponges as carriers for anti-cancer hydrophobic agents: overcoming limitations of host-guest complexes in a comparative evaluation. *Pharmaceutics, 14*, 1059. https://doi.org/10.3390/pharmaceutics14051059
147. Pedrazzo, R. (2019). Smarra, caldera, musso, dhakar, cecone, hamedi, corsi, trotta, eco-friendly β-cyclodextrin and linecaps polymers for the removal of heavy metals. *Polymers (Basel), 11*, 1658. https://doi.org/10.3390/polym11101658
148. Berto, S., Bruzzoniti, M. C., Cavalli, R., Perrachon, D., Prenesti, E., Sarzanini, C., Trotta, F., & Tumiatti, W. (2007). Synthesis of new ionic β-cyclodextrin polymers and characterization of their heavy metals retention. *Journal of Inclusion Phenomena and Macrocyclic Chemistry, 57*, 631–636. https://doi.org/10.1007/s10847-006-9273-0
149. Cecone, C., Caldera, F., & Trotta, F. (2020). Sustainable synthesis of cyclodextrin-based solvents †. *Green Chemistry, 22*, 5806–5814. https://doi.org/10.1039/d0gc02247k
150. Girek, T., & Ciesielski, W. (2011). Polymerization of β-cyclodextrin with maleic anhydride along with thermogravimetric study of polymers. *Journal of Inclusion Phenomena and Macrocyclic Chemistry, 69*, 445–451. https://doi.org/10.1007/s10847-010-9778-4
151. Girek, T., Shin, D.-H., & Lim, S.-T. (2000). Polymerization of β-cyclodextrin with maleic anhydride and structural characterization of the polymers. *Carbohydrate Polymers, 42*, 59–63. https://doi.org/10.1016/S0144-8617(99)00138-1
152. Pifferi, V., Ferrari, E., Manfredi, A., Ferruti, P., Alongi, J., Ranucci, E., & Falciola, L. (2023). Nanosponges by the oxo-Michael polyaddition of cyclodextrins as sorbents of water pollutants: The o-toluidine case. *Environmental Science and Pollution Research, 30*, 6592–6603. https://doi.org/10.1007/s11356-022-22501-2
153. Swaminathan, S., Cavalli, R., Trotta, F., Ferruti, P., Ranucci, E., Gerges, I., Manfredi, A., Marinotto, D., & Vavia, P. R. (2010). In vitro release modulation and conformational stabilization of a model protein using swellable polyamidoamine nanosponges of β-cyclodextrin. *Journal of Inclusion Phenomena and Macrocyclic Chemistry, 68*, 183–191. https://doi.org/10.1007/s10847-010-9765-9
154. Yang, G., Fang, D., Yang, L., Wei, Z., Tu, Y., Shao, P., Hua, Z., Wang, Z., & Luo, X. (2022). Tailored construction of β-cyclodextrin covalently-supported tannic acid polymer nanosponge towards highly selective lead recovery. *Journal of Cleaner Production, 330*, 129882. https://doi.org/10.1016/j.jclepro.2021.129882
155. Utzeri, G., Verissimo, L., Murtinho, D., Pais, A. A. C. C., Perrin, F. X., Ziarelli, F., Iordache, T.-V., Sarbu, A., & Valente, A. J. M. (2021). Poly(β-cyclodextrin)-activated carbon gel composites for removal of pesticides from water. *Molecules, 26*, 1426. https://doi.org/10.3390/molecules26051426
156. Skuredina, A. A., Tychinina, A. S., Le-Deygen, I. M., Golyshev, S. A., Kopnova, T. Y., Le, N. T., Belogurova, N. G., & Kudryashova, E. V. (2022). Cyclodextrins and their polymers affect the lipid membrane permeability and increase levofloxacin's antibacterial activity in vitro. *Polymers (Basel), 14*, 4476. https://doi.org/10.3390/polym14214476
157. Govardhane, S., & Shende, P. (2022). Colloidal complexed nanocarriers: A modulated aspect in fabrication and characterization for streptozotocin-induced diabetic rats. *Colloids Surfaces A Physicochemical and Engineering Aspects, 651*, 129755. https://doi.org/10.1016/j.colsurfa.2022.129755
158. Zhang, X., Chen, R., Gao, X., Weng, J., Liu, Y., Gui, T., Yang, S., Wang, D., Chen, X., & Liu, J. (2023). Mechanochemical synthesis of reticular β-cyclodextrin polyurethanes for the decontamination of phenolic micropollutants. *Chemical Engineering Journal, 453*, 139987. https://doi.org/10.1016/j.cej.2022.139987
159. Wilson, L. D., Mohamed, M. H., & Headley, J. V. (2011). Surface area and pore structure properties of urethane-based copolymers containing β-cyclodextrin. *Journal of Colloid and Interface Science, 357*, 215–222. https://doi.org/10.1016/j.jcis.2011.01.081

160. Mohamed, M. H., Wilson, L. D., & Headley, J. V. (2010). Estimation of the surface accessible inclusion sites of β-cyclodextrin based copolymer materials. *Carbohydrate Polymers, 80*, 186–196. https://doi.org/10.1016/j.carbpol.2009.11.014
161. Cesteros, L. C., Ramírez, C. A., Peciña, A., & Katime, I. (2007). Synthesis and properties of hydrophilic networks based on poly(ethylene glycol) and β-Cyclodextrin. *Macromolecular Chemistry and Physics, 208*, 1764–1772. https://doi.org/10.1002/macp.200700109
162. Zhou, L., Liang, Q., Chai, K., Tong, Z., & Ji, H. (2020). A cost-effective β-cyclodextrin polymer for selective adsorption and separation of acetophenone and 1-phenylethanol via specific noncovalent molecular interactions. *Reactive & Functional Polymers, 146*, 104448. https://doi.org/10.1016/j.reactfunctpolym.2019.104448
163. Yilmaz, E., Memon, S., & Yilmaz, M. (2010). Removal of direct azo dyes and aromatic amines from aqueous solutions using two β-cyclodextrin-based polymers. *Journal of Hazardous Materials, 174*, 592–597. https://doi.org/10.1016/j.jhazmat.2009.09.093
164. Mhlongo, S. H., Mamba, B. B., & Krause, R. W. (2009). Monitoring the prevalence of nitrosamines in South African waters and their removal using cyclodextrin polyurethanes. *Physics and Chemistry of the Earth, Parts A/B/C, 34*(2009), 819–824. https://doi.org/10.1016/j.pce.2009.07.008
165. Bhaskar, M., Aruna, P., Ganesh Jeevan, R. J., & Radhakrishnan, G. (2004). β-Cyclodextrin-polyurethane polymer as solid phase extraction material for the analysis of carcinogenic aromatic amines. *Analytica Chimica Acta, 509*(2004), 39–45. https://doi.org/10.1016/j.aca.2003.12.015
166. Skwierawska, A. M., Nowacka, D., Nowicka, P., Rosa, S., & Kozłowska-tylingo, K. (2021). Structural adaptive, self-separating material for removing ibuprofen from waters and sewage. *Materials (Basel)., 14*, 7697. https://doi.org/10.3390/ma14247697
167. Vasconcelos, D. A., Kubota, T., Santos, D. C., Araujo, M. V. G., Teixeira, Z., & Gimenez, I. F. (2016). Preparation of Au quantum clusters with catalytic activity in β-cyclodextrin polyurethane nanosponges. *Carbohydrate Polymers, 136*, 54–62. https://doi.org/10.1016/j.carbpol.2015.09.010
168. Yazdani, M., Tavakoli, O., Khoobi, M., Wu, Y. S., Faramarzi, M. A., Gholibegloo, E., & Farkhondeh, S. (2022). Beta-carotene/cyclodextrin-based inclusion complex: Improved loading, solubility, stability, and cytotoxicity. *Journal of Inclusion Phenomena and Macrocyclic Chemistry, 102*, 55–64. https://doi.org/10.1007/s10847-021-01100-7
169. Kawano, S., Kida, T., Miyawaki, K., Fukuda, Y., Kato, E., Nakano, T., & Akashi, M. (2015). Adsorption capability of urethane-crosslinked heptakis(2,6-di-O-methyl)-β-cyclodextrin polymers toward polychlorobiphenyls in nonpolar organic media. *Polymer Journal, 47*, 443–448. https://doi.org/10.1038/pj.2015.13
170. Dai, Y., Li, Q., Zhang, S., Shi, S., Li, Y., Zhao, X., Zhou, L., Wang, X., Zhu, Y., & Li, W. (2021). Smart GSH/pH dual-bioresponsive degradable nanosponges based on β-CD-appended hypercross-linked polymer for triggered intracellular anticancer drug delivery. *Journal of Drug Delivery Science and Technology, 64*, 102650. https://doi.org/10.1016/j.jddst.2021.102650
171. Russo, M., Saladino, M. L., Chillura Martino, D., Lo Meo, P., & Noto, R. (2016). Polyaminocyclodextrin nanosponges: Synthesis, characterization and pH-responsive sequestration abilities. *RSC Advances, 6*(2016), 49941–49953. https://doi.org/10.1039/C6RA06417E
172. Russo, M., Spinella, A., Di Vincenzo, A., Lazzara, G., Correro, M. R., Shahgaldian, P., Lo Meo, P., & Caponetti, E. (2018). Synergistic activity of silver nanoparticles and polyaminocyclodextrins in nanosponge architectures. *ChemistrySelect, 4*(2019), 873–879. https://doi.org/10.1002/slct.201803424
173. Utzeri, G., Cova, T. F., Murtinho, D., Pais, A. A. C. C., & Valente, A. J. M. (2023). Insights on macro- and microscopic interactions between Confidor and cyclodextrin-based nanosponges. *Chemical Engineering Journal, 455*, 140882. https://doi.org/10.1016/j.cej.2022.140882
174. Utzeri, G., Murtinho, D., Maria, T. M. R., Pais, A. A. C. C., Sannino, F., & Valente, A. J. M. (2022). Amine-β- cyclodextrin-based nanosponges. The role of cyclodextrin amphiphilicity in the imidacloprid uptake. *Colloids Surfaces A Physicochemical and Engineering Aspects, 635*(2022), 128044. https://doi.org/10.1016/j.colsurfa.2021.128044

175. Khalid, Q., Ahmad, M., Minhas, M. U., Batool, F., Malik, N. S., & Rehman, M. (2021). Novel β-cyclodextrin nanosponges by chain growth condensation for solubility enhancement of dexibuprofen: Characterization and acute oral toxicity studies. *Journal of Drug Delivery Science and Technology, 61*, 102089. https://doi.org/10.1016/j.jddst.2020.102089
176. Klemes, M. J., Ling, Y., Chiapasco, M., Alsbaiee, A., Helbling, D. E., & Dichtel, W. R. (2018). Phenolation of cyclodextrin polymers controls their lead and organic micropollutant adsorption. *Chemical Science, 9*, 8883–8889. https://doi.org/10.1039/c8sc03267j
177. Dai, J., Yin, H., Yu, L., Hong, T., Zhou, L., & Liu, M. (2021). Novel poly(β-cyclodextrin) porous material as solid phase extraction sorbent for aniline derivatives in rubber samples. *BioResources, 16*, 5746–5765.
178. Zhang, J., Liu, D., Shi, Y., Sun, C., Niu, M., Wang, R., & Hu, F. (2017). Determination of quinolones in wastewater by porous β-cyclodextrin polymer based solid-phase extraction coupled with HPLC. *Journal of Chromatography B, 1068–1069*, 24–32. https://doi.org/10.1016/j.jchromb.2017.09.046
179. Ling, Y., Klemes, M. J., Xiao, L., Alsbaiee, A., Dichtel, W. R., & Helbling, D. E. (2017). Benchmarking micropollutant removal by activated carbon and porous β-cyclodextrin polymers under environmentally relevant scenarios. *Environmental Science and Technology, 51*, 7590–7598. https://doi.org/10.1021/acs.est.7b00906
180. Li, H., Qi, S., Li, X., Qian, Z., Chen, W., & Qin, S. (2021). Tetrafluoroterephthalonitrile-crosslinked β-cyclodextrin polymer as a binding agent of diffusive gradients in thin-films for sampling endocrine disrupting chemicals in water. *Chemosphere, 280*, 130774. https://doi.org/10.1016/j.chemosphere.2021.130774
181. Klemes, M. J., Ling, Y., Ching, C., Wu, C., Xiao, L., Helbling, D. E., & Dichtel, W. R. (2019). Reduction of a tetrafluoroterephthalonitrile-b-cyclodextrin polymer to remove anionic micropollutants and perfluorinated alkyl substances from water communications. *Angewandte Chemie—International Edition, 58*, 12049–12053. https://doi.org/10.1002/anie.201905142
182. Liao, X., & Zhang, Q. (2019). Mesoporous polymer nanosponges immobilized with functional polyols for rapid removal of boric acid and organic micropollutants. *ACS Applied Polymer Materials, 1*, 2089–2098. https://doi.org/10.1021/acsapm.9b00399
183. Wang, J., & Harrison, M. (2018). Removal of organic micro-pollutants from water by β-cyclodextrin triazine polymers. *Journal of Inclusion Phenomena and Macrocyclic Chemistry, 92*, 347–356. https://doi.org/10.1007/s10847-018-0851-8
184. Varan, C., Anceschi, A., Sevli, S., Bruni, N., Giraudo, L., Bilgiç, E., Korkusuz, P., İskit, A. B., Trotta, F., & Bilensoy, E. (2020). Preparation and characterization of cyclodextrin nanosponges for organic toxic molecule removal. *International Journal of Pharmaceutics, 585*, 119485. https://doi.org/10.1016/j.ijpharm.2020.119485
185. Lo Meo, P., Lazzara, G., Liotta, L., Riela, S., & Noto, R. (2014). Cyclodextrin–calixarene co-polymers as a new class of nanosponges. *Polymer Chemistry, 5*(2014), 4499–4510. https://doi.org/10.1039/C4PY00325J
186. Massaro, M., Labbozzetta, M., Lazzara, G., Lo Meo, P., Poma, P., Riela, S., & Noto, R. (2016). Chemical and pharmaceutical evaluation of the relationship between triazole linkers and pore size on cyclodextrin–calixarene nanosponges used as carriers for natural drugs †. *RSC Advance, 6*(2016) , 50858–50866. https://doi.org/10.1039/C6RA06143E
187. Cinà, V., Russo, M., Lazzara, G., Chillura, D., & Lo, P. (2017). Pre- and post-modification of mixed cyclodextrin-calixarene co-polymers: A route towards tunability. *Carbohydrate Polymers, 157*, 1393–1403. https://doi.org/10.1016/j.carbpol.2016.11.018
188. Cataldo, S., Lo, P., Conte, P., Di, A., Milea, D., & Pettignano, A. (2021). Evaluation of adsorption ability of cyclodextrin-calixarene nanosponges towards Pb^{2+} ion in aqueous solution. *Carbohydrate Polymers, 267*, 118151. https://doi.org/10.1016/j.carbpol.2021.118151
189. Massaro, M., Colletti, C. G., Lazzara, G., Guernelli, S., Noto, R., & Riela, S. (2017). Synthesis and characterization of halloysite−cyclodextrin nanosponges for enhanced dyes adsorption. *ACS Sustainable Chemistry & Engineering, 5*, 3346–3352. https://doi.org/10.1021/acssuschemeng.6b03191

Cyclodextrin-based nanosponges: overview and opportunities

II

G Utzeri, P. M.C. Matias, D. Murtinho, A. J.M. Valente

Frontiers in Chemistry

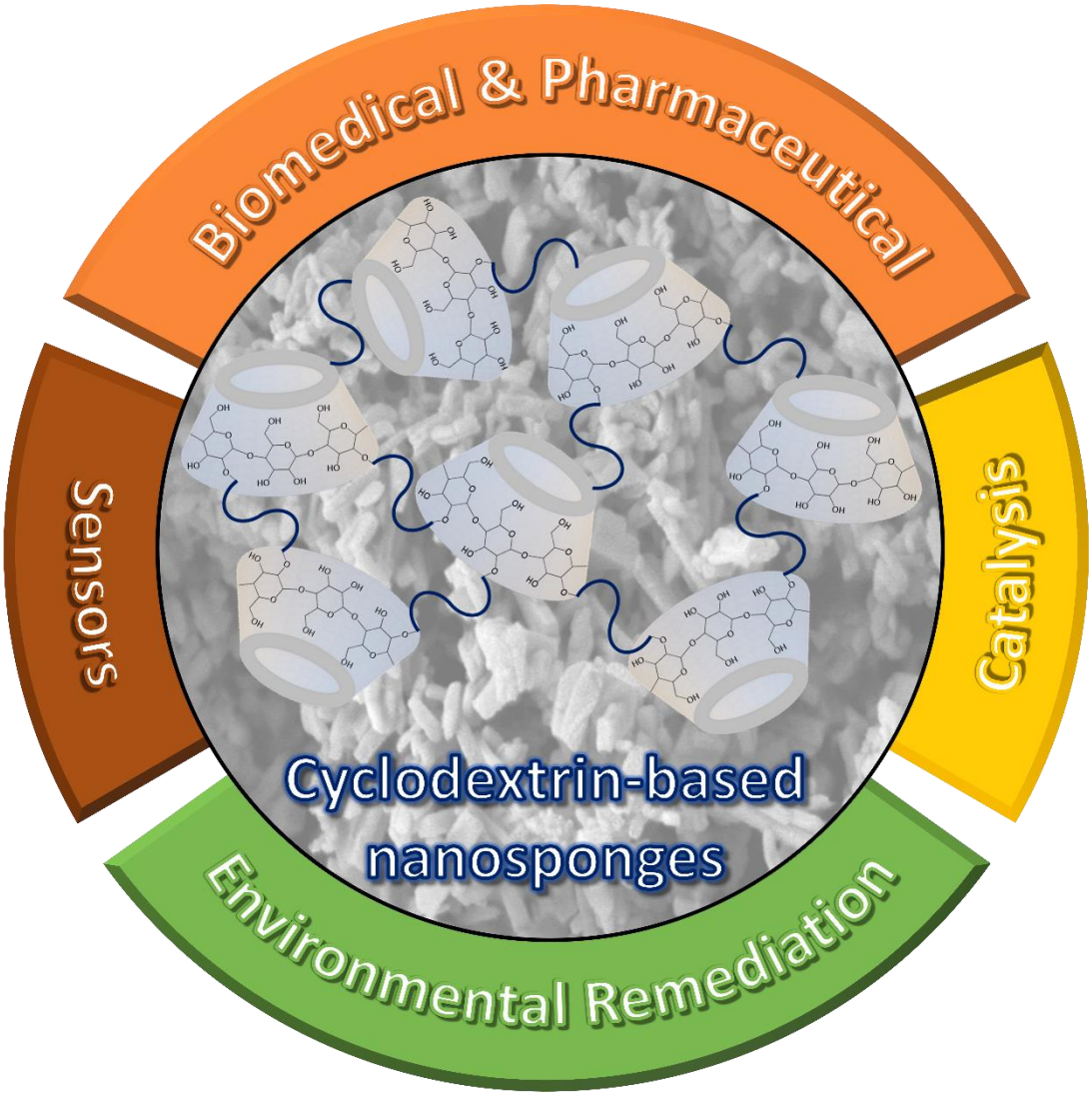

frontiers in Chemistry

REVIEW
published: 24 March 2022
doi: 10.3389/fchem.2022.859406

Cyclodextrin-Based Nanosponges: Overview and Opportunities

*Gianluca Utzeri, Pedro M. C. Matias, Dina Murtinho and Artur J. M. Valente**

CQC, IMS, Department of Chemistry, University of Coimbra, Coimbra, Portugal

Nanosponges are solid cross-linked polymeric nano-sized porous structures. This broad concept involves, among others, metal organic frameworks and hydrogels. The focus of this manuscript is on cyclodextrin-based nanosponges. Cyclodextrins are cyclic oligomers of glucose derived from starch. The combined external hydrophilicity with the internal hydrophobic surface constitute a unique "microenvironment", that confers cyclodextrins the peculiar ability to form inclusion host–guest complexes with many hydrophobic substances. These complexes may impart beneficial modifications of the properties of guest molecules such as solubility enhancement and stabilization of labile guests. These properties complemented with the possibility of using different crosslinkers and high polymeric surface, make these sponges highly suitable for a large range of applications. Despite that, in the last 2 decades, cyclodextrin-based nanosponges have been developed for pharmaceutical and biomedical applications, taking advantage of the nontoxicity of cyclodextrins towards humans. This paper provides a critical and timely compilation of the contributions involving cyclodextrins nanosponges for those areas, but also paves the way for other important applications, including water and soil remediation and catalysis.

Keywords: cyclodextrins, nanosponges, crosslinked polymers, supramolecular interactions, responsive materials, multipurpose structures

OPEN ACCESS

Edited by:
Pellegrino Musto,
National Research Council (CNR), Italy

Reviewed by:
Angela Scala,
University of Messina, Italy
Khaleel Assaf,
Al-Balqa Applied University, Jordan

****Correspondence:***
Artur J. M. Valente
avalente@ci.uc.pt

Specialty section:
This article was submitted to Polymer Chemistry, a section of the journal Frontiers in Chemistry

Received: *21 January 2022*
Accepted: *02 March 2022*
Published: *24 March 2022*

Citation:
Utzeri G, Matias PMC, Murtinho D and Valente AJ (2022) Cyclodextrin-Based Nanosponges: Overview and Opportunities. Front. Chem. 10:859406. doi: 10.3389/fchem.2022.859406

INTRODUCTION

Cyclodextrins (CDs) are amazing molecules because of their peculiar and amphiphilic structure. They are natural oligosaccharides formed by α-(1,4)-linked glucopyranose units where the first three members are formed by 6, 7, or 8 glucopyranose units, labelled as α-, β-, or γ-cyclodextrin, respectively. Since the glucopyranose units are in the chair conformation (Figueiras et al., 2007; Messner et al., 2010), CDs have the form of a truncated cone or torus (Saenger et al., 1998), with a hydrophobic cavity. Due to their Lewis base character, they are able to form host–guest supramolecular structures (Schibilla et al., 2017; Neva et al., 2019; Usacheva et al., 2020; Wang J.-W. et al., 2021), and a hydrophilic outer surface as a consequence of hydroxyl groups positioned at both ends of the cavity (Saenger et al., 1998), allowing the interaction with polar compounds and, concomitantly, making them water soluble. The most varied compounds are those that can establish supramolecular interactions either through the hydrophobic effect or through, e.g., hydrogen bonds. To give some examples we can mention surfactants (Valente and Söderman, 2014; dos Santos Silva Araújo et al., 2021), drugs (Uekama et al., 1998; Rajbanshi et al., 2018; Saokham et al., 2018; Tian et al., 2020), organic pollutants (Cova T. F. G. G. et al., 2018; Filho et al., 2018; Liu Q. et al., 2020), dyes (Bezerra et al., 2020), and metal ions (Buvári and Barcza, 1989; Ribeiro et al., 2006; Prochowicz et al., 2017). The versatility of these oligosaccharides makes their application highly attractive in distinct fields such as pharmaceutical (the main one among them all) (Loftsson and Brewster, 1996; Loftsson

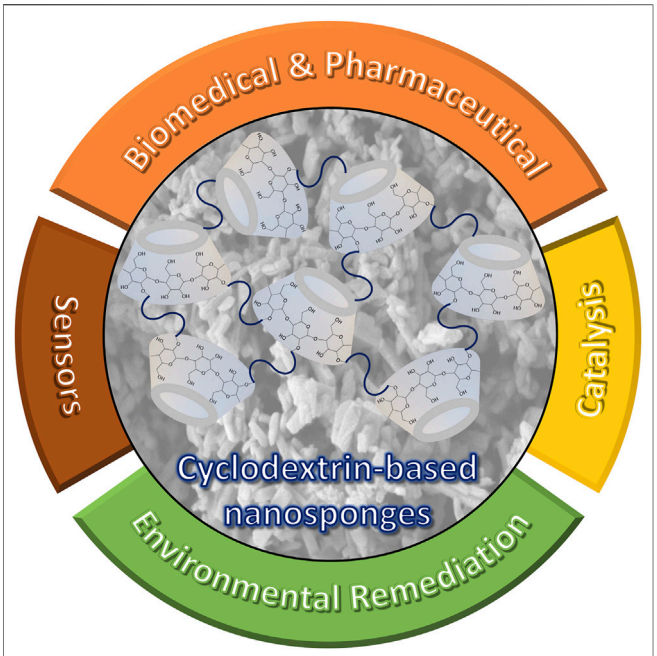

GRAPHICAL ABSTRACT |

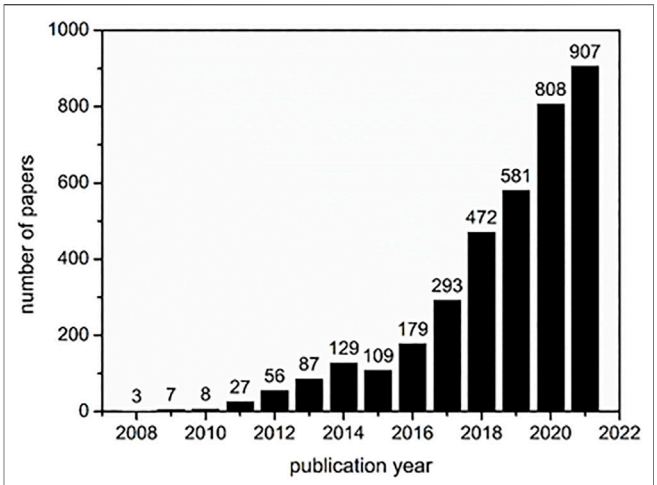

FIGURE 1 | Number of papers that includes the keywords "cyclodextrin" and "nanosponge" cited by the Web of Science till 23.12.2021 (accessed at 12:41 GMT).

and Duchene, 2007), food technology (Matencio et al., 2020c; Gonzalez Pereira et al., 2021), textile (Bezerra et al., 2020), wastewater treatment (Sikder et al., 2019; Chodankar et al., 2021; Cova et al., 2021), detergency (Schlüter et al., 2020) and paper (Aguado et al., 2019).

Cyclodextrins show high reactivity as a consequence of their hydroxyl groups able to suffer substitution or elimination. Due to these properties, cyclodextrins can be directly copolymerized with other monomers or grafted onto organic or inorganic materials (Mocanu et al., 2001; Cova T. F. et al., 2018, 2021; Gómez-Graña et al., 2021; Real et al., 2021) allowing a significant increase in the range of applications for CDs. Due to the high content in hydroxyl groups, cyclodextrins can easily form reticulated structures by co-polymerization with appropriate crosslinkers. Among the most used crosslinkers, epichlorohydrin (EPI) originates a hydrophilic gel with CD monomers connected by repeating glyceryl units. The polymerization with EPI occurs according to a well-known mechanism and the experimental conditions of synthesis are straightforward (Morin-Crini et al., 2018).

In recent decades a new type of crosslinked material, so called nanosponges (NSs) has emerged (Blasco-Tamarit et al., 2018; Trotta and Mele, 2019; Pawar and Shende, 2020a; Krabicová et al., 2020; Larin et al., 2020). Nanosponges can be defined as a hydrophilic, water-insoluble, supramolecular 3D–hyper-reticulated nanoporous structures, showing a high stability over a wide range of temperatures and pH (Sherje et al., 2017). Thus, it is not surprising that cyclodextrins have also been used to synthesize these materials providing cooperative properties between the amphiphilicity and high surface area. However, it should be stressed that the application of cyclodextrin nanosponges (CDNSs) is still at an early stage. As can be seen from **Figure 1**, although the number of publications involving the keywords "cyclodextrin" and "nanosponge" is increasing exponentially, the absolute numbers are relatively low.

A meticulous analysis of data shows that the majority of published studies involving CDNSs is, by far, from the pharmaceutical area (Shrestha and Bhattacharya, 2020). The porosity, together with the amphiphilic properties of the cyclodextrin, permits the loading and solubilization of both hydrophilic and lipophilic molecules, allowing the increase in stability and bioavailability of drugs; on the other hand, the relatively low association constants characterizing the cyclodextrin-guest complexes (Houk et al., 2003; Kumar et al., 2020) [when compared with e.g., cucurbit(*n*)urils (Liu et al., 2005)] can be seen as an opportunity, since it enables not only the encapsulation (binding) but also the release and permeation of active substances (Mane et al., 2021; Pushpalatha et al., 2019). The same properties shown by CDNSs for an efficient drug encapsulation can also be used for the removal of toxic substances from the body, as is suggested in a few publications [e.g., (Varan et al., 2020)]. Other areas with identical relevance for the application of CDNSs are the removal of pollutants from wastewater (Kumari et al., 2020) and drinking water (Mhlanga et al., 2007) and heterogeneous catalysis (Jafari Nasab et al., 2018). Of course, given the versatility of these materials, their application in areas such as flame retardancy (Alongi et al., 2012), electrochemistry (Alidoost et al., 2022) and floriculture (at pre- and postharvest) (Seglie et al., 2012, 2013) can also be found.

All these applications, as highlighted in **Figure 2**, will be discussed in detail in the following sections, along with the different paths and strategies for the synthesis of cyclodextrin-nanosponges. Finally, a critical assessment on the future perspectives for the application of these materials will be proposed.

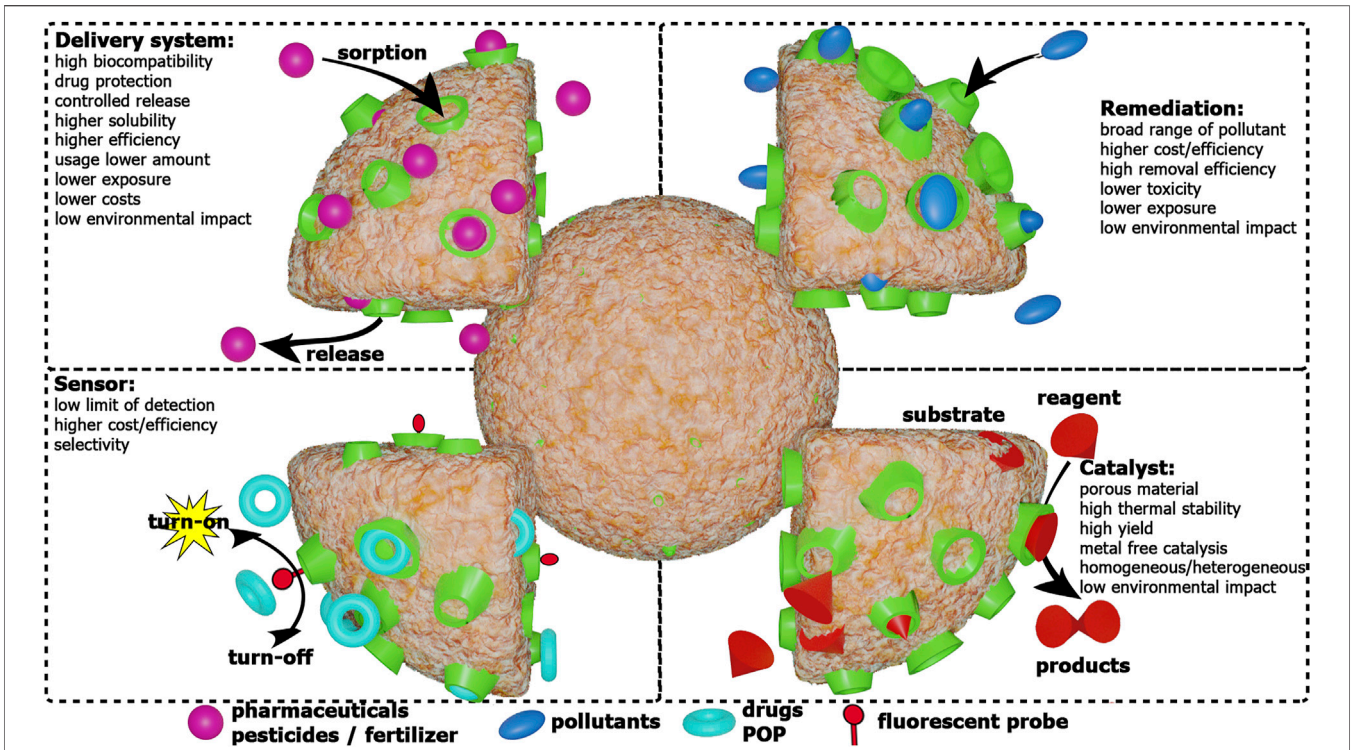

FIGURE 2 | Schematic representation of CDNSs main applications and their advantages.

TABLE 1 | Crosslinking agents used in the preparation of different categories of CDNSs.

CDNSs classes	Crosslinkers
Carbonate	Carbonyls: diphenyl carbonate (DPC); 1,1′-carbonyl diimidazole (CDI); dimethyl carbonate (DMC) and triphosgene
Carbamate	Diisocyanates: 1,6-hexamethylene diisocyanate (HDI); methylene diphenyl diisocyanate (MDI) Appell et al. (2018); toluene 2,4-diisocyanate (TDI) and toluene 2,6-diisocyanate Krabicová et al. (2020)
Ester	Dianhydrides: pyromellitic dianhydride (PMA); ethylenediaminetetraacetic acid dianhydride (EDTA) Ferro et al. (2017); Epiclon-B-4400 Gholibegloo et al. (2019a); dialcohol 2-hydroxyethyl disulfide (2-HEDS) can be use together with PMA to introduce disulfide bonds Trotta et al. (2016b) Carboxylic acids: citric acid (CA) Rubin Pedrazzo et al. (2019) and 2,6-naphthalene dicarboxylic acid (NDCA) Nait Bachir et al. (2019)
Ether	Epoxides: epichlorohydrin; 1,4-butanediol diglycidylether (BDE) Rizzi et al. (2021); E-51 epoxy resin Lai et al. (2012)
Polyamidoamine	2,2′-bis(acrylamido)acetic acid and its polyamidoamine derivates (PAA) formed by reaction with amines (such as 2-methylpiperazine) Swaminathan et al. (2010a)
Polyamine	Polyamines: 1,6-hexanediamine (am_6), 1,8-octanediamine, 1,12-dodecanediamine (am_{12}) Russo et al. (2016); Utzeri et al. (2022)
Other linkers	Dichloromethane Noothi et al. (2020) and *N*,*N*′-methylene bisacrylamide (MBA) Pawar et al. (2019)

CYCLODEXTRIN-BASED NANOSPONGES: SYNTHESIS AND PROPERTIES

As a new family of spongy materials, CDNSs are solid, hyper-reticulated and nanoporous three-dimensional polymeric colloidal biodegradable nanostructures, typically having spherical shape (Cecone et al., 2020; Rizzi et al., 2021; Sadjadi and Koohestani, 2021a; Suvarna et al., 2021). In terms of structural regularity, CDNSs can be amorphous or crystalline frameworks (Singh et al., 2017). They can be directly obtained through the covalent binding between cyclodextrins and a multifunctional reactant (crosslinker)—see **Table 1**, which is possible thanks to the existence of reactive hydroxyl groups spatially located in the hydrophilic outer leaflet of CDs (**Figure 3**) (Morin-Crini et al., 2018; Gupta et al., 2021; Rubin Pedrazzo et al., 2022). Regarding CDs, both natural (αCD, βCD and γ CD) or chemically modified derivatives, such as 2-hydroxypropyl-βCD (Argenziano et al., 2019), sulfobutylether-βCD (Olteanu et al., 2014), carboxymethyl-βCD (Yakavets et al., 2020), tosylated-βCD (Sadjadi et al., 2019a) or halide-βCD (Utzeri et al., 2022) can be used. Nevertheless, βCD forms are preferred in the construction of CDNSs due to their cavity size,

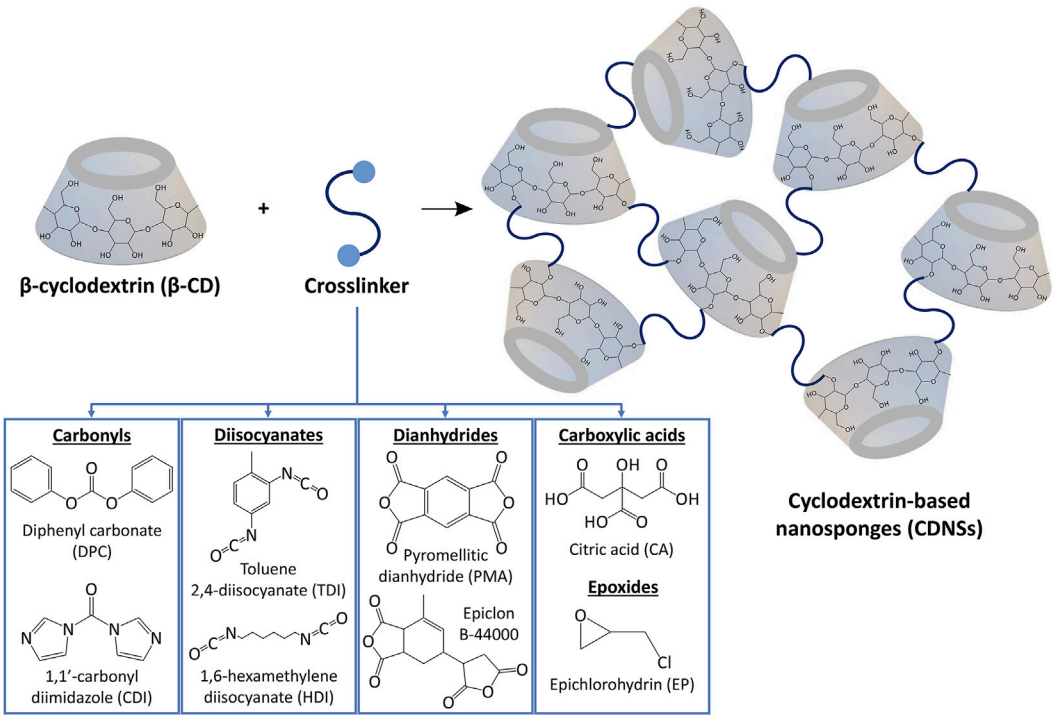

FIGURE 3 | Synthesis of CDNSs through the reaction between β-cyclodextrin and a crosslinker, being carbonyls, diisocyanates, dianhydrides, carboxylic acids and epoxides the most common.

which confers greater stability, complexation ability and a larger number of encapsulation sites, as well as low cost and higher rates of production (Andaç et al., 2021; Guineo-Alvarado et al., 2021).

Synthetic Methods

Different crosslinkers and the crosslinking degree allow the construction of polymeric structures of distinct polarity and dimension, leading to macromolecules (CDNSs) with unique properties (Rubin Pedrazzo et al., 2022). The existence of lipophilic cavities in the building units (CDs) and the hydrophilic network in CDNSs, depending on the crosslinker's nature, make these materials ideal candidates to increase the stability of sensitive and volatile compounds, as well as the solubility of lipophilic or lipophobic analytes (Asela et al., 2021; Guineo-Alvarado et al., 2021; Rezaei et al., 2021). Furthermore, the variety of synthetic methods used for the preparation of CDNSs also leads to polymers with distinct properties:

Hot Melting Procedure

This simple, reproducible, and solvent-free approach is based on the joint fusion of CD and typically a carbonyl linker, being diphenyl carbonate the most used. In general, the homogenization occurs at 90–130°C during at least 5 h, to ensure a complete crosslinking reaction (Sadjadi et al., 2019b; Iriventi et al., 2020). For further crosslinking, the mixture must be incubated for a longer period (Rezaei et al., 2021). At the end of the reaction a fine homogeneous powder is obtained (Jasim et al., 2020; Moin et al., 2020; Sadjadi and Koohestani, 2021a, 2021b; Srivastava et al., 2021). The powdered substance is repeatedly washed with water and/or acetone, and, generally, it is also subjected to Soxhlet extraction with ethanol or acetone, and even to an additional washing with sodium hydroxide (NaOH) solution (Kumar A. and Rao R., 2021; Sadjadi and Koohestani, 2021a, 2021b; Suvarna et al., 2021). Water allows the removal of CD in excess and ethanol/acetone allows the elimination of the unreacted crosslinker and still other impurities such as phenol or imidazole, formed when DPC or CDI linkers are used, respectively. Typically, the phenoxide ion formed from phenol is soluble in water, so the rinse with a base (NaOH) will ensure the total removal of this impurity, which can be observed using a ferric salt (Garrido et al., 2019; Kumar et al., 2021), UV-vis spectroscopy or HPLC (Sadjadi et al., 2018c).

Solvent Condensation Method

This strategy involves dissolving CD and a crosslinker in an appropriate solvent, namely, petroleum-based polar aprotic solvents such as DMF, DMSO, butanone or pyridine (Anandam and Selvamuthukumar, 2014), or green solvents to make the process more sustainable, such as water or aqueous solutions (Swaminathan et al., 2010a; Jafari Nasab et al., 2018) and deep natural eutectic solvents (NADES) (Cecone et al., 2020). If necessary, a catalyst can be added to reduce reaction time (Demasi et al., 2021). Typically, an excess of crosslinking agent is used in CD:crosslinker molar ratios in the range of 1:2 to 1:16

(Jain et al., 2020). In general, after the reaction, the recovery of NSs may involve precipitation using water, acetone (Khajeh Dangolani et al., 2019) or ethyl acetate (Cecone et al., 2018, 2019; Matencio et al., 2020b) among other possible solvents (Ferro et al., 2014; Appell et al., 2018; Garrido et al., 2019; Lo Meo et al., 2020; Pawar and Shende, 2021).

In the case of using dianhydride linkers alone or with 2-hydroxyethyl disulphide (Daga et al., 2016), the addition of triethylamine (Et_3N) as basic catalyst is required, and the exothermic reaction occurs quickly at room temperature (Nazerdeylami et al., 2021; Suvarna et al., 2021; Yazdani et al., 2021). Using other linkers, such as HDI (Yazdani et al., 2021), MDI (Khajeh Dangolani et al., 2019), DMC and DPC (Singh et al., 2018), Et_3N can also be introduced to increase the rate of the reaction, with or without an increase in temperature. Furthermore, the use of another base, 1,4-diazabicyclo(2,2,2) octane (DABCO), was reported to catalyse the reaction involving BDE as crosslinker in aqueous NaOH solution at 90°C or to catalyse the process using HDI and βCD at r. t. (Ramírez-Ambrosi et al., 2014). Basic conditions (NaOH) are also required for the reticulation of CD with EPI (Olteanu et al., 2014; Jafari Nasab et al., 2018; Liu X. et al., 2020). Other bases such as ammonia, pyridine and collidine can be used as catalysts as well (Trotta, 2011). According to the literature, when CA is chosen as linker, the reaction takes place under vacuum in water and at a temperature equal to or above its normal boiling point (Varan et al., 2020; Rubin Pedrazzo et al., 2022) or in NADES, such as a choline chloride/CA mixture, which acts both as solvent and co-reactant (Cecone et al., 2020). Sometimes, the addition of sodium hypophosphite monohydrate as catalyst is also required with this linker. Another example of this method involves the reaction between βCD and NDCA crosslinker, in aqueous media and using sulfuric acid as catalyst, to obtain the corresponding CDNSs after 2 days at 100°C (Nait Bachir et al., 2019).

Interfacial Condensation Method

This method involves the complete dissolution of the CD in an alkaline aqueous phase, pH > 10, and the crosslinking agent in an organic one (methylene chloride, butanone or chloroform) (Shende P. et al., 2015; Desai and Shende, 2021).

Emulsion Solvent Diffusion Method

Based on the phenomenon of emulsification, this process consists of two immiscible phases: one internal and one external. The internal phase is formed when the crosslinker is added dropwise, under constant magnetic stirring, to a solution containing CD and an inclusion analyte in a polar aprotic solvent (usually DMF). The external phase is an aqueous solution to which the internal phase is then added drop by drop, under vigorous stirring, at room temperature. The suspension obtained is lyophilized and the CDNSs are subsequently dried (Gangadharappa et al., 2017).

Ultrasound-Assisted Synthesis

Through the application of ultrasonic vibration, it is possible to promote crosslinking of CD with an appropriate linker, in a certain molar ratio, and in the absence of solvents, thus constituting an environmentally friendly process. Spherical uniform size particles are formed (Ciesielska et al., 2020; Jain et al., 2020; Omar et al., 2020). The sonication is useful either for the melting or for the solvent condensation method (Swaminathan et al., 2013).

Microwave-Assisted Synthesis

Conventional and ultrasound heating methods lead to non-uniform transformations due to the occurrence of thermal gradients and, consequently, to longer reaction times and scalability problems. As such, the promotion of reactions by microwave irradiation makes them four times faster than the melting approach (Andaç et al., 2021), and more reproducible and scalable due to uniform and controlled heating provided by microwave irradiation. Thus, using microwave synthesis, it is possible to obtain highly crystalline CDNSs with a narrow particle size distribution (Ciesielska et al., 2020) by reacting CD with an appropriate crosslinker (mostly DPC), using polar aprotic solvents such as DMF (Anandam and Selvamuthukumar, 2014; Zainuddin et al., 2017; Sharma et al., 2021). As the solvent condensation synthesis can be performed using microwave irradiation, Vasconcelos et al. (Vasconcelos et al., 2016) reported the use of tin octanoate catalyst to promote the reaction between βCD and HDI crosslinker using DMF as solvent in a microwave system at 80°C for 30 min.

Mechanochemical Synthesis

CD-crosslinker reaction can also be induced by mechanochemistry (Jicsinszky and Cravotto, 2021), the direct absorption of mechanical energy, capable of activating chemical bonds. Usually, this type of activation occurs between solids or solidified reactants in ball mills, in the absence of solvents or minimizing their use as much as possible, contrary to what happens conventionally, whereby a large quantity of solvents, mostly derived from fossil fuels, are used. So, mechanosynthesis is a more sustainable method, where mass transport and energy dispersion are guaranteed through efficient grinding in the solid state. Although solvents such as acetone and ethanol continue to be used in CDNSs' purification, they are relatively volatile, in contrast with high boiling point polar aprotic solvents (DMSO or DMF), that have complex recycling processes. The use of ball mills has disadvantages such as difficult scalability, the impossibility of precise temperature control (although it does not exceed 72°C in CDNSs' synthesis), and the use of closed containers that increase the polycondensation reaction time due to the impossibility of water removal during these batch processes. These drawbacks can be overcome by using twin-screw extruder reactors, which allow not only a tight temperature control but also makes processes more scalable by transitioning from a batch approach to a continuous process. In general, mechanosynthesis is a simple, economical, and faster strategy for obtaining CDNSs. Two examples are: 1) the use of ball mills to obtain CDNSs using CDI as cross-linker in 3 h; and 2) the use of said extruder for the preparation of CDNSs using βCD, CA crosslinker, and

TABLE 2 | Comparative properties of different types of CDNSs.

Nanosponge		Method	Structure	Mean size/nm	PDI	ζ-Potential/mV	S_{BET}/m^2 g^{-1}	Pore diameter/nm	Pore volume/cm^3g^{-1}
βCD:DPC Kumar et al. (2021); Liu et al. (2020b); Sharma et al. (2021); Sadjadi et al. (2018a); Sadjadi et al. (2017b); Rao et al. (2013)		Melt	C/A	<664	<0.45	− (3–22)	9.7 (1:2)	~ 11.1 (1:2)	~ 0.03 (1:2)
βCD:DPC Shringirishi et al. (2017); Pushpalatha et al. (2018b); Singireddy et al. (2016); Liu et al. (2020b); Gupta et al. (2021)		Solvent	A	135–500	<0.43	± (12–35)	2.2 (1:2)	13.3 (1:2)	0.0075 (1:2)
βCD:DPC 1:4 Guineo-Alvarado et al. (2021); Singireddy et al. (2016)		MW	C	153 ± 8	0.11 ± 0.01	28 ± 2	<2.0	—	—
βCD:CDI 1:4 Rao et al. (2018); Sabzi and Kiasat (2018); Kardooni et al. (2020); Desai and Shende (2021)		Solvent	A	473 ± 1	0.24 ± 0.06	−(39 ± 1)	10.9	4.86	0.013
		Interfacial	—	173 ± 1	0.22 ± 0.03	−(33 ± 1)	—	—	—
CD:HDI Salgın et al. (2017); Mhlanga et al. (2007)		Solvent	A	420×10^3	—	—	1.7–3.5	—	0.01
CD:TDI Mhlanga et al. (2007); Deshmukh and Shende (2018); Varan et al. (2020)		Solvent	A	367 ± 2	0.25 ± 0.02	−(26 ± 2)	1.7–3.5	—	0.01
αCD:MDI 1:10 Khajeh Dangolani et al. (2019)		Solvent	A	100–200	—	—	11.9	35.9	0.11
βCD:PMA Gabr et al. (2018); Rao et al. (2018); Pushpalatha et al. (2018b)	1:4	Solvent	A	605 ± 18	0.31 ± 0.03	−(61 ± 2)	1.21	120.3	0.04
	1:6			264 ± 16	0.26 ± 0.01	−(60 ± 2)	0.573	484.8	0.07
	1:8			477 ± 23	0.72 ± 0.06	−(60 ± 3)	0.393	299.9	0.03
GSH-NS: βCD:PMA/2-HEDS Palminteri et al. (2021); Daga et al. (2020)		Solvent	A	203 ± 14	0.20 ± 0.01	−(32 ± 3)	—	—	—
βCD: Epiclon Gholibegloo et al. (2019b)	1:2	Solvent	A	300 ± 10	0.27	−(24 ± 2)	0.4	105	-
	1:4			206 ± 9	0.20	−(27 ± 2)	6.0	22	
	1:8			140 ± 6	0.19	−(37 ± 2)	9.3	16	
βCD:CA Cecone et al. (2020)		NADES	A	<20×10^3	—	5–18	9.0	—	—
βCD:CA 1:8 Rubin Pedrazzo et al. (2022)		Solvent	—	800	—	−(29 ± 11)	1.30	—	—
		Extrusion	—		—	−(26 ± 7)	0.93	—	—
βCD:EPI Jafari Nasab et al. (2018); Liu et al. (2020b)		Solvent	A	167 ± 8 (1:8)	0.58 (1:8)	−(37 ± 2) (1:8)	10.9 (1:10)	4.86 (1:10)	0.014 (1:10)
CD:am_6 Utzeri et al. (2022); Russo et al. (2016)		Solvent	A	446 ± 30	0.38 ± 0.05	41 ± 6	21.8	24.3	0.13
CD:am_{12} Utzeri et al. (2022); Russo et al. (2016)		Solvent	A	438 ± 38	0.43 ± 0.03	54 ± 7	17.9	7.5	0.03
PAA:NS Swaminathan et al. (2010a)		Solvent	—	410–502	0.10–0.12	−(32–35)	—	—	—
βCD:acrylic acid Khalid et al. (2021)		Chain-growth	A	275 ± 29	0.28	−(41 ± 5)	—	—	—

A: amorphous; C: crystalline.

sodium hypophosphite monohydrate as catalyst. In the latter case, the equipment is preheated to a temperature between 120 and 180°C and the solid blend is slowly inserted into it and the process lasts between 5 and 25 min, contrary to the conventional approach that takes place in vacuum for at least 4 h, using water as solvent (Rubin Pedrazzo et al., 2020, 2022; Trotta and Pedrazzo, 2020).

Chain-Growth Polycondensation Method

The conventional step growth procedures are based on a polycondensation reaction in which monomers react with each other and, subsequently, a new monomer reacts with the polymer under construction, presenting both functional groups with identical reactivity. However, it is possible to evolve to a chain-growth polycondensation method, in the case of the reactive group at the polymer chain's end, formed by reaction with the monomer, is stable and more reactive than the monomer itself (Yokozawa and Ohta, 2016). Thus, an initiator can be used to promote polymer growth by creating points of high reactivity at its tip, so that the binding of a new monomer readily occurs, and so on, in these reactive ends, allowing the increase of the chain. CDNSs with reduced polydispersity are obtained, as the monomers do not interact with each other, but selectively connect with the reactive terminals. A chain-growth approach reported by Khalid et *al.* (Khalid et al., 2021) is based on the use of βCD together with acrylic acid monomer in the presence of ammonium persulfate as initiator and MBA as crosslinking agent.

Properties

CDNSs are colloidal systems with an average diameter size generally below 1 μm and with a narrow size distribution, denoted by a polydispersity index (PDI) less than 0.7, which is

typical of monodispersed particles (Kumar et al., 2021). Their high ζ-potential (±30 mV), mostly showing a negatively charged surface, means that the particles easily disperse in water to form stable suspensions, whereby they tend to repel electrostatically, not acting as surfactants, as they do not aggregate (Trotta et al., 2012; Suvarna et al., 2021). However, NSs can swell upon water absorption appearing to have a gel structure, as hydrogels. Thus, although swelling is not directly related to uptake capacity in CDNSs, PMA and CA CDNSs have a greater degree of swelling at small quantities of crosslinker compared to carbonate and carbamate ones, decreasing with the increase of crosslinker:CD ratio, because of strong crosslinking formation and loss of structural elasticity (Trotta, 2011; Hoti et al., 2021; Rubin Pedrazzo et al., 2022). Polyamidoamine CDNSs also have a huge swelling in aqueous media and they bear both acidic and basic groups (Swaminathan et al., 2010a). In addition to crosslinking, there may also be some branching with PMA and CA linkers, culminating in the formation of carboxylic acid groups, which can cause ζ-potential oscillations, as they are pH-sensitive, giving them the possibility to host cations and organic molecules simultaneously (Varan et al., 2020). The use of EPI linker leads to more hydrophilic NSs than those obtained with carbonyl, dianhydride or diisocyanate linkers.

Characteristics of nanosponges' dimension, surface area (S_{BET}), porous network, charge, and ζ-potential are determinant factors for the interaction with an analyte. These properties (in **Table 2**) are greatly affected by CDNS structure, which depends on the linker and CD form chosen, CD:crosslinker proportion, solvent, catalyst and synthetic conditions. All parameters play an important role on the properties of CDNSs in terms of loading capacity and efficiency (in general, higher in crystalline CDNSs and in native CDs) (Osmani et al., 2018; Sharma et al., 2021), release profile and solubility, being cross-linked cyclodextrin polymers often insoluble in water and organic solvents (Sherje et al., 2017; Venuti et al., 2017).

The amount of crosslinker influences the surface area and porosity. Normally, with the increase in its proportion in relation to CD, the smaller the pore diameter will be, and a higher degree of crosslinking will lead to a greater S_{BET} value, which can create a superior polymeric interconnection forming a material with greater porosity. This situation is denoted in βCD:Epiclon NSs (**Table 2**), in which the degree of crosslinking increases from 61 to 94% with the increase of crosslinker amount (from 1:2 to 1:8 M ratios) (Gholibegloo et al., 2019b).

The NSs are thermally stable structures up to 300°C and resistant to organic solvents, and their formation can be screened by infrared spectroscopy, through bands that do not exist in the original CDs. For example, carbonate CDNSs present C=O elongation of the carbonate linkage (Darandale and Vavia, 2013) (Singireddy et al., 2016) at 1720–1780 cm^{-1}; carbamate CDNSs show characteristic peaks at 1700, 1630 (due to amide-I-like carbonyl stretching) and 1550 cm^{-1} (assignable to amide-II-like N–H bending) (Lo Meo et al., 2020), and the absence of the N=C=O vibration band at 2270 cm^{-1} (Leudjo Taka et al., 2020); ester CDNSs have a band at 1720–1735 cm^{-1} corresponding to the C=O ester bonds (Gholibegloo et al., 2019a; Varan et al., 2020).

As tiny mesh-like structures, CDNSs may encapsulate many molecules, making them useful in solubility, cytotoxicity and bioavailability enhancement, drug delivery, protection and transport of unstable molecules, catalysis, environmental remediation, chemical and biological sensing (important in diseases diagnosis), gas carrying and in release of enzymes, proteins, vaccines, and antibodies, as a form of treatment. Their safe, biodegradable, non-toxic and biocompatible nature make them promising materials for the aforementioned applications.

Compared with activated carbon (with S_{BET} = 600–700 $m^2 g^{-1}$), CDNSs have lower surface area but similar interaction capacities for lipophilic molecules, which means that these guests are both adsorbed on the surface and carried into the bulk of the NSs during inclusion complex formation or internal diffusion, leading to higher apparent stability constants compared to those using free CDs (non-bond) ($\leq 10^4 M^{-1}$), which do not have the ability of host hydrophilic or high molar mass analytes. Despite the formation of inclusion compounds being highly favoured in water, it is reversible in organic solvents (such as ethanol), which makes CDNSs' full recover and reuse easy, without requiring hazardous burning techniques for partial regeneration, as is the case with activated carbon (Trotta, 2011).

APPLICATIONS

Pharmaceutical and Biomedical Applications

Cyclodextrin-based nanosponges have shown a great potential for applicability in pharmaceuticals and have been widely explored for this purpose in the last decade. (Caldera et al., 2017; Sherje et al., 2017; Krabicová et al., 2020). One of the most relevant applications is in drug delivery, highlighting in this field the use of CDNSs for cancer therapy (Subramanian et al., 2012; Trotta et al., 2012, 2014; Lakkakula and Krause, 2013; Swaminathan et al., 2016; Venuti et al., 2017; Lembo et al., 2018; Osmani et al., 2018; Allahyari et al., 2019; Kumar and Rao, 2019; Menezes et al., 2019). This topic has been the subject of numerous review articles and book chapters, some of which are quite recent (Ciesielska et al., 2020; Jain et al., 2020; Tannous et al., 2020, 2021; Andaç et al., 2021; Babadi et al., 2021).

Although a vast array of drugs is currently available for a variety of pathologies, some of them exhibit bioavailability problems that limit their therapeutic potential. Factors such as reduced solubility, low permeability, reduced lifetime and low stability of some drugs, make their formulation a challenging task (Swaminathan et al., 2016; Babadi et al., 2021). CDNSs, as a result of their spongy structure, have the ability to form inclusion and non-inclusion complexes with different drugs, and thus constitute an effective therapeutic vehicle for the delivery of drugs with low bioavailability. The cavity of the CDs allows the inclusion of hydrophobic molecules and the more hydrophilic outer polymeric network is able to accommodate less lipophilic molecules. Furthermore, CDNSs combine high biocompatibility, biodegradability and low cytotoxicity, conferred by the cyclodextrins, with high thermal stability and

insolubility that arises from the fact that they are highly crosslinked polymers (Tejashri et al., 2013; Shende P. et al., 2015; Krabicová et al., 2020; Deng et al., 2021; Mashaqbeh et al., 2021). Thus, it is not surprising that this type of nanomaterials has been explored for the oral, topical and parenteral delivery of numerous drugs, in controlled drug delivery systems as, for example, for target cancer therapy (Allahyari et al., 2022). It is worth noticing that the same ability and selectivity of CD towards drug encapsulation and delivery can be used for drug scavengers. In fact, the use of βCD-NS as reactive oxygen species scanvanger has been reported by Kumar and Rao (2022).

Caldera et al. (Caldera et al., 2017) categorized CDNSs into four generations, according to their chemical composition and properties, which also represent the evolution of these systems in pharmaceutical applications. First generation CDNSs are synthesized by reacting CDs with a crosslinking agent (diisocyanate, active carbonyl compounds, anhydrides, polyacids or epoxides), leading to the formation of NSs containing urethane, carbonate, ester and ether functionalities. Among these, CD-based NSs containing carbonate and ester functionalities are the most used in pharmaceutical applications. This type of nanomaterials has been used in the oral delivery of drugs with low solubility and/or high degradability, such as ferulic (antioxidant, anticancer) (Rezaei et al., 2019) and kynurenic acids (antioxidant, neuroprotector) (Dhakar et al., 2019) paliperidone (antipsychotic) (Sherje et al., 2019), tamoxifen (anticancer) (Torne et al., 2013), paclitaxel (anticancer) (Torne et al., 2010; Ansari et al., 2011a; Mognetti et al., 2012), rosuvastatin (antipsychotic) (Gabr et al., 2018), repaglinide (antidiabetic) (Olteanu et al., 2014), rilpivirine (antiretroviral) (Rao et al., 2018), norfloxacin (antibiotic) (Mendes et al., 2018), erlotinib (anticancer) (Dora et al., 2016), resveratrol (anti-inflammatory, antioxidant, anticancer) (Ansari et al., 2011b; Pushpalatha et al., 2018a) curcumin (anti-inflammatory, antioxidant, anticancer) (Pushpalatha et al., 2018b; Möller et al., 2021) camptothecin (antitumor) (Swaminathan et al., 2010b; Minelli et al., 2012; Gigliotti et al., 2016, 2017) and dithranol (drug for psoriasis) (Kumar S. and Rao R., 2021), among others.

The experimental results obtained show that the solubility/degradability of drugs is improved when they are incorporated into NSs, thus increasing their bioavailability. In the case of drugs used in the cancer treatment, there is generally a reduction in side effects and toxicity of these drugs and greater tumor inhibition, when compared to the free drug (Trotta et al., 2012, 2014).

Recently, Pivato et al. have reported the synthesis of a βCDNS hydrogel using pyromellitic dianhydride as crosslinker. The loading and release of piroxicam showed that a two-step release kinetics is occurring: at short-range times the kinetics is characterized by a pseudo-Fickian mechanism, whilst for long times the release is dominated by the drug previously encapsulated in the CD cavities. This 3D material will offer a sustained release of drug over 75 h (Pivato et al., 2021).

The interaction of CDNSs with drugs and the stability of formulations is usually confirmed using various analytical techniques, including zeta potential, FTIR, DSC, and XRD. The determination of zeta potentials allows to validate the stability of the prepared formulations. The interaction of drugs with NSs can be confirmed using FTIR, by the presence of characteristic drug peaks in loaded NSs and by the shift observed in those peaks when the drug is incorporated into NSs. DSC thermograms often show a reduction/suppression or shift in drug crystalline peaks after encapsulation due to the formation of inclusion complexes. XRD studies show that, in general, crystalline drugs adopt an amorphous form when complexation with the NSs occurs (Shende P. K. et al., 2015; Pushpalatha et al., 2018a; Allahyari et al., 2020, 2021; Pawar and Shende, 2021; Suvarna et al., 2021).

One of the major problems concerning conventional drug delivery is that the concentration of drug in the bloodstream reaches a maximum, followed by a sharp decrease. Thus, the concentration of the drug in the body is not stable, which reduces its effectiveness. The use of controlled release systems makes it possible to maintain more stable drug levels, reducing the frequency of doses and the side effects that result from dose peaks. NSs have shown to be promising materials in this field (Subramanian et al., 2012; Menezes et al., 2019). In particular, CDNSs have been used for the controlled release of some drugs, including meloxicam (anti-inflammatory) (Shende P. K. et al., 2015), nifedipine (antihypertensive) (Shringirishi et al., 2017), telmisartan (antihypertensive) (Rao et al., 2013) and curcumin (Darandale and Vavia, 2013; Gholibegloo et al., 2019b; Rafati et al., 2019).

Other relevant applications in pharmaceuticals include the dermal transport of active principles, such as diclofenac (anti-inflammatory) (Conte et al., 2014), imiquimod (antitumor) (Argenziano et al., 2020a) or curcumin and resveratrol (Pushpalatha et al., 2019), the encapsulation of essential oils which exhibit antioxidant and antimicrobial activity (Nait Bachir et al., 2019; Silva et al., 2019; Simionato et al., 2019), and oxygen delivery (Coviello et al., 2017). **Table 3** summarizes recent examples of the use of first generation CDNSs in pharmaceutical applications.

In second generation of CDNSs other functional groups, in addition to those already existing in the CDs or in the crosslinker, are introduced through functionalization before, after or concomitantly with the crosslinking. This functionalization allows to modulate the polarity or charge of the NSs, according to the characteristics of the drugs to be encapsulated, or the coupling of fluorescent compounds, which can be useful for diagnosis and cancer therapy (Trotta, 2011; Mognetti et al., 2012; Caldera et al., 2017). For example, the use of negatively charged NSs, obtained by reacting βCD with succinic anhydride and functionalized with fluorescein isothiocyanate, were used for acyclovir delivery. *In vitro* studies showed prolonged drug release kinetics and increased antiviral activity. The coupling of fluorescein allowed to observe the internalization of CDNSs in cells (Lembo et al., 2013). CDNSs prepared by condensation of βCD with 1–(3–dimethylaminopropyl)–3–ethylcarbodiimide hydrochloride (AMD) and modified with fluorescent compounds (carbon quantum dots) (Pei et al., 2018) and CDNSs (obtained using βCD and Epiclon B-4400 as crosslinker) anchored on magnetite

TABLE 3 | Some recent examples (2020–2021) of first generation CDNSs applications in pharmaceuticals.

Nanosponge	Drug	Application	Main results
α-, βCD:CDI Matencio et al. (2020a)	Oxyresveratrol	Anticancer drug delivery	Strong cell viability inhibition for HT-29 and HCT-116 cancer cell lines
βCD:PMA; βCD:DPC Suvarna et al. (2021)	Irbesartan	Solubility enhancement	PMA crosslinker enhanced the drug solubility (81.86 folds) and drug release to a greater extent than DPC crosslinker; encapsulation efficiency up to 38%
βCD:PMA Appleton et al. (2020)	Insulin	Protein delivery	Loading capability 14%; encapsulation efficiency >90%; *In vitro* release of insulin negligible at a gastric pH (<2%) and sustained at intestinal pH
HPβCD + βCD:CDI Pawar and Shende (2020b)	Artemether Lumefantrine	Drug delivery	Entrapment efficiencies of 70.6% for artemether and 88.3% for lumefantrine; *In-vitro* release study showed controlled-release of actives up to 24 h; *In vitro* antimalarial study showed significant action towards RKL-9 strains in comparison to MRC-2 strains
βCD:DPC Kumar et al. (2021)	Clobetasol propionate	Topical delivery	Drug release 86.25%; Appreciable anti-psoriatic activity and alleviated severity of side effects
βCD:DPC Gupta et al. (2021)	Sesamol	Photostability enhancement	Encapsulation efficiency 90.66%; Enhancement of stability, while retaining antioxidant and anti-tyrosinase potential
βCD:DPC Amin et al. (2020)	Febuxostat	Oral bioavailability enhancement	≥30% release at first hour followed by controlled release (≥75%) at 6 h
βCD:DMC Moin et al. (2020)	Paracetamol + aceclofenac + caffeine	Solubility/combination therapy enhancement	*In vitro* studies indicate rapid dissolution compared to pure drugs; Formulation stable up to 45 days
βCD:CDI Srivastava et al. (2021)	Econazole nitrate	Topical delivery	Entrapment efficiency 70.13%; nanogel was able to impede the fungal growth both *in vitro* and *in vivo*
βCD:CDI Yaşayan et al. (2020)	Sulfamethoxazole	Solubility enhancement	Improved solubility up to 30-fold
βCD:PMA Clemente et al. (2020)	ICOS-Fc	Cancer therapy	*In vivo* experiments showed that treatment of C57BL6/J mice with ICOS-Fc[a] loaded in CDNPs inhibits the growth of subcutaneous B16-F10 tumors
βCD:CDI Allahyari et al. (2021)	flutamide	Anticancer drug delivery	Increased dissolution rate, sustained release and considerable uptake into PC3 cell line was observed
βCD:CDI Allahyari et al. (2020)	Bortezomib	Anticancer drug delivery	Uptake of 93.9% in 3 h against MCF-7 cell line; Higher IC_{50} in comparison with the plain drug
βCD:PMA Argenziano et al. (2020b)	Doxorubicin	Cancer therapy	Higher accumulation in the tumor and neoplastic cells; Reduced cardiotoxicity
βCD:DPC Rezaei et al. (2021)	Thyme essential oil	Solubility and volatility reduction enhancement	Increased antibacterial activity; Aqueous solubility enhanced 15-folds; Minimum inhibitory concentration decreased up to 29.4 fold after encapsulation
βCD:DPC Salehi et al. (2021)	Limonene essential oil	Solubility and volatility reduction enhancement	Enhanced solubility and thermal stability; Higher antibacterial activity; Minimum inhibitory decreased after encapsulation
βCD:DMC Iriventi et al. (2020)	curcumin + caffeine	Topical delivery	69.72% *in vitro* drug release; Promising anti-psoriatic activity

[a]*ICOS-Fc: soluble recombinant form of inducible T-cell costimulatory.*

nanoparticles and modified with folic acid (Gholibegloo et al., 2019a) have also been described and used in tumor theranostics, with good results. Another paper refers the use of CDNSs modified with carboxylate groups and impregnated with lysozyme with the aim of being used as antibacterial agents (Deshmukh et al., 2016).

Recent examples of the application of second generation CDNSs in pharmaceuticals include the use of CDNSs, functionalized with cholesterol hydrogen succinate (CHS), as site-specific drug delivery carriers. Doxorubicin was used as model drug and it was observed that modification with CHS increased drug absorption and improved the uptake into the cells (Singh et al., 2018). Another recent study showed that the use of CDNSs functionalized with gold NPs constitutes an efficient drug transport system, with high loading capacities for phenylethylamine and 2-amino-4-(4-chlorophenyl)-thiazole (90 and 150%, respectively), eight times higher than those obtained with native βCD (Asela et al., 2021).

The third generation CDNSs can be categorized as responsive nanomaterials, whose behavior depends on external stimuli such as variations in pH, temperature, light, redox potential or electromagnetic field. (Caldera et al., 2017). NSs of this type can be very useful for controlled drug release induced by a specific stimulus (Krabicová et al., 2020). For example, glutathione-responsive nanosponges were developed by Trota *et al.* (Trotta et al., 2016b; Daga et al., 2016) and prepared by reaction of βCD with 2-HEDS and PMA. The NSs were loaded with a model anticancer drug, doxorubicin, and drug release was observed to be dependent on the glutathione content present in the tumor cells. This same system was also used for the delivery of erlotinib hydrochloride and resveratrol, two drugs used in cancer therapy (Momin et al., 2018; Palminteri et al., 2021), and their *in vitro* biological effects in HCT116, HT–29, DU145, and PC-3 cancer cell lines was also assessed (Argenziano et al., 2020a). Following a similar approach a dual glutathione/pH dual responsive CDNS was reported (Dai et al., 2021). Another type of pH-responsive NS was obtained by co-polymerization between CD and calixarene derivatives, covalently linked by triazole units (CyCaNSs). CyCaNSs are useful in environmental remediation (Cataldo et al., 2021) and in drug delivery, as the triazole acts actively

TABLE 4 | Recap of the main results of heavy metals removal by different nanosponge formulations.

Nanosponge	Pore size/ (nm)	Surface area/(m^2 g^{-1})	Heavy metal/q_m (mg g^{-1})/RE%	q_m/ (mg g^{-1})	Removal efficiency (RE%)	References
βCD:CA (1:8)[a]	n.a	n.a	n.a./20–70 (high conc.); 80 (Cu(II), Zn(II) at low conc.); 80, 60 (Cu(II), Zn(II) in artificial sea water)	n.a	20–70 (high conc.); 80 (Cu(II), Zn(II) at low conc.); 80, 60 (Cu(II), Zn(II) in artificial sea water)	Rubin Pedrazzo et al. (2019)
βCD:EPI (1:6)	n.a	n.a	Cu(II)/23/≥ 90 in water; Cd(II)/43/≥ 90 in water			Zhao et al. (2015)
βCD:EDTA (1:17)	n.a	n.a	Cu(II)/79/95 in a model textile effluent Cd(II)/124/95 in a model textile effluent			
βCD:PMA (1:8)	n.a	n.a	n.a./20–70 (high conc.); 80 (Cu(II), Zn(II) at low conc.); 80, 60 (Cu(II), Zn(II) in artificial sea water)	n.a	20–70 (high conc.); 80 (Cu(II), Zn(II) at low conc.); 80, 60 (Cu(II), Zn(II) in artificial sea water)	Rubin Pedrazzo et al. (2019)
β-MCD:VI (1:100)	0.02	27.5	Pb(II)/18/n.a Cu(II)/55/n.a Cd(II)/65/n.a Zn(II)/50/n.a Ni(II)/25/n.a Co(II)/20/n.a			Qin et al. (2019)
βCD:TFP (1:3)	3	271	Pb(II)/196/70 Cu(II)/164/77 Cd(II)/136/83			He et al. (2017)
βCD:TDI (1:10)	1.6	2.4	As(V)/n.a./≈10			Raoov et al. (2014)
βBZMCD:TDI (1:10)	77.6	1.3	As(V)/n.a./≈95			
βCD:TPC:TA (1:4)	<10	2.3	Pb(II)/136/≈90			Yang et al. (2022)

[a]*Molar ratio values in mol/mol.*

as antibacterial, antifungal, antitumor and cytotoxic agent (Lo Meo et al., 2014; Pawar et al., 2019).

CDNSs prepared by molecular imprinting techniques allow the preparation of materials that exhibit high selectivity for specific molecules, being considered the fourth generation of NSs (Caldera et al., 2017; Ciesielska et al., 2020; Jain et al., 2020; Krabicová et al., 2020). Work by Trotta *et al.* reports the preparation of MIP-CDNSs by reacting βCD with CDI, in the presence of the template, L-Dopa, a prodrug used in the treatment of Parkinson's disease. The release of L-Dopa using the synthesized MIP-CDNSs was studied and the results obtained showed good encapsulation efficiencies and a slow and prolonged release of the drug, as a result of the strong interactions established between the drug, the polymeric network of NS and the cavity of the CD (Trotta et al., 2016a).

Beside pharmaceutical applications, cyclodextrin–based nanosponges have found a growing interest for application in the biomedical field. In this context, βCD–based materials prepared using PMA as crosslinker seems to be the most applied. For example, βCD:PMA at molar ratio 1:12 found application in health promoting and anti–aging studies by release of oxyresveratrol (OXY), a compound with antioxidant activity. The study showed an increase of 9.6% in life expectancy *in vitro* using *Caenorhabditis elegans* as animal model (Matencio et al., 2020b). A different biomedical application of βCD:PMA microparticles is as probe for glucose estimation via molecular and non–molecular imprinting. The molecular imprinting βCD:PMA, synthesized by reacting βCD with PMA and using glucose as the template, present a porous structure and a surface area ranging from 70 to 52 m^2 g^{-1} and shows an extremely high glucose binding capacity (95%) (Deshmukh et al., 2015).

The volume of studies already carried out using CDNSs shows that these systems are very promising for pharmaceutical and biomedical applications, especially for the delivery and controlled release of drugs. *In vitro* and *in vivo* studies show higher bioavailability of drugs encapsulated in CDNSs when compared to non-encapsulated ones. However, further studies are needed regarding the stability and toxicity of CDNSs and their *in vivo* degradation products (Lembo et al., 2013; Menezes et al., 2019).

Environmental Remediation

The 3D-structure of CDNSs shows several advantages in their application in environmental remediation, with removal percentages of pollutants similar to those found for activated carbon (AC). Despite the high cost of AC production, CDs and their derivatives are getting cheaper and of easy functionalization, allowing the synthesis of a wide range of highly structured sorbent materials. Moreover, taking advantage of the properties of CDNSs, three different sorption mechanisms can occur simultaneously; they are: 1) the formation of host–guest complexes by taking advantage of the hydrophobic cavities of CDs; 2) diffusion through pores and channels of the hydrophilic network; and 3) interaction at active sites on the NS surface. Hence, their application in environmental remediation processes lead to remarkable results (Kumari et al., 2020). Moreover, studies have demonstrated that different synthetic conditions, including solvents, aliphatic or aromatic linkers and CDs:crosslinker molar

ratio, affect the physico–chemical properties of the material and thus the removal efficiency of pollutants.

Moreover, considering the monomers used for CD coupling in environmental remediation, EPI is one of the most used aliphatic linkers along with citric acid, HDI and EDTA. As common examples of aromatic linkers we can mention TDI and tetrafluoroterephtalonitrile (TFP).

In this section, we evaluate and compare the role of NSs' physico–chemical properties on the sorption mechanisms and removal efficiencies for five different classes of pollutants: heavy metals, pesticides, pharmaceuticals and other aromatic compounds (biphenyls).

Heavy Metals

Heavy metals constitute one of the major classes of pollutant worldwide because of their easy absorption by living organisms leading to bioaugmentation and bioaccumulation. Particularly, the exposure to heavy metals can produce allergic reactions, mental disability, dementia, vision problem as well as liver and kidney diseases (Vareda et al., 2016) (Vareda et al., 2019).

CDNSs prepared by using either aliphatic or aromatic crosslinkers for the removal of a broad range of heavy metals (e.g., Cu(II), Zn(II), Pb(II), Cd(II), Ni(II), Co(II), Hg(II), Fe(III), and Cr(III), and As(V)) have been synthesised and tested. **Table 4** summarizes the most relevant data on the NSs and sorption parameters.

Concerning aliphatic-based CDNSs, citric acid (Rubin Pedrazzo et al., 2019) and EDTA (Zhao et al., 2015) are relevant crosslinkers, not only because they form highly crosslinked materials but also due to the number of available carboxylic acid groups, which allows a significant increase in active sites for interaction with metal ions. Moreover, the sorption ability of these materials is pH responsive. βCD:EDTA shows the highest removal efficiency for Cd(II) and Cu(II) reaching values higher than 90% (Zhao et al., 2015).

A different approach is the modification of chitosan by EDTA, followed by the crosslinking to βCD using pentafluoropyridine (βCD–PFP–CTS/EDTA). This βCD–PFP–CTS/EDTA NS exploits the simultaneous chelating ability of CTS and EDTA. As for pure βCD–EDTA, the sorption process is promoted at acidic pH with a removal higher than 90% for Pb(II), Ni(II), Cu(II), Co(II), Hg(II) and Cr(III) in about 1 min (Yu et al., 2018b). Likewise, the removal of Pb(II), Cu(II) and Cd(II) was studied by using NSs of βCD and TFP and methacrylic-βCD with 1–vinylimidazole (VI) (MCD:VI). βCD:TFP exhibits the largest active surface area which plays a key role on the significant amount of heavy metals sorbed per gram of material (Pb(II): 196.4 mg g^{-1}, Cu(II): 164.4 mg g^{-1} and Cd(II): 136.4 mg g^{-1}). However, its removal efficiency diminishes along cycles of sorption/desorption (He et al., 2017). The pH responsive MCD:VI adsorbent was synthesized at different molar ratios. At 1:100 mol/mol, it has revealed the best sorbent performance for Pb(II), Cu(II), Cd(II), Zn(II), Ni(II) and Co(II). The sorption ability of MCD:VI via coordinative interaction decreases in the order Cd(II)>Cu(II)>Zn(II)>Ni(II)>Co(II)>Pb(II) within 70–15 mg g^{-1} (Qin et al., 2019). Moreover, βCD crosslinked with pyromellitic dianhydride (βCD:PMA) was tested for Cu(II), Zn(II), Pb(II), Cd(II) and Fe(III) removal and the results were compared to those obtained for βCD:CA. Both materials show similar removal efficiencies (from 20 to 70%), however, the highest removal efficiencies (ca. 80%) are obtained for initial low concentrations of Cu(II) and Zn(II) (Rubin Pedrazzo et al., 2019).

Toluene diisocyanate was used to synthesize βCD and (6–deoxy)–(6–benzylimidazolium)–βCD NSs. The latter shows higher efficiency in the removal of metal ions, due to electrostatic interactions and chelating ability of the imidazolium groups, as well as higher thermal stability (Raoov et al., 2014). The hydroxyl-rich tannic acid (TA) is an interesting monomer used to synthesise βCD-TA nanosponge crosslinked by terephthaloyl chloride (TPC) and applied for Pb(II) removal. βCD:TPC:TA shows a selective and high removal efficiency of 97% for Pb(II) at alkaline pH, in the presence of salt, humic acid and other interferents (Yang et al., 2022).

Dyes

Dyes are used in many industries, mainly involving the production of consumables, including textiles, inks and paper. The textile industry is one of the activities that consumes greatest amounts of water, either in quality or in quantity, associated with the use of dyes, which makes this industry one of the biggest water body pollutants. Moreover, dyes are, in general, water soluble compounds, making them difficult to remove from wastewaters (Lellis et al., 2019). Being a relevant issue, several CDNSs have shown effectiveness in removing dyes (**Table 5**). For instance, βCD:EPI macroparticles show a spontaneous and exothermic sorption of DirectBlue78 (Murcia-Salvador et al., 2019). The effect of other cyclodextrins, αCD and hydroxypropyl-αCD, on the synthesis of NSs and consequent performance on Direct Red83:1 dye removal has been evaluated. The removal efficiency (*RE*) and the maximum amount sorbed (q_m) of *RE* = 92.8% and q_m = 31.5 mg g^{-1} and *RE* = 75% and q_m = 23.41 mg g^{-1}, for αCD:EPI and HP-αCD:EPI, respectively, have been obtained (Pellicer et al., 2018).

The βCD:EDTA was also applied for the removal of different dyes (methylene blue (MB), safranin O (SF) and crystal violet (CV)), highlighting the removal efficiency higher than 90% for the MB. As mentioned above, the presence of carboxylate groups in EDTA are relevant for the interaction with dye molecules (Zhao et al., 2015).

On the other hand, MCD:VI obtained via free radical copolymerization at different molar ratios (from 1:10 to 1: 150 mol/mol) was tested for sorption of rhodamine B (RB) and Congo red (CR); it has been demonstrated that pH strongly influences the electrostatic and π–π interactions occurring between NSs and dye molecules. Moreover the affinity of dyes towards MCD depends on the VI molar ratio; i.e., for CR the q_m increases by increasing the molar ratio, reaching a maximum q_m value (1.12 mg g^{-1}) for MCD:VI150 and for RB, the opposite is observed (the highest q_m value is obtained for MCD:VI10, 336 mg g^{-1}) (Qin et al., 2019).

The effect of benzyl-βCD hyperlinked with 4,4′-bipyridine (PD), synthesised through the Menshutkin reaction, in the sorption of two cationic (RB and MB) and two anionic (CR

TABLE 5 | Selected examples of nanosponges application for dye removal.

Nanosponge[a]	Pore size/(nm)	Surface area/ (m^2 g^{-1})	Dye/qm (mg g^{-1})/RE (%)	References
βCD:EPI (1:135)[b]	n.a	n.a	DirectBlue 78/24/n.a	Murcia-Salvador et al. (2019)
αCD:EPI (1:115)	n.a	n.a	DirectRed83:1/32/93	Pellicer et al. (2018)
HP-αCD:EPI	n.a	n.a	DirectRed83:1/23/75	
βCD:EPI (1:6)	n.a	n.a	Methylene blue/50/≥ 90; Safranin/6/≥ 90; Crystal violet/42/≥ 90	Zhao et al. (2015)
βCD:EDTA (1:17)	n.a	n.a	Methylene blue/84/n.a.; Safranin/60/n.a.; Crystal violet/114/n.a	
MCD:MPP (1:1)	2–10	n.a	Rhodamine B/10/n.a.; Congo Red	Qin et al. (2019)
β-MCD:VI (1:100)	0.02	28	Rhodamine B/175/60; Congo red/712/100	Qin et al. (2019)
β-BCD:PD	no porous	22	Methyl orange/285/77; Congo red/288/80; Rhodamine B/n.a./n.a.; Methylene blue/n.a./n.a	Li et al. (2018b)
βCD–P5 (1:1)	4	479	Methylene blue/135/78	Lu et al. (2019)
βCD:FPS (1:2)	5–6	n.a	2–naphthol/n.a./>80 2–naphthol/n.a./>99 (flow through)	Wang et al. (2017)
βCD:CMP(H)	1–10	1,099	nitrobenzene/325/80 2–nitrophenol/310/75 2–nitroaniline/290/70 4–nitroaniline/275/65 2–chloroaniline/300/75	Huang et al. (2020)

[a]*MPP [2,2′–azobis (2–methylpropionitrile)].*
[b]*Values of molar ratio in mol/mol.*

and methyl orange, MO) dyes has been reported by Li et al. This NS is effective in the removal of anionic dyes: RE = 80 and 77% for CR and MO, respectively (Li X. et al., 2018).

MB is a molecule used very often as a drug and dye model. Therefore, the interaction between MB and NS goes beyond the interest in the sorption of MB onto NSs. The copolymerization of two molecules containing cavity gates [the βCD and the pillar (5) arene (P5)], using TFP as crosslinker, provides the ability to form two different types of host–guest complexes as well as to manage the hydrophilic/hydrophobic balance of the NS. Lu et al. (Lu et al., 2019) have found that by increasing the molar fraction of P5 the hydrophobicity increases and the best removal efficiency of MB is attained (78%).

Different classes of dye intermediates and dyes derived from benzene were studied using two uncommon linkers: the 4,4′–difluorodiphenylsulfone (FPS) and the 4,4′-bis(chloromethyl)-1,1′-biphenyl (CMP) for βCD and βBCD, respectively. βCD:FPS was tested for 2-naphthol removal allowing >80 and 99% removal efficiency for in batch and in flow-through sorption experiments, respectively (Wang et al., 2017). On the other hand, the adsorption of different aromatic compounds, such as nitrobenzene, 2-nitrophenol, 2-nitroaniline, 4-nitroaniline and 2–chloroaniline, onto βCD:CMP has also been evaluated. It is worth mentioning that, for this NS, the percentage of crosslinker significantly modifies the active surface area; i.e., an increase in the crosslinking degree may result in an increase in the surface area up to 5 times. Thus, surface area and the phenyls groups play a crucial role on the sorption efficiency by enhancing the π–π interactions with removal efficiency >70% for any dye intermediates (Huang et al., 2020).

Pesticides

Nowadays pesticides are one of the most concerning classes of substances related with environmental pollution and human health issues. Recently, nanosponges have been considered promising sorbent materials and they were applied for removal of pesticides and their intermediates such as, atrazine, benalaxyl, bromacil, butachlor, butylene fipronil, fenamiphos, fipronil, fluprifole, fomesafen, pretilachlor, simazine, 4–*n*–nonylphenol (4*n*NP), 4–*n*–octylphenol (4*n*OP) and 4–*tert*–octyphenol (4*t*OP) (**Table 6**).

Macroparticles of αCD:EPI, βCD:EPI and γCD:EPI, with diameter ranging from 0.212 to 0.250 mm, were used for atrazine sorption. αCD:EPI and βCD:EPI have similar removal efficiencies (around 60%) with sorption isotherms characterized by the Freundlich model, whilst the RE of γCD:EPI is only 50%, in agreement with the highest ratio between the volume of γCD cavity and the aromatic ring of atrazine (Romita et al., 2019). Additionally, atrazine, benalaxyl, bromacil, butachlor, butylene fipronil, fenamiphos, fipronil, fomesafen, pretilachlor and simazine were tested in a screening study of sorption ability of βCD:EPI, γCD:EPI, HPβCD:EPI, randomly methylated βCD:EPI (RM-βCD:EPI), equimolar mixture of β-γ-CD:EPI, βHPβCD:EPI and γHPβCD:EPI and a physical mixture of βCD:EPI, HPβCD:EPI and RM-βCD:EPI with mass ratio of 40:30:30 (w/w) (multiplex). Multiplex NSs combining the physico–chemical properties of the three materials, show the best performance as sorbent material, even at low concentrations either in deionized water or in sea water, even after five cycles of regeneration (Liu et al., 2011). In a similar way βCD:EPI and γCD:EPI were initially synthesised and, subsequently, oxidized with $KMnO_4$. Albeit swelling ratio, particle and pore sizes, the

TABLE 6 | The main types of CDNSs applied for the adsorption of pesticides.

Nanosponge	Pore size/(nm)	Surface area/(m^2 g^{-1})	Pesticide/q_m (mg g^{-1})/RE %	References
αCD:EPI (1:115)[a]	n.a	n.a	Atrazine/≈0.07/≈60	Romita et al. (2019)
βCD:EPI (1:115)	n.a	n.a	Atrazine/≈0.07/≈60	Romita et al. (2019)
Multiplex	5	1–4	Atrazine/10/30 Benalaxyl/23/65 Bromacil/11/25 Butachlor 115/85; butene fipronil/6/98 fenamiphos/21/60 fipronil/8/85 fomesafen/25/25 pretilachlor/83/55 simazine/1/28	Liu et al. (2011)
βCD:EPI/$KMnO_4$	4	1	Atrazine/n.a./17 Benalaxyl/n.a./70 Bromacil/n.a./19 Butachlor/n.a./80 Fenamiphos/n.a./58 Fipronil/n.a./48 Flufiprole/n.a./80 Pretilachlor/n.a./40	Wang et al. (2021b)
βCD:am_6 (1:20)	24	22	Imidacloprid/68/97	Utzeri et al. (2022)
BZM-βCD:TDI (1:10)	78	1	2–chlorophenol/n.a./25 4–chloro–3–methylphenol/n.a./90 4–nitrophenol/n.a./80 2,4,6–trichlorophenol/n.a./85 2–nitrophenol/n.a./70 2,4–dinitrophenol/n.a./85 2,4–dichlorophenol/n.a./70	Raoov et al. (2014)
βCD:TTI3% (1:2)	n.a	34	2,4–dichlorophenol/145/68	Zhou et al. (2019a)
βCD:TFP (1:3)	2–4	263	2,4–dichlorophenol/14/85 1–naphtyl amine/13/92 Metolachlor/26/92	Alsbaiee et al. (2016)
βCD:TFP:THTS (1:1:2)	2–25	231	2,4–dichlorophenol/≈500/≈90	Wang et al. (2019b)
βCD:DPC (1:4)	2	3	4–chlorophenoxyacetic acid/1/91 2,3,4,6–tetrachlorophenol/1/78	Salazar et al. (2018)
αCD/βCD/γCD:DCO	non-porous	n.a	Carbendazim/0.3/90 (after 5 h)	Rizzi et al. (2021)

[a]*Molar ratio values in mol/mol.*

crosslinking degree and hydrophilicity increase by increasing the amount of $KMnO_4$, while the CD content and surface area decrease concomitantly. It has also be found that γCD:EPI is more efficient for hydrophobic compound removal (*i.e.* benalaxyl, butachlor, fipronil and flufiprole) whereas βCD:EPI performs better for hydrophilic pesticides (i.e. atrazine, bromacil, fenamiphos, pretilachlor) (Wang M. et al., 2021). The sorption experiments involving 4*n*NP, 4*n*OP and 4*t*OP and CD-based:EPI NSs, where the mixture of α- β- and γCD NS, using EPI as crosslinker, stands out, have shown high removal efficiencies for all the adsorbates. In general, all sorbents have *RE* around 90%. However, the HP-βCD shows the highest performance, in the order 4*t*OP>4*n*NP≈4*n*OP, due to its higher hydrophilicity and host–guest complex formation (Crini et al., 2021).

In a recent study, βCDNSs were synthesized using as linker two diamine monomers: 1,6–hexane diamine and 1,12–dodecane diamine. Physico–chemical properties were characterized and their influence on the sorption process assessed. Both materials present similar particle size (430 nm) but the CD-am_6 shows lower thermal stability but higher hydrophilicity, surface area and pore size. These properties seem to have relevance for the highest removal efficiency of imidacloprid (>90%), obtained for initial concentrations of IMD ranging from 20 to 300 mg L^{-1} (Utzeri et al., 2022). On the other hand, for βCD crosslinked with hexamethylene diisocyanate (βCD:HDI) the removal efficiencies for imidacloprid and cymoxanil were low; however, by forming composite gels with just 10% (w/w) of AC the removal efficiency increases to 81 and 73%, respectively (Utzeri et al., 2021).

Spherical βCD:HDI (10 equivalents of crosslinker) with high thermal stability was applied for the removal of 2,4–dinitrophenol (2,4NP) in different environmental water samples (tap water, lake water, river water and sea water). A higher removal efficiency (ca. 74%), at acidic pH and low analyte concentration, was observed; the RE remained constant along five sorption/desorption cycles (Anne et al., 2018). In the same study, the performance of βCD:TDI for the removal of 2,4NP has been compared with that obtained by using βCD:HDI. The porous βCD:TDI presents higher efficiency (ca. 85%) than the non-porous βCD:HDI. However, results can also be justified by considering the presence of the phenyl groups of the linkers, which can

TABLE 7 | Nanosponges developed for drug removal (2015–2019).

Nanosponge	Pore size/(nm)	Surface area/ ($m^2\ g^{-1}$)	Drugs/q_m ($mg\ g^{-1}$)/RE %	References
αCD:CA	n.a	—	Progesterone/n.a./95	Moulahcene et al. (2015)
βCD:CHI (1:1)[a]	n.a	n.a	Testosterone/n.a./98–100; epitestosterone/n.a./98–100; androsterone/n.a./98–100; etiocholanolone/n.a./98–100; 5α–androstane–3α,17β–diol/n.a./98–100; 5β–androstane–3α,17β–diol/n.a./98–100	Manaf et al. (2018)
βCD:PFP:CTS/EDTA (1:2,900)	1	48	6–bromo–2–naphtol/0.30/> 90	Yu et al. (2018b)
βCD:TFP:THTS (1:1:2)	2–25	231	Propranolol hydrochloride/≈100/n.a	Wang et al. (2019b)
βCD:TFP (1:3)	2–4	21	ethynyl oestradiol/n.a./≈60; propranolol hydrochloride/n.a./≈90	Alsbaiee et al. (2016)
	n.a		Chloroxylenol/144/91; Carbamazepine/136/65	Zhou et al. (2019b)
βBCD:CMP	2–5	1,107	Albendazole/180/96	Wang et al. (2019a)
βCD:HDI (1:4)	n.a	n.a	Ibuprofen/86/<70	Skwierawska et al. (2021)

[a]*Values of molar ratio in mol/mol.*

form π–π interactions with 2,4-dichlorophenoxy acid (2,4D) (Anne et al., 2018).

As was pointed out in the previous section, β-BZMCD:TDI was applied for the removal of a set of phenols with different substitutions. The β-BZMCD:TDI shows higher ability than the non-substituted βCD:TDI, with an average removal percentage equal to 85%, which can be justified by its higher porosity (Raoov et al., 2014). The sorption of 2,4CP onto βCD:TTI (triphenylmethane–4,4′,4″–trisocyanate), synthesised using 2–butanone as solvent, has been studied. The properties of the NS is highly affected by the catalyst/linker ratio, temperature and βCD:TTI molar ratio (Zhou L. et al., 2019). Another example of a common aromatic linker is TFP. A study comparing the sorbent performance of porous and non-porous βCD:TFP has also been reported. Sorption tests were performed with 2,4CP, 1-naphtyl amine and metolachlor. Porous βCD:TFP has a lower water uptake, compared with non-porous material, but has shown better removal efficiency ≥85% (Alsbaiee et al., 2016). Pure βCD:TFP was also used as control material in comparison with a mixture of two monomers, TFP and 5,5′,6,6′–tetrahydroxy-3,3,3′,3′-tetramethylspirobisindande (THTS), prepared in dimethylacetamide. Overall, NS particles exhibit dimensions ca. 90 nm diameter with micro– and meso–pores and higher active surface area; these properties are improved by increasing the THTS percentage. The βCD:TFP:THTS0.5 is the most efficient material for various micropollutants. Particularly, it sorbs 460 $mg\ g^{-1}$ of 2,4CP per gram of sorbent corresponding to around 90% of removal efficiency. βCD:P5 at molar ratio 1:1 presents the best hydrophilic behaviour, higher surface area (479 $m^2\ g^{-1}$) than βCD:TFP and larger pore size (3.5 nm) than P5:TFP. They represent an advantage on sorption processes of 1–naphthylamine with removal efficiency of around 80% in aqueous solution and environmental conditions (Lu et al., 2019). An interesting study reported by Klemes et al. shows how solvent, catalyst (K_2CO_3) and crosslinker ratio influence both reaction yield and physico–chemical properties of βCD:TFP NS. Higher TFP amount led to a decrease in reaction yield and phenolate incorporation. Moreover, depending on the method of addition of K_2CO_3, a porous material may result, with 346 $m^2\ g^{-1}$ of active surface, or even a non–porous material. NSs obtained using different methods were tested towards 83 pesticides. In general, a stronger affinity of the micropollutants was observed for the porous βCD:TFP synthesised by using DMSO, with higher surface area and phenolate content (Klemes et al., 2018). Another extensive study involving βCD:TFP, was carried out by Li *et al.* (Li C. et al., 2018). It has been demonstrated that for almost all pesticides the removal efficiency of the NS is higher than 70%.

NSs based on aromatic linkers such as FPS, CMP and DPC have also been prepared and their performance towards pesticide sorption evaluated. The sorption of 2,4CP by βCD:FPS (1:2 mol/mol) showed a removal efficiency higher than 80% (Wang et al., 2017). The aromatic crosslinker can act synergetically in the sorption process of organic adsorbates; for example, the sorption of 2NP, 2,4CP, 2,6CP and 2,4,6CP onto βCD:CMP increases by increasing the amount of crosslinker (Huang et al., 2020).

The incorporation of Fe_3O_4 nanoparticles into βCD:DPC for the sorption of aromatic chlorinated pesticides [4–chlorophenoxyacetic acid (CPA) and 2,3,4,6–tetrachlorophenol (TCP)] has demonstrated that no variation of removal efficiency occurs; however, the sorption kinetics seem to be facilitated by the presence of NPs (Salazar et al., 2018). The same research group has also tested this composite for dinotefuran removal with similar results (Salazar et al., 2020).

Non–porous materials with high thermal stability were synthesized using BDE as linker for α-, β- and γCDs. The materials were mainly applied for ciprofloxacin removal, although they were also tested for carbendazim (a broad-spectrum fungicide) with 70% of active substance sorbed in 30 min and a value of 90% can be reached after 5 h sorption (Rizzi et al., 2021).

Hybrid NSs, which include CD and a polymer, have also been synthesised and tested for the removal of pesticides. Recently, poly (vinyl alcohol)-βCD has been synthesised and its adsorption performance evaluated towards paraquat. The obtained material shows a very fast adsorption of pesticide, with a RE of around 96%

in just 3 min, following a Langmuir mechanism (Martwong et al., 2021, 2022).

Drug Removal

As the other classes of pollutants, pharmaceuticals represent one of the biggest concern in relation with ecosystem pollution and its side effects. In Europe, they were detected in surface and groundwater that are used in agriculture and drinking water production. Thus, strategical actions are made to face this issue. One of these strategies is the development of efficient sorbent materials, including nanosponges (**Table 7**). βCD:EPI particles were employed in a pilot scale test for the simultaneous removal of eight different drugs (β–estradiol, ethynyl estradiol, estriol, ibuprofen, diclofenac, naproxen, ketoprofen and cholesterol) from greenhouse municipal wastewater. Particles reach up ca. 99% of removal efficiency for hormones and 85% for ibuprofen and diclofenac, in–flow sorption process (Fenyvesi et al., 2020). Commercial βCD:EPI macroparticles were used for the removal of twenty one different drugs existing in wastewater effluents. The adsorption process is carried out together with a photodegradation treatment. The results show a removal efficiency of 71% after 5 min for most of the drugs, whereas a 99% removal is reached for metoprolol, paroxetine and propranolol. Generally, the removal efficiency follows the order: β–blockers > psychiatric drugs > lipid regulators > antibiotics > anti–inflammatories > diuretics (Gómez-Morte et al., 2021). Additionally, fibers of HP-βCD:EPI have been evaluated as adsorbent for removal of phenanthrene—a compound used for the synthesis of bile acids and steroids. It has been found that these fibers were able to remove 80% of phenantrene (Celebioglu et al., 2019).

Nanosponges of αCD, βCD and γCD crosslinked with citric acid have been evaluated by Moulahcene et al. for the sorption of progesterone. The αCD:CA NS showed the best sorption performance in continuous flow column (95%); that was justified by the lower swelling ability, higher surface area and number of acidic groups (among all three NSs). (Moulahcene et al., 2015).

βCD:EDTA was applied for the removal of ciprofloxacin, a quimolone antibiotic, having reached a maximum sorbed amount of 327 mg g^{-1}, at a pH range 4–6. The sorption mechanism is sensitive to the ionic strength, probably due to screening effect caused by the counterions (Yu F. et al., 2018). The ciprofloxacin removal was further studied with αCD, βCD and γCD crosslinked with BDE and the removal efficiency was also quite promising (i.e., 90%). In a similar way, the sorption capacity is impaired by the presence of salts and pH changes (Rizzi et al., 2021).

In an interesting study, βCD nanosponges obtained using aliphatic and aromatic linkers of the diisocyanate class, dicyclohexylmethane-4,4′-diisocyanate (CHI) and MDI, respectively, were compared. Three molar ratios, 1:1, 1:2 and 1:3 mol/mol were used. The polymers present different hydrophilic/hydrophobic ratios. Tests were performed on artificial and human urines to analyse sorption abilities for testosterone, epitestosterone, androsterone, etiocholanolone, 5*α*–androstane-3*α*,17*β*-diol and 5*β*-androstane-3*α*,17*β*–diol. βCD:CHI at molar ratio 1:1 showed the best performance for each analyte with accuracy and recovery within 96 and 106%, respectively. The superior performance of βCD:CHI can be justified considering the higher mobility and flexibility of the aliphatic linker, making the active sites more easily accessible (Manaf et al., 2018).

Materials already mentioned in previous sections were also applied for pharmaceutical removal. βCD:TFP has been used for a number of studies involving the adsorption of many drugs. The properties of βCD:TFP are dependent on the solvent and CD: crosslinker molar ratio (Klemes et al., 2018) (Li C. et al., 2018). Among the adsorbates evaluated we can mention ethynyl oestradiol and propranolol hydrochloride (Alsbaiee et al., 2016; Wang Z. et al., 2019), and chloroxylenol and carbamazepine (Zhou Y. et al., 2019). With few exceptions, this NS reached efficiencies higher than 70%, which shows a high affinity of NSs for different kinds of pharmaceutical molecules.

Moreover, four types of nanosponges with different crosslinkers, namely, PMA, CDI, CA and TDI, were synthesised. βCD:PMA and βCD:CA show the higher level of swelling justified by the larger number of donator and acceptor hydrogen bonding. The removal efficiency of the NSs was tested for indole in three different media: water, simulated gastric fluid and intestinal fluid. Indole is produced by tryptophan conversion, and it is a precursor of uremic toxins responsible of several severe health illnesses. The removal ability of the materials for indole decrease in the following order: βCD:TDI (≈91%)>βCD:CA>βCD:PMA>βCD:CDI (Varan et al., 2020).

Other Aromatic Compounds

Biphenols are derivatives of phenol used in the manufacture of plastic furniture and are key components of liquid crystal polymers. Nonetheless, due to their high volume of production and usage, they are classified as persistent organic pollutants. They are hazardous for the environment and for human health. Bisphenol A (BPA) is the most produced and thus the most common in water bodies. Consequently, there is a demand for adsorbents capable of removing these pollutants. The aromatic ring of these compounds can strongly interact, via host-guest interaction, with CD, making CDNSs ideal for that purpose. In fact, several CDNS adsorbents were studied and high removal efficiencies were reported. For example, βCD:EPI, βCD:PFP:CTS/EDTA, βCD:P5 and βCD:TFP:THTS have RE greater than 90% in the removal of Bisphenol A (Alsbaiee et al., 2016; Yu et al., 2018c; Wang Z. et al., 2019; Lu et al., 2019).

Other biphenols with less environmental impact were also tested. Thus, the bisphenol S (BPS) (an endocrine disruptor) has a significant interaction with βCD:FPS (1:2 mol/mol) leading to a removal efficiency ≥80% (Wang et al., 2017). The removal of bisphenol F (BPF) and bisphenol AF (BPAF) was also studied by using βCD:CMP. This NS shows a high sorption efficiency due to its larger surface area and a significant number of π–π interactions (Huang et al., 2020).

Particularly interesting is a study carried out for assessing the adsorption capacity of *heptakis*(2,6–di–*O*–methyl)βCD crosslinked with three different diisocyanates [MDI, 1,4–phenylene diisocyanate (PDS) and HDI]. Sixty six different biphenyls, from mono to decachlorobiphenyls, using isooctane as solvent, were tested. The highest crosslinked βCD:MDI and βCD:PDS showed adsorption performances around 100%. This

behaviour is also dependent on the CD concentration (Kawano et al., 2015).

Other Applications

Pesticide and Fertilizer Delivery System

In a previous section, the ability of CDNSs for the removal of pesticides and other pollutants has been summarized. In this section, we discuss the role of CDs based on a different approach. In order to reduce the amount of pesticides applied in agriculture, the exposure of workers, and to ameliorate the efficiency of the phytopharmaceuticals, a broad range of materials have been developed. Nanosponges of αCD, βCD and γCD were prepared using 1,1′-carbonyldiimidazole (CDI) and PMA as crosslinkers. Both types of nanosponges were loaded in methanol with ailanthone, a natural herbicide characterized by low persistence and rapid degradation. γCD-based materials showed higher interaction for ailanthone with 55% of encapsulation efficiency (EE) and remarkable efficacy on index growth of garden cress and radish after 10 days. The highest EE is found for γCD-based NS, probably due to proper fit between cavity and analyte sizes (Demasi et al., 2021) (Demasi et al., 2021). Additionally, βCD:PMA was synthesized at molar ratio 1:12 mol/mol by electrospinning in fibers with 3 μm diameter. It was applied as micropesticide, loaded with a maximum of 130 mg g^{-1} of *N,N*-diethyl-3-toluamide (DEET), a common insecticide, with a release of 60% in 72 h and 100% at about 350 h (Cecone et al., 2018).

Sensors

Cyclodextrin–materials can be applied as direct or indirect sensor materials via turn–on or turn–off of fluorescence both via host–guest complexation or molecular assembly with fluorescent/luminescent probe molecules.

Fluorescent cyclodextrin–based probe was obtained via cross-linking of βCD with 4,4′–diisocyanato–3,3′–dimethyl biphenyl (IMP) and tetrakis (4–hydroxyphenyl)ethane (TPE) as fluorescent ligands. The fluorescent βCD–polymer was successfully applied for the detection of trinitrophenol and nitrobenzene by turn–off. These aromatic compounds are used for dye and pesticide synthesis, presenting hazardous effects for human health and possible environment contamination (Danquah et al., 2019). βCD:PMA was prepared at molar ratio of 1:7 mol/mol as fluorescent probe with emission wavelength at 423 nm. The polymeric material has an heterogeneous size distribution with a high polydispersity index. It presents an excellent selectivity for diclofenac (LOD 0.92 μM) in aqueous solution and tablets, whose value is not significantly influenced by the presence of different drugs, probably due to more hydrophobic behaviour of the diclofenac (Nazerdeylami et al., 2021).

Catalysts

Being CD nanosponges porous polymeric materials, often with a large active surface area and numerous available active sites, they are considered promising materials to be used as heterogeneous catalysts.

βCD:CDI with 11 m^2 g^{-1} of active surface and nanoporous structure (5 nm) has promising activity as a metal free catalyst in a one-pot three component condensation reaction (between aromatic aldehydes, methylene compounds and amines) for the synthesis of *N*-containing organic scaffolds (Sabzi and Kiasat, 2018). βCD:EPI (surface area of 11 m^2 g^{-1} and 5 nm of pore diameter) was applied in a four component solvent-free reaction for the synthesis of spiro [indoline–3,4′–pyrano(2,3–c) pyrazole] and pyranopyrazole derivatives. However, the reaction only proceeds with high yield at 100°C (Jafari Nasab et al., 2018). In another paper, a heteropolyacid was immobilized onto βCD: DPC (3 m^2 g^{-1} and pore size 14 nm) and applied as catalyst for the synthesis of xanthenes in high yields (87–95%), at reflux, in short reaction times (Sadjadi et al., 2017b). The same authors also described the use of NSs modified with an ionic liquid, that was used in a cascade reaction for the synthesis of benzochromeno-pyrazole derivatives (Sadjadi et al., 2017a). High yields were obtained using solvent-free conditions, at 80°C.

Amino-βCD NSs were covalently bonded to chitosan beads to prepare a thermally stable porous composite, with surface area 11 m^2 g^{-1}. βCD:CS was applied as metal free catalyst for the synthesis of dihydropyrimidinone and octahydroquinazolinone in water, via the Biginelli reaction. The composite reveals excellent catalyst activity, with yields up to 100%, using an ultrasonic assisted procedure at 25°C. The composite was reused and a yield decrease of approximately 10% was observed, after five cycles (Sadjadi and Koohestani, 2021a).

Heterogeneous catalysts based on CD nanosponges and containing embedded inorganic nanoparticles were also described. However, since the aim of this review is focused on pure CDNSs, these studies will not be reported in detail, just a brief classification based on the type of metal used is given: 1) Pd^0/Pd^{2+} for hydrogenation reactions (Sadjadi and Koohestani, 2021b), cyanation reactions (Khajeh Dangolani et al., 2019), Sonogashira and Heck (Sadjadi et al., 2018b; 2019b); 2) Ag^+ for redox reactions (Russo et al., 2019); 3) Au for 4–nitrophenol synthesis (Vasconcelos et al., 2016).

FUTURE PERSPECTIVES

The use of cyclodextrin nanosponges is still at an early stage of wide application in the most diverse areas. Currently, many of the studies described in the literature are based on their application in the pharmaceutical and biomedical areas. However, relevant studies have recently been published on the application of nanosponges in water and, to a lesser extent, soil remediation. However, in this area, it is interesting to note that a 2007 study (Mhlanga et al., 2007) describes the potential of CDNSs for removing chlorinated disinfection by-products (DBPs). Fifteen years later, this issue has become a priority topic for the European Community, so the use of NSs for this purpose should be developed. Concomitantly, other pollutants such as antibiotics, antidepressants and pesticides have molecular structures that suggests a potential high removal efficiency by CDNSs.

The stiffness of cyclodextrins in NSs, due to hyper crosslinking, decreases the degree of freedom of guest molecules that interact with them by supramolecular host-guest interactions. This effect can be used effectively for the development of matrices for Aggregation-Induced Emission

(Hong et al., 2009). In general, it is expected that chromophore aggregation leads to a luminescence quenching. However, some molecules have the opposite effect, which is called: Aggregation-Induced Emission. This may result from the restriction of intramolecular rotation (RIR). CDNSs seem to be potential matrices to promote the RIR mechanism and, thus, lead to luminescence emission by the chromophores. The impact of this phenomenon might be relevant in areas such as optoelectronics and sensors.

Using a similar approach, we think that nanosponges could play an important role in the development of sensors with very low detection limits. The preconcentration of pollutants is often a necessary condition for their detection. NSs could have a similar effect through their use in monoliths or by using membranes. In the latter case, we envisage the use of, e.g., cellulose acetate or PVA as matrices for incorporation of CDNSs.

We also believe that the use of NSs for heterogeneous catalysis is incipient. Most of the conventional asymmetric synthesis methods involve the use of toxic organic solvents, chiral metal complexes and homogeneous catalysis methods, which makes them unsustainable. On the other hand, usage of heterogeneous matrices with high density of hydrophobic cavities capable of enantiomeric discrimination could be a valuable alternative. CDNSs can accommodate hydrophobic molecules inside and interact efficiently with aqueous media in the exterior, opening the way to the development of greener asymmetric chemical reactions. Additionally, CDNSs can also be modified with metallic nanoparticles, allowing the development of more sustainable organometallic heterogeneous catalysts.

It should be mentioned that some of these suggestions and views have been tested by authors and preliminary results are available. However, we strong believe that CDNSs either alone or in the presence of other polymers still have a promising future not only for fundamental interest but especially for a wide range of not yet unveiled applications.

AUTHOR CONTRIBUTIONS

GU: Writing—original draft, Writing—review and editing. PM: Writing—original draft, Writing—review and editing. DM: Writing—original draft, Conceptualization, Resources, Writing—review and editing, supervision. AV: Conceptualization, Resources, Writing—original draft, Writing—review and editing, Supervision.

FUNDING

This work was funded by the Coimbra Chemistry Centre, which is supported by the Fundação para a Ciência e a Tecnologia (FCT) through the programmes UID/QUI/00313/2020 and COMPETE, and PhD grant (SFR/BD/146358/2019), and also by the project "BIOSHELL", Ref. "BLUEBIO/0003/2019—Recycling Crustaceans Shell Wastes for Developing Biodegradable Wastewater Cleaning Composites", financed by FCT within program ERA-NET Cofund on Blue Bioeconomy (BlueBio)—Unlocking the Potential of Aquatic Bioresources.

ACKNOWLEDGMENTS

GU thanks Fundação para a Ciência e a Tecnologia (FCT, Portugal) for PhD grant (SFR/BD/146358/2019).

REFERENCES

A. Ansari, K., J. Torne, S., Pradeep R. Vavia, P., Trotta, F., and Cavalli, R. (2011a). Paclitaxel Loaded Nanosponges: *In-Vitro* Characterization and Cytotoxicity Study on MCF-7 Cell Line Culture. *Cdd* 8, 194–202. doi:10.2174/156720111794479934

Aguado, R., Murtinho, D., and Valente, A. J. M. (2019). A Broad Overview on Innovative Functionalized Paper Solutions. *Nordpulp Pap. Res. J.* 34, 395–416. doi:10.1515/npprj-2019-0036

Alidoost, M., Mangini, A., Caldera, F., Anceschi, A., Amici, J., Versaci, D., et al. (2022). Micro-Mesoporous Carbons from Cyclodextrin Nanosponges Enabling High-Capacity Silicon Anodes and Sulfur Cathodes for Lithiated Si-S Batteries. *Chem. A Eur. J* 28, 1. doi:10.1002/chem.202104201

Allahyari, S., Esmailnezhad, N., Valizadeh, H., Ghorbani, M., Jelvehgari, M., Ghazi, F., et al. (2021). *In-vitro* Characterization and Cytotoxicity Study of Flutamide Loaded Cyclodextrin Nanosponges. *J. Drug Deliv. Sci. Tech.* 61, 102275. doi:10.1016/j.jddst.2020.102275

Allahyari, S., Trotta, F., Valizadeh, H., Jelvehgari, M., and Zakeri-Milani, P. (2019). Cyclodextrin-based Nanosponges as Promising Carriers for Active Agents. *Expert Opin. Drug Deliv.* 16, 467–479. doi:10.1080/17425247.2019.1591365

Allahyari, S., Valizadeh, H., Roshangar, L., Mahmoudian, M., Trotta, F., Caldera, F., et al. (2020). Preparation and Characterization of Cyclodextrin Nanosponges for Bortezomib Delivery. *Expert Opin. Drug Deliv.* 17, 1807–1816. doi:10.1080/17425247.2020.1800637

Allahyari, S., Zahednezhad, F., Khatami, M., Hashemzadeh, N., Zakeri-Milani, P., and Trotta, F. (2022). Cyclodextrin Nanosponges as Potential Anticancer Drug Delivery Systems to Be Introduced into the Market, Compared with Liposomes. *J. Drug Deliv. Sci. Tech.* 67, 102931. doi:10.1016/j.jddst.2021.102931

Alongi, J., Poskovic, M., P.M., V., and Malucelli, G. (2012). Cyclodextrin Nanosponges as Novel green Flame Retardants for PP, LLDPE and PA6. *Carbohydr. Polym.* 88, 1387–1394. doi:10.1016/j.carbpol.2012.02.038

Alsbaiee, A., Smith, B. J., Xiao, L., Ling, Y., Helbling, D. E., and Dichtel, W. R. (2016). Rapid Removal of Organic Micropollutants from Water by a Porous β-cyclodextrin Polymer. *Nature* 529, 190–194. doi:10.1038/nature16185

Amin, O. M., Ammar, A., and Eladawy, S. A. (2020). Febuxostat Loaded β-cyclodextrin Based Nanosponge Tablet: an *In Vitro* and *In Vivo* Evaluation. *J. Pharm. Investig.* 50, 399–411. doi:10.1007/s40005-019-00464-w

Anandam, S., and Selvamuthukumar, S. (2014). Optimization of Microwave-Assisted Synthesis of Cyclodextrin Nanosponges Using Response Surface Methodology. *J. Porous Mater.* 21, 1015–1023. doi:10.1007/s10934-014-9851-2

Anne, J. M., Boon, Y. H., Saad, B., Miskam, M., Yusoff, M. M., Shahriman, M. S., et al. (2018). β-Cyclodextrin Conjugated Bifunctional Isocyanate Linker Polymer for Enhanced Removal of 2,4-dinitrophenol from Environmental Waters. *R. Soc. Open Sci.* 5, 180942. doi:10.1098/rsos.180942

Ansari, K. A., Vavia, P. R., Trotta, F., and Cavalli, R. (2011b). Cyclodextrin-based Nanosponges for Delivery of Resveratrol: *In Vitro* Characterisation, Stability, Cytotoxicity and Permeation Study. *AAPS PharmSciTech* 12, 279–286. doi:10.1208/s12249-011-9584-3

Appell, M., Evans, K. O., Jackson, M. A., and Compton, D. L. (2018). Determination of Ochratoxin A in Grape Juice and Wine Using Nanosponge Solid Phase Extraction Clean-Up and Liquid Chromatography with Fluorescence Detection. *J. Liquid Chromatogr. Relat. Tech.* 41, 949–954. doi:10.1080/10826076.2018.1544148

Appleton, S. L., Tannous, M., Argenziano, M., Muntoni, E., Rosa, A. C., Rossi, D., et al. (2020). Nanosponges as Protein Delivery Systems: Insulin, a Case Study. *Int. J. Pharmaceutics* 590, 119888. doi:10.1016/j.ijpharm.2020.119888

Argenziano, M., Foglietta, F., Canaparo, R., Spagnolo, R., Della Pepa, C., Caldera, F., et al. (2020a). Biological Effect Evaluation of Glutathione-Responsive Cyclodextrin-Based Nanosponges: 2D and 3D Studies. *Molecules* 25, 2775. doi:10.3390/molecules25122775

Argenziano, M., Gigliotti, C. L., Clemente, N., Boggio, E., Ferrara, B., Trotta, F., et al. (2020b). Improvement in the Anti-tumor Efficacy of Doxorubicin Nanosponges in *In Vitro* and in Mice Bearing Breast Tumor Models. *Cancers* 12, 162–180. doi:10.3390/cancers12010162

Argenziano, M., Haimhoffer, A., Bastiancich, C., Jicsinszky, L., Caldera, F., Trotta, F., et al. (2019). *In Vitro* Enhanced Skin Permeation and Retention of Imiquimod Loaded in β-Cyclodextrin Nanosponge Hydrogel. *Pharmaceutics* 11, 138. doi:10.3390/pharmaceutics11030138

Asela, I., Donoso-González, O., Yutronic, N., and Sierpe, R. (2021). β-Cyclodextrin-Based Nanosponges Functionalized with Drugs and Gold Nanoparticles. *Pharmaceutics* 13, 513. doi:10.3390/pharmaceutics13040513

Babadi, D., Dadashzadeh, S., Osouli, M., Abbasian, Z., Daryabari, M. S., Sadrai, S., et al. (2021). Biopharmaceutical and Pharmacokinetic Aspects of Nanocarrier-Mediated Oral Delivery of Poorly Soluble Drugs. *J. Drug Deliv. Sci. Tech.* 62, 102324. doi:10.1016/j.jddst.2021.102324

Bergal, A., Andaç, M., and Andaç, M. (2021). Nanosponges (NSs): Using as a Nanocarrier for Anti Cancer Drug Delivery Applications. *actapharm* 59, 306–320. doi:10.23893/1307-2080.APS.05918

Bezerra, F. M., Lis, M. J., Firmino, H. B., Dias da Silva, J. G., Curto Valle, R. d. C. S., Borges Valle, J. A., et al. (2020). The Role of β-Cyclodextrin in the Textile Industry-Review. *Molecules* 25, 3624. doi:10.3390/molecules25163624

Blasco-Tamarit, E., Muñoz-Portero, M.-J., Sánchez-Tovar, R., Fernández-Domene, R. M., and García-Antón, J. (2018). The Effect of Reynolds Number on TiO2 Nanosponges Doped with Li+ Cations. *New J. Chem.* 42, 11054–11063. doi:10.1039/C8NJ00800K

Buvari, g., and Barcza, L. (1989). Complex Formation of Inorganic Salts With?-Cyclodextrin. *J. Incl Phenom Macrocycl Chem.* 7, 379–389. doi:10.1007/BF01076992

Caldera, F., Tannous, M., Cavalli, R., Zanetti, M., and Trotta, F. (2017). Evolution of Cyclodextrin Nanosponges. *Int. J. Pharmaceutics* 531, 470–479. doi:10.1016/j.ijpharm.2017.06.072

Cataldo, S., Lo Meo, P., Conte, P., Di Vincenzo, A., Milea, D., and Pettignano, A. (2021). Evaluation of Adsorption Ability of Cyclodextrin-Calixarene Nanosponges towards Pb2+ Ion in Aqueous Solution. *Carbohydr. Polym.* 267, 118151. doi:10.1016/j.carbpol.2021.118151

Cecone, C., Caldera, F., Trotta, F., Bracco, P., and Zanetti, M. (2018). Controlled Release of DEET Loaded on Fibrous Mats from Electrospun PMDA/Cyclodextrin Polymer. *Molecules* 23, 1694. doi:10.3390/molecules23071694

Cecone, C., Hoti, G., Krabicová, I., Appleton, S. L., Caldera, F., Bracco, P., et al. (2020). Sustainable Synthesis of Cyclodextrin-Based Polymers by Exploiting Natural Deep Eutectic Solvents. *Green. Chem.* 22, 5806–5814. doi:10.1039/D0GC02247K

Cecone, C., Zanetti, M., Anceschi, A., Caldera, F., Trotta, F., and Bracco, P. (2019). Microfibers of Microporous Carbon Obtained from the Pyrolysis of Electrospun β-cyclodextrin/pyromellitic Dianhydride Nanosponges. *Polym. Degrad. Stab.* 161, 277–282. doi:10.1016/j.polymdegradstab.2019.02.001

Celebioglu, A., Topuz, F., and Uyar, T. (2019). Water-Insoluble Hydrophilic Electrospun Fibrous Mat of Cyclodextrin-Epichlorohydrin Polymer as Highly Effective Sorbent. *ACS Appl. Polym. Mater.* 1, 54–62. doi:10.1021/acsapm.8b00034

Chodankar, D., Vora, A., and Kanhed, A. (2021). β-Cyclodextrin and its Derivatives: Application in Wastewater Treatment. *Environ. Sci. Pollut. Res.* 29, 1585–1604. doi:10.1007/s11356-021-17014-3

Ciesielska, A., Ciesielski, W., Girek, B., Girek, T., Koziel, K., Kulawik, D., et al. (2020). Biomedical Application of Cyclodextrin Polymers Cross-Linked via Dianhydrides of Carboxylic Acids. *Appl. Sci.* 10, 8463. doi:10.3390/app10238463

Clemente, N., Boggio, E., Gigliotti, L. C., Raineri, D., Ferrara, B., Miglio, G., et al. (2020). Immunotherapy of Experimental Melanoma with ICOS-Fc Loaded in Biocompatible and Biodegradable Nanoparticles. *J. Controlled Release* 320, 112–124. doi:10.1016/j.jconrel.2020.01.030

Conte, C., Caldera, F., Catanzano, O., D'Angelo, I., Ungaro, F., Miro, A., et al. (2014). β-Cyclodextrin Nanosponges as Multifunctional Ingredient in Water-Containing Semisolid Formulations for Skin Delivery. *J. Pharm. Sci.* 103, 3941–3949. doi:10.1002/jps.24203

Cova, T. F. G. G., Murtinho, D., Pais, A. A. C. C., and Valente, A. J. M. (2018a). Cyclodextrin-based Materials for Removing Micropollutants from Wastewater. *Coc* 22, 2150–2181. doi:10.2174/1385272822666181019125315

Cova, T. F., Murtinho, D., Aguado, R., Pais, A. A. C. C., and Valente, A. J. M. (2021). Cyclodextrin Polymers and Cyclodextrin-Containing Polysaccharides for Water Remediation. *Polysaccharides* 2, 16–38. doi:10.3390/polysaccharides2010002

Cova, T. F., Murtinho, D., Pais, A. A. C. C., and Valente, A. J. M. (2018b). Combining Cellulose and Cyclodextrins: Fascinating Designs for Materials and Pharmaceutics. *Front. Chem.* 6. doi:10.3389/fchem.2018.00271

Coviello, V., Sartini, S., Quattrini, L., Baraldi, C., Gamberini, M. C., and La Motta, C. (2017). Cyclodextrin-based Nanosponges for the Targeted Delivery of the Anti-restenotic Agent DB103: A Novel Opportunity for the Local Therapy of Vessels wall Subjected to Percutaneous Intervention. *Eur. J. Pharmaceutics Biopharmaceutics* 117, 276–285. doi:10.1016/j.ejpb.2017.04.028

Crini, G., Bradu, C., Fourmentin, M., Cosentino, C., Ribeiro, A. R. L., and Morin-Crini, N. (2021). Sorption of 4-N-Nonylphenol, 4-N-Octylphenol, and 4-Tert-Octyphenol on Cyclodextrin Polymers. *Environ. Sci. Pollut. Res.* 29, 171–181. doi:10.1007/s11356-021-14435-y

Daga, M., de Graaf, I. A. M., Argenziano, M., Barranco, A. S. M., Loeck, M., Al-Adwi, Y., et al. (2020). Glutathione-responsive Cyclodextrin-Nanosponges as Drug Delivery Systems for Doxorubicin: Evaluation of Toxicity and Transport Mechanisms in the Liver. *Toxicol. Vitro* 65, 104800. doi:10.1016/j.tiv.2020.104800

Daga, M., Ullio, C., Argenziano, M., Dianzani, C., Cavalli, R., Trotta, F., et al. (2016). GSH-targeted Nanosponges Increase Doxorubicin-Induced Toxicity "*In Vitro*" and "*In Vivo*" in Cancer Cells with High Antioxidant Defenses. *Free Radic. Biol. Med.* 97, 24–37. doi:10.1016/j.freeradbiomed.2016.05.009

Dai, Y., Li, Q., Zhang, S., Shi, S., Li, Y., Zhao, X., et al. (2021). Smart GSH/pH Dual-Bioresponsive Degradable Nanosponges Based on β-CD-appended Hyper-Cross-Linked Polymer for Triggered Intracellular Anticancer Drug Delivery. *J. Drug Deliv. Sci. Tech.* 64, 102650. doi:10.1016/j.jddst.2021.102650

Danquah, M. K., Wang, S., Wang, Q., Wang, B., and Wilson, L. D. (2019). A Porous β-cyclodextrin-based Terpolymer Fluorescence Sensor for *In Situ* Trinitrophenol Detection. *RSC Adv.* 9, 8073–8080. doi:10.1039/C8RA06192K

Darandale, S. S., and Vavia, P. R. (2013). Cyclodextrin-based Nanosponges of Curcumin: Formulation and Physicochemical Characterization. *J. Incl. Phenom. Macrocycl. Chem.* 75, 315–322. doi:10.1007/s10847-012-0186-9

Demasi, S., Caser, M., Caldera, F., Dhakar, N. K., Vidotto, F., Trotta, F., et al. (2021). Functionalized Dextrin-Based Nanosponges as Effective Carriers for the Herbicide Ailanthone. *Ind. Crops Prod.* 164, 113346. doi:10.1016/j.indcrop.2021.113346

Deng, J., Chen, Q. J., Li, W., Zuberi, Z., Feng, J. X., Lin, Q. L., et al. (2021). Toward Improvements for Carrying Capacity of the Cyclodextrin-Based Nanosponges: Recent Progress from a Material and Drug Delivery. *J. Mater. Sci.* 56, 5995–6015. doi:10.1007/s10853-020-05646-8

Desai, D., and Shende, P. (2021). Drug-Free Cyclodextrin-Based Nanosponges for Antimicrobial Activity. *J. Pharm. Innov.* 16, 258–268. doi:10.1007/s12247-020-09442-4

Deshmukh, K., and Shende, P. (2018). Toluene Diisocyanate Cross-Linked β-cyclodextrin Nanosponges as a pH-Sensitive Carrier for Naproxen. *Mater. Res. Express* 5, 075008. doi:10.1088/2053-1591/aac93d

Deshmukh, K., Tanwar, Y. S., Sharma, S., Shende, P., and Cavalli, R. (2016). Functionalized Nanosponges for Controlled Antibacterial and Antihypocalcemic Actions. *Biomed. Pharmacother.* 84, 485–494. doi:10.1016/j.biopha.2016.09.017

Deshmukh, K., Tanwar, Y. S., Shende, P., and Cavalli, R. (2015). Biomimetic Estimation of Glucose Using Non-molecular and Molecular Imprinted Polymer Nanosponges. *Int. J. Pharmaceutics* 494, 244–248. doi:10.1016/j.ijpharm.2015.08.022

Dhakar, N. K., Caldera, F., Bessone, F., Cecone, C., Pedrazzo, A. R., Cavalli, R., et al. (2019). Evaluation of Solubility Enhancement, Antioxidant Activity, and

Cytotoxicity Studies of Kynurenic Acid Loaded Cyclodextrin Nanosponge. *Carbohydr. Polym.* 224, 115168. doi:10.1016/j.carbpol.2019.115168

Dora, C. P., Trotta, F., Kushwah, V., Devasari, N., Singh, C., Suresh, S., et al. (2016). Potential of Erlotinib Cyclodextrin Nanosponge Complex to Enhance Solubility, Dissolution Rate, *In Vitro* Cytotoxicity and Oral Bioavailability. *Carbohydr. Polym.* 137, 339–349. doi:10.1016/j.carbpol.2015.10.080

dos Santos Silva Araújo, L., Lazzara, G., and Chiappisi, L. (2021). Cyclodextrin/surfactant Inclusion Complexes: An Integrated View of Their Thermodynamic and Structural Properties. *Adv. Colloid Interf. Sci.* 289, 102375. doi:10.1016/j.cis.2021.102375

Fenyvesi, É., Barkács, K., Gruiz, K., Varga, E., Kenyeres, I., Záray, G., et al. (2020). Removal of Hazardous Micropollutants from Treated Wastewater Using Cyclodextrin Bead Polymer - A Pilot Demonstration Case. *J. Hazard. Mater.* 383, 121181. doi:10.1016/j.jhazmat.2019.121181

Ferro, M., Castiglione, F., Pastori, N., Punta, C., Melone, L., Panzeri, W., et al. (2017). Dynamics and Interactions of Ibuprofen in Cyclodextrin Nanosponges by Solid-State NMR Spectroscopy. *Beilstein J. Org. Chem.* 13, 182–194. doi:10.3762/bjoc.13.21

Ferro, M., Castiglione, F., Punta, C., Melone, L., Panzeri, W., Rossi, B., et al. (2014). Anomalous Diffusion of Ibuprofen in Cyclodextrin Nanosponge Hydrogels: an HRMAS NMR Study. *Beilstein J. Org. Chem.* 10, 2715–2723. doi:10.3762/bjoc.10.286

Figueiras, A., Sarraguça, J. M. G., Carvalho, R. a., Pais, A. A. C. C., and Veiga, F. J. B. (2007). Interaction of Omeprazole with a Methylated Derivative of β-Cyclodextrin: Phase Solubility, NMR Spectroscopy and Molecular Simulation. *Pharm. Res.* 24, 377–389. doi:10.1007/s11095-006-9161-8

Filho, C. M. C., Bueno, P. V. A., Matsushita, A. F. Y., Rubira, A. F., Muniz, E. C., Durães, L., et al. (2018). Synthesis, Characterization and Sorption Studies of Aromatic Compounds by Hydrogels of Chitosan Blended with β-cyclodextrin- and PVA-Functionalized Pectin. *RSC Adv.* 8, 14609–14622. doi:10.1039/C8RA02332H

F. Trotta and A. Mele (Editors) (2019). *Nanosponges: Synthesis and Applications* (Weinheim, Germany, Germany: Wiley VCH).

Gabr, M. M., Mortada, S. M., and Sallam, M. A. (2018). Carboxylate Cross-Linked Cyclodextrin: A Nanoporous Scaffold for Enhancement of Rosuvastatin Oral Bioavailability. *Eur. J. Pharm. Sci.* 111, 1–12. doi:10.1016/j.ejps.2017.09.026

Gangadharappa, H. V., Chandra Prasad, S. M., and Singh, R. P. (2017). Formulation, *In Vitro* and *In Vivo* Evaluation of Celecoxib Nanosponge Hydrogels for Topical Application. *J. Drug Deliv. Sci. Tech.* 41, 488–501. doi:10.1016/j.jddst.2017.09.004

Garrido, B., González, S., Hermosilla, J., Millao, S., Quilaqueo, M., Guineo, J., et al. (2019). Carbonate-β-Cyclodextrin-Based Nanosponge as a Nanoencapsulation System for Piperine: Physicochemical Characterization. *J. Soil Sci. Plant Nutr.* 19, 620–630. doi:10.1007/s42729-019-00062-7

Gholibegloo, E., Mortezazadeh, T., Salehian, F., Forootanfar, H., Firoozpour, L., Foroumadi, A., et al. (2019a). Folic Acid Decorated Magnetic Nanosponge: An Efficient Nanosystem for Targeted Curcumin Delivery and Magnetic Resonance Imaging. *J. Colloid Interf. Sci.* 556, 128–139. doi:10.1016/j.jcis.2019.08.046

Gholibegloo, E., Mortezazadeh, T., Salehian, F., Ramazani, A., Amanlou, M., and Khoobi, M. (2019b). Improved Curcumin Loading, Release, Solubility and Toxicity by Tuning the Molar Ratio of Cross-Linker to β-cyclodextrin. *Carbohydr. Polym.* 213, 70–78. doi:10.1016/j.carbpol.2019.02.075

Gigliotti, C. L., Ferrara, B., Occhipinti, S., Boggio, E., Barrera, G., Pizzimenti, S., et al. (2017). Enhanced Cytotoxic Effect of Camptothecin Nanosponges in Anaplastic Thyroid Cancer Cells *In Vitro* and *In Vivo* on Orthotopic Xenograft Tumors. *Drug Deliv.* 24, 670–680. doi:10.1080/10717544.2017.1303856

Gigliotti, C. L., Minelli, R., Cavalli, R., Occhipinti, S., Barrera, G., Pizzimenti, S., et al. (2016). *In Vitro* and *In Vivo* Therapeutic Evaluation of Camptothecin-Encapsulated β-Cyclodextrin Nanosponges in Prostate Cancer. *J. Biomed. Nanotechnol.* 12, 114–127. doi:10.1166/jbn.2016.2144

Gómez-Graña, S., Pérez-Juste, J., and Hervés, P. (2021). Cyclodextrins and Inorganic Nanoparticles: Another Tale of Synergy. *Adv. Colloid Interf. Sci.* 288, 102338. doi:10.1016/j.cis.2020.102338

Gómez-Morte, T., Gómez-López, V. M., Lucas-Abellán, C., Martínez-Alcalá, I., Ayuso, M., Martínez-López, S., et al. (2021). Removal and Toxicity Evaluation of a Diverse Group of Drugs from Water by a Cyclodextrin Polymer/pulsed Light System. *J. Hazard. Mater.* 402, 123504. doi:10.1016/j.jhazmat.2020.123504

Gonzalez Pereira, A., Carpena, M., García Oliveira, P., Mejuto, J. C., Prieto, M. A., and Simal Gandara, J. (2021). Main Applications of Cyclodextrins in the Food Industry as the Compounds of Choice to Form Host-Guest Complexes. *Ijms* 22, 1339. doi:10.3390/ijms22031339

Guineo-Alvarado, J., Quilaqueo, M., Hermosilla, J., González, S., Medina, C., Rolleri, A., et al. (2021). Degree of Crosslinking in β-cyclodextrin-based Nanosponges and Their Effect on Piperine Encapsulation. *Food Chem.* 340, 128132. doi:10.1016/j.foodchem.2020.128132

Gupta, B., Dalal, P., and Rao, R. (2021). Cyclodextrin Decorated Nanosponges of Sesamol: Antioxidant, Anti-tyrosinase and Photostability Assessment. *Food Biosci.* 42, 101098. doi:10.1016/j.fbio.2021.101098

He, J., Li, Y., Wang, C., Zhang, K., Lin, D., Kong, L., et al. (2017). Rapid Adsorption of Pb, Cu and Cd from Aqueous Solutions by β-cyclodextrin Polymers. *Appl. Surf. Sci.* 426, 29–39. doi:10.1016/j.apsusc.2017.07.103

Hong, Y., Lam, J. W. Y., and Tang, B. Z. (2009). Aggregation-induced Emission: Phenomenon, Mechanism and Applications. *Chem. Commun.* 2009, 4332. doi:10.1039/b904665h

Hoti, G., Caldera, F., Cecone, C., Rubin Pedrazzo, A., Anceschi, A., Appleton, S. L., et al. (2021). Effect of the Cross-Linking Density on the Swelling and Rheological Behavior of Ester-Bridged β-Cyclodextrin Nanosponges. *Materials* 14, 478. doi:10.3390/ma14030478

Houk, K. N., Leach, A. G., Kim, S. P., and Zhang, X. (2003). Binding Affinities of Host-Guest, Protein-Ligand, and Protein-Transition-State Complexes. *Angew. Chem. Int. Ed.* 42, 4872–4897. doi:10.1002/anie.200200565

Huang, Q., Chai, K., Zhou, L., and Ji, H. (2020). A Phenyl-Rich β-cyclodextrin Porous Crosslinked Polymer for Efficient Removal of Aromatic Pollutants: Insight into Adsorption Performance and Mechanism. *Chem. Eng. J.* 387, 124020. doi:10.1016/j.cej.2020.124020

Iriventi, P., Gupta, N. V., Osmani, R. A. M., and Balamuralidhara, V. (2020). Design & Development of Nanosponge Loaded Topical Gel of Curcumin and Caffeine Mixture for Augmented Treatment of Psoriasis. *DARU J. Pharm. Sci.* 28, 489–506. doi:10.1007/s40199-020-00352-x

Jafari Nasab, M., Kiasat, A. R., and Zarasvandi, R. (2018). β-Cyclodextrin Nanosponge Polymer: a Basic and Eco-Friendly Heterogeneous Catalyst for the One-Pot Four-Component Synthesis of Pyranopyrazole Derivatives under Solvent-free Conditions. *Reac Kinet Mech. Cat* 124, 767–778. doi:10.1007/s11144-018-1373-5

Jain, A., Prajapati, S. K., Kumari, A., Mody, N., and Bajpai, M. (2020). Engineered Nanosponges as Versatile Biodegradable Carriers: An Insight. *J. Drug Deliv. Sci. Tech.* 57, 101643. doi:10.1016/j.jddst.2020.101643

Jasim, I. K. S., Abd Alhammid, S., and Abdulrasool, A. (2020). Synthesis and Evaluation of B-Cyclodextrin Based Nanosponges of 5- Fluorouracil by Using Ultrasound Assisted Method. *Ijps* 29, 88–98. doi:10.31351/vol29iss2pp88-98

Jicsinszky, L., and Cravotto, G. (2021). Toward a Greener World-Cyclodextrin Derivatization by Mechanochemistry. *Molecules* 26, 5193. doi:10.3390/molecules26175193

Kardooni, R., Kiasat, A. R., and Eskandari Sabzi, N. (2020). Hyper-cross-linked β-cyclodextrin Nanosponge: a Three-Dimensional, Porous and Biodegradable Catalyst in the One-Pot Synthesis of Kojic Acid-Based Heterocyclic Compounds. *Res. Chem. Intermed.* 46, 1857–1868. doi:10.1007/s11164-019-04067-w

Kawano, S., Kida, T., Miyawaki, K., Fukuda, Y., Kato, E., Nakano, T., et al. (2015). Adsorption Capability of Urethane-Crosslinked Heptakis(2,6-Di-O-Methyl)-β-Cyclodextrin Polymers toward Polychlorobiphenyls in Nonpolar Organic media. *Polym. J.* 47, 443–448. doi:10.1038/pj.2015.13

Khajeh Dangolani, S., Sharifat, S., Panahi, F., and Khalafi-Nezhad, A. (2019). Immobilized Palladium Nanoparticles on a Cyclodextrin-Polyurethane Nanosponge (Pd-CD-PU-NS): An Efficient Catalyst for Cyanation Reaction in Aqueous media. *Inorg. Chim. Acta* 494, 256–265. doi:10.1016/j.ica.2019.05.021

Khalid, Q., Ahmad, M., Minhas, M. U., Batool, F., Malik, N. S., and Rehman, M. (2021). Novel β-cyclodextrin Nanosponges by Chain Growth Condensation for Solubility Enhancement of Dexibuprofen: Characterization and Acute Oral Toxicity Studies. *J. Drug Deliv. Sci. Tech.* 61, 102089. doi:10.1016/j.jddst.2020.102089

Klemes, M. J., Ling, Y., Chiapasco, M., Alsbaiee, A., Helbling, D. E., and Dichtel, W. R. (2018). Phenolation of Cyclodextrin Polymers Controls Their lead and

Organic Micropollutant Adsorption. *Chem. Sci.* 9, 8883–8889. doi:10.1039/C8SC03267J

Krabicová, I., Appleton, S. L., Tannous, M., Hoti, G., Caldera, F., Rubin Pedrazzo, A., et al. (2020). History of Cyclodextrin Nanosponges. *Polymers* 12, 1122. doi:10.3390/polym12051122

Kumar, A., and Rao, R. (2021a). Enhancing Efficacy and Safety of Azelaic Acid via Encapsulation in Cyclodextrin Nanosponges: Development, Characterization and Evaluation. *Polym. Bull.* 78, 5275–5302. doi:10.1007/s00289-020-03366-2

Kumar, A., and Rao, R. (2022). Formulation and Modification of Physicochemical Parameters of P-Coumaric Acid by Cyclodextrin Nanosponges. *J. Incl. Phenom. Macrocycl. Chem.* 102, 313–326. doi:10.1007/s10847-021-01121-2

Kumar, S., Dalal, P., and Rao, R. (2020). "Cyclodextrin Nanosponges: A Promising Approach for Modulating Drug Delivery," in *Colloid Science in Pharmaceutical Nanotechnology* (London: IntechOpen). doi:10.5772/intechopen.90365

Kumar, S., Prasad, M., and Rao, R. (2021). Topical Delivery of Clobetasol Propionate Loaded Nanosponge Hydrogel for Effective Treatment of Psoriasis: Formulation, Physicochemical Characterization, Antipsoriatic Potential and Biochemical Estimation. *Mater. Sci. Eng. C* 119, 111605. doi:10.1016/j.msec.2020.111605

Kumar, S., and Rao, R. (2019). Analytical Tools for Cyclodextrin Nanosponges in Pharmaceutical Field: a Review. *J. Incl. Phenom. Macrocycl. Chem.* 94, 11–30. doi:10.1007/s10847-019-00903-z

Kumar, S., and Rao, R. (2021b). Novel Dithranol Loaded Cyclodextrin Nanosponges for Augmentation of Solubility, Photostability and Cytocompatibility. *Cnano* 17, 747–761. doi:10.2174/1573413716666201215165552

Kumari, P., Singh, P., and Singhal, A. (2020). Cyclodextrin-based Nanostructured Materials for Sustainable Water Remediation Applications. *Environ. Sci. Pollut. Res.* 27, 32432–32448. doi:10.1007/s11356-020-09519-0

Lai, X., Zeng, X., Li, H., Yin, C., Zhang, H., and Liao, F. (2012). Synergistic Effect of Phosphorus-Containing Nanosponges on Intumescent Flame-Retardant Polypropylene. *J. Appl. Polym. Sci.* 125, 1758–1765. doi:10.1002/app.35646

Lakkakula, J., and Krause, R. W. M. (2013). "Cyclodextrin-Based Nanoengineered Drug Delivery System," in *Nanomedicine for Drug Delivery and Therapeutics* (Springer), 311–335. doi:10.1002/9781118636299.ch11

Larin, A. O., Nominé, A., Ageev, E. I., Ghanbaja, J., Kolotova, L. N., Starikov, S. V., et al. (2020). Plasmonic Nanosponges Filled with Silicon for Enhanced white Light Emission. *Nanoscale* 12, 1013–1021. doi:10.1039/C9NR08952G

Lellis, B., Fávaro-Polonio, C. Z., Pamphile, J. A., and Polonio, J. C. (2019). Effects of Textile Dyes on Health and the Environment and Bioremediation Potential of Living Organisms. *Biotechnol. Res. Innovation* 3, 275–290. doi:10.1016/j.biori.2019.09.001

Lembo, D., Swaminathan, S., Donalisio, M., Civra, A., Pastero, L., Aquilano, D., et al. (2013). Encapsulation of Acyclovir in New Carboxylated Cyclodextrin-Based Nanosponges Improves the Agent's Antiviral Efficacy. *Int. J. Pharmaceutics* 443, 262–272. doi:10.1016/j.ijpharm.2012.12.031

Lembo, D., Trotta, F., and Cavalli, R. (2018). Cyclodextrin-based Nanosponges as Vehicles for Antiviral Drugs: Challenges and Perspectives. *Nanomedicine* 13, 477–480. doi:10.2217/nnm-2017-0383

Leudjo Taka, A., Doyle, B. P., Carleschi, E., Youmbi Fonkui, T., Erasmus, R., Fosso-Kankeu, E., et al. (2020). Spectroscopic Characterization and Antimicrobial Activity of Nanoparticle Doped Cyclodextrin Polyurethane Bionanosponge. *Mater. Sci. Eng. C* 115, 111092. doi:10.1016/j.msec.2020.111092

Li, C., Klemes, M. J., Dichtel, W. R., and Helbling, D. E. (2018a). Tetrafluoroterephthalonitrile-crosslinked β-cyclodextrin Polymers for Efficient Extraction and Recovery of Organic Micropollutants from Water. *J. Chromatogr. A* 1541, 52–56. doi:10.1016/j.chroma.2018.02.012

Li, X., Zhou, M., Jia, J., and Jia, Q. (2018b). A Water-Insoluble Viologen-Based β -cyclodextrin Polymer for Selective Adsorption toward Anionic Dyes. *Reactive Funct. Polym.* 126, 20–26. doi:10.1016/j.reactfunctpolym.2018.03.004

Liu, H., Cai, X., Wang, Y., and Chen, J. (2011). Adsorption Mechanism-Based Screening of Cyclodextrin Polymers for Adsorption and Separation of Pesticides from Water. *Water Res.* 45, 3499–3511. doi:10.1016/j.watres.2011.04.004

Liu, Q., Zhou, Y., Lu, J., and Zhou, Y. (2020a). Novel Cyclodextrin-Based Adsorbents for Removing Pollutants from Wastewater: A Critical Review. *Chemosphere* 241, 125043. doi:10.1016/j.chemosphere.2019.125043

Liu, S., Ruspic, C., Mukhopadhyay, P., Chakrabarti, S., Zavalij, P. Y., and Isaacs, L. (2005). The Cucurbit[n]uril Family: Prime Components for Self-Sorting Systems. *J. Am. Chem. Soc.* 127, 15959–15967. doi:10.1021/ja055013x

Liu, X., Li, W., and Xuan, G. (2020b). Preparation and Characterization of β-Cyclodextrin Nanosponges and Study on Enhancing the Solubility of Insoluble Nicosulfuron. *IOP Conf. Ser. Mater. Sci. Eng.* 774, 012108. doi:10.1088/1757-899X/774/1/012108

Lo Meo, P., Lazzara, G., Liotta, L., Riela, S., and Noto, R. (2014). Cyclodextrin-calixarene Co-polymers as a New Class of Nanosponges. *Polym. Chem.* 5, 4499–4510. doi:10.1039/C4PY00325J

Lo Meo, P., Mundo, F., Terranova, S., Conte, P., and Chillura Martino, D. (2020). Water Dynamics at the Solid-Liquid Interface to Unveil the Textural Features of Synthetic Nanosponges. *J. Phys. Chem. B* 124, 1847–1857. doi:10.1021/acs.jpcb.9b11935

Loftsson, T., and Brewster, M. E. (1996). Pharmaceutical Applications of Cyclodextrins. 1. Drug Solubilization and Stabilization. *J. Pharm. Sci.* 85, 1017–1025. doi:10.1021/js950534b

Loftsson, T., and Duchene, D. (2007). Cyclodextrins and Their Pharmaceutical Applications. *Int. J. Pharmaceutics* 329, 1–11. doi:10.1016/j.ijpharm.2006.10.044

Lu, P., Cheng, J., Li, Y., Li, L., Wang, Q., and He, C. (2019). Novel Porous β-cyclodextrin/pillar[5]arene Copolymer for Rapid Removal of Organic Pollutants from Water. *Carbohydr. Polym.* 216, 149–156. doi:10.1016/j.carbpol.2019.04.015

Manaf, N. A., Saad, B., Mohamed, M. H., Wilson, L. D., and Latiff, A. A. (2018). Cyclodextrin Based Polymer Sorbents for Micro-solid Phase Extraction Followed by Liquid Chromatography Tandem Mass Spectrometry in Determination of Endogenous Steroids. *J. Chromatogr. A* 1543, 23–33. doi:10.1016/j.chroma.2018.02.032

Mane, P. T., Wakure, B. S., and Wakte, P. S. (2021). Cyclodextrin Based Nanosponges: A Multidimensional Drug Delivery System and its Biomedical Applications. *Cdd* 18, 1467–1493. doi:10.2174/1567201818666210423091250

Martwong, E., Chuetor, S., and Junthip, J. (2022). Adsorption of Cationic Contaminants by Cyclodextrin Nanosponges Cross-Linked with 1,2,3,4-Butanetetracarboxylic Acid and Poly(vinyl Alcohol). *Polymers* 14, 342. doi:10.3390/polym14020342

Martwong, E., Chuetor, S., and Junthip, J. (2021). Adsorption of Paraquat by Poly(Vinyl Alcohol)-Cyclodextrin Nanosponges. *Polymers* 13, 4110. doi:10.3390/polym13234110

Mashaqbeh, H., Obaidat, R., and Al-Shar'i, N. (2021). Evaluation and Characterization of Curcumin-β-Cyclodextrin and Cyclodextrin-Based Nanosponge Inclusion Complexation. *Polymers* 13, 4073. doi:10.3390/polym13234073

Matencio, A., Dhakar, N. K., Bessone, F., Musso, G., Cavalli, R., Dianzani, C., et al. (2020a). Study of Oxyresveratrol Complexes with Insoluble Cyclodextrin Based Nanosponges: Developing a Novel Way to Obtain Their Complexation Constants and Application in an Anticancer Study. *Carbohydr. Polym.* 231, 115763. doi:10.1016/j.carbpol.2019.115763

Matencio, A., Guerrero-Rubio, M. A., Caldera, F., Cecone, C., Trotta, F., García-Carmona, F., et al. (2020b). Lifespan Extension in *Caenorhabditis elegans* by Oxyresveratrol Supplementation in Hyper-Branched Cyclodextrin-Based Nanosponges. *Int. J. Pharmaceutics* 589, 119862. doi:10.1016/j.ijpharm.2020.119862

Matencio, A., Navarro-Orcajada, S., García-Carmona, F., and López-Nicolás, J. M. (2020c). Applications of Cyclodextrins in Food Science. A Review. *Trends Food Sci. Tech.* 104, 132–143. doi:10.1016/j.tifs.2020.08.009

Mendes, C., Meirelles, G. C., Barp, C. G., Assreuy, J., Silva, M. A. S., and Ponchel, G. (2018). Cyclodextrin Based Nanosponge of Norfloxacin: Intestinal Permeation Enhancement and Improved Antibacterial Activity. *Carbohydr. Polym.* 195, 586–592. doi:10.1016/j.carbpol.2018.05.011

Menezes, P. d. P., Andrade, T. d. A., Frank, L. A., de Souza, E. P. B. S. S., Trindadedas, G. d. G. G. G. G., Trindade, I. A. S., et al. (2019). Advances of Nanosystems Containing Cyclodextrins and Their Applications in Pharmaceuticals. *Int. J. Pharmaceutics* 559, 312–328. doi:10.1016/j.ijpharm.2019.01.041

Messner, M., Kurkov, S. V., Jansook, P., and Loftsson, T. (2010). Self-assembled Cyclodextrin Aggregates and Nanoparticles. *Int. J. Pharmaceutics* 387, 199–208. doi:10.1016/j.ijpharm.2009.11.035

Mhlanga, S. D., Mamba, B. B., Krause, R. W., and Malefetse, T. J. (2007). Removal of Organic Contaminants from Water Using Nanosponge Cyclodextrin Polyurethanes. *J. Chem. Technol. Biotechnol.* 82, 382–388. doi:10.1002/jctb.1681

Minelli, R., Cavalli, R., Ellis, L., Pettazzoni, P., Trotta, F., Ciamporcero, E., et al. (2012). Nanosponge-encapsulated Camptothecin Exerts Anti-tumor Activity in Human Prostate Cancer Cells. *Eur. J. Pharm. Sci.* 47, 686–694. doi:10.1016/j.ejps.2012.08.003

Mocanu, G., Vizitiu, D., and Carpov, A. (2001). Cyclodextrin Polymers. *J. Bioactive Compatible Polym.* 16, 315–342. doi:10.1106/JJUV-8F2K-JGYF-HNGF

Mognetti, B., Barberis, A., Marino, S., Berta, G., Francia, S., Trotta, F., et al. (2012). *In Vitro* enhancement of Anticancer Activity of Paclitaxel by a Cremophor Free Cyclodextrin-Based Nanosponge Formulation. *J. Incl. Phenom. Macrocycl. Chem.* 74, 201–210. doi:10.1007/s10847-011-0101-9

Moin, A., Roohi, N. K. F., Rizvi, S. M. D., Ashraf, S. A., Siddiqui, A. J., Patel, M., et al. (2020). Design and Formulation of Polymeric Nanosponge Tablets with Enhanced Solubility for Combination Therapy. *RSC Adv.* 10, 34869–34884. doi:10.1039/D0RA06611G

Möller, K., Macaulay, B., and Bein, T. (2021). Curcumin Encapsulated in Crosslinked Cyclodextrin Nanoparticles Enables Immediate Inhibition of Cell Growth and Efficient Killing of Cancer Cells. *Nanomaterials* 11, 489. doi:10.3390/nano11020489

Momin, M. M., Zaheer, Z., Zainuddin, R., and Sangshetti, J. N. (2018). Extended Release Delivery of Erlotinib Glutathione Nanosponge for Targeting Lung Cancer. *Artif. Cell Nanomedicine, Biotechnol.* 46, 1064–1075. doi:10.1080/21691401.2017.1360324

Morin-Crini, N., Winterton, P., Fourmentin, S., Wilson, L. D., Fenyvesi, É., and Crini, G. (2018). Water-insoluble β-cyclodextrin-epichlorohydrin Polymers for Removal of Pollutants from Aqueous Solutions by Sorption Processes Using Batch Studies: A Review of Inclusion Mechanisms. *Prog. Polym. Sci.* 78, 1–23. doi:10.1016/j.progpolymsci.2017.07.004

Moulahcene, L., Skiba, M., Senhadji, O., Milon, N., Benamor, M., and Lahiani-Skiba, M. (2015). Inclusion and Removal of Pharmaceutical Residues from Aqueous Solution Using Water-Insoluble Cyclodextrin Polymers. *Chem. Eng. Res. Des.* 97, 145–158. doi:10.1016/j.cherd.2014.08.023

Murcia-Salvador, A., Pellicer, J. A., Fortea, M. I., Gómez-López, V. M., Rodríguez-López, M. I., Núñez-Delicado, E., et al. (2019). Adsorption of Direct Blue 78 Using Chitosan and Cyclodextrins as Adsorbents. *Polymers* 11, 1003. doi:10.3390/polym11061003

Nait Bachir, Y., Nait Bachir, R., Hadj-Ziane-Zafour, A., Bachir, Y. N., Bachir, R. N., and Hadj-Ziane-Zafour, A. (2019). Nanodispersions Stabilized by β-cyclodextrin Nanosponges: Application for Simultaneous Enhancement of Bioactivity and Stability of Sage Essential Oil. *Drug Dev. Ind. Pharm.* 45, 333–347. doi:10.1080/03639045.2018.1542705

Nazerdeylami, S., Ghasemi, J. B., Mohammadi Ziarani, G., Amiri, A., and Badiei, A. (2021). Direct Monitoring of Diclofenac Using a Supramolecular Fluorescent Approach Based on β-cyclodextrin Nanosponge. *J. Mol. Liquids* 336, 116104. doi:10.1016/j.molliq.2021.116104

Neva, T., Carmona, T., Benito, J. M., Przybylski, C., Ortiz Mellet, C., Mendicuti, F., et al. (2019). Dynamic Control of the Self-Assembling Properties of Cyclodextrins by the Interplay of Aromatic and Host-Guest Interactions. *Front. Chem.* 7. doi:10.3389/fchem.2019.00072

Noothi, S., Malothu, N., Kulandaivelu, U., Rao, G. K. G. K., Alavala, R. R., and Pulavarthy, V. (2020). Preparation and Evaluation of Simvastatin Nanosponges. *ijpr* 12, 855–861. doi:10.31838/ijpr/2020.12.03.047

Olteanu, A. A., Aramă, C.-C., Radu, C., Mihăescu, C., Monciu, C.-M., Aramə, C. C., et al. (2014). Effect of β-cyclodextrins Based Nanosponges on the Solubility of Lipophilic Pharmacological Active Substances (Repaglinide). *J. Incl. Phenom. Macrocycl. Chem.* 80, 17–24. doi:10.1007/s10847-014-0406-6

Omar, S. M., Ibrahim, F., and Ismail, A. (2020). Formulation and Evaluation of Cyclodextrin-Based Nanosponges of Griseofulvin as Pediatric Oral Liquid Dosage Form for Enhancing Bioavailability and Masking Bitter Taste. *Saudi Pharm. J.* 28, 349–361. doi:10.1016/j.jsps.2020.01.016

Osmani, R. A., Kulkarni, P., Manjunatha, S., Vaghela, R., and Bhosale, R. (2018). "Cyclodextrin Nanosponge-Based Systems in Drug Delivery and Nanotherapeutics," in *Organic Materials as Smart Nanocarriers for Drug Delivery* (Elsevier), 659–717. doi:10.1016/B978-0-12-813663-8.00016-6

Palminteri, M., Dhakar, N. K., Ferraresi, A., Caldera, F., Vidoni, C., Trotta, F., et al. (2021). Cyclodextrin Nanosponge for the GSH-Mediated Delivery of Resveratrol in Human Cancer Cells. *Nanotheranostics* 5, 197–212. doi:10.7150/ntno.53888

Pawar, S., and Shende, P. (2020a). A Comprehensive Patent Review on β-cyclodextrin Cross-Linked Nanosponges for Multiple Applications. *Nanotec* 14, 75–89. doi:10.2174/1872210513666190603083930

Pawar, S., and Shende, P. (2021). Design and Optimization of Cyclodextrin-Based Nanosponges of Antimalarials Using central Composite Design for Dry Suspension. *J. Incl. Phenom. Macrocycl. Chem.* 99, 169–183. doi:10.1007/s10847-020-01038-2

Pawar, S., and Shende, P. (2020b). Dual Drug Delivery of Cyclodextrin Cross-Linked Artemether and Lumefantrine Nanosponges for Synergistic Action Using 23 Full Factorial Designs. *Colloids Surf. A: Physicochemical Eng. Aspects* 602, 125049. doi:10.1016/j.colsurfa.2020.125049

Pawar, S., Shende, P., and Trotta, F. (2019). Diversity of β-cyclodextrin-based Nanosponges for Transformation of Actives. *Int. J. Pharmaceutics* 565, 333–350. doi:10.1016/j.ijpharm.2019.05.015

Pei, M., Pai, J.-Y., Du, P., and Liu, P. (2018). Facile Synthesis of Fluorescent Hyper-Cross-Linked β-Cyclodextrin-Carbon Quantum Dot Hybrid Nanosponges for Tumor Theranostic Application with Enhanced Antitumor Efficacy. *Mol. Pharmaceutics* 15, 4084–4091. doi:10.1021/acs.molpharmaceut.8b00508

Pellicer, J. A., Rodríguez-López, M. I., Fortea, M. I., Gabaldón Hernández, J. A., Lucas-Abellán, C., Mercader-Ros, M. T., et al. (2018). Removing of Direct Red 83:1 Using α- and HP-α-CDs Polymerized with Epichlorohydrin: Kinetic and Equilibrium Studies. *Dyes Pigm.* 149, 736–746. doi:10.1016/j.dyepig.2017.11.032

Pivato, R. V., Rossi, F., Ferro, M., Castiglione, F., Trotta, F., and Mele, A. (2021). β-Cyclodextrin Nanosponge Hydrogels as Drug Delivery Nanoarchitectonics for Multistep Drug Release Kinetics. *ACS Appl. Polym. Mater.* 3, 6562–6571. doi:10.1021/acsapm.1c01262

Prochowicz, D., Kornowicz, A., and Lewiński, J. (2017). Interactions of Native Cyclodextrins with Metal Ions and Inorganic Nanoparticles: Fertile Landscape for Chemistry and Materials Science. *Chem. Rev.* 117, 13461–13501. doi:10.1021/acs.chemrev.7b00231

Pushpalatha, R., Selvamuthukumar, S., and Kilimozhi, D. (2018a). Carbonyl and Carboxylate Crosslinked Cyclodextrin as a Nanocarrier for Resveratrol: In Silico, *In Vitro* and *In Vivo* Evaluation. *J. Incl. Phenom. Macrocycl. Chem.* 92, 261–272. doi:10.1007/s10847-018-0843-8

Pushpalatha, R., Selvamuthukumar, S., and Kilimozhi, D. (2018b). Cross-linked, Cyclodextrin-Based Nanosponges for Curcumin Delivery - Physicochemical Characterization, Drug Release, Stability and Cytotoxicity. *J. Drug Deliv. Sci. Tech.* 45, 45–53. doi:10.1016/j.jddst.2018.03.004

Pushpalatha, R., Selvamuthukumar, S., and Kilimozhi, D. (2019). Cyclodextrin Nanosponge Based Hydrogel for the Transdermal Co-delivery of Curcumin and Resveratrol: Development, Optimization, *In Vitro* and *Ex Vivo* Evaluation. *J. Drug Deliv. Sci. Tech.* 52, 55–64. doi:10.1016/j.jddst.2019.04.025

Qin, X., Bai, L., Tan, Y., Li, L., Song, F., and Wang, Y. (2019). β-Cyclodextrin-crosslinked Polymeric Adsorbent for Simultaneous Removal and Stepwise Recovery of Organic Dyes and Heavy Metal Ions: Fabrication, Performance and Mechanisms. *Chem. Eng. J.* 372, 1007–1018. doi:10.1016/j.cej.2019.05.006

Rafati, N., Zarrabi, A., Caldera, F., Trotta, F., and Ghias, N. (2019). Pyromellitic Dianhydride Crosslinked Cyclodextrin Nanosponges for Curcumin Controlled Release; Formulation, Physicochemical Characterization and Cytotoxicity Investigations. *J. Microencapsulation* 36, 715–727. doi:10.1080/02652048.2019.1669728

Rajbanshi, B., Saha, S., Das, K., Barman, B. K., Sengupta, S., Bhattacharjee, A., et al. (2018). Study to Probe Subsistence of Host-Guest Inclusion Complexes of α and β-Cyclodextrins with Biologically Potent Drugs for Safety Regulatory Dischargement. *Sci. Rep.* 8, 13031. doi:10.1038/s41598-018-31373-x

Ramírez-Ambrosi, M., Caldera, F., Trotta, F., Berrueta, L. Á., and Gallo, B. (2014). Encapsulation of Apple Polyphenols in β-CD Nanosponges. *J. Incl. Phenom. Macrocycl. Chem.* 80, 85–92. doi:10.1007/s10847-014-0393-7

Rao, M., Bajaj, A., Khole, I., Munjapara, G., and Trotta, F. (2013). *In Vitro* and *In Vivo* Evaluation of β-cyclodextrin-based Nanosponges of Telmisartan. *J. Incl. Phenom. Macrocycl. Chem.* 77, 135–145. doi:10.1007/s10847-012-0224-7

Rao, M. R. P., Chaudhari, J., Trotta, F., and Caldera, F. (2018). Investigation of Cyclodextrin-Based Nanosponges for Solubility and Bioavailability

Enhancement of Rilpivirine. *AAPS PharmSciTech* 19, 2358–2369. doi:10.1208/s12249-018-1064-6

Raoov, M., Mohamad, S., and Abas, M. (2014). Synthesis and Characterization of β-Cyclodextrin Functionalized Ionic Liquid Polymer as a Macroporous Material for the Removal of Phenols and As(V). *Ijms* 15, 100–119. doi:10.3390/ijms15010100

Real, D. A., Bolaños, K., Priotti, J., Yutronic, N., Kogan, M. J., Sierpe, R., et al. (2021). Cyclodextrin-Modified Nanomaterials for Drug Delivery: Classification and Advances in Controlled Release and Bioavailability. *Pharmaceutics* 13, 2131. doi:10.3390/pharmaceutics13122131

Rezaei, A., Khavari, S., and Sami, M. (2021). Incorporation of Thyme Essential Oil into the β-cyclodextrin Nanosponges: Preparation, Characterization and Antibacterial Activity. *J. Mol. Struct.* 1241, 130610. doi:10.1016/j.molstruc.2021.130610

Rezaei, A., Varshosaz, J., Fesharaki, M., Farhang, A., and Jafari, S. M. (2019). Improving the Solubility and *In Vitro* Cytotoxicity (Anticancer Activity) of Ferulic Acid by Loading it into Cyclodextrin Nanosponges. *Ijn* 14, 4589–4599. doi:10.2147/IJN.S206350

Ribeiro, A. C. F., Esteso, M. A., Lobo, V. M. M., Valente, A. J. M., Simões, S. M. N., Sobral, A. J. F. N., et al. (2006). Interactions of Copper (II) Chloride with β-Cyclodextrin in Aqueous Solutions. *J. Carbohydr. Chem.* 25, 173–185. doi:10.1080/07328300600732469

Rizzi, V., Gubitosa, J., Signorile, R., Fini, P., Cecone, C., Matencio, A., et al. (2021). Cyclodextrin Nanosponges as Adsorbent Material to Remove Hazardous Pollutants from Water: The Case of Ciprofloxacin. *Chem. Eng. J.* 411, 128514. doi:10.1016/j.cej.2021.128514

Romita, R., Rizzi, V., Semeraro, P., Gubitosa, J., Gabaldón, J. A., Gorbe, M. I. F., et al. (2019). Operational Parameters Affecting the Atrazine Removal from Water by Using Cyclodextrin Based Polymers as Efficient Adsorbents for Cleaner Technologies. *Environ. Tech. Innovation* 16, 100454. doi:10.1016/j.eti.2019.100454

Rubin Pedrazzo, A., Caldera, F., Zanetti, M., Appleton, S. L., Dhakar, N. K., and Trotta, F. (2020). Mechanochemical green Synthesis of Hyper-Crosslinked Cyclodextrin Polymers. *Beilstein J. Org. Chem.* 16, 1554–1563. doi:10.3762/bjoc.16.127

Rubin Pedrazzo, A., Smarra, A., Caldera, F., Musso, G., Dhakar, N. K., Cecone, C., et al. (2019). Eco-Friendly β-cyclodextrin and Linecaps Polymers for the Removal of Heavy Metals. *Polymers* 11, 1658. doi:10.3390/polym11101658

Rubin Pedrazzo, A., Trotta, F., Hoti, G., Cesano, F., and Zanetti, M. (2022). Sustainable Mechanochemical Synthesis of β-cyclodextrin Polymers by Twin Screw Extrusion. *Environ. Sci. Pollut. Res.* 29, 251–263. doi:10.1007/s11356-021-15187-5

Russo, M., Saladino, M. L., Chillura Martino, D., Lo Meo, P., and Noto, R. (2016). Polyaminocyclodextrin Nanosponges: Synthesis, Characterization and pH-Responsive Sequestration Abilities. *RSC Adv.* 6, 49941–49953. doi:10.1039/C6RA06417E

Russo, M., Spinella, A., Di Vincenzo, A., Lazzara, G., Correro, M. R., Shahgaldian, P., et al. (2019). Synergistic Activity of Silver Nanoparticles and Polyaminocyclodextrins in Nanosponge Architectures. *ChemistrySelect* 4, 873–879. doi:10.1002/slct.201803424

Subramanian, S., Krishnamoorthy, K., and Rajappan, M. (2012). Nanosponges: A Novel Class of Drug Delivery System - Review. *J. Pharm. Pharm. Sci.* 15, 103–111. doi:10.18433/j3k308

Sabzi, N. E., and Kiasat, A. R. (2018). β-Cyclodextrin Based Nanosponge as a Biodegradable Porous Three-Dimensional Nanocatalyst in the One-Pot Synthesis of N- Containing Organic Scaffolds. *Catal. Lett.* 148, 2654–2664. doi:10.1007/s10562-018-2484-3

Sadjadi, S., Heravi, M. M., and Daraie, M. (2017a). A Novel Hybrid Catalytic System Based on Immobilization of Phosphomolybdic Acid on Ionic Liquid Decorated Cyclodextrin-Nanosponges: Efficient Catalyst for the green Synthesis of Benzochromeno-Pyrazole through cascade Reaction: Triply green. *J. Mol. Liquids* 231, 98–105. doi:10.1016/j.molliq.2017.01.072

Sadjadi, S., Heravi, M. M., and Daraie, M. (2017b). Cyclodextrin Nanosponges: a Potential Catalyst and Catalyst Support for Synthesis of Xanthenes. *Res. Chem. Intermed.* 43, 843–857. doi:10.1007/s11164-016-2668-7

Sadjadi, S., Heravi, M. M., and Malmir, M. (2018a). Bio-assisted Synthesized Ag(0) Nanoparticles Immobilized on SBA-15/cyclodextrin Nanosponge Adduct: Efficient Heterogeneous Catalyst for the Ultrasonic-Assisted Synthesis of Benzopyranopyrimidines. *Appl. Organometal Chem.* 32, e4286. doi:10.1002/aoc.4286

Sadjadi, S., Heravi, M. M., and Malmir, M. (2018b). Pd@HNTs-CDNS-g-C3N4: A Novel Heterogeneous Catalyst for Promoting Ligand and Copper-free Sonogashira and Heck Coupling Reactions, Benefits from Halloysite and Cyclodextrin Chemistry and G-C3n4 Contribution to Suppress Pd Leaching. *Carbohydr. Polym.* 186, 25–34. doi:10.1016/j.carbpol.2018.01.023

Sadjadi, S., Heravi, M. M., and Raja, M. (2019a). Composite of Ionic Liquid Decorated Cyclodextrin Nanosponge, Graphene Oxide and Chitosan: A Novel Catalyst Support. *Int. J. Biol. Macromolecules* 122, 228–237. doi:10.1016/j.ijbiomac.2018.10.160

Sadjadi, S., Heravi, M. M., Raja, M., and Kahangi, F. G. (2018c). Palladium Nanoparticles Immobilized on Sepiolite-Cyclodextrin Nanosponge Hybrid: Efficient Heterogeneous Catalyst for Ligand- and Copper-free C─C Coupling Reactions. *Appl. Organometal Chem.* 32, e4508. doi:10.1002/aoc.4508

Sadjadi, S., and Koohestani, F. (2021a). Composite of Cross-Linked Chitosan Beads and a Cyclodextrin Nanosponge: A Metal-free Catalyst for Promoting Ultrasonic-Assisted Chemical Transformations in Aqueous media. *J. Phys. Chem. Sol.* 156, 110157. doi:10.1016/j.jpcs.2021.110157

Sadjadi, S., and Koohestani, F. (2021b). Palladated Composite of MOF and Cyclodextrin Nanosponge: A Novel Catalyst for Hydrogenation Reaction. *J. Mol. Struct.* 1245, 131068. doi:10.1016/j.molstruc.2021.131068

Sadjadi, S., Malmir, M., Heravi, M. M., and Raja, M. (2019b). Magnetic Hybrid of Cyclodextrin Nanosponge and Polyhedral Oligomeric Silsesquioxane: Efficient Catalytic Support for Immobilization of Pd Nanoparticles. *Int. J. Biol. Macromolecules* 128, 638–647. doi:10.1016/j.ijbiomac.2019.01.181

Saenger, W., Jacob, J., Gessler, K., Steiner, T., Hoffmann, D., Sanbe, H., et al. (1998). Structures of the Common Cyclodextrins and Their Larger AnaloguesBeyond the Doughnut. *Chem. Rev.* 98, 1787–1802. doi:10.1021/cr9700181

Salazar, S., Guerra, D., Yutronic, N., and Jara, P. (2018). Removal of Aromatic Chlorinated Pesticides from Aqueous Solution Using β-Cyclodextrin Polymers Decorated with Fe3O4 Nanoparticles. *Polymers* 10, 1038. doi:10.3390/polym10091038

Salazar, S., Yutronic, N., and Jara, P. (2020). Magnetic β-Cyclodextrin Nanosponges for Potential Application in the Removal of the Neonicotinoid Dinotefuran from Wastewater. *Ijms* 21, 4079. doi:10.3390/ijms21114079

Salehi, O., Sami, M., and Rezaei, A. (2021). Limonene Loaded Cyclodextrin Nanosponge: Preparation, Characterization, Antibacterial Activity and Controlled Release. *Food Biosci.* 42, 101193. doi:10.1016/j.fbio.2021.101193

Salgın, S., Salgın, U., and Vatansever, Ö. (2017). Synthesis and Characterization of β-Cyclodextrin Nanosponge and its Application for the Removal Ofp-Nitrophenol from Water. *CLEAN. - Soil Air Water* 45, 1500837. doi:10.1002/clen.201500837

Saokham, P., Muankaew, C., Jansook, P., and Loftsson, T. (2018). Solubility of Cyclodextrins and Drug/Cyclodextrin Complexes. *Molecules* 23, 1161. doi:10.3390/molecules23051161

Schibilla, F., Voskuhl, J., Fokina, N. A., Dahl, J. E. P., Schreiner, P. R., and Ravoo, B. J. (2017). Host-Guest Complexes of Cyclodextrins and Nanodiamonds as a Strong Non-Covalent Binding Motif for Self-Assembled Nanomaterials. *Chem. Eur. J.* 23, 16059–16065. doi:10.1002/chem.201703392

Schlüter, F., Bela, M. M., Glikman, D., Braunschweig, B., and Ravoo, B. J. (2020). A Cyclodextrin Surfactant for Stable Emulsions with an Accessible Cavity for Host-Guest Complexation. *Chem. Commun.* 56, 15434–15437. doi:10.1039/D0CC06657E

Seglie, L., Devecchi, M., Trotta, F., and Scariot, V. (2013). β-Cyclodextrin-based Nanosponges Improve 1-MCP Efficacy in Extending the Postharvest Quality of Cut Flowers. *Scientia Horticulturae* 159, 162–165. doi:10.1016/j.scienta.2013.05.019

Seglie, L., Spadaro, D., Trotta, F., Devecchi, M., Gullino, M. L., and Scariot, V. (2012). Use of 1-methylcylopropene in Cyclodextrin-Based Nanosponges to Control Grey Mould Caused by Botrytis Cinerea on Dianthus Caryophyllus Cut Flowers. *Postharvest Biol. Tech.* 64, 55–57. doi:10.1016/j.postharvbio.2011.09.014

Sharma, K., Kadian, V., Kumar, A., Mahant, S., and Rao, R. (2021). Evaluation of Solubility, Photostability and Antioxidant Activity of Ellagic Acid Cyclodextrin Nanosponges Fabricated by Melt Method and Microwave-Assisted Synthesis. *J. Food Sci. Technol.* 59, 898–908. doi:10.1007/s13197-021-05085-6

Shende, P. K., Gaud, R. S., Bakal, R., and Patil, D. (2015a). Effect of Inclusion Complexation of Meloxicam with β-cyclodextrin- and β-cyclodextrin-based Nanosponges on Solubility, *In Vitro* Release and Stability Studies. *Colloids Surf. B: Biointerfaces* 136, 105–110. doi:10.1016/j.colsurfb.2015.09.002

Shende, P., Kulkarni, Y. A., Gaud, R. S., Deshmukh, K., Cavalli, R., Trotta, F., et al. (2015b). Acute and Repeated Dose Toxicity Studies of Different β-Cyclodextrin-Based Nanosponge Formulations. *J. Pharm. Sci.* 104, 1856–1863. doi:10.1002/jps.24416

Sherje, A. P., Dravyakar, B. R., Kadam, D., and Jadhav, M. (2017). Cyclodextrin-based Nanosponges: A Critical Review. *Carbohydr. Polym.* 173, 37–49. doi:10.1016/j.carbpol.2017.05.086

Sherje, A. P., Surve, A., and Shende, P. (2019). CDI Cross-Linked β-cyclodextrin Nanosponges of Paliperidone: Synthesis and Physicochemical Characterization. *J. Mater. Sci. Mater. Med.* 30, 74. doi:10.1007/s10856-019-6268-0

Shrestha, S., and Bhattacharya, S. (2020). Versatile Use of Nanosponge in the Pharmaceutical Arena: A Mini-Review. *Nanotec* 14, 351–359. doi:10.2174/1872210514999200901200558

Shringirishi, M., Mahor, A., Gupta, R., Prajapati, S. K., Bansal, K., and Kesharwani, P. (2017). Fabrication and Characterization of Nifedipine Loaded β-cyclodextrin Nanosponges: An *In Vitro* and *In Vivo* Evaluation. *J. Drug Deliv. Sci. Tech.* 41, 344–350. doi:10.1016/j.jddst.2017.08.005

Sikder, M. T., Rahman, M. M., Jakariya, M., Hosokawa, T., Kurasaki, M., and Saito, T. (2019). Remediation of Water Pollution with Native Cyclodextrins and Modified Cyclodextrins: A Comparative Overview and Perspectives. *Chem. Eng. J.* 355, 920–941. doi:10.1016/j.cej.2018.08.218

Silva, F., Caldera, F., Trotta, F., Nerín, C., and Domingues, F. C. (2019). Encapsulation of Coriander Essential Oil in Cyclodextrin Nanosponges: A New Strategy to Promote its Use in Controlled-Release Active Packaging. *Innovative Food Sci. Emerging Tech.* 56, 102177. doi:10.1016/j.ifset.2019.102177

Simionato, I., Domingues, F. C., Nerín, C., and Silva, F. (2019). Encapsulation of Cinnamon Oil in Cyclodextrin Nanosponges and Their Potential Use for Antimicrobial Food Packaging. *Food Chem. Toxicol.* 132, 110647. doi:10.1016/j.fct.2019.110647

Singh, P., Ren, X., Guo, T., Wu, L., Shakya, S., He, Y., et al. (2018). Biofunctionalization of β-cyclodextrin Nanosponges Using Cholesterol. *Carbohydr. Polym.* 190, 23–30. doi:10.1016/j.carbpol.2018.02.044

Singh, V., Xu, J., Wu, L., Liu, B., Guo, T., Guo, Z., et al. (2017). Ordered and Disordered Cyclodextrin Nanosponges with Diverse Physicochemical Properties. *RSC Adv.* 7, 23759–23764. doi:10.1039/C7RA00584A

Singireddy, A., Rani Pedireddi, S., Nimmagadda, S., and Subramanian, S. (2016). Beneficial Effects of Microwave Assisted Heating versus Conventional Heating in Synthesis of Cyclodextrin Based Nanosponges. *Mater. Today Proc.* 3, 3951–3959. doi:10.1016/j.matpr.2016.11.055

Skwierawska, A. M., Nowacka, D., Nowicka, P., Rosa, S., and Kozłowska-Tylingo, K. (2021). Structural Adaptive, Self-Separating Material for Removing Ibuprofen from Waters and Sewage. *Materials* 14, 7697. doi:10.3390/ma14247697

Srivastava, S., Mahor, A., Singh, G., Bansal, K., Singh, P. P., Gupta, R., et al. (2021). Formulation Development, *In Vitro* and *In Vivo* Evaluation of Topical Hydrogel Formulation of Econazole Nitrate-Loaded β-Cyclodextrin Nanosponges. *J. Pharm. Sci.* 110, 3702–3714. doi:10.1016/j.xphs.2021.07.008

Suvarna, V., Singh, V., Sharma, D., and Murahari, M. (2021). Experimental and Computational Insight of the Supramolecular Complexes of Irbesartan with β-cyclodextrin Based Nanosponges. *J. Drug Deliv. Sci. Tech.* 63, 102494. doi:10.1016/j.jddst.2021.102494

Swaminathan, S., Cavalli, R., and Trotta, F. (2016). Cyclodextrin-based Nanosponges: a Versatile Platform for Cancer Nanotherapeutics Development. *WIREs Nanomed Nanobiotechnol* 8, 579–601. doi:10.1002/wnan.1384

Swaminathan, S., Cavalli, R., Trotta, F., Ferruti, P., Ranucci, E., Gerges, I., et al. (2010a). *In Vitro* release Modulation and Conformational Stabilization of a Model Protein Using Swellable Polyamidoamine Nanosponges of β-cyclodextrin. *J. Incl. Phenom. Macrocycl. Chem.* 68, 183–191. doi:10.1007/s10847-010-9765-9

Swaminathan, S., Pastero, L., Serpe, L., Trotta, F., Vavia, P., Aquilano, D., et al. (2010b). Cyclodextrin-based Nanosponges Encapsulating Camptothecin: Physicochemical Characterization, Stability and Cytotoxicity. *Eur. J. Pharmaceutics Biopharmaceutics* 74, 193–201. doi:10.1016/j.ejpb.2009.11.003

Swaminathan, S., Vavia, P. R., Trotta, F., Cavalli, R., Tumbiolo, S., Bertinetti, L., et al. (2013). Structural Evidence of Differential Forms of Nanosponges of Beta-Cyclodextrin and its Effect on Solubilization of a Model Drug. *J. Incl. Phenom. Macrocycl. Chem.* 76, 201–211. doi:10.1007/s10847-012-0192-y

Tannous, M., Caldera, F., Hoti, G., Dianzani, U., Cavalli, R., and Trotta, F. (2021). Drug-Encapsulated Cyclodextrin Nanosponges. *Methods Mol. Biol.* 2207, 247–283. doi:10.1007/978-1-0716-0920-0_19

Tannous, M., Trotta, F., and Cavalli, R. (2020). Nanosponges for Combination Drug Therapy: State-Of-The-Art and Future Directions. *Nanomedicine* 15, 643–646. doi:10.2217/nnm-2020-0007

Tejashri, G., Amrita, B., and Darshana, J. (2013). Cyclodextrin Based Nanosponges for Pharmaceutical Use: A Review. *Acta Pharm.* 63, 335–358. doi:10.2478/acph-2013-0021

Tian, B., Hua, S., and Liu, J. (2020). Cyclodextrin-based Delivery Systems for Chemotherapeutic Anticancer Drugs: A Review. *Carbohydr. Polym.* 232, 115805. doi:10.1016/j.carbpol.2019.115805

Torne, S., Darandale, S., Vavia, P., Trotta, F., and Cavalli, R. (2013). Cyclodextrin-based Nanosponges: Effective Nanocarrier for Tamoxifen Delivery. *Pharm. Dev. Tech.* 18, 619–625. doi:10.3109/10837450.2011.649855

Torne, S. J., Ansari, K. A., Vavia, P. R., Trotta, F., and Cavalli, R. (2010). Enhanced Oral Paclitaxel Bioavailability after Administration of Paclitaxel-Loaded Nanosponges. *Drug Deliv.* 17, 419–425. doi:10.3109/10717541003777233

Trotta, F., Caldera, F., Cavalli, R., Soster, M., Riedo, C., Biasizzo, M., et al. (2016a). Molecularly Imprinted Cyclodextrin Nanosponges for the Controlled Delivery of L-DOPA: Perspectives for the Treatment of Parkinson's Disease. *Expert Opin. Drug Deliv.* 13, 1671–1680. doi:10.1080/17425247.2017.1248398

Trotta, F., Caldera, F., Dianzani, C., Argenziano, M., Barrera, G., and Cavalli, R. (2016b). Glutathione Bioresponsive Cyclodextrin Nanosponges. *Chempluschem* 81, 439–443. doi:10.1002/cplu.201500531

Trotta, F. (2011). "Cyclodextrin Nanosponges and Their Applications," in *Nanosponges*. Editors F. Trotta and E. Bilensoy (New York: John Wiley & Sons), 323–342. doi:10.1002/9780470926819.ch17

Trotta, F., Dianzani, C., Caldera, F., Mognetti, B., and Cavalli, R. (2014). The Application of Nanosponges to Cancer Drug Delivery. *Expert Opin. Drug Deliv.* 11, 931–941. doi:10.1517/17425247.2014.911729

Trotta, F., and Pedrazzo, R. (2020). *A Process for Preparing a Nanosponge*. Springer, 1–54.

Trotta, F., Zanetti, M., and Cavalli, R. (2012). Cyclodextrin-based Nanosponges as Drug Carriers. *Beilstein J. Org. Chem.* 8, 2091–2099. doi:10.3762/bjoc.8.235

Uekama, K., Hirayama, F., and Irie, T. (1998). Cyclodextrin Drug Carrier Systems. *Chem. Rev.* 98, 2045–2076. doi:10.1021/cr970025p

Usacheva, T., Pham, T. L., Nguyen, T. D., Kabirov, D., Alister, D., Vu, X. M., et al. (2020). Host-guest Inclusion Complex of β-cyclodextrin and Benzoic Acid in Water-Ethanol Solvents: Spectroscopic and Thermodynamic Characterization of Complex Formation. *J. Therm. Anal. Calorim.* 142, 2015–2024. doi:10.1007/s10973-020-09807-4

Utzeri, G., Murtinho, D., Maria, T. M. R., Pais, A. A. C. C., Sannino, F., and Valente, A. J. M. (2022). Amine-β-cyclodextrin-based Nanosponges. The Role of Cyclodextrin Amphiphilicity in the Imidacloprid Uptake. *Colloids Surf. A: Physicochemical Eng. Aspects* 635, 128044. doi:10.1016/j.colsurfa.2021.128044

Utzeri, G., Verissimo, L., Murtinho, D., Pais, A. A. C. C., Perrin, F. X., Ziarelli, F., et al. (2021). Poly(β-cyclodextrin)-Activated Carbon Gel Composites for Removal of Pesticides from Water. *Molecules* 26, 1426. doi:10.3390/molecules26051426

Valente, A. J. M., and Söderman, O. (2014). The Formation of Host-Guest Complexes between Surfactants and Cyclodextrins. *Adv. Colloid Interf. Sci.* 205, 156–176. doi:10.1016/j.cis.2013.08.001

Varan, C., Anceschi, A., Sevli, S., Bruni, N., Giraudo, L., Bilgiç, E., et al. (2020). Preparation and Characterization of Cyclodextrin Nanosponges for Organic Toxic Molecule Removal. *Int. J. Pharmaceutics* 585, 119485. doi:10.1016/j.ijpharm.2020.119485

Vareda, J. P., Valente, A. J. M., and Durães, L. (2019). Assessment of Heavy Metal Pollution from Anthropogenic Activities and Remediation Strategies: A Review. *J. Environ. Manage.* 246, 101–118. doi:10.1016/j.jenvman.2019.05.126

Vareda, J. P., Valente, A. J. M., and Durães, L. (2016). Heavy Metals in Iberian Soils: Removal by Current Adsorbents/amendments and Prospective for Aerogels. *Adv. Colloid Interf. Sci.* 237, 28–42. doi:10.1016/j.cis.2016.08.009

Vasconcelos, D. A., Kubota, T., Santos, D. C., Araujo, M. V. G., Teixeira, Z., and Gimenez, I. F. (2016). Preparation of Au Quantum Clusters with Catalytic Activity in β-cyclodextrin Polyurethane Nanosponges. *Carbohydr. Polym.* 136, 54–62. doi:10.1016/j.carbpol.2015.09.010

Venuti, V., Rossi, B., Mele, A., Melone, L., Punta, C., Majolino, D., et al. (2017). Tuning Structural Parameters for the Optimization of Drug Delivery Performance of Cyclodextrin-Based Nanosponges. *Expert Opin. Drug Deliv.* 14, 331–340. doi:10.1080/17425247.2016.1215301

Wang, D., Chen, G., Li, X., and Jia, Q. (2019a). Hypercrosslinked β-cyclodextrin Porous Polymer as Adsorbent for Effective Uptake towards Albendazole from Aqueous media. *Sep. Purif. Tech.* 227, 115720. doi:10.1016/j.seppur.2019.115720

Wang, J.-W., Yu, K.-X., Ji, X.-Y., Bai, H., Zhang, W.-H., Hu, X., et al. (2021a). Structural Insights into the Host-Guest Complexation between β-Cyclodextrin and Bio-Conjugatable Adamantane Derivatives. *Molecules* 26, 2412. doi:10.3390/molecules26092412

Wang, M., Li, G., Xia, C., Jing, X., Wang, R., Liu, Q., et al. (2021b). Facile Preparation of Cyclodextrin Polymer Materials with Rigid Spherical Structure and Flexible Network for Sorption of Organic Contaminants in Water. *Chem. Eng. J.* 411, 128489. doi:10.1016/j.cej.2021.128489

Wang, Z., Cui, F., Pan, Y., Hou, L., Zhang, B., Li, Y., et al. (2019b). Hierarchically Micro-mesoporous β-cyclodextrin Polymers Used for Ultrafast Removal of Micropollutants from Water. *Carbohydr. Polym.* 213, 352–360. doi:10.1016/j.carbpol.2019.03.021

Wang, Z., Zhang, P., Hu, F., Zhao, Y., and Zhu, L. (2017). A Crosslinked β-cyclodextrin Polymer Used for Rapid Removal of a Broad-Spectrum of Organic Micropollutants from Water. *Carbohydr. Polym.* 177, 224–231. doi:10.1016/j.carbpol.2017.08.059

Yakavets, I., Guereschi, C., Lamy, L., Kravchenko, I., Lassalle, H.-P., Zorin, V., et al. (2020). Cyclodextrin Nanosponge as a Temoporfin Nanocarrier: Balancing between Accumulation and Penetration in 3D Tumor Spheroids. *Eur. J. Pharmaceutics Biopharmaceutics* 154, 33–42. doi:10.1016/j.ejpb.2020.06.022

Yang, G., Fang, D., Yang, L., Wei, Z., Tu, Y., Shao, P., et al. (2022). Tailored Construction of β-cyclodextrin Covalently-Supported Tannic Acid Polymer Nanosponge towards Highly Selective lead Recovery. *J. Clean. Prod.* 330, 129882. doi:10.1016/j.jclepro.2021.129882

Yaşayan, G., Şatıroğlu Sert, B., Tatar, E., and Küçükgüzel, İ. (2020). Fabrication and Characterisation Studies of Cyclodextrin-Based Nanosponges for Sulfamethoxazole Delivery. *J. Incl. Phenom. Macrocycl. Chem.* 97, 175–186. doi:10.1007/s10847-020-01003-z

Yazdani, M., Tavakoli, O., Khoobi, M., Wu, Y. S., Faramarzi, M. A., Gholibegloo, E., et al. (2021). Beta-carotene/cyclodextrin-based Inclusion Complex: Improved Loading, Solubility, Stability, and Cytotoxicity. *J. Incl. Phenom. Macrocycl. Chem.* 102, 55–64. doi:10.1007/s10847-021-01100-7

Yokozawa, T., and Ohta, Y. (2016). Transformation of Step-Growth Polymerization into Living Chain-Growth Polymerization. *Chem. Rev.* 116, 1950–1968. doi:10.1021/acs.chemrev.5b00393

Yu, F., Chen, D., and Ma, J. (2018a). Adsorptive Removal of Ciprofloxacin by Ethylene Diaminetetraacetic Acid/β-Cyclodextrin Composite from Aqueous Solution. *New J. Chem.* 42, 2216–2223. doi:10.1039/c7nj03770h

Yu, T., Xue, Z., Zhao, X., Chen, W., and Mu, T. (2018b). Green Synthesis of Porous β-cyclodextrin Polymers for Rapid and Efficient Removal of Organic Pollutants and Heavy Metal Ions from Water. *New J. Chem.* 42, 16154–16161. doi:10.1039/C8NJ03438A

Yu, T., Xue, Z., Zhao, X., Chen, W., and Mu, T. (2018c). Green Synthesis of Porous β-cyclodextrin Polymers for Rapid and Efficient Removal of Organic Pollutants and Heavy Metal Ions from Water. *New J. Chem.* 42, 16154–16161. doi:10.1039/c8nj03438a

Zainuddin, R., Zaheer, Z., Sangshetti, J. N., and Momin, M. (2017). Enhancement of Oral Bioavailability of Anti-HIV Drug Rilpivirine HCl through Nanosponge Formulation. *Drug Dev. Ind. Pharm.* 43, 2076–2084. doi:10.1080/03639045.2017.1371732

Zhao, F., Repo, E., Yin, D., Meng, Y., Jafari, S., and Sillanpää, M. (2015). EDTA-Cross-Linked β-Cyclodextrin: An Environmentally Friendly Bifunctional Adsorbent for Simultaneous Adsorption of Metals and Cationic Dyes. *Environ. Sci. Technol.* 49, 10570–10580. doi:10.1021/acs.est.5b02227

Zhou, L., Xu, Z., Yi, K., Huang, Q., Chai, K., Tong, Z., et al. (2019a). Efficient Remediation of 2,4-dichlorophenol from Aqueous Solution Using β-cyclodextrin-based Submicron Polymeric Particles. *Chem. Eng. J.* 360, 531–541. doi:10.1016/j.cej.2018.11.196

Zhou, Y., Cheng, G., Chen, K., Lu, J., Lei, J., and Pu, S. (2019b). Adsorptive Removal of Bisphenol A, Chloroxylenol, and Carbamazepine from Water Using a Novel β-cyclodextrin Polymer. *Ecotoxicology Environ. Saf.* 170, 278–285. doi:10.1016/j.ecoenv.2018.11.117

Conflict of Interest: The authors declare that the research was conducted in the absence of any commercial or financial relationships that could be construed as a potential conflict of interest.

Publisher's Note: All claims expressed in this article are solely those of the authors and do not necessarily represent those of their affiliated organizations, or those of the publisher, the editors and the reviewers. Any product that may be evaluated in this article, or claim that may be made by its manufacturer, is not guaranteed or endorsed by the publisher.

GLOSSARY

4C3MP 4–chloro–3–methylphenol
2,4CP 2,4–dichlorophenol
2CP 2–chlorophenol
2,4,6CP 2,4,6–trichlorophenol
2,4D 2,4-dichlorophenoxy acid
2-HEDS 2-hydroxyethyl disulfide
2NP 2–nitrophenol
4NP 4–nitrophenol
2,4NP 2,4–dinitrophenol
4nNP 4–n–nonylphenol
4nOP 4–n–octylphenol
4tOP 4–tert–octyphenol
AC activated carbon
am6 1,6-hexanediamine
am12 1,12-dodecanediamine
AMD 1–(3–dimethylaminopropyl)–3–ethylcarbodiimide hydrochloride
BDE 1,4-butanediol diglycidylether
BPA Bisphenol A
BPAF Bisphenol AF
BPF Bisphenol F
BPS bisphenol S
CA citric acid
CDs cyclodextrins
CDI 1,1′-carbonyl diimidazole
CDNSs cyclodextrin nanosponges
CHI dicyclohexylmethane-4,4′-diisocyanate
CHS cholesterol hydrogen succinate
CMP 4,4′-bis(chloromethyl)-1,1′-biphenyl
CPA 4–chlorophenoxyacetic acid
CyCa NSs CD-calixarene NSs
CR congo red
CTS chitosan
CV cristal violet
DABCO 1,4-diazabicyclo(2,2,2)octane
DBPs chlorinated disinfection by-products
DEET N,N–diethyl–3–toluamide
DMC dimethyl carbonate
DPC diphenyl carbonate
EDTA ethylenediaminetetraacetic acid dianhydride
EE encapsulation efficiency
EPI epichlorohydrin
Et3N triethylamine
FPS 4,4′–difluorodiphenylsulfone
GSH-NS glutathione-responsive NSs
HDI 1,6-hexamethylene diisocyanate
IMP 4,4′–diisocyanato–3,3′–dimethyl biphenyl
MB methylene blue
MBA N,N′-methylene bisacrylamide
MDI methylene diphenyl diisocyanate
MIPs molecularly imprinted polymers
MO methyl orange
MPP 2,2′–azobis(2–methylpropionitrile)
NADES deep natural eutectic solvents
NDCA 2,6-naphthalene dicarboxylic acid
NIP-NSs non-molecularly imprinted polymers
NSs nanosponges
OXY oxyresveratrol
P5 pillar(5)arene
PAA polyamidoamine
PD 4,4′-bipyridine
PDI polydispersity index
PDS 1,4–phenylene diisocyanate
PFP pentafluoropyridine
PMA pyromellitic dianhydride
RB rhodamine B
RIR restriction of intramolecular rotation
SBET surface area
SFsafranin O; TA safranin O; TAtannic acid
TCP 2,3,4,6–tetrachlorophenol
TDI oluene 2,4-diisocyanate
TFP tetrafluoroterephtalonitrile
THTS 5,5′,6,6′–tetrahydroxy-3,3,3′,3′-tetramethylspirobisindande
TPC terephthaloyl chloride
TPE tetrakis(4–hydroxyphenyl)ethane
TTI triphenylmethane–4,4′,4″–trisocyanate

References of chapter 3

[1] A.R. Khan, P. Forgo, K.J. Stine, V.T. D'Souza, Methods for Selective Modifications of Cyclodextrins, Chem. Rev. 98 (1998) 1977–1996. https://doi.org/10.1021/cr970012b.

[2] B.I. Gorin, R.J. Riopelle, G.R.J. Thatcher, Efficient perfacial derivatization of cyclodextrins at the primary face, Tetrahedron Lett. 37 (1996) 4647–4650. https://doi.org/10.1016/0040-4039(96)00916-1.

[3] M. Agnes, E. Pancani, M. Malanga, E. Fenyvesi, I. Manet, Implementation of Water-Soluble Cyclodextrin-Based Polymers in Biomedical Applications: How Far Are We?, Macromol. Biosci. 22 (2022) 2200090. https://doi.org/10.1002/mabi.202200090.

[4] S. Farooq, L. Xu, A. Ostovan, C. Qin, Y. Liu, Y. Pan, J. Ping, Y. Ying, Assessing the greenification potential of cyclodextrin-based molecularly imprinted polymers for pesticides detection, Food Chem. 429 (2023) 136822. https://doi.org/10.1016/j.foodchem.2023.136822.

[5] M.A. Przybyla, G. Yilmaz, C.R. Becer, Natural cyclodextrins and their derivatives for polymer synthesis, Polym. Chem. 11 (2020) 7582–7602. https://doi.org/10.1039/D0PY01464H.

[6] M. Hussain Asim, M. Ijaz, A.C. Rösch, A. Bernkop-Schnürch, Thiolated cyclodextrins: New perspectives for old excipients, Coord. Chem. Rev. 420 (2020) 213433. https://doi.org/10.1016/j.ccr.2020.213433.

[7] L.M.A. Pinto, L.F. Fraceto, M.H.A. Santana, T.A. Pertinhez, S.O. Junior, E. de Paula, Physico-chemical characterization of benzocaine-β-cyclodextrin inclusion complexes, J. Pharm. Biomed. Anal. 39 (2005) 956–963. https://doi.org/10.1016/j.jpba.2005.06.010.

[8] C.I.A. V. Santos, A.C.F. Ribeiro, M.A. Esteso, Drug Delivery Systems: Study of Inclusion Complex Formation between Methylxanthines and Cyclodextrins and Their Thermodynamic and Transport Properties, Biomolecules. 9 (2019) 196. https://doi.org/10.3390/biom9050196.

[9] Q. Khalid, M. Ahmad, M.U. Minhas, F. Batool, N.S. Malik, M. Rehman, Novel β-cyclodextrin nanosponges by chain growth condensation for solubility enhancement of dexibuprofen: Characterization and acute oral toxicity studies, J. Drug Deliv. Sci. Technol. 61 (2021) 102089. https://doi.org/10.1016/j.jddst.2020.102089.

[10] V.S. Ghorpade, A.V. Yadav, R.J. Dias, Citric acid crosslinked cyclodextrin/hydroxypropylmethylcellulose hydrogel films for hydrophobic drug delivery, Int. J. Biol. Macromol. 93 (2016) 75–86. https://doi.org/10.1016/j.ijbiomac.2016.08.072.

[11] L. Moulahcene, M. Skiba, O. Senhadji, N. Milon, M. Benamor, M. Lahiani-Skiba, Inclusion and removal of pharmaceutical residues from aqueous solution using water-

insoluble cyclodextrin polymers, Chem. Eng. Res. Des. 97 (2015) 145–158. https://doi.org/10.1016/j.cherd.2014.08.023.

[12] A.M. Skwierawska, D. Nowacka, P. Nowicka, S. Rosa, K. Kozłowska-Tylingo, Structural Adaptive, Self-Separating Material for Removing Ibuprofen from Waters and Sewage, Materials (Basel). 14 (2021) 7697. https://doi.org/10.3390/ma14247697.

[13] E. Martwong, S. Chuetor, J. Junthip, Adsorption of Paraquat by Poly(Vinyl Alcohol)-Cyclodextrin Nanosponges, Polymers (Basel). 13 (2021) 4110. https://doi.org/10.3390/polym13234110.

[14] C. Yañez, M. Araya, S. Bollo, Complexation of herbicide bentazon with native and modified β-cyclodextrin, J. Incl. Phenom. Macrocycl. Chem. 68 (2010) 237–241. https://doi.org/10.1007/s10847-010-9750-3.

[15] K. Köse, M. Tüysüz, D. Aksüt, L. Uzun, Modification of cyclodextrin and use in environmental applications, Environ. Sci. Pollut. Res. 29 (2022) 182–209. https://doi.org/10.1007/s11356-021-15005-y.

[16] G. Crini, S. Fourmentin, É. Fenyvesi, G. Torri, M. Fourmentin, N. Morin-Crini, Cyclodextrins, from molecules to applications, Environ. Chem. Lett. 16 (2018) 1361–1375. https://doi.org/10.1007/s10311-018-0763-2.

[17] S. Swaminathan, F. Trotta, Cyclodextrin Nanosponges, in: F. Trotta, A. Mele (Eds.), Nanosponges, Wiley-VCH Verlag GmbH & Co. KGaA, Weinheim, Germany, 2019: pp. 27–57. https://doi.org/10.1002/9783527341009.ch2.

[18] G. Utzeri, P.M.C. Matias, D. Murtinho, A.J.M. Valente, Cyclodextrin-Based Nanosponges: Overview and Opportunities, Front. Chem. 10 (2022) 1–25. https://doi.org/10.3389/fchem.2022.859406.

[19] A. Marican, E.F. Durán-Lara, A review on pesticide removal through different processes, Environ. Sci. Pollut. Res. 25 (2018) 2051–2064. https://doi.org/10.1007/s11356-017-0796-2.

[20] J.M. Anne, Y.H. Boon, B. Saad, M. Miskam, M.M. Yusoff, M.S. Shahriman, N.N.M. Zain, V. Lim, M. Raoov, β-Cyclodextrin conjugated bifunctional isocyanate linker polymer for enhanced removal of 2,4-dinitrophenol from environmental waters, R. Soc. Open Sci. 5 (2018) 180942. https://doi.org/10.1098/rsos.180942.

[21] P.R. Ashton, R. Königer, J.F. Stoddart, D. Alker, V.D. Harding, Amino Acid Derivatives of β-Cyclodextrin, J. Org. Chem. 61 (1996) 903–908. https://doi.org/10.1021/jo951396d.

[22] P. Lo Meo, F. D'Anna, M. Gruttadauria, S. Riela, R. Noto, Synthesis and characterization of new polyamino-cyclodextrin materials, Carbohydr. Res. 347 (2012) 32–39. https://doi.org/10.1016/j.carres.2011.10.029.

[23] M. Russo, M.L. Saladino, D. Chillura Martino, P. Lo Meo, R. Noto, Polyaminocyclodextrin nanosponges: synthesis, characterization and pH-responsive

sequestration abilities, RSC Adv. 6 (2016) 49941–49953. https://doi.org/10.1039/C6RA06417E.

[24] J. Toit, N.H. Casey, Iodine as an alleviator of bromine toxicity in thyroid , liver and kidney of broiler chickens, Livest. Sci. 144 (2012) 269–274. https://doi.org/10.1016/j.livsci.2011.12.011.

[25] G. Utzeri, D. Murtinho, T.M.R. Maria, A.A.C.C. Pais, F. Sannino, A.J.M. Valente, Amine-β-cyclodextrin-based nanosponges. The role of cyclodextrin amphiphilicity in the imidacloprid uptake, Colloids Surfaces A Physicochem. Eng. Asp. 635 (2022) 128044. https://doi.org/10.1016/j.colsurfa.2021.128044.

[26] G. Utzeri, D. Murtinho, A.J.M. Valente, Introduction to Cyclodextrin-Based Nanosponges, in: S. Gulati (Ed.), Nanosponges Environ. Remediat., 1st ed., Springer Nature Switzerland, Cham, 2023: pp. 87–115. https://doi.org/10.1007/978-3-031-41077-2_5.

Chapter 4.

4. Insight to the characterization of the systems

In this chapter, the fundamentals of the main methods used throughout the thesis for the characterization of the synthesized materials are presented. A comparison of the polymer properties will be provided, highlighting their variations according to the use of α-CD or β-CD and different crosslinkers in the synthesis process. The idea is to provide to the reader a deeper overlook of the sorbent materials for a better understanding of the scientific papers reported in Chapter 6.

4.1.Physical characterization

Physical properties of a solid phase such size distribution, porosity, surface area and morphology are important factors conferring and/or correlating with other properties like mechanical ones, swelling capability, permeability, degradability, thermal and electrical conductivity, optical and catalytic properties. Hence, they are directly or indirectly related with the final application areas of the materials such as gas adsorption and storage, catalysis, biomedical-imaging, semiconductors, environmental remediation, sensors, and drug delivery, among others [1]. Thus, extensive research have been focused on the development of rational design for successful synthesis of materials either crystalline or amorphous [2].

4.1.1. Morphology

The morphological or topographical analysis of surface sample can be performed by several techniques: optic, fluorescence, and electron microscopy such as scanning and transmission electron microscopies (SEM and TEM), scanning tunneling microscopy (STM) or atomic force microscopy (AFM). The selection of the technique must consider the required resolution and properties, advantages and disadvantages, such cost of the analysis. For example, optical microscopy has a low magnification and is typically applied for membrane components. Multicolor imaging can be obtained by fluorescence microscopy. Both are applicable at environmental conditions [3].

On the other hand, the electron microscopy techniques reach a lower limit resolution ≈ 1 nm, with a magnification range from ×10 to 500 k, employing an electron beam with an accelerating voltage within 2-30 kV, and a condenser lens. Thus, SEM and TEM are commonly used for morphological or topographical analysis, elemental composition and porosity of nano- or submicron-particles [4]. According to IUPAC recommendations, particles with size range within 1-100 nm are defined as nanoparticles (NP), 0.1 to 1 μm are considered submicron particles (SMP) and > 1 μm as microparticles. SEM analysis permits the imaging of the material from different perspectives which is not possible with the AFM. The SEM performance is dependent on different parameters like the brightness (A cm^{-2} $steradian^{-2}$) ($b = 4I/\pi^2\alpha^2d^2 - I$ (A) is the beam current, α (steradian) is the angle of divergence and d (cm) is the incident spot diameter). The magnification can be enhanced by increasing the voltage applied to the electron gun, or the magnetic field to the lenses. The SEM analysis is based on two types of signals collected by the detector (*e.g.* secondary or backscattered electrons detector, X-ray detector): *i*) secondary electrons emitted from the external orbitals of the atoms constituting the solid surface irradiated (inelastic scattering), which gives high resolution and depth-of-field images; *ii*) backscattered electrons of the beam gives chemical information of the analyzed material (elastic scattering) [5,6]. However, the analysis must be performed in high vacuum and the electron beam can damage the sample surface. The resolution depends on the electron conductivity of the material, that can cause a beam broadening and scattering effects dependent on the thickness of the sample and electron interaction with the surface [7]. The resolution may be improved by handling different parameters like increasing the brightness, the voltage and the current applied to the electron gun, among others.

SEM analysis was used along the thesis in order to morphologically characterize the two families of sorbent materials, urethane- and amine-cyclodextrin-based (Figures 4.1 - 4.2 - 4.3).

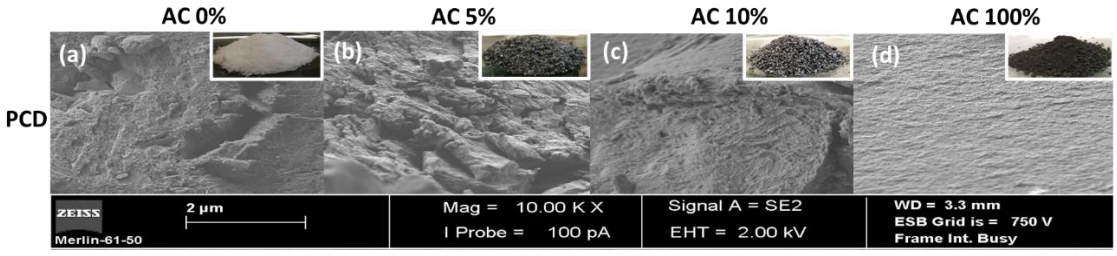

Figure 4.1. SEM micrographs of poly-*β*cyclodextrin (a) PCD, (b) PCD-AC5%, (c) PCD-AC10%, (d) AC; (magnification ×10 k).

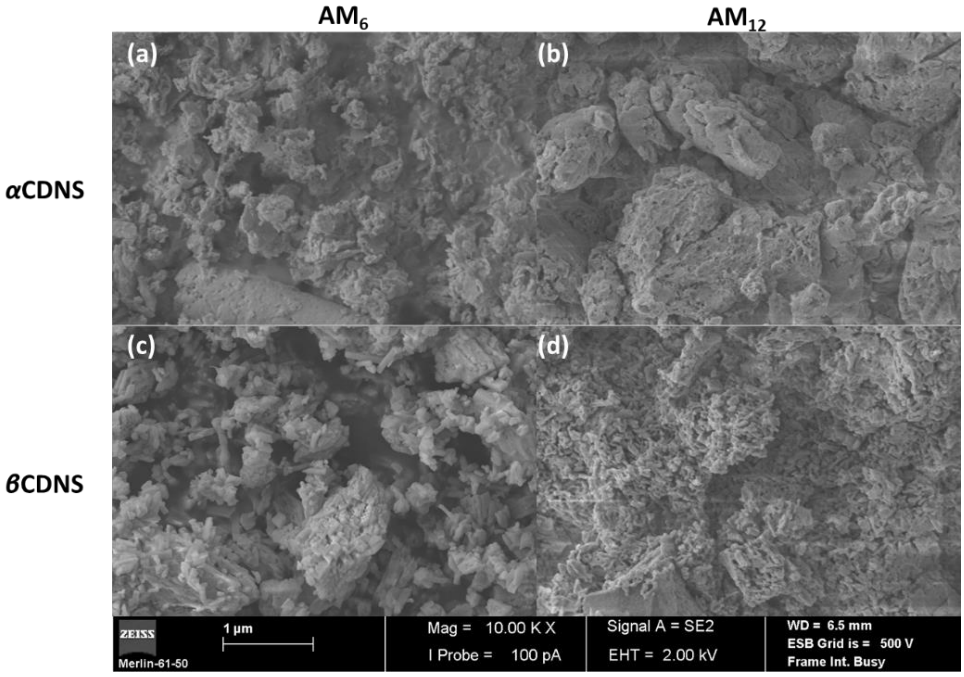

Figure 4.2. SEM micrographs of (a) αCDAM$_6$, (b) αCDAM$_{12}$, (c) βCDAM$_6$, (d) βCDAM$_{12}$; (magnification ×10 k).

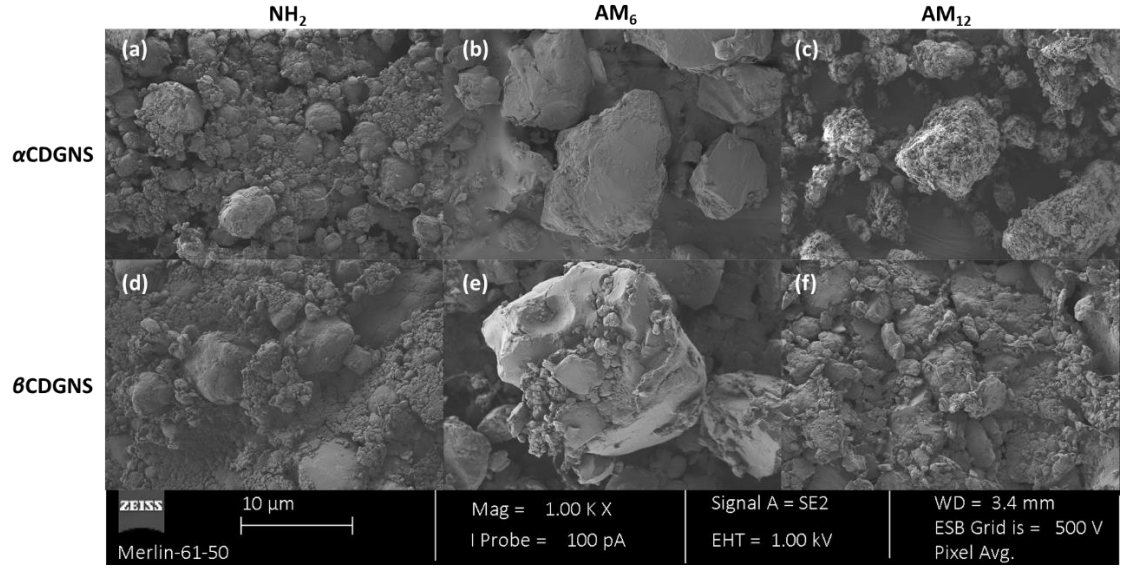

Figure 4.3. SEM micrographs of (a) αCDGNH$_2$, (b) αCDGAM$_6$, (c) αCDGAM$_{12}$, (d) βCDGNH$_2$, (e) βCDGAM$_6$, (f) βCDGAM$_{12}$; (magnification ×1 k).

It can be observed that the poly-*β*cyclodextrin presents a different morphology from the second family of cyclodextrin-based nanosponges. The polymer surfaces presented from Figure 4.1-a to Figure 4.1-c show a typical morphology of a break-zone in a hard material. Smoothed areas are alternated to wide channels probably created in the grinding process. This behaviour can be explained taking into account that the polymerization product is a hydrogel with reduced or non-elasticity. The low elasticity can be explained by the efficiently catalysed polymerization reaction which led to a 3D-crosslinked and hard polymeric material in the dehydrated state. In the smooth homotattic surface regions [8], the presence of narrow pores can be observed (see subparagraph 4.1.4). These zones increase with higher percentage of AC added. The inserts in the right corner of the micrographs show the microscopic size of the sorbents.

The CDAM-NS are a powder-like materials synthesized using two different routes of polymerization. Generally, they have a heterogeneous morphology, suggesting the presence of aggregates as shown in Figure 4.2 and Figure 4.3. Yet, the two classes of amine-CDNS exhibit differences. The micrographs in Figure 4.2 are related with *α*$CDAM_6$, *α*$CDAM_{12}$, *β*$CDAM_6$, and *β*$CDAM_{12}$ obtained by crosslinking of CD-I with ammine-*per*substituted cyclodextrins. This class of CDNS presents a rod-like shape which are more visible for *β*$CDAM_6$, and *β*$CDAM_{12}$. Smaller aggregates of rod-like shape are still visible in *α*$CDAM_6$ upon a smooth surface blocks. The difference may be justified by using *α*-CD as substrate which is smaller than *β*-CD. It gives more degree of freedom for the structural rearrangement and/or entanglement of the aliphatic chains resulting in a tighter packed structure. That is more evident in *α*$CDAM_{12}$ with a longer aliphatic chain of crosslinker, which presents bigger aggregates with a dense structure.

The second class of amine-CDNSs was obtained by click-condesation reaction using the GLT as crosslinker. It is noticeable from the micrographs in Figure 4.3 that the morphology seems dependent only on the length of the branches and not on *α*-CD or *β*-CD used as substrate. Indeed, the *α*$CDGNH_2$ and *β*$CDGNH_2$ present an alveolar structure with a miscellany of spherical-like agglomerates of various dimensions. The morphology also suggests the presence of channels probably due to an irregular packing. In *α*$CDGAM_{12}$ and *β*$CDGAM_{12}$, a jagged morphology is observed, with bigger agglomerates of roughed surface. Differently, *α*$CDGAM_6$ and *β*$CDGAM_6$ show homotattic surfaces, consisting in smooth monoliths, probably due to strong hydrophobic interaction of the aliphatic chains, resulting in a dense structural packing.

The morphology of both classes of amine-CDNS suggests that by dynamic light scattering analysis (DLS) the particle size distribution could be determined, albeit the high agglomeration behaviour can led to a probably high polydispersity index (PDI).

4.1.2. Particles size distribution

Many methods can be used to determine the particle size distribution of a powder, granulate, suspension or emulsion. Their suitability is a function of the material properties and size range of the particles as well as their availability and cost of the analysis. Commonly used methods are sieve analysis, laser diffraction, DLS, AFM, SEM and TEM (Table 4.1) [9]. The particle size distribution influences either the application fields of the materials such as pharmaceutical, cosmetic, food or environmental areas as well as their impact on the environment and health concerns because of their mobility [10].

Table 4.1. Comparison of the methods of analysis for particle size distribution measurement.

Method	**Size range**	**Advantages**	**Disadvantages**
Sieve	10 µm to 200 mm	- broad size range; - weight percent distribution; - sample recovery.	- irregular shape cause interference; - not useful below 10 µm; - hygroscopic or electrostatic properties cause interferences; - large amount of sample.
Laser diffraction	0.1 nm to 3 mm	- fast; - *on-line* and *off-line* analysis.	- low resolution
Dynamic Light scattering (DLS)	0.3 nm to 10 µm	- low cost; - easy analysis; - broad distribution; - sample recovery.	- time-consuming sample preparation; - poor for polydispersity.
Scanning electron microscopy (SEM)	> 10 nm	- direct assessment of size and shape; - high resolution.	- time-consuming sample preparation; - high cost materials; - vacuum condition; - charging effects.
Transmission electron microscopy (TEM)	> 0.7 nm		
Atomic force microscopy (ATM)	1nm to 1 µm	- 3D images; - mild operative conditions	- support needed; - limited vertical range; - limited magnification range.

The size distribution of the cyclodextrin-based nanosponges applied throughout the thesis was determined by DLS. Exception is the poly-*β*cyclodextrin because of the micro-dimensions of the ground material as shown in the inserts in Figure 4.1 - subparagraph 4.1.1.

Dynamic light scattering (or photon correlation spectroscopy) enables the determination of the size distribution in the whole population and its stability over time. The analysis is based on the assumption that the particles are spherical. Particles in colloidal suspension scatter the monochromatic helium-neon laser beam (633 nm – red wavelength), at 4 mW [11]. The scattering light is detected at 90° angle or 173° angle backscattering. The intensity is a function of the incident light, scattering angle, sample parameters and light polarization [12]. The scattering of the incident light due to Brownian motion of the particles, can lead to: *i*) elastic scattering with same energy as respect to the angle, for particle size << λ (Rayleigh scattering) ($I = r^6/\lambda^4$ – I is the intensity of the scattered light and r is the particle radius); *ii*) inelastic scattering, due to particle size >> λ (Mie scattering), with different energy depending on the scattering angle [13,14]. The result is a constructive/destructive interaction of the light with intensity fluctuation over time (count rate, kcps). Due to the motion and size of the particles, the decay of the light intensity in a short interval of time (τ) is observed for reduced size in contrast to large particle. Thus, the correlation function ($G2(\tau)$) (Figure 4.4-a) is estimated by the equation 4.1:

$$G2(\tau) = \int_0^\infty I(t)I(t+\tau)dt = B + Ae^{-2\Gamma\tau} \qquad \text{(eq. 4.1)}$$

where B is the baseline, A is the amplitude and Γ is the translation diffusion coefficient associated with the diffusion coefficient (D) of the particle ($\Gamma = Dq^2$). q is the magnitude of the scattering vector (eq. 4.2) [15],

$$q = \frac{4\pi n_0}{\lambda} \sin\left(\theta/_2\right) \qquad \text{(eq. 4.2)}$$

where n_0 is the solvent refractive index, λ (nm) is the wavelength of the laser beam and θ is the scattering angle [16].

In this way, it can be established the relation of the diffusion coefficient with the hydrodynamic radius (R_h) of the particle through the Stoke-Einstein equation (eq. 4.3),

$$D = \frac{k_b T}{6\pi\eta R_h} \qquad \text{(eq. 4.3)}$$

where k_b is the Boltzmann constant (1.4×10^{-23} kg m^2 s^{-2} K^{-1}), T (K) is the temperature, η (kg m^{-1} s^{-1}) is the dispersant viscosity and R_h (m) is the hydrodynamic radius.

From the first cumulant, which corresponds to the initial slope of cumulative function (see insertion in Figure 4.4-b), the *Z-average* value is determined. Instead, the PDI corresponds to

the deviation from the linearity of the first cumulant. The PDI is related to the particle size heterogeneity, which varies within 0 and 1 (eq. 4.4), where PDI < 0.1 indicates monodisperse particles, 0.1 < PDI < 0.5 and PDI > 0.5 suggest moderately and highly polydisperse particles (ISO standards 22.412:2017) [17]. For heterogeneous and polydisperse samples, the *Z-average* size value may be fallacious [18]. Experimental conditions such as ionic strength, pH, temperature, sample concentration, colored or fluorescent sample, and solvent are influencing factors [19],

$$PDI = (\frac{\sigma}{d})^2 \qquad \text{(eq. 4.4)}$$

where σ is the standard deviation and d (nm) is the average particle diameter [20].

Otherwise, the particle size can be evaluated by intensity distribution obtained from the distribution fit based on default algorithms such as *General Purpose, Multiple Narrow Modes* and *Protein Analysis*, through a non-negative least square analysis. From the intensity distribution, the volume and number size distribution are derived.

For the determination of the cyclodextrin-based nanosponges size, the analysis was performed using an He-Ne laser at λ = 633 nm, detector at 173° backscatter. Dispersion of within 0.1 and 0.2 mg mL^{-1} was prepared in distilled water used as dispersant solvent with refractive index of 1.33 (RI) and viscosity value of 0.0008 kg m^{-1} s^{-1}, at 25 °C. Default algorithm of the Zetasizer software v. 7.12, *General Purpose* analysis was used for the intensity distribution determination.

Figure 4.4-a shows that αCDAM$_{12}$ and βCDAM$_{12}$ present a decay of the correlation function at higher time, associated with larger particles as shown in Figure 4.4-b and 4.4-d. Moreover, *Z-average* value for αCDAM$_{12}$ can provides an overestimation of the size particles because the correlation function does not consider both size distribution (Figure 4.4-b and the cumulant fit as insertion). In Figure 4.4-c is represented the effect of the pH in the *Z-average* value for αCDAM$_6$, αCDAM$_{12}$, βCDAM$_6$, and βCDAM$_{12}$ (Table 4.2). As it can be seen, pH between 3.5 and 6.5 does not influence the polymer size. Differently, at alkaline pH an enhancement of the nanosponges size is observed probably caused by aggregation phenomena due to the presence of low charged or neutral functional groups on the polymer surface (Figure 4.7 – subparagraph 4.1.3). This is confirmed by the enhancement of the PDI values from acidic to alkaline pH (Figure 4.4-d). At pH = 3.5, PDI ≤ 0.16 was observed for αCDAM$_6$ and βCDAM$_6$ indicating a monodispersion, instead PDI > 0.4 was obtained for αCDAM$_{12}$ and βCDAM$_{12}$ associated to polydisperse materials.

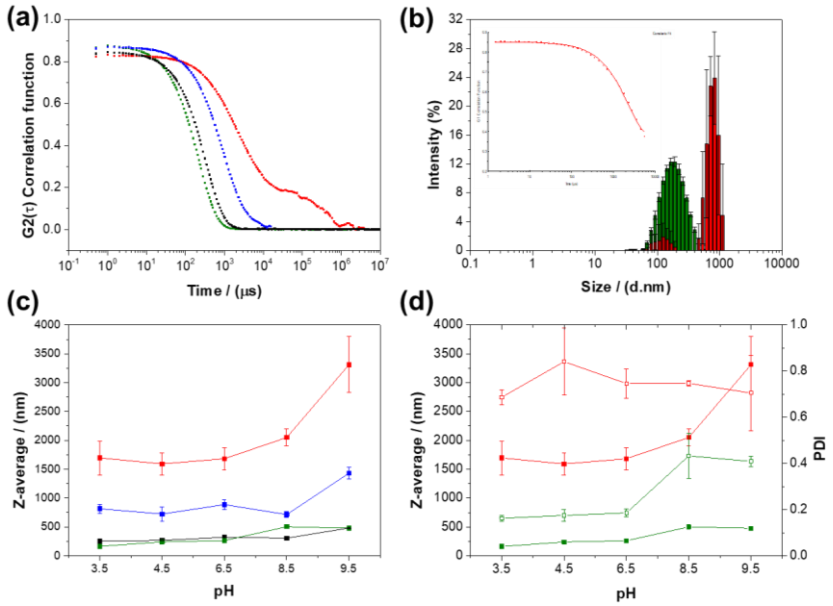

Figure 4.4. Representation of (a) correlation function; (b) particle size distribution based on intensity; (c) *Z-average* mean diameter values as function of pH; (d) effect of the pH to *Z-average* mean diameter (full square) and PDI values (empty square). αCDAM$_6$ (green line), αCDAM$_{12}$ (red line), βCDAM$_6$ (black line), and βCDAM$_{12}$ (blue line).

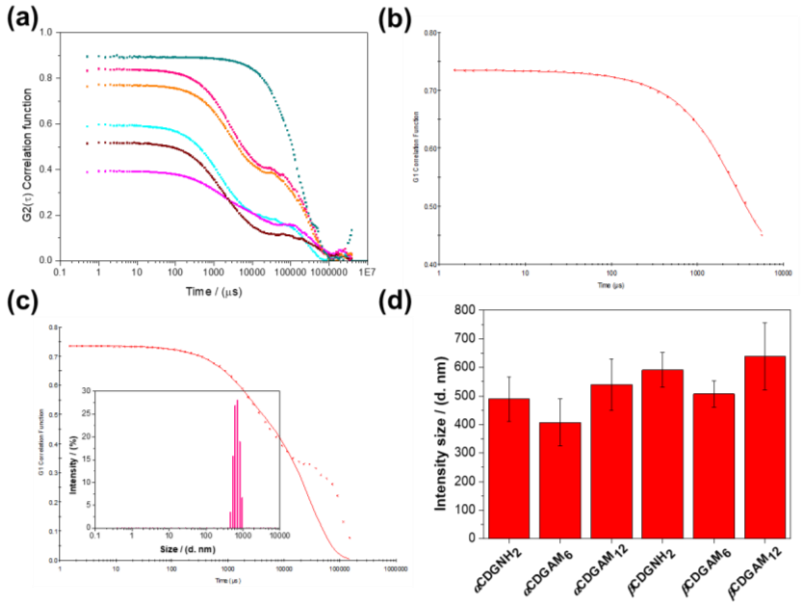

Figure 4.5. Representation of (a) correlation function of αCDGNH$_2$ (azure line), αCDGAM$_6$ (magenta line), αCDGAM$_{12}$ (brown line); (d) βCDGNH$_2$ (pink line), βCDGAM$_6$ (orange line), βCDGAM$_{12}$ (dark-cyan line); (b) cumulative function of βCDGNH$_2$; (c) distribution fit and intensity size distribution as insert of βCDGNH$_2$; (d) particle size values determined by the intensity distribution.

Table 4.2. DLS parameters of the first class of amine-CDNS as function of pH.

Nanosponges	pH	*Z–average* ± std (d.nm)	PDI ± std
αCDAM$_6$	3.5	163 ± 2	0.16 ± 0.01
	4.5	241 ± 4	0.18 ± 0.02
	6.5	263 ± 3	0.19 ± 0.02
	8.5	503 ± 36	0.46 ± 0.08
	9.5	478 ± 24	0.41 ± 0.02
αCDAM$_{12}$	3.5	1696 ± 293 *	0.79 ± 0.08
	4.5	1592 ± 193 *	0.8 ± 0.2
	6.5	1682 ± 193 *	0.75 ± 0.06
	8.5	2050 ± 145 *	0.747 ± 0.008
	9.5	3311 ± 485 *	0.7 ± 0.2
βCDAM$_6$	3.5	253.7 ± 0.2	0.137 ± 0.006
	4.5	267 ± 3	0.13 ± 0.02
	6.5	320 ± 6	0.20 ± 0.03
	8.5	306 ± 5	0.28 ± 0.01
	9.5	481 ± 4	0.37 ± 0.01
βCDAM$_{12}$	3.5	814 ± 78 *	0.44 ± 0.04
	4.5	725 ± 122 *	0.6 ± 0.1
	6.5	886 ± 84 *	0.6 ± 0.1
	8.5	714 ± 52 *	0.51 ± 0.04
	9.5	1432 ± 99 *	0.61 ± 0.08

* Values obtained considering two nodal distributions.

For the second class of CDAM-NS, which correlograms are shown in Figure 4.5-a, the *Z-average* values give an overestimation of the particle size for the batch of 6 polymers. This is due to the presence of what is called “number fluctuations”, which is represented by elevated baseline, and/or discontinuity in the correlation function (Figure 4.5-a). Moreover, as observed in the cumulant fit in Figure 4.5-b a lower number of points of the correlogram function is fitted compared to the distribution fit (Figure 4.5-c). Thus, for a qualitative assessment of the size value of the particle diameter, the mean value of the intensity distribution has been considered, which is in good agreement with the volume and number distribution, in duplicate (Table 4.3). Overall, the second class of amine-nanosponges has values of PDI ≥ 0.8 related to the highly polydisperse particles. That is usually associated with the aggregate formation, big particles or their precipitation, in agreement with the morphological results presented in Figure 4.3 –

subparagraph 4.1.1. From the intensity size values, it can be observed that the *α*CD-based nanosponges have lower size than the *β*CD-based nanosponges. However, other techniques should be employed to quantitatively accept the size values, such as SEM or TEM that can be compared with the mean number value.

Table 4.3. Particle size parameters of the second class of CDAM-NS, in aqueous dispersion.

Nanosponges	Intensity size (d. nm)	Volume size (d. nm)	Number size (d.nm)	PDI
*α*CDGNH$_2$	489 ± 77	505 ± 96	467 ± 91	0.80 ± 0.06
*α*CDGAM$_6$	493 ± 5	507 ± 3	474 ± 9	0.82 ±0.14
*α*CDGAM$_{12}$	584 ± 62	619 ± 76	562 ± 62	0.90 ± 0.2
*β*CDGNH$_2$	600 ± 12	616 ± 14	596 ± 12	0.96 ± 0.05
*β*CDGAM$_6$	545 ± 55	558 ± 62	539 ± 52	1 ± 0
*β*CDGAM$_{12}$	663 ± 33	624 ± 33	569 ± 27	1 ± 0

4.1.3. Zeta Potential

The presence of functional groups in NP structure is of outstanding importance since it confer peculiar properties such as specific active sites for physical or chemical interactions, pH-responsiveness, optical properties, among others. Moreover, depending on the type of functional groups, the material can present a neutral, negatively or positively charged surface that can electrically stabilize the sample in suspension media avoiding aggregation phenomena by electrostatic repulsion. The potential at the particle surface known as *Nernst potential* (E_0) is not directly measurable and exponentially decreases with the distance from the particle (eq. 4.5):

$$E = E_S e^{-kx} \qquad \text{(eq. 4.5)}$$

where E_S and E (mV) are the surface potential at the Stern layer (x) and at $x + \Delta x$, respectively. k is the Debye-Hückel parameter, dependent on the ionic strength. E_S can be substituted with ζ-potential when the electrical double layer is strictly close to the Stern layer ($E_S \approx \zeta$).

Hence, the ζ-potential (or electrokinetic potential) is a measure of the surface charge of a particle in colloidal systems as potential difference between the electrical double layer (slipping plane) and the thin layer of the media. It expresses the potential at the interface particle-fluid, as the charge at the particle surface [16] (Figure 4.6). The ζ-potential is directly related with the stability of a colloidal system, based on the DLVO theory. It explains the aggregation and kinetic stability of aqueous dispersion taken into account the van der Waals attraction forces and

the electrostatic repulsion. The higher the value of ζ-potential in absolute terms, the more stable is the system [21]. Experimentally, the analysis is performed by measuring the electrophoretic mobility ($\mu_e = V/E$ – where V (μm s^{-1}) is the mobility speed and E (V cm^{-1}) is the electrical field) of the particle under an electrical field. The most applied model to calculate the ζ-potential is Smoluchowski's theory, which is independent from the shape of the particle and their concentration but is limited to thin double layer and negligible surface conductivity. The Helmholtz-Smoluchowski function is included in Henry's equation used to measure the μ_e [22],

$$\mu_e = \frac{2\varepsilon_r \varepsilon_0 \zeta f(K_a)}{3\eta} \qquad \text{(eq. 4.6)}$$

where ε_0 ($A^2 \cdot s^4 \cdot kg^{-1} \cdot m^{-3}$) and ε_r are the permittivity of vacuum and the relative permittivity (dielectric constant), respectively. $f(K_a)$ is the Helmholtz-Smoluchowski function varying between 1 and 1.5 as function of the experimental conditions, and η ($kg \cdot m^{-1} \cdot s^{-1}$) is the viscosity.

It is generally accepted that 25 mV < ζ < −25 mV leads to an excess of repulsion forces, electrical stability. However, the ζ-potential values are highly affected by the chemical composition of the surface, concentration, size of particle, pH, temperature, solvent and ionic strength, among others [12].

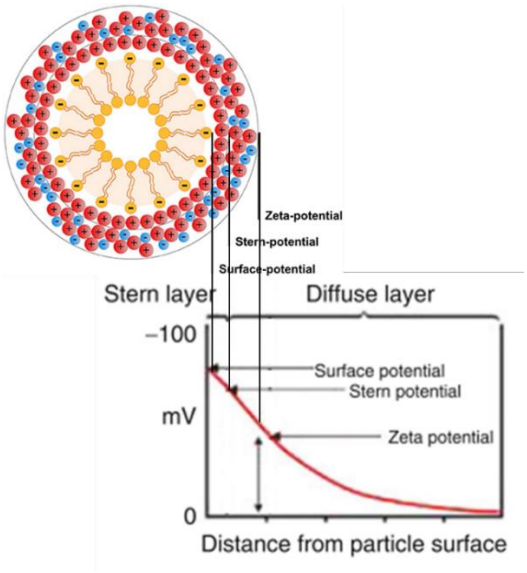

Figure 4.6. Representation of the charge layers involved in ζ-potential measurements and their dependence to the distance.

The Figure 4.7 states the behavior of the first class of the CDNS, which maintain a positively charged surface in the whole pH range. In particular, αCDAM$_6$ and βCDAM$_6$ show a ζ-potential

> 30 mV also at pH 9.5, so, they are more electrically stable than αCDAM$_{12}$ and βCDAM$_{12}$, which ζ-potential value is < 20 mV at pH 9.5. The variation of the ζ-potential seems to be correlated with ratio between the total and free moles of nitrogen per gram of NS determined by potentiometric titration of the nanosponges (see Figure 4.14 and Table 4.6 – paragraph 4.2 - subparagraph 4.2.4) and the CD% content in the polymers indirectly calculated from the data of CHNSO elemental analysis (see Table 4.5 – paragraph 4.2 - sub-paragraph 4.2.2.). However, the CD% content is inversely correlated with the degree of crosslinking and the free moles of nitrogen in the structure. It suggests that beyond the primary amine groups also the secondary amine groups can contribute to the electrical stability, confirming that lower CD content led to higher degree of crosslinking, so, denser structure (Figure 4.2. – paragraph 4.1. – subparagraph 4.1.1.), and higher Z-average values (Figure 4.4. and Table 4.2.– paragraph 4.1. – subparagraph 4.1.2.). Higher values of ζ-potential for αCDAM$_6$ and βCDAM$_6$ led to their lower size due to the electrostatic repulsion, reducing the aggregation. At contrary to αCDAM$_{12}$ and βCDAM$_{12}$ have higher degree of crosslinking, with a dense 3D-network, which means that more amine groups in the bulk phase are not easily available.

The ζ-potential of the second class of CDNSs, αCDGNH$_2$, αCDGAM$_6$, αCDGAM$_{12}$, βCDGNH$_2$, βCDGAM$_6$, βCDGAM$_{12}$, will be measured by *Malvern Zetasizer nanoZS*.

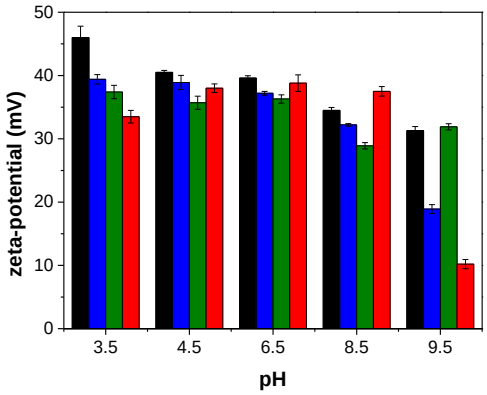

Figure 4.7. ζ-potential values as function of pH for αCDAM$_6$ (green bar), αCDAM$_{12}$ (red bar), βCDAM$_6$ (black bar), and βCDAM$_{12}$ (blue bar).

4.1.4. Porosity and surface area

The porosity is a fundamental property, influencing the free volume and the active surface area of the material. They have a crucial role in the application areas regulating, for example, the rate of sorbent-sorbate interaction in the uptake, delivery, separation and catalytic processes as well as the loading capability and entrapment efficiency. Based on IUPAC definition, a material is classified as microporous (≤ 2 nm), mesoporous (2 < nm < 50) or macroporous (> 50 nm). It can be determined by several methods like He-pycnometry, gas adsorption, mercury intrusion porosimetry, small and ultra small angle neutron scattering (SANS and USANS), and TEM [23]. The pore diameter (P_d), pore volume (V_p) and specific surface area (S_{BET}), were calculated by gas-adsorption analysis which will be discussed in more detail.

Gas-adsorption is a non-destructive method based on the capillary condensation of liquid or gas [24] into the open pores. Different gases can be used as, for example, N_2, Ar, O_2, CO_2, Kr and H_2O, as function of the average area occupied per molecule in the monolayer. The use of an inert gas allows to avoid interferences from chemical interactions. In particular, N_2 permits to determine pore diameter within 0.35 - 500 nm. The gas-solid interaction is influenced either by the experimental conditions or the interaction nature, with them being physical (physisorption) or chemical (chemisorption). It must be stressed that the determination of the pore size distribution of a solid phase depends on the sorption and its counterpart, the desorption process, at certain pressure and temperature. Both processes indicate the direction of the analysis with the respective curves, where the point of non-overlapping is called hysteresis (Figure 4.8) [25,26]. The hysteresis loop is a reversible process due to capillary condensation at relative pressure (p/p_0) > 0.4/0.5. The desorption process permits a better assessment of the pore diameter and pore shape due to the thermodynamic stability (Figure 4.8.) (eq. 4.7), based on the Kelvin equation or Barrett-Joyner-Halenda model (BJH) [30,31], from which is possible to obtain a pore distribution.

$$\Delta G = RT \ln\left(\frac{p}{p_0}\right) \qquad \text{(eq. 4.7)}$$

where R (8.314 m^3 Pa $K^{-1}mol^{-1}$) is the gas constant and T (K) is the temperature. Thus, for the same amount of volume adsorbed $\Delta G_{des} < \Delta G_{ads}$.

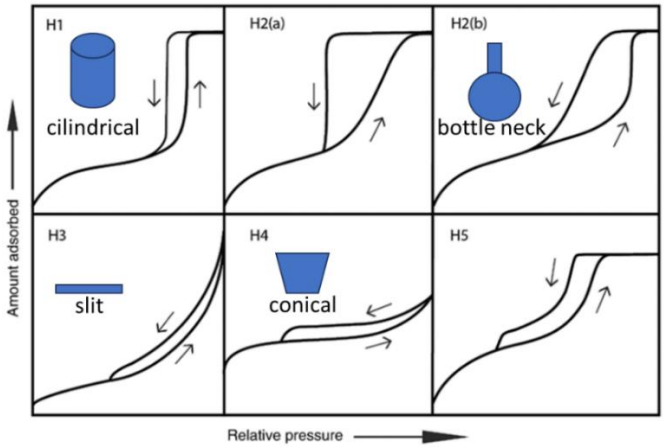

Figure 4.8. Classification of the sorption-desorption hysteresis [25].

The Brunauer-Emmett-Teller model (BET) is the most prevalent for surface area determination [25][24]. The mathematical expression of the BET model is shown in (eq. 4.8),

$$\frac{p}{X(p_0-p)} = \frac{1}{X_m C} + \frac{(C-1)p}{X_m C p_0} \qquad \text{(eq. 4.8)}$$

where p and p_0 (Pa) are the pressures at the equilibrium state and at saturated vapor pressure, respectively, X and X_m (mol g^{-1}) are the adsorption capacity at specific relative pressure values and the saturated adsorption capacity of the monolayer, respectively, and C is the BET constant related to the interaction strength sorbent-sorbate [26]. Plotting the left-hand side of the eq. 4.8 as function of the narrow linear range of relative pressure ($0.05 < p/p_0 < 0.3$), X_m and C are determined from intercept and slope values. Thus, it is possible to calculate the specific surface area (eq. 4.9) [27],

$$S_{BET} = \frac{X_m a_m N}{M} \qquad \text{(eq. 4.9)}$$

where a_m (m^2 molec.$^{-1}$) is the area occupied per adsorbate's molecule in the monolayer, N is the Avogadro's constant (6.023×10^{23} molec. mol^{-1}), and M (g mol^{-1}) is the molecular weight of the adsorbate [28][29]. The total amount of nitrogen taken up gives the total pore volume value, then the average pore diameter can be calculated as $P_d = 4V_p/S_{BET}$, assuming an energetical homogeneous interaction at the active sites, giving more importance to the sorbent-sorbate interaction at the monolayer. The pore volume and diameter are calculated considering a cylindric pore geometry.

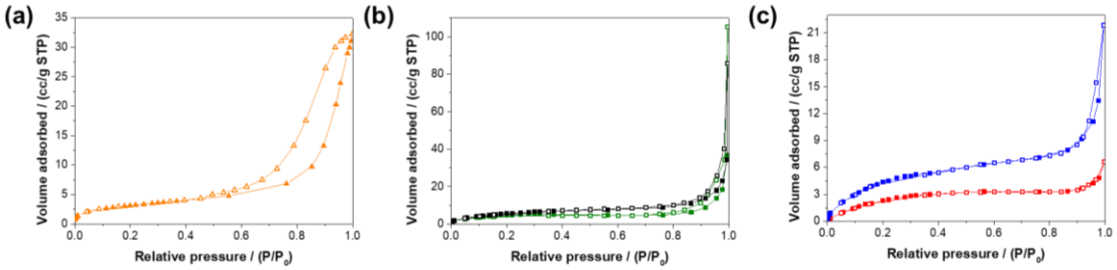

Figure 4.9. Sorption hysteresis of (a) PCD (orange curve) (b) αCDAM$_6$ (green curve), βCDAM$_6$ (black curve) and (c) αCDAM$_{12}$ (red curve), βCDAM$_{12}$ (blue curve). Sorption curve (full square) and desorption curves (empty square).

For the pure PCD, the isotherm type IV (Figure 4.9-a) indicates a mesoporous material with a H1 hysteresis loop which suggests a cylindrical pore shape. Due to the higher thermodynamic stability, the desorption process was considered to determine the pore diameter (10.85 nm). The surface area was obtained by the eq. 4.9, S_{BET} = 11.3 m^2 g^{-1}. The continuous increase of the volume of gas adsorbed as a function of the relative pressure is related to the multilayer formation.

For αCDAM$_6$ and βCDAM$_6$, the monolayer formation is well defined, with a type IV isotherm and H3 hysteresis loop (Figure 4.9-b). H3 hysteresis loop is also suggested for βCDAM$_{12}$, but the multilayer formation is more significant (Figure 4.9-c). The H3 hysteresis indicates a slit-shaped pores for αCDAM$_6$ (31.7 nm), βCDAM$_6$ (27.4 nm) and βCDAM$_{12}$ (16.5 nm). Differently, for αCDAM$_{12}$ an isotherm type I was obtained, which is typical of microporous material (3.8 nm) characterized by low surface area. The surface areas follow the increasing order αCDAM$_{12}$ (10.7 m^2 g^{-1}) < αCDAM$_6$ (17.2 m^2 g^{-1}) ≈ βCDAM$_{12}$ (17.9 m^2 g^{-1}) < βCDAM$_6$ (21.8 m^2 g^{-1}). These results agree with the size of particles (Table 4.2 – subparagraph 4.1.2., *CD%* and *DC* (Table 4.5 – paragraph 4.2 – subparagraph 4.2.2.).

For the second class of nanosponges, namely αCDGNH$_2$, αCDGAM$_6$, αCDGAM$_{12}$, βCDGNH$_2$, βCDGAM$_6$ and βCDGAM$_{12}$, it was not possible to determine a specific pore-shape due to the absence of hysteresis loop in the adsorption/desorption curves, indicating possible non-porous materials, at least within the range of the equipment analysis. Nevertheless, it was possible to determine the S_{BET}, V_p and P_d, through the BET model and the values are reported in Table 4.4. Generally, the polymers present P_d values ≤ 50 nm, exhibiting a direct relation with the degree of crosslinking, cyclodextrin content (Table 4.5 – paragraph 4.2 – subparagraph 4.2.2.) and amine groups distribution (Table 4.6. – paragraph 4.2 – subparagraph 4.2.4.) (with the data available so far). V_p values seem directly correlated with the surface area, indeed, higher volume

led to higher surface area, with the lowest value for βCDGAM$_6$ (9.3 m^2 g^{-1}) and the highest S_{BET} values for αCDGAM$_6$ and βCDGNH$_2$.

Table 4.4. Parameters of gas-sorption analysis of the second class of CDAM-NS.

N_2-adsorption analysis			
Nanosponges	**Average pore diameter (nm)**	**Pore volume (cm^3 g^{-1})**	**Surface area (m^2 g^{-1})**
αCDGNH$_2$	30.5	0.16	20.6
αCDGAM$_6$	54.8	0.33	23.8
αCDGAM$_{12}$	39.6	0.12	12.6
βCDGNH$_2$	32.2	0.19	23.2
βCDGAM$_6$	42.9	0.10	9.3
βCDGAM$_{12}$	38.2	0.13	14.1

4.2.Chemical characterization

4.2.1. Fourier transform infrared spectroscopy

The infrared spectroscopy is a common method performed using the electromagnetic spectrum between the visible and microwave region, in particular in the wavenumber range 4000 - 400 cm^{-1}. The infrared spectrum is characteristic of each molecule, permitting the identification of functional groups peak-by-peak. IR-spectroscopy can be performed to gas, liquid or solid samples. Solid sample is usually analyzed via mull or pellet preparation. Pellet preparation is performed by mixing a maximum of 5% (w/w) of sample with KBr, under pressure [32]. The resolution depends on good mixing of the components, thickness and transparency of the pellet. The radiation is absorbed by the molecule, converted into vibrational modes and quantified by bands. The wavenumber of absorption depends on the relative mass of the atoms and their geometry, the bond strength and the molecular environment. *Y* is directly proportional to the energy of the light in agreement with the Planck equation. The intensity of the bands can be expressed as transmittance or absorbance. The vibrational modes usually observed are stretching or bending (Figure 4.10) and only the vibrational modes that imply a rhythmical change of the dipole moment of a molecule or a functional group can be observed [33]. Stronger dipole moment of the functional group led to higher IR signal. The permitted vibrational modes are function of the degree of freedom of a molecule of *n* atoms (3*n*), distinguished in linear (3*n*-5) and non-linear molecules (3*n*-6), which include rotational and translational modes. However,

the experimental number of theoretical vibrational modes can be increased by overtones or overlaps of the bands and decreased by low intensity of the signal or coalescence of two vibrational modes [34].

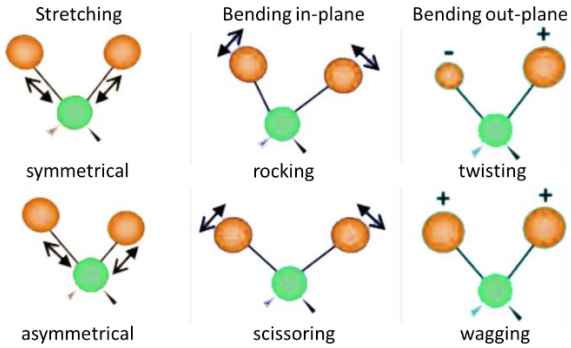

Figure 4.10. Representation of the vibrational modes.

Particularly, the Fourier transform infrared spectrometer (FTIR) has a high signal-to-noise ratio resulting from the sum of numerous scans as function of the time. FTIR has also a high resolution (± 0.01 cm^{-1}) due to the high-intensity of radiation reaching the detector based on the constructive-destructive interferogram, directly proportional to the frequency of the light. In a IR spectrum three important regions can be identified: *i)* within 4000-1300 cm^{-1} defined as high-frequency region and characteristic of specific functional groups as -OH, -NH_x and -C=O; *ii*) the complex finger-print region between 1300-950 cm^{-1} originated from the interaction of the vibrational modes of the functional groups; *iii*) the low-frequency region between 950-650 cm^{-1}, where strong bands can indicate the presence of aromatic or halide groups.

The FTIR analysis of the different sorbent materials were performed via KBr pellets, with a maximum of 2% (w/w) of the sample (Figure 4.11). From a first evaluation of the spectrograms in Figure 4.11, it is possible to observe that PCD present different vibrational bands than the CDAM-NS.

In PCD synthesis, the HDI was used as a crosslinker with formation of the carbamate group (Figure 4.12-a). In the spectra in Figure 4.11-a related to the PCD, the strong band at 1710 cm^{-1} indicates the -C=O vibrational stretching (1765-1720 cm^{-1}) of the esther groups. The amide group is confirmed by the presence of the bands at 1643 cm^{-1} and 1550 cm^{-1} associated with the stretching of -C=O in amide I (1680-1640 cm^{-1}) and -NH bending (1560-1530 cm^{-1}). The medium stretching band at 1265 cm^{-1} (1310-1290 cm^{-1}) is associated with the -CN group.

Considering the CDAM-NS, primary and secondary amine groups are the main functional groups, both as free groups and as a result of the polymerization reaction, respectively (Figure 4.12-b). As expected, the two classes of amine-nanosponges exhibit similar vibrational bands. The two bands around 2900 cm^{-1} are associated with asymmetrical and symmetrical stretching vibration of -CH_2- groups. The alkyl chain of the glutaraldehyde for the amine-CDNS spectra represented in Figure 4.11-c and 4.11-d must be also taken in consideration. In the second class of nanosponges, the effect of the aliphatic chain length of the crosslinker is also noticeable by a medium band at 1463 cm^{-1} due to the scissoring vibration mode of -CH_2- groups. The strong band at *ca.* 1660 cm^{-1} is associated with -NH- groups. Instead, the band with lower intensity at *ca.* 1550 cm^{-1} indicates the presence of -NH_2 groups. Primary and secondary ammine groups make them pH-responsive materials. The strong bands at 1150 cm^{-1}, 1080 cm^{-1} and 1040 cm^{-1} are related with stretching vibration of -C-C-N- or -C-O-C- groups (1230-1100 cm^{-1}), -C-NH- group (1120-1030 cm^{-1}) and -CH-OH group (1065-1015 cm^{-1}), respectively. Shifting of the bands from the associated ranges can be due to inter- and intra-molecular interactions.

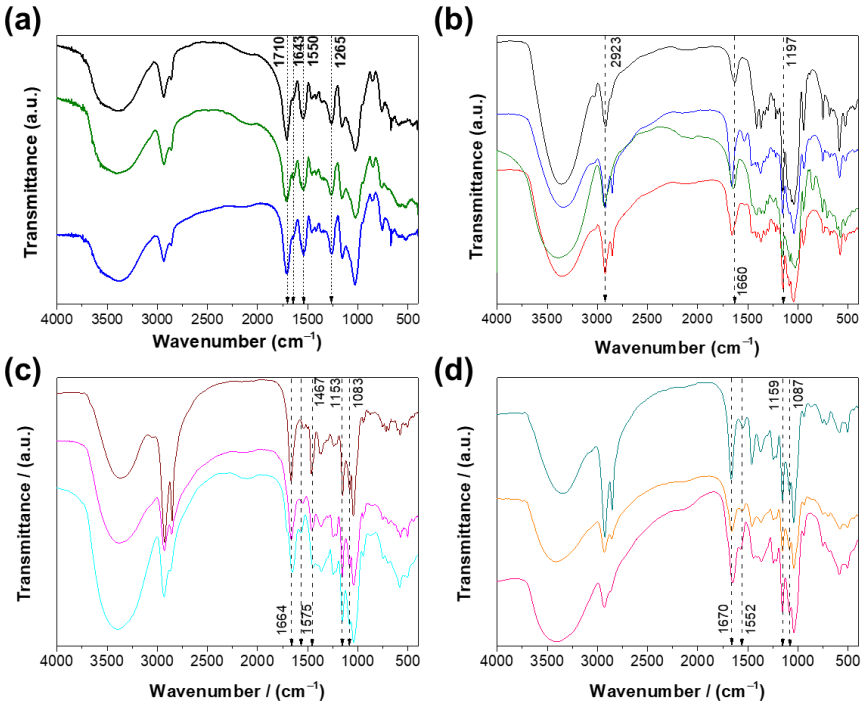

Figure 4.11. FTIR spectra of (a) PCD (black line), PCD-AC5% (green line), PCD-AC10% (blue line); (b) αCDAM$_6$ (green line), αCDAM$_{12}$ (red line), βCDAM$_6$ (black line), and βCDAM$_{12}$ (blue line); (c) αCDGNH$_2$ (light-blue line), αCDGAM$_6$ (magenta line), αCDGAM$_{12}$ (brown line); (d) βCDGNH$_2$ (pink line), βCDGAM$_6$ (orange line), βCDGAM$_{12}$ (dark-cyan line).

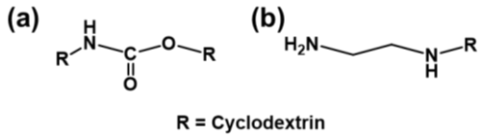

Figure 4.12. Representation of the characteristic functional groups in the sorbent materials.

4.2.2. Elemental analysis

The elemental analysis is employed for the determination of the amount of carbon, hydrogen, nitrogen and sulphur for a wide range of substances. The measurements are performed on solids, liquids or gases by combustion at high temperature (1000 °C), in static or flow of O_2 atmosphere, with addition of a catalyst (*e.g.* Pt, Pd, Re). The O_2 in the combustion step transforms C into CO_2, H into H_2O, N into N_2 or NO_x, S into SO_2. The products are carried out from the chamber by an inert gas passing to high purity copper for reductive reaction. In this way, O_2 residues and other elements are also removed passing to a sorbent trap. Then, the gas goes through a separation technique, such as gas-chromatography, and the elements are finally detected by thermal conductivity. The result permits to calculate the crude empirical formula of a compound [35]. Disadvantages are represented by air-sensitivity, random errors, and calibration.

CHNSO elemental analysis was performed for a better understanding of the physical structural parameters related to the porosity and surface area. Indeed, it enabled the indirectly estimation of the unit of CD and the degree of crosslinking. The values are reported in Table 4.5.

Qualitatively, it was possible to extract the respective empirical formula of the CDNSs: αCDAM$_6$ ($C_{31}H_{45}N_1I_3O_{57}$), αCDAM$_{12}$ ($C_{22}H_{32}N_1I_2O_{33}$), βCDAM$_6$ ($C_{63}H_{81}N_1I_9O_{120}$), βCDAM$_{12}$ ($C_{14}H_{25}N_1I_1O_{14}$), αCDGNH$_2$ ($C_{15}H_{28}N_1O_9$), βCDGNH$_2$ ($C_{12}H_{24}N_1O_7$), βCDGAM$_6$ ($C_{10}H_{18}N_1O_4$). From the empirical formula an increment in terms of moles of carbon is registered as βCDAM$_{12}$ < αCDAM$_{12}$ < αCDAM$_6$ < βCDAM$_6$, which agree with the CD% values reported in Table 4.5. However, higher amount of CD% led to lower DC values due to the presence of higher number of active sites reacted in the polymerization reaction (Table 4.6 – subparagraph 4.2.4.). Moreover, the higher *DC* of αCDAM$_{12}$ and βCDAM$_{12}$ can also be determined by the higher chain length which is less influenced by steric hindrance. This is in agreement with the denser morphology obtained by SEM (Figure 4.2-b and 4.2-d - paragraph 4.1 – subparagraph 4.1.1)

Considering the data available until now (Table 4.5), the second class of amine-CDNS present a direct correlation between the *CD%* and the *DC* values. The result suggests that the click-condensation with glutaraldehyde and the higher length of the arms compared to the first class

of CDAM-NS led to a drastic reduction of the steric hindrance influence; indeed, the *DC* of αCDGAM$_6$ and βCDGAM$_6$ are ≈ 2 and 5-fold higher than for αCDGAM$_6$ and βCDAM$_6$. Additionally, with higher *CD%* increases the amount in terms of moles of nitrogen per gram of NS (Figure 4.14 and Table 4.6 – subparagraph 4.2.4.), in agreement with the *DC* values and the morphological results (Figure 4.3 – paragraph 4.1 – subparagraph 4.1.1.).

Table 4.5. CHNO values from elemental analysis of cyclodextrin-based nanosponges.

	Elemental						
CDNSs	**N% (w/w)**	**C% (w/w)**	**H% (w/w)**	**I% (w/w)**	**O% (w/w)**	**CD% (w/w)**	**DC**
αCDAM$_6$	1.04 ± 0.01	27.93 ± 0.19	3.39 ± 0.21	31.91 ± 1.45[a]	35.74 ± 1.50[b]	0.69[c]	1.5[d]
αCDAM$_{12}$	1.69 ± 0.01	31.43 ± 0.02	4.10 ± 0.16	36.71 ± 1.17[a]	26.25 ± 1.19[b]	0.59[c]	2.9[d]
βCDAM$_6$	0.51 ± 0.02	27.37 ± 0.06	2.95 ± 0.09	40.11 ± 1.50[a]	29.07 ± 1.51[b]	0.62[c]	0.8[d]
βCDAM$_{12}$	3.25 ± 0.02	38.78 ± 0.07	5.72 ± 0.31	33.13 ± 3.29[a]	19.14 ± 3.32[b]	0.46[c]	7.0[d]
αCDGNH$_2$	3.84 ± 0.08	50.80 ± 0.02	7.59 ± 0.19	n.a.	37.58 ± 0.08	0.64[e]	1.4[f]
αCDGAM$_6$	6.60 ±	61.05 ±	8.46 ±	n.a.	23.67 ±	1.10[e]	3.1[f]
αCDGAM$_{12}$	–	–	–	–	–	–	–
βCDGNH$_2$	4.70 ± 0.30	48.71 ± 0.23	8.04 ± 1.35	n.a.	38.15 ± 2.34	0.67[e]	2.3[f]
βCDGAM$_6$	6.56 ± 0.1	56.55 ± 0.05	8.33 ± 0.59	n.a.	28.46 ± 0.57	0.94[e]	3.8[f]
βCDGAM$_{12}$	–	–	–	–	–	–	–

[a] I% (w/w) values reported on the table are obtained by EDX analysis, for CDNSs involving CD-I in the polymerization;
[b] O% = 100 − (N% + C% + H% + I%);
[c] CD% = (C% − C_{linker}%)/C_{CD}; [e] CD% = C_{CDNS}% / C_{CD}
[d] DC (degree of crosslinking) is calculated as the amount of N per mole of cyclodextrin as obtained by elemental analysis;
[f] DC is calculated as the amount of N per mole of glutaraldehyde obtained as difference of C% − C_{CDNS}%.
–: values still not available.

4.2.3. Free-cyclodextrin content determination via inclusion complex

More in detail, albeit from the elemental analysis was possible to calculate the unit of CD for both classes of CDAM-NS, the value encompass free-CD (available to form host-guest complex in the sorption process) and trapped-CD. In order to estimate the free-CDs, an indirect measurement was performed exploiting the CD's capacity to form inclusion complexes [36–38]. Considering the stoichiometric ratio 1:1, phenolphthalein (PP) was used as a guest probe for the βCD-based nanosponges, because of the known high binding constant (K_{11} = 2.4 × 10^4 or 1.05 × 10^4) [39,40]. Stock aqueous solution of phenolphthalein 0.3 mmol L^{-1} was prepared in aqueous solution of Na_2CO_3 0.02 mol L^{-1}. Alkaline pH ≈10 ensures the complete deprotonation of the

phenolphthalein. Calibration was performed in the [PP] range within 0 - 4 × 10^{-5} mol L^{-1}, at λ_{max} = 553 nm (Figure 4.13-a). Considering the reversible process of host-guest complex formation described by the equation below (eq. 4.10), the binding constant at equilibrium state can be written via the following equation (eq. 4.11):

$$\mathbf{CD + PP} \overset{K_{1,1}}{\rightleftharpoons} \mathbf{CD\text{-}PP} \qquad \text{(eq. 4.10)}$$

$$K_{1,1} = \frac{[CD-PP]}{[CD]_f[PP]_f} \qquad \text{(eq. 4.11)}$$

where $[CD]_f$ and $[PP]_f$ are the concentration of free or uncomplexed CD and PP, respectively, at the equilibrium state. Considering the fraction of PP complexed with βCD_f, $K_{1,1}$ can be reformulated:

$$K_{1,1} = \frac{f}{(1-f)([CD]_T - f[PP]_T)} \qquad \text{(eq. 4.12)}$$

The complexation was quantified by UV-Vis through variation of the absorbance for the guest molecule, expressed by the eq. 4.13:

$$Abs_{obs} = (1-f)Abs_{PP,f} + fAbs_{CD-PP} \qquad \text{(eq. 4.13)}$$

where $Abs_{PP,f}$ and $Abs_{CD\text{-}PP}$ represent the contribution to the measured signal of free and complexed PP, respectively. Thus, the variation in presence or not of the guest is $\Delta Abs_{obs} = Abs_{obs} - Abs_{PP}$, also expressed by the following eq. 4.14:

$$\Delta Abs_{obs} = \Delta Abs_{CD-PP}\left(\left[CD - PP\right]/[PP]_T\right) \qquad \text{(eq. 4.14)}$$

Considering the reaction expressed in the eq. 4.10, the law of conservation of mass for the two reactants gives the eq. 4.15 and 4.16:

$$[CD]_f = [CD]_T - [CD - PP] \qquad \text{(eq. 4.15)}$$

$$[PP]_f = [PP]_T - [CD - PP] \qquad \text{(eq. 4.16)}$$

Combining the eq. 4.11 with the eq. 4.15 and 4.16, resolving for the complex and substituting the expression in the eq. 4.14, the result is the following eq. 4.17 [41][42]:

$$\Delta Abs_{obs} = \frac{\Delta Abs_{CD-PP}}{2[CD]_T}\left\{\left([PP]_T + [CD]_T + \frac{1}{K_1}\right) - \left(\left([PP]_T + [CD]_T + \frac{1}{K_1}\right)^2 - 4([PP]_T[CD]_T)\right)^{\frac{1}{2}}\right\} \qquad \text{(eq. 4.17)}$$

By fitting the ΔAbs_{obs} as function of the [βCD] with a non-linear least-squares algorithm, the values of $K_{1,1}$ = (2.2 ± 0.2) × 10^4 and $\Delta Abs_{CD\text{-}PP}$ (1.17 ± 0.03) were calculated (Figure 4.13-b). The binding constant value, $K_{1,1}$, was applied to indirectly determine the content of available βCD in the structure of the nanosponges. The analysis was performed by letting in contact 1 mg of nanosponge with different [PP] for 24 hours, to ensure the equilibrium state. By fitting the ΔAbs_{obs} as function of the [*PP*] (Figure 4.13-c), with pre-established value of $K_{1,1}$, the $[CD]_T$ were determined for the βCDAM-NS (Figure 4.13-d). βCDAM$_6$ shows a CD content 1 × 10^{22}-fold higher than βCDAM$_{12}$, which can explain its superior removal efficiency towards IMD as a pure active ingredient or commercial formulation. For the second class of amine-CDNS, it seems that longer aliphatic chains led to higher CD content, that for βCDGAM$_6$ is 3.7 × 10^{12} times higher than βCDGNH$_2$. Moreover, βCDGAM$_6$ has a content of free-CD moles per gram of NS ≈ 5 times lower than βCDAM$_6$, that can justify its higher degree of crosslinking. The CD content in βCDGAM$_{12}$ was not determinable as the ΔAbs_{obs} values were of the same magnitude of the equipment sensitivity.

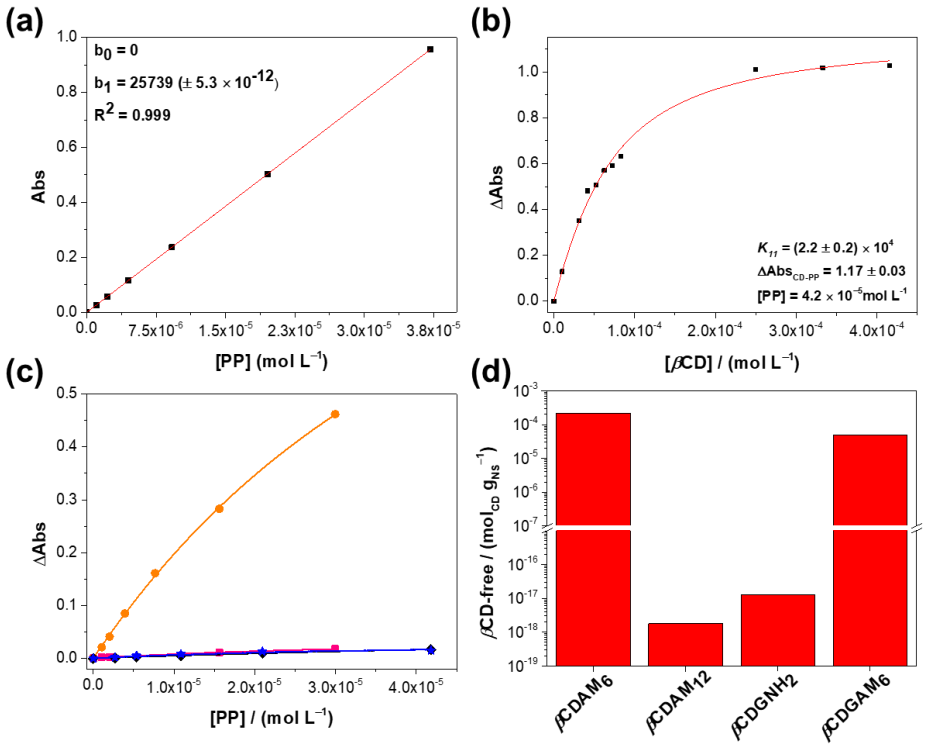

Figure 4.13. Representation of phenolphthalein host-guest analysis: (a) calibration curve of phenolphthalein aqueous solution of Na_2CO_3 0.02 mol L^{-1}; (b) determination of constant binding, $K_{1,1}$, by using titration; (c) determination of free-βCD content in βCDAM$_6$ (black curve), βCDAM$_{12}$ (blue curve), βCDGNH$_2$ (pink curve) and βCDGAM$_6$ (orange curve), by using titration; (d) histogram of the free-βCD values in term of mol_{CD} g_{NS}^{-1}.

The free-CDs were also measured in αCD-based nanosponges, however the low binding constant value, $K_{1,1}$, and the low values of ΔAbs_{obs} suggest that phenolphthalein is not suitable guest molecule. That can be due to the smaller cavity diameter which does not permit the formation of the host-guest complex. In this light, smaller molecules must be used as guest probes.

4.2.4. Potentiometric titration

The presence of primary and secondary amine groups was suggested by the bands at 1550 cm^{-1} and 1660 cm^{-1} (Figure 4.11-b, 4.11-c and 4.11-d – subparagraph 4.2.1), respectively, but quantitative data could not be extracted. In order to calculate the mole of amine groups responsive to pH, a potentiometric micro-titration was performed. A weighted amount of amine-CDNS (≈ 0.01 g) was dispersed in 5 mL of aqueous HCl 0.02 mol L^{-1} and titrated with NaOH 0.1 mol L^{-1} (Figure 4.14-a). To highlight the point of inflection, the derivative (dpH/dV) was calculated, determining two points of equivalence (Figure 4.14-b). The first point of equivalence is related to the neutralization of the excess of moles of HCl, whereas the second point of equivalence corresponds to the ammonium groups in the 3D-structure. The moles of free-nitrogen per gram of NS and its ratio *vs.* moles of total-nitrogen per gram of NS are shown in Table 4.6, in terms of percentage (Figure 4.14-c). The moles of total-nitrogen were calculated based on the N% (w/w) determined by elemental analysis (Table 4.5 – subparagraph 4.2.2.). The βCDAM$_6$ shows the highest ratio of molN_f g_{NS}^{-1}/molN_t g_{NS}^{-1}, which means a higher availability of the ammine groups in the surface, thanks to the higher S_{BET}. The presence of more molN_f g_{NS}^{-1} agrees with the lower *DC* value and is directly related with the higher *CD%* value (Table 4.5 – subparagraph 4.2.2). The high molN_f can contribute to the formation of sorbent/sorbate interactions, justifying its higher removal capability compared to the other NS of the first class of CDAM-NS. For the second class of CDNS, the histogram shows that the amount of molN_f g_{NS}^{-1} increases with the length of the amine arms in the cyclodextrin derivatives. Comparing the two class of CDAM-NS, it is possible to observe that the second class of nanosponges have higher amount of molN_t g_{NS}^{-1} and molN_f g_{NS}^{-1} than the first class of CDAM-NS, but their ratio is between 0.1% and 0.5%. This indicates that mostly of the molN_t g_{NS}^{-1} are involved in the polymerization process which increases the degree of crosslinking based on the presence of higher CD content in the general order αCDGNH$_2$ < βCDGNH$_2$ < αCDAM$_6$ < βCDGAM$_6$.

Table 4.6. Values of the total moles and free moles of nitrogen per gram of nanosponges.

Nanosponge	**molN_t g$^{-1}_{NS}$**	**molN_f g$^{-1}_{NS}$**	**(molN_f g$^{-1}_{NS}$)/(molN_t g$^{-1}_{NS}$) %**
αCDAM$_6$	0.7×10^{-3}	1.5×10^{-6}	0.2
αCDAM$_{12}$	1.2×10^{-3}	1.1×10^{-6}	0.1
αCDGNH$_2$	2.7×10^{-3}	7.4×10^{-6}	0.3
αCDGAM$_6$	4.7×10^{-3}	21.9×10^{-6}	0.5
βCDAM$_6$	0.4×10^{-3}	4.0×10^{-6}	1.1
βCDAM$_{12}$	2.3×10^{-3}	12.4×10^{-6}	0.5
βCDGNH$_2$	3.3×10^{-3}	2.7×10^{-6}	0.1
βCDGAM$_6$	4.7×10^{-3}	13.7×10^{-6}	0.3

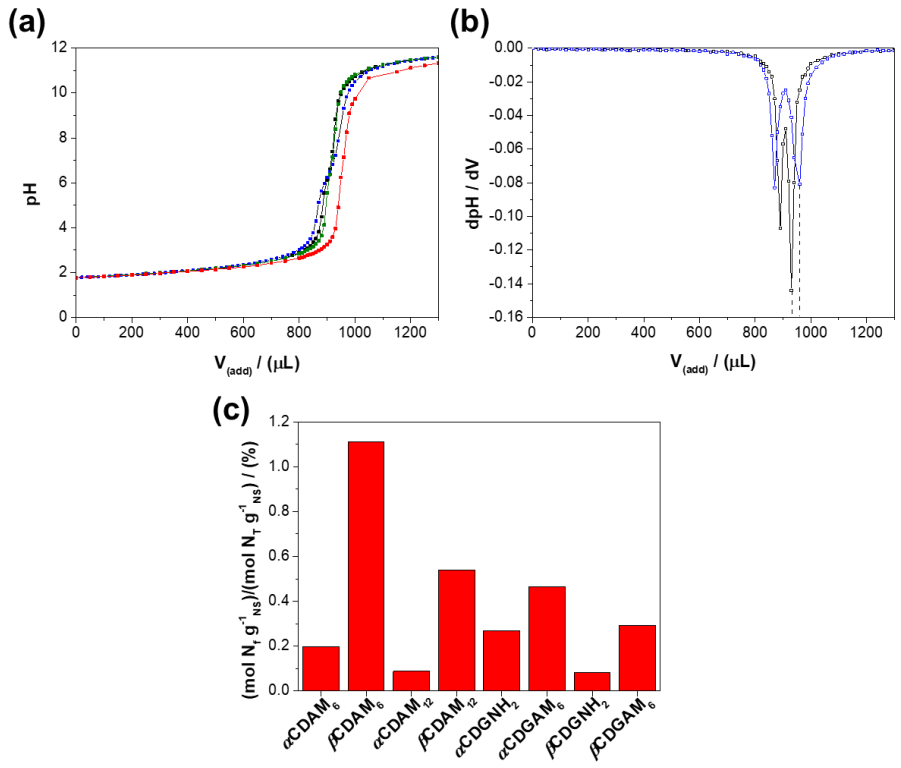

Figure 4.14. Representation of (a) pH versus titrant volume; (b) *d*pH/*d*V curves; (c) histogram of the ratio of molesN_f g$_{NS}^{-1}$/molesN_t g$_{NS}^{-1}$. In figure (a) and (b), αCDAM$_6$ (green line), αCDAM$_{12}$ (red line), βCDAM$_6$ (black line), and βCDAM$_{12}$ (blue line).

4.3. Thermal characterization

The most relevant thermal methods include differential scanning calorimetry (DSC), differential thermal analysis (DTA), thermogravimetric analysis (TGA) and dielectric thermal analysis (DETA). These permit to analyse small amounts of solid, liquid or gaseous state samples, via temperature programmes, in non-equilibrium state. Depending on the sample properties, these techniques can be employed to determine physical and chemical properties through controlled heat exchange [43]. The change in a sample property is determined as a function of the temperature in the time (Figure 4.15). The analysis can be performed in gradient of temperature or in isothermal conditions. It must be considered that a homogeneous heat exchange with the sample is a function of its mass, volume, composition and structure complexity. Moreover, several experimental parameters can influence the analysis such as heating rate, pressure and atmosphere. The heat exchange can be performed by three transfer mechanisms as conduction, convection and radiation. It must be kept in attention that indirect complementary analytical data (*e.g.* TGA/DSC or DTA/DSC) is needed to understand molecular processes at thermodynamic level [44].

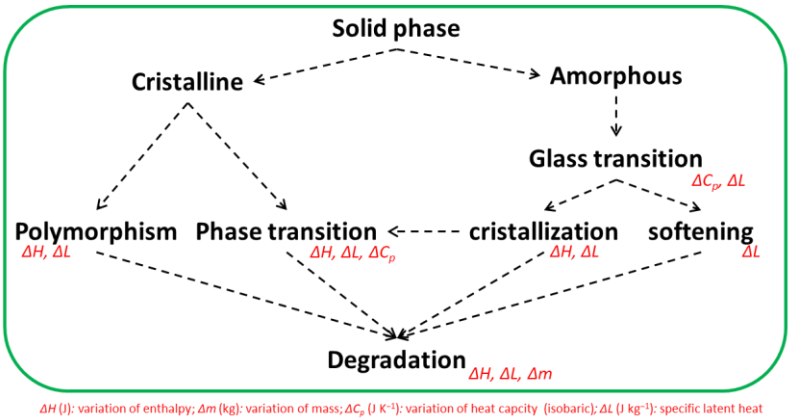

Figure 4.15. Physical and chemical properties obtained by thermal analysis in solid sample.

Thermogravimetric analysis is based on thermodynamic events; but the molecular processes involved are usually not known. Thermogravimetry measurement involves sample properties changes via mass variation (absorption/desorption, decomposition, oxidation, reduction or sublimation) as function of the temperature or time in an open system. The respective graph is called “thermal analysis curve”. In this sense when complex polymeric structures are studied, the internal network, heterogeneity, presence of numerous functional groups, shape and size particle and porosity are important factors such as mass and volume. These can make phase

transitions unobservable, because the thermal decomposition or crystolysis, which are directly related to break of chemical linkage via thermolysis, may occur before the melting point [45]. The equipment employed for the thermogravimetric analysis records the mass variation by a thermobalance, which is a combination of a microbalance with an electromagnetic power compensation and furnace. This system presents a maximum load of 2 g and sensitivity of 0.01 μg. More sensitive is the quartz crystal microbalance at expense of stability and working temperature range. The microbalance is enclosed by a gas-tight thermostatically controlled housing, which reduces temperature influences. Then, the heat exchange is obtained by radiative mechanism through an air or inert gas gap between furnace and sample. An alternative is the infrared heating with faster heating-rate of the sample, but the development of gases absorbing the radiation represents a disadvantage. Different gases can be used (*e.g.* He, Ar, N_2, air, O_2, CO_2) in static or flowing mode, influencing the resultant curves. The gas-flowing reduces gas condensation, corrosion phenomena and helps in the cooling process. Their choice must consider the reactivity, cost, purity, density and thermal conductivity. The temperature control is the most critical point obtained by a thermocouple sensor. As shown in Figure 4.16, several thermogravimetric curves can result from TGA which are related to dehydration, single- or multi-step decomposition and oxidation processes [46]. It must be stressed that the heating rate can strongly affect the resulting curve. As an example, high heating rate as well as dense polymeric materials enhance the decomposition temperature and decrease the temperature interval. Furthermore, from the mass change associated with a thermal decomposition step, it is possible to calculate the rate of mass loss (M_L) (eq. 4.18),

$$M_L = \frac{(m_i - m_{s)}}{m_s} \times 100 \qquad \text{(eq. 4.18)}$$

where m_i and m_s (g) are the initial and final mass of the sample before and after a thermal event, respectively.

In multi-step decomposition, thermal events can result in overlapping, that is hardly resolved. Improved resolution can be obtained modifying the experimental conditions such as lower heating rate. Another possibility is to plot the first derivative of the TG curve (dTG) as a function of temperature (dm/dT), evidencing the temperature of maximum degradation rate (T_{max}) of a thermal event. The area under the peak, in a dTG, represents the percentage of mass loss and the height indicates the rate of mass variation at a specific temperature [47].

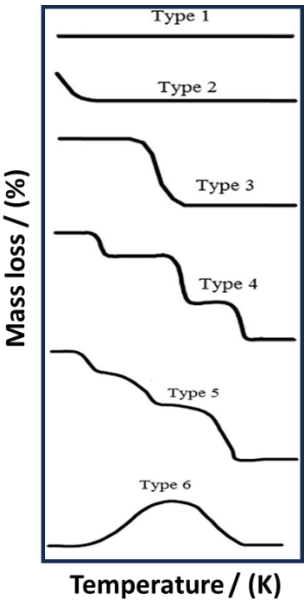

Figure 4.16. representation of the main thermogravimetric curves [46].

For the thermogravimetric analysis, ground polymeric materials in powder-state (2-5 mg) were used to ensure a homogeneous heat exchange, as much as possible. Nitrogen-gas was used during the measurement due to its chemical unreactivity, at flow rate of 50 mL min^{-1}. The analysis was usually performed with temperature increment, dT/dt = 10 K min^{-1}. The thermal analysis curves and the corresponding dTG are represented in Figure 4.17; the values are reported in Table 4.7. Generally, from the values reported in Table 4.7, it is possible to observe that the decomposition of the sorbent materials is a multistep process.

In detail, the $T_{1,max}$ temperature values inherent to the dehydration process are higher for PCD hydrogels than for CDAM-NS powders. It can be explained considering that a hydrogel is defined as an insoluble condensed matter with high water retention capability. The bigger solids size and its density can also influence the heat exchange to the bulk phase reducing the dehydration rate. The second thermal event, $T_{2,max}$, is reported around 250 °C for all the cyclodextrin-based sorbents, which can be associated with a first degradation process of the glucopyranose units. Exception are αCDAM$_6$, βCDAM$_6$, and αCDAM$_{12}$, which shown a single thermal step of degradation at 200 °C, 210 °C and 204 °C, with values of mass loss of 61.5%, 63.6% and 71.0%, respectively. This behaviour can be due to the lower DC of these materials and suggests a homogeneous structure of the material; degradation temperature lower than pure cyclodextrin [48] points out a decrease of inter- and intra-molecular interactions. The addition of AC in the hydrogel matrix of PCD at 5% and 10% (w/w) splits the $T_{2,max}$ peak of PCD, at *ca.* 275 °C and 330 °C. AC probably acts as a spacer of the crosslinker branches allowing more degrees of freedom to establish functional group interactions, with denser and softer regions.

The peak, $T_{3,max}$, at 310 °C is also present in βCDAM$_{12}$ which present the highest degree of crosslinking (Table 4.5. – paragraph 4.2 – subparagraph 4.2.2.) and size particle (Table 4.2. – paragraph 4.1 – subparagraph 4.1.2.) in the first class of CDAM-NS, with a dense morphological structure (Figure 4.2 - paragraph 4.1. – paragraph 4.1.1.). In the nanosponges synthesized using the glutaraldehyde, the peak shifts to higher temperature, $T_{3,max} \approx 430$ °C; and an additional peak at $T_{4,max} = 560$ °C is shown in αCDGAM$_6$ thermal cruve. The enhancement of the decomposition temperatures can be an outcome of a higher degree of reticulation and CD content, as well as the stronger hydrophobic interactions and entanglement due to the extended aliphatic chain of the branches, and the higher particle size.

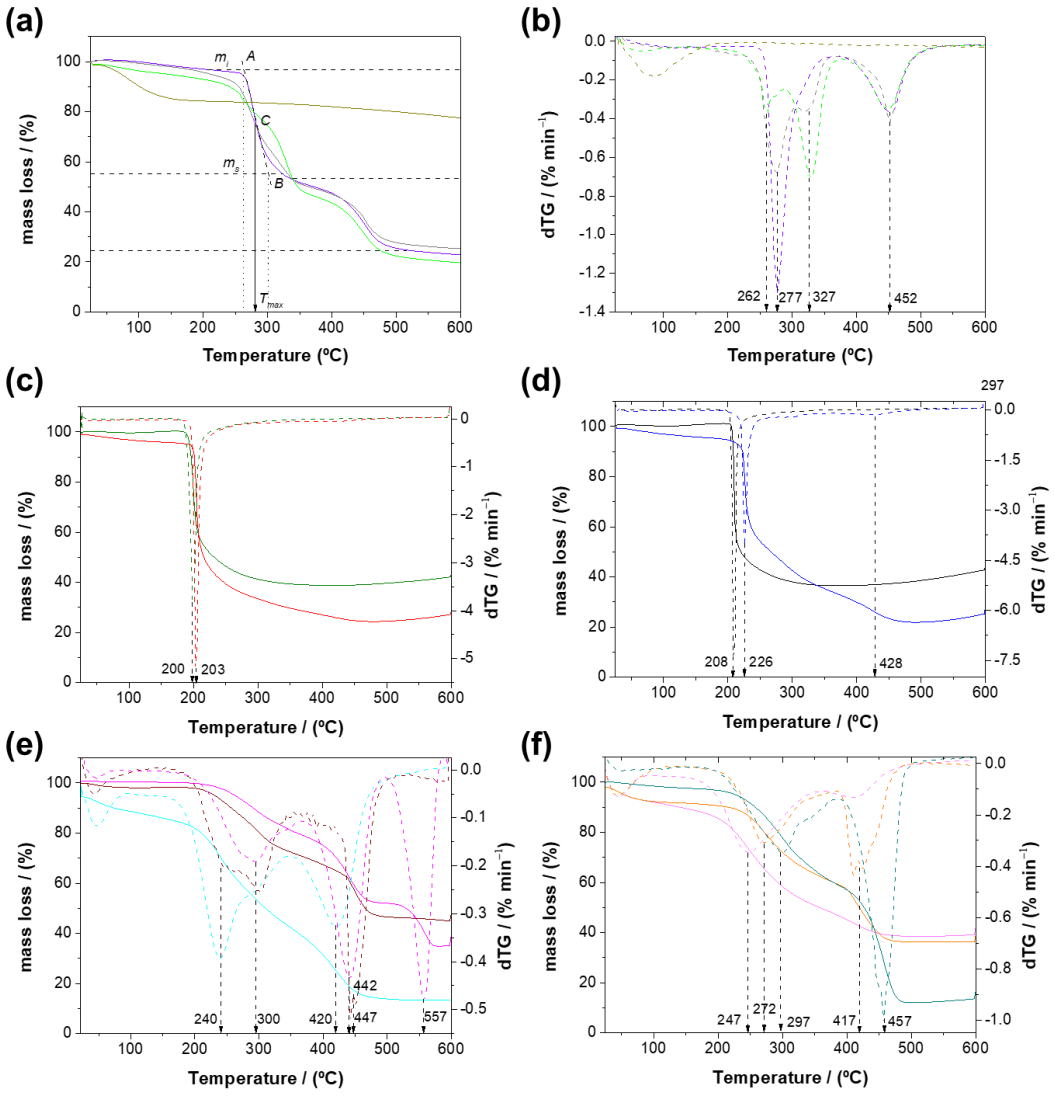

Figure 4.17. Thermal analysis curves of TG (line) and DTG (dashed line) of (a) and (b) PCD (violet line), PCD-ACD5% (grey line), PCD-AC10% (light green line), AC (dark yellow line); (c) αCDAM$_6$ (green line), αCDAM$_{12}$ (red line); (d) βCDAM$_6$ (black line), βCDAM$_{12}$ (blue line); (e) αCDGNH$_2$ (light-blue line), αCDGAM$_6$ (magenta line), αCDGAM$_{12}$ (brown line); (f) βCDGNH$_2$ (pink line), βCDGAM$_6$ (orange line), βCDGAM$_{12}$ (cyan line).

Table 4.7. Thermal parameters of thermogravimetric analysis and derivative TG curves of the cyclodextrin-based sorbent materials.

Compounds	Temperature range / (°C)	T_{max} / (°C)	Weight loss / (%)
PCD	T_1: 55-215	$T_{1,max}$: 95	T_1: 2.1
	T_2: 250-350	$T_{2,max}$: 288	T_2: 45
	T_3: 350-520	$T_{3,max}$: 470	T_3: 25
PCD-AC5%	T_1: 33-217	$T_{1,max}$: 96	T_1: 5.7
	T_2: 235-300	$T_{2,max}$: 277	T_2: 28.0
	T_3: 300-375	$T_{3,max}$: 327	T_3: 16.3
	T_4: 375-525	$T_{4,max}$: 452	T_4: 22.4
PCD-AC10%	T_1: 30-210	$T_{1,max}$: 95	T_1: 6.6
	T_2: 210-310	$T_{2,max}$: 262	T_2: 19.1
	T_3: 310-375	$T_{3,max}$: 327	T_3: 27.1
	T_4: 375-515	$T_{4,max}$: 452	T_4: 24.5
AC	T_1: 30-164	$T_{1,max}$: 85	T_1: 14.0
αCDAM$_6$	T_1: 160-415	$T_{1,max}$: 200	T_1: 61.5
βCDAM$_6$	T_1: 30-110	$T_{1,max}$: 98	T_1: 0.6
	T_2: 165-382	$T_{2,max}$: 210	T_2: 63.6
αCDAM$_{12}$	T_1: 186-481	$T_{1,max}$: 204	T_1: 71.0
βCDAM$_{12}$	T_1: 30-195	$T_{1,max}$: 140	T_1: 4.4
	T_2: 200-255	$T_{2,max}$: 226	T_2: 41.6
	T_3: 255-325	$T_{3,max}$: 310	T_3: 15
	T_4: 325-480	$T_{4,max}$: 415	T_4: 16.3
αCDGNH$_2$	T_1: 20-156	$T_{1,max}$: 55	T_1: 9.3
	T_2: 156-330	$T_{2,max}$: 239	T_2: 40.1
	T_3: 330-538	$T_{3,max}$: 424	T_3: 32.2
βCDGNH$_2$	T_1: 20-152	$T_{1,max}$: 49	T_1: 8.6
	T_2: 152-354	$T_{2,max}$: 248	T_2: 39.0
	T_3: 354-583	$T_{3,max}$: 417	T_3: 11.5

αCDGAM$_6$	T_1: 20-175	$T_{1,max}$: n.a.	T_1: 0.1
	T_2: 175-361	$T_{2,max}$: 282	T_2: 20.3
	T_3: 361-495	$T_{3,max}$: 444	T_3: 27.8
	T_4: 495-586	$T_{4,max}$: 559	T_4: 17.2
βCDGAM$_6$	T_1: 20-169	$T_{1,max}$: 55	T_1: 6.8
	T_2: 169-338	$T_{2,max}$: 270	T_2: 26.4
	T_3: 338-486	$T_{3,max}$: 418	T_3: 28.5
αCDGAM$_{12}$	T_1: 20-157	$T_{1,max}$: 45	T_1: 1.5
	T_2: 157-374	$T_{2,max}$: 254	T_2: 28.2
	T_3: 374-600	$T_{3,max}$: 446	T_3: 25.0
βCDGAM$_{12}$	T_1: 20-178	$T_{1,max}$: n.a.	T_1: 2.7
	T_2: 178-379	$T_{2,max}$: 301	T_2: 37.3
	T_3: 379-522	$T_{3,max}$: 455	T_3: 47.9

References of chapter 4

[1] S. Das, P. Heasman, T. Ben, S. Qiu, Porous Organic Materials: Strategic Design and Structure–Function Correlation, Chem. Rev. 117 (2017) 1515–1563. https://doi.org/10.1021/acs.chemrev.6b00439.

[2] T.D. Bennett, F.-X. Coudert, S.L. James, A.I. Cooper, The changing state of porous materials, Nat. Mater. 20 (2021) 1179–1187. https://doi.org/10.1038/s41563-021-00957-w.

[3] E. Ortiz Ortega, H. Hosseinian, M.J. Rosales López, A. Rodríguez Vera, S. Hosseini, Characterization Techniques for Morphology Analysis, in: J. Atai, R. Liang (Eds.), Prog. Opt. Sci. Photonics, 1st ed., Springer Singapore, 2022: pp. 1–45. https://doi.org/10.1007/978-981-16-9569-8_1.

[4] A. Popelka, S. Zavahir, S. Habib, Morphology analysis, in: M. Al Ali AlMaadeed, D. Ponnamma, M.A. Carignano (Eds.), Polym. Sci. Innov. Appl., 1st ed., Elsevier, 2020: pp. 21–68. https://doi.org/10.1016/B978-0-12-816808-0.00002-0.

[5] C.R. Brooks, B.L. McGill, The application of scanning electron microscopy to fractography, Mater. Charact. 33 (1994) 195–243. https://doi.org/10.1016/1044-5803(94)90045-0.

[6] L. Reimer, Scanning Electron Microscopy, Springer Berlin Heidelberg, Berlin, Heidelberg, 1998. https://doi.org/10.1007/978-3-540-38967-5.

[7] E. Müller, M. Hugenschmidt, D. Gerthsen, Electron-beam broadening in electron microscopy by solving the electron transport equation, Phys. Rev. Res. 2 (2020) 043313. https://doi.org/10.1103/PhysRevResearch.2.043313.

[8] C. Sanford, S. Ross, Homotattic Surface—A Suggested New Word, J. Phys. Chem. 58 (1954) 288–288. https://doi.org/10.1021/j150513a026.

[9] J. Dodds, Techniques to analyse particle size of food powders, in: B. Bhandari, N. Bansal, M. Zhang, P. Schuck (Eds.), Handb. Food Powders, Elsevier, 2013: pp. 309–338. https://doi.org/10.1533/9780857098672.2.309.

[10] J.W. Hickey, J.L. Santos, J.-M. Williford, H.-Q. Mao, Control of polymeric nanoparticle size to improve therapeutic delivery, J. Control. Release. 219 (2015) 536–547. https://doi.org/10.1016/j.jconrel.2015.10.006.

[11] M. Kaszuba, D. McKnight, M.T. Connah, F.K. McNeil-Watson, U. Nobbmann,

Measuring sub nanometre sizes using dynamic light scattering, J. Nanoparticle Res. 10 (2008) 823–829. https://doi.org/10.1007/s11051-007-9317-4.

[12] T. Mudalige, H. Qu, D. Van Haute, S.M. Ansar, A. Paredes, T. Ingle, Characterization of Nanomaterials, in: A.L. Rubio, M.J.F. Rovira, M.M. Snaz, L.G. Gómez-Mascaraque (Eds.), Nanomater. Food Appl., Elsevier, 2019: pp. 313–353. https://doi.org/10.1016/B978-0-12-814130-4.00011-7.

[13] J.W. Strutt, On the light from the sky, its polarization and colour, London, Edinburgh, Dublin Philos. Mag. J. Sci. 41 (1871) 274–279. https://doi.org/10.1080/14786447108640479.

[14] S.K. Brar, M. Verma, Measurement of nanoparticles by light-scattering techniques, TrAC Trends Anal. Chem. 30 (2011) 4–17. https://doi.org/10.1016/j.trac.2010.08.008.

[15] J.C. Thomas, Photon correlation spectroscopy: technique and instrumentation, in: K.S. Schmitz (Ed.), Phot. Correl. Spectrosc. Multicomponent Syst., 1991: p. 2. https://doi.org/10.1117/12.44153.

[16] P.M. Carvalho, M.R. Felício, N.C. Santos, S. Gonçalves, M.M. Domingues, Application of Light Scattering Techniques to Nanoparticle Characterization and Development, Front. Chem. 6 (2018) 1–17. https://doi.org/10.3389/fchem.2018.00237.

[17] N. Raval, R. Maheshwari, D. Kalyane, S.R. Youngren-Ortiz, M.B. Chougule, R.K. Tekade, Importance of Physicochemical Characterization of Nanoparticles in Pharmaceutical Product Development, in: R.K. Tekade (Ed.), Basic Fundam. Drug Deliv., Academic Press, Elsevier, 2019: pp. 369–400. https://doi.org/10.1016/B978-0-12-817909-3.00010-8.

[18] C.I.C. Crucho, M.T. Barros, Polymeric nanoparticles: A study on the preparation variables and characterization methods, Mater. Sci. Eng. C. 80 (2017) 771–784. https://doi.org/10.1016/j.msec.2017.06.004.

[19] V.A. Hackley, J.D. Clogston, Measuring the Size of Nanoparticles in Aqueous Media Using Batch-Mode Dynamic Light Scattering, Gaithersburg, MD, 2007. https://doi.org/10.6028/NIST.SP.1200-6.

[20] S. Bhattacharjee, In relation to the following article “DLS and zeta potential — What they are and what they are not?” Journal of Controlled Release, 2016, 235, 337–351, J. Control. Release. 238 (2016) 311–312. https://doi.org/10.1016/j.jconrel.2016.07.002.

[21] P.M. Williams, Zeta Potential, in: Encycl. Membr., Springer Berlin Heidelberg, Berlin, Heidelberg, 2016: pp. 2063–2064. https://doi.org/10.1007/978-3-662-44324-8_612.

[22] S. Bhattacharjee, DLS and zeta potential – What they are and what they are not?, J. Control. Release. 235 (2016) 337–351. https://doi.org/10.1016/j.jconrel.2016.06.017.

[23] K. Mergia, K.L. Stefanopoulos, N. Ordás, C. García-Rosales, A comparative study of the porosity of doped graphites by small angle neutron scattering, nitrogen adsorption and helium pycnometry, Microporous Mesoporous Mater. 134 (2010) 141–149. https://doi.org/10.1016/j.micromeso.2010.05.019.

[24] E.P. Barrett, L.G. Joyner, P.P. Halenda, The Determination of Pore Volume and Area Distributions in Porous Substances. I. Computations from Nitrogen Isotherms, J. Am. Chem. Soc. 73 (1951) 373–380. https://doi.org/10.1021/ja01145a126.

[25] M. Thommes, K. Kaneko, A. V. Neimark, J.P. Olivier, F. Rodriguez-Reinoso, J. Rouquerol, K.S.W. Sing, Physisorption of gases, with special reference to the evaluation of surface area and pore size distribution (IUPAC Technical Report), Pure Appl. Chem. 87 (2015) 1051–1069. https://doi.org/10.1515/pac-2014-1117.

[26] M. Naderi, Surface Area, in: S. (Department of C.E. Tarleton (Ed.), Prog. Filtr. Sep., Elsevier, 2015: pp. 585–608. https://doi.org/10.1016/B978-0-12-384746-1.00014-8.

[27] N. Gibson, P. Kuchenbecker, K. Rasmussen, V.-D. Hodoroaba, H. Rauscher, Volume-specific surface area by gas adsorption analysis with the BET method, in: V. Dan Hodoroaba, W. Unger E.S., A. Shard G. (Eds.), Charact. Nanoparticles, Elsevier, 2020: pp. 265–294. https://doi.org/10.1016/B978-0-12-814182-3.00017-1.

[28] D.P. Lapham, J.L. Lapham, BET surface area measurement of commercial magnesium stearate by krypton adsorption in preference to nitrogen adsorption, Int. J. Pharm. 568 (2019) 118522–118536. https://doi.org/10.1016/j.ijpharm.2019.118522.

[29] D. Dollimore, P. Spooner, A. Turner, The bet method of analysis of gas adsorption data and its relevance to the calculation of surface areas, Surf. Technol. 4 (1976) 121–160. https://doi.org/10.1016/0376-4583(76)90024-8.

[30] S. Lowell, J.E. Shields, M.A. Thomas, M. Thommes, Characterization of Porous Solids and Powders: Surface Area, Pore Size and Density, Springer, Dordrecht, New York, 2004. https://doi.org/10.1007/978-1-4020-2303-3.

[31] R. Bardestani, G.S. Patience, S. Kaliaguine, Experimental methods in chemical engineering: specific surface area and pore size distribution measurements—BET, BJH, and DFT, Can. J. Chem. Eng. 97 (2019) 2781–2791. https://doi.org/10.1002/cjce.23632.

[32] R.M. Silverstein, F.X. Webster, D.J. Kiemle, Infrared Spectrometry, in: D. Brennan, J. Yee, S. Wolfman-Robichaud (Eds.), Spectrom. Identif. Org. Compd., seventh ed, John

Wiley & Sons, Inc., 2005: pp. 72–126.

[33] B.C. Smith, Fundamentals of Fourier Transform Infrared Spectroscopy, 2nd ed., CRC Press, Boca Raton, 2011. https://doi.org/10.1201/b10777.

[34] B.H. Stuart, Infrared Spectroscopy: Fundamentals and Applications, John Wiley & Sons, Ltd, 2004. https://doi.org/10.1002/0470011149.

[35] W. Kandioller, J. Theiner, K. Keppler, C.R. Kowol, INORGANIC CHEMISTRY FRONTIERS Elemental analysis : an important purity control but prone to manipulations †, RSC Inorg. Chem. Front. 9 (2022) 412–416. https://doi.org/10.1039/d1qi01379c.

[36] E. Martwong, S. Chuetor, J. Junthip, Adsorption of Paraquat by Poly(Vinyl Alcohol)-Cyclodextrin Nanosponges, Polymers (Basel). 13 (2021) 4110. https://doi.org/10.3390/polym13234110.

[37] D. Zhao, L. Zhao, C. Zhu, Z. Tian, X. Shen, Synthesis and properties of water-insoluble β-cyclodextrin polymer crosslinked by citric acid with PEG-400 as modifier, Carbohydr. Polym. 78 (2009) 125–130. https://doi.org/10.1016/j.carbpol.2009.04.022.

[38] V.S. Ghorpade, A.V. Yadav, R.J. Dias, Citric acid crosslinked cyclodextrin/hydroxypropylmethylcellulose hydrogel films for hydrophobic drug delivery, Int. J. Biol. Macromol. 93 (2016) 75–86. https://doi.org/10.1016/j.ijbiomac.2016.08.072.

[39] Á. Buvári, L. Barcza, M. Kajtár, Complex formation of phenolphthalein and some related compounds with β-cyclodextrin, J. Chem. Soc., Perkin Trans. 2. (1988) 1687–1690. https://doi.org/10.1039/P29880001687.

[40] P.K. Zarzycki, H. Lamparczyk, The equilibrium constant of β-cyclodextrin-phenolphtalein complex; Influence of temperature and tetrahydrofuran addition, J. Pharm. Biomed. Anal. 18 (1998) 165–170. https://doi.org/10.1016/S0731-7085(98)00150-2.

[41] B.F.F. Medronho, S. Gonçalves, R. Rodríguez-Solana, A.J.M. Valente, A. Romano, Interactions between Bio-Based Compounds and Cyclodextrins, in: P. Arora, N. Dhingra (Eds.), Cyclodext. - A Versatile Ingred., IntechOpen, Rijeka, 2018: pp. 70–93. https://doi.org/10.5772/intechopen.73531.

[42] A.J.M. Valente, O. Söderman, The formation of host–guest complexes between surfactants and cyclodextrins, Adv. Colloid Interface Sci. 205 (2014) 156–176. https://doi.org/10.1016/j.cis.2013.08.001.

[43] M.E. Brown, ed., Introduction to Thermal Analysis, 2nd ed., Kluwer Academic Publishers, Dordrecht, 2004. https://doi.org/10.1007/0-306-48404-8.

[44] M.E. Brown, A.K. Galwey, Handbook of Thermal Analysis and Calorimetry, 1st ed., Elsevier, 1998. https://doi.org/10.1016/S1573-4374(13)60004-7.

[45] B. Wunderlich, Thermal Analysis of Polymeric Materials, 1st ed., Springer-Verlag, Berlin/Heidelberg, 2005. https://doi.org/10.1007/b137476.

[46] S. Loganathan, R.B. Valapa, R.K. Mishra, G. Pugazhenthi, S. Thomas, Thermogravimetric Analysis for Characterization of Nanomaterials, in: S. Thomas, R. Thomas, A.K. Zachariah, R.K. Mishra (Eds.), Therm. Rheol. Meas. Tech. Nanomater. Charact., Elsevier, 2017: pp. 67–108. https://doi.org/10.1016/B978-0-323-46139-9.00004-9.

[47] T. Hatakeyama, F.X. Quinn, eds., Thermal Analysis — Fundamentals and Applications to Polymer Science, 2nd ed., John Wiley & Sons, Ltd, Chichester, UK, 2000. https://doi.org/10.1016/S0039-9140(99)00304-5.

[48] A.P. Gerola, D.C. Silva, S. Jesus, R.A. Carvalho, A.F. Rubira, E.C. Muniz, O. Borges, A.J.M. Valente, Synthesis and controlled curcumin supramolecular complex release from pH-sensitive modified gum-arabic-based hydrogels, RSC Adv. 5 (2015) 94519–94533. https://doi.org/10.1039/C5RA14331D.

Chapter 5.

In the current chapter the methodologies applied in order to understand the mechanisms and the interactions occurring at level of the two interface systems, liquid-liquid (L-L) and solid-liquid (S-L), involving two or more components identifiable by the state of the species studied, will be discussed.

5.1. L-L interface

The interface L-L is of particular interest when pollutant species, like pesticides, are considered. As discussed along the Chapter 1, their physico-chemical properties such as solubility, polarity, K_a, K_{oc}, and K_{ow} as well as the environmental conditions can influence their fate in the environment. The understanding of the transport phenomena is necessary to predict or evaluate the pesticide spreading and impact. One of the main mechanisms of transport is based on mass transport which driving-force is the concentration gradient of the solute [1]. Thus, the study of the molecular diffusion process has be employed to understand the pesticides behaviour in the environment, particularly, in aqueous media (Chapter 6-III). The diffusion is a spontaneous process that occurs in presence of a concentration gradient in solution. This is the result of the casual motion of the particles, Brownian motion, which lead to an irreversible process in a state of non-thermodynamic equilibrium [2]. The fundamentals are based on the Fourier's theory for energy transport [3], adopted by Fick to quantify the mutual diffusion coefficient (D – $cm^2\ s^{-1}$) driven by a chemical potential gradient (μ) [4]. Considering different assumption such as, an isotropic medium and constant temperature, the mass transport as unidimensional process; the thermodynamic transport coefficient, in a system of n components, is directly proportional to the rate of transfer (J) crossing a unit area section along the axes x, expressed by the Fick's first law equation (eq. 5.1):

$$J_i = -\sum_{j=1}^{n} D_{ij} \left(\frac{\partial \mu}{\partial x}\right)_j \ (i = 1,2, \dots n) \qquad \text{(eq. 5.1)}$$

where μ is the chemical potential defined in terms of Gibbs energy (eq. 5.2), $\partial\mu/\partial x$ indicates the changes of μ in the axes x, ij take in consideration the contribute of each component in the system. The chemical potential can be described as:

$$\mu_i = \left[\frac{\partial G_i}{\partial n_i}\right]_{T,P,n_j} = \mu_i^0(T,P) + RTlna_i \qquad \text{(eq. 5.2)}$$

where a_i is the activity of the specie i in solution. Considering an isotropic system at an infinitesimal concentration, the chemical potential can be substituted with the concentration (C).

J can be also described as the amount of matter diffused per unit of time, so, the variation of the flux along x can be rewritten as the Fick's second law equation:

$$\frac{\partial C}{\partial t} = D\left(\frac{\partial^2 C}{\partial x^2}\right) \qquad \text{(eq. 5.3)}$$

The Fick's first and second law equations can be described in the three Cartesian dimensions x, y and z. One of the methods of solution consider an unidimensional process, with diluted and fixed concentration of solute C(x, t), in an infinite cylindrical path of infinite perpendicular cross-section areas, in which D is assumed to be constant and the unique driving force is the chemical potential [4]. In those conditions the diffusion coefficient can be computed by eqs. 5.2 and 5.3 [5]. The boundary conditions required by geometry and experimental analysis are that $C = 0$ per $t = 0$ and $C = C_0$ per $t > 0$.

For a binary system, the equation 5.1 can be rewritten in terms of the component A and B, with a rate of transport J_i across a perpendicular section, at the time t and constant volume,

$$J_A = -D_A\left(\frac{\partial C_A}{\partial x}\right) \text{ and } J_B = -D_B\left(\frac{\partial C_B}{\partial x}\right) \qquad \text{(eq. 5.3)}$$

assuming that no volume changes occur, the flux rate of each component can be expressed in terms of partial molar volume as:

$$D_A V_A\left(\frac{\partial C_A}{\partial x}\right) + D_B V_B\left(\frac{\partial C_B}{\partial x}\right) = 0 \qquad \text{(eq. 5.4)}$$

where V_i (cm^3) is the partial volume of each component and for the law of mass conservation:

$$V_A C_A + V_B C_B = 1 \text{ (for } V_i \neq 0) \qquad \text{(eq. 5.5)}$$

by which $D_A = D_B$, defined as the mutual coefficients of diffusion, simplifying the system as uni-component.

These fundamentals have been applied in unsteady-state methods (Taylor technique) to study the diffusion in water of three pesticide active ingredients: ammonium glufosinate (organophosphate - herbicide), cymoxanil (cyanoacetamide oxime – fungicide) and imidacloprid (neonicotinoid – insecticide), as binary system (Figure 5.1).

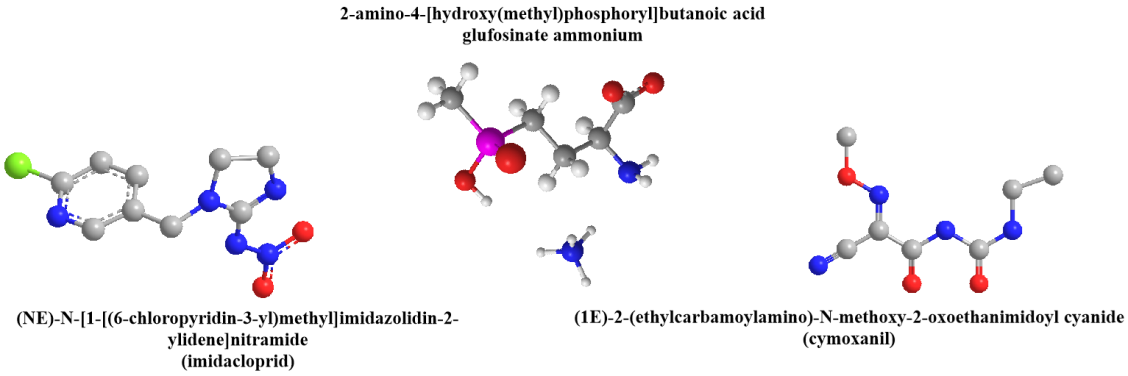

Figure 5.1. 3D-molecular structure of imidacloprid, glufosinate ammonium and cymoxanil.

The Taylor dispersion technique (see schematic representation in Figure 5.2) was employed to determine the diffusion coefficient, *D*. In brief, the pesticide solution, at specific concentration, is injected into a constant flow of solvent, D^0 (water or aqueous solution). The analysis is based on the assumption that the diffusion results from the gradient concentration and the gradient speed along the capillary tube of length, *L*, and radius, *r* (Figure 5.2). Then, the analyte flux is measured by a differential refractometer [6].

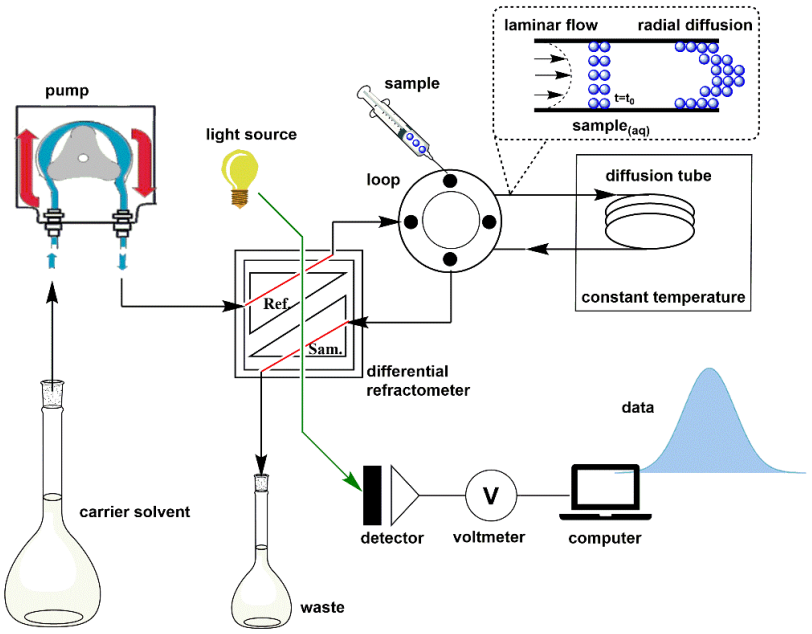

Figure 5.2. Design of the Taylor dispersion technique.

Experimentally, the quantification is obtained by detection of refractive index changes as function of the analyte concentration along the tube. Assuming the cylindrical coordinates of the capillary of side *r* and diffusion in *x*, the diffusion coefficient for a solute of known molar concentration:

$$D = \left[\frac{\partial^2 C}{\partial r^2} + \frac{1}{r}\frac{\partial C}{\partial r} + \frac{\partial^2 C}{\partial x^2}\right] = u(r)\frac{\partial C}{\partial x} + \frac{\partial C}{\partial t} \qquad \text{(eq. 5.6)}$$

where *u(r)* is the rate of the flux respect the experimental coordinates.

Now, considering the radial component *D* constant at infinite dilution, in absence of chemical interactions, constant density in overall media and a length of the capillary $L >> r$ (radius) which make negligible the axial diffusion component; it is possible to calculate the diffusion coefficient of an injected solute of known molecular weight quantifying the concentration via potentiometer measurement as function of the time [7]:

$$V(t) = V_0 + V_1 t + k\Delta R\Delta C(t) \qquad \text{(eq. 5.7)}$$

where $V_0 + V_1$ correspond to the baseline voltage and slope, respectively, $k = dV/dn$ represents the signal/noise ratio (sensitivity), $\Delta R = \partial n/\partial C$ considers the change of the refractive index as function of the average radial concentration and $\Delta C = C(t) - \bar{C}$. By mathematical rearrangement:

$$V(t) = V_0 + V_1 t + V_{max}(\frac{t_r}{r})^{\frac{1}{2}}\exp\left[-\frac{12D(t-\bar{t})^2}{r^2 t}\right] \qquad \text{(eq. 5.8)}$$

where V_{max} is the analytical signal at the maximum peak height, t_r is the retention time, *r* is the capillary radius.

The value of *D* can be calculated by plotting *V(t)* as function of *t* and the fitting is obtained by varying the values of V_0, V_1, V_{max} and *t*, to the gaussian distribution of the concentration [4].

In order to mimic the environmental condition, the effect of the ionic strength was also assessed for the GLF, by diffusion measurement of the pesticide in aqueous solution of NH_4NO_3 used as solvent and media. In presence of ions, *D* can changes to highly positive values indicating a *salting-out* effect, or negative values suggesting electrostatic interactions. The analysis permits to determine the named tracer diffusion coefficient (D_T) in a supposed ternary system. However, maintaining the $[NH_4NO_3] >> [GLF]$, and constant in overall system, the ternary system can be simplified to a binary system, being $D_T = D$.

From the *D* values, it is possible to derive the molar conductivity of the ionic species by the Nernst equation 5.9 [4],

$$D_i = \frac{RT}{z_i^2 F^2}\lambda_{m,i}^0 \qquad \text{(eq. 5.9)}$$

where R (8.31 J $K^{-1}mol^{-1}$) is the constant of a gas in ideal conditions, T (K) is the absolute temperature, F (9.65×10^4 C mol^{-1}) is the Faraday's constant, z and $\lambda_{m,i}$ (S m^2 mol^{-1}) are the valence and the molar conductivity, respectively, of the ion *i*.

From the coefficient of diffusion is also possible to determine the hydrodynamic radius through the Stoke-Einstein equation already presented in the equation 4.6 - Chapter 4 - paragraph 4.1. - subparagraph 4.1.2.

5.2.S-L interface

At the interface S-L beyond the analyte, the physico-chemical properties of the sorbent must be considered [8]. These were deeply discussed in Chapter 4, emphasizing how the characteristics of a polymer changes as function of the synthesis route, substrate and crosslinker. In S-L interface over the physical mass transport, chemical interactions can occur due to the presence of functional groups at the surface of the sorbent materials.

In order to evaluate the sorption mechanism, as result of the sorbate-sorbent interactions, kinetic and equilibrium analysis can be performed and kinetic and isothermal models applied [9][10] (Chapter 6-IV/-V/-VI). In addition, molecular dynamics simulation has been developed for an atomistic evaluation of the mechanism, as a complementary analysis (Chapter 6-VII/VIII).

Sorption is thermodynamically considered an exothermic process based on the Gibbs energy formula $\Delta G^0 = \Delta H^0 - T\Delta S^0$ [11]. In the process atoms or molecules of gases or liquids are accumulated on the surface of a solid condensed material; inter- and intra-molecular sorbent-sorbate and sorbate-sorbate interactions can occur by physisorption ($2 < \Delta H^0$ (kJ mol^{-1}) < 21) ($-20 < \Delta G^0$ (kJ mol^{-1}) < 0) involving mass transfer processes, coordination, electrostatic or van der Waals interactions [12]; or chemisorption ($80 < \Delta H^0$ (kJ mol^{-1}) < 200) ($-400 < \Delta G^0$ (kJ mol^{-1}) < -80) via dipole-dipole, ionic interactions, hydrogen or covalent bonds [13]. Hence, the activation energy values make the difference between a faster and reversible process as in the former case and a slower and irreversible, but active site-specific process as in the chemisorption (Figure 5.3.) [14].

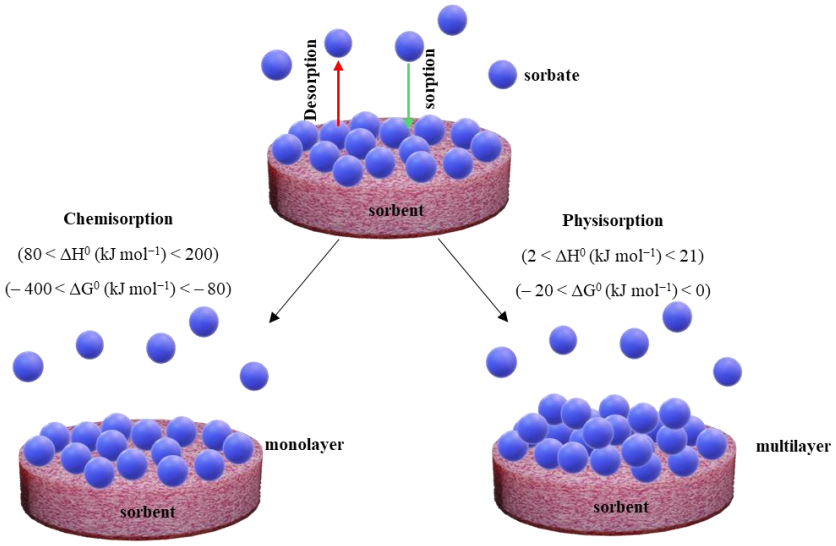

Figure 5.3. Schematic representation of the mechanisms involved in sorption process.

5.2.1. Equilibrium sorption

The equilibrium sorption models provide information about the sorption capability and efficiency of a sorbent material towards a sorbate in a range of concentration, at constant temperature. It is based on the condition that sorption and desorption rate are constant, providing important information to understanding the adsorption mechanism. This is firstly driven by gradient of concentration during the external diffusion step. In a second step the contaminant enters in the structure through the pores of the sorbent via internal diffusion. The last step regards the establishment of interaction in the active sites [10]. The amount of sorbed analyte (q_e – mg g^{-1}) correlates the concentration of the analyte at the steady state with a constant amount of sorbent and volume solution (eq. 5.10):

$$q_e = (C_i - C_e)(\frac{V}{m}) \qquad \text{(eq. 5.10)}$$

where C_i and C_e (mg L^{-1}) are the initial and the equilibrium state concentrations of the pesticide, respectively, V (L) is the volume of the solution and m (g) is the sorbent amount.

Another way to determine the performance of the sorbent material, independent from its amount and volume of solution, is the removal efficiency (*RE%*) (eq. 5.11),

$$RE\% = (\frac{C_i - C_e}{C_i}) \times 100 \qquad \text{(eq. 5.11)}$$

To evaluate the isotherm process, various mathematical models have been developed [9,14–16]: *i*) Henry model – one parameter; *ii*) Langmuir and Freundlich models – two independent parameters; *iii*) Redlich-Peterson, Sips, Toth, Koble-Corrigan, Khan and BET models – three

independent parameters; and models with multiple independent parameters. Herein, only the isotherm models applied along the thesis will be discussed more in detail.

The Langmuir isotherm model (eq. 5.12) can be used to describe homogeneous phenomena at S-L interface, assuming the presence of finite specific active sites, energetically equivalents, with formation of a monolayer in absence of sorbate-sorbate interactions and steric hindrance. It is usually applied to fit isotherm of type-I,

$$q_e = \frac{q_{max} K_L C_e}{1 + K_L C_e} \qquad \text{(eq. 5.12)}$$

where q_{max} (mg g^{-1}) is the maximum amount of sorbed solute per gram of sorbent, K_L (L mg^{-1}) is the Langmuir constant correlated with the binding affinity. Graphically, the value of q_{max} is extrapolated from the plateau, at the monolayer saturation point. The Figure 5.4 shows the typical profile obtained by fitting of the Langmuir isotherm model to the experimental data. By the value of K_L is possible to determine the value of ΔG^0 through the equation 5.13,

$$\Delta G^0 = -RTln(K_{eq}) \qquad \text{(eq. 5.13)}$$

after conversion of K_L units L mg^{-1} to L mol^{-1} [17]. The analytical parameters reported in Table 5.1 gives a fast overlook about the influence of the physico-chemical properties of the CDNS discussed in Chapter 4, sorbate and experimental conditions (*e.g.* sorbent amount, pH and volume of solution) which optima conditions were assessed by full factorial experimental design (paragraph 5.3). From the Langmuir isotherm model, the dimensionless separation factor (R_L) can be calculated (eq. 5.14), where $R_L > 1$ is for unfavourable, $R_L = 1$ is for linear, $0 < R_L < 1$ is for favourable and $R_L = 0$ is for irreversible processes, respectively.

$$R_L = \frac{1}{1 + K_L C_0} \qquad \text{(eq. 5.14)}$$

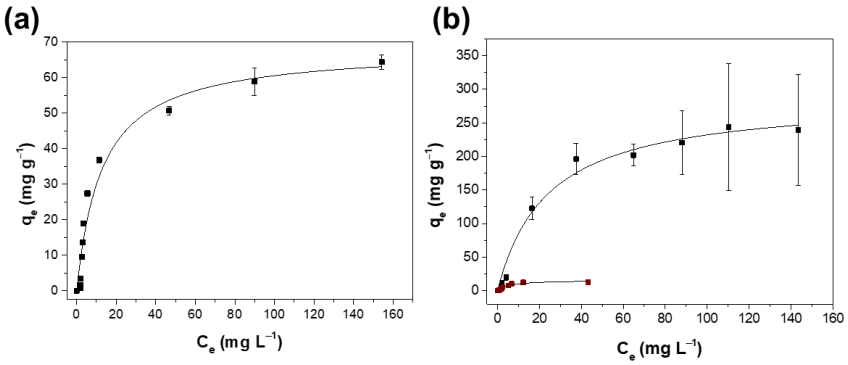

Figure 5.4. Langmuir isotherm for removal of βCDAM$_6$ towards (a) pure imidacloprid, at S/L = 5, at pH 3.8 and (b) imidacloprid in Confidor O-TEQ®, S/L = 0.1 (black square) and S/L = 10 (Bordeaux square), at pH = 6.5.

Table 5.1. Analytical parameters of Langmuir sorption model for imidacloprid removal by βCDAM$_6$.

Model		**βCDAM$_6$**		
pH		3.8	6.5	6.5
S/L (mg mL^{-1})		0.5	0.1	10
Langmuir	q_m (mg g^{-1})	68.3 (± 4.8)	287.8 (± 18.7)	15.8 (± 1.8)
	K_L (L mg^{-1})	0.08 (± 0.02)	0.04 (± 0.01)	17.2 (± 5.0)
	R_L	0.7 – 0.02	0.9 – 0.1	0.9 - 0.1
	R^2	0.9502	0.9784	0.9272

Differently, the Freundlich model is related to type-III isotherm, with formation of multilayers, in reversible sorption processes (eq. 5.15). This empirical model mainly describes the sorption process of organic molecules, in which binding sites have different activation energies where the stronger sites are occupied first. The model can be described by the following equation:

$$q_e = K_f C_e^{1/n} \qquad \text{(eq. 5.15)}$$

where K_f (L mg^{-1}) is the Freundlich constant associated to the sorption capacity and n indicates the sorption intensity or heterogeneity of the sorbent. $1/n < 1$ suggests heterogeneous surface with a favourable chemisorption process, and $1/n > 1$ is related to homogeneous surfaces involving cooperative interactions with multilayer formation. The Figure 5.5-a shows the curves obtained by fitting of the Freundlich isotherm model for $1/n \leq 1$ [18].

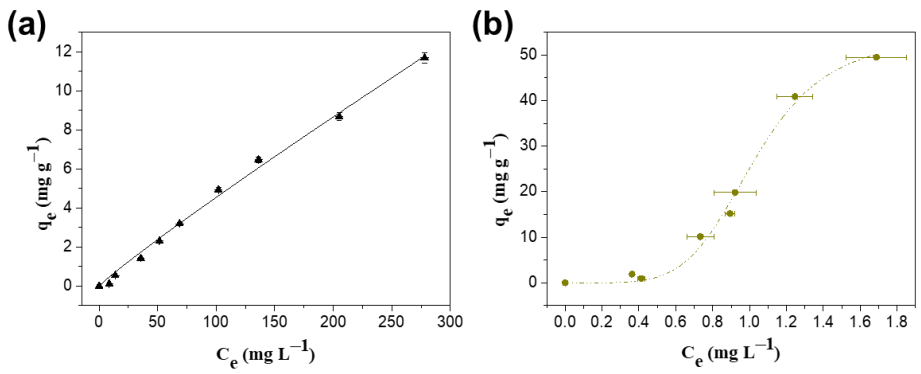

Figure 5.5. (a) Freundlich isotherm model of PCD, and (b) Sips isotherm model of AC; for imidacloprid sorption, at 25 °C.

Coupling the Langmuir and Freundlich isotherm models, it is achieved the three parameters model, named Sips isotherm (eq. 5.16) available within type-I to type-V isotherms. The Sips model can overcome the limits of both models. At low concentration, the model returns to the Freundlich isotherm model, but at high concentration it predicts the typical Langmuir isotherm (Figure 5.5-b).

$$q_e = \frac{q_m K_S C_e^{1/n_S}}{(1+K_S C_e^{1/n_S})} \qquad \text{(eq. 5.16)}$$

where K_S ($L^{1/n}$ $mol^{-1/n}$) is the Sips constant and $1/n_s$ is a factor related with the heterogeneity of the system, analogously to the Freundlich parameter.

Similarly, type-S isotherm (II, IV or V) can be described by fitting of the theoretical BET model (eq. 5.17) (Figure 5.6), at three independent parameters [19],

$$q_e = \frac{q_S C_{BET} C_e}{\left[C_S+(C_{BET}-2)C_e-\left((C_{BET}-1)C_e^2/C_S\right)\right]} \qquad \text{(eq. 5.17)}$$

where q_s (mg g^{-1}), C_{BET} (L mg^{-1}) and C_s (mg L^{-1}) are the theoretical isotherm saturation capacity, BET constant of sorption isotherm and sorbate monolayer saturation concentration, respectively.

The BET model was developed specifically for gas sorption, with the same assumptions of the Langmuir isotherm model. As discussed in Chapter 4 – paragraph 4.1. - subparagraph 4.1.2., the BET model can be employed to determine the surface area and porosity.

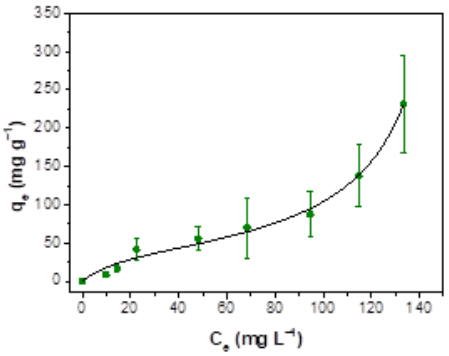

Figure 5.6. Representation of the experimental data of the sorption process of imidacloprid in Confidor O-TEQ® into *α*CDAM$_6$, by fitting of the BET isotherm model, at S/L 0.1 mg mL^{-1}, at pH = 6.5 and 25°C.

5.2.2. Sorption kinetic

Complementary information can be obtained by sorption kinetic which describes the rate of intake or release of a solute, into or from a polymeric material, as function of the time. Several sorption kinetic models are presented in the literature [20]. The two most used models to describe the sorption kinetics processes were the Lagergren's pseudo first–order (PFO) (eq.5.18), and pseudo second–order (PSO) (eq. 5.19) kinetic models [10,21], obtained by integration:

$$\frac{dq_t}{dt} = k_1(q_e - q_t) \qquad \text{resulting in} \qquad q_t = q_e(1 - e^{-k_1 t}) \qquad \text{(eq. 5.18)}$$

$$\frac{dq_t}{dt} = k_2(q_e - q_t)^2 \qquad \text{resulting in} \qquad q_t = \frac{k_2 q_e^2 t}{1 + k_2 q_e t} \qquad \text{(eq. 5.19)}$$

where q_t (mg g^{-1}) is the amount of sorbate uptaken per gram of sorbent at time t (min), k_1 (h^{-1}) and k_2 (g mg^{-1} h^{-1}) are the corresponding rate constants.

In Lagergren's model is considered that the sorption process only occurs on existing specific active sites and does not involve interactions between sorbate molecule, atoms or ions. It is limited to monolayer formation associated with a maximum of sorption. The external or internal diffusion is the rate controlling step; indeed the process is dependent only to the solute concentration. On the other hand, the PSO model considers mechanism of chemisorption occurring at the active sites with formation of mono- or multi-layers. The interaction at level of the active sites is the rate controlling step.

The goodness of the fitting between two or more isotherm or kinetic sorption models was assessed through determination of the likelihood as a metric. In this sense, the Akaike's Information Criterion (AIC) was applied. The AIC was chosen because, even if the increment of parameter number in a model increases the likelihood of goodness-of the fit, that is penalized by the higher complexity of the model in terms of free parameters [22]. The AIC for a general model can be expressed as:

$$AIC_i = -2LL(\widehat{\theta}|y, M_i) + 2K_i \qquad \text{(eq. 5.20)}$$

where $LL(\widehat{\theta}|y, M_i)$ is the log-likelihood for a model M_i for its parameters θ, based on the experimental data y, K_i is related with number of free parameters in the considered model. A more in-depth description can be found in published article of Akaike H. [23]. In particular for model comparison, it was used the default expression of the program used for data analysis, expressed as follow:

$$AIC = Nln\left(\frac{RSS}{N}\right) + 2K + \frac{2K(K+1)}{N-K-1} \qquad \text{(for } N/K < 40\text{)} \qquad \text{(eq. 5.21)}$$

where N is the number of experimental data, RSS is the residual sum of square and K is the number of free parameters.

5.3.Experimental design

In order to determine the optima experimental conditions to study the sorption process, an experimental design can be a powerful tool. A full 2^k factorial planning experimental design has been performed [24]. The total number of tests is established by:

$$N = 2^k \qquad \text{(eq. 5.22)}$$

where N is the total number of tests needed for a complete design to determine the effect of the k factors setting ($k=n, m...p$), at 2 levels. To investigate the effect of the parameters, a polynomial equation derived from a first-order model was applied:

$$y = b_0 + b_n X_n + b_m X_m + \cdots + b_{nm} X_n X_m \qquad \text{(eq. 5.23)}$$

where y is the chosen parameter affected by the k factors, b_0 is the average of the y values, b_n, b_m ... are the linear coefficients, b_{nm} takes into account the contribution of the factor interactions, and X_n, X_m and X_{nm} represent the isolated and combined parameters in exam. For each parameter is established a maximum and minimum value associated to the level (+1 and −1) to build-up the model matrix of the system. It is important for a full factorial design that the matrix is orthogonal and the sum of the columns is zero, in order to have a balanced design and avoid replicates.

5.4.Molecular dynamic simulation

Molecular dynamic (MD) simulation is a strong and complementary tool that can be employed to evaluate the driving forces involved in the interaction of two species, in aqueous media, at the molecular level. The binding enthalpies and the type and strength of non-covalent interactions (NCI) between sorbate and sorbent, which involve attractive/repulsive forces such as van der Waals and hydrogen-bonds, were further characterized. The interaction is thermodynamically described by the standard Gibbs energy ($\Delta G_{bind}^0 = \Delta H_{bind}^0 - T\Delta S_{bind}^0$), which gives a robust and quantitative understanding of the equilibrium between the favourable enthalpy and unfavourable entropy changes [25]. Considering the reactants, generically, as A and B, the simulations were

performed from non-interacting (bulk phase, used as reference system) to A-B interacting distance favouring the formation of AB complex. Thus, the enthalpy change can be calculated from:

$$\Delta H = \langle H_{AB} \rangle + \langle H_{solvent} \rangle - \langle H_A \rangle - \langle H_B \rangle \quad \text{(eq. 5.24)}$$

where each term corresponds to the Boltzmann averaged total potential energies of each component considered, corresponding to independent simulations performed at the same conditions. The solvated reactant molecules were always considered as system reference [26]. Optimized structural geometries and the respective topologies were constructed using semi-empirical methods [27]. Specifically, all simulations were performed using a cubic box of 7.5 nm edge-length containing one solvated species or two reactant species, at 300 K and 1 bar. The systems were equilibrated during 50 ns as equilibration time, and the total potential energy for representative interacting systems were calculated after 200 ns simulation runs [26]. In order to identify and quantify the NCI interactions governing the association between the two species A and B, the Independent Gradient Model (IGM) was employed [28]. The IGM model, based on the electronic densities of each atom in the molecular system, permits to quantify and visualize the areas of stabilizing/destabilizing interactions (isosurface) due to NCI. Considering the electronic density (ρ) of each component as the point of minimum effect (initial state), NCI interactions are quantified in terms of distortion of the electronic density, as result of the interactions (eq. 5.25). The overall NCI value is determined from the sum of the *N* atoms in A and B in a unidimensional system (axis *x*) (eq. 5.26). Hydrogen bonds usually gives high negative values indicating strong stabilizing interactions, whereas values tending to zero are correlated to van der Waals forces [25].

$$\delta g^{inter} = \left|\nabla \delta g^{IGM,inter}\right| - |\nabla \rho| \quad \text{(eq. 5.25)}$$

$$\left(\frac{\delta_\rho}{\delta_x}\right)^{IGM,inter} = \left|\sum_{i=1}^{N_A} \frac{\delta_{\rho_i}}{\delta x}\right| + \left|\sum_{i=1}^{N_B} \frac{\delta_{\rho_i}}{\delta x}\right| \quad \text{(eq. 5.26)}$$

Reference chapter 5

[1] M.L. Brusseau, Physical Processes Affecting Contaminant Transport and Fate, in: M.L. Brusseau, I.L. Pepper, C.P. Gerba (Eds.), Environ. Pollut. Sci., 3rd ed., Elsevier, 2019: pp. 103–112. https://doi.org/10.1016/B978-0-12-814719-1.00007-0.

[2] S.R. De Groot, On the thermodynamics of irreversible heat and mass transfer, Int. J. Heat Mass Transf. 4 (1961) 63–70. https://doi.org/10.1016/0017-9310(61)90061-8.

[3] I.-S. Liu, On Fourier's law of heat conduction, Contin. Mech. Thermodyn. 2 (1990) 301–305. https://doi.org/10.1007/BF01129123.

[4] N.E. Helwig, S. Hong, E.T. Hsiao-wecksler, Diffusion: mass transfer in fluid systems, 3rd ed., Cambridge, n.d. www.cambridge.org/9780521871211.

[5] J. Crank, THE MATHEMATICS OF DIFFUSION, second edi, Clarendon Press Oxford, Bristol, England, 1975.

[6] G. Taylor, P.R.S.L. A, The dispersion of matter in turbulent flow through a pipe, Proc. R. Soc. London. Ser. A. Math. Phys. Sci. 223 (1954) 446–468. https://doi.org/10.1098/rspa.1954.0130.

[7] G. Taylor, P.R.S.L. A, Conditions under which dispersion of a solute in a stream of solvent can be used to measure molecular diffusion, Proc. R. Soc. London. Ser. A. Math. Phys. Sci. 225 (1954) 473–477. https://doi.org/10.1098/rspa.1954.0216.

[8] D. Debnath, A.K. Gupta, P.S. Ghosal, Recent advances in the development of tailored functional materials for the treatment of pesticides in aqueous media: A review, J. Ind. Eng. Chem. 70 (2019) 51–69. https://doi.org/10.1016/j.jiec.2018.10.014.

[9] A. Syafiuddin, S. Salmiati, J. Jonbi, M.A. Fulazzaky, Application of the kinetic and isotherm models for better understanding of the behaviors of silver nanoparticles adsorption onto different adsorbents, J. Environ. Manage. 218 (2018) 59–70. https://doi.org/10.1016/j.jenvman.2018.03.066.

[10] J. Wang, X. Guo, Adsorption kinetic models: Physical meanings, applications, and solving methods, J. Hazard. Mater. 390 (2020) 122156. https://doi.org/10.1016/j.jhazmat.2020.122156.

[11] I. Anastopoulos, G.Z. Kyzas, Are the thermodynamic parameters correctly estimated in liquid-phase adsorption phenomena?, J. Mol. Liq. 218 (2016) 174–185. https://doi.org/10.1016/j.molliq.2016.02.059.

[12] J.E. House, K.A. House, Ionic Bonding, Crystals, and Intermolecular Forces, in: J.E. House, K.A. House (Eds.), Descr. Inorg. Chem., third, Elsevier, 2016: pp. 47–66. https://doi.org/10.1016/B978-0-12-804697-5.00004-X.

[13] J.E. House, K.A. House, Covalent Bonding and Molecular Structure, in: J.E. House, K.A. House (Eds.), Descr. Inorg. Chem., third, Elsevier, 2016: pp. 23–46. https://doi.org/10.1016/B978-0-12-804697-5.00003-8.

[14] R. Kecili, C.M. Hussain, Mechanism of Adsorption on Nanomaterials, in: C. Hussain Mustansa (Ed.), Nanomater. Chromatogr., first, Elsevier, 2018: pp. 89–115. https://doi.org/10.1016/B978-0-12-812792-6.00004-2.

[15] K.Y. Foo, B.H. Hameed, Insights into the modeling of adsorption isotherm systems, Chem. Eng. J. 156 (2010) 2–10. https://doi.org/10.1016/j.cej.2009.09.013.

[16] P.S. Ghosal, A.K. Gupta, Determination of thermodynamic parameters from Langmuir isotherm constant-revisited, J. Mol. Liq. 225 (2017) 137–146. https://doi.org/10.1016/j.molliq.2016.11.058.

[17] E.C. Lima, A. Hosseini-Bandegharaei, J.C. Moreno-Piraján, I. Anastopoulos, A critical review of the estimation of the thermodynamic parameters on adsorption equilibria. Wrong use of equilibrium constant in the Van't Hoof equation for calculation of thermodynamic parameters of adsorption, J. Mol. Liq. 273 (2019) 425–434. https://doi.org/10.1016/j.molliq.2018.10.048.

[18] J.P. Vareda, A.J.M. Valente, L. Durães, Heavy metals in Iberian soils: Removal by current adsorbents/amendments and prospective for aerogels, Adv. Colloid Interface Sci. 237 (2016) 28–42. https://doi.org/10.1016/j.cis.2016.08.009.

[19] N. Gibson, P. Kuchenbecker, K. Rasmussen, V.-D. Hodoroaba, H. Rauscher, Volume-specific surface area by gas adsorption analysis with the BET method, in: V. Dan Hodoroaba, W. Unger E.S., A. Shard G. (Eds.), Charact. Nanoparticles, Elsevier, 2020: pp. 265–294. https://doi.org/10.1016/B978-0-12-814182-3.00017-1.

[20] X. Guo, J. Wang, A general kinetic model for adsorption: Theoretical analysis and modeling, J. Mol. Liq. 288 (2019) 111100. https://doi.org/10.1016/j.molliq.2019.111100.

[21] J.-P. Simonin, On the comparison of pseudo-first order and pseudo-second order rate laws in the modeling of adsorption kinetics, Chem. Eng. J. 300 (2016) 254–263. https://doi.org/10.1016/j.cej.2016.04.079.

[22] F.A.A. Kingdom, N. Prins, Model Comparisons, in: F.A.A. Kingdom, N. Prins (Eds.), Psychophysics, second, Elsevier, 2016: pp. 247–307. https://doi.org/10.1016/B978-0-12-

407156-8.00009-8.

[23] H. Akaike, A new look at the statistical model identification, IEEE Trans. Automat. Contr. 19 (1974) 716–723. https://doi.org/10.1109/TAC.1974.1100705.

[24] J. Antony, Full Factorial Designs, in: J. Antony (Ed.), Des. Exp. Eng. Sci., Second Edi, Elsevier, 2014: pp. 63–85. https://doi.org/10.1016/B978-0-08-099417-8.00006-7.

[25] A.T. Fenley, N.M. Henriksen, H.S. Muddana, M.K. Gilson, Bridging Calorimetry and Simulation through Precise Calculations of Cucurbituril–Guest Binding Enthalpies, J. Chem. Theory Comput. 10 (2014) 4069–4078. https://doi.org/10.1021/ct5004109.

[26] T.F. Cova, B.F. Milne, A.A.C.C. Pais, Host flexibility and space filling in supramolecular complexation of cyclodextrins: A free-energy-oriented approach, Carbohydr. Polym. 205 (2019) 42–54. https://doi.org/10.1016/j.carbpol.2018.10.009.

[27] G. Utzeri, T.F. Cova, D. Murtinho, A.A.C.C. Pais, A.J.M. Valente, Insights on macro- and microscopic interactions between Confidor and cyclodextrin-based nanosponges, Chem. Eng. J. 455 (2023) 140882. https://doi.org/10.1016/j.cej.2022.140882.

[28] T.F.G.G. Cova, B.F. Milne, S.C.C. Nunes, A.A.C.C. Pais, Drastic Stabilization of Junction Nodes in Supramolecular Structures Based on Host–Guest Complexes, Macromolecules. 51 (2018) 2732–2741. https://doi.org/10.1021/acs.macromol.8b00154.

Chapter 6.

Limiting diffusion coefficients of glufosinate ammonium, cymoxanil and imidacloprid in aqueous solutions

III

Luis M.P. Verissimo, Gianluca Utzeri, M. Luísa Ramos, Ana C.F. Ribeiro, Artur J.M Valente

Journal of Molecular Liquids, vol. 293 (2019) 111459

Journal of Molecular Liquids 293 (2019) 111459

Contents lists available at ScienceDirect

Journal of Molecular Liquids

journal homepage: www.elsevier.com/locate/molliq

Limiting diffusion coefficients of glufosinate ammonium, cymoxanil and imidacloprid in aqueous solutions☆

Luis M.P. Verissimo, Gianluca Utzeri, M. Luísa Ramos, Ana C.F. Ribeiro, Artur J.M. Valente *

CQC, Department of Chemistry, University of Coimbra, 3004-535 Coimbra, Portugal

ARTICLE INFO

Article history:
Received 30 April 2019
Received in revised form 28 June 2019
Accepted 27 July 2019
Available online 29 July 2019

Keywords:
Glufosinate ammonium
Cymoxanil
Imidacloprid
Diffusion coefficients
Taylor technique
^{1}H and ^{31}P NMR spectroscopy

ABSTRACT

We have measured the limiting diffusion coefficients of three different pesticides in aqueous solutions: glufosinate ammonium, cymoxanil and imidacloprid, highly used for tomato production. The experiments were carried in aqueous solutions, at 25 °C, at concentrations below 3 mmol dm^{-3} (depending on the solubility of pesticides). Mutual diffusion coefficients (D) obtained by using the Taylor dispersion technique, and by using pure water and different solutions of concentration c, as carrier stream and injection solutions, respectively, show that the systems can be analyzed as binary ones. The hydrodynamic radii and the respective limiting diffusion coefficients of the glufosinate anion, cymoxanil and imidacloprid have also been estimated. For the electrolyte glufosinate ammonium, by using the Nernst equation, it is also possible to estimate the limiting molar conductivity of the glufosinate anion.

In order to mimic field conditions, we have measured the tracer diffusion coefficients of glufosinate ammonium in aqueous solutions of ammonium nitrate at different concentrations, permitting us to analysis the salting-in effects on the diffusion of this pesticide.

From these measurements useful information on the thermodynamic, transport and structural parameters can be obtained, allowing a better understanding of the behaviour of these compounds in aqueous solution.

These studies have been complemented with ^{1}H and ^{31}P NMR spectroscopy in order to obtain more additional structural information on the interaction of ammonium nitrate with glufosinate-ammonium in aqueous solution. The results obtained support the hypothesis of salting-in effects on the diffusion of this pesticide in aqueous solution.

1. Introduction

Pesticides provide the primary means for controlling organisms that compete with man for food and fibre or cause injury to man, livestock and crops. However, pesticides persistence is the key-factor in the formation of resistant species, which consequently demands of higher amounts of pesticides or to the development of new plant production products [1]. Besides, the pesticides efficiency is very low; in fact, only ca. 0.5% of pesticides reach the target, while 99.5% is dispersed in the environment [2]. Their persistence, toxicity, bio-accumulation and non-specificity as well as the capacity to permeate the soil, inquinate surface and ground waters after leaching, run-off and volatilize made them an issue of increasing concern [3]. Thus, the environmental issues related with the use and disposal of pesticides is nowadays a key concern that needs to be solved.

The knowledge of phenomena transport, in particular the diffusion, is a key point in the assessment of pesticide impact on the biotic and environment. Examples of that, can be found for the assessment of pesticide permeation through plant cuticles [1,2], soil sorption [4–7] or wastewater and ground water treatment [8–10]. In the latter, the knowledgment of diffusion coefficients of the diffusing pesticides are of outmost importance once it corresponds to the maximum limit values for diffusion [11]. However, at the best of our knowledge only few papers are reporting diffusion coefficients of pesticides. In the 90s of the last century, Reviejo et al. have measured self-diffusion coefficients of dieldrin, heptachlor, endolsufan and endosulfan sulfate, in a emulsified solution (containing, e.g., Triton-X and ethyl acetate), by using polarography. The results range from 2.2×10^{-11} m^2 s^{-1} for heptachlor to 6.9×10^{-11} m^2 s^{-1} for endosulfan sulfate [12]. More recently, limiting diffusion coefficients of six different pesticides (tebuconazole, pirimicarb, metazachlor, chlorotoluron, sulcotrione and cyromazine) have been reported, and range in ascending order from

☆ This paper is dedicated to the memory of Prof. Josef Barthel.

* Corresponding author at: Department of Chemistry, University of Coimbra, 3004-535 Coimbra, Portugal.
E-mail address: avalente@ci.uc.pt (A.J.M. Valente).

https://doi.org/10.1016/j.molliq.2019.111459
0167-7322/

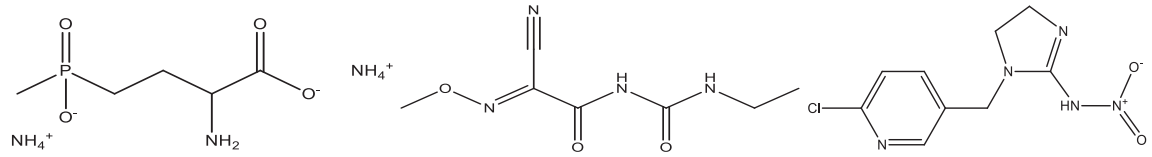

Scheme 1. Molecular structures of glufosinate ammonium, cymoxanil and imidacloprid (from left to right).

3.5×10^{-10} m^2 s^{-1} to 7.3×10^{-10} m^2 s^{-1}, respectively, at 25 °C [13]. The later work also make a review of few papers related to the measurement of mutual diffusion and self-diffusion coefficients of some herbicides [14,15].

In this work we aim to characterize the diffusion properties of three different pesticides: glufosinate ammonium, cymoxanil and imidacloprid (Scheme 1) [16]. For that, mutual diffusion coefficients for all those pesticides in aqueous solutions, at 25 °C, were measured by using the Taylor dispersion technique. The corresponding mutual diffusion coefficients (D) were obtained by using pure water and solutions of concentration, c, as carrier stream and injection solutions, respectively. The computed D values, as well as the dispersion profiles, have shown that all systems can be analyzed as binary ones. Consequently, the corresponding limiting diffusion coefficients (D^0) and the hydrodynamic radii have been estimated. In particular, for the glufosinate ammonium, and through the Nernst-equation, the limiting molar conductivity of glufosinate anion was also computed. The major drawback for using the Taylor dispersion technique is its low detection limit; for that reason, the effect of ionic strength on the diffusion behaviour of pesticides was only evaluated for aqueous solutions of glufosinate ammonium (the pesticide with highest solubility). Thus, we have measured the tracer diffusion coefficients (D_T) of glufosinate ammonium in aqueous solutions of ammonium nitrate at different concentrations, permitting us to analysis the salting-in effects on the diffusion of this pesticide. For the sake of clarification both tracer and limiting diffusion coefficients are quantitative measures of the mutual diffusion phenomenon but obtained under different experimental conditions. Limiting diffusion coefficients are computed by extrapolation of the experimental diffusion coefficients. The diffusion coefficients are measured by using water as the carrier stream and pesticide solutions, at different concentrations, in the injection solution. On the other hand, the tracer diffusion measurement is made in a way that an ion (e.g., glufosinate) at very low concentration is diffusing in the presence of other (in the present case, nitrate) whose concentration is essentially constant at all points in the solution [17].

Some additional structural information on the interaction of glufosinate ammonium with ammonium nitrate was obtained by ^{1}H and ^{31}P NMR spectroscopy.

2. Experimental section

2.1. Materials

Three different pesticides were tested: glufosinate ammonium (2-amino-4-[hydroxy(methyl)phosphoryl]butanoic acid), imidacloprid (*N*-[1-[(6-chloropyridin-3-yl)methyl]-4,5-dihydroimidazol-2-yl] nitramide) and cymoxanil ((1*E*)-2-(ethylcarbamoylamino)-*N*-methoxy-2-oxoethanimidoyl cyanide); all pesticides are Pestanal-analytical standard grade and were obtained from Sigma-Aldrich. All solutions were prepared by using Millipore-Q water.

For the NMR experiments, the solutions were prepared in D_2O (Aldrich, >0.99).

2.2. Diffusion measurements

The theory of the Taylor dispersion technique has been presented in detail in the literature [18–20] and, thus, only a brief description of the apparatus and the procedure used in our study is presented here [21–24].

This method is based on the dispersion of small amounts of solution injected into laminar carrier streams of solution of different composition flowing through a long capillary tube. At the start of each run, a 6-port Teflon injection valve (Rheodyne, model 5020) was used to introduce 63 mm^3 of solution into a laminar carrier stream of slightly different composition. A flow rate of 0.17 cm^3 min^{-1} was maintained by a metering pump (Gilson model Minipuls 3) to give retention times of about 1.1×10^4 s. The dispersion tube (length 32.799 (±0.001) m) and the injection valve were kept at 298.15 K (±0.01 K) in an air thermostat.

Dispersion of the injected samples was monitored using a differential refractometer (Waters model 2410) at the outlet of the dispersion tube. Detector voltages, $V(t)$, were measured at 5 s intervals with a digital voltmeter (Agilent 34,401 A) with an IEEE interface.

Binary diffusion coefficients were evaluated by fitting the dispersion equation (Eq. (1))

$$V(t) = V_0 + V_1 t + V_{max}(t_R/t)^{0.5} \exp\left[-12D(t-t_R)^2/r^2 t\right] \quad (1)$$

to the detector voltages. The additional fitting parameters were the mean sample retention time t_R, radius of the dispersion tube r, peak height V_{max}, baseline voltage V_0, and baseline slope V_1.

In the first experimental part of this work, we have measured values of D for three pesticides in water. That is, for each pesticide, solutions of different concentrations were injected into pure water to confirm that the measured diffusion coefficients were independent of the initial concentration gradient and therefore represented the differential value of D at the carrier-stream composition. The diffusion data D were obtained from, at least, three independent runs, using different concentrations of the injected solutions in water. The uncertainty of these values is lower than 2%.

In second part of this work, values of tracer diffusion coefficients, D_T, for glufosinate ammonium (NH_4Glu) in aqueous solutions of ammonium nitrate were measured. For the $(NH_4)_2Glu(1)/NH_4NO_3(2)$ system the following dispersion equation should be considered

$$V(t) = V_0 + V_1 t + V_{max}(t_R/t)^{0.5}\left[W_1 \exp\left(-\frac{12D_1(t-t_R)^2}{r^2 t}\right) + (1-W_1)\exp\left(-\frac{12D_2(t-t_R)^2}{r^2 t}\right)\right] \quad (2)$$

where D_1 and D_2, are the eigenvalues of the matrix of main and cross D_{ik} diffusion coefficients and W_1 and (1-W_1) are the normalized pre-exponential factors. However, in our experimental set up, the concentrations of $NH_4NO_3(2)$ in the injection and carrier solutions are equal and, consequently, the 2nd term inside square brackets is null. Additionally, the concentration of $NH_4NO_3(2)$ is significantly higher than the concentration of $(NH_4)_2Glu(1)$ which ensures the occurrence of tracer diffusion. In these conditions, Eq. (2) becomes equal to the Eq. (1), being $D = D_T$ [25–27].

2.3. NMR experiments

The ^{1}H and ^{31}P NMR spectra were obtained on a Bruker Avance III HD 500 MHz NMR spectrometer. The methyl signal of *tert*-butyl alcohol was used as the internal reference for ^{1}H (δ 1.3) and the ^{31}P signal of a D_2O solution of H_3PO_4 (85%) used as the external reference for ^{31}P. The pH values measured with a pH metter Crison Basic 20, equipped with a glass microelectrode 50/28, pH 0–14. The pH values quoted are the direct pH-meter readings (room temperature) after standardization with aqueous buffers.

3. Results and discussion

3.1. Analysis of the mutual diffusion coefficients of some pesticides in aqueous solutions

Mutual diffusion coefficients, D, of glufosinate ammonium, cymoxanil and imidacloprid, in aqueous solutions, at 298.15 K, were measured and are shown in Fig. 1.

By fitting a linear model equation in the form of $D = f(c^{1/2})$, for the electrolyte glufosinate ammonium, and $D = f(c)$ for cymoxanil and imidacloprid (which are non-electrolytes) [17], to the experimental D values, the limiting diffusion coefficient at infinitesimal concentration ($c_1 \rightarrow 0$) D^0 can be computed by extrapolation. The obtained values are 1.091 ($\pm$0.001) $\times 10^{-9}$, 8.333 ($\pm$0.001) $\times 10^{-10}$ and 6.593 ($\pm$ 0.005) $\times 10^{-10}$ m^2 s^{-1}, respectively. From these values, $D^0((NH_4)_2Glu) > D^0$(cymoxanil) > D^0(imidacloprid), it can be concluded that $(NH_4)_2Glu$ offers less frictional resistance to motion through the liquid, which can be related with the electrolytic character of the glufosinate ammonium.

From the limiting diffusion coefficients at infinitesimal concentration other physico-chemical parameters characterizing the systems can be calculated. Thus, the limiting diffusion coefficient of the glufosinate anion (D_a^0) can be estimated by using the Nernst Eq. (3)

$$D^0 = \frac{RT|Z_c| + |Z_a|}{F^2\ |Z_c \times Z_a|}\frac{\lambda_c^0\lambda_a^0}{\lambda_c^0 + \lambda_a^0} \tag{3}$$

where R is the gas constant in J K^{-1} mol^{-1}, F is the Faraday constant, T is the absolute temperature, Z_c and Z_a are the algebraic valences of the cation (NH_4^+) and the anion (Glu^{2-}), respectively, and the λ_c^0 and λ_a^0 are the corresponding limiting molar conductivities. Thus, by knowing the limiting conductivity for the ammonium ion, λ_c^0, which is equal to 73.70 $\times 10^{-4}$ Ω^{-1} m^2 mol^{-1} [28], the limiting molar conductivity of the glufosinate anion can be computed: λ_a^0 = 43.40 $\times 10^{-4}$ Ω^{-1} m^2 mol^{-1}. The limiting molar conductivity of the specie i is related to ion diffusivity by the equation.

$$D_i^0 = RT\lambda_i^0/FZ_i^2 \tag{4}$$

Consequently, the limiting glufosinate ion diffusion coefficient can also be calculated and is equal to 0.578 $\times 10^{-9}$ m$^2\cdot$s^{-1}.

Our calculation demonstrates that the mutual diffusion coefficient of the glufosinate ammonium at infinitesimal concentration (D^0 = 1.091 $\times 10^{-9}$ m^2 s^{-1}) is ca. two times higher than the corresponding limiting diffusion coefficient for the glufosinate anion (D_a^0 = 0.578 $\times 10^{-9}$ m^2 s^{-1}). Such a difference may indicate a non-negligible electrostatic dragging effect of the ammonium ions on the glufosinate anion.

From the Stokes-Einstein equation [17,29], and being aware of its limitations, it is possible to estimate the hydrodynamic radius, R_h, for all three pesticides, in aqueous solution, by the equation,

$$D^0 = k_BT/(6\pi\eta^0R_h) \tag{5}$$

where k_B and η^0 are the Boltzmann's constant and the viscosity of water at temperature T, respectively. The following values were obtained: $R_h(Glu^{2-})$ = 0.424 $\times 10^{-10}$ m, R_h(cymoxanil) = 0.294 $\times 10^{-10}$ m and R_h(imidacloprid) = 0.372 $\times 10^{-10}$ m. As it was expected the radius of the glufosinate ion is significantly higher than the other two pesticides. In fact, due to its nature, the interactions between these entities and water molecules are most favoured.

3.2. Tracer diffusion coefficients of glufosinate ammonium in ammonium nitrate aqueous solutions

Table 1 presents the experimental tracer diffusion coefficients, D_T, for aqueous $(NH_4)_2Glu/NH_4NO_3$ mix solutions, at 25 °C. The use of ammonium nitrate has the objective of mimetizing the effect of ionic strength in real pesticide applications in soil and water, often in the presence of fertilizers. Comparing the tracer diffusion coefficients of glufosinate ammonium in the presence of ammonium nitrate with the corresponding limiting diffusion coefficients (see $\Delta D_T/D^0$ in the Table 1), it can be concluded that the presence of the salt in the solution leads to a significant decrease in the diffusion coefficient. Such negative deviation, ranging from 17 to 24%, may be interpreted as the occurrence

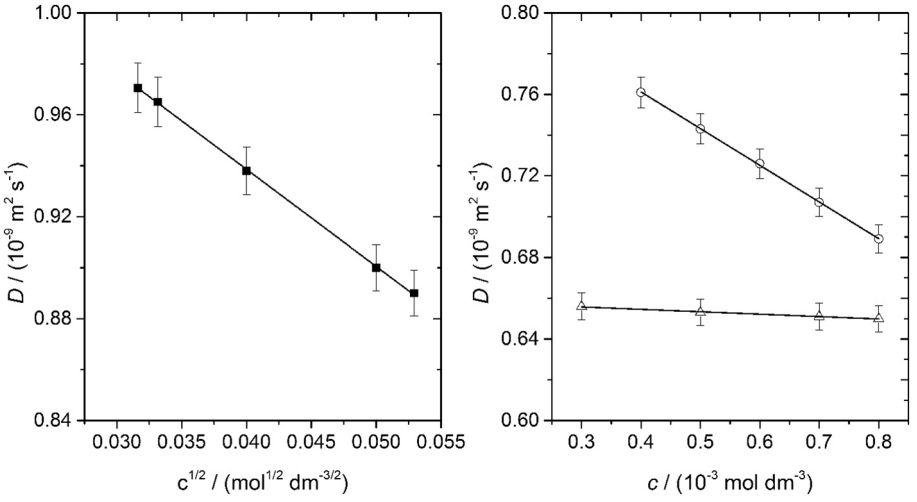

Fig. 1. Mutual diffusion coefficients, D, of glufosinate ammonium (■), cymoxanil (○) and imidacloprid (△), in aqueous solutions, at 298.15 K.

Table 1
Tracer diffusion coefficients, D_T, for $(NH_4)_2Glu$ in aqueous solutions containing NH_4NO_3, at 25 °C.[a]

c_1/(mol dm^{-3})	$D_T/10^{-9}$ m^2 s^{-1}	$\Delta D_T/D^0$ [b] %	$D_T/10^{-9}$ m^2 s^{-1}	$\Delta D_T/D^0$ [b] %
	$c_2 = 0.01$/(mol dm^{-3})		$c_2 = 0.02$/(mol dm^{-3})	
0.001	0.788	−19	0.744	−24
0.002	0.751	−17	0.733	−19
0.003	0.733	−17	0.721	−19

[a] This table shows the values of tracer diffusion coefficients of glufosinate ammonium in ammonium nitrate aqueous solutions. To get those values, 70 μL of $(NH_4)_2Glu + NH_4NO_3$ at concentrations, c_1 and c_2, respectively, was injected into the flow ammonium salt solution, at concentration c_2.
[b] $\Delta D_T/D^0$ represent the deviations between tracer and limiting diffusion coefficients of $(NH_4)_2Glu$.

Table 2
pH* values for a D_2O solution of glufosinate ammonium 1.8 mmol kg^{-1} as a function of increasing concentrations of NH_4NO_3.

[NH_4NO_3] (mol kg^{-1})	pH*
0	7.34
0.0089	6.34
0.0178	6.23
0.0356	6.08

of a salting-in effect [30,31]. That is, the presence of ammonium nitrate contributes to more favourable interactions between $(NH_4)_2Glu$ and water molecules. Subsequently, the entities of $(NH_4)_2Glu$ offer more frictional resistance to motion through the liquid thus, lowering the diffusion coefficient of this aqueous system. However, such effect is not particularly sensitive to the ionic strength.

Some insights on the structure of the solution of glufosinate ammonium and its structural changes with increasing concentrations of the salt have been obtained from ^1H and ^{31}P NMR spectroscopy. The combination of ^1H and ^{31}P NMR parameters should provide informations on the degree of protonation and on the conformational changes of the ligand in the presence of a large excess of the salt [32–34].

Scheme 2 shows the glufosinate hydrolysis equilibria, as a function of pH. Accordingly, four different ionized forms of glufosinate are assigned (H_2L^+, H_2L, HL^- and L^{2-}) as a consequence of the differences in the degree of protonation/deprotonation of the three acidic functions present in the molecule, the phosphonate group $RP(CH_3)OOH \rightarrow RP(CH_3)OO^-$ ($H_2L^+ \rightarrow H_2L$) ($pK_{a1} = 2.00$), the carboxylic group, $R'CO_2H \rightarrow R'CO_2^-$ (($H_2L \rightarrow HL^-$), ($pK_{a2} = 2.90$), and the amino group, $R''NH_3^+ \rightarrow R''NH_2$ ($HL^- \rightarrow L^{2-}$) ($pK_{a3} = 9.80$), at 298.15 K, respectively [35,36].

The proton and phosphorous chemical shifts have been measured for a solution of glufosinate ammonium, at pH* of dissolution, alone and in the presence of increasing concentrations of NH_4NO_3. It is worth noting that the pH* of $(NH_4)_2Glu(1)/NH_4NO_3(2)$ solutions decreases by increasing the concentration (Table 2).

Figs. 2 and 3 show, respectively, the dependence of the ^1H and ^{31}P NMR spectra as a function of the concentration of the NH_4NO_3 added to a solution of glufosinate ammonium (1.8 mmol kg^{-1}) in D_2O, at pH* of dissolution (pH* 7.34). The numbering used in the ^1H assignment is defined in the Scheme 2.

According with the Fig. 2, the ^1H signal of proton H-2 is the most affected, showing a slight shift to higher frequencies with increasing concentrations of NH_4NO_3 added to the solution, whereas in the same conditions, the chemical shifts of the corresponding signals of protons H-3, H-4 and H-6 are not affected. Similarly to H-2, the ^{31}P NMR signal shows a slight shift to higher frequencies (Fig. 3). The pattern of the dependence is very similar for both H-2 and P-5 nuclei which, for better visualization, is shown in the graphs of the Fig. 4. From the observed deshielding of H-2 nuclei in the ^1H NMR spectra, the increasing of negative charge of carboxylate group is suggested, in consequence of the polarization of the bonding electrons from C-2 towards C-1. Likewise, the ^{31}P NMR spectra indicate for the phosphonate group some conformational changes as a result of the increasing of negative charge of the atom O-5 [32–34]. As the dominant species of glufosinate in solution is HL^- (Scheme 2), the increasing of the negative charge of the two terminal negative functional groups (carboxylate and phosphonate) with increasing concentrations of NH_4NO_3 should be regarded as a result of the increment of the electrostatic interactions of these sites with the excess of NH_4^+ species. These findings should have a particular impact on the decreasing of diffusion coefficients with the increasing concentration of the salt based on "salting in" effect.

4. Conclusions

The limiting mutual diffusion coefficients for three pesticides (glufosinate ammonium, cymoxanil and imidacloprid) in water and the tracer diffusion coefficients of glufosinate ammonium, at 25 °C, were measured.

In water, the differences found for the limiting diffusion coefficients of these pesticides may be interpreted on the basis of their electrolytic character.

The effect of ionic strength, simulated by using ammonium nitrate, on the diffusion of glufosinate ammonium in aqueous solutions has been studied. It has been found that, in these conditions, a salting-in effect is affecting the diffusion behaviour. The salting-in effect is more favourable at high salt concentrations ($c = 0.02$ mol dm^{-3}). Consequently, the entities of $(NH_4)_2Glu$ offer more frictional resistance to motion through the liquid, and, consequently, the diffusion coefficient of

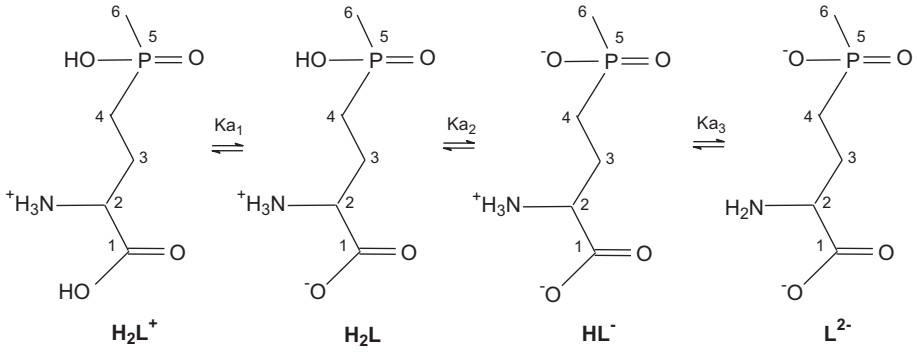

Scheme 2. Glufosinate hydrolysis equilibria. For the sake of simplicity the hydronium ions have been omitted.

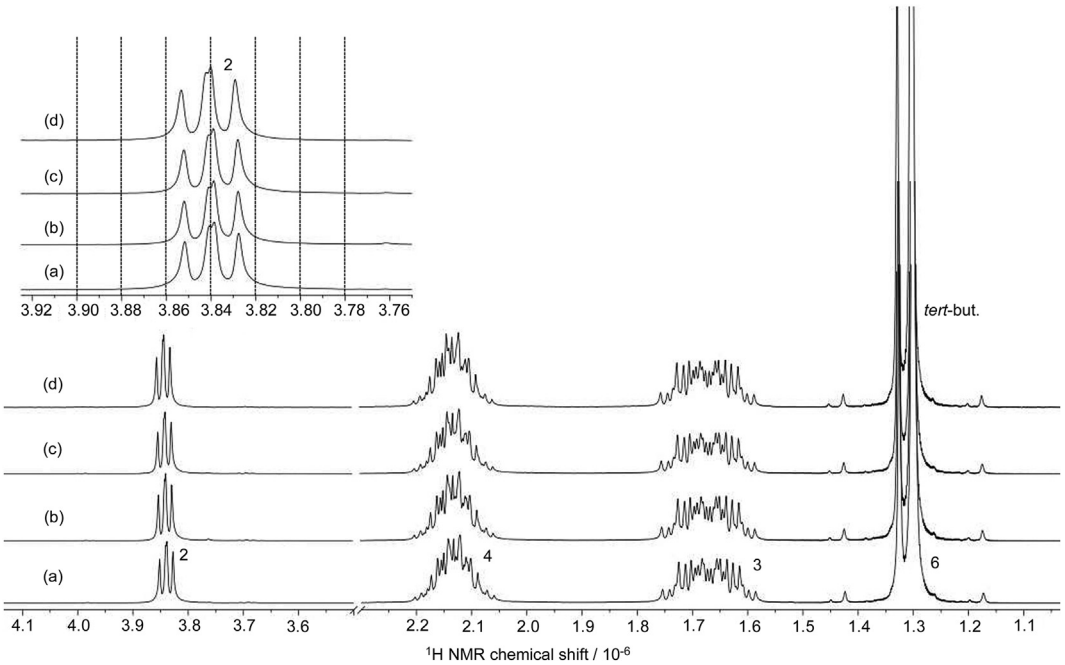

Fig. 2. ^{1}H NMR spectra of a D_2O solutions of glufosinate ammonium, at 298.15 K as a function of increasing concentrations of NH_4NO_3: (a) $(NH_4)_2Glu$ 1.8 mmol kg^{-1}, pH* 7.34 and (b) $(NH_4)_2Glu/NH_4NO_3$ 1.8:8.9 mmol kg^{-1}, pH* 6.34; (c) $(NH_4)_2Glu/NH_4NO_3$ 1.8:17.8 mmol kg^{-1}, pH* 6.23; (d) $(NH_4)_2Glu/NH_4NO_3$ 1.8:35.6 mmol kg^{-1}, pH* 6.08. Inset containing an expansion from 3.75 to 3.93 ppm for better visualization of H-2 signals of $(NH_4)_2Glu$ alone and in the presence of increasing concentrations of NH_4NO_3.

this aqueous system becomes smaller, as a consequence of stronger interactions between ions and water molecules. This is supported by NMR experiments. In the presence of an excess of ammonium ions, the electrostatic interactions due to an increase of the negative charge in the phosphonate and carboxylate groups increase, contributing for a diffusion slow down.

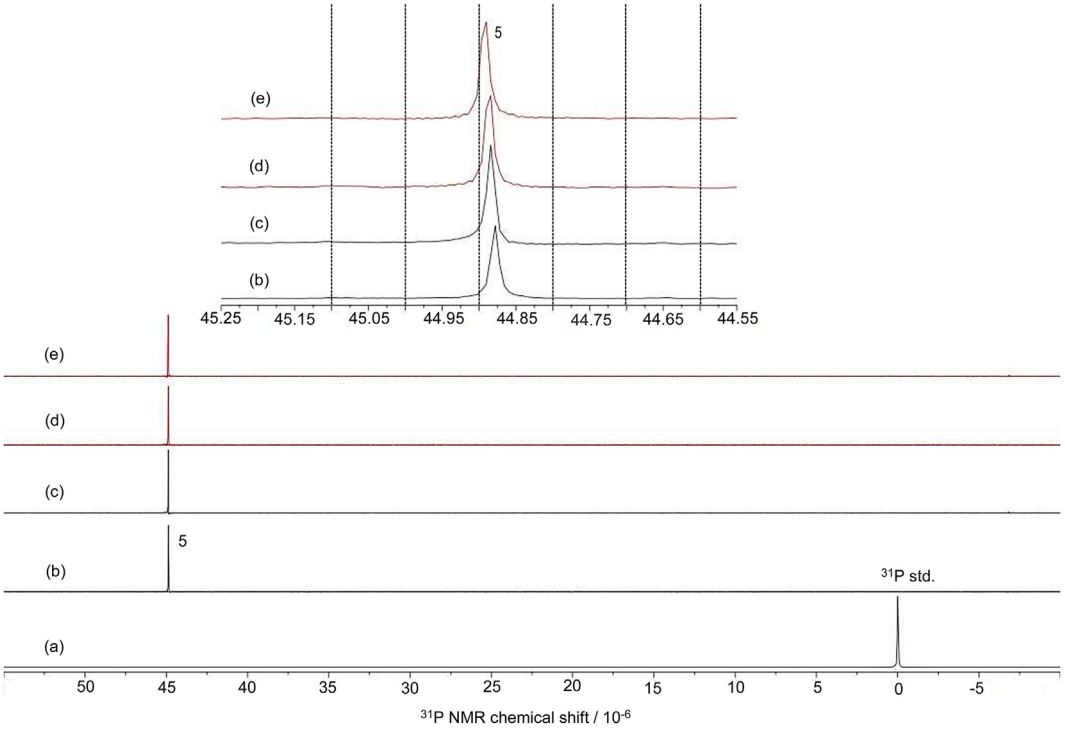

Fig. 3. ^{31}P NMR spectra of a D_2O solutions of glufosinate ammonium, at 298.15 K, as a function of increasing concentrations of NH_4NO_3: (a) H_3PO_4 85% alone (standard - std) and (b) $(NH_4)_2Glu$ 1.8 mmol kg^{-1}, pH* 7.34; (c) $(NH_4)_2Glu/NH_4NO_3$ 1.8:8.9 mmol kg^{-1}, pH* 6.34; (d) $(NH_4)_2Glu/NH_4NO_3$ 1.8:17.8 mmol kg^{-1}, pH* 6.23; (e) $(NH_4)_2Glu/NH_4NO_3$ 1.8:35.6 mmol kg^{-1}, pH* 6.08. Inset containing an expansion from 44.55 to 45.25 ppm for better visualization of ^{31}P signals of $(NH_4)_2Glu$ alone and in the presence of increasing concentrations of NH_4NO_3.

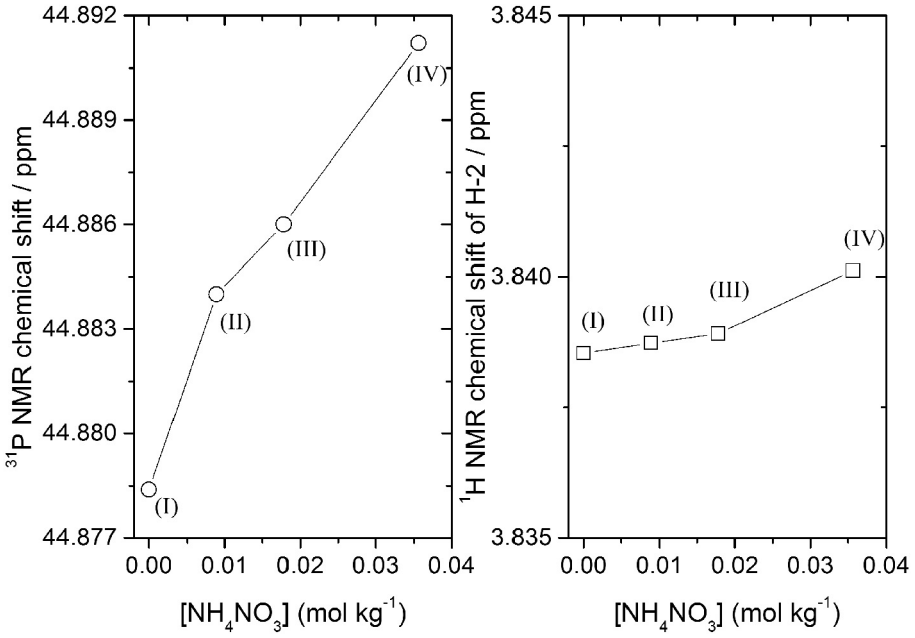

Fig. 4. ^{1}H NMR chemical shifts (ppm) for proton H-2 and ^{31}P NMR chemical shifts (ppm), relative to the signals of tert-butanol (□) and H_3PO_4 85% (○) (standards) of a D_2O solution of $(NH_4)_2$Glu 1.8 mmol kg^{-1}, pH* 7.34, at 298.15 K as a function of increasing concentrations of NH_4NO_3: (I) $(NH_4)_2$Glu 1.8 mmol kg^{-1}, pH* 7.34; (II) $(NH_4)_2$Glu/NH_4NO_3 1.8:8.9 mmol kg^{-1}, pH* 6.34; (III) $(NH_4)_2$Glu/NH_4NO_3 1.8:17.8 mmol kg^{-1}, pH* 6.23; (IV) $(NH_4)_2$Glu/NH_4NO_3 1.8:35.6 mmol kg^{-1}, pH* 6.08.

Acknowledgements

This work was financed by Portuguese funds through FCT - Fundação para a Ciência e a Tecnologia in the framework of the projects WaterJPI/0006/2016 and UID/QUI/00313/2019. NMR data were obtained at the UC-NMR facility which is supported in part by FEDER–European Regional Development Fund through the COMPETE Programme (Operational Programme for Competitiveness) and by National Funds through FCT — Fundação para a Ciência e Tecnologia (Portuguese Foundation for Science and Technology) through grants REEQ/481/QUI/2006, RECI/QEQ-QFI/0168/2012, CENTRO-07-CT62-FEDER-002012, and Rede Nacional de Ressonância Magnética Nuclear (RNRMN).

References

[1] R.L. Metcalf, Insect control, Ullmann's Encycl. Ind. Chem, Wiley-VCH Verlag GmbH & Co. KGaA, Weinheim, Germany, 2000https://doi.org/10.1002/14356007.a14_263.
[2] D. Pimentel, Amounts of pesticides reaching target pests: environmental impacts and ethics, J. Agric. Environ. Ethics 8 (1995) 17–29, https://doi.org/10.1007/BF02286399.
[3] A.E. Akay Demir, F.B. Dilek, U. Yetis, A new screening index for pesticides leachability to groundwater, J. Environ. Manag. 231 (2019) 1193–1202, https://doi.org/10.1016/j.jenvman.2018.11.007.
[4] J. Villaverde, W. van Beinum, S. Beulke, C.D. Brown, The kinetics of sorption by retarded diffusion into soil aggregate pores, Environ. Sci. Technol. 43 (2009) 8227–8232, https://doi.org/10.1021/es9015052.
[5] W.M. Daniels, W.A. House, B.V. Zhmud, J.E. Rae, A. Parker, Diffusive movement of simazine and lindane in river-bed sediments, Pestic. Sci. 54 (1998) 212–222, https://doi.org/10.1002/(SICI)1096-9063(1998110)54:3<212::AID-PS810>3.0.CO;2-6.
[6] P. Moldrup, T. Olesen, T. Komatsu, S. Yoshikawa, P. Schjonning, D. Rolston, Modeling diffusion and reaction in soils: X. A unifying model for solute and gas diffusivity in unsaturated soil, Soil Sci. 168 (2003) 321–327.
[7] F.G. Renaud, P.B. Leeds-Harrison, C.D. Brown, W. van Beinum, Determination of time-dependent partition coefficients for several pesticides using diffusion theory, Chemosphere 57 (2004) 1525–1535, https://doi.org/10.1016/j.chemosphere.2004.08.059.
[8] M.Z. Momčilović, M.S. Ranđelović, M. Purenović, A.E. Onjia, B.M. Babić, B.Z. Matović, Synthesis and characterization of resorcinol formaldehyde carbon cryogel as efficient sorbent for imidacloprid removal, Desalin. Water Treat. 52 (2014) 7306–7316, https://doi.org/10.1080/19443994.2013.836993.
[9] B.M. Patterson, G.B. Davis, A.J. McKinley, Laboratory column experiments using polymer mats to remove selected VOCs, PAHs, and pesticides from ground water, Groundw. Monit. Remediat. 22 (2002) 99–106, https://doi.org/10.1111/j.1745-6592.2002.tb00318.x.
[10] S.G. Kumbar, A.M. Dave, T.M. Aminabhavi, Release kinetics and diffusion coefficients of solid and liquid pesticides through interpenetrating polymer network beads of polyacrylamide-g-guar gum with sodium alginate, J. Appl. Polym. Sci. 90 (2003) 451–457, https://doi.org/10.1002/app.12675.
[11] S. Yedla, A.K. Dikshit, Removal mechanism of endosulfan sorption onto wood charcoal, Int. J. Environ. Pollut. 15 (2001) 528, https://doi.org/10.1504/IJEP.2001.004921.
[12] A.J. Reviejo, A. Samprón, J.M. Pingarrón, L.M. Polo, Determination of organochlorine pesticides by polarography in emulsified medium, Electroanalysis 4 (1992) 111–120, https://doi.org/10.1002/elan.1140040120.
[13] S. Sarraute, P. Husson, M.C. Gomes, Effect of the diffusivity on the transport and fate of pesticides in water, Int. J. Environ. Sci. Technol. 16 (2019) 1857–1872, https://doi.org/10.1007/s13762-018-1815-7.
[14] H.D. Scott, R.E. Phillips, Self-diffusion coefficients of selected herbicides in water and estimates of their transmission factors in soil1, Soil Sci. Soc. Am. J. 37 (1973) 965, https://doi.org/10.2136/sssaj1973.03615995003700060046x.
[15] M. Raveton, A. Schneider, C. Desprez-Durand, P. Ravanel, M. Tissut, Comparative diffusion of atrazine inside aqueous or organic matrices and inside plant seedlings, Pestic. Biochem. Physiol. 65 (1999) 36–43, https://doi.org/10.1006/pest.1999.2422.
[16] F.G.A. Estrada, J.M.C. Marques, A.J.M. Valente, Molecular dynamics insights for screening the ability of polymers to remove pesticides from water, ChemistryOpen 8 (2019) 438–446, https://doi.org/10.1002/open.201800293.
[17] H.J.V. Tyrrell, K.R. Harris, Diffusion in Liquids, Butterworths, London, 1984.
[18] G.I. Taylor, Dispersion of soluble matter in solvent flowing slowly through a tube, Proc. R. Soc. London. Ser. A. Math. Phys. Sci. 219 (1953) 186–203, https://doi.org/10.1098/rspa.1953.0139.
[19] G.I. Taylor, The dispersion of matter in turbulent flow through a pipe, Proc. R. Soc. London. Ser. A. Math. Phys. Sci. 223 (1954) 446–468, https://doi.org/10.1098/rspa.1954.0130.
[20] G.I. Taylor, Conditions under which dispersion of a solute in a stream of solvent can be used to measure molecular diffusion, Proc. R. Soc. London. Ser. A. Math. Phys. Sci. 225 (1954) 473–477, https://doi.org/10.1098/rspa.1954.0216.
[21] A.C.F. Ribeiro, D.G. Leaist, M.A. Esteso, V.M.M. Lobo, A.J.M. Valente, C.I.A.V. Santos, et al., Binary mutual diffusion coefficients of aqueous solutions of β-cyclodextrin at temperatures from 298.15 to 312.15 K, J. Chem. Eng. Data 51 (2006) 1368–1371, https://doi.org/10.1021/je060092t.
[22] A.C.F. Ribeiro, J.J.S. Natividade, M.A. Esteso, Differential mutual diffusion coefficients of binary and ternary aqueous systems measured by the open ended conductometric capillary cell and by the Taylor technique, J. Mol. Liq. 156 (2010) 58–64, https://doi.org/10.1016/j.molliq.2010.04.020.
[23] L.M.P. Verissimo, M.L. Ramos, L.L.G. Justino, H.D. Burrows, P.F. Cruz, A.M.T.D.P.V. Cabral, et al., The structure and diffusion behaviour of the 1:1 copper(II) complex of ethambutol in aqueous solution, J. Mol. Liq. 262 (2018) 63–70, https://doi.org/10.1016/j.molliq.2018.04.039.
[24] A. Malagón, L.F. Velásquez, D.M. Galindres, A.C.F. Ribeiro, A.J.M. Valente, L.M.P. Verissimo, et al., Diffusion and conductance properties of aqueous solutions of tetrasodium 5,11,17,23-tetrakissulfonatemethylen-2,8,14,20-tetra(2-(methylthio)ethyl)resorcinarene, J. Mol. Liq. 276 (2019) 897–901, https://doi.org/10.1016/j.molliq.2018.12.007.
[25] R. Callendar, D.G. Leaist, Diffusion coefficients for binary, ternary, and polydisperse solutions from peak-width analysis of Taylor dispersion profiles, J. Solut. Chem. 35 (2006) 353–379, https://doi.org/10.1007/s10953-005-9000-2.

[26] D.M. Rodriguez, L.M.P. Verissimo, M.C.F. Barros, D.F.S.L. Rodrigues, M.M. Rodrigo, M.A. Esteso, et al., Limiting values of diffusion coefficients of glycine, alanine, α-amino butyric acid, norvaline and norleucine in a relevant physiological aqueous medium, Eur. Phys. J. E. 40 (2017), 21. https://doi.org/10.1140/epje/i2017-11511-y.
[27] T. Grossmann, J. Winkelmann, Ternary diffusion coefficients of cyclohexane + toluene + methanol by Taylor dispersion measurements at 298.15 K. Part 1. Toluene-rich area †, J. Chem. Eng. Data 54 (2009) 405–410, https://doi.org/10.1021/je800444e.
[28] R. Robinson, R. Stokes, Electrolyte Solutions, 2nd ed. Butterworths, London, 1959.
[29] T. Erdey-Gruz, Transport Phenomena in Aqueous Solutions, 2nd ed. Adam Hilger, London, 1974.
[30] R.L. Baldwin, How Hofmeister ion interactions affect protein stability, Biophys. J. 71 (1996) 2056–2063, https://doi.org/10.1016/S0006-3495(96)79404-3.
[31] A.M. Hyde, S.L. Zultanski, J.H. Waldman, Y.-L. Zhong, M. Shevlin, F. Peng, General principles and strategies for salting-out informed by the Hofmeister series, Org. Process. Res. Dev. 21 (2017) 1355–1370, https://doi.org/10.1021/acs.oprd.7b00197.
[32] M.L. Ramos, L.L.G. Justino, V.M.S. Gil, H.D. Burrows, NMR and DFT studies of the complexation of W(VI) and Mo(VI) with 3-phospho-D-glyceric and 2-phospho-D-glyceric acids, Dalt. Trans. (2009) 9616, https://doi.org/10.1039/b905933d.
[33] D. Costa, M. Luísa Ramos, H.D. Burrows, M. José Tapia, M. da Graça Miguel, Using lanthanides as probes for polyelectrolyte–metal ion interactions. Hydration changes on binding of trivalent cations to nucleotides and nucleic acids, Chem. Phys. 352 (2008) 241–248, https://doi.org/10.1016/j.chemphys.2008.06.014.
[34] L. Ramos, V.M.S. Gil, Multinuclear NMR study of the complexes of 6-phospho-d-gluconic acid with W(VI) and Mo(VI), Carbohydr. Res. 339 (2004) 2225–2232, https://doi.org/10.1016/j.carres.2004.06.014.
[35] Q. Li, B. Liu, W. Mu, Q. Yu, Y. Tian, G. Liu, et al., Protonation states of glufosinate in aqueous solution, J. Solut. Chem. 47 (2018) 705–714, https://doi.org/10.1007/s10953-018-0751-y.
[36] R. Devendra, V. Umamahesh, T. Prasad, T. Prasad, S. Asha, A. Ashok, Influence of surfactants on efficacy of different herbicides in control of Cyperus rotundus and Oxalis latifolia, Curr. Sci. Assoc. 86 (2004) 1148–1151.

Poly(β-cyclodextrin)-Activated Carbon Gel Composites for Removal of Pesticides from Water

IV

Gianluca Utzeri, Luis Verissimo, Dina Murtinho, Alberto A.C.C. Pais, F. Xavier Perrin, Fabio Ziarelli, Tanta-Verona Iordache, Andrei Sarbu, Artur J.M Valente

Molecules, vol. 26 (2021) 1426

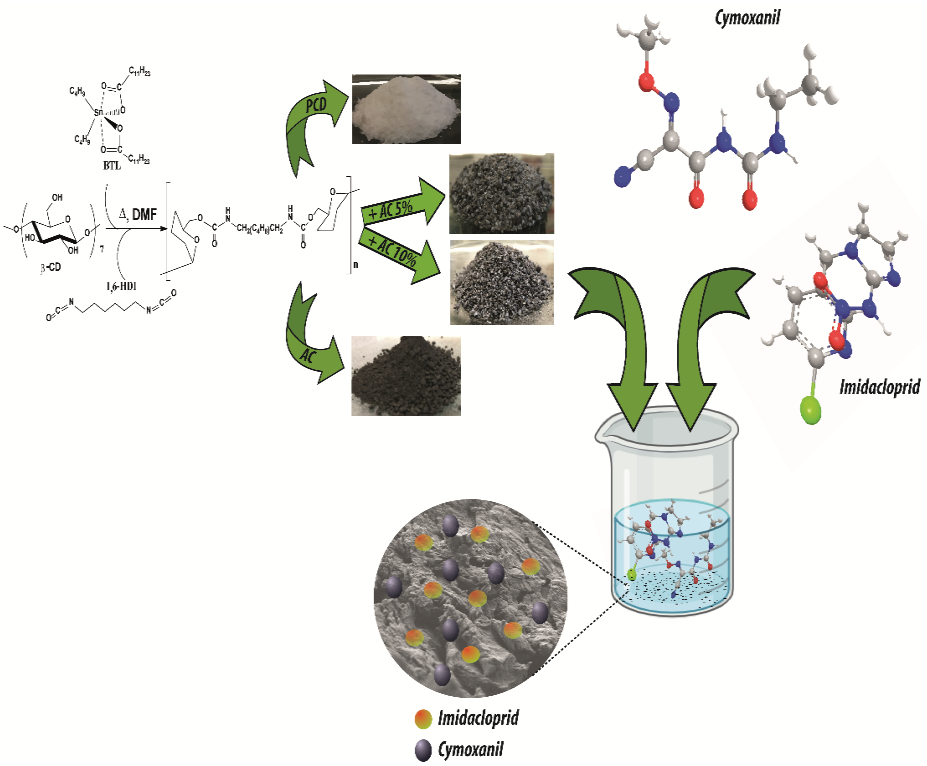

molecules

MDPI

Article

Poly(β-cyclodextrin)-Activated Carbon Gel Composites for Removal of Pesticides from Water

Gianluca Utzeri [1], Luis Verissimo [1], Dina Murtinho [1], Alberto A. C. C. Pais [1], F. Xavier Perrin [2], Fabio Ziarelli [3], Tanta-Verona Iordache [4], Andrei Sarbu [4] and Artur J. M. Valente [1,*]

1 Coimbra Chemistry Centre, Department of Chemistry, University of Coimbra, 3004-535 Coimbra, Portugal; uc2015276036@student.uc.pt (G.U.); luisve@gmail.com (L.V.); dmurtinho@ci.uc.pt (D.M.); pais@ci.uc.pt (A.A.C.C.P.)
2 Laboratoire MAPIEM, Université de Toulon, 83041 Toulon CEDEX 9, France; francois-xavier.perrin@univ-tln.fr
3 CNRS, Centrale Marseille, FSCM, Aix Marseille University, 13397 Marseille CEDEX 20, France; fabio.ziarelli@univ-amu.fr
4 National Institute for Research & Development in Chemistry and Petrochemistry-ICECHIM, Splaiul Independenței 202, 060021 București, Romania; iordachev.icechim@gmail.com (T.-V.I.); andr.sarbu@gmail.com (A.S.)
* Correspondence: avalente@ci.uc.pt; Tel.: +351-966047336

Abstract: Pesticides are widely used in agriculture to increase and protect crop production. A substantial percentage of the active substances applied is retained in the soil or flows into water courses, constituting a very relevant environmental problem. There are several methods for the removal of pesticides from soils and water; however, their efficiency is still a challenge. An alternative to current methods relies on the use of effective adsorbents in removing pesticides which are, simultaneously, capable of releasing pesticides into the soil when needed. This reduces costs related to their application and waste treatments and, thus, overall environmental costs. In this paper, we describe the synthesis and preparation of activated carbon-containing poly(β-cyclodextrin) composites. The composites were characterized by different techniques and their ability to absorb pesticides was assessed by using two active substances: cymoxanil and imidacloprid. Composites with 5 and 10 wt% of activated carbon showed very good stability, high removal efficiencies (>75%) and pesticide sorption capacity up to ca. 50 mg g^{-1}. The effect of additives (NaCl and urea) was also evaluated. The composites were able to release around 30% of the initial sorbed amount of pesticide without losing the capacity to keep the maximum removal efficiency in sorption/desorption cycles.

Keywords: β-cyclodextrin; activated carbon; hydrogels; pesticides; remediation

Citation: Utzeri, G.; Verissimo, L.; Murtinho, D.; Pais, A.A.C.C.; Perrin, F.X.; Ziarelli, F.; Iordache, T.-V.; Sarbu, A.; Valente, A.J.M. Poly(β-cyclodextrin)-Activated Carbon Gel Composites for Removal of Pesticides from Water. *Molecules* **2021**, *26*, 1426. https://doi.org/10.3390/molecules26051426

Academic Editors: João Valente Nabais and Giorgio Vilardi

Received: 18 January 2021
Accepted: 2 March 2021
Published: 6 March 2021

1. Introduction

One of the major challenges facing society nowadays is the development of effective methodologies to eliminate or reduce air, soil and water (surface and groundwater) contamination as a consequence of growing anthropogenic activities. Urbanization and industrialization has led to a massive release of different contaminant classes such as heavy metal ions [1], volatile organic compounds (VOCs) [2], polyfluoroalkyl substances (PFAs) [3], persistent organic pollutants (POPs) [4] and pesticides [5] into the environment. These xenobiotics can be harmful for both human health and ecosystems, causing sizable changes in the flora and fauna equilibria. Depending on their physical–chemical properties, they show different toxicity levels and mechanisms of action. Pesticides, which include biocides and plant protection products (PPPs), are mainly applied in the agriculture for improving harvests. Due to soil persistence, water contamination and food chain concentration, pesticides can affect directly or indirectly a wide range of organisms [6]. It is consensual that pesticides can cause adverse effects to human health leading to acute or chronic disorders, with effects being a function of time and amount of exposure [7,8].

Ideally, these products should be highly specific and, thus, selectively toxic to the target organisms. However, most of the pesticides have a broad spectrum of action and only ca. 0.1% reach the intended target [9]. Due to the agrochemicals' highly negative impacts, its removal from soil and water is a major challenge [10,11]. Hence, the improvement of environmental remediation techniques [12], e.g., biological treatment [13] and advanced oxidation processes [14], is pivotal. Sorption processes and materials have wakened great attention being straightforward in application and often reusable, showing good efficiency and advantageous cost effectiveness. A wide range of adsorbent materials, including clays [15], alumina, mesoporous metal oxide [16–18] and zeolites [19–21], can be used for an extensive range of applications [22], albeit, activated carbon (AC) remains a most prominent material for environmental contaminants removal due to its high sorption efficiency. This includes the effective sorption of different pesticides as summarized in Table 1.

Table 1. Sorption efficiency of pesticides from activated carbon (AC).

Pesticide	AC Source	q_m [(a)] (mg g^{-1})	*RE* [(b)] (%)	Ref.
Acetamiprid, Atrazine, Azoxystrobin, Chlorantraniliprole, Difeconazole, Diuron, Imazalil, Pymetrozine, Pyraclostrobin, Thiacloprid, Trifloxyztrobin	Starch	66.2 (Pyraclostrobin)	>80	[23]
2,4-dichlorophenoxyacetic acid	*Lagenaria vulgaris*	333.3	100	[24]
2,4-dichlorophenoxyacetic acid	Date stone	238.1	91.8	[25]
4-chloro-2-methylphenoxyacetic acid	Norit 0.8, Aquacarb 207C, Aquacarb 208C, Aquacarb 208EA	133.6, 117.6, 106.2, 105.3	n/a	[26]
Acetamiprid	Tangerine peels	35.7	92	[27]
Alachlor	*Juglans regia*	n/a	≥72	[28]
Ametryn, Aldicarb, Dinoseb, Diuron	Carbon-cloth	354.6, 421.6, 301.8, 213.1	n/a	[29]
Atrazine	Mangosteen peels	51	n/a	[30]
Atrazine, deethylatrazine, deisopropylatrazine, simazine	Rayon	238.1, 303, 119, 370.4	n/a	[31]
Bentazon	CAT, Carbopal	718	n/a	[32]
Bentazon	Sky fruit husk	166.7	≥70	[33]
Benzimidazole	*Arachis hypogaea*	n/a	70	[34]
Carbofuran	Banana stalks	64	97	[35]
Diazinon	NH_4Cl-AC	250	97.5	[36]
Endosulfan	*Saccharum officinarum*	2.3	≥93	[37]
Ethaboxam	*Juglans regia*	n/a	≥89	[38]
Furadan, Metribuzin, 2,4-dichlorophenoxyacetic acid	Bamboo	869, 756.5, 274.7	92.3, 93, 96.7	[39]
Imidacloprid	Peach stone	39.4	≥80	[40]
Imidacloprid	*Ricinodendron heudelotii*	43.5	90	[41]
Hinosan	Rice husk	81.4	≥65	[42]
Methoxychlor, atrazine, methyl parathion	Rubber tire	112, 104.9, 88.9	91, 82, 71	[43]

[(a)] q_m maximum sorption capacity per unit weight of the adsorbent; [(b)] *RE* is the removal efficiency; n/a: not available.

Despite that, two major AC drawbacks can be pointed out: the high production cost and the low regeneration capacity [44]. Low-cost materials are vital as AC alternatives and a wide range of sorbents have gained increasing attention. Amidst them, hydrogels—materials formed by 3D hydrophilic polymer network capable of sorption large amounts of water—have been applied to environmental remediation processes [45,46]. Among these polymers, natural polysaccharides such as starch, chitosan and pectin have been increasingly used as adsorbents due to being biodegradable, inexpensive, non-toxic, abundant, and renewable [47,48]. The presence of reactive chemical groups such as amine, hydroxyl or carboxyl permit easy modification as well as notable selective interactions. For these reasons, polysaccharides and their derivatives are smart alternative sorbent materials with remarkable sorption efficiency and might as well be easily regenerated by desorption cycles. Cyclodextrins (CDs) are cyclic oligosaccharides with outstanding properties, including the

ability to form host-guest supramolecular complexes [49–51]. Consequently, the use of CDs arises as a natural choice for preparing sorbent materials [52–54] as they can be used as monomers for hydrogel formation [55–57] and, simultaneously, provide a significant number of active sites for interaction with less water soluble pollutants as, e.g., pesticides [58]. The synthesis of CD-based hydrogels relies on a covalent binding of a CD to a solid matrix or a direct linkage of CDs by using a crosslinker (epichlorohydrin and diisocyanates are commonly used [59–61]).

Additionally, we also want to address the question: is it feasible preparing sorbent material with the capability to provide for active substances to the soil, when it is needed, without further maintenance? For such purpose, the sorbent material should be able to show high sorption-desorption cyclic performance.

In this paper, we describe the synthesis and characterization of poly(β-cyclodextrin)s (PCD) and activated carbon composites, at different weight ratios. The PCD hydrogels were initially prepared by copolymerization of β-CD with hexamethylene diisocyanate (1,6-HDI), acting as crosslinker, through a carbamate forming reaction. The activated carbon has been used due to its high sorption performance for a vast type of pollutants, whilst the PCD was chosen due to its low swelling degree, allowing for a long-term encapsulation of the AC and concomitantly keeping high permeation rates. The obtained hydrogel composites were assessed towards the removal of two active agrochemical substances: cymoxanil (CYM) and imidacloprid (IMD), a fungicide of the cyanoacetamide oximes class and an insecticide of the neonicotinoid class, respectively (Scheme 1). The evaluation was made on the basis of a thorough study on sorption kinetics and isotherms as well as on the structural characterization of composites before and after sorption. Besides, the effect of different additives (NaCl and urea) and sorption/desorption cycles on the gel performance was also evaluated.

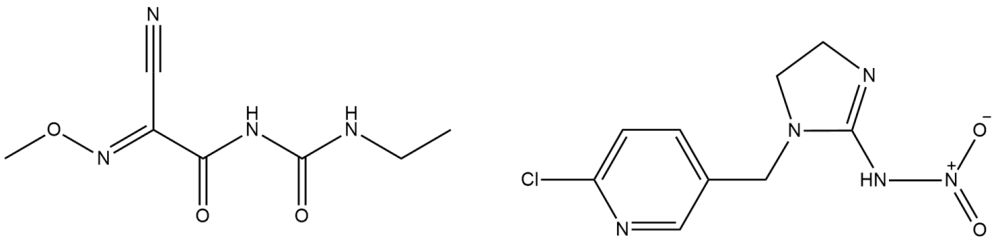

Scheme 1. Molecular structures of cymoxanil (**left**) and imidacloprid (**right**).

2. Results and Discussion

2.1. Poly(β-cyclodextrin) Synthesis and Characterization

Crosslinked PCD was prepared by reaction of the primary hydroxyl groups of β-CD with the isocyanate groups of 1,6-HDI (Figure 1a), forming a urethane linkage. The reaction is catalyzed by BTL, which acts as Lewis acid by coordination of the Sn with the nitrogen atom of the isocyanate and, thus, facilitates the attack of the oxygen of the hydroxyl group to the carbonyl of the isocyanate.

In the PCD/AC composites, the AC is retained by the PCD crosslinked matrix (Figure 1b,c).

A thermogravimetric characterization has been performed to assess the effect of AC addition at 5% and 10% (*w*/*w*) on the thermal stability of poly(*β*-CD). The TGA and dTG curves of adsorbent materials are shown in Figure 2a,b. All adsorbents showed an initial loss of mass up to ca. 12% with a maximum temperature around 100 °C, associated with solvent evaporation. PCD showed a typical second degradation step between 250 °C and 350 °C with a maximum degradation rate at 277 °C and weight loss of ca. 50%; such thermal event can be assigned to the *β*-CD degradation [62,63]. All poly(β-CD)-based materials revealed a further thermal degradation at around 452 °C. That can be justified by the cleavage of the ester bond between *β*-CD and 1,6-HDI [64]. It should be stressed that the latter can also be indicative of a successful synthesis of PCD. Taking into account just these two thermal changes, it can also be noticed that the corresponding maximum degradation

temperatures, for PCD/$AC_{10\%}$, show a slightly decrease; i.e., they occur at 262 °C and 449 °C, suggesting that the incorporation of a higher content of AC has a negligible effect on the stability of the poly(β-cyclodextrin). We can hypothesize that an increase in the AC content might decrease the intermolecular H-bonds interactions between CDs affecting its thermal stability. An interesting process is also observed as an additional thermal transition for PCD/$AC_{5\%}$ and PCD/$AC_{10\%}$ at 322 °C and 327 °C. These transitions seem to indicate that the incorporation of AC does not affect equally the polymeric structure; i.e., the hypothetical (microscopically) heterogeneous density of AC might induce polymeric zones of higher and lower stability. This is supported by the weight loss percentage for these two regions being similar to that observed just for PCD. Finally, the decrease in the mass loss shown in the TG of AC can be assigned to devolatilization [65].

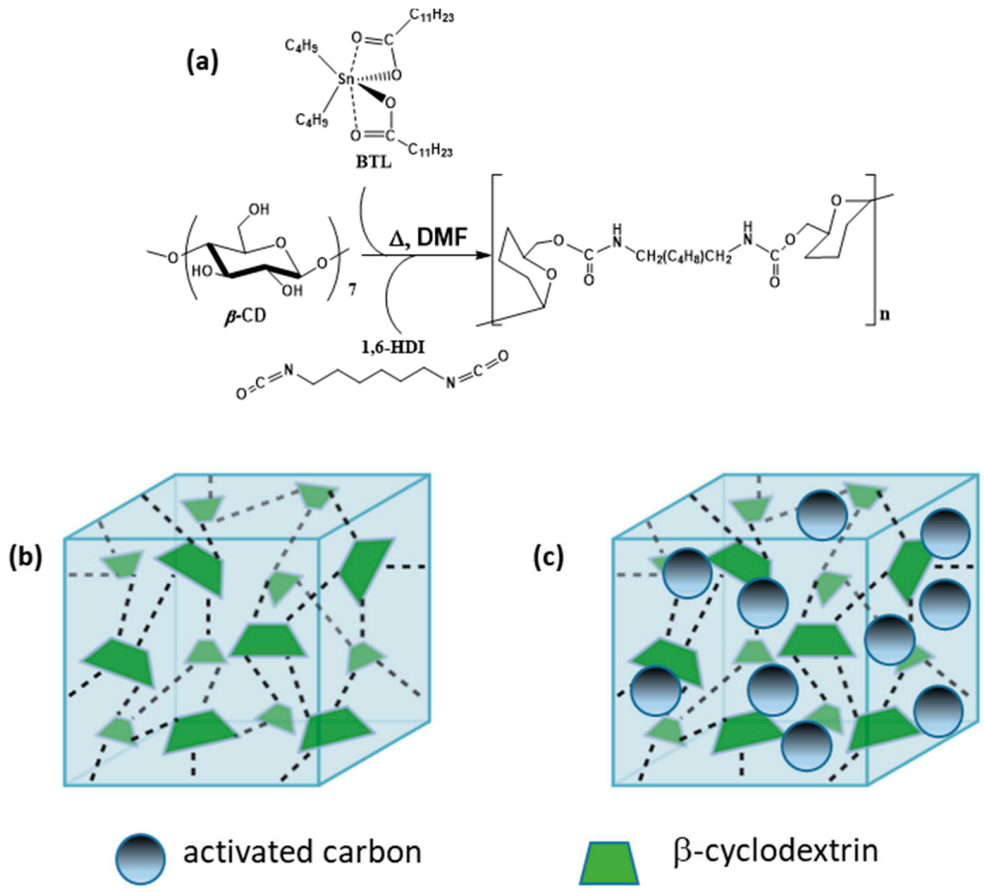

Figure 1. Representation of (**a**) synthesis route of poly(β-cyclodextrin) (PCD), (**b**) schematic structure of PCD and (**c**) schematic representation of PCD/AC matrix. Cyclodextrin (CD) and activated carbon (AC) structures are not at the same scale.

The synthesis of PCD and its composites was also analyzed by FT-IR. The corresponding spectra are shown in Figure 2c. Considering the FTIR spectrum of the PCD it is possible to observe a broad band around 3400 cm^{-1} due to the asymmetrical and symmetrical stretching vibration of the -OH groups. The two bands at 2935 cm^{-1} and 2862 cm^{-1} are associated to the methylene groups stretching vibrations of the 1,6-HDI crosslinker. The absence of a peak at 2270 cm^{-1}, corresponding to the isocyanate group, indicates a complete polymerization reaction [64]. A characteristic band appears at 1710 cm^{-1}, which is due to the stretching vibration of the carbonyl group of the ester bond between the -OH at C-6 position of the *β*-CD and the terminal carbonyl of the isocyanate group of 1,6-HDI. The presence of the amide groups is also confirmed by the band at 1547 cm^{-1} relative to the bending vibration of the -NH group in secondary amide. The band at 1265 cm^{-1} results from the overlapping of bands due to the interaction of the -NH bending vibration and

-CN stretching vibration of the amide groups. The band at 850 cm^{-1} is characteristic of the α - 1 $\rightarrow$ 4 glycosidic bond [66]. Finally, the weak bands between 800 and 600 cm^{-1} can be assigned to the -NH wagging vibrations of the secondary amide groups [67].

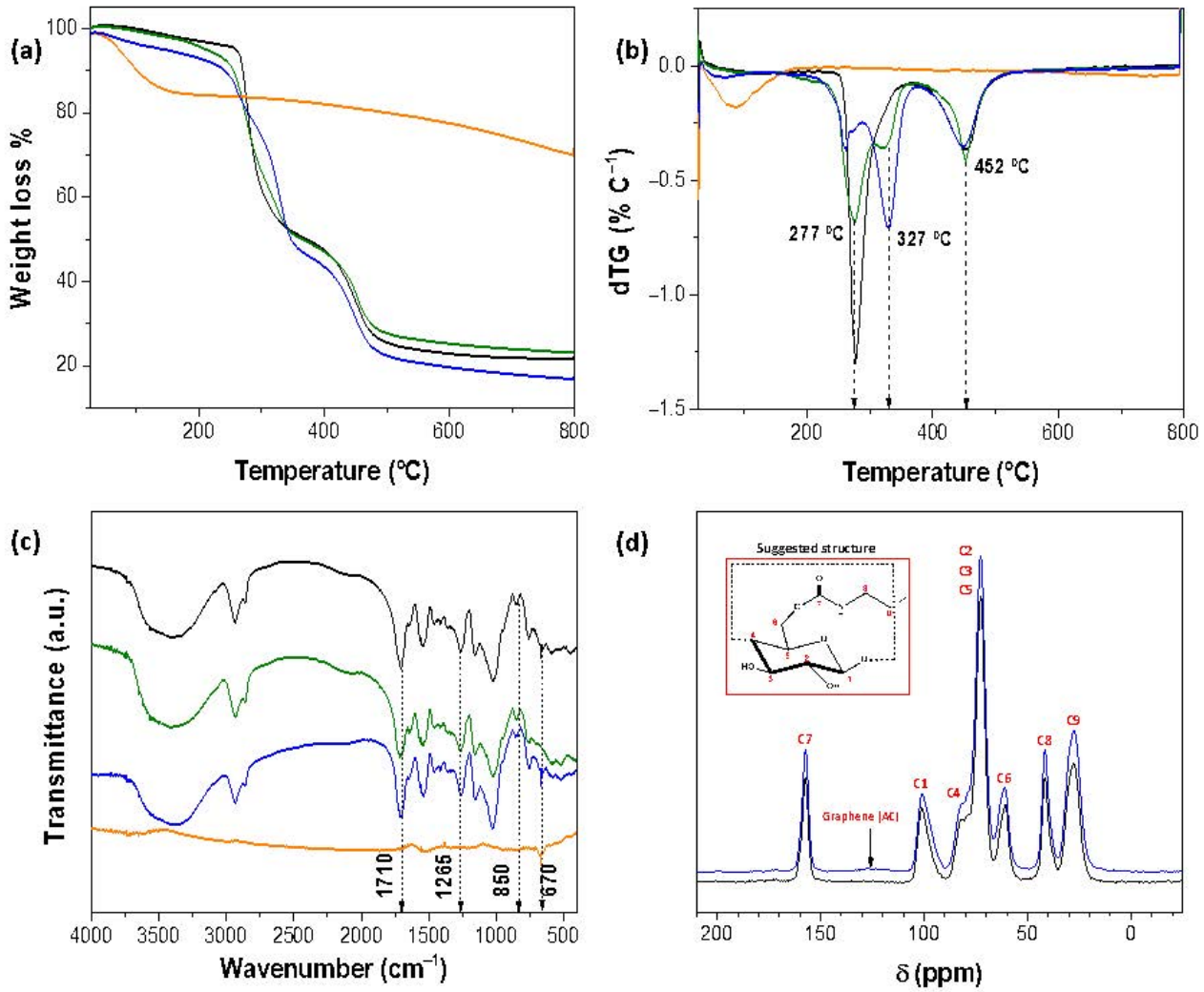

Figure 2. Thermograms (**a**) and corresponding dTGs (**b**) for PCD (black line), PCD/$AC_{5\%}$ (green line), PCD/$AC_{10\%}$ (blue line) and AC (orange line). FTIR and ^{13}C CPMAS solid state NMR spectra are shown in (**c**,**d**), respectively.

Comparing the spectra of neat-PCD and its composites with activated carbon at 5% and 10%, it is not possible to observe any characteristic bands that can confirm or reveal the presence of the activated carbon, probably due to the weak adsorption bands of the AC. However, in a more detailed analysis, it is possible to observe two weak peaks at the high frequency region around 3700–3600 cm^{-1}, indicating the presence of hydroxyl groups. The bands between 1500 and 1000 cm^{-1} can be assigned to C-O stretching and -OH bending vibrations. The bands in the region 950–800 cm^{-1} are probably associated to the C-H vibration [68]. However, from the ^{13}C CPMAS solid-state NMR spectra (Figure 2d), which compares the spectrum of PCD with that of PCD/$AC_{10\%}$, it is observed a broad and low carbon resonance, around 125.5 ppm, associated with aromatic structures of AC moiety [69]. The other resonances can be assigned to four carbon resonances of the glucopiranose unit: C1 (101.1 ppm), C4 (82.1 ppm), C2/C3/C5 (72.7 ppm) and C6 (60.7 ppm) [70]. Moreover, it can be noticed at low field a carbon resonance C7 (157.3 ppm) associated to the carbonyl in the carbamate (urethane) group while at high field two carbon resonances—C8 (41.6 ppm)

and C9 (27.7ppm)—related to the carbon of the methylene groups in the aliphatic chain of 1,6-HDI, can be observed.

The swelling behavior of different gels were also evaluated by the analysis of the water uptake capacity (Table 2). It can be seen that the swelling degree for the PCD is not high, in line with a semi-rigid (not soft) gel when handled, and the encapsulation of AC leads to a decrease in the *SW*. This might be related with the structural effect produced by the AC into CD structure as seen by the thermogravimetric and BET analysis. Concerning the latter, it can be observed that the incorporation of AC into pBC increases by 3 times the surface area of the composite. This increase is accompanied by a continuously decrease in the average pore diameter with an increase in the AC percentage.

Table 2. Swelling degree and structural properties of the adsorbent materials.

Adsorbents	*SW*%	S_{BET}/(m^2 g^{-1})	D_{pore} [(a)]/nm
PCD	55 ± 10	11.3 ± 0.2	17.7
PCD/AC$_{5\%}$	50 ± 4	36.1 ± 0.7	10.8
PCD/AC$_{10\%}$	33 ± 3	33.3 ± 0.9	7.91
AC		1272 ± 38	2.05

[(a)] Average pore diameter (D_{pore}) was determined by $4V_P/S_{BET}$.

2.2. Sorption Kinetics

The adsorption kinetic analysis provides valuable information about the adsorption efficiency of an adsorbent material and a better understanding of the adsorption mechanism. It should be stressed that these experiments were carried out at two initial pesticide concentrations 200 ppm and 500 ppm.

Figure 3 shows representative sorption kinetic data for IMD and CYM onto PCD/AC$_{10\%}$. In general, the maximum sorption capacity is attained (taking a cumulative sorption capacity of 80%) after ca. 10 and 20 h. Such slow sorption rate might be related to the relatively low swelling degree of these gels. In fact, independently of the model [71], there is an inverse relationship between the diffusion coefficient (or rate constant) and the polymer volume fraction and thus with the swelling degree; i.e., the fractional drag action on adsorbate movement inside the gels increase by decreasing the swelling degree, and consequently, their kinetic rate constant [72]. It is also worth noticing that the time needed to reach the sorption equilibrium is also high and similar in magnitude to that found for PCD-based hydrogels.

Additionally, the kinetic data were evaluated by the PFO and PSO (Equations (7) and (8)); the fitting parameters for all sorption systems are summarized in Tables 3 and 4 and are represented by solid and dashed lines in Figure 3. Generally, the determination coefficients (R^2) values are higher than 0.95, indicating a good fit. However, once the R^2 values are similar for the fitting of both equations to the experimental data, the AIC are used to conclude on the best fitting. It can be concluded that for all systems the sorption kinetic follows a pseudo-second order mechanism. It is worth noticing that the q_e values obtained by Equation (8), representing the amount of pesticide sorbed at equilibrium time, denote that the constancy of q_e value is not completely reached after 4 days. Hence, a chemisorption nature is suggested which can be justified by the occurrence of hydrogen bonds or inclusion complexes formation. That hypothesis can also explain the higher adsorbed amount of pesticide at higher concentration and larger contact time as observed in the experimental design and kinetic and equilibrium analysis. Another issue that deserves a comment is the effect of the initial concentration on the k_2 rate constants: by increasing the initial concentration from 200 ppm to 500 ppm, k_2 values decrease significantly. This indicates that other phenomena than sorbent-sorbate interaction occur; an example of that might be an increase of sorbate-sorbate interactions upon concentration increase [46]. Both these findings are in agreement with the sorption isotherms as will be discussed in the next section.

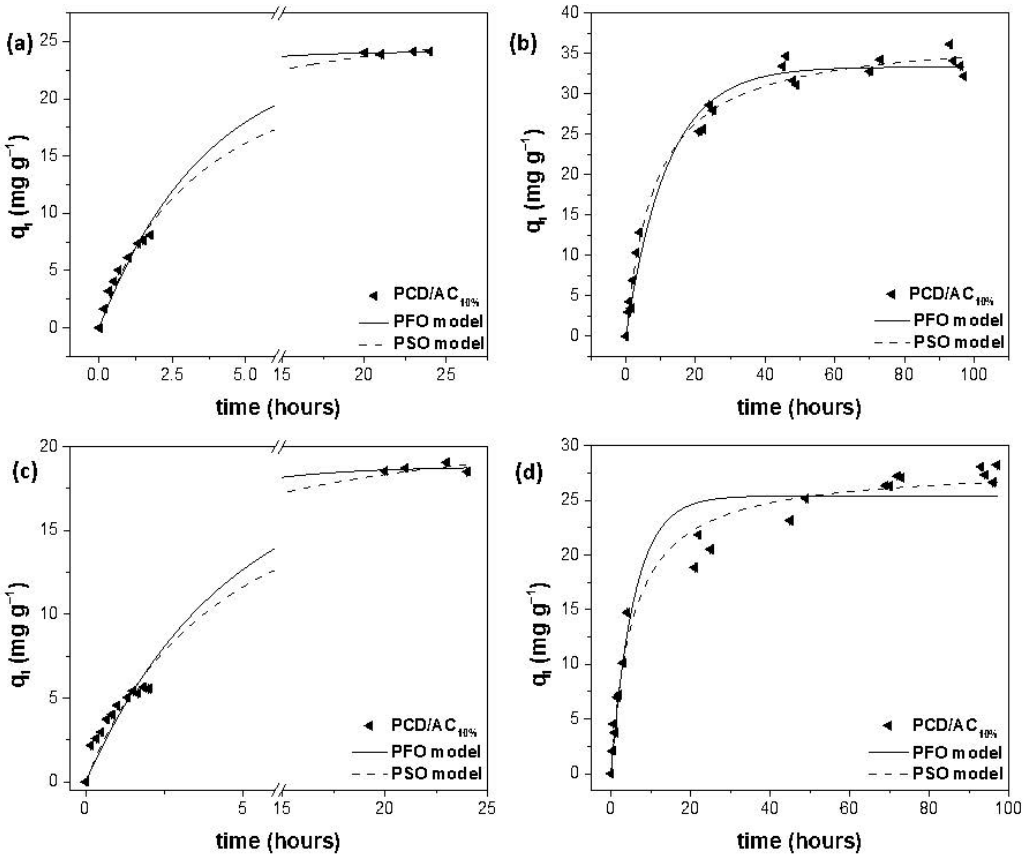

Figure 3. Sorption kinetic of imidacloprid (IMD) solution at 200 ppm (**a**) and 500 ppm (**b**); and cymoxanil (CYM) solution at 200 ppm (**c**) and 500 ppm (**d**) onto PCD/AC$_{10\%}$. Solid and dashed lines represent the fitting of Equations (7) and (8), respectively, to the experimental data, at 25 °C. The fitting parameters are shown in Tables 3 and 4.

Table 3. Fitting parameters for the fitting of pseudo-first order (up) and pseudo-second order (down) kinetic equations for the sorption of imidacloprid, at 25 °C and 200 or 500 ppm.

C_i = 200 ppm	**PCD**	**PCD/AC$_{5\%}$**	**PCD/AC$_{10\%}$**	**AC**
$q_{e,exp}$ (mg g^{-1})	10.3 (±0.6)	14.6 (±0.5)	24.1 (±0.3)	37.4 (±0.6)
q_e (mg g^{-1})	10.4 (±0.2)	15.0 (±0.2)	24.1 (±0.4)	37.2 (±0.9)
k_1 (10^{-2} min^{-1})	75 (±4)	18.4 (±0.7)	27.4 (±0.2)	67 (±5)
R^2	0.9869	0.9984	0.9953	0.9758
AIC	−20.6	−31.5	−6.2	23.0
q_e (mg g^{-1})	11.0 (±0.1)	19.0 (±0.3)	28.1 (±0.4)	39.2 (±0.5)
k_2 (10^{-2} g mg^{-1} min^{-1})	9.7 (±0.5)	0.83 (±0.01)	0.96 (±0.07)	2.4 (±0.1)
R^2	0.9953	0.9983	0.9970	0.9951
AIC	−33.0	−28.7	−9.8	2.6
C_i = 500 ppm	**PCD**	**PCD/AC$_{5\%}$**	**PCD/AC$_{10\%}$**	**AC**
$q_{e,exp}$ (mg g^{-1})	23 (±3)	31 (±3)	32 (±2)	223.9 (±0.3)
q_e (mg g^{-1})	24.3 (±0.4)	31.1 (±0.5)	33.3 (±0.6)	219 (±2)
k_1 (10^{-2} min^{-1})	7.1 (±0.7)	6.5 (±0.5)	8.4 (±0.8)	5.7 (±0.2)
R^2	0.9834	0.9890	0.9821	0.9975
AIC	15.0	15.6	27.9	75.7
q_e (mg g^{-1})	27.8 (±0.7)	36.0 (±0.7)	37.6 (±0.7)	258(±1)
k_2 (10^{-2} g mg^{-1} min^{-1})	0.33 (±0.05)	0.23 (±0.02)	0.31 (±0.03)	0.030 (±0.001)
R^2	0.9844	0.9931	0.9898	0.9996
AIC	15.9	7.6	18.2	32.21

Table 4. Fitting parameters for the fitting of pseudo-first order (up) and pseudo-second order (down) kinetic equations for the sorption of cymoxanil, at 25 °C and 200 and 500 ppm.

C_i = 200 ppm	**PCD**	**PCD/AC$_{5\%}$**	**PCD/AC$_{10\%}$**	**AC**
$q_{e,exp}$ (mg g^{-1})		10 (±2)	18.7 (±0.1)	35.2 (±0.1)
q_e (mg g^{-1})	n/a	10.2 (±0.3)	18.8 (±0.4)	35.6 (±0.2)
k_1 (10^{-2} min^{-1})	n/a	12 (±1)	22 (±2)	21.5 (±0.5)
R^2	n/a	0.9938	0.9858	0.9990
AIC	n/a	−32.9	−1.9	−21.4
q_e (mg g^{-1})	n/a	14.2 (±0.7)	22.7 (±0.7)	43.6 (±0.6)
k_2 (10^{-2} g mg^{-1} min^{-1})	n/a	0.6 (±0.1)	0.9 (±0.1)	0.44 (±0.02)
R^2	n/a	0.9930	0.9883	0.9980
AIC	n/a	−29.0	−3.0	−9.1
C_i = 500 ppm	**PCD**	**PCD/AC$_{5\%}$**	**PCD/AC$_{10\%}$**	**AC**
$q_{e,exp}$ (mg g^{-1})	11 (±4)	18 (±4)	27 (±4)	259 (±1)
q_e (mg g^{-1})	10.4 (±0.8)	19.2 (±0.8)	25.4 (±0.7)	253 (±6)
k_1 (10^{-2} min^{-1})	5 (±1)	3.8 (±0.5)	17 (±3)	11 (±2)
R^2	0.9171	0.9651	0.9478	0.9608
AIC	7.6	14.8	40.1	145.5
q_e (mg g^{-1})	11 (±1)	23 (±1)	28.1 (±0.6)	277 (±1)
k_2 (10^{-2} g mg^{-1} min^{-1})	0.7 (±0.3)	0.18 (±0.04)	0.65 (±0.09)	0.081(±0.002)
R^2	0.9384	0.9714	0.9794	0.9992
AIC	5.8	13.0	22.6	54.0

2.3. Sorption Isotherms

Sorption isotherms for IMD and CYM onto gel composites and activated carbon have been measured and are shown in Figures 4 and 5, respectively. It can be seen that the sorption mechanism changes with the sorbent. In fact, for PCD the sorption isotherms are almost linear, following a quasi-Henry model, suggesting a diffusion of pesticides into the gel water free volume or a weak interaction between the pesticides and the cyclodextrins. By increasing the incorporation of AC into PCD the dependence of the q_e as function of C_e becomes more concave and the sorption becomes clearly favorable. For the activated carbon, the sorption follows an s-shape isotherm, with significantly low C_e values, suggesting an initial highly favorable sorption towards AC. Such behavior is independent on the IMD or CYM. A deeper analysis has been done by fitting the Freundlich and Sips equations to the experimental data (see fitting lines in Figures 4 and 5); the corresponding fitting parameters are gathered in Tables 5 and 6. In general, the Sips model fits better the experimental sorption data, considering the determination coefficient and the AIC data. From the analysis of the fitting parameters reported in Tables 5 and 6, it can be noticed that the maximum sorption capacity increases by increasing the amount of AC into the gel matrix. It can also be observed a similar stability constant, for IMD and CYM, registered for PCD and PCD/AC$_{5\%}$; however, for the PCD/AC$_{10\%}$ and AC the interaction between IMD and the adsorbents is significantly higher. This might be justified by the occurrence in higher extent of London dispersion forces between the activated carbon and the more hydrophobic pesticide, IMD.

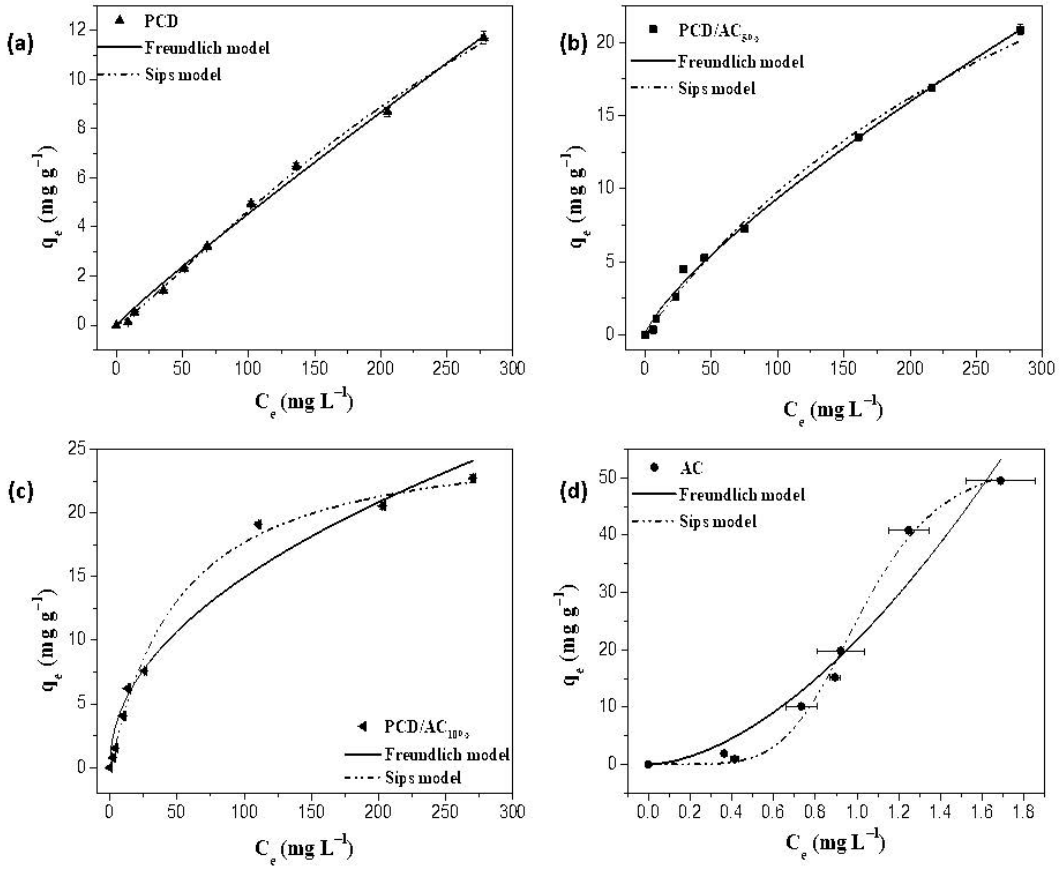

Figure 4. Sorption isotherms of IMD onto: (**a**) PCD, (**b**) PCD/$AC_{5\%}$, (**c**) PCD/$AC_{10\%}$ and (**d**) AC, at 25 °C.

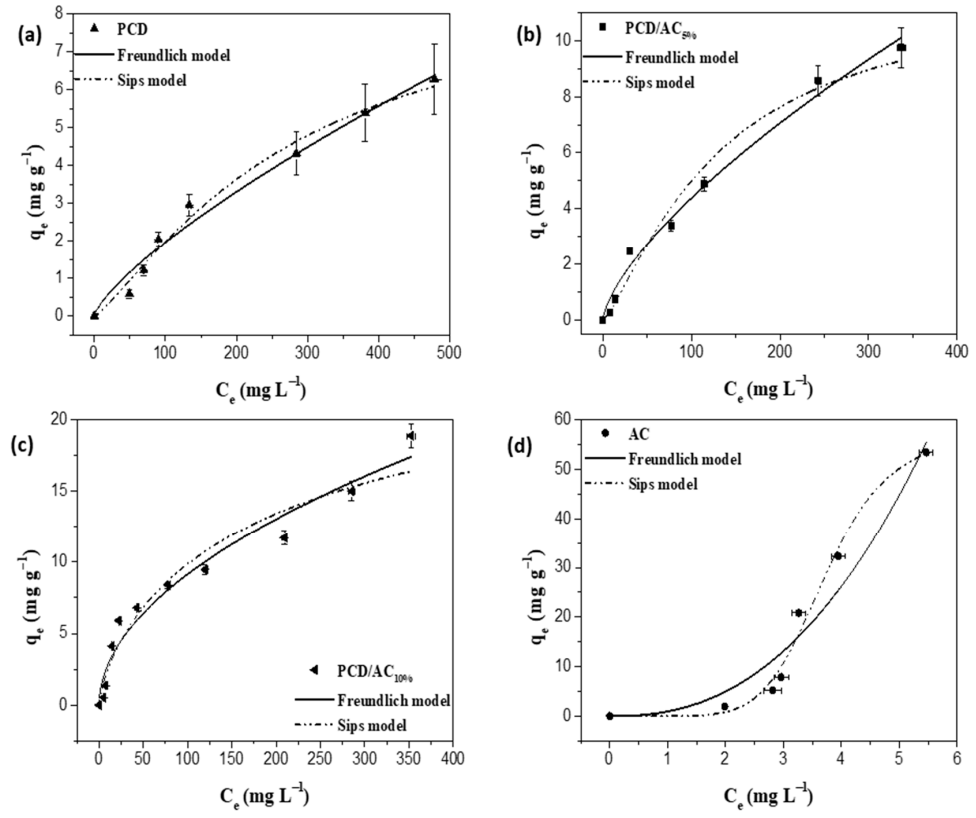

Figure 5. Sorption isotherms of CYM onto: (**a**) PCD, (**b**) PCD/$AC_{5\%}$, (**c**) PCD/$AC_{10\%}$ and (**d**) AC, at 25 °C.

Table 5. Sorption fitting parameters for imidacloprid (see Figure 4).

Model		PCD	PCD/AC$_{5\%}$	PCD/AC$_{10\%}$	AC
Freundlich	K_F (mg g^{-1} mg^{-n} L^n)	0.06 (±0.01)	0.27 (±0.04)	1.6 (±0.5)	21 (±2)
	1/n	0.93 (±0.03)	0.77 (±0.03)	0.48 (±0.05)	1.7 (±0.3)
	R^2	0.9953	0.9958	0.9651	0.9375
	AIC	−18.6	−8.6	13.2	26.6
Sips	q_m (L mg^{-1})	31 (±9)	48 (±22)	26 (±2)	54 (±3)
	K_S (10^{-2} L mg^{-1})	0.2 (±0.1)	0.2 (±0.2)	2.0 (±0.5)	97 (±4)
	1/n	1.20 (±0.1)	1.0 (±0.1)	1.0 (±0.1)	5.2 (±0.8)
	R^2	0.9979	0.9944	0.9945	0.9935
	AIC	−27.4	−5.0	−0.2	13.6

Table 6. Sorption fitting parameters for cymoxanil (see Figure 5).

Model		PCD	PCD/AC5%	PCD/AC10%	AC
Freundlich	K_F (mg g^{-1} mg$^{-1/n}$ L$^{1/n}$)	0.06 (±0.02)	0.18 (±0.05)	0.9 (±0.2)	0.9 (±0.6)
	1/n	0.75 (±0.07)	0.70 (±0.05)	0.51 (±0.05)	2.4 (±0.4)
	R^2	0.9736	0.986	0.9576	0.9265
	AIC	−9.8	−6.6	8.5	25.1
Sips	q_m (L mg^{-1})	9 (±3)	12 (±3)	28 (±18)	57 (±5)
	K_S (10^{-2} L mg^{-1})	0.4 (±0.2)	0.8 (±0.4)	0.4 (±0.7)	27 (±1)
	1/n	1.3 (±0.3)	1.3 (±0.4)	0.7 (±0.3)	8 (±1)
	R^2	0.9871	0.9804	0.9527	0.9865
	AIC	−14.6	−3.4	13.0	17.9

The interaction between IMD and CYM and the four different adsorbents was complementary evaluated by scanning electron microscopy (Figure 6).

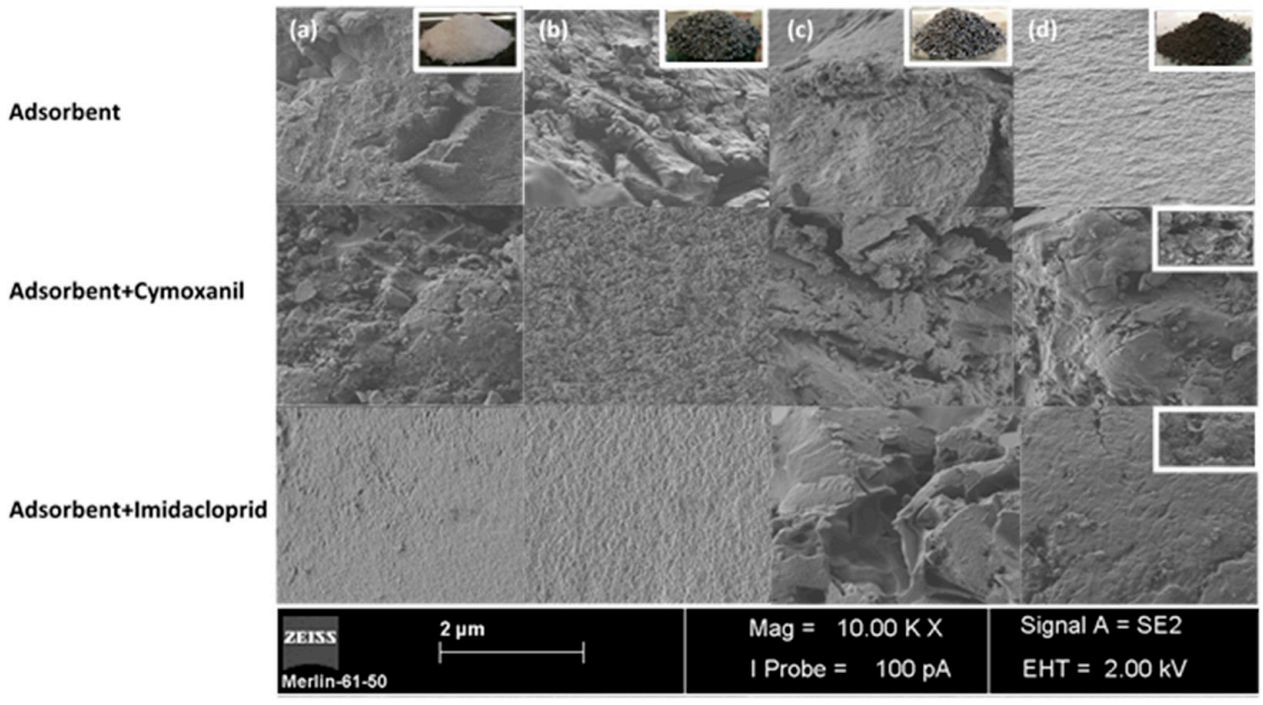

Figure 6. SEM micrographs of sorbent materials before (top row) and after 24 h in contact with aqueous solutions of cymoxanil (middle row) and imidacloprid (bottom row), respectively (magnification ×10,000). (**a**) PCD); (**b**) PCD/AC$_{5\%}$; (**c**) PCD/AC$_{10\%}$ and (**d**) AC. Inset figures are photos of the adsorbents.

The micrographs show an irregular and amorphous surface for PCD and PCD/$AC_{5\%}$ (Figure 6a,b—top row) and become smoother by increasing the amount of AC. After 24h in contact with the aqueous solution of CYM and IMD, respectively, significant morphological alterations have been observed. Thus, the surface morphology of PCD becomes significantly more featureless in the presence of IMD and a similar behavior occurs for PCD/$AC_{5\%}$, showing that for this gel composite, the cyclodextrin effect is predominant. On the other hand, an opposite effect is observed for PCD/$AC_{10\%}$ and AC; i.e., the sorption of CYM by PCD/$AC_{10\%}$ (c)-middle row) leads to a highly jagged surface, which is enhanced in the presence of IMD. In the case of AC the effect of both pesticides on the adsorbent surface morphology do not follow the same trend, although they are different when compared with the pristine adsorbent. The former evidence is in close agreement with the fact that IMD interacts more strongly with the gel than the CYM thus producing a more significant surface modification; the latter might be related with the high performance of the activated carbon for the sorption of both pesticides reaching a removal efficiency higher than 98% (Figure 7) and a maximum amount of sorbed CYM and IMD of 53.4(±0.7) and 49.5(±0.3) mg g^{-1} (Figure S2) respectively. The analysis of Figure 7 and Figure S2 deserves further comments. The performance of PCD is the poorest of all adsorbents (tested with *RE* lower than 35% and 20% for IMD and CYM, respectively), in agreement with the higher affinity of the aromatic towards the hydrophobic cavity of the CD. However, for the composite gel adsorbents, the removal efficiency increases by increasing the amount of encapsulated AC and, as a general trend, decreases by increasing the initial concentration of pesticide. Such a behavior might be linked to the tendency of pesticides to form dimers [73], which might hamper the sorption process—as previously discussed. It should be noticed, however, that there is an increase in the q_e values with an increase in the initial concentration of pesticides (Figure S2). The maximum removal efficiencies of CYM by PCD/$AC_{5\%}$ and PCD/$AC_{10\%}$ are 45(±2) and 73(±2)%, respectively, whilst for IMD are 55.9(±0.6) and 80.9(±0.7)%, respectively. Such behavior is remarkable for two different reasons: the removal efficiency is higher for the lowest initial concentration (i.e., 50 ppm) and the use of lower amounts of AC leads to a significant level of removal. Looking at the q_e values, an increase in the amount of AC from 5% to 10% doubles and triples the q_e values for CYM, compared to PCD; again, the AC is playing a main role on the sorption efficiency.

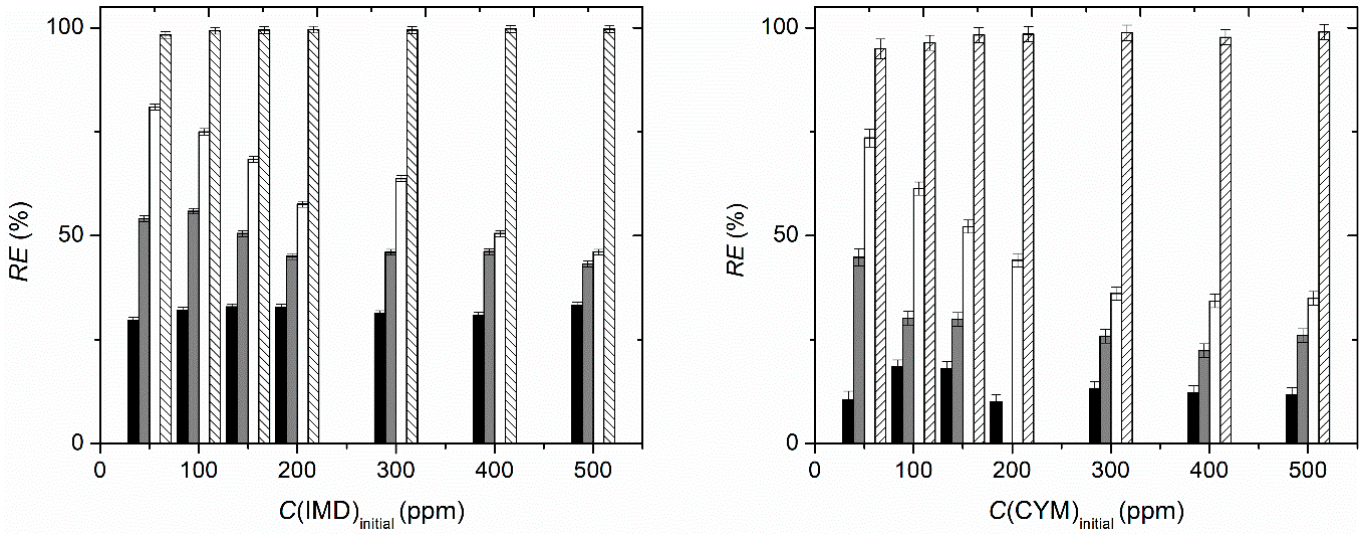

Figure 7. Removal efficiency (*RE*%) of IMD (**left**) and CYM (**right**) by different adsorbents: PCD (black columns), PCD/$AC_{5\%}$ (grey), PCD/$AC_{10\%}$ (white) and AC (lines).

For the sake of comparison, the values of *RE* and q_m reported in the Table 1 for the removal of IMD by using AC [40,41] are lower than those obtained by us, and are similar to those corresponding to the use of PCD/$AC_{5\%}$ and PCD/$AC_{10\%}$.

2.4. Effect of Additives on the Pesticide Sorption Isotherms

Saline soils are composed of several types of dissolved salts but NaCl is the most prevalent one, which is why the effect of salinity on the sorption of pesticides is of great importance [74]. Furthermore, urea is a nutrient often used in cropping together with different types of pesticides and has proved to be suitable as a carrier for some of the herbicides [75]. Hence, the influence of additives like NaCl and urea has been assessed in the attempt to evaluate the sorption efficiency of composite materials in simulated environments. The effect of ionic strength and additives on the sorption isotherms of CYM and IMD have been evaluated by using NaCl (1 g L^{-1}) and urea (1 g L^{-1}) as model molecules and data are shown in Figures S3 and S4, respectively. Generally, it can be observed an analogous behavior of the adsorbent materials for IMD in presence of urea and NaCl, with favorable and cooperative adsorption process as it is suggested from the value of n and K_s parameters (Tables S4 and S5).

However, there are some issues that deserve further discussion. The amount of sorbed cymoxanil and the corresponding removal efficiencies for cymoxanil onto PCD and PCD/$AC_{5\%}$, in the presence of NaCl, are higher than in its absence. Namely, the *RE* is twice higher than in the NaCl absence. The structure of cymoxanil shows a significant number of amine groups able to interact with primary and secondary hydroxyl groups of β-CD by H-bonding. Simultaneously, it is known that intermolecular CD interactions might occur strongly [76]. Once this effect is more significant for the gels with lower amount of AC, we may hypothesize that the screening effect [77] caused by an increase in the ionic strength decreases the number of CD-CD interactions (in spite of its short-range nature) [78,79], leaving the CD available to interact with CYM. The sorption enhancement obtained for PCD/$AC_{5\%}$ might also be related to a more porous surface morphology. Even so, and although urea can be removed by activated carbon [80], it is worth noting that no modification of the pesticide *RE* is observed. In the case of IMD removal no significant changes are observed in the presence of either NaCl or urea.

2.5. Reusability Assessment

Three cycles of adsorption/desorption have been performed using ca. 0.1 g of each adsorbent in 10 mL of 500 ppm solution of IMD and CYM, respectively. The results are shown in Figure 8. In general, it can be noticed a slightly increase of the sorption capability along the three cycles of sorption/desorption for both pesticides. The average values of q_e and *RE*% for IMD sorption onto PCD, PCD/$AC_{5\%}$ and PCD/$AC_{10\%}$ agree with the experimental values obtained by equilibrium analysis. That behavior is more pronounced for CYM where it can be also observed a decrease of the desorption rate for the three adsorbent materials. The same result is achieved with PCD/$AC_{10\%}$ for IMD while PCD and PCD/$AC_{5\%}$ reach the equilibrium at the first cycle both in sorption and desorption steps. Hence, it can be suggested that the presence of sorbate molecules plays a prominent role promoting the sorption process via cooperative mechanism due to sorbate-sorbate interaction. The results also suggest that the sorption mechanism occurs via dual physi- and chemisorption.

In addition, AC does not show any ability to desorb either of these pesticides by diffusion (data not shown). Thus, we can conclude that the desorbed capacity of the composite gels is mainly due to the PCD. Besides this, it is interesting to observe from the data in Table S6 that the presence of AC on the composite significantly ruled the IMD release in contrast with CYM release probably determined by concentration gradient.

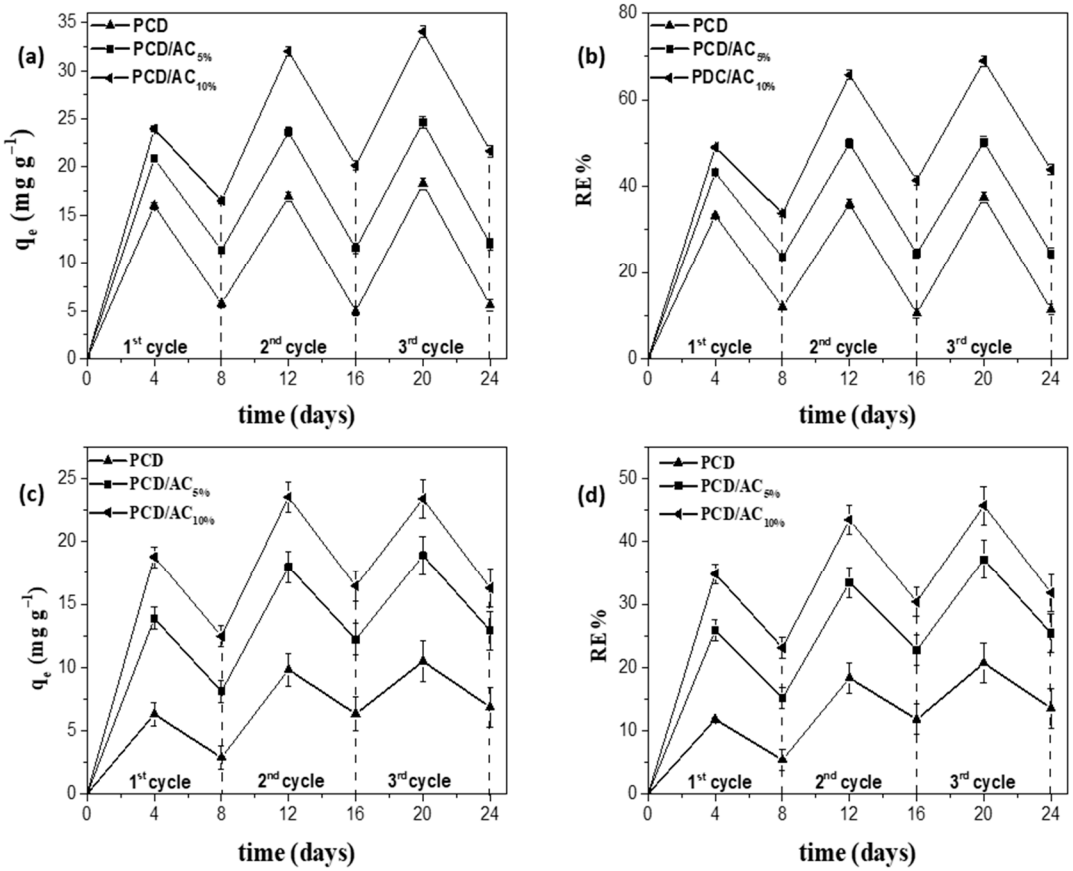

Figure 8. Graphical representation of q_e (**a**) and *RE*% (**b**) values for IMD and q_e (**c**) and *RE*% (**d**) values for CYM on three cycles of sorption/desorption.

3. Materials and Methods

3.1. Materials

β-cyclodextrin (*β*-CD) was purchased from ACROS-Organics (MW = 1134.98 g·mol^{-1}, 98%, CAS 7585–39–9). For the poly(*β*-cyclodextrin) synthesis, hexamethylene diisocyanate (MW = 168.19 g·mol^{-1}, purity $\geq$ 98%, CAS 822–06–0, 1,6-HDI) and dibutyltin dilaurate (MW = 631.56 g·mol^{-1}, 95%, CAS 77–58–7, BTL) were supplied by Sigma-Aldrich (Steinhem, Germany). The *N*,*N*-dimethylformamide (DMF) used in the syntheses was dried by treatment with CaO (previously activated at 500 °C) for 24 h, followed by decanting and stirring with NaOH (solid) for 1 h. After further decantation, the solvent is distilled and stored over 4 Å molecular sieves. Activated carbon (AC, granular, pure) was purchased from Riedel-de Haën (Seelze, Germany). Cymoxanil (MW = 198.18 g·mol^{-1}, 98.9%, CAS 57966–95–7, CYM) and imidacloprid (MW = 255.66 g mol^{-1}, 100%, CAS 138261–41–3, IMD) were supplied by Sigma-Aldrich (Steinhem, Germany).

The other chemicals were used without further purification process. All solutions were prepared with Millipore-Q water obtained with gradient water purification system *Direct*-Q® 3UV-R.

3.2. Synthesis of Poly(β-cyclodextrin) and Its Composites

Poly(*β*-cyclodextrin) was synthesized following a previous work reported in literature [81]. Briefly, 1.8 mmol of *β*-CD was solubilized in anhydrous DMF, under stirring and in a nitrogen atmosphere. After complete dissolution, one drop of BTL was added, as catalyst. Then, a DMF solution of 1,6-HDI (7.2 mmol) as crosslinker was added dropwise to the mixture and heated at 70 °C for 24 h. Likewise, two PCD composites (PCD/AC) were prepared by encapsulating 5% and 10% (*w*/*w*) of activated carbon. The size of AC

powder has been measured by sieving and the following size distribution was obtained: 300–212 μm: 49%; 212–180 μm: 7%; 180–75 μm: 3%; 75–38 μm: 17%; 38–25 μm: 13%; and <25 μm: 9%.

The obtained polymers were washed first with an excess of chloroform, under stirring for 12 h at room temperature, to remove the organic solvent and then, with ultrapure water, under stirring at room temperature, to remove the unreacted β-CD [81].

Finally, the solids were collected by filtration in filter paper and dried in an oven at 60 °C. Afterwards, a second drying step was performed at 160 °C by using a thermobalance (A&D MS-70, Tokyo, Japan) until reaching a mass variation $\leq$0.001% min^{-1}, ensuring a complete solvent removal. The xerogels of PCD and PCD/ACs appear as macroscopically homogeneous solids, white and dark grey, respectively. The adsorbents were used as powder. Obtained percentage yields (weight): PCD = 89.3%; PCD-$AC_{5\%}$ = 92.5%; PCD-$AC_{10\%}$ = 78.0%.

3.3. Physico–Chemical Characterization of Absorbent Materials

The chemical structure of neat-PCD, AC and their composites was evaluated by Fourier transform infrared spectroscopy (FT-IR) (Nicolet 6700 FT-IR, Thermo Scientific, Waltham, MA, USA) in a wavelength interval of 4000 and 400 cm^{-1} using KBr pellets as reference. Pellets were prepared at 1% (*w*/*w*) for PCD and PCD/$AC_{5\%}$ and at 0.5% (*w*/*w*) for PCD/$AC_{10\%}$ and AC with KBr.

The incorporation of AC into PCD was further assessed by solid-state nuclear magnetic resonance (NMR) using ^{13}C cross polarization magic angle spinning (CPMAS) technique.

The ^{13}C CPMAS solid state NMR spectra were obtained on a Bruker Avance HD-400 MHz NMR spectrometer operating at a ^{13}C resonance frequency of 106 MHz and using a commercial Bruker double-channel probe. To obtain a good signal-to-noise ratio in ^{13}C CPMAS experiment 20 K scans were accumulated using a delay of 2.5 s. The ^{13}C chemical shifts were referenced to tetramethylsilane and calibrated with glycine carbonyl signal, set at 176.5 ppm.

Thermogravimetric (TGA) and differential thermogravimetric (dTG) analysis of PCD, PCD/AC (5% and 10%) and AC in xerogel forms have been carried out by using TG209-F3 Tarsus (Netzsch Instruments, Selb, Germany). The analysis was performed in TiO_2 plates using approximately 4–5 mg of adsorbent, in the 25 to 800 °C temperature range, at a heating rate of 10 °C·min^{-1}, under nitrogen atmosphere with a flow rate of 50 mL·min^{-1}.

The surface morphology of the xerogel was characterized by scanning electron microscopy (SEM) (Gemini 2-Zeiss, Merlin-Zeiss, Oberkochen, Germany,) at 2.00 kV with magnification 10,000×. The samples were previously frozen using liquid nitrogen followed by freeze drying (Labconco, Kansas City, MO, USA, model Free-Zone 4.5) before being sputter-coated with a thin gold layer. PCD, PCD/$AC_{5\%}$, PCD/$AC_{10\%}$ and AC were analyzed before and after 24 h of contact with 200 mg L^{-1} IMD and CYM aqueous solutions, respectively, to determine the morphological effects.

The Brunauer Emmett Teller (BET) specific surface area was obtained through nitrogen adsorption (ASAP 2000, Micrometrics, Norcross, GA, USA).

The water uptake capacity was determined by swelling analysis, performed in triplicate, using ca. 50 mg of adsorbent at 25 °C. The swelling degree (*SW*) was calculated by Equation (1):

$$SW\% = \frac{(m_e - m_0)}{m_0} \times 100 \quad (1)$$

where m_0 and m_e (g) are the masses of the adsorbent as xerogel and swollen state at equilibrium, respectively.

3.4. Sorption Analysis

The optimal experimental conditions for the equilibrium and kinetic sorption analysis were assessed by performing a 2^3 factorial analysis. The effect of three parameters: volume (5 and 10 mL), amount of adsorbent (50 and 100 mg) and concentration of CYM (7.5 and

22.5 ppm) and IMD (5.0 and 15 ppm) was considered. The concentration values were decided taking the analytical range into account. The linearity of the analytical methods, the analytical range, limit of detection (LOD) and limit of quantification (LOQ) were statistically determined. The quantification of CYM and IMD concentrations were obtained by UV-Vis spectroscopy (Shimadzu UV-2450, Kyoto, Japan) between 200 nm and 500 nm, at the maximum wavelengths: 242 nm and 270 nm, respectively. The statistical parameters supporting the normal data distribution, absence of outliers as well as the linearity of the calibration data are reported in Tables S1 and S2, respectively. UV-Vis spectra and calibration curve are shown in Figure S1 while the analytical parameters of IMD and CYM are reported in Table S3.

Sorption analysis of CYM or IMD were performed in aqueous solutions at 25 °C and shaken at 120 rpm in an incubator LABWIT (ZWI-100H, Shangai, China) using a weighted mass of neat–PCD, PCD/$AC_{5\%}$, PCD/$AC_{10\%}$ and pristine AC. Nylon teabags (100-mesh nylon screen) were used to ensure a complete immersion of the adsorbents in the bulk phase. In the concentration range at which pesticide sorption was evaluated, control experiments were carried out showing that no measurable sorption of pesticides onto teabags has been detected. The efficiency of removal (*RE*%) of both active ingredients was calculated by using Equation (2),

$$RE\% = \frac{(C_0 - C_e)}{C_0} \times 100 \quad (2)$$

where, C_0 and C_e (mg L^{-1}) are initial and equilibrium concentration in the analytical samples, respectively. The amount of CYM or IMD adsorbed was computed by using Equation (3)

$$q_e = \frac{(C_0 - C_e)}{m} \times V \quad (3)$$

where, q_e (mg g^{-1}) is the amount of active ingredient adsorbed per gram of adsorbent at equilibrium state, V (L) is the volume of the analytical solutions and m (g) is the mass of the adsorbent. Sorption isotherms were performed by using a concentration range from 0 to 500 mg L^{-1} for CYM and IMD. Additionally, sorption isotherms in a pesticide aqueous solution, containing either NaCl or urea (both at 1.0 g L^{-1}) were also performed. A mass of adsorbate of ca. 0.1 g was used.

Based on the experimental data, and assuming a heterogeneous adsorbent, two isotherm models have been chosen: Freundlich [82] and Sips [83,84] (Equations (4) and (5)), respectively,

$$q_e = K_F C_e^{1/n} \quad (4)$$

$$q_e = \frac{q_m K_s C_e^{1/n_s}}{\left(1 + K_s C_e^{1/n_s}\right)} \quad (5)$$

where, K_F (mg g^{-1} $L^{1/n}$ $mol^{-1/n}$) and K_S ($L^{1/n}$ $mol^{-1/n}$) are the Freundlich and Sips constants, q_m (mg g^{-1}) is the maximum sorption capacity per unit weight of the adsorbent and $1/n$ and $1/n_S$ are heterogeneous related factors. Equation (5) predicts a monolayer sorption, characteristic of the Langmuir equation [85], to higher adsorbate concentrations or when n_S equals to 1. The goodness of the fitting was assessed by the determination coefficient (R^2) and the Akaike information criterion (*AIC*)—Equation (6) [86]:

$$AIC = Nln\frac{SS}{N} + 2k \quad (6)$$

where, N is the number of experimental points, SS is the sum of squared errors and k is related to the number of fitted parameters.

Sorption kinetic analysis were performed using ca. 0.1 g of PCD, PCD/$AC_{5\%}$, PCD/$AC_{10\%}$ and AC in 10 mL of IMD and CYM aqueous solutions at 200 ppm and 500 ppm. The

sorption kinetic mechanism was assessed by using the pseudo–first order (PFO) and pseudo–second order (PSO) kinetic models (Equations (7) and (8)), respectively.

$$q_t = q_e\left(1 - e^{-k_1 t}\right) \tag{7}$$

$$q_t = \frac{k_2 q_e^2 t}{1 + q_e k_2 t} \tag{8}$$

where, q_t (mg g^{-1}) is the amount of adsorbate at defined interval of times t (min). k_1 (min^{-1}) and k_2 (g mg^{-1} min^{-1}) are the rate constants for PFO and PSO, respectively.

Sorption kinetics and isotherms were performed in triplicate.

3.5. Reusability Assessment

The reusability of the adsorbent materials was evaluated by performing three sorption/desorption cycles, using experimental conditions similar to those used for sorption kinetics. Desorption capability (*DC*%) was computed by using Equation (9)

$$DC\% = \frac{C_{e_{des}}}{C_{e_{sor}}} \times 100 \tag{9}$$

where, Ce_{sor} and Ce_{des} (mg·L^{-1}) are the equilibrium concentrations of the sorbed and desorbed pesticide, respectively. The analysis was performed in triplicate.

4. Conclusions

Poly(β-cyclodextrin)-activated carbon composite materials were synthesized and their performance for the removal of cymoxanil and imidacloprid—pesticides highly used in agriculture of the South of Europe—was evaluated. The use of poly(β-cyclodextrin) and activated carbon allows to use a highly efficient material (AC) with an amphiphilic material (CD) with high capacity to interact with low molecular weight compounds. Additionally, the use of PCD enables to obtain a hydrogel with a low swelling degree. This feature seems to be of utmost importance because it prevents the release of AC and simultaneously allows the partial release of pesticides.

Cyclodextrin was polymerized by using 1,6-HDI as crosslinker; two composites, with 5 and 10 wt% AC, were synthesized. The encapsulation was monitored by FT-IR and ^{13}C-NMR. The presence of AC into the gel matrix has no significant effect on the thermal degradation of the composite but has a significant effect on the swelling degree, suggesting that the AC might interact with CDs, thus, acting as a further crosslinker. The performance of hydrogel composites towards pesticide removal was evaluated. Activated carbon has shown the best performance as adsorbent for IMD and CYM. It has also been shown that by increasing the amount of AC inside gel-matrix increases the RE and the maximum amount of sorbed pesticide. This cannot be solely explained by the modification of the BET surface area. Although those values are significant (higher than 56% and 80% RE for IMD-PCD/$AC_{5\%}$ and IMD-PCD/$AC_{10\%}$, respectively and maximum q_e of around 20 mg g^{-1} for both composites), they are lower than those obtained for the sorption of CYM and IMD onto AC—this work—but better than the majority of data reported for AC systems. Furthermore, the sorption mechanism follows the Sips model, suggesting that there is a dual (physical and chemical) interaction between the pesticides and the adsorbent. This is observed in the surface morphology of the adsorbent, in the absence and presence of pesticides, as well as it is in agreement with pseudo-second order sorption kinetics. It has been found that ionic strength (NaCl) and soil additive (urea) has no significant effect on the sorption isotherms of CYM and IMD, indicating that the interactions sorbent-sorbate are weak (e.g., London dispersion forces).

A relevant achievement of this work was to allow to conclude that these composites, unlike the AC, are able to sorb and desorb both pesticides, in significant amounts, after three cycles, without losing the ability to reach the maximum amount of sorbed/desorbed

pesticide; in fact, it has been found that with the reuse cycles the maximum removal capacity of composites slightly increases. This accomplishment clearly paves the way for the development of new materials capable of acting simultaneously as sorbents and carriers, thus, contributing to the decrease of pesticides amounts applied in agriculture and, consequently, reducing the environmental damages.

Supplementary Materials: The following are available online at, Figure S1: Representation of IMD and CYM (a) UV-Vis spectra, and (b) curve of calibration., Figure S2: Removal efficiency (*RE*%) of CYM (left) and IMD (right) by different adsorbents: PCD (black columns), PCD/$AC_{5\%}$ (grey), PCD/$AC_{10\%}$ (white) and AC (lines), Figure S3: Adsorption isotherm of IMD (0–500) ppm onto PCD (a), PCD/$AC_{5\%}$ (b), PCD/$AC_{10\%}$ (c) and AC (d), in 1.0 g L^{-1} urea solution; and onto PCD (a'), PCD/$AC_{5\%}$ (b'), PCD/$AC_{10\%}$ (c') and AC (d'), in 1.0 g L^{-1} NaCl solution, at 25 °C, Figure S4: Adsorption isotherm of CYM (0–500) ppm onto PCD (a), PCD/$AC_{5\%}$ (b), PCD/$AC_{10\%}$ (c) and AC (d), in 1.0 g L^{-1} urea solution; and onto PCD (a'), PCD/$AC_{5\%}$ (b'), PCD/$AC_{10\%}$ (c') and AC (d'), in 1.0 g L^{-1} NaCl solution, at 25 °C. Table S1: One-tailored Grubb's test parameters. Table S2: Two-tailored F-test parameters for equality variance, Table S3: Analytical parameters of imidacloprid and cymoxanil, Table S4: Fitting parameters for the fitting of Equations (4) and (5) to the sorption isotherm data for imidacloprid in the presence of urea and NaCl, Table S5: Fitting parameters for the fitting of Equations (4) and (5) to the sorption isotherm data for cymoxanil in presence of urea and NaCl, Table S6: Characterization values for three sorption/desorption cycles.

Author Contributions: Conceptualization, D.M., A.A.C.C.P., F.X.P., T.-V.I., A.S. and A.J.M.V.; methodology, G.U., L.V., D.M., A.A.C.C.P., F.Z., F.X.P., T.-V.I., A.S. and A.J.M.V.; validation, A.J.M.V., D.M., A.A.C.C.P. and F.X.P.; formal analysis, G.U., D.M., A.A.C.C.P. and A.J.M.V.; investigation, G.U., L.V., A.J.M.V., F.Z. and F.X.P.; resources, D.M., A.A.C.C.P., F.X.P., T.-V.I., A.S. and A.J.M.V.; writing—original draft preparation and review and editing, G.U., L.V., D.M., A.A.C.C.P., F.Z., F.X.P., T.-V.I., A.S. and A.J.M.V.; visualization, G.U. and A.J.M.V.; supervision, D.M. and A.J.M.V.; project administration, A.J.M.V., T.-V.I. and F.X.P.; funding acquisition, A.J.M.V., T.-V.I. and F.X.P. All authors have read and agreed to the published version of the manuscript.

Funding: This work was funded by the Coimbra Chemistry Centre, which is supported by the Fundação para a Ciência e a Tecnologia (FCT) through the programmes UID/QUI/00313/2020 and COMPETE, and by Portuguese funds through FCT in the framework of the ERA-NET project ProWsper—WaterJPI/0006/2016.

Institutional Review Board Statement: Not applicable.

Informed Consent Statement: Not applicable.

Data Availability Statement: The data presented in this study are available within the article and in the supplementary material.

Acknowledgments: Gianluca Utzeri thanks the grant from the project ERA-NET ProWsper—WaterJPI/0006/2016 (contract: DPA 19-182) and the Ph.D. grant from Fundação de Ciência e Tecnologia (FCT) (reference: SFRH/BD/146358/2019).

Conflicts of Interest: The authors declare no conflict of interest.

Sample Availability: Samples of gels are available from the authors.

References

1. Vareda, J.P.; Valente, A.J.M.; Durães, L. Assessment of heavy metal pollution from anthropogenic activities and remediation strategies: A review. *J. Environ. Manag.* **2019**, *246*, 101–118. [CrossRef]
2. Paciência, I.; Madureira, J.; Rufo, J.; Moreira, A.; Fernandes, E.D.O. A systematic review of evidence and implications of spatial and seasonal variations of volatile organic compounds (VOC) in indoor human environments. *J. Toxicol. Environ. Health Part B* **2016**, *19*, 47–64. [CrossRef]
3. Mahinroosta, R.; Senevirathna, L. A review of the emerging treatment technologies for PFAS contaminated soils. *J. Environ. Manag.* **2020**, *255*, 109896. [CrossRef] [PubMed]
4. Pariatamby, A.; Kee, Y.L. Persistent Organic Pollutants Management and Remediation. *Procedia Environ. Sci.* **2016**, *31*, 842–848. [CrossRef]
5. Silva, V.; Mol, H.G.J.; Zomer, P.; Tienstra, M.; Ritsema, C.J.; Geissen, V. Pesticide residues in European agricultural soils—A hidden reality unfolded. *Sci. Total Environ.* **2019**, *653*, 1532–1545. [CrossRef] [PubMed]

6. Parween, T.; Jan, S. Pesticide consumption and threats to biodiversity. In *Ecophysiology of Pesticides*; Elsevier: Amsterdam, The Netherlands, 2019; pp. 39–73. ISBN 9780128176146.
7. Kaur, H.; Garg, H. Pesticides: Environmental Impacts and Management Strategies. In *Pesticides—Toxic Aspects*; Larramendy, L.M., Soloneski, S., Eds.; InTech: London, UK, 2014; Volume 395, pp. 116–124.
8. Quarcoo, F.; Bonsi, C.; Tackie, N. Pesticides, the Environment, and Human Health. In *Pesticides–Toxic Aspects*; Larramendy, L.M., Soloneski, S., Eds.; InTech: London, UK, 2014; p. 13.
9. Pimentel, D. Amounts of pesticides reaching target pests: Environmental impacts and ethics. *J. Agric. Environ. Ethics* **1995**, *8*, 17–29. [CrossRef]
10. Lushchak, V.I.; Matviishyn, T.M.; Husak, V.V.; Storey, J.M.; Storey, K.B. Pesticide toxicity: A mechanistic approach. *Excli J.* **2018**, *17*, 1101–1136. [CrossRef]
11. Marican, A.; Durán-Lara, E.F. A review on pesticide removal through different processes. *Environ. Sci. Pollut. Res.* **2018**, *25*, 2051–2064. [CrossRef]
12. Morillo, E.; Villaverde, J. Advanced technologies for the remediation of pesticide-contaminated soils. *Sci. Total Environ.* **2017**, *586*, 576–597. [CrossRef]
13. Encarnação, T.; Palito, C.; Pais, A.A.C.C.; Valente, A.J.M.; Burrows, H.D. Removal of Pharmaceuticals from Water by Free and Imobilised Microalgae. *Molecules* **2020**, *25*, 3639. [CrossRef]
14. Hu, L.; Wang, P.; Shen, T.; Wang, Q.; Wang, X.; Xu, P.; Zheng, Q.; Zhang, G. The application of microwaves in sulfate radical-based advanced oxidation processes for environmental remediation: A review. *Sci. Total Environ.* **2020**, *722*, 137831. [CrossRef]
15. Diagboya, P.N.; Olu-Owolabi, B.I.; Mtunzi, F.M.; Adebowale, K.O. Clay-carbonaceous material composites: Towards a new class of functional adsorbents for water treatment. *Surf. Interfaces* **2020**, *19*, 100506. [CrossRef]
16. Lamy-Mendes, A.; Torres, R.B.; Vareda, J.P.; Lopes, D.; Ferreira, M.; Valente, V.; Girão, A.V.; Valente, A.J.M.; Durães, L. Amine Modification of Silica Aerogels/Xerogels for Removal of Relevant Environmental Pollutants. *Molecules* **2019**, *24*, 3701. [CrossRef] [PubMed]
17. Filho, C.M.C.; Matias, T.; Durães, L.; Valente, A.J.M. Efficient simultaneous removal of petroleum hydrocarbon pollutants by a hydrophobic silica aerogel-like material. *Colloids Surf. A Phys. Eng. Asp.* **2017**, *520*, 550–560. [CrossRef]
18. Addorisio, V.; Pirozzi, D.; Esposito, S.; Sannino, F. Decontamination of waters polluted with simazine by sorption on mesoporous metal oxides. *J. Hazard. Mater.* **2011**, *196*, 242–247. [CrossRef] [PubMed]
19. Reeve, P.J.; Fallowfield, H.J. Natural and surfactant modified zeolites: A review of their applications for water remediation with a focus on surfactant desorption and toxicity towards microorganisms. *J. Environ. Manag.* **2018**, *205*, 253–261. [CrossRef] [PubMed]
20. Hosseini Hashemi, M.S.; Eslami, F.; Karimzadeh, R. Organic contaminants removal from industrial wastewater by CTAB treated synthetic zeolite Y. *J. Environ. Manag.* **2019**, *233*, 785–792. [CrossRef]
21. Marocco, A.; Dell'Agli, G.; Sannino, F.; Esposito, S.; Bonelli, B.; Allia, P.; Tiberto, P.; Barrera, G.; Pansini, M. Removal of Agrochemicals from Waters by Adsorption: A Critical Comparison among Humic-Like Substances, Zeolites, Porous Oxides, and Magnetic Nanocomposites. *Processes* **2020**, *8*, 141. [CrossRef]
22. Yi, Y.; Huang, Z.; Lu, B.; Xian, J.; Tsang, E.P.; Cheng, W.; Fang, J.; Fang, Z. Magnetic biochar for environmental remediation: A review. *Bioresour. Technol.* **2020**, *298*, 122468. [CrossRef]
23. Suo, F.; Liu, X.; Li, C.; Yuan, M.; Zhang, B.; Wang, J.; Ma, Y.; Lai, Z.; Ji, M. Mesoporous activated carbon from starch for superior rapid pesticides removal. *Int. J. Biol. Macromol.* **2019**, *121*, 806–813. [CrossRef]
24. Bojic, D.; Kostic, M.; Radovic-Vucic, M.; Velinov, N.; Najdanovic, S.; Petrovic, M.; Bojic, A. Removal of the herbicide 2,4-dichlorophenoxyacetic acid from water by using an ultrahighly efficient thermochemically activated carbon. *Hem. Ind.* **2019**, *73*, 223–237. [CrossRef]
25. Hameed, B.H.; Salman, J.M.; Ahmad, A.L. Adsorption isotherm and kinetic modeling of 2,4-D pesticide on activated carbon derived from date stones. *J. Hazard. Mater.* **2009**, *163*, 121–126. [CrossRef]
26. Gimeno, O.; Plucinski, P.; Kolaczkowski, S.T.; Rivas, F.J.; Alvarez, P.M. Removal of the Herbicide MCPA by Commercial Activated Carbons: Equilibrium, Kinetics, and Reversibility. *Ind. Eng. Chem. Res.* **2003**, *42*, 1076–1086. [CrossRef]
27. Mohammad, S.G.; Ahmed, S.M.; Amr, A.E.-G.E.; Kamel, A.H. Porous Activated Carbon from Lignocellulosic Agricultural Waste for the Removal of Acetampirid Pesticide from Aqueous Solutions. *Molecules* **2020**, *25*, 2339. [CrossRef]
28. Ahmad, K.S. Sorption and Juglans regia-derived activated carbon-mediated removal of aniline-based herbicide Alachlor from contaminated soils. *Environ. Earth Sci.* **2018**, *77*, 437. [CrossRef]
29. Ayranci, E.; Hoda, N. Adsorption kinetics and isotherms of pesticides onto activated carbon-cloth. *Chemosphere* **2005**, *60*, 1600–1607. [CrossRef]
30. Amézquita-Marroquín, C.P.; Torres-Lozada, P.; Giraldo, L.; Húmpola, P.D.; Rivero, E.; Poon, P.S.; Matos, J.; Moreno-Piraján, J.C. Sustainable production of nanoporous carbons: Kinetics and equilibrium studies in the removal of atrazine. *J. Colloid Interface Sci.* **2020**, *562*, 252–267. [CrossRef]
31. Faur, C.; Métivier-Pignon, H.; Le Cloirec, P. Multicomponent Adsorption of Pesticides onto Activated Carbon Fibers. *Adsorption* **2005**, *11*, 479–490. [CrossRef]
32. Spaltro, A.; Simonetti, S.; Torrellas, S.A.; Rodriguez, J.G.; Ruiz, D.; Juan, A.; Allegretti, P. Adsorption of bentazon on CAT and CARBOPAL activated carbon: Experimental and computational study. *Appl. Surf. Sci.* **2018**, *433*, 487–501. [CrossRef]

33. Njoku, V.O.; Islam, M.A.; Asif, M.; Hameed, B.H. Utilization of sky fruit husk agricultural waste to produce high quality activated carbon for the herbicide bentazon adsorption. *Chem. Eng. J.* **2014**, *251*, 183–191. [CrossRef]
34. Ahmad, K.S. Arachis hypogaea derived activated carbon steered remediation of Benzimidazole based fungicide adsorbed soils. *Chem. Ecol.* **2019**, *35*, 576–591. [CrossRef]
35. Salman, J.M.; Hameed, B.H. Removal of insecticide carbofuran from aqueous solutions by banana stalks activated carbon. *J. Hazard. Mater.* **2010**, *176*, 814–819. [CrossRef] [PubMed]
36. Moussavi, G.; Hosseini, H.; Alahabadi, A. The investigation of diazinon pesticide removal from contaminated water by adsorption onto NH4Cl-induced activated carbon. *Chem. Eng. J.* **2013**, *214*, 172–179. [CrossRef]
37. Ahmad, K.S. Adsorption removal of endosulfan through Saccharum officinarum derived activated carbon from selected soils. *J. Cent. South Univ.* **2019**, *26*, 146–157. [CrossRef]
38. Ahmad, K.S. Exploring the potential of Juglans regia-derived activated carbon for the removal of adsorbed fungicide Ethaboxam from soils. *Environ. Monit. Assess.* **2018**, *190*, 737. [CrossRef] [PubMed]
39. Santana, G.M.; Lelis, R.C.C.; Jaguaribe, E.F.; Morais, R.d.M.; Paes, J.B.; Trugilho, P.F. Development of activated carbon from bamboo (bambusa vulgaris) for pesticide removal from aqueous solutions. *Cerne* **2017**, *23*, 123–132. [CrossRef]
40. Mohammad, S.G.; El-Sayed, M.M.H. Removal of imidacloprid pesticide using nanoporous activated carbons produced via pyrolysis of peach stone agricultural wastes. *Chem. Eng. Commun.* **2020**, 1–12. [CrossRef]
41. Urbain, K.Y.; Fodjo, E.K.; Ardjouma, D.; Serge, B.Y.; Aimé, E.S.; Irié Marc, G.B.; Albert, T. Removal of imidacloprid using activated carbon produced from ricinodendron heudelotii shells. *Bull. Chem. Soc. Ethiop.* **2018**, *31*, 397. [CrossRef]
42. Hashemi, M.M.R.; Abolghasemi, S.S.; Ashournia, M.; Modaberi, H. Removal of hinosan from underground water using NH4Cl-modified activated carbon from rice husk. *Environ. Sci. Pollut. Res.* **2019**, *26*, 20344–20351. [CrossRef] [PubMed]
43. Gupta, V.K.; Gupta, B.; Rastogi, A.; Agarwal, S.; Nayak, A. Pesticides removal from waste water by activated carbon prepared from waste rubber tire. *Water Res.* **2011**, *45*, 4047–4055. [CrossRef]
44. Premarathna, K.S.D.; Rajapaksha, A.U.; Sarkar, B.; Kwon, E.E.; Bhatnagar, A.; Ok, Y.S.; Vithanage, M. Biochar-based engineered composites for sorptive decontamination of water: A review. *Chem. Eng. J.* **2019**, *372*, 536–550. [CrossRef]
45. Alves, D.C.S.; Gonçalves, J.O.; Coseglio, B.B.; Burgo, T.A.L.; Dotto, G.L.; Pinto, L.A.A.; Cadaval, T.R.S. Adsorption of phenol onto chitosan hydrogel scaffold modified with carbon nanotubes. *J. Environ. Chem. Eng.* **2019**, *7*, 103460. [CrossRef]
46. Filho, C.M.C.; Bueno, P.V.A.; Matsushita, A.F.Y.; Rubira, A.F.; Muniz, E.C.; Durães, L.; Murtinho, D.M.B.; Valente, A.J.M. Synthesis, characterization and sorption studies of aromatic compounds by hydrogels of chitosan blended with β-cyclodextrin- and PVA-functionalized pectin. *Rsc Adv.* **2018**, *8*, 14609–14622. [CrossRef]
47. Thakur, S.; Chaudhary, J.; Kumar, V.; Thakur, V.K. Progress in pectin based hydrogels for water purification: Trends and challenges. *J. Environ. Manag.* **2019**, *238*, 210–223. [CrossRef]
48. Sharma, G.; Sharma, S.; Kumar, A.; Al-Muhtaseb, A.H.; Naushad, M.; Ghfar, A.A.; Mola, G.T.; Stadler, F.J. Guar gum and its composites as potential materials for diverse applications: A review. *Carbohydr. Polym.* **2018**, *199*, 534–545. [CrossRef] [PubMed]
49. Szejtli, J. Introduction and General Overview of Cyclodextrin Chemistry. *Chem. Rev.* **1998**, *98*, 1743–1753. [CrossRef] [PubMed]
50. Li, S.; Purdy, W.C. Cyclodextrins and their applications in analytical chemistry. *Chem. Rev.* **1992**, *92*, 1457–1470. [CrossRef]
51. Cova, T.F.G.G.; Cruz, S.M.A.; Valente, A.J.M.; Abreu, P.E.; Marques, J.M.C.; Pais, A.A.C.C. Aggregation of Cyclodextrins: Fundamental Issues and Applications. In *Cyclodextrin—A Versatile Ingredient*; InTech: London, UK, 2018. [CrossRef]
52. Sikder, M.T.; Rahman, M.M.; Jakariya, M.; Hosokawa, T.; Kurasaki, M.; Saito, T. Remediation of water pollution with native cyclodextrins and modified cyclodextrins: A comparative overview and perspectives. *Chem. Eng. J.* **2019**, *355*, 920–941. [CrossRef]
53. Cova, T.F.G.G.; Murtinho, D.; Pais, A.A.C.C.; Valente, A.J.M. Cyclodextrin-based Materials for Removing Micropollutants From Wastewater. *Curr. Org. Chem.* **2018**, *22*, 2150–2181. [CrossRef]
54. Tian, B.; Hua, S.; Tian, Y.; Liu, J. Cyclodextrin-based adsorbents for the removal of pollutants from wastewater: A review. *Environ. Sci. Pollut. Res.* **2021**, *28*, 1317–1340. [CrossRef] [PubMed]
55. Fenyvesi, É.; Barkács, K.; Gruiz, K.; Varga, E.; Kenyeres, I.; Záray, G.; Szente, L. Removal of hazardous micropollutants from treated wastewater using cyclodextrin bead polymer—A pilot demonstration case. *J. Hazard. Mater.* **2020**, *383*, 121181. [CrossRef]
56. Topuz, F.; Uyar, T. Poly-cyclodextrin cryogels with aligned porous structure for removal of polycyclic aromatic hydrocarbons (PAHs) from water. *J. Hazard. Mater.* **2017**, *335*, 108–116. [CrossRef] [PubMed]
57. Russo, M.; Saladino, M.L.; Chillura Martino, D.; Lo Meo, P.; Noto, R. Polyaminocyclodextrin nanosponges: Synthesis, characterization and pH-responsive sequestration abilities. *Rsc Adv.* **2016**, *6*, 49941–49953. [CrossRef]
58. Crini, G.; Fourmentin, S.; Fenyvesi, É.; Torri, G.; Fourmentin, M.; Morin-Crini, N. Cyclodextrins, from molecules to applications. *Environ. Chem. Lett.* **2018**, *16*, 1361–1375. [CrossRef]
59. Gidwani, B.; Vyas, A. Synthesis, characterization and application of Epichlorohydrin-β-cyclodextrin polymer. *Colloids Surf. B Biointerfaces* **2014**, *114*, 130–137. [CrossRef]
60. Morin-Crini, N.; Crini, G. Environmental applications of water-insoluble β-cyclodextrin–epichlorohydrin polymers. *Prog. Polym. Sci.* **2013**, *38*, 344–368. [CrossRef]
61. Mohamed, M.H.; Wilson, L.D.; Headley, J.V. Design and characterization of novel β-cyclodextrin based copolymer materials. *Carbohydr. Res.* **2011**, *346*, 219–229. [CrossRef] [PubMed]

62. Gerola, A.P.; Silva, D.C.; Jesus, S.; Carvalho, R.A.; Rubira, A.F.; Muniz, E.C.; Borges, O.; Valente, A.J.M. Synthesis and controlled curcumin supramolecular complex release from pH-sensitive modified gum-arabic-based hydrogels. *RSC Adv.* **2015**, *5*, 94519–94533. [CrossRef]
63. Abarca, R.L.; Rodríguez, F.J.; Guarda, A.; Galotto, M.J.; Bruna, J.E. Characterization of beta-cyclodextrin inclusion complexes containing an essential oil component. *Food Chem.* **2016**, *196*, 968–975. [CrossRef] [PubMed]
64. Anne, J.M.; Boon, Y.H.; Saad, B.; Miskam, M.; Yusoff, M.M.; Shahriman, M.S.; Zain, N.N.M.; Lim, V.; Raoov, M. β-Cyclodextrin conjugated bifunctional isocyanate linker polymer for enhanced removal of 2,4-dinitrophenol from environmental waters. *R. Soc. Open Sci.* **2018**, *5*, 180942. [CrossRef] [PubMed]
65. Yi, Q.; Qi, F.; Cheng, G.; Zhang, Y.; Xiao, B.; Hu, Z.; Liu, S.; Cai, H.; Xu, S. Thermogravimetric analysis of co-combustion of biomass and biochar. *J. Therm. Anal. Calorim.* **2013**, *112*, 1475–1479. [CrossRef]
66. Jin, Z. (Ed.) *Cyclodextrin Chemistry*; World Scientific Publishing: Singapore, 2013; ISBN 978-981-4436-79-3.
67. Silverstein, R.M.; Webster, F.X.; Kiemle, D.J. Infrared Spectrometry. In *Spectrometric Identification of Organic Compounds*; Brennan, D., Yee, J., Wolfman-Robichaud, S., Eds.; John Wiley & Sons, Inc.: New York, NY, USA, 2005; pp. 72–126. ISBN 0-471-39362-2.
68. Park, J.H.; Choppala, G.; Lee, S.J.; Bolan, N.; Chung, J.W.; Edraki, M. Comparative Sorption of Pb and Cd by Biochars and Its Implication for Metal Immobilization in Soils. *WaterAirSoil Pollut.* **2013**, *224*, 1711. [CrossRef]
69. Omri, A.; Benzina, M.; Ammar, N. Preparation, modification and industrial application of activated carbon from almond shell. *J. Ind. Eng. Chem.* **2013**, *19*, 2092–2099. [CrossRef]
70. Mallard, I.; Baudelet, D.; Castiglione, F.; Ferro, M.; Panzeri, W.; Ragg, E.; Mele, A. Polydisperse methyl β-cyclodextrin–epichlorohydrin polymers: Variable contact time 13 C CP-MAS solid-state NMR characterization. *Beilstein J. Org. Chem.* **2015**, *11*, 2785–2794. [CrossRef] [PubMed]
71. Amsden, B. Solute Diffusion within Hydrogels. Mechanisms and Models. *Macromolecules* **1998**, *31*, 8382–8395. [CrossRef]
72. Naghash, H.J.; Okay, O. Formation and structure of polyacrylamide gels. *J. Appl. Polym. Sci.* **1996**, *60*, 971–979. [CrossRef]
73. Estrada, F.G.A.; Marques, J.M.C.; Valente, A.J.M. Molecular Dynamics Insights for Screening the Ability of Polymers to Remove Pesticides from Water. *ChemistryOpen* **2019**, *8*, 438–446. [CrossRef] [PubMed]
74. Spark, K.; Swift, R. Effect of soil composition and dissolved organic matter on pesticide sorption. *Sci. Total Environ.* **2002**, *298*, 147–161. [CrossRef]
75. Riah, W.; Laval, K.; Laroche-Ajzenberg, E.; Mougin, C.; Latour, X.; Trinsoutrot-Gattin, I. Effects of pesticides on soil enzymes: A review. *Environ. Chem. Lett.* **2014**, *12*, 257–273. [CrossRef]
76. Medronho, B.; Andrade, R.; Vivod, V.; Ostlund, A.; Miguel, M.G.; Lindman, B.; Voncina, B.; Valente, A.J.M. Cyclodextrin-grafted cellulose: Physico-chemical characterization. *Carbohydr. Polym.* **2013**, *93*, 324–330. [CrossRef]
77. Piculell, L.; Lindman, B. Association and segregation in aqueous polymer/polymer, polymer/surfactant, and surfactant/surfactant mixtures: Similarities and differences. *Adv. Colloid Interface Sci.* **1992**, *41*, 149–178. [CrossRef]
78. Painter, P.C.; Veytsman, B.; Kumar, S.; Shenoy, S.; Graf, J.F.; Xu, Y.; Coleman, M.M. Intramolecular Screening Effects in Polymer Mixtures. 1. Hydrogen-Bonded Polymer Blends. *Macromolecules* **1997**, *30*, 932–942. [CrossRef]
79. Sung, S.-S. Dielectric screening effect of electronic polarization and intramolecular hydrogen bonding. *Protein Sci.* **2017**, *26*, 2003–2009. [CrossRef] [PubMed]
80. Ooi, C.-H.; Cheah, W.-K.; Yeoh, F.-Y. Comparative study on the urea removal by different nanoporous materials. *Adsorption* **2019**, *25*, 1169–1175. [CrossRef]
81. Yamasaki, H.; Makihata, Y.; Fukunaga, K. Efficient phenol removal of wastewater from phenolic resin plants using crosslinked cyclodextrin particles. *J. Chem. Technol. Biotechnol.* **2006**, *81*, 1271–1276. [CrossRef]
82. Hemine, K.; Skwierawska, A.; Kernstein, A.; Kozłowska-Tylingo, K. Cyclodextrin polymers as efficient adsorbents for removing toxic non-biodegradable pimavanserin from pharmaceutical wastewaters. *Chemosphere* **2020**, *250*, 126250. [CrossRef] [PubMed]
83. Limousin, G.; Gaudet, J.-P.; Charlet, L.; Szenknect, S.; Barthès, V.; Krimissa, M. Sorption isotherms: A review on physical bases, modeling and measurement. *Appl. Geochem.* **2007**, *22*, 249–275. [CrossRef]
84. Langmuir, I. The adsorption of gases on plane surfaces of glass, mica and platinum. *J. Am. Chem. Soc.* **1918**, *40*, 1361–1403. [CrossRef]
85. Al-Ghouti, M.A.; Da'ana, D.A. Guidelines for the use and interpretation of adsorption isotherm models: A review. *J. Hazard. Mater.* **2020**, *393*, 122383. [CrossRef] [PubMed]
86. Kingdom, F.A.A.; Prins, N. Model Comparisons. In *Psychophysics*; Kingdom, F.A.A., Prins, N., Eds.; Elsevier: Amsterdam, The Netherlands, 2016; pp. 247–307. ISBN 9780124071568.

Amine-β-cyclodextrin-based nanosponges. The role of cyclodextrin amphiphilicity in the imidacloprid uptake

V

Gianluca Utzeri, Dina Murtinho, Teresa M.R. Maria, Alberto A.C.C. Pais, Filomena Sannino, Artur J.M Valente

Colloids and Surfaces A: Physicochemical and Engineering Aspects, vol. 635 (2022) 128044

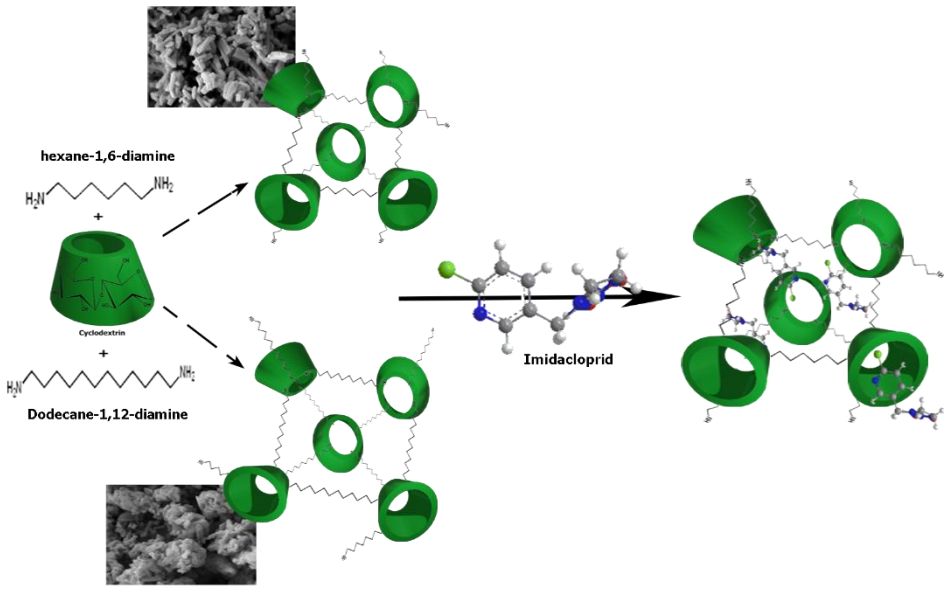

Colloids and Surfaces A: Physicochemical and Engineering Aspects 635 (2022) 128044

Contents lists available at ScienceDirect

Colloids and Surfaces A: Physicochemical and Engineering Aspects

journal homepage: www.elsevier.com/locate/colsurfa

Amine-β-cyclodextrin-based nanosponges. The role of cyclodextrin amphiphilicity in the imidacloprid uptake

Gianluca Utzeri [a], Dina Murtinho [a], Teresa M.R. Maria [a], Alberto A.C.C. Pais [a], Filomena Sannino [b], Artur J.M. Valente [a,*]

[a] University of Coimbra, Department of Chemistry, CQC, 3004-535 Coimbra, Portugal
[b] Department of Agricultural Sciences, University of Naples "Federico II", Italy

HIGHLIGHTS

- Synthesis of NSs of amine-β-cyclodextrin with linkers with different chain lengths.
- Dependency of the physico-chemical properties on the chain length of the crosslinker.
- NS with shorter linker presents higher active surface and lower thermal stability.
- High dependency on the physico-chemical characteristic of the NSs as sorbents.
- Superior performance of amine-β-cyclodextrin nanosponges for pesticide sorption.

GRAPHICAL ABSTRACT

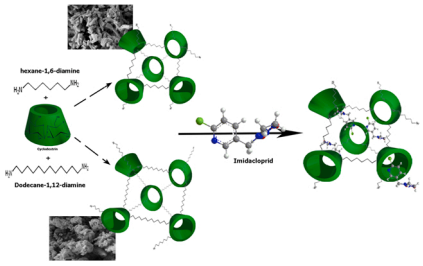

ARTICLE INFO

Keywords:
β-cyclodextrin
Nanosponge
Chain length effect
Imidacloprid
Agrochemical

ABSTRACT

This paper describes the synthesis, characterization and sorption performance of cyclodextrin nanosponges (NSs). Cyclodextrins are cyclic oligosaccharides with remarkable amphiphilic properties, allowing for a vast range of applications. The synthesis of nanosponges of β-cyclodextrins was carried out using two uncommon cross-linkers: hexane-1,6-diamine (am_6) and dodecane-1,12-diamine (am_{12}). It has been found that the physico-chemical properties of the nanosponges are highly influenced by the chain length of the crosslinker. Nanosponge with crosslinker with shorter chain length is characterized by a higher active surface area (21.8 m^2 cm^{-1}), pore size (24.3 nm) and structural disorder; on the other hand, the use of am_{12} leads to a higher thermal stability but lower porosity (7.5 nm), suggesting the occurrence of intermolecular alkyl chain interactions. It can also be concluded that by increasing the crosslinker alkyl chain length, the CD gains additional degrees of freedom and, consequently, a higher structural organization is favored. The more compact structure of the CD-am_{12}-CD led to less available amine groups, consequently it shows a more pronounced response to pH variation. Such properties make the am_6–containing NS a better sorbent for imidacloprid – an active substance used as systemic foliar insecticide and veterinary substance. A preliminary factorial study was performed to determine the effect of several parameters (IMD concentration, amount of sorbent, volume of solution and pH) on sorption abilities of the NSs. Hence, the sorption analysis were performed at the optimal experimental conditions pH 3.8, s/l ratio 5

* Corresponding author.
E-mail address: avalente@ci.uc.pt (A.J.M. Valente).

https://doi.org/10.1016/j.colsurfa.2021.128044
Received 26 October 2021; Received in revised form 29 November 2021; Accepted 30 November 2021
Available online 3 December 2021

and 25 °C in which CD-am$_6$-CD shows the ability for an efficient sorption of the active substance. From the application perspective, the maximum adsorption capability is 68 ± 5 mg g^{-1} and the removal efficiency is 95%.

1. Introduction

The cyclic oligomers α-, β- and γ-cyclodextrins (CDs) and their derivatives have been studied for over a half-century [1]. They show a fascinating structure of truncated-cone-shaped with 6, 7 and 8 α-(1→4)-D-glucopyranosyl linked units, respectively. The combined external hydrophilicity with the internal hydrophobic surface constitute a unique "microenvironment", that confer them the peculiar ability to form host-guest complexes with many hydrophobic substances by hydrophobic interaction, dipole-dipole, electrostatic interaction, Van der Waals, dispersion forces and reduction of conformational strain [2,3]. Hence, physical, chemical and/or biological characteristics of the guest molecules can be modified and/or improved. CDs were explored in a wide range of applications and areas including drug-delivery system, catalysis, agricultural industries, food and cosmetic industries, pollution remediation, among others [4–7]. Due to their ability to form inclusion complexes, CDs and derivatives are also applied for analyte extraction/isolation or remediation/decontamination applied to heavy metals, dyes, pharmaceuticals and agrochemical [8–11] compounds.

Pesticides are becoming one of the most relevant environmental global issues [12,13]. Albeit they have positive effects for maximizing crop production, studies demonstrate that only ca. 0.1% reach their targets, which means high-cost implication and soil, water streams and air pollution [14]. Moreover, due to their broad spectra of action, persistence, bioaccumulation and bioaugmentation, they can indirectly affect the biodiversity with species loss and/or resistant species formation, and they have impact upon human health, leading to chronic or acute illness [15–17].

The sequestrating ability of CDs and their derivatives are widely studied for pesticide removal. Derivatives can be prepared via facile mono- or per-functionalization due to the intrinsic nucleophilicity of the primary and secondary hydroxyl groups [18,19]. In the last few years, attention was focused on the use of CDs and derivatives to develop versatile supramolecular nanostructures such as nanosponges (NSs) and nanogels (NGs) [20,21]. Nanosponges can be defined as 3D-hyper-reticulated nanoporous structures with high thermal stability that allows more applications with hydrophilic compounds. Several classes of linkers can be used to synthesize CD-based nanosponges (CD-NSs) and common examples are dicarboxylic acid chlorides, anhydrides, diisocyanates, dicarboxylic acids, alkyl dihalides and chlorohydrins [8,22]. CD-NSs are recently being explored as promising environmentally friendly sorbent materials for pesticides, taking advantage of the hydrophobic cavities of the CDs and the hydrophilic network of the porous structure (Table 1).

In this study we are investigating the sequestrating capability of two CD-NSs for imidacloprid (IMD). Imidacloprid is one of the most widely used neonicotinoids, accounting for a third of the world market for insecticides. IMD is widely applied as veterinary substance and systemic neurotoxic broad-spectrum insecticide [23]; however, because of the massive amount used and long half-life, it promotes soil and water-streams contamination. Moreover, studies have demonstrated the presence of IMD residues on European topsoil samples [15], plants and human urine [24]. Herein, we synthesized CD-NSs using two uncommon linkers, hexane-1,6-diamine (am$_6$) and dodecane-1,12–diamine (am$_{12}$), namely CD-am$_6$-CD and CD-am$_{12}$-CD. NSs were characterized by different techniques and the influence of the chain length of the linker was assessed. The chemical structure was characterized by ^{1}H-NMR, FTIR and thermal stability via TGA and DSC. Particle size and stability were determined by DLS and ζ-potential measurements, whereas the morphology was analyzed by SEM before and after contact with an aqueous solution of the pesticide active ingredient. The removal efficiency and the mechanism of sorption of the IMD into both NSs were evaluated via sorption isotherm and sorption kinetic. The optimal experimental conditions were determined through a 2^k experimental design, while also evaluating the pH effect on the sorption capability of CD-am$_6$-CD and CD-am$_{12}$-CD, since both materials are pH responsive.

2. Materials and methods

2.1. Materials

For the synthesis of NSs, *β*-cyclodextrin (*β*-CD) was supplied by Sigma Aldrich (purity 98%, CAS 7585–39–9), triphenylphosphine (Ph_3P) was purchased from Alpha Aesar and iodine, I_2, was supplied as resublimed pearls by PanReac. Hexane-1,6-diamine (am$_6$) (CAS 124–09-4) and dodecane-1,12–diamine (am$_{12}$) (purity 98%, CAS 2783–17-7), used as crosslinkers, were purchased from Sigma-Aldrich. *N,N*-Dimethylformamide (DMF) was obtained from Honeywell (purity ≥ 99.8%, CAS 68–12-2) and dried using molecular sieves. Methanol (MeOH) was obtained from Chem-Lab (purity 99.8% HPLC grade, CAS 67–56-1). Imidacloprid was supplied by Sigma-Aldrich (purity 100%, CAS 138261–41-3). The other chemicals were used without further purification processes. For NMR analysis dimethylsulfoxide-d$_6$ (DMSO-d$_6$) (purity 99.80%, CAS 2206–27-1) and 3–(trimethylsilyl) propionic acid-d$_4$ sodium salt (TMSP) (M_W = 172.27 g mol^{-1}, purity 98%, CAS 24493–21-8) were purchased from Eurisotop and used as solvent and internal reference, respectively.

2.2. Synthesis of amine-cyclodextrin nanosponges

The amine-cyclodextrin-based nanosponges are obtained by reaction of *heptakis*-(6–amine)-(6–deoxy)-*β*-cyclodextrins (am$_x$-CD) with

Table 1
Sorption efficiency of pesticides from cyclodextrin-based nanosponges.

Nanosponges	Pesticide	q_m [(a)] (mg g^{-1})	*RE* [(b)] (%)	Ref.
*β*CD-EPI	flufiprole	n.a.	60–80	[25]
HP-*β*CD-EPI	fomesafen	1.5, 0.7	n.a.	[26]
	simazine	0.3, 0.01		
	bromacil	n.a	10–60	[25]
		0.7, 0.7	n.a.	[26]
	fenamiphos	n.a.	10–60	[25]
		9.5, 18.2	n.a.	[26]
	pretilachlor	n.a.	10–60	[25]
		28.7, 28.4	n.a.	[26]
	butachlor	n.a.	60–80	[25]
		37.4, 19.2	n.a.	[26]
	butylenefipronil	n.a.	10–60	[25]
		3.7, 2.8	n.a	[26]
	fipronil	n.a.	60–80	[25]
		2.8, 6.2	n.a	[26]
	benalaxyl	n.a.	60–80	[25]
		14.2, 28.0	n.a	[26]
	atrazine	n.a.	10–60	[25]
		0.8, 1.2	n.a.	[26]
*β*CD-HDI	2,4–dinitrophenol	3.4	76	[27]
	methyl parathion	n.a.	55	[28]
*β*CD-CTR	paraquat dichloride hydrate	20.8	n.a.	[29]
*β*CD-EDTA-CS	2,4,5–trichlorophenol	9.2	90	[30]
*β*CD-TDI	2,4–dinitrophenol	3.9	86	[27]
*β*CD-DPC	dinotefuran	0.9	90	[31]
*β*CD-BDE	ciprofloxacin	2	90	[32]

[(a)] q_m maximum sorption capacity per unit of weight of the sorbent; [(b)] *RE* is the removal efficiency.

heptakis-(6–iodo)-(6–deoxy)-β-cyclodextrin (I-CD). The am_x-CDs has been obtained by previous modification of native β-CD via nucleophilic substitution using excess of I_2.

The synthesis of I-CD was relied on an experimental procedure described elsewhere [33]. Briefly, Ph_3P (30.0 mmol) was dissolved in 30 mL of anhydrous DMF. I_2 (30.0 mmol) was carefully added to the previous solution and, after complete dissolution, dried β-CD (2.0 mmol) was added to the mixture. The solution was stirred under a N_2 atmosphere, at 70 °C, overnight. Then, the solution was cooled to r.t. and concentrated by solvent removal (ca. 40%). A fresh solution of NaOMe (3 M, 12 mL) was added to the reaction mixture for 30 min, under cooling and stirring. The solution was then poured in an excess of MeOH and the precipitate is collected by filtration in vacuum. The precipitate is superficially washed and Soxhlet extracted with MeOH until no more discoloration by the solvent is detected. Finally, the purified product was collected, frozen with liquid nitrogen and freeze dried (*Labconco* model Free Zone 4.5). The product, a solid white powder, is stored in desiccator until further use.

The synthesis of am_x-CDs was carried out using two diamines with different chain length, hexane-1,6-diamine and dodecane-1,12–diamine. The intrinsic nucleophilicity of polyamines was exploited to easily react with the I-CD. Based on a published research [34], the amine-functionalized CD was prepared by nucleophilic substitution of the iodine in position C6 with the amine group. I-CD was mixed with a 20–fold excess of the proper linker. Particularly, to synthesize am_{12}-CD, 15 mL of DMF is needed to ensure the dissolution of am_{12} at 60 °C. After complete dissolution, 5 mL of DMF containing I-CD was added. The reaction mixtures of am_6-CD and am_{12}-CD were heated at 60 °C and 70 °C, respectively, and stirred under a nitrogen atmosphere for 48 h. Then, 20 mL of MeOH were added and the resulting solution was added dropwise in ca. 200 mL of cold diethyl ether under vigorous stirring. The solution was decanted, after settling of the brown gum product, dissolved in 10 mL of MeOH and precipitated once more in cold diethyl ether. The cycles of dissolution-precipitation were repeated until a pale-yellow solid was obtained. The products were collected by centrifugation at 4500 rpm, for 20 min, frozen and freeze-dried. Due to the high time consuming, the synthetic routes for am_6-CD and am_{12}-CD were also performed via microwave-assisted procedure (MW), based on the literature [35]. A minimum amount of anhydrous DMF is used to ensure the dissolution of the 20–fold excess of am_6 and am_{12}. The MW-synthesis of am_6-CD and am_{12}-CD were performed in a CEM Discover microwave using a fixed temperature method, 85 °C and 95 °C, for 30 min, respectively. This procedure allows a drastic reduction of the reaction time, with good yield for am_6-CD and am_{12}-CD.

Finally, the synthesis of the amine cyclodextrin-based nanosponges was carried out by reaction of am_x-CD with I-CD, using 1:1 equivalent ratio. The reactants were mechanically mixed and anhydrous DMSO was used as media to ameliorate the blending of the reactants. The mixtures were heated at 60 °C and 70 °C, during 48 h, for CD-am_6-CD and CD-am_{12}-CD, respectively. The product, with a like brown gum appearance, was transferred to 10 mL of water and mechanically smashed. The solid was collected by centrifugation at 4500 rpm for 20 min. Three cycles of washing were performed by sonicating the solid for 10 min in 10 mL MeOH. The solid was collected through centrifugation. A final washing with diethyl ether was performed and the final product was frozen, freeze-dried and stored in a desiccator until further use.

2.3. Physico-chemical characterization of the cyclodextrin-based materials

The substitution efficiency of I-CD and am_x-CDs was determined by ^{1}H-nuclear magnetic resonance (^{1}H-NMR) at 400 MHz using ca. 10 mg of compounds in 1 mL of DMSO-d^6 solution containing 0.5% (w/v) of TMSP.

The chemical structure of β-CD, am_{12}, I-CD, am_6-CD, am_{12}-CD, CD-am_6-CD and CD-am_{12}-CD were characterized by Fourier transform infrared spectroscopy (FTIR) in a wavelength interval of 4000–400 cm^{-1}.

The thermal stability of the pristine compounds, intermediates and final products was determined by thermogravimetric analysis (TGA) (*Netzsch Instruments*, model TG209–F3 Tarsus) and power-compensated differential scanning calorimetry (DSC) (*PerkinElmer*, model DSC 7). The TGA analysis was performed using ca. 3 mg of sample in a temperature range from 20° to 600°C, heating rate of 10 °C min^{-1}, under a 50 mL min^{-1}flow rate of nitrogen. The DSC experiments were performed in a Perkin Elmer DSC7 calorimeter, with an intracooler cooling unit at − 20 °C (ethylene glycol-water(1:1, v/v) cooling mixture). The analyses were carried out using ca. 3 mg of compound in 30 µL aluminum vented pans, in the temperature range from 0° to 200°C, with a heating rate of 20 °C min^{-1}, under a 20 mL min^{-1} nitrogen flow rate.

Dynamic light scattering (DLS) and ζ-potential measurements were performed using 1 mL of nanosponge dispersion in aqueous solution of KCl 0.01 mM at 25 °C (*Malvern Zetasizer NanoZS*). For the DLS measurements, a scattering angle of 173° was used and the average diameter was calculated before and after ζ-potential analysis, verifying the effect of the applied potential. The size values were retrieved from the intensity distribution values using the cumulants method. ζ-potential measurements were performed by aqueous electrophoresis measurements and the values were calculated from electrophoretic mobility using the Smoluchowski relationship. Moreover, the change of the ζ-potential of both materials as function of pH at four values (3.5, 4.5, 6.5, 8.5 and 9.5) was determined. The pH was adjusted by micro-adding of HCl or NaOH 0.01 mol L^{-1}.

Nitrogen adsorption-desorption analysis (*ASAP 2000, Micrometrics*) was performed to determine the specific surface area (S_{BET}) with pore size given by the Brunauer-Emmet-Teller (BET) model

$$Pore \quad size = \frac{4V_{pore}}{S_{BET}} \tag{1}$$

where V_{pore} is the volume of the pores.

Scanning electron microscopy (SEM) (*Gemini 2-Zeiss, Merlin-Zeiss*, Oberkochen, Germany) micrographs were taken at 4.00 kV and 10000 × of magnification to analyze the morphology of the NSs before and after contact with aqueous solutions of IMD at 500 mg L^{-1}.

2.4. Sorption analysis

Experimental conditions for the sorption analysis were determined by experimental design. A full 2^k factorial design was performed considering three factors, namely concentration of pesticide, amount of adsorbent and volume of solution (Table 2). Their influence on the amount of pesticide sorbed per gram of sorbent (q_e) was determined using

$$q_e = \frac{C_0 - C_e}{m} \times V \tag{2}$$

where q_e (mg g^{-1}) is the amount of analyte sorbed by unit of sorbent, C_0 and C_e (mg L^{-1}) are concentration of IMD at initial and equilibrium state, respectively. In turn, m (g) is the mass of the sorbent, and V (L) the volume of the solution.

The total number of tests for a complete design is given as $N = 2^k$, where k is related with the factors varied over 2 levels. In this case, k has

Table 2
Experimental factors and their designation.

Code (X_i)	Factor	Experimental field	
		Min. (−1)	Max. (+1)
X_1	IMD concentration (mg L^{-1})	150	500
X_2	Adsorbent amount (g)	0.010	0.020
X_3	Solution volume (L)	0.002	0.010

the value 3.

A polynomial equation based on the first-order model was used in order to determine the effect of the three parameters (X_1, X_2 and X_3) and their terms of interaction, as shown in

$$q_e = b_0 + b_1X_1 + b_2X_2 + b_3X_3 + b_{12}X_1X_2 + b_{13}X_1X_3 + b_{23}X_2X_3 + + \quad b_{123}X_1X_2X_3 \tag{3}$$

where b_0 is the average of the q_e values, b_1, b_2 and b_3 are the linear coefficients and b_{12}, b_{13}, b_{23} and b_{123} represent the coefficients of the interactions. X_1, X_2 and X_3 are the single factors studied in the model whereas X_1X_2, X_1X_3, X_2X_3 and $X_1X_2X_3$ are products of factor values. The IMD quantification was performed by UV-Vis spectroscopy. Calibration and analytical parameters for IMD quantification were determined and reported on our previous study [36].

Furthermore, based on the supposition that CD-am$_6$-CD and CD-am$_{12}$-CD are pH responsive materials, due to the presence of amine groups, the effect of the pH on q_e, removal efficiency (*RE*) and degradation rate (*DR*) of IMD was also assessed. The *RE* and *DR* were calculated using

$$RE\% = \frac{C_0 - C_e}{C_0} \tag{4}$$

$$DR\% = (1 - \frac{C_t}{C_0}) \times 100 \tag{5}$$

where C_t is the concentration of IMD solution determined at a defined interval of time, 24 h.

At the same pH values, the degradation rate (*DR%*) (Eq. 5) was assessed for aqueous solution of imidacloprid (500 mg L^{-1}) within 7 days, at 25 °C with agitation at 120 rpm.

The study was performed at four different pH values (3.8, 5.8, 7.8 and 9.8) by using HCl and NaOH 0.1 M. The initial pH of the IMD aqueous solution is 5.8.

2.4.1. Adsorption kinetics and isotherms

The experimental best conditions to carry out the sorption kinetics and sorption isotherms were established from factorial analysis and pH effect studies. The sorption analysis for both NSs were performed in aqueous solution of IMD at pH = 3.8, solid/liquid (s/l) ratio of 5, shaken at 120 rpm and at 25 °C. The sorption kinetic was performed with IMD aqueous solution of 500 mg L^{-1} and the mechanism was evaluated through modified pseudo-first order (PFO) and pseudo-second (PSO) order kinetic model, respectively

$$q_t = q_e\left(1 - e^{-k_1 t}\right) + c \tag{6}$$

$$q_t = \frac{k_2 q_e^2 t}{1 + k_2 q_e t} + c \tag{7}$$

where, q_t (mg g^{-1}) is the amount of sorbate at defined interval of times (min). k_1 (min^{-1}) and k_2 (g mg^{-1} min^{-1}) are the rate constants for PFO and PSO, respectively, and c (mg g^{-1}) is the estimated initial concentration.

The goodness of the fitting for the models was established by the coefficient of determination (R^2) and the Akaike information criterion (AIC) calculated as follows [37].

$$AIC = Nln\left(\frac{RSS}{N}\right) + 2k + \frac{2k(k+1)}{N-k-1} \quad for \quad \frac{N}{k} < 40 \tag{10}$$

where N is the number of the experimental points, *RSS* the residual sum of squares and k the number of fitted parameters.

Sorption isotherms were performed in the range of IMD concentration from 0 to 500 mg L^{-1}, for 24 h as determined from the kinetic analysis, at pH 3.8 and a solid/liquid ratio equal to 5. Albeit different models were fitted to the experimental data, the Langmuir and modified Langmuir-Henry isotherm model were used in this work due to a higher fitting ability to the experimental data

$$q_e = \frac{q_m K_L C_e}{1 + K_L C_e} \tag{11}$$

$$q_e = \frac{q_m K_L C_e}{1 + K_L C_e} + K_H C_e \tag{12}$$

where q_m (mg g^{-1}) is the maximum sorption capacity per unit weight of sorbent and K_L (L mg^{-1}) and K$_H$ (L g^{-1}) are the Langmuir and Henry constants, respectively.

Sorption kinetics and isotherm analysis relied in, at least, duplicates.

3. Results and discussion

3.1. Synthesis and characterization of amine-cyclodextrin nanosponges

As previously described, the *heptakis*-iodination at C6 position of the β-CD was carried out using I_2, DMF as solvent and Ph_3P as catalyst. The amination was performed via nucleophilic displacement of the iodine atom by the amine groups of the diamine linker. Finally, the CD-am$_6$-CD and CD-am$_{12}$-CD were synthesized via nucleophilic substitution of the iodine atoms of I-CD by the amine groups of the proper am$_x$-CDs, using a1:1 molar ratio. The synthetic sequences are schematized in Fig. 1.

The structures of β-CD, am$_{12}$, I-CD, am$_6$-CD and am$_{12}$-CD were confirmed by ^{1}H NMR and the following information was obtained: ***β*-cyclodextrin (*β*-CD)**: ^{1}H-NMR ((CD$_3$)$_2$SO): 3.29–3.41 (m, 14 H); 3.56–3.72 (m, 28 H); 4.49 (t, *J*=5.6 Hz, 7 H); 4.85 (d, *J*=3.2 Hz, 7 H); 5.75 (bs, 7 H); 5.80 (d, *J*=6.4 Hz, 7 H); **Dodecane-1,12-diamine (am$_{12}$)**: ^{1}H-NMR ((CDCl$_3$): 1.20–1.34 (m, 20 H); 1.43 (q, *J*=3.5, 4 H); 2.68 (t, *J*=3.0 Hz, 4 H); ***Heptakis*-(6-deoxy)-(6-iodo)-*β*-CD (I-CD)**: yield 3.04 g (91%); ^{1}H-NMR ((CD$_3$)$_2$SO): 3.32 (t, *J*=4.0 Hz, 7 H); 3.38–3.44 (m, 7 H); 3.44–3.53 (m, 7 H); 3.60–3.74 (m, 14 H); 3.84 (bd, *J*=4.0 Hz, 7 H); 5.02 (d, *J*=2.0 Hz, 7 H); 6.03 (bs, 7 H); 6.12 (bd, *J*=4.0 Hz, 7 H); ***Heptakis*-(6-deoxy)-[6-(6-amino-1-hexylamine)]-*β*-CD (am$_6$-CD):** yield 0.341 g (96%); ^{1}H-NMR ((CD$_3$)$_2$SO): 1.08–1.66 (m, 56 H); 2.53–2.98 (m, 42 H); 3.24–3.46 (m, 14 H); 3.56–3.83 (m, 14 H); 4.86 (bs, 7 H); and ***Heptakis*-(6-deoxy)-[6-(12-amino-1-dodecylamine)]-*β*-CD (am$_{12}$-CD):** yield 0.239 g (78%); ^{1}H-NMR ((CD$_3$)$_2$SO): 0.90–1.63 (m, 140 H); 2.51–2.79 (m, 42 H); 3.05–3.34 (m, 14 H); 3.56–3.84 (m, 14 H); 4.86 (s, 7 H); 5.77 (bs, 7 H); 5.84 (bs, 7 H).

The chemical interactions and functional groups of precursors and NSs were screened by FTIR spectroscopy. The spectra of all materials are shown in Fig. S1, whereas in Fig. 2–a and 2–b are represented the spectra of am$_6$-CD and CD-am$_6$-CD, am$_{12}$–CD and CD-am$_{12}$-CD, respectively. As expected, all spectra, with exception of that for am$_{12}$, present the typical peaks of β-CD at 3300 cm^{-1} corresponding to primary and secondary -OH groups stretching vibration. At 1640, 1150, 1080 and 1024 cm^{-1} the vibrational modes related to stretching and bending vibration of -C-O-C- and -OH groups can be observed and at 855 cm^{-1} appears the one related with the α-1→4 glycosidic bond [38–44].

In the FTIR spectrum of the dodecane-1,12-diamine, bands at 3329, 3250 and 3160 cm^{-1}, associated with the asymmetric and symmetric stretching vibration and the Fermi resonance of the aliphatic primary amine groups, can be observed; at 2917 and 2847 cm^{-1} the typical bands of the asymmetric and symmetric stretching vibrations of the methylene groups of linear chain alkanes are also observed. The medium bending and strong wagging vibration bands of -NH$_2$ are present at 1606 and 900 cm^{-1}. Weak/medium stretching bands due to -CN stretching vibrations are visible between 1100 and 1000 cm^{-1}. The strong peaks at 1462 and 720 cm^{-1} are related with scissoring and doublet rocking bands of the -CH$_2$ groups.

The per-iodination of β-CD leads to a narrower peak at 3300 cm^{-1} that can be assigned to a decrease of the -OH functional groups at C6 and, consequently, to the intermolecular hydrogen bonding. The

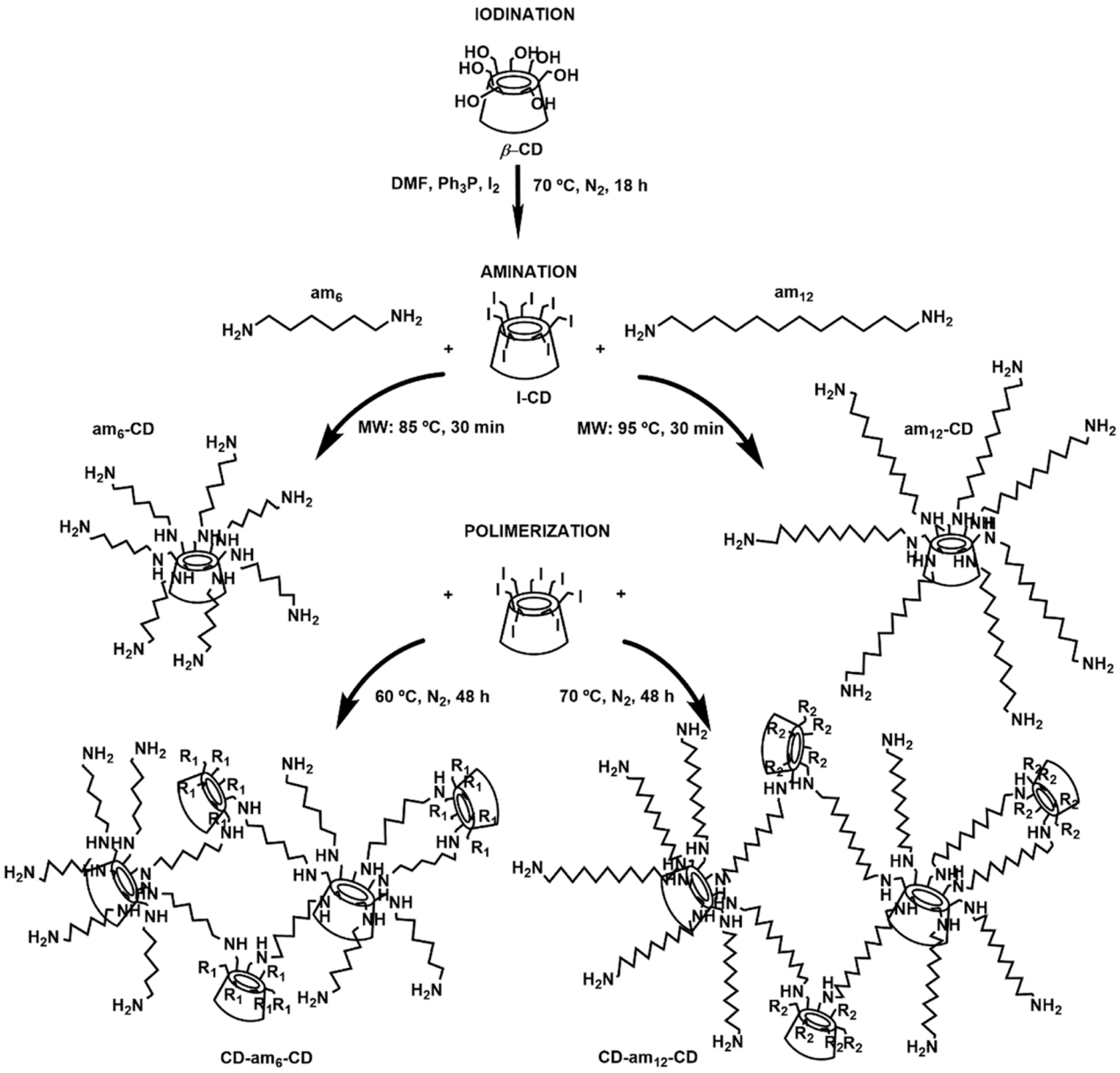

Fig. 1. Synthetic routes for amine-cyclodextrin-based nanosponges.

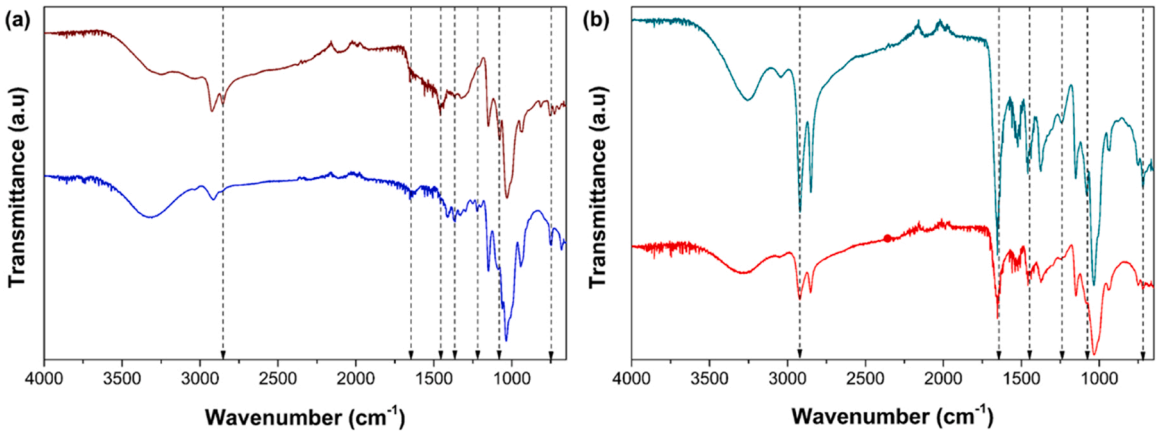

Fig. 2. FTIR spectra of (a) am_6-CD (wine), CD-am_6-CD (blue) and (b) am_{12}-CD (dark cyan), CD-am_{12}-CD (red).

Table 3
TGA and dTG data of am_x-CD and CD-am_x-CD.

	temperature range (°C)	T_{max} (°C)	weight loss (%)
am_6-CD			
	(1)	(1)	(1)
	160–275	261	23.6
	(2) 275–344	(2) 320	(2) 27.7
	(3) 344–441	(3) 395	(3) 24.0
am_{12}-CD			
	(1)	(1)	(1)
	220–315	272	25.7
	(2) 315–382	(2) 339	(2) 26.4
	(3) 382–497	(3) 435	(3) 34.1
CD-am_6-CD			
	(1)	(1)	(1)
	200–290	211	62.4
CD-am_{12}-CD			
	(1)	(1)	(1)
	229–310	226	32.2
	(2) 310–375	(2) 310	(2) 18.2
	(3) 375–465	(3) 440	(3) 14.8

presence of iodine is also confirmed by a sharp and strong band at 1150 and 755 cm^{-1} associated to CH_2-I wagging and C-I stretching vibration, respectively.

On the other hand, the amination of β-CD leads to a broader band at 3300 cm^{-1} due to contributions of the asymmetrical and symmetrical stretching vibrations of the primary and secondary amine groups, indicative of the successful substitution. am_6-CD and am_{12}-CD also show two high peaks around 2900 cm^{-1} and a peak at 1460 cm^{-1} associated to stretching and scissoring vibrations of the -CH_2- groups of the aliphatic chains. The presence of the primary and secondary amine groups is confirmed by peaks in the region 1650–1500 cm^{-1}, associated to their bending vibrations [45]. It can also be seen at 720 cm^{-1} a weak band related to -N-H wagging band. Once again, the successful of the nucleophilic substitution is confirmed by the disappearance of the -C-I peak at 755 cm^{-1}. Considering the spectra of the CD-am_6-CD [34] and CD-am_{12}-CD, a decrease of intensity of the peaks described for am_6-CD and am_{12}-CD was observed, probably due to the effect of crosslinking.

The thermal stability was determined by thermogravimetrical analysis. The thermograms of all compounds, and the corresponding dTGs, are depicted in Fig. S2. An initial weight loss is observed for all compounds in the temperature range 25–150 °C, associated with water evaporation. As described in the literature, β-CD shows a maximum

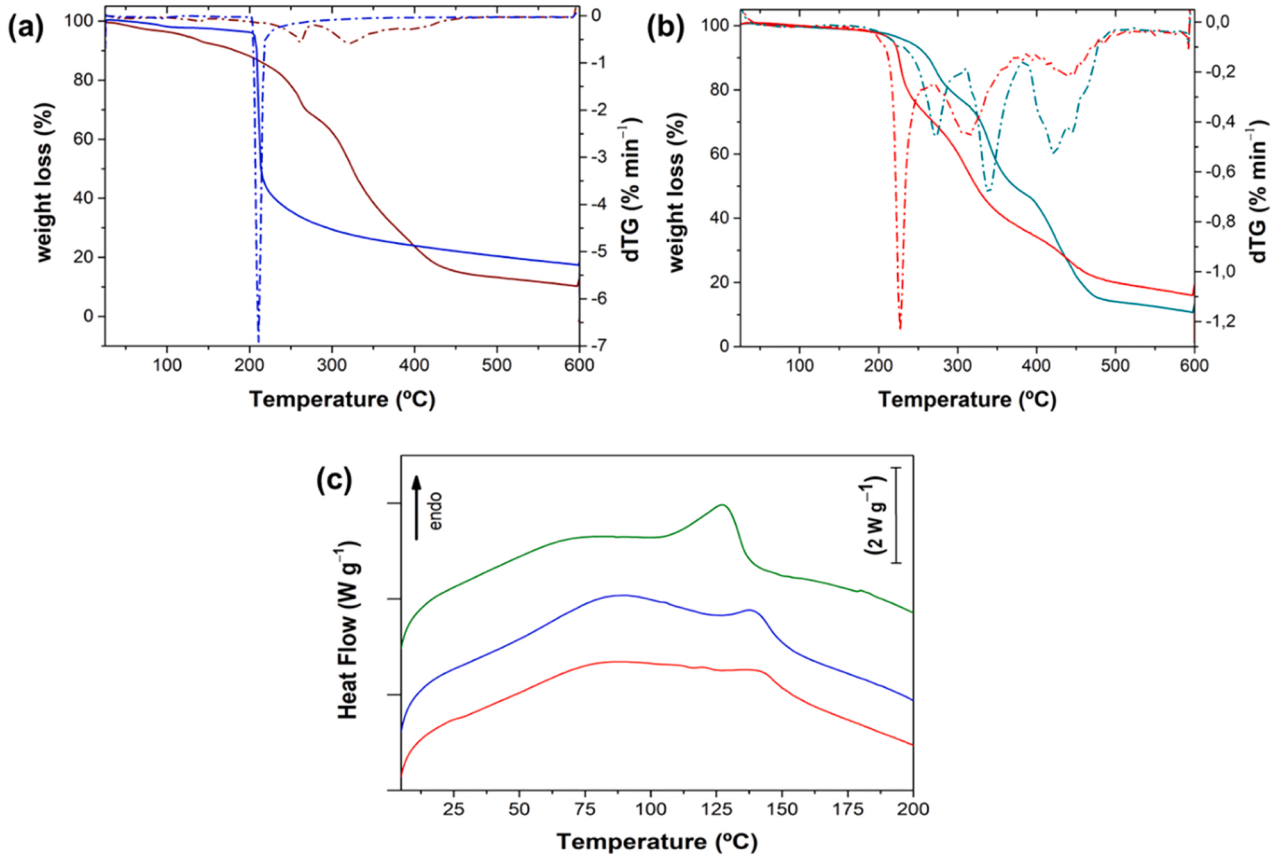

Fig. 3. TGA (solid line) and dTG (dash dot line) curves of (a) am_6-CD (wine), CD-am_6-CD (blue), (b) am_{12}-CD (dark cyan), CD-am_{12}-CD (red); (c) DSC of I-CD (green), CD-am_6-CD (blue) and CD-am_{12}-CD (red).

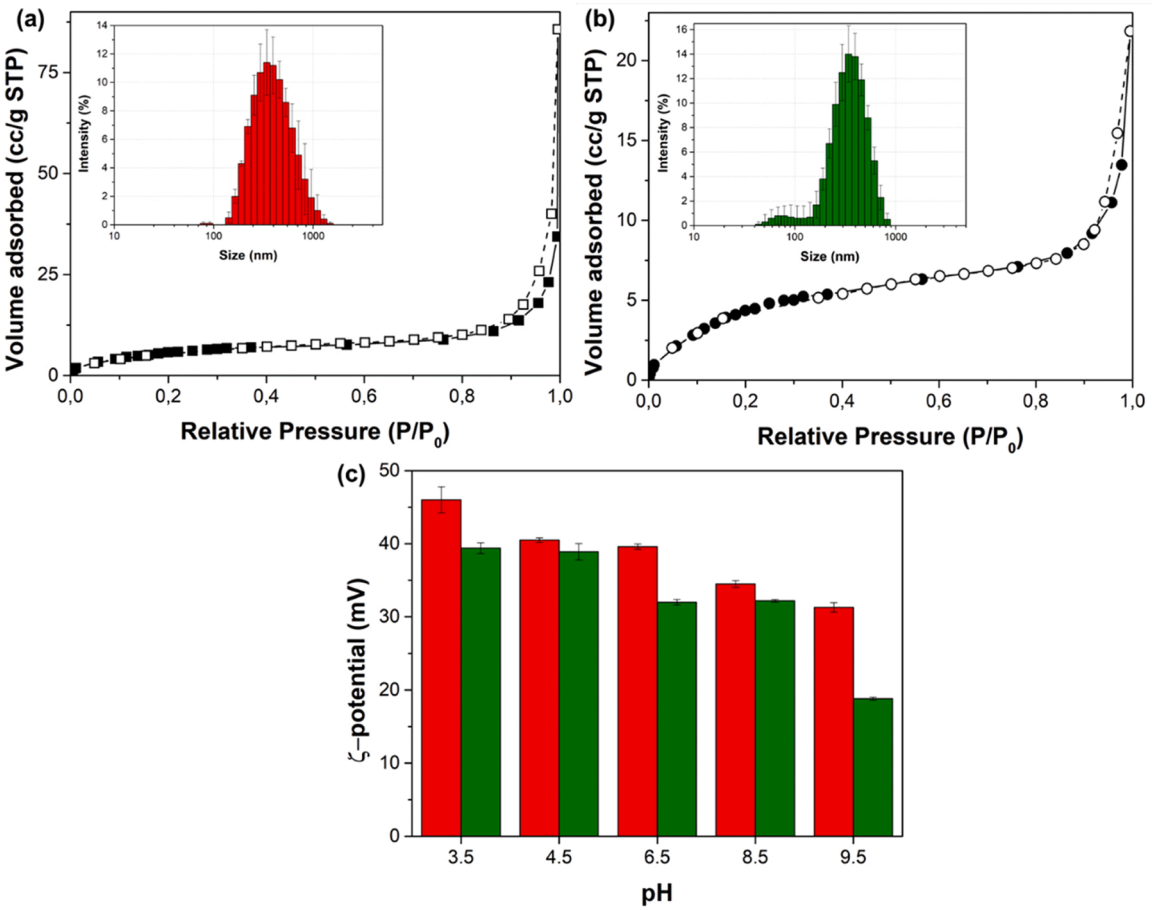

Fig. 4. N_2 adsorption-desorption isotherms of CD-am$_6$-CD (a) and CD-am$_{12}$-CD (b); effect of pH on the ζ-potential of both NSs (c). Insets show the corresponding particle size distributions.

Table 4
DLS, ζ—potential and BET parameters.

Nanosponges	Z-average (d.nm) ± std	PDI ± std	ζ—potential (mV) ± std	S_{BET} ($m^2\ g^{-1}$)	Pore volume ($cm^3\ g^{-1}$)	Pore diameter (nm)
CD-am$_6$-CD	446 ± 30	0.38 ± 0.05	41 ± 6	21.8	0.13	24.3
CD-am$_{12}$-CD	438 ± 38	0.43 ± 0.03	54 ± 7	17.9	0.03	7.5

thermal degradation rate temperature, T_{max}, at around 312 °C with a weight loss of 84% [39,46,47]. Pure am$_{12}$ exhibits a unique T_{max} at 176 °C. I-CD shows a T_{max} = 232 °C [46]. The degradation at lower temperatures, compared with β-CD suggests a weaker stability, probably due to a decrease in intra- and inter-molecular hydrogen bonding, as previously hypothesized based on the FTIR analysis. TG data of am$_6$-CD, CD-am$_6$-CD and am$_{12}$-CD, CD-am$_{12}$-CD are summarized in Table 3 and the thermograms are shown in Fig. 3–a and 3–b. Both amino-cyclodextrin derivatives present a similar thermal behavior with three degradation steps. However, am$_{12}$-CD always display higher T_{max} values, which can be explained by the longer chain length and, consequently, higher melting temperature. More in detail, $T_{max(1)}$ might be associated with a first melting process of β-CD. The $T_{max(2)}$ is associated with β-CD, while the $T_{max(3)}$ is related to the cleavage of the secondary amine bond at position C6. Herein, the shift to higher temperature can be associated with an increase in the stability, probably due to a better intermolecular alkyl chain packing.

The TGs of NSs show significant differences. In fact, it is worth noticing that for CD-am$_6$-CD, only a weight loss transition is occurring, with $T_{max(1)}$= 211 °C whereas CD-am$_{12}$-CD exhibits a thermal profile similar to that of am$_{12}$-CD. However, for both NSs, T_{max} values are lower than those observed for the respective am$_x$-CDs.

The DSC curves in Fig. 3(c) presents two endothermic events attributed to solvent loss, since no transitions were observed for these samples when analyzed by polarized light thermomicroscopy. For CD-am$_6$-CD and CD-am$_{12}$-CD the peak with a maximum at 140 °C, corresponds to the loss of solvation water from β-CD cavity [32,48]. The lower temperature value observed for I-CD suggests weaker interactions between water molecules with the β-CD cavity in this derivative.

Dynamic light scattering and ζ-potential values of the NSs at constant ionic strength are reported in Fig. 4 and Table 4.

Graphical distributions of particle size are shown as insert in Fig. 4 as well as the trend of the ζ-potential as pH function. CD-am$_6$-CD and CD-am$_{12}$-CD present a similar particles size of ca. 440 nm. After the ζ-potential analysis performed with application of 151 V, CD-am$_6$-CD undergoes negligible size variation (1.8%) while CD-am$_{12}$-CD presents a significant size variation (20.6%). This size deviation can be explained considering the higher structural flexibility and conformational organization of CD-am$_{12}$-CD due to the longer chain length of am$_{12}$. It must be stressed that this is an unexpected result taking into account ζ-potential values of (41 ± 6) mV and (54 ± 7) mV for CD-am$_6$-CD and CD-am$_{12}$-CD, respectively, which in principle are high enough to prevent

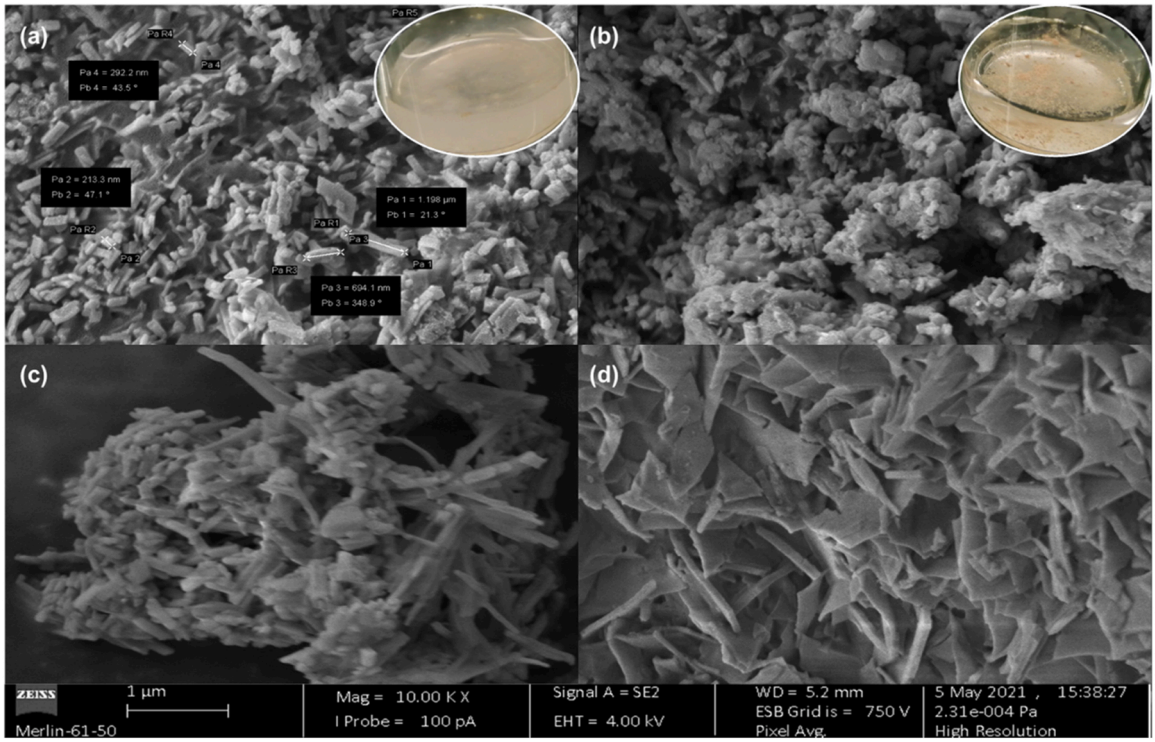

Fig. 5. SEM micrographs of CD-am$_6$-CD (a, c) and CD-am$_{12}$-CD (b, d) before (a,b) and after (c,d) immersion in an aqueous solution of IMD. Inset figures show NSs in water.

interparticle interactions (Fig. S3). Moreover, we can observe in Fig. 4–c that overall either CD-am$_6$-CD and CD-am$_{12}$-CD keep a significant positive surface charge albeit ζ-potential decreases with increase of the pH. It can be notice that the effect of the pH is higher for CD-am$_{12}$-CD probably because of the lower surface area and condensed structure which lead to low availability of the amine groups. The suggestion of higher CD-am$_{12}$-CD interparticle interactions is supported by nitrogen sorption analysis. Type-II gas sorption isotherms were obtained for both poly(aminocyclodextrins), suggesting a mesoporous structure. The slightly marked shoulder for CD-am$_{12}$-CD and particularly for CD-am$_6$-CD indicates an overlap of monolayer and multilayer gas sorption (Fig. 4). Additionally, the surface area (S_{BET}), volume and pore diameter with ca. 22 m^2 g^{-1}, 18 m^2 g^{-1} and 24 nm, 7.5 nm for CD-am$_6$-CD and CD-am$_{12}$-CD were determined, respectively, as reported in Table 4. In fact, the use of am$_6$ and am$_{12}$ promotes an anchor between CDs and thus it will be expected that am$_{12}$ will allow the occurrence of am$_{12}$-am$_{12}$ intermolecular hydrophobic interactions and, consequently, a higher packing, as observed in other systems such as gemini surfactants and CDs [49,50], bolaform surfactants and cyclodextrins [51] or chain entanglements between crosslinker chains [52]. On the other hand, the shorter spacer am$_6$ leads to a more definite CD-am$_6$-CD structure essentially dominated by CDs as it is also suggested by TG analysis. Such features are also confirmed by SEM analysis (Fig. 5).

Micrographs of pristine NSs show two different surface morphologies. For CD-am$_6$-CD (Fig. 5–a) the surface in composed by rod-like structures, some of them with more than 1 mm long. On the other hand, CD-am$_{12}$-CD (Fig. 5–b) is characterized by the occurrence of very small rod-shape and spherical structures. The former surface suggests a more diffuse, porous, surface, whilst the latter is characterized by the occurrence of a compact structure, with alveolar architecture, probably due to the reorganization of the lipophilic chain of am$_{12}$. Such an effect is also observed by the size of particles by visual observation – see inset pictures in Fig. 5(a) and 5(b).

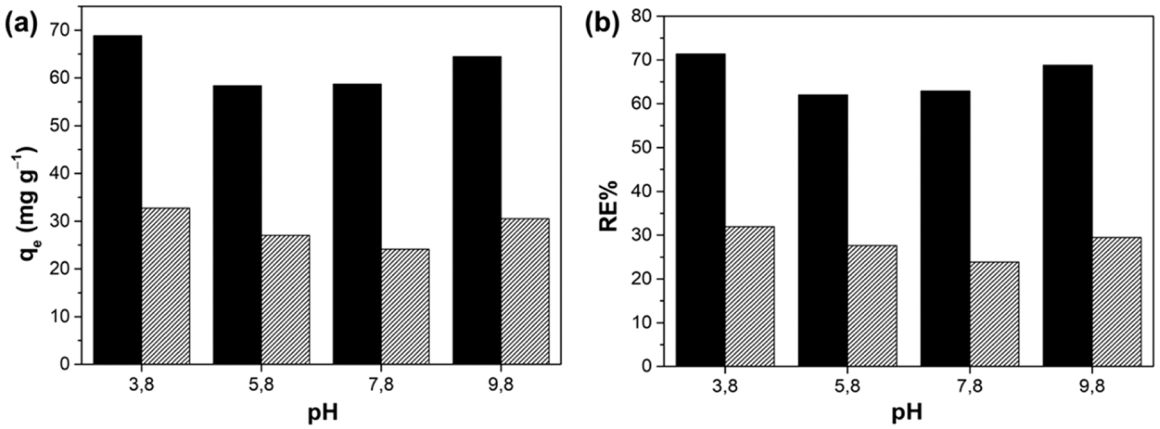

Fig. 6. Effect of pH to sorbed amount (q_e) and removal efficiency (RE %) of IMD into CD-am$_6$-CD (black columns) and CD-am$_{12}$-CD (lines).

3.2. Optimization of the sorption process

The best experimental conditions to carry out the sorption analysis were evaluated by experimental design. The matrix scheme of the experimental design, taking into account three different factors (IMD concentration, sorbent amount, volume solution) and the corresponding q_e values for both NS$_s$ are shown in table S1. The influence of those in the experimental domain can be observed substituting the obtained values of b_i in Eq. 1, obtaining the following expressions for CD-am$_6$–CD and CD-am$_{12}$-CD, respectively

$$q_e = 28.98 + 6.12X_1 - 1.37X_2 + 1.55X_3 + 0.38X_{12} - 2.21X_{13} + + 2.27X_{23} - 0.45X_{123} \quad (13)$$

$$q_e = 10.60 + 5.15X_1 - 0.86X_2 + 0.87X_3 - 0.35X_{12} + 0.01X_{13} + + 0.12X_{23} + 0.34X_{123} \quad (14)$$

The pesticide concentration and the volume of solution have positive effects; on contrary, the amount of sorbent has a negative effect on the adsorbate per gram of adsorbent. That is, lower amounts of adsorbent and higher volume solution and IMD concentration enhance the sorption of pesticide onto both NSs. The effects are more pronounced for CD-am$_6$–CD. A different perspective is offered if the interaction coefficients are considered. The combination of a higher amount of sorbent and a larger volume have a positive effect on the sorption performance. An approximate optimal ratio between sorbent amount and volume of solution was indirectly determined as s/l ratio of 5. The results of the interaction coefficients are graphically represented as 3D color map surface in Fig. S4.

Additionally, the stability of IMD in different aqueous solutions, at different pH values (3.8, 5.8, 7.8 and 9.8), was assessed and data are reported in Fig. S5. It has been found that IMD remains stable up to 7 days.

Degradation rate and the effect of pH were assessed for aqueous solution of IMD at 500 mg L^{-1} in four pH values (3.8, 5.8, 7.8 and 9.8). It has been found that IMD remains stable up to 7 days (Fig. S5).

3.3. Sorption of IMD onto CD nanosponges

Fig. 6-a and 6-b show the effect of pH on the removal efficiency and maximum removal amount of adsorbate (RE% and q_e, respectively). It can be noticed that highest sorption is achieved in acidic media (pH 3.8) due to protonation of amine groups, resulting in high positively charged surface. The presence of the abundant primary and secondary amine groups promotes sorbent-sorbate interactions by hydrogen bonding. Thus, the higher efficiency of CD-am$_6$-CD is justified by its higher active surface area, pore size and availability of functional groups as well as by its higher hydrophilicity.

Table 5
Fitting parameters of the Langmuir isotherm model for IMD sorption.

Model		CD-am$_6$-CD	CD-am$_{12}$-CD
Langmuir	q_m (mg g^{-1})	68.3 (± 4.8)	52.4 (± 12.2)
	K_L (L mg^{-1})	0.08 (± 0.02)	0.004 (± 0.002)
	R_L	0.7 – 0.02	1.0 – 0.3
	R^2	0.9502	0.9379
Langmuir-Henry	q_m (mg g^{-1})	66.6 (± 15.3)	6.6 (± 1.2)
	K_L (L mg^{-1})	0.08 (± 0.03)	0.27 (± 0.21)
	K_H (L g^{-1})	0.01 (± 0.1)	0.08 (± 0.006)
	R^2	0.9553	0.9852

From the analysis of Fig. 6, it can be concluded that CD-am$_6$-CD shows q_e and RE% values about twice those corresponding to CD-am$_{12}$-CD (a similar picture is clearly visible in the values of the independent term in Eqs. 13 and 14). That is, at pH 3.8, the maximum sorption reaches q_e values of 68.8 mg g^{-1} and 32.7 mg g^{-1} and RE% of 71.4% and 32% for CD-am$_6$-CD and CD-am$_{12}$-CD, respectively. These values show that the low porosity (Table 4) and the close-packed surface (Fig. 5-b) of CD-am$_{12}$-CD are relevant for the IMD sorption process.

The sorption mechanism was then assessed and Fig. 7 and Table 5 show the representative sorption isotherms for IMD into CD-am$_6$-CD and CD-am$_{12}$-CD and the fitting parameters of the Langmuir and Langmuir-Henry models, respectively. It must be noticed that for CD-am$_6$-CD the isotherm models are in agreement, indicating a homogeneous sorption system whereas the Langmuir-Henry model presents a higher R^2 value for CD-am$_{12}$-CD, suggesting a more heterogeneous system. We can justify the increased goodness of fit considering a high contribution of the Henry term. That consideration is in agreement with the curve shown in Fig. 7–b where we can observe a burst sorption within 0 and 25 mg L^{-1}, followed by a linear relationship q_e-C_0 between 25 and 300 mg L^{-1}. Herein, the q_e value (7 ± 1 mg g^{-1}) obtained via Lagmuir-Henry model for CD-am$_{12}$-CD represents the sorbed amount for monolayer formation at low initial sorbate concentration when the Langmuir term has higher influence. Additionally, the more concave curve for CD-am$_6$-CD indicates a more favorable process as confirmed by the higher value of K_L associated with the sorption capacity and the lower values of R_L in Table 5. Once again, CD-am$_6$-CD shows an excellent sorption capability of IMD ($q_m = 68 \pm 5$ mg g^{-1}).

As previously mentioned, the different performance of the two nanosponges can be explained by their physical properties. We suggest that the lower removal efficiency of CD-am$_{12}$-CD is due to the smaller active surface, pore volume and size as well as its lower hydrophilicity compared to CD-am$_6$-CD. These properties play a key role on the

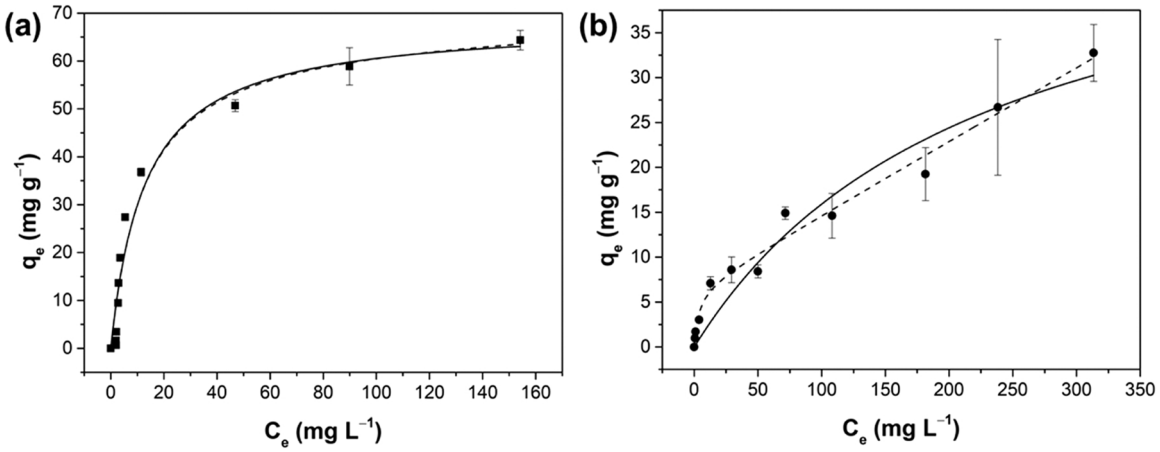

Fig. 7. Sorption isotherm of IMD into CD-am$_6$-CD (square) (a) and CD-am$_{12}$-CD (circle) (b) at 25 °C and pH 3.8. Langmuir isotherm model (solid line), Langmuir-Henry isotherm model (dash line).

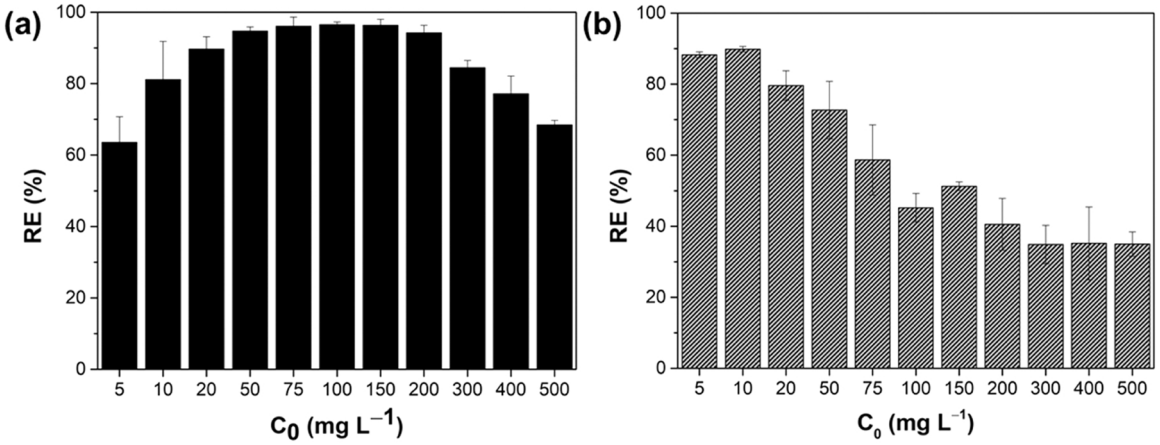

Fig. 8. Removal efficiency (RE %) of IMD by CD-am$_6$-CD (black columns) and CD-am$_{12}$-CD.

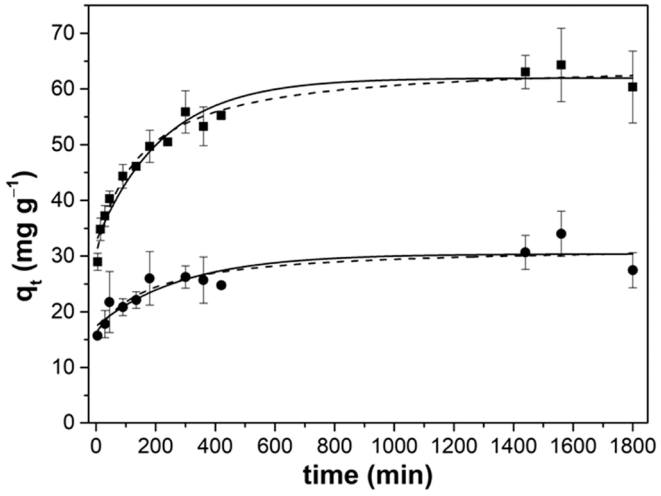

Fig. 9. Sorption kinetic of imidacloprid at 500 mg L^{-1} into CD-am$_6$-CD (square) and CD-am$_{12}$-CD (circle) at 25 °C, s/l ratio 5, pH 3.8. Fitting of PFO and PSO models are represented by solid and dashed lines, respectively.

Table 6
Fitting parameters of the pseudo-first and pseudo-second order kinetic models.

PFO parameters	CD-am$_6$-CD	CD-am$_{12}$-CD
$q_{e,\,exp}$ (mg g^{-1})	62.6 (± 5.3)	30.7 (± 3.4)
q_e (mg g^{-1})	62.0 (± 2.2)	30.4 (± 2.4)
k_1 (10^{-2} min^{-1})	26.7 (± 3.8)	20.9 (± 7.5)
R^2	0.9629	0.8396
AIC	31.9	30.1
PSO parameters	**CD-am$_6$-CD**	**CD-am$_{12}$-CD**
q_e (mg g^{-1})	64.9 (± 2.1)	31.8 (± 2.8)
k_2 (10^{-2} g mg^{-1} min^{-1})	1.2 (± 0.2)	2.1 (± 1.2)
R^2	0.9772	0.8572
AIC	25.1	28.7

sorption process, reducing the movement to the pores of adsorbent and the availability of the amine groups in the internal part of the network. This suggestion is compatible with the SEM micrographs of CD NSs in the presence of the IMD (Fig. 5); it can be seen that whilst for CD-am$_6$-CD (Fig. 5–c) the surface morphology remains similar with rod-shape structures, in the case of CD-am$_{12}$-CD a significant surface morphology modification is occurring; i.e., instead of a compact heterogeneous structure the surface shows a sheet-like morphology, resembling a supramolecular structure [53]. An interpretation for this come from the paper published by Guan et al. [54], where SEM images of sheet-like IMD structures are also showed. On the other hand, no significant morphological variations were observed for CD-am$_6$-CD (Fig. 5–c) probably due to the internal diffusion of IMD (octanol/water partition coefficient, logP 0.57) inside the structure favored by NS hydrophilicity. Consequently, we can conclude that, sorbent-sorbate interaction mainly occurs at the CD-am$_{12}$-CD outer surface.

The effect of the initial IMD concentration on the removal efficiency of nanosponges are shown in Fig. 8. It can be seen that CD-am$_6$-CD and CD-am$_{12}$-CD reach the maximum RE % value of 96.5% and 89.8% at 150 mg L^{-1} and 10 mg L^{-1} of IMD, respectively. We must also stress that CD-am$_6$-CD achieves a removal efficiency in excess of 90% in a wider range of IMD concentration (20–200 mg L^{-1}) than CD-am$_{12}$-CD, which is limited to 5 mg L^{-1} and 10 mg L^{-1}.

3.4. Sorption kinetics of IMD onto CD nanosponges

For a better understanding of the sorption mechanism and to determine the sorption efficiency of IMD into CD-am$_6$-CD and CD-am$_{12}$-CD, the sorption kinetic analysis was performed in the optimal experimental conditions. The experimental data are shown in Fig. 9 and the fitting parameters of the PFO and PSO models are reported in Table 6. For both materials, the PSO model performs a better fitting to the experimental data as confirmed by R^2 and *AIC* values. The PSO model suggests a chemisorption mechanism justified by hydrogen bonds or formation of inclusion complexes [55–57]. However, due to little difference to the goodness of fit in the case of PFO, we cannot exclude the occurrence of physisorption phenomena via electrostatic interactions. Those interactions can be explained considering the positive charges on the sorbent surface due to the presence of the amine groups and the zwitterionic character of the IMD structure. It should also be emphasized that the chain length of the linker not only can influence the physical properties but also the sorption abilities of the materials. CD-am$_6$-CD displays an IMD sorption efficiency that is twice that of CD-am$_{12}$-CD, which can be explained considering the less aggregated structure and hydrophilicity bearing a higher active surface, volume and size of the pores as indicated by BET and SEM analysis and consequent higher availability for interaction with the amine groups. Contrarily, the lipophilicity of CD-am$_{12}$-CD limits the interactions adsorbent-adsorbate on the surface of the material and the IMD internal diffusion.

4. Conclusions

The two nanosponges, CD-am$_6$-CD and CD-am$_{12}$-CD were synthesized and applied for the removal of imidacloprid. The 3D-hyperreticulated structure of the cyclodextrin-based nanosponges allows to exploit both the hydrophilic nanoporous structure and the hydrophobic cavity of the cyclodextrin, resulting in a highly efficient material. Additionally,

resorting to linkers with different chain lengths allows the modulation of physical properties which have shown to be of fundamental importance on the material performance. It was observed that hydrophobic interactions between the linker's hydrocarbon chains play an important role on the physical-chemical properties. That can be noticed in CD-am$_{12}$-CD in which significant hydrophobic interactions led to reorganization of the structure with higher tendency to aggregate and higher hydrophobicity than CD-am$_6$-CD. Furthermore, the more compact structure leads to a decrease in S_{BET}, volume and size of pores. Hence, the sorption abilities of two materials towards IMD was assessed. An initial factorial analysis and the study of the pH effect upon these two pH responsive materials, has permitted to establish the optimal experimental conditions. The sorption kinetics and isotherms were carried out at s/l ratio of 5 and pH 3.8 and both materials have shown an excellent performance with a maximum q_e of (68 ± 5) mg L^{-1} and (52 ± 12) mg L^{-1} and RE % of 96% and 90% for CD-am$_6$-CD and CD-am$_{12}$-CD, respectively. More in detail, CD-am$_6$-CD shows a high removal efficiency in a wide range of concentration, contrarily to CD-am$_{12}$-CD. Kinetic analysis suggests that both physi- and chemi-sorption contribute to the sorption process. The physical interactions sorbent-sorbate are also confirmed by the Langmuir model with monolayer formation. The lower efficiency of CD-am$_{12}$-CD is explained by the higher tendency for interparticle interaction and higher lipophilicity which limit the internal diffusion of IMD on the inner active surface, restricting the interaction to the outer surface. Contrarily, the hydrophilic behavior of CD-am$_6$-CD promotes the internal diffusion of IMD and therefore the interaction with the internal amine groups. That is compatible with the observed alteration of the sorbent morphology in the presence of IMD via SEM analysis.

CRediT authorship contribution statement

Gianluca Utzeri: Conceptualization; Methodology; Formal analysis; Investigation; Writing - Original Draft; Writing - Review & Editing. **Dina Murtinho:** Conceptualization; Methodology; Investigation; Writing - Original Draft; Writing - Review & Editing. **Teresa M.R. Maria:** Investigation; Writing - Original Draft. **Filomena Sannino:** Conceptualization, Methodology; Writing - Original Draft. **Alberto Pais:** Conceptualization; Methodology; Resources; Validation; Writing - Review & Editing. **Artur Valente:** Conceptualization, Validation, Resources, Writing - Original Draft; Writing - Review & Editing, Supervision.

Declaration of Competing Interest

The authors declare that they have no known competing financial interests or personal relationships that could have appeared to influence the work reported in this paper.

Acknowledgements

G. Utzeri thanks Fundação para a Ciência e a Tecnologia (FCT, Portugal) for PhD grant (SFR/BD/146358/2019). The Coimbra Chemistry Centre is supported by the FCT, through Projects UIDB/00313/2020 and UIDP/00313/2020.

Appendix A. Supporting information

Supplementary data associated with this article can be found in the online version at doi:10.1016/j.colsurfa.2021.128044.

References

[1] J. Szejtli, E. Bánky-Elöd, Inclusion Complexes of Unsaturated Fatty Acids with Amylose and Cyclodextrin, Starch - Stärke 27 (1975) 368–376, https://doi.org/10.1002/star.19750271104.
[2] J. Wankar, N.G. Kotla, S. Gera, S. Rasala, A. Pandit, Y.A. Rochev, Recent Advances in Host–Guest Self-Assembled Cyclodextrin Carriers: Implications for Responsive Drug Delivery and Biomedical Engineering, Adv. Funct. Mater. 30 (2020), 1909049, https://doi.org/10.1002/adfm.201909049.
[3] A.J.M. Valente, O. Söderman, The formation of host–guest complexes between surfactants and cyclodextrins, Adv. Colloid Interface Sci. 205 (2014) 156–176, https://doi.org/10.1016/j.cis.2013.08.001.
[4] G. Crini, Review: A History of Cyclodextrins, Chem. Rev. 114 (2014) 10940–10975, https://doi.org/10.1021/cr500081p.
[5] G. Crini, S. Fourmentin, É. Fenyvesi, G. Torri, M. Fourmentin, N. Morin-Crini, Cyclodextrins, from molecules to applications, Environ. Chem. Lett. 16 (2018) 1361–1375, https://doi.org/10.1007/s10311-018-0763-2.
[6] P. Saokham, C. Muankaew, P. Jansook, T. Loftsson, Solubility of Cyclodextrins and Drug/Cyclodextrin Complexes, Molecules 23 (2018) 1161, https://doi.org/10.3390/molecules23051161.
[7] T.F. Cova, D. Murtinho, A.A.C.C. Pais, A.J.M. Valente, Combining Cellulose and Cyclodextrins: Fascinating Designs for Materials and Pharmaceutics, Front. Chem. 6 (2018), https://doi.org/10.3389/fchem.2018.00271.
[8] A.P. Sherje, B.R. Dravyakar, D. Kadam, M. Jadhav, Cyclodextrin-based nanosponges: A critical review, Carbohydr. Polym. 173 (2017) 37–49, https://doi.org/10.1016/j.carbpol.2017.05.086.
[9] T.F.G.G. Cova, D. Murtinho, A.A.C.C. Pais, A.J.M. Valente, Cyclodextrin-based Materials for Removing Micropollutants From Wastewater, Curr. Org. Chem. 22 (2018) 2150–2181, https://doi.org/10.2174/1385272822666181019125315.
[10] C. Zou, P. Zhao, J. Ge, Y. Lei, P. Luo, β-Cyclodextrin modified anionic and cationic acrylamide polymers for enhancing oil recovery, Carbohydr. Polym. 87 (2012) 607–613, https://doi.org/10.1016/j.carbpol.2011.08.031.
[11] S. Lin, C. Zou, H. Liang, H. Peng, Y. Liao, The effective removal of nickel ions from aqueous solution onto magnetic multi-walled carbon nanotubes modified by β-cyclodextrin, Colloids Surf. A Physicochem. Eng. Asp. 619 (2021), 126544, https://doi.org/10.1016/j.colsurfa.2021.126544.
[12] D. McNaught, A. Wilkinson, pesticide, in: IUPAC Compend. Chem. Terminol., 2nd ed..,, IUPAC, Research Triagle Park, NC, 1997, p. 4519, https://doi.org/10.1351/goldbook.P04519.
[13] A.E. Akay Demir, F.B. Dilek, U. Yetis, A new screening index for pesticides leachability to groundwater, J. Environ. Manag. 231 (2019) 1193–1202, https://doi.org/10.1016/j.jenvman.2018.11.007.
[14] D. Pimentel, Amounts of pesticides reaching target pests: Environmental impacts and ethics, J. Agric. Environ. Ethics 8 (1995) 17–29, https://doi.org/10.1007/BF02286399.
[15] V. Silva, H.G.J. Mol, P. Zomer, M. Tienstra, C.J. Ritsema, V. Geissen, Pesticide residues in European agricultural soils – A hidden reality unfolded, Sci. Total Environ. 653 (2019) 1532–1545, https://doi.org/10.1016/j.scitotenv.2018.10.441.
[16] G. Utzeri, L.M.P. Verissimo, A.C.F. Ribeiro, A.J.M. Valente, Pesticides and their environment and health impact: an approach to remediation using hydrogels, in: O.V. Haghi, A.K. Faria Ribeiro, A.C. Pogliani, L. Balkose, D. Torrens, F. Mukbaniani (Eds.), Opt. Mol. PHYSICS. Theorecital Princ. Exp. Methods, Apple Academic Press, Inc./CRC, New Jersey, 2018, p. 514.
[17] J.E. Casida, R.J. Bryant, The ABCs of pesticide toxicology: Amounts, biology, and chemistry, Toxicol. Res. (Camb.). 6 (2017) 755–763, https://doi.org/10.1039/c7tx00198c.
[18] A.R. Khan, P. Forgo, K.J. Stine, V.T. D'Souza, Methods for Selective Modifications of Cyclodextrins, Chem. Rev. 98 (1998) 1977–1996, https://doi.org/10.1021/cr970012b.
[19] J. Tang, W. Tang, Modification of Cyclodextrin, in: W. Tang, S.-C. Ng, D. Sun (Eds.), Modif. Cyclodextrins Chiral Sep., Springer Berlin Heidelberg, Berlin, Heidelberg, 2013, pp. 1–25, https://doi.org/10.1007/978-3-642-37648-1_1.
[20] M.T. Sikder, M.M. Rahman, M. Jakariya, T. Hosokawa, M. Kurasaki, T. Saito, Remediation of water pollution with native cyclodextrins and modified cyclodextrins: A comparative overview and perspectives, Chem. Eng. J. 355 (2019) 920–941, https://doi.org/10.1016/j.cej.2018.08.218.
[21] W. Tang, C. Zou, C. Da, Y. Cao, H. Peng, A review on the recent development of cyclodextrin-based materials used in oilfield applications, Carbohydr. Polym. 240 (2020), 116321, https://doi.org/10.1016/j.carbpol.2020.116321.
[22] B. Tian, S. Hua, Y. Tian, J. Liu, Cyclodextrin-based adsorbents for the removal of pollutants from wastewater: a review, Environ. Sci. Pollut. Res. (2020), https://doi.org/10.1007/s11356-020-11168-2.
[23] A. Singh, A.K. Kar, D. Singh, R. Verma, N. Shraogi, A. Zehra, et al., pH-responsive eco-friendly chitosan modified cenosphere/alginate composite hydrogel beads as carrier for controlled release of Imidacloprid towards sustainable pest control, Chem. Eng. J. 427 (2022), 131215, https://doi.org/10.1016/j.cej.2021.131215.
[24] L. Wang, T. Liu, F. Liu, J. Zhang, Y. Wu, H. Sun, Occurrence and Profile Characteristics of the Pesticide Imidacloprid, Preservative Parabens, and Their Metabolites in Human Urine from Rural and Urban China, Environ. Sci. Technol. 49 (2015) 14633–14640, https://doi.org/10.1021/acs.est.5b04037.
[25] M. Wang, G. Li, C. Xia, X. Jing, R. Wang, Q. Liu, et al., Facile preparation of cyclodextrin polymer materials with rigid spherical structure and flexible network for sorption of organic contaminants in water, Chem. Eng. J. 411 (2021), 128489, https://doi.org/10.1016/j.cej.2021.128489.
[26] H. Liu, X. Cai, Y. Wang, J. Chen, Adsorption mechanism-based screening of cyclodextrin polymers for adsorption and separation of pesticides from water, Water Res 45 (2011) 3499–3511, https://doi.org/10.1016/j.watres.2011.04.004.
[27] J.M. Anne, Y.H. Boon, B. Saad, M. Miskam, M.M. Yusoff, M.S. Shahriman, et al., β-Cyclodextrin conjugated bifunctional isocyanate linker polymer for enhanced

removal of 2,4-dinitrophenol from environmental waters, R. Soc. Open Sci. 5 (2018), 180942, https://doi.org/10.1098/rsos.180942.
[28] Y. Lee, A. Singh, Poly-β-Cyclodextrins: Multifunctional Polymer Support for the Hydrolysis and Removal of Methyl Parathion, Mater. Res. Soc. Symp. - Proc. (2003) 99–104, https://doi.org/10.1557/proc-774-o7.32.
[29] J. Junthip, Water-insoluble cyclodextrin polymer crosslinked with citric acid for paraquat removal from water, J. Macromol. Sci. Part A. 56 (2019) 555–563, https://doi.org/10.1080/10601325.2019.1586444.
[30] T. Yu, Z. Xue, X. Zhao, W. Chen, T. Mu, Green synthesis of porous β-cyclodextrin polymers for rapid and efficient removal of organic pollutants and heavy metal ions from water, N. J. Chem. 42 (2018) 16154–16161, https://doi.org/10.1039/C8NJ03438A.
[31] S. Salazar, N. Yutronic, P. Jara, Magnetic β-Cyclodextrin Nanosponges for Potential Application in the Removal of the Neonicotinoid Dinotefuran from Wastewater, Int. J. Mol. Sci. 21 (2020) 4079, https://doi.org/10.3390/ijms21114079.
[32] V. Rizzi, J. Gubitosa, R. Signorile, P. Fini, C. Cecone, A. Matencio, et al., Cyclodextrin nanosponges as adsorbent material to remove hazardous pollutants from water: The case of ciprofloxacin, Chem. Eng. J. 411 (2021), 128514, https://doi.org/10.1016/j.cej.2021.128514.
[33] P.R. Ashton, R. Königer, J.F. Stoddart, D. Alker, V.D. Harding, Amino Acid Derivatives of β-Cyclodextrin, J. Org. Chem. 61 (1996) 903–908, https://doi.org/10.1021/jo951396d.
[34] M. Russo, M.L. Saladino, D. Chillura Martino, P. Lo Meo, R. Noto, Polyaminocyclodextrin nanosponges: synthesis, characterization and pH-responsive sequestration abilities, RSC Adv. 6 (2016) 49941–49953, https://doi.org/10.1039/C6RA06417E.
[35] A. Puglisi, J. Spencer, J. Clarke, J. Milton, Microwave-assisted synthesis of 6-amino-β-cyclodextrins, J. Incl. Phenom. Macrocycl. Chem. 73 (2012) 475–478, https://doi.org/10.1007/s10847-011-0054-z.
[36] G. Utzeri, L. Verissimo, D. Murtinho, A.A.C.C. Pais, F.X. Perrin, F. Ziarelli, et al., Poly(β-cyclodextrin)-Activated Carbon Gel Composites for Removal of Pesticides from Water, Molecules 26 (2021) 1426, https://doi.org/10.3390/molecules26051426.
[37] F.A.A. Kingdom, N. Prins, Model Comparisons, in: F.A.A. Kingdom, N. Prins (Eds.), Psychophysics, second, Elsevier, 2016, pp. 247–307, https://doi.org/10.1016/B978-0-12-407156-8.00009-8.
[38] V.S. Ghorpade, A.V. Yadav, R.J. Dias, Citric acid crosslinked β -cyclodextrin/carboxymethylcellulose hydrogel films for controlled delivery of poorly soluble drugs, Carbohydr. Polym. 164 (2017) 339–348, https://doi.org/10.1016/j.carbpol.2017.02.005.
[39] R.L. Abarca, F.J. Rodríguez, A. Guarda, M.J. Galotto, J.E. Bruna, Characterization of beta-cyclodextrin inclusion complexes containing an essential oil component, Food Chem. 196 (2016) 968–975, https://doi.org/10.1016/j.foodchem.2015.10.023.
[40] Z. Jin, Cyclodextrin Chemistry, WORLD SCIENTIFIC, CHEMICAL INDUSTRY PRESS,, CHINA, 2013, https://doi.org/10.1142/8630.
[41] N.V. Roik, L.A. Belyakova, Thermodynamic, IR spectral and X-ray diffraction studies of the "β-cyclodextrin-para-aminobenzoic acid" inclusion complex, J. Incl. Phenom. Macrocycl. Chem. 69 (2011) 315–319, https://doi.org/10.1007/s10847-010-9737-0.
[42] Z. Fallah, H.N. Isfahani, M. Tajbakhsh, Cyclodextrin-triazole-titanium based nanocomposite: Preparation, characterization and adsorption behavior investigation, Process Saf. Environ. Prot. 124 (2019) 251–265, https://doi.org/10.1016/j.psep.2019.02.016.
[43] J. Pellicer, M. Rodríguez-López, M. Fortea, C. Lucas-Abellán, M. Mercader-Ros, S. López-Miranda, et al., Adsorption Properties of β- and Hydroxypropyl-β-Cyclodextrins Cross-Linked with Epichlorohydrin in Aqueous Solution. A Sustainable Recycling Strategy in Textile Dyeing Process, in: Polymers, 11, Basel,, 2019, p. 252, https://doi.org/10.3390/polym11020252.
[44] Z. Zhou, F. Guo, N. Wang, M. Meng, G. Li, Dual pH-sensitive supramolecular micelles from star-shaped PDMAEMA based on β-cyclodextrin for drug release, Int. J. Biol. Macromol. 116 (2018) 911–919, https://doi.org/10.1016/j.ijbiomac.2018.05.092.
[45] R.M. Silverstein, F.X. Webster, D.J. Kiemle, Infrared Spectrometry, in: D. Brennan, J. Yee, S. Wolfman-Robichaud (Eds.), Spectrom. Identif. Org. Compd., seventh.,, John Wiley & Sons, Inc, 2005, pp. 72–126.
[46] F. Trotta, M. Zanetti, G. Camino, Thermal degradation of cyclodextrins, Polym. Degrad. Stab. 69 (2000) 373–379, https://doi.org/10.1016/S0141-3910(00)00084-7.
[47] A.P. Gerola, D.C. Silva, S. Jesus, R.A. Carvalho, A.F. Rubira, E.C. Muniz, et al., Synthesis and controlled curcumin supramolecular complex release from pH-sensitive modified gum-arabic-based hydrogels, RSC Adv. 5 (2015) 94519–94533, https://doi.org/10.1039/C5RA14331D.
[48] L.M.A. Pinto, L.F. Fraceto, M.H.A. Santana, T.A. Pertinhez, S.O. Junior, E. de Paula, Physico-chemical characterization of benzocaine-β-cyclodextrin inclusion complexes, J. Pharm. Biomed. Anal. 39 (2005) 956–963, https://doi.org/10.1016/j.jpba.2005.06.010.
[49] R.A. Carvalho, H.A. Correia, A.J.M. Valente, O. Söderman, M. Nilsson, The effect of the head-group spacer length of 12-s-12 gemini surfactants in the host-guest association with β-cyclodextrin, J. Colloid Interface Sci. 354 (2011) 725–732, https://doi.org/10.1016/j.jcis.2010.11.024.
[50] M. Nilsson, C. Cabaleiro-Lago, A.J.M. Valente, O. Söderman, Interactions between Gemini Surfactants, 12- s -12, and β-cyclodextrin As Investigated by NMR Diffusometry and Electric Conductometry, Langmuir 22 (2006) 8663–8669, https://doi.org/10.1021/la061220e.
[51] M. Nilsson, A.J.M. Valente, G. Olofsson, O. Söderman, M. Bonini, Thermodynamic and Kinetic Characterization of Host−Guest Association between Bolaform Surfactants and α- and β-Cyclodextrins, J. Phys. Chem. B. 112 (2008) 11310–11316, https://doi.org/10.1021/jp802963x.
[52] M. Arslan, R. Sanyal, A. Sanyal, Cyclodextrin embedded covalently crosslinked networks: synthesis and applications of hydrogels with nano-containers, Polym. Chem. 11 (2020) 615–629, https://doi.org/10.1039/C9PY01679A.
[53] R.F.P.R.F.P. Pereira, A.J.M.A.J.M. Valente, H.D.H.D. Burrows, V. De Zea Bermudez, R.A.R. a Carvalho, R. a E.R.A.E. Castro, Structural characterization of solid trivalent metal dodecyl sulfates: from aqueous solution to lamellar superstructures, RSC Adv. 3 (2013) 1420, https://doi.org/10.1039/c2ra21906a.
[54] H. Guan, D. Chi, J. Yu, X. Li, A novel photodegradable insecticide: Preparation, characterization and properties evaluation of nano-Imidacloprid, Pestic. Biochem. Physiol. 92 (2008) 83–91, https://doi.org/10.1016/j.pestbp.2008.06.008.
[55] Y. Liu, X. Liu, W. Dong, L. Zhang, Q. Kong, W. Wang, Efficient Adsorption of Sulfamethazine onto Modified Activated Carbon: A Plausible Adsorption Mechanism, Sci. Rep. 7 (2017) 12437, https://doi.org/10.1038/s41598-017-12805-6.
[56] N. Neghi, M. Kumar, D. Burkhalov, Synthesis and application of stable, reusable TiO2 polymeric composites for photocatalytic removal of metronidazole: Removal kinetics and density functional analysis, Chem. Eng. J. 359 (2019) 963–975, https://doi.org/10.1016/j.cej.2018.11.090.
[57] L. Zhou, Z. Xu, K. Yi, Q. Huang, K. Chai, Z. Tong, et al., Efficient remediation of 2,4-dichlorophenol from aqueous solution using β-cyclodextrin-based submicron polymeric particles, Chem. Eng. J. 360 (2019) 531–541, https://doi.org/10.1016/j.cej.2018.11.196.

Synthesis of β-cyclodextrin-based nanosponges for remediation of 2,4-D polluted waters

VI

Artur J.M Valente, Domenico Pirozzi, Alessia Cinquegrana, Gianluca Utzeri, Dina Murtinho, Filomena Sannino

Environmental Research, vol. 215 (2022) 114214

Environmental Research 215 (2022) 114214

Contents lists available at ScienceDirect

Environmental Research

journal homepage: www.elsevier.com/locate/envres

Synthesis of β-cyclodextrin-based nanosponges for remediation of 2,4-D polluted waters

Artur J.M. Valente [a], Domenico Pirozzi [b], Alessia Cinquegrana [c], Gianluca Utzeri [a], Dina Murtinho [a], Filomena Sannino [c,*]

[a] University of Coimbra, Department of Chemistry, CQC, 3004-535 Coimbra, Portugal
[b] University of Naples "Federico II", Department of Chemical Engineering, Materials and Industrial Production (DICMaPI), Laboratory of Biochemical Engineering, Piazzale Tecchio, 80, 80125, Naples, Italy
[c] University of Naples "Federico II", Department of Agricultural Sciences, Via Università 100, 80055 Portici, Naples, Italy

ARTICLE INFO

Keywords:
Wastewater remediation
2,4-D removal
Agrochemicals
β-Cyclodextrin-based nanosponges
Effect of crosslinkers
Sustainable regeneration

ABSTRACT

Two cyclodextrin-based nanosponges (CD-NSs) were synthesized using diamines with 6 and 12 methylene groups, CDHD6 and CDHD12, respectively, and used as adsorbents to remove 2,4-D from aqueous solutions. The physico-chemical characterization of the CD−NSs demonstrated that, when using the linker with the longest chain length, the nanosponges show a more compact structure and higher thermal stability, probably due to hydrophobic interactions. SEM micrographs showed significant differences between the two nanosponges used.

The adsorption of 2,4-D was assessed in terms of different parameters, including solid/liquid ratio, pH, kinetics and isotherms. Adsorption occurred preferentially at lower pH values and for short-chain crosslinked nanosponges; while the former is explained by the balance of acid-base characteristics of the adsorbent and adsorbate, the latter can be justified by the increase in the crosslinker-crosslinker interactions, predominantly hydrophobic, rather than adsorbent-adsorbate interactions. The maximum adsorption capacity at the equilibrium (q_e) was 20,903 mmol/kg, obtained using CDHD12 with an initial 2,4-D concentration of 2 mmol/L. An environmentally friendly strategy, based on alkali desorption, was developed to recycle and reuse the adsorbents. On the basis of the results obtained, cyclodextrin-based nanosponges appear promising materials for an economically feasible removal of phenoxy herbicides, to be used as potential adsorbents for the sustainable management of agricultural wastewaters.

1. Introduction

The use of agrochemicals can be responsible of a number of diseases as a consequence of their carcinogenic, mutagenic and teratogenic effects (Srivastava et al., 2009). Additionally, their mobility and persistence in water bodies and soils lead to harmful consequences not only for the environment but also for the food chain (Derylo-Marczewska et al., 2010). The (2,4-dichlorophenoxy)acetic acid ($Cl_2C_6H_3OCH_2COOH$, 2,4-D), is a herbicide widely used around the world due to its effectiveness in eliminating broadleaf weeds in a wide variety of crops, including rice, soybean and wheat. However, according to WHO, this herbicide is toxic and highly persistent, in particular in its salt and acid forms (Tayeb et al., 2010; Jaafarzadeh et al., 2017). Thus, it is not surprising that 2,4-D is one of the most studied pollutants and its removal from effluents and soil is of paramount importance.

Nowadays, significant efforts are made to develop new and effective methods, targeting recalcitrant and priority pollutants, for remediation of water and soils. Those methods should have advantages over conventional ones, such as advanced oxidative processes and photocatalysis (Peziak-Kowalska et al., 2019), in addition to low cost, absence of by-products and intermediates and high removal efficiency, among others.

The adsorption processes, depending on the adsorbent materials, have paired these advantages. So far, many different adsorbent materials such as clays (Cornejo et al., 2008; Biswas et al., 2020; Mahy et al., 2022), mesoporous metal oxides (Addorisio et al., 2010), zeolites (Andrunik and Bajda, 2021), activated carbon Derylo-Marczewska et al. (2010); Blachnio et al. (2020) and biopolymers (Wang and Zhao, 2013; Russo et al., 2021; Yaashikaa et al., 2022) have been commonly used for the removal of environmental contaminants.

* Corresponding author. University of Naples "Federico II", Department of Agricultural Sciences, Via Università 100, 80055 Portici, Naples, Italy.
E-mail address: fsannino@unina.it (F. Sannino).

https://doi.org/10.1016/j.envres.2022.114214
Received 8 June 2022; Received in revised form 5 August 2022; Accepted 23 August 2022
Available online 1 September 2022

Among those adsorbents, the use of environmentally friendly bio-based materials is increasingly a priority. Consequently, it is expected that polysaccharides are among the most immediate choices for adsorption processes, due to their natural origin, abundance, renewability, price and, most important, the absence of toxicity (Thakur et al., 2019; Sharma et al., 2018). From the chemical point of view, polysaccharides are also quite attractive, since the presence of reactive groups such as $–NH_2$, –OH and –COOH on the surface of polysaccharides allows for notable selective interactions, as well as their easy modification in order to improve adsorption efficiency.

Taking that into consideration, cyclodextrins have been used to synthesise different adsorbents either by functionalization of (bio) polymers or by polymerization of the cyclodextrins themselves (Morin-Crini et al., 2018), due to their excellent sequestering ability for amphiphilic molecules, including agrochemicals (Waris et al., 2021; Utzeri et al., 2021). Cyclodextrins (CDs) are well-known cyclic oligosaccharides, the most common being those with 6–8 glucopyranose units. The abundance of hydroxyl groups makes their outer face highly hydrophilic. However, their ability to form supramolecular host-guest inclusion compounds is justified by its hydrophobic cavity (Gao et al., 2005). Those complexes contain lipophilic cavities in which the guest molecules are well retained if their size fits with that of the CD molecule. The cavities provide a good microenvironment for guest molecules, especially if the latter are hydrophobic, forming highly stable host–guest complexes (Wankar et al., 2020; Valente and Söderman, 2014) which significantly change the guest properties. As a consequence, the range of applications is wide, covering areas as diverse as pharmaceuticals (Loftsson and Brewster, 2010), water remediation (Cova et al., 2018) and food technology (Tian et al., 2020).

The properties of cyclodextrins allow the development of innovative materials such as NanoSponges(NSs), versatile supramolecular 3D–hyperreticulated materials, with high surface area and thermal stability, and extraordinary ability to adsorb compounds with different degrees of hydrophilicity/hydrophobicity (Utzeri et al., 2022a), including agrochemicals (Salazar et al., 2018, 2020).

This work describes the synthesis of oligosaccharide-based nanosponges, using diamines with different chain lengths as crosslinkers, and their performance on the adsorption of 2,4-D. Optimal adsorption conditions were evaluated and justified based on the physicochemical and surface features of the nanosponges.

2. Materials and methods

2.1. Materials

β–Cyclodextrin (purity >98%), hexane-1,6-diamine and dodecane-1,12-diamine (both with purity higher than 98%), (2,4-dichlorophenoxy)acetic acid (99.0% purity) and acetonitrile (HPLC grade) were purchased from Sigma-Aldrich. Triphenylphosphine (Ph_3P) was obtained from Alpha-Aesar and iodine was supplied from PanReac. *N,N*-dimethylformamide (purity ≥99.8%, CAS 68–12–2) and methanol (MeOH) were supplied from Honeywell and Chem-Lab, respectively.

2.2. Synthesis of nanosponges

Amine-nanosponges were synthesized using a three-step route as described below: initially, Ph_3P and I_2, 30 mmol each, were dissolved in DMF (30 mL); after that 2 mmol of β-cyclodextrin were added and the mixture was kept under stirring overnight, under N_2 atmosphere, at 70 °C. The obtained solution of *heptakis*–(6–iodo)–(6–deoxy)–β–cyclodextrin was then concentrated by solvent removal and sodium methoxide (3 M, 12 mL) was added under cooling and stirring. The product was precipitated in an excess of methanol followed by filtration. The purification was performed by Soxhlet extraction with MeOH until no more discoloration of the product was observed.

The synthesis of the heptakis–(6–amine)–(6–deoxy)–β–cyclodextrins with HD6 or HD12 was carried out by nucleophilic substitution of the iodine groups in β-cyclodextrin C-6 carbon. The synthesis was performed with an excess of the diamine monomer, which was mixed with the *heptakis*–(6–iodo)–(6–deoxy)–*β*–cyclodextrin. This synthetic step was improved by the use of a microwave-assisted process (CEM Discover microwave). The advantage was the drastic reduction of time consuming from 48 h to 30 min at 85 °C for HD6 and 45 min at 95 °C for HD12 functionalized cyclodextrins. After that, 10 mL of methanol were added and the solution was added dropwise in an excess of cold diethyl ether in order to precipitate. Several cycles of dissolution in MeOH (10 mL) and precipitation in diethyl ether (200 mL) were carried out. The final pale-yellow products were collected by centrifugation (Utzeri et al., 2022a).

The final step consists in the reaction of heptakis–(6–amine)–(6–deoxy)–β–cyclodextrin with *heptakis*–(6–iodo)–(6–deoxy)–*β*–cyclodextrin (1:1) achieving the amine-*β*-cyclodextrin nanosponges. The two CD derivatives were mechanically mixed, and a minimum amount of DMSO was added as media. The polymers CDHD6 and CDHD12 mixtures were heated at ca. 60 °C for 48 h. The obtained brown gum product was poured into water and mechanically smashed. Next, the nanosponge is separated from water by centrifugation and washed 3 times with MeOH with sonication (10 min) and finally washed with diethyl ether. A pale-brown product was collected by centrifugation for both NSs (Russo et al., 2016) (Utzeri et al., 2022b) (Scheme 1).

2.3. Physico–chemical characterization of the CD-NSs

The chemical structures of CDHD6 and CDHD12 were characterized by infrared spectroscopy (FTIR) in the wavelength range of 4000 to 400 cm^{-1}. KBr was used as reference and pellets at 2% were used for the NSs.

Thermograms of CDHD6 and CDHD12 samples (ca. 3–5 mg) were obtained in a TG209–F3 Tarsus, from Netzsch Instruments, using a heating rate of 5 K/min and a 50 mL/min N_2 flow rate.

The specific surface area (S_{BET}) of the CDHD6 and CDHD12 was determined by N_2 adsorption using a ASAP 2000 from *Micrometrics*, and the pore size was computed by using the BET model.

Dynamic light scattering and *ζ*–potential were performed in a *Malvern Zetasizer NanoZS*. For the DLS measurements a neon-laser at scattering angle of 173° was used. The hydrodynamic diameter (Z-average) and the polydispersity index (PDI) were determined from the intensity distribution obtained by cumulant analysis. The reported values are an average of, at least, three independent measurements, carried out at 25 °C.

The morphology of the NSs before and after contact with aqueous solutions of 2,4-D was evaluated by Scanning Electron Microscopy (SEM). The images were acquired with FEI Inspect S, Hillsboro, Oregon, United States of America, in the range between 15.00 and 25.00 kV and at 24,000-25000 x of magnification.

2.4. Analytical determination

An Agilent 1200 Series HPLC apparatus (Wilmington U.S.), equipped with a DAD, a ChemStation Agilent Software, and a Macharey-Nagel Nucleosil 100−5C18 column (stainless steel 250 × 4 mm) was used to evaluate the concentration of 2,4-D in solution. A binary system of 40:60 acetonitrile:phosphate buffer (0.1%, pH 2.95), used as mobile phase, was pumped at 1.2 mL/min flow in isocratic mode.

The detector was set at 283 nm. The injection volume was 20 μL. The quantitative determination was performed using a calibration curve obtained with concentrations of 2,4-D ranging from 0.01 to 2.0 mmol/L (Sannino et al., 2015).

2,4-D concentration in solution was analyzed with an Agilent 1200 Series HPLC apparatus (Wilmington U.S.), equipped with a DAD and a ChemStation Agilent Software. A Macharey-Nagel Nucleosil 100−5C18 column (stainless steel 250 × 4 mm) was used. The mobile phase composed of a binary system of 40:60 acetonitrile: phosphate buffer

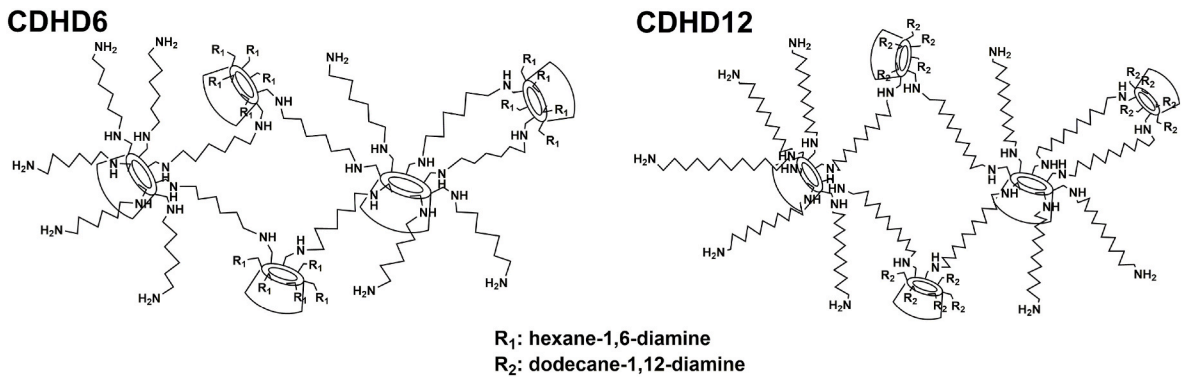

Scheme 1. Representation of the theoretical molecular structure of the CDHD6 and CDHD12.

(0.1%, pH 2.95) was pumped at 1.2 mL/min flow in isocratic mode. The detector was set at 283 nm. The injection volume was 20 μL. The quantitative determination was performed using a calibration curve. The following concentration ranges were adopted 0.01–2.0 mmol/L (Sannino et al., 2015).

2.5. Adsorption experiments

In each test, 221 mg of herbicide were dissolved in 500 mL of Milli-Q ultrapure water thus obtaining a stock solution with a final concentration of 2.0 mmol/L.

The obtained solution was kept refrigerated and subsequently used to prepare all the solutions tested within this work.

2,4-D removal tests from waters by adsorption on CDHD6 and CDHD12 were carried out using batch experiments.

Aqueous solutions of 2,4-D were placed in contact with each NS sample in glass vials with Teflon caps at 25 °C; the vessels were continuously stirred on an orbital shaker at 150 rpm until steady state conditions were attained. Successively, the samples were centrifuged at 5000 rpm for 30 min at 4 °C and the supernatant liquid was analyzed by HPLC for 2,4-D quantification.

The amount of 2,4-D adsorbed was calculated as the difference between its initial and final concentrations in solution. Blanks of 2,4-D in ultrapure water were analyzed in order to evaluate 2,4-D stability and sorption on vials. The following experimental factors were evaluated:

(a) Solid/liquid (S/L) ratio: a constant volume of 2,4-D solution (0.1 mmol/L) was placed in contact with different amounts of CDHD6 and CDHD12 sample, at pH 3.0 for an incubation time of 24 h. The S/L ratios (R = mg of adsorbent/mL of 2,4-D aqueous solution) were 0.1, 0.3, 0.5, 1.0, and 2.0.
(b) pH: NSs samples, CDHD6 and CDHD12 were immersed in a 0.10 mmol/L 2,4-D solution at solid/liquid ratio S/L = 0.1 for 24 h (this time was shown to be sufficient to attain a steady state). The pH of this solution varied between 2.0 and 8.0, by adding the proper amount of 0.01 or 0.10 mmol/L HCl or NaOH aqueous solution.
(c) Adsorption kinetics: kinetic studies were performed by using 2,4-D aqueous solutions at two different concentrations: 0.10 and 0.5 mmol/L, at solid/liquid ratio S/L = 0.1 and at two different pH values, namely: pH 3.0 for CDHD6 and pH 4.0 for CDHD12.

Removal tests were performed at different incubation times, 10, 30, 60, 120, 240, 360, 900 and 1440 min. Successively, the suspensions were subjected to the separation procedure as described.

(d) Sorption isotherm: CDHD6 and CDHD12 were placed in contact with solutions at concentrations of 2,4-D up to 2.0 mmol/L, S/L = 0.1, T = 25 °C and pH = 3.0 or pH 4.0, respectively, for 24 h. The pH of each suspension was kept constant by adding proper amounts of 0.01 or 0.10 mmol/L HCl or NaOH solution.

2.6. Desorption and reuse experiments

The desorption and reuse experiments were carried out by alkali desorption. In particular, CDHD6 and CDHD12 adsorbents were preliminarily used to adsorb 2,4-D at the initial concentration of 0.5 mmol/L at pH 4.0 and 3.0, respectively, for 24 h. The samples were centrifuged at 5000 rpm for 30 min at 4 °C and the concentration of 2,4-D in the supernatant liquid quantified, by using the method above described.

Successively, the exhausted samples were put in contact with a NaOH solution at 0.1 M concentration for an incubation time of 24 h. Thus, the adsorbents were separated by centrifugation, and the concentration of the desorbed 2,4-D, in the liquid phase, measured. For CDHD6, new adsorption tests were carried out to measure the efficiency of the regenerated adsorbent; that was achieved by incubating the sample for 24 h in a 2,4-D solution, at the initial concentration of 0.5 mmol/L, at optimal pH.

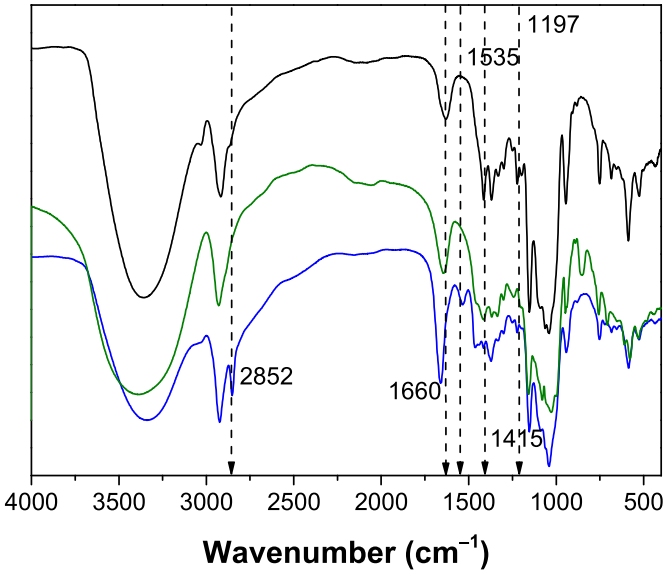

Fig. 1. FTIR spectra of CD (green line), CDHD6 (black line) and CDHD12 (blue line). Reference sample: KBr pellets at 2%. (For interpretation of the references to color in this figure legend, the reader is referred to the Web version of this article.)

3. Results and discussion

3.1. Physico-chemical characterization

CDHD6 and CDHD12 were characterized by FTIR analysis (Fig. 1). The corresponding assignments of the main vibrational modes are summarized in Table 1. The vibrational mode at 3335 cm^{-1} shows the presence of amine and hydroxyl groups, being sharper than that observed for pure cyclodextrin (Abarca et al., 2016). Comparing both NSs, it can be seen that the vibrational mode at 2852 cm^{-1} is only characteristic of CDHD12, once it is related with the hydrocarbon chain length. On the other hand, the higher intensity of the mode at 1631 cm^{-1}, for CDHD12, can be justified considering its more compact structure. It is worthy notice that the $–CH_2$- bending vibration (ca. 1415 cm^{-1}) of the aliphatic chain and the stretching vibration of primary and secondary amine groups (at around 1197 cm^{-1}) are only detectable for the NS with the shorter linker.

The comparison between nanosponges was also done by thermogravimetric analysis (Fig. 2). The NS with a shorter linker only shows a single thermal transition with a maximum at 210 °C, as a consequence of β-cyclodextrin degradation. On the other hand, for the CDHD12, three different thermal steps are observed: the first one occurring at 226 °C, the second at 310 °C and the third at 415 °C. The latter might be assigned to the breakup of the secondary amine bond at the C-6 of the cyclodextrin, whilst at 310 °C the degradation of the cyclodextrin is occurring (Trotta et al., 2000). Such thermal behaviour suggests that the NS with a longer alkyl chain length crosslinker has higher thermal stability, most probably due to hydrophobic interactions among alkyl chains, entanglements and more compact spatial arrangement.

The thermal behaviour agrees with N_2 adsorption data (Table 2); i.e., it has been found that CDHD12 has a more compact structure with a pore volume and diameter equal to 0.03 $cm^3\ g^{-1}$ and 7.5 nm, respectively, much lower than those measured for CDHD6 (0.13 $cm^3\ g^{-1}$ and 24.3 nm, respectively). However, the BET surface of the CDHD6 is just 20% higher than that observed for the CDHD12 (21.8 and 17.9 $m^2\ g^{-1}$, respectively). The average size, polydispersion index (PDI) and the corresponding ζ-potential, for both nanosponges, are summarized in Table 2. The size of the nanosponges, as well as their distribution, are similar independently of the crosslinker chain length but the PDI and the potential are slightly higher for the CDHD12.

Micrographs of pristine NSs show two different surface morphologies. The surface of CDHD6 (Fig. 3A) is composed by rod-like structures which tend to be less compact with each other, i.e. to open after 2,4-D adsorption. On the other hand, CDHD12 (Fig. 3B) is characterized by the occurrence of very small rod-shape and spherical structures. The former sample (CDHD6) suggests a more diffuse porous surface, whilst the latter (CDHD12) is characterized by the occurrence of a compact structure, with alveolar architecture, probably due to the reorganization of the lipophilic chain of HD12. After the adsorption of 2,4-D solution, a significant surface morphology modification is occurring.

Table 1
Main FTIR vibrational mode assignments for CD-NSs.

Wavelength (cm^{-1})	Assignment	Reference
3330, 1153,1087, 1040, 950	-OH str. vb., -C-O-C- str. vb., –OH bd. vb., α-1→4-glycosidic bond	(Abarca et al., 2016); (Utzeri et al., 2021); (Russo et al., 2016); (Utzeri et al., 2022a); (Silverstein et al., 2005).
3335	-NH-, NH_2 str. vb.	
2850	$-CH_2$- str. vb.	
1631, 1660	$-NH_2$ bd. vb.	
1415	$-CH_2$- bd. vb.	
1197	-NH-, $–NH_2$ str. vb.	

3.2. Effect of solid/liquid ratio

The effects of CD−NSs dosages on 2,4-D adsorption were firstly investigated at 25 °C with different amounts of sample (3.0–60 mg/30 mL final volume) at an initial 2,4-D concentration of 0.1 mmol/L at pH 3.0. The results reported in Fig. 4 demonstrate that the lower the solid/liquid ratio, the higher is the adsorption capacity. As a matter of fact, lower values of solid/liquid ratio were obtained reducing the amount of adsorbent added while keeping constant the total volume of 2,4-D solution, and consequently the adsorption equilibrium is shifted towards a larger amount of solute adsorbed per mass unit of adsorbent. The highest amounts of 2,4-D adsorbed on CDHD6 and CDHD12, were 250 and 1000 mmol/kg, respectively, at a solid/liquid ratio equal to 0.1.

Therefore, for the same final volume, a mass of 3.0 mg exposed an adequate number of sites available for 2,4-D molecules uptake. Previous studies performed by our research group showed that the adsorption of simazine, 2-chloro-4,6-bis(ethylamino)-s-triazine, on porous silicas decreased with increasing s/l ratio (Sannino et al., 2013). Based on these considerations, the optimal CDHD6 and CDHD12 dosages for both the samples is 3.0 mg/30 mL.

3.3. Effect of pH

Fig. 5 reports the amounts of 2,4-D adsorbed on CDHD6 and CDHD12, respectively at s/l ratio of 0.1 after a contact time of 24 h, as a function of pH. The 2,4-D uptake was found to be low for CDHD6 (about 130 mmol/kg) and negligible for CDHD12 at very acidic pH values (pH = 2.0). The amount adsorbed increased rapidly up to pH 4.0 and pH 3.0, in the presence of CDHD6 and CDHD12, respectively, then decreased up to pH 8.0. The decreasing effect was very noticeable for the CDHD6 sample, whereas it was moderate for CDHD12 sample.

The maximum adsorption occurs at pH 4.0 and 3.0 for CDHD6 and CDHD12, respectively, whereby all further experiments were performed at these pH values.

The pH of the solution plays an essential role in adsorption in the aqueous phase, especially when adsorbates or adsorbents have several functional groups such as –COOH, $–NH_2$, primary and secondary –OH, and $–CH_2$ of the aliphatic chains. As a matter of facts, the pH of the solution directly controls the charges of these groups on both the adsorbents and adsorbate via deprotonation or protonation reactions.

The optimal pH values observed for nanosponges were both higher than the 2,4-D pKa (2.73), suggesting that the adsorption is favoured when the herbicide molecule is present as a deprotonated acid and the amine groups of the nanosponsponge are protonated, thus allowing ionic interactions.

Lower amounts of 2,4-D, consisting of 15.977 and 665.790 mmol/kg for CDHD6 and CDHD12, respectively, were found to be adsorbed at pH 8.0. At alkaline pHs, the hydroxyl anions - stronger bases than 2,4-D molecules - preferentially react with hydrogen atoms of the nanosponges, thus hindering the 2,4-D molecules uptake. In particular, an increase in the pH from 3.0 to 8.0 (for CDHD12) decreases the adsorption efficiency from 100 to 66.6%.

Hence, lower pH values favour the adsorption of 2,4-D by NSs, which is consistent with the reported literature (Herrera-Garcia et al., 2019; Aparecida Matias et al., 2019).

3.4. Kinetic and equilibrium features of the adsorption process

Fig. 6A and B report 2,4-D uptake from water by CDHD6 and CDHD12, using two solutions with an initial herbicide concentration of 0.1 and 0.5 mmol/L respectively, as a function of time. Whatever the experimental conditions adopted, the curves showed initially a fast uptake, that gradually slow down and eventually reach a steady state in about 24 h. In the tests carried out at higher concentration of herbicide, the adsorption kinetics was faster.

The kinetic data were fitted using four widely adopted models,

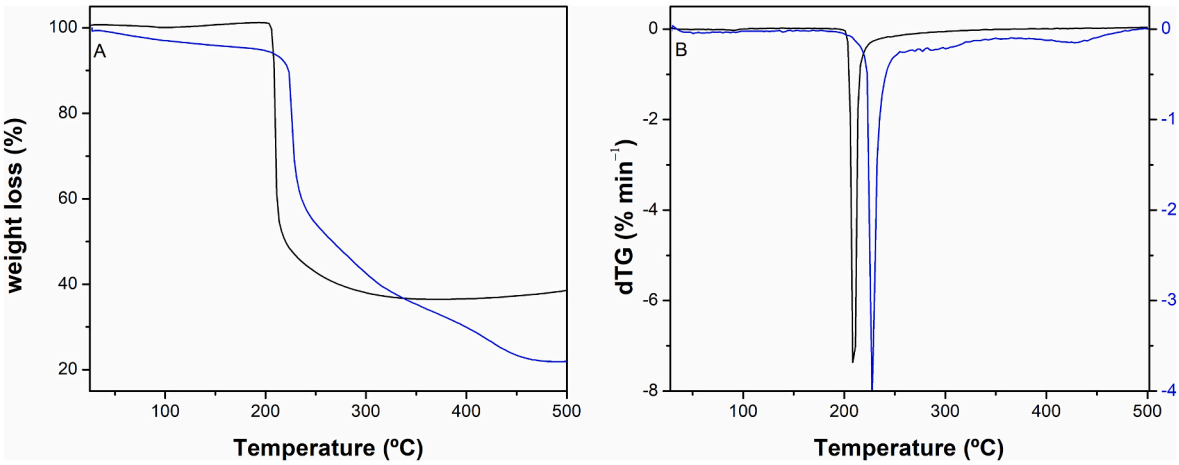

Fig. 2. TGA and dTG of CDHD6 (black line) and CDHD12 (blue line). Heating rate: 5 K/min. N_2 flow rate: 50 mL/min. (For interpretation of the references to color in this figure legend, the reader is referred to the Web version of this article.)

Table 2
Z-average size and ζ—potential for nanosponges (Utzeri et al., 2022b).

NSs	Z-average (d.nm)	PDI	ζ potential (mV)
CDHD6	446 ± 30	0.38 ± 0.05	41 ± 6
CDHD12	438 ± 38	0.43 ± 0.03	54 ± 7

namely:

- the pseudo-first order equation (PFO) of Lagergren (Yuh-Shan, 2004; Lagergren, 1898)

$$\frac{dq_t}{dt} = k_1(q_e - q_t) \tag{1}$$

where q_t and q_e are the adsorption capacities of the adsorbent material (mmol/kg) at the time t and at the equilibrium, respectively, $k_1(min^{-1})$ is the adsorption rate constant.

The integrated form of Eq. (1) is:

$$q_t = q_e\left(1 - e^{-k_1 t}\right) \tag{2}$$

- the pseudo-second order equation (PSO) (Blanchard et al., 1984):

$$\frac{dq_t}{dt} = k_2(q_e - q_t)^2 \tag{3}$$

where k_2 (kg/mmol min) is the adsorption rate constant.

The integrated form of Eq. (3) is:

$$q_t = \frac{tk_2q_e^2}{1 + tk_2q_e} \tag{4}$$

- the Elovich model (Elovich and Larinov, 1962)

$$\frac{dq_t}{dt} = a \cdot e^{-b \cdot q_t} \tag{5}$$

The integrated form of Eq. (5) is:

$$q_t = \frac{1}{b} ln(1 + a \cdot b \cdot t) \tag{6}$$

- the simplified intraparticle diffusion model (Boyd et al., 1947)

$$\frac{dq_t}{dt} = a \cdot e^{-b \cdot q_t} \tag{7}$$

The integrated form of Eq. (7) is:

$$q_t = \frac{1}{b} ln(1 + a \cdot b \cdot t) \tag{8}$$

The experimental data were elaborated by nonlinear regressions using the mathematical models (2),(4),(6),(8). It should be noticed that none of these models was able to satisfactorily describe the experimental curves.

Consequently, a composite model was adopted to describe the kinetics of the adsorption of 2,4 D by β-cyclodextrin-based NSs. The composite model was obtained adopting the Elovich and the pseudo first-order models to describe the initial and the later stages of the adsorption process, respectively. Fig. 6A and B shows the interpolation curves obtained using the composite model. The parameters of the composite model obtained by nonlinear regression are reported in Tables 3a and 3b.

The adoption of a composite model is justified by the fact that, in the adsorption system studied, the overall driving force responsible for the inclusion phenomenon is the sum of several types of contributions (Pereira et al., 2015). As a matter of facts, the inclusion process comprises several host-guest interactions, most of them of hydrophobic nature. The inclusion process is also affected by other weak interactions such as van der Waals, hydrophobic or hydrogen-bonding, though none of these is enough to form a supramolecular complex.

It is worth noting that the Elovich model is usually valid to describe chemiadsorption processes (Wang and Guo, 2020a), justified by the formation of inclusion complexes by hydrophobic interactions occurring between the lipophilic aromatic ring of 2,4-D and the cavity of nanosponges. Consequently, the Elovich model can be responsible for the formation of the adsorbed first layer of 2,4 D onto nanosponges. The formation of the subsequent 2,4-D layers can be described by the pseudo first-order model. In fact, previous works (Ezzati, 2020) have demonstrated that pseudo first-order model can describe the adsorption process when the system is close to equilibrium.

Fig. 7 (left side) reports the isotherm for CDHD6. This isotherm, showing a quite complex behaviour, can be considered a type IV isotherm. The best model to describe this isotherm was obtained by the additive superposition of the models of Langmuir and Sips (Buttersack, 2019), yielding the following mathematical expression:

$$q_e = Q_0 \cdot \left(\frac{C_e}{\frac{1}{b'} + C_e} + \frac{C_e^5}{\frac{1}{b''} + C_e^5}\right) \tag{9}$$

where C_e is the equilibrium concentration (mmol/L) and q_e is the amount of 2,4-D adsorbed per kilogram at equilibrium (mmol/kg). Q_0 is

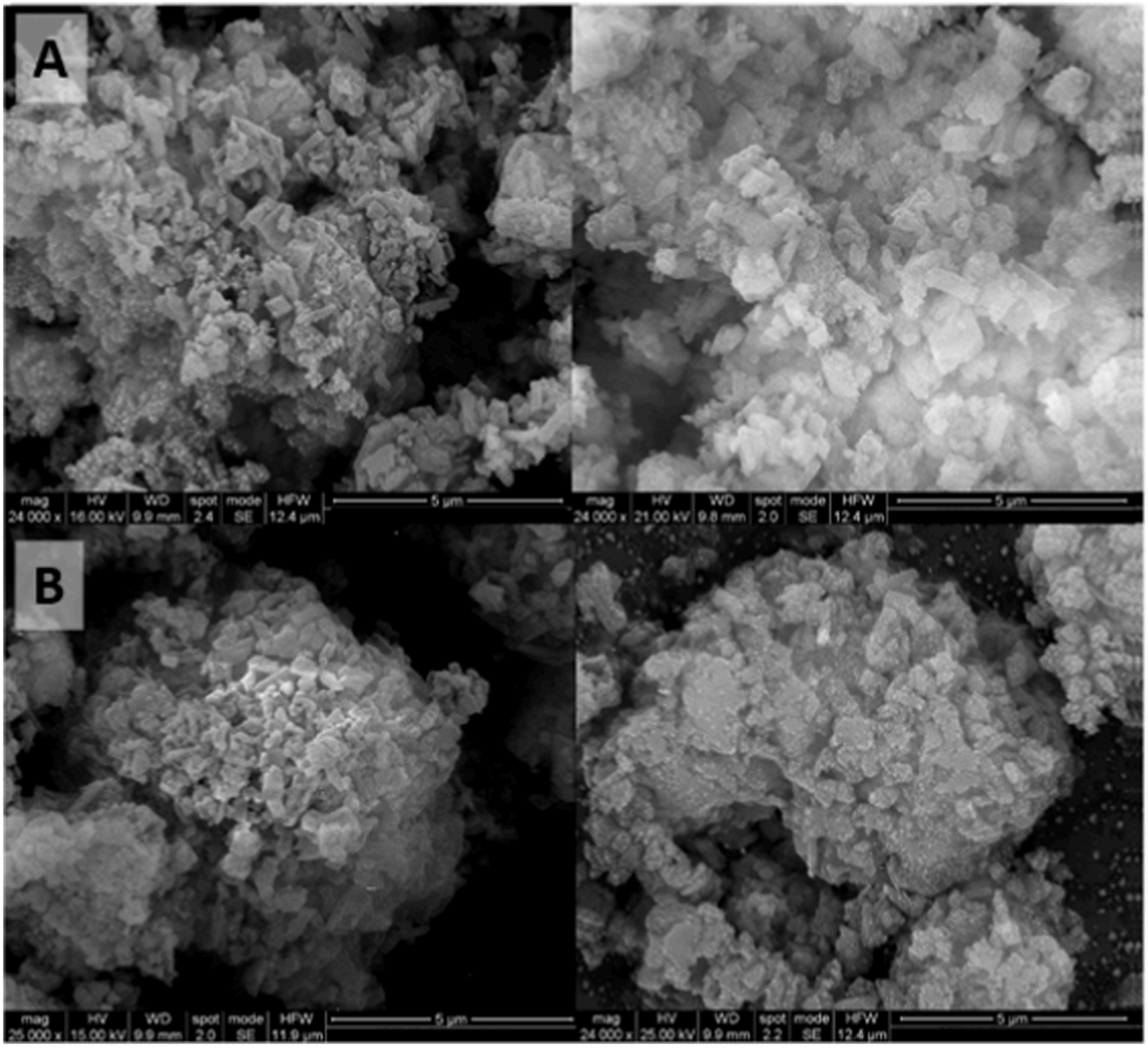

Fig. 3. Micrographs of CDHD6 (A) and CHD12(B) before (left) and after (right) 2,4-D adsorption. Images acquired in the range between 15.00 and 25.00 kV and at 24,000–25000 x of magnification.

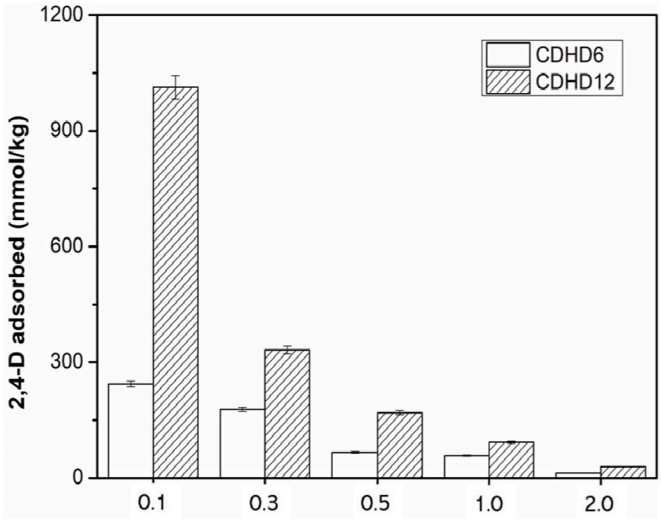

Fig. 4. Effect of solid/liquid ratio on the adsorption of 2,4-D by CDHD6 and CDHD12, respectively. Experimental conditions: T = 25 °C, pH 3.0, orbital shaking at 150 rpm. S/L units are mg/mL.

a constant related to the adsorption capacity (mmol/kg), *b'* is the energy of adsorption (L/mmol), and *b''* is a parameter of the model of Sips ($L^5/mmol^5$). The computed values of Q_0, *b'* and *b''*, obtained by nonlinear interpolation, are: 1.22×10^3 (mmol/kg), 5.30 (L/mmol) and 8.56×10^{-3} (L/mmol), respectively.

In order to understand the physical meaning of the Langmuir-Sips model, we can observe that, at lower values of C_e, eq. (9) becomes the Langmuir model, thus describing a monolayer adsorption where the interaction between adsorbate molecules is negligible (Wang and Guo, 2020b). On the contrary, at higher values of C_e, a multilayer adsorption is likely to occur, due to noncovalent π−π stacking interactions between cyclodextrins, and consequently the experimental data are described by the more complex Langmuir-Sips model. It should be considered that the Sips model combines the Langmuir and Freundlich models, and in many studies the Freundlich isotherm has been applied to represent multi-layer adsorption processes (Wang and Guo, 2020b). Different alternative models suitable to describe multilayer adsorption, such as Temkin and BET models, have been tested, although less satisfactory results have been obtained.

With regard to the CDHD12 isotherm (Fig. 7), it can be seen that, at the analyzed concentration range, the adsorption can be described by the Henry model:

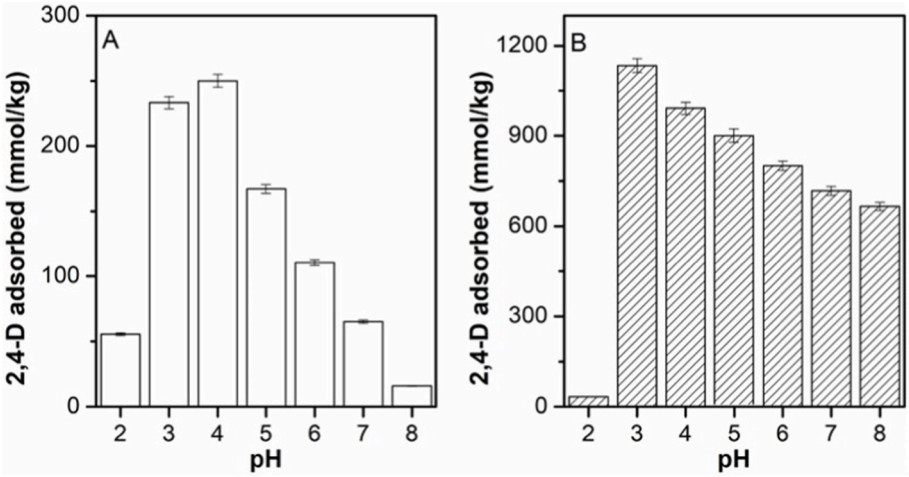

Fig. 5. 2,4-D adsorbed on (A) CDHD6 and (B) CDHD12 respectively, from a 0.1 mmol/L 2,4-D solution as a function of pH. Experimental conditions: T = 25 °C, orbital shaking at 150 rpm contact time 24 h.

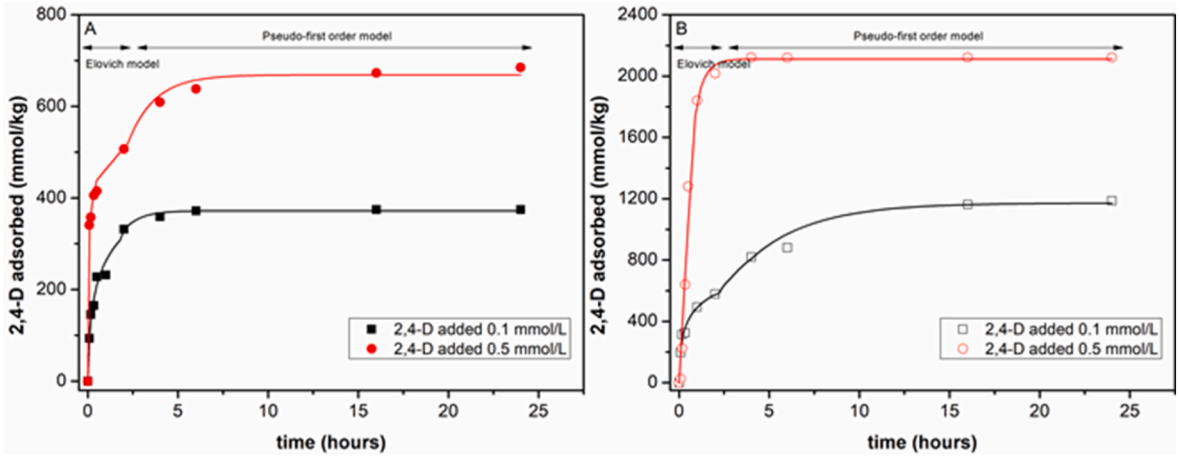

Fig. 6. Adsorption kinetics of 2,4-D on (A) CDHD6 and (B) CDHD12. Experimental conditions: T = 25 °C, pH 3.0 (for CDHD6) or 4.0 (for CDHD12), solid/liquid ratio (S/L) = 0.1, orbital shaking at 150 rpm.

Table 3
a Fitting kinetic parameters for the adsorption of 2,4-D onto CDHD6.
b.Fitting kinetic parameters for the adsorption of 2,4-D onto CDHD12.

	(2,4-D) = 0.1 mmol/L	(2,4-D) = 0.5 mmol/L
	CDHD6	
Elovich model (initial stage)	$a = 3.35 \times 10$ mmol kg^{-1} min^{-1}	$a = 1.29 \times 10^3$ mmol kg^{-1} min^{-1}
	$b = 1.24 \times 10^{-2}$ kg mmol^{-1}	$b = 1.44 \times 10^{-2}$ kg mmol^{-1}
Pseudo I order (final stage)	$q_e = 3.72 \times 10^2$ mmol kg^{-1}	$q_e = 6.69 \times 10^2$ mmol kg^{-1}
	$k_1 = 1.82 \times 10^{-2}$ min^{-1}	$k_1 = 1.13 \times 10^{-2}$ min^{-1}
R^2	0.991	0.995
	(2,4-D) = 0.1 mmol/L	(2,4-D) = 0.5 mmol/L
	CDHD12	
Elovich model (initial stage)	$a = 1.04 \times 10^2$ mmol kg^{-1} min^{-1}	$a = 3.73 \times 10$ mmol kg^{-1} min^{-1}
	$b = 8.04 \times 10^{-3}$ kg mmol^{-1}	$b = 1.61 \times 10^{-4}$ kg mmol^{-1}
Pseudo I order (final stage)	$q_e = 1.17 \times 10^3$ mmol kg^{-1}	$q_e = 2.11 \times 10^3$ mmol kg^{-1}
	$k_1 = 4.87 \times 10^{-3}$ min^{-1}	$k_1 = 3.33 \times 10^{-2}$ min^{-1}
R^2	0.996	0.976

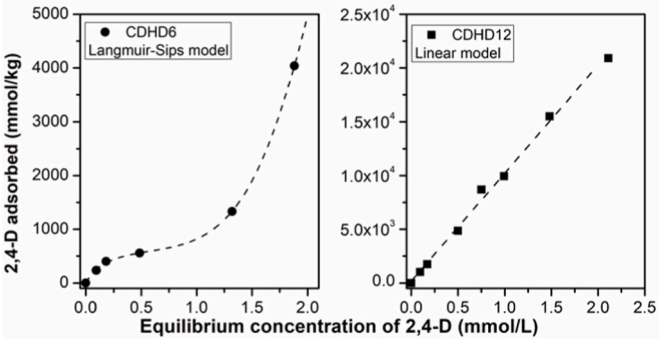

Fig. 7. Adsorption isotherms of 2,4-D on CDHD6 (spheres) and CDHD12 (squares). Experimental conditions: T = 25 °C, pH 3.0 (for CDHD6) or 4.0 (for CDHD12), solid/liquid ratio (S/L) = 0.1, orbital shaking at 150 rpm.

$$q_e = q_0 + C_e \cdot b \quad (10)$$

The values of q_0 and b obtained by linear interpolation were 168 (μmol/kg) and 1.01×10^4 (L/μmol), respectively.

The maximum values of q_e measured in our experiments were 4040 mmol/kg for CDHD6 and 20,903 mmol/kg for CDHD12, when the

Table 4
Comparison of the maximum values of q_e measured in our experiments with the values observed in previous studies focused on the adsorption of 2,4-D.

Adsorbent	q_e (mmol/kg)	Reference
Organically modified bentonite	36.2	Salcedo et al. (2021)
Activated carbon	1809	Vedenyapina et al. (2017)
OPAC (Orange Peel Activated Carbon)	2332	Pandiarajan et al. (2018)
Nitrogen-enriched carbon, derived from melamine@metal-azolate framework-6	3166	Bhadra et al. (2022)
MOF (metal–organic framework)	2515	Jung et al. (2013)
Activated carbon	1293	Jung et al. (2013)
USY, zeolite	1158	Jung et al. (2013)
Organo-modified bentonite clay	227	de Souza et al. (2019)
Aminosilane grafted mesoporous carbons	642–864	Goscianska and Olejnik (2019)
Fly ash	31.7	Kuśmierek and Świątkowski (2016)
[Co–Al–Cl] layered double hydroxide	136	Calisto et al. (2019)
Activated carbon	167	Dornelas Marsolla et al. (2022)
Amino-functionalized magnetite	525	Zadeh et al. (2020)
Single-walled carbon nanotubes	4434	Bazrafshan et al. (2013)
Fe-crosslinked chitosan	5317	Zhou et al. (2017)
CDHD6	4040	This study
CDHD12	20,903	This study

equilibrium concentration of 2,4-D in solution was 2 mmol/L (see Fig. 7). These values are compared in Table 4 to those observed in previous studies focused on the adsorption of 2,4-D using different materials. On the basis of these results, it can be concluded that the adsorption performance of both CDHD6 and CDHD12 was satisfactory.

3.5. Desorption and reuse of β-cyclodextrin nanosponge adsorbents

In order to find an environmentally friendly strategy, an alkali desorption procedure was developed, based on the incubation of exhausted samples of CDHD6 and CDHD12 in a NaOH solution. Different conditions were tested in terms of incubation times and NaOH concentration. The best results were obtained carrying out the incubation in a 0.1 M NaOH aqueous solution under stirring at 25 °C for 24 h. CDHD6 adsorbent was subjected to four consecutive washing cycles to evaluate the efficiency of the desorption method. The completely desorption of 2,4-D is achieved after 4 washing cycles (Fig. 8).

Successively, the adsorption capacity of regenerated CDHD6 was evaluated by contacting with a 0.5 mmol/L 2,4-D solution. The results obtained showed that CDHD6 kept unchanged its adsorption capacity, i.e. about 700 mmol/kg, in the experiments carried out both before and after the regeneration procedure.

Experimental conditions of adsorption: T = 25 °C, contact time = 24 h, pH 3.0, initial 2,4-D concentration = 0.5 mmol/L, orbital shaking at 150 rpm.

Experimental conditions of desorption: T = 25 °C, incubation time = 24 h, initial NaOH concentration = 0.1 M, orbital shaking at 150 rpm.

4. Conclusions

Two cyclodextrin-based nanosponges were employed as adsorbents to remove the herbicide 2,4-D from aqueous solutions. Two different linkers were used, namely hexane–1,6–diamine (HD6) and dodecane–1,12–diamine (HD12), to assess the influence of the chain length of the linker on sorption performance.

The FTIR analysis demonstrated that, when using a linker with a longer chain length (HD12), the nanosponges show a more compact structure. The higher structural compactness of the CDHD12 was confirmed by the lower values of pore volume and diameter, obtained from N_2 adsorption data, and by the lower specific surface, measured by BET analysis.

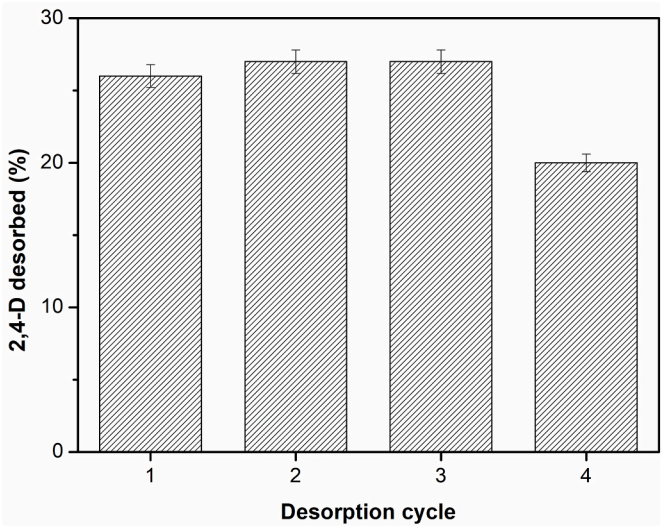

Fig. 8. Desorption of 2,4-D (%) from CDHD6 as a function of cycles.

The TGA and dTA analyses showed that linkers with a longer chain confer higher thermal stability to the CD–NSs, probably due to the generation of stronger hydrophobic interactions.

The average size and the polydispersion index were not significantly affected by the crosslinker chain length. SEM micrographs showed significant differences in surface morphology between the two nanosponges tested. The morphology underwent further changes during the adsorption of 2,4-D.

The maximum adsorption for CDHD6 and CDHD12 was obtained at pH 4.0 and 3.0, respectively. We demonstrated that, under these conditions, the 2,4-D molecules are deprotonated, whereas the amine groups of the nanosponge are protonated, thus causing electrostatic attraction.

A composite model was adopted to describe the kinetics of the adsorption of 2,4-D by CD-NSs, obtained by adopting the Elovich and the pseudo first-order models to describe the initial and the later stages of the adsorption process, respectively.

The isotherm for CDHD12 could be described by the Henry model, whereas that pertaining to the CDHD6 required a more complex model, obtained by the additive superposition of the models of Langmuir and Sips.

In order to find an environmentally friendly strategy for the reuse of the nanosponges, an alkali desorption procedure was developed, allowing a full recycle and reuse of the adsorbents.

On the basis of the results obtained, it can be concluded that the CDHD6 and CDHD12 nanosponges showed a remarkable ability for 2,4-D removal, making them suitable to be used as potential adsorbents for the sustainable management of agricultural wastewaters. Consequently, the use of CDHD6 and CDHD12 with real wastewaters is worthy of further research efforts.

Funding

This research received no external funding.

Declaration of competing interest

The authors declare that they have no known competing financial interests or personal relationships that could have appeared to influence the work reported in this paper.

Data availability

Data will be made available on request.

References

Abarca, R.L., Rodríguez, F.J., Guarda, A., Galotto, M.J., Bruna, J.E., 2016. Characterization of beta-cyclodextrin inclusion complexes containing an essential oil component. Food Chem. 196, 968–975.

Addorisio, V., Esposito, S., Sannino, F., 2010. Sorption capacity of mesoporous metal oxides for the removal of MCPA from polluted waters. J. Agric. Food Chem. 58, 5011–5016.

Andrunik, M., Bajda, T., 2021. Removal of pesticides from waters by adsorption: comparison between synthetic zeolites and mesoporous silica materials. A review. Materials 14, 3532–3570.

Aparecida Matias, C., Vilela, P.B., Becegato, V.A., Paulino, A.T., 2019. Adsorption kinetic, isotherm and thermodynamic of 2,4-dichlorophenoxyacetic acid herbicide in novel alternative natural adsorbents. Water. Air and Soil Pollution 230, 276. https://doi.org/10.1007/s11270-019-4324-5.

Bhadra, B.N., Lee, H.J., Jhung, S.H., 2022. Adsorptive removal of herbicides with similar structures from water over nitrogen-enriched carbon, derived from melamine@ metal-azolate framework-6. Environ. Res. 204, 111991 https://doi.org/10.1016/j.envres.2021.111991.

Bazrafshan, E., Kord Mostafapour, F., Faridi, H., Farzadkia, M., Sargazi, S., Sohrabi, A., 2013. Removal of 2,4-Dichlorophenoxyacetic acid (2,4-D) from aqueous environments using single-walled carbon nanotubes. Health Scope 2, 39–46.

Biswas, B., Labille, J., Prelot, B., 2020. Clays and modified clays in remediating environmental pollutants. Environ. Sci. Pollut. Control Ser. 27, 38381–38383.

Blachnio, M., Derylo-Marczewska, A., Charmas, B., Zienkiewicz-Strzalka, M., Bogatyrov, V., Galaburda, M., 2020. Activated carbon from agricultural wastes for adsorption of organic pollutants. Molecules 25, 5105. https://doi:10.3390/molecules25215105.

Blanchard, G., Maunaye, M., Martin, G., 1984. Removal of heavy metals from waters by means of natural zeolites. Water Res. 18, 1501–1507.

Boyd, G.E., Adamson, A.W., Myers, L.S., 1947. The exchange adsorption of ions from aqueous solutions by organic zeolites. II. Kinetics. Journal of American Chemistry Society 69, 2836–2848.

Buttersack, C., 2019. Modeling of type IV and V sigmoidal adsorption isotherms. Phys. Chem. Chem. Phys. 21, 5614.

Calisto, J.S., Pacheco, I.S., Freitas, L.L., Santana, L.K., Fagundes, W.S., Amaral, F.A., Canobre, S.C., 2019. Adsorption kinetic and thermodynamic studies of the 2,4–dichlorophenoxyacetate (2,4-D) by the [Co–Al–Cl] layered double hydroxide. Heliyon 5, e02553.

Cornejo, J., Celis, R., Pavlovic, I., Ulibarri Cormenzana, M.A., 2008. Interactions of pesticides with clays and layered double hydroxides: a review. Clay Miner. 43, 155–175. https://doi.org/10.1180/claymin.2008.043.2.01.

Cova, T.F., Murtinho, D., Pais, A.A.C.C., Valente, A.J.M., 2018. Combining cellulose and cyclodextrins: fascinating designs for materials and pharmaceutics. Front. Chem. 6, 271. https://doi.org/10.3389/fchem.2018.00271.

Derylo-Marczewska, A., Blachnio, M., Marczewski, A.W., Swiatkowski, A., Tarasiuk, B., 2010. Adsorption of selected herbicides from aqueous solutions on activated carbon. J. Therm. Anal. Calorim. 101, 785–794. https://doi.org/10.1007/s10973-010-0840-7.

Dornelas Marsolla, L., Maia Brito, G., Checon Freitas, J.C., Cabral Coelho, E.R., 2022. Removing 2,4-D micropollutant herbicide using powdered activated carbons: the influence of different aqueous systems on adsorption process. J. Environm. Sci. Health, Part B 57, 588–596.

de Souza, F.M., dos Santos, O.A.A., Vieira, M.G.A., 2019. Adsorption of herbicide 2,4-D from aqueous solution using organo-modified bentonite clay. Environ. Sci. Pollut. Control Ser. 26, 18329–18342.

Elovich, S.Y., Larinov, O.G., 1962. Theory of adsorption from solutions of non-electrolytes on solid (I) equation adsorption from solutions and the analysis of its simplest form, (II) verification of the equation of adsorption isotherm from solutions. Izvestiya Akademii Nauk. SSSR, Otdelenie Khimicheskikh Nauk 2, 209–216.

Ezzati, R., 2020. Derivation of pseudo-first-order, pseudo-second-order and modified pseudo-first-order rate equations from Langmuir and Freundlich isotherms for adsorption. Chem. Eng. J. 392, 123705 https://doi.org/10.1016/j.cej.2019.123705.

Gao, Y.A., Li, Z.H., Du, J.M., Han, B.X., Li, G.Z., Hou, W.G., Shen, D., Zheng, L.Q., Zhang, G.Y., 2005. Preparation and characterization of inclusion complexes of β-cyclodextrin with ionic liquid. Chem. Eur J. 11, 5875–5880.

Goscianska, J., Olejnik, A., 2019. Removal of 2,4-D herbicide from aqueous solution by aminosilane-grafted mesoporous carbons. Adsorption 25, 345–355.

Herrera-Garcia, U., Castillo, J., Patino-Ruiz, D., Solano, R., Herrera, A., 2019. Activated carbon from yam peels modified with Fe3O4 for removal of 2,4-dichlorophenoxy-acetic acid in aqueous solution. Water 11, 2342. https://doi.org/10.3390/w11112342.

Jaafarzadeh, N., Ghanbari, F., Ahmadi, M., 2017. Efficient degradation of 2,4-dichlorophenoxyacetic acid by peroxymonosulfate/magnetic copper ferrite nanoparticles/ozone: a novel combination of advanced oxidation processes. Chem. Eng. J. 320, 436–447.

Jung, B.K., Hasan, Zubair, Jhung, S., 2013. Adsorptive removal of 2,4-dichlorophenoxyacetic acid (2,4-D) from water with a metal–organic framework. Chem. Eng. J. 234, 99–105.

Kuśmierek, K., Świątkowski, A., 2016. Adsorption of 2,4-Dichlorophenoxyacetic acid from an aqueous solution on fly ash. Water Environ. Res. 88, 231–238.

Lagergren, S., 1898. Zur theorie der sogenannten adsorption geloster stoffe, Kungliga Svenska Vetenskapsakademiens. Handlingar 24, 1–39.

Loftsson, T., Brewster, M.E., 2010. Pharmaceutical applications of cyclodextrins: basic science and product development. J. Pharmaceut. Sci. 62, 1607–1621.

Mahy, J.G., Mbognou, M.H.T., Léonard, C., Fagel, N., Woumfo, E.D., Lambert, S.D., 2022. Natural clay modified with ZnO/TiO_2 to enhance pollutant removal from water. Catalysts 12, 148. https://doi.org/10.3390/catal12020148, 2022.

Morin-Crini, N., Winterton, P., Fourmentin, S., Wilson, L.D., Fenyvesi, E., Crini, G., 2018. Water-insoluble β-cyclodextrin–epichlorohydrin polymers for removal of pollutants from aqueous solutions by sorption processes using batch studies: a review of inclusion mechanisms. Prog. Polym. Sci. 78, 1–23.

Pandiarajan, A., Kamaraj, R., Vasudevan, S., Vasudevan, S., 2018. OPAC (orange peel activated carbon) derived from waste orange peel for the adsorption of chlorophenoxyacetic acid herbicides from water: adsorption isotherm, kinetic modelling and thermodynamic studies. Bioresour. Technol. 261, 329–341.

Pereira, R.A., Anconi, C.P.A., Nascimento Jr., C.S., De Almeida, W.B., Dos Santos, H.F., 2015. Stability and spatial arrangement of the 2,4-dichlorophenoxyacetic acid and -cyclodextrin inclusion compound: a theoretical study. Chem. Phys. Lett. 633, 158–162.

Peziak-Kowalska, D., Syguda, A., Lawniczak, L., Borkowski, A., Fourcade, F., Heipieper, H.J., Lota, G., Chrzanowski, L., 2019. Hybrid electrochemical and biological treatment of herbicidal ionic liquids comprising the MCPA anion. Ecotoxicol. Environ. Saf. 181, 172–179.

Russo, T., Fucile, P., Giacometti, R., Sannino, F., 2021. Sustainable removal of contaminants by biopolymers: a novel approach for wastewater treatment. Current state and future perspectives. Processes 9, 719–739. https://doi.org/10.3390/pr9040719.

Russo, M., Saladino, M.L., Chillura Martino, D., Lo Meo, P., Noto, R., 2016. Polyaminocyclodextrin nanosponges: synthesis, characterization and pH-responsive sequestration abilities. RSC Adv. 6, 49941–49954.

Salazar, S., Guerra, D., Yutronic, N., Jara, P., 2018. Removal of aromatic chlorinated pesticides from aqueous solution using β-cyclodextrin polymers decorated with Fe_3O_4 nanoparticles. Polymers 10, 1038–1057. https://doi.org/10.3390/polym10091038.

Salazar, S., Yutronic, N., Jara, P., 2020. Magnetic β-cyclodextrin nanosponges for potential application in the removal of the neonicotinoid dinotefuran from wastewater. Int. J. Mol. Sci. 21, 4079–4092. https://10.3390/ijms21114079.

Salcedo, M.F., Mansilla, A.Y., Colman, S.L., Iglesias, M.J., Alvarez, V.A., Casalonguè, C. A., 2021. Efficacy of an organically modified bentonite to adsorb 2,4-dichlorophenoxyacetic acid (2,4-D) and prevent its phytotoxicity. J. Environ. Manag. 297, 113427.

Sannino, F., Ruocco, S., Marocco, A., Esposito, S., Pansini, M., 2013. Simazine removal from waters by adsorption on porous silicas tailored by sol–gel technique. Microporous Mesoporous Mater. 180, 178–186.

Sannino, F., Pernice, P., Minieri, L., Camandona, G.A., Aronne, A., Pirozzi, D., 2015. Oxidative degradation of different chlorinated phenoxyalkanoic acid herbicides by a hybrid ZrO_2 gel-derived catalyst without light irradiation. ACS Appl. Mater. Interfaces 7, 256–263.

Sharma, G., Sharma, S., Kumar, A., Al-Muhtaseb, A.H., Naushad, M., Ghfar, A.A., Mola, G.T., Stadler, F.J., 2018. Guar gum and its composites as potential materials for diverse applications: a review. Carbohydr. Polym. 199, 534–545.

Silverstein, R.M., Webster, F.X., Kiemle, D.J., 2005. Infrared spectrometry. In: Brennan, D., Yee, J., Wolfman-Robichaud, S. (Eds.), Spectrom. Identif. Org. Compd, seventh. John Wiley & Sons, Inc, pp. 72–126.

Srivastava, B., Jhelum, V., Basu, D.D., Patanjali, P.K., 2009. Adsorbents for pesticide uptake from contaminated water: a review. J. Sci. Ind. Res. (India) 68, 839–850.

Tayeb, W., Nakbi, A., Trabelsi, M., Attia, N., Miled, A., Hammami, M., 2010. Hepatotoxicity induced by sub-acute exposure of rats to 2,4-Dichlorophenoxyacetic acid based herbicide “Desormone lourd. J. Hazard Mater. 180, 225–233.

Thakur, S., Chaudhary, J., Kumar, V., Thakur, V.K., 2019. Progress in pectin based hydrogels for water purification: trends and challenges. J. Environ. Manag. 238, 210–223.

Tian, B., Xiao, D., Hei, T., Ping, R., Hua, S., Liu, J., 2020. The application and prospects of cyclodextrin inclusion complexes and polymers in the food industry: a review. Polym. Int. 69, 597–603.

Utzeri, G., Verissimo, L., Murtinho, D., Pais, Alberto A.C.C., Perrin, F.X., Ziarelli, F., Iordache, T.V., Sarb, A., Valente, A.J.M., 2021. Poly(β-cyclodextrin)-Activated carbon gel composites for removal of pesticides from water. Molecules 126, 1426–1446. https://doi.org/10.3390/molecules26051426.

Trotta, F., Zanetti, M., Camino, G., 2000. Thermal degradation of cyclodextrins. Polym. Degrad. Stabil. 69, 373–379.

Utzeri, G., Matias, P.M.C., Murtinho, D., Valente, A.J.M., 2022a. Cyclodextrin-Based nanosponges: overview and opportunities. Front. Chem. 10, 859406–859431.

Utzeri, G., Murtinho, D., Maria, T.M.R., Pais, A.A.C.C., Sannino, F., Valente, A.J.M., 2022b. Amine-β-cyclodextrin based nanosponges. The role of cyclodextrin amphiphilicity in the imidacloprid uptake. Coll. Surf. A: Physicochem. Eng. Aspects 635, 128044.

Valente, A.J.M., Söderman, O., 2014. The formation of host–guest complexes between surfactants and cyclodextrins. Adv. Colloid Interface Sci. 205, 156–176. https://doi.org/10.1016/j.cis.2013.08.001.

Vedenyapina, M.D., Sharifullina, L.R., Kulaishin, S.A., Vedenyapin, A.A., Lapidus, A.L., 2017. Adsorption of 2,4-dichlorophenoxyacetic acid on activated carbon. Solid Fuel Chem. 51, 115–121.

Wang, J., Guo, X., 2020a. Adsorption kinetic models: physical meanings, applications, and solving methods. J. Hazard Mater. 390, 122156.
Wang, J., Guo, X., 2020b. Adsorption isotherm models: classification, physical meaning, application and solving method. Chemosphere 258, 127279. https://doi.org/10.1016/j.chemosphere.2020.127279.
Wang, X., Zhao, J., 2013. Encapsulation of the herbicide picloram by using polyelectrolyte biopolymers as layer-by-layer materials. J. Agric. Food Chem. 61, 3789–3796.
Wankar, J., Kotla, N.G., Gera, S., Rasala, S., Pandit, A., Rochev, Y.A., 2020. Recent advances in host–guest self- assembled cyclodextrin carriers: implications for responsive drug delivery and biomedical engineering. Adv. Funct. Mater. 30, 1909049 https://doi.org/10.1002/adfm.201909049.
Waris, K.H., Lee, V.S., Mohamad, S., 2021. Pesticide remediation with cyclodextrins: a review. Environ. Sci. Pollut. Control Ser. 28, 47785–47799. https://doi.org/10.1007/s11356-021-15434-9.
Yaashikaa, P.R., Kumar, P.S., Karishma, S., 2022. Review on biopolymers and composites – evolving material as adsorbents in removal of environmental pollutants. Environ. Res. 212, 113114 https://doi.org/10.1016/j.envres.2022.113114.
Yuh-Shan, H., 2004. Citation review of Lagergren kinetic rate equation on adsorption reactions. Scientometrics 59, 171–177.
Zadeh, R.J., Sayadi, M., Rezaei, M., 2020. Removal of 2, 4-dichlorophenoxyacetic acid from aqueous solutions by modified magnetic nanoparticles with amino functional groups. J. Wat. Env. Nanotech. 5 (2), 147–156.
Zhou, T., Fang, L., Wang, X., Han, M., Zhang, S., Han, R., 2017. Adsorption of the herbicide 2,4-dichlorophenoxyacetic acid by Fe-crosslinked chitosan complex in batch mode. Desalination Water Treat. 70, 294–301.

Insights on macro- and microscopic interactions between Confidor and cyclodextrin-based nanosponge

VII

Gianluca Utzeri, Tânia F. Cova, Dina Murtinho, Alberto A.C.C. Pais, Artur J.M Valente

Chemical Engineering Journal, vol. 455 (2023) 140882

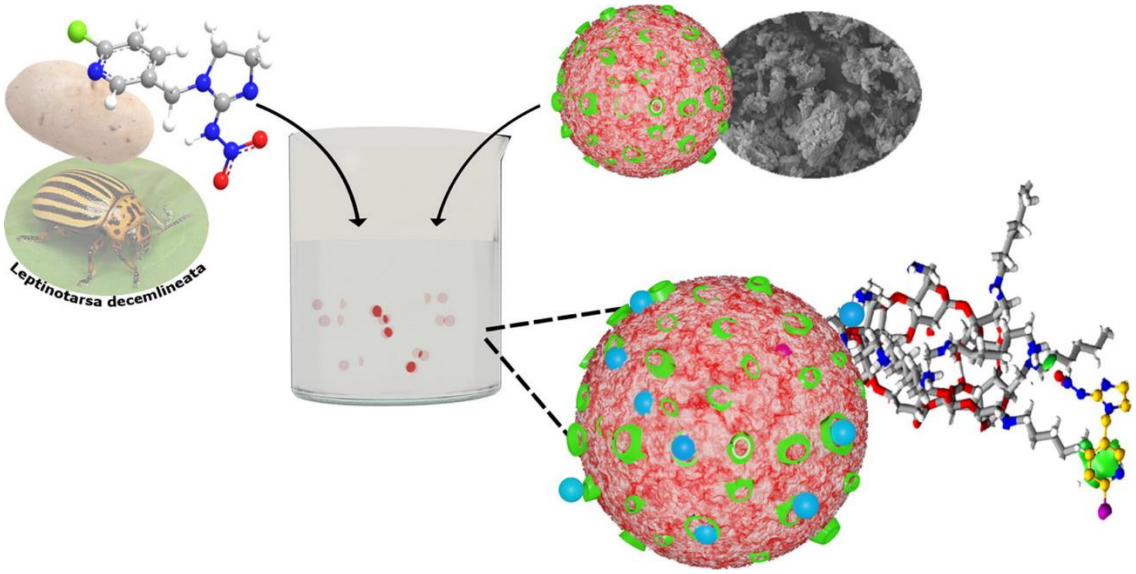

Chemical Engineering Journal 455 (2023) 140882

Contents lists available at ScienceDirect

Chemical Engineering Journal

journal homepage: www.elsevier.com/locate/cej

Insights on macro- and microscopic interactions between Confidor and cyclodextrin-based nanosponges

Gianluca Utzeri, Tânia F. Cova, Dina Murtinho, Alberto A.C.C. Pais, Artur J.M. Valente *

Coimbra Chemistry Centre, Department of Chemistry, Institute of Molecular Sciences (IMS), Faculty of Sciences and Technology, University of Coimbra, 3004-535 Coimbra, Portugal

ARTICLE INFO

Keywords:
Cyclodextrins
Commercial pesticide formulation
Imidacloprid
Nanosponges
Sorption
Molecular dynamics simulations

ABSTRACT

Imidacloprid is one of the most widely used soluble neonicotinoid insecticide, which is non–volatile and persists in the soil, with hazardous effects on birds, honeybees, and mammals. It is used in both agricultural and veterinary applications, and is found in at least 7% of European topsoils. One of the commercially available formulations is Confidor O–TEQ® that exhibits higher retention, spreading, and penetration capacity being in form of an oil suspension. In this work, porous materials based on cyclodextrin nanosponges (CDNSs) were developed for the efficient removal of imidacloprid. In the synthesis of CDNSs, α– and β–cyclodextrin and two diamine monomers, hexane–1,6–diamine (HDA) and dodecane–1,12–diamine (DDA) were used. It was found that linkers with longer aliphatic chains resulted in CDNSs with higher thermal stability and crosslinking degree. αCD_2–HDA and βCD_2–HDA showed superior sorption efficiency for Confidor O–TEQ®, as evaluated by kinetic and equilibrium sorption analyses at optimal conditions. To better understand the effects of monomer chain length and type of cyclodextrin, the sorption performance of αCD and βCD, αCD–HDA and βCD–HDA, αCD–DDA and βCD–DDA, dimeric αCD_2–HDA and βCD_2–HDA, and αCD_2–DDA and βCD_2–DDA with imidacloprid was also investigated by atomistic molecular dynamics simulations. Relevant contact patterns based on the identification of the stabilizing/destabilizing noncovalent interactions within the CD-based complexes were described in detail. Results suggest that significant modulation of the sorption performance of CDNSs for imidacloprid can be achieved by imposing various features, with direct implications for the rational design of supramolecular materials with high sorption capacity for pesticides.

1. Introduction

Persistent organic pesticides have long been responsible for controlling human disease vectors and significantly increased agricultural productivity. In recent years, however, the effects of pesticides on the environment, biodiversity, and human health became a major concern. These chemicals include organochlorines, such as imidacloprid, a systemic chloronicotinyl insecticide that can persist in the environment for prolonged periods and is readily absorbed by living organisms. It acts by contact and ingestion as postsynaptic nicotinic acetylcholine receptors and blocks insect neurotransmission.

Sorption systems have integrated efficient technologies to prevent or eliminate pesticides from the environment, as they are based on low-cost materials such as clay minerals, zeolites, aluminum, and iron oxides or oxyhydroxides, and biomaterials [1–10]. Within the latter, nanosponges (NSs) proved to be versatile materials with application in catalysis [11], sensors [12], biomedicine [13], and remediation processes [14–17]; especially for efficient removal of organic and inorganic pollutants from water and soil [18,19]. The most studied types of pollutants have been heavy metals, dyes and drugs, and to a lesser extent, pesticides [18–23]. In the case of pesticides, it should be emphasized that the agrochemical active ingredients most studied in recent years have been atrazine [24,25] and 2,4–dichlorophenol [26–29]; other examples of studied pesticides or their percursors can be found in the literature [30–33].

Imidacloprid has been used for seed treatment, in soil and veterinary applications [34], but it has been considered highly toxic to bees and birds even at low concentrations [35–37]. For this reason, neonicotinoids have been banned in Europe, and a recent study reported the presence of imidacloprid in 7 % of topsoil samples [38]. Thus, due to the large amount of imidacloprid used and the respective long half–life, it can have a serious impact on the environment and biodiversity, which requires cost-effective solutions for its removal.

* Corresponding author.
E-mail address: avalente@ci.uc.pt (A.J.M. Valente).

https://doi.org/10.1016/j.cej.2022.140882
Received 9 September 2022; Received in revised form 5 December 2022; Accepted 7 December 2022
Available online 10 December 2022

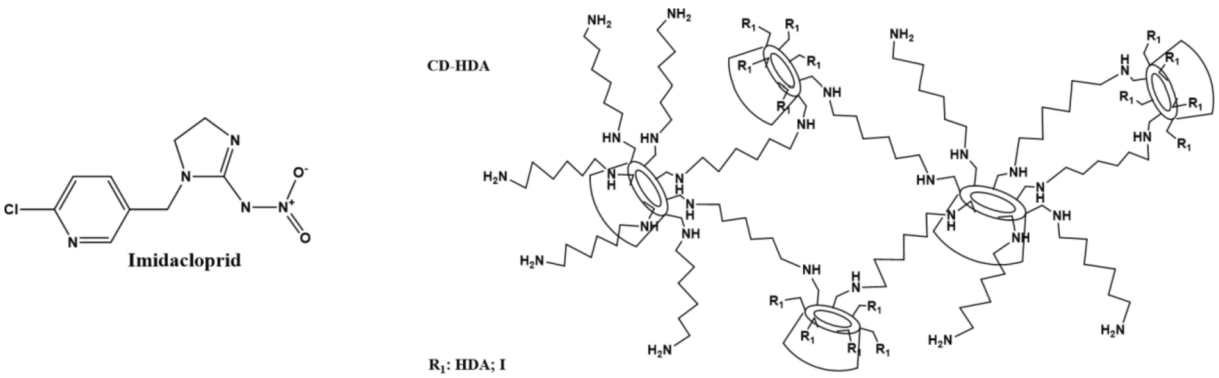

Scheme 1. Molecular structure of Imidacloprid (left); representative structure of NS with HDA as linker.

NSs are defined as water insoluble, supramolecular, porous 3D polymeric materials with high thermal stability [19]. Among the various monomers suitable for their synthesis, cyclodextrins (CDs) are the most common, due to their amphiphilic properties and high ability to form host–guest complexes. Moreover, CDs are characterized by a large number of hydroxyl groups, located at the major and minor edges of the truncated cone, which are susceptible to functionalization. Cyclodextrin-based nanosponges (CDNSs), nanoporous 3D-dimensional structures, with high degree of crosslinking and unique physicochemical properties, have recently been recognized as promising environmentally friendly sorbents for pesticides, taking advantage from the hydrophobic cavities of CDs and the hydrophilic network of the porous structure.[39 18,19,40]. The synthetic conditions (e.g., molar ratios, temperature, and pH), type and dosage of adsorbent, thermodynamics signatures, isothermal adsorption models, kinetics, contact time, competing ions, toxicity and safety of CDNSs are important factors affecting the adsorption and removal of pesticides and requiring a thorough evaluation [41]. The synthesis of CDNSs can be tailored to the desirable properties for the required functions by varying the synthetic routes, the crosslinkers and solvents, among other factors [42,43].

In this work, the effect of alkyl chain length of crosslinkers, for two different natural cyclodextrins (α-CD and β-CD), obtained by a new synthetic route, for the sorption of imidacloprid from a commercial formulation (Confidor O–TEQ® [44]), is reported (Scheme 1). The synthetic route is characterized by a faster microwave assisted procedure and by the use of hexane–1,6–diamine (HDA) and dodecane–1,12–diamine (DDA) as linkers.

The novelty thus consists in the synthetic route, and on the ability to explain, at the molecular level, the role of the HDA and DDA crosslinkers in the adsoprtion efficiency of α-CD and β-CD NSs, with Confidor O-TEQ as guest.

The O–TEQ family brand represents an oil dispersion formulation that contains adjuvants and vegetable oil to provide better retention, distribution and penetration properties [45]. This oil dispersion is defined as a stable suspension of the active ingredient in a water immiscible fluid [46].

NSs were characterized using a range of techniques for complete morphological, physicochemical and thermal characterization. The influence of the oil component was also evaluated by measures of surface tension. In addition, the sorption mechanism and efficiency were assessed by kinetic and isothermal sorption analysis at the optimal experimental conditions in term of S/L ratio and pH. The sorption performance of the polymeric materials was further tested in the presence of ionic and non–ionic fertilizers as model interfering factors as well as their reusability. Finally, the binding enthalpies and stabilizing/destabilizing noncovalent interactions within the complexes between αCD/βCD, αCD/βCD–HDA, αCD/βCD–DDA, and α/βCDNSs in dimeric models and imidacloprid were investigated by explicit water molecular dynamics simulations (MD), together with a description of the noncovalent interactions (NCI) including their spatial distribution features. The analysis of NCI was performed using the Independent Gradient Method (IGM) [47], which allows to visualize the regions of low charge density corresponding to stabilizing/destabilizing NCI. These are based on the analysis of the electronic charge density of the interacting molecules and their gradients, as well as on the quantitative comparison of the strength of NCI by calculating the IGM descriptor δg, which directly corresponds to the charge density gradient(s) in real space (for details, see ref. [47]).

2. Materials and methods

2.1. Materials

For the synthesis of NSs, α– and β–cyclodextrins were supplied by Sigma Aldrich (purity 98 %), triphenylphosphine (Ph_3P) by Alpha Aesar, and iodine (I_2) as resublimed pearls by PanReac. Hexane–1,6–diamine (HDA) and dodecane–1,12–diamine (DDA) crosslinkers were purchased from Sigma-Aldrich. *N,N*–dimethylformamide (DMF) was obtained from Honeywell (purity ≥ 99.8 %) and dried using molecular sieves and methanol (MeOH) was obtained from Chem–Lab (purity 99.8 %). Commercial Confidor O–TEQ® (206 g/L in imidacloprid content) was acquired under license from Direção-Geral de Alimentação e Veterinária (Portugal). Urea and ammonium nitrate, used as additive models, were obtained from Fagron (purity 100 %) and Chem–Lab (purity greater than 99 %), respectively. The other chemicals were used without further purification, unless otherwise stated.

2.2. Synthesis of amine–cyclodextrin nanosponges

Four different nanosponges were synthesized using a similar procedure, which was described in a previous work [18]. Anhydrous cyclodextrins were modified with iodine to obtain *per*–(6–iodo)–(6–deoxy)–cyclodextrin (CD-I) [48]. The *per*-6-iodo cyclodextrins were subject to a second *per*–nucleophilic substitution with the crosslinker (either HDA or DDA), in a 20–fold excess, using a microwave-assisted procedure with temperature control (85 °C for 40 min). Finally, the synthesis of nanosponges was carried out by reacting CD–I with CD–HDA or CD–DDA in 1:1 (mol iodine per mol amine). The mixture was mechanically grinded and homogenized, a minimal amount of DMSO was used to facilitate the interaction of the reactants, and the reaction was carried out at 70 °C for 48 hr. In the following, the different NSs are referred as: αCD_2–HDA, αCD_2–DDA, βCD_2–HDA and βCD_2–DDA. All NSs were freeze–dried and grinded for storage. NMR characterization of the αCDs is reported below. The yield and substitution efficiencies for CD–I and CD–HDA (or DDA) were determined by ^{1}H–nuclear magnetic resonance (^{1}H NMR) at 400 MHz, using 10 mg mL^{-1} of compounds in DMSO-d_6 containing trace amounts of sodium salt of trimethylsilylpropionic acid-d_4.

The synthesis of *hexakis*– (6–iodo)–(6–deoxy)–*α*–cyclodextrin

(αCD–I), yield (73 %), was confirmed by ^{1}H NMR in DMSO–d_6: 3.32–3.42 (m, 12H); 3.47–3.56 (m, 6H); 3.58–3.67 (m, 6H); 3.71–3.78 (m, 6H); 3.79–3.85 (m, 6H); 4.95 (d, $J = 3.2$ Hz, 6H); 5.65 (d, $J = 2.4$ Hz, 6H); 5.80 (d, $J = 7.2$ Hz, 6H).

Substitution with HDA or DDA was confirmed by NMR. *Hexakis*–[(6–(6–amine–1–hexylamine)–(6–deoxy)–α–cyclodextrin (αCD–HDA), yield (85 %), ^{1}H NMR in DMSO–d_6: 1.30–1.53 (m, 48H); 2.77–2.81 (m, 24H); 3.02–3.14 (m, 6H); 3.25–3.37 (m, 6H); 3.59–3.97 (m, 24H); 4.81 (bs, 6H). *Hexakis*–[(6–(12–amine–1–dodecylamine)–(6–deoxy)–α–cyclodextrin (αCD–DDA), yield (80 %), ^{1}H NMR in DMSO-d_6:Hexakis–[(6–(12–amine–1–dodecylamine)–(6–deoxy)–α–cyclodextrin (αCD–DDA), yield (80 %), ^{1}H NMR in DMSO-d_6: 1.13–1.58 (m, 120H); 2.52–2.54 (m, 12H); 2.63–2.78 (m, 24H); 2.98–3.11 (m, 6H); 3.23–3.35 (m, 6H); 3.67–3.87 (m, 12H); 4.79 (bs, 6H).

Solubility assays were carried out by using the following solvents: water, methanol, acetone, dimethylformamide, chloroform and toluene. The solubility measurements were performed by adding a weighed amount of nanosponge to 5 mL of solvent and left in equilibrium, with helical stirring, during 1 week. After that time, the samples were centrifuged. The supernatant was collected and the corresponding UV–vis spectrum was obtained by using a Shimadzu UV–vis 2600 I spectrophotometer; the solid was lyophilized and weighed (by using a RADWAG AS 220/C/2 balance). Gravimetric analysis showed negligible changes on the weight taking into account an uncertainty of 5 %. On the other hand, supernatant spectra, for all solvents, do not show any band characteristic of CD-HDA and CD-DDA. We can conclude that, in the aforementioned conditions, no solubilization occurs.

2.3. Characterization of nanosponges

The chemical structure of CDNSs, such as the presence of functional groups were characterized by Fourier transform infrared spectroscopy (*Thermo Scientific,* model Nicolet 6700 FT–IR) in a wavelength range of 4000–400 cm^{-1} using KBr pellets. The percentage (w/w) of N, C and H of CDNSs, in powder state, was determined by elemental analysis (EA 1108 CHNS–O, Fisons); the experiments were carried out in triplicate.

The thermal stability of the polymers was determined by thermogravimetric analysis (TGA) (*Netzsch Instruments*, model TG209–F3 Tarsus), and differential scanning calorimetry (DSC) (PerkinElmer, model DSC 7). For TGA, data were acquired using the *NETZSCH Measurement v. 6.0* program and processed using *NETZSCH Proteus Thermal Analysis*. The analysis were performed using approximately 3–5 mg of powdered material at a temperature range between 25 and 500 °C, at a heating rate of 5 K min^{-1}, and a nitrogen flow rate of 50 mL min^{-1}. Thermal analysis was performed before and after contact of NSs with an aqueous suspension of Confidor O–TEQ® at approximately 150 mg L^{-1} of IMD for 24 h, at 25 °C. The DSC experiments were performed using ca. 3 mg of compound in 30 μL aluminum vented pans, in the temperature range from 0° to 200 °C, with a heating rate of 20 °C min^{-1}, under a 20 mL min^{-1} nitrogen flow rate.

Particle size distribution and surface charge were determined by dynamic light scattering (DLS) and ζ–potential analysis (*Malvern Zetasizer NanoZS*), using an aqueous suspension of CDNSs (0.2 mg mL^{-1}) sonicated before measurements. These measurements were performed at four pH values (3.5, 4.5, 6.5, 8.5, 9.5) to evaluate the effect of pH. A neon laser with scattering angle of 173° was used for the DLS measurements. The hydrodynamic diameter (ζ–average) and polydispersity index (PDI) of NSs were determined from the intensity distribution obtained by cumulative analysis. ζ–potential values were calculated from electrophoretic mobility using the Smoluchowski relationship. Values are averages of three independent measurements. The active surface area (S_{BET}), pore volume and pore size distribution were determined by nitrogen adsorption–desorption analysis (*ASAP 2000, Micrometrics*). Surface morphology and near-surface elemental composition of NSs were determined by scanning electron microscopy (SEM), and energy dispersive X-ray (EDX), operating at 4 kV and 7 kV, respectively (*Gemini 2-Zeiss, Merlin-Zeiss*, Oberkochen, Germany). EDS data represents an average of three measurements carried out in three different areas of the sample. Prior to analysis, the samples were sputter-coated with a thin gold layer.

To determine the role of the oil formulation of Confidor O–TEQ®, the surface tension of the aqueous suspension and the aqueous imidacloprid solution, both at 150 mg L^{-1} of IMD, were measured and compared. The analysis was performed using a tensiometer (*Sigma702, Biolin Scientific*) at constant temperature of 25 °C (HAAKE AC150 coupled with HAAKE A10, *Thermo-Scientific*). Measurements were performed in triplicate using the Du Noüy ring of platinum and the Huh-Mason correction method [49].

2.4. Sorption analysis

For the sorption experiments, we took into account the preparative indication for Confidor O–TEQ® concentration, the dosage value of 75 mL hL^{-1} (ca. 150 mg L^{-1} of imidacloprid) in water recommended for use against Colorado potato beetle (*Leptinotarsa decemlineata*) in potato crops.

The rate of degradation (*DR*) of Confidor O–TEQ®,

$$DR = \left(1 - \left(\frac{C_t}{C_0}\right)\right) \times 100 \quad (1)$$

Measured by quantification of the active ingredient, imidacloprid, was also tested at four pH values (3.5, 4.5, 6.5, 8.5 and 9.5) within 7 days, at 25 °C and under stirring, at 120 rpm. The pH was adjusted by micro addition of HCl or NaOH 0.01 M. The natural pH of an aqueous suspension of Confidor O–TEQ® at 150 mg L^{-1} of IMD is 6.5.

The sorption analysis can be divided into two phases. First, the optimal conditions were determined hence, the effect of the solid/liquid ratio (S/L ratio, mg of sorbent per mL of solution) and the influence of pH were evaluated. The experiments were performed at 25 °C, with agitation at 120 rpm, for at least 24 h.

The effects of S/L (mg mL^{-1}) ratio and pH were evaluated as a function of the amount of pesticide sorbed per gram of sorbent (q_e as mg g^{-1}) and removal efficiency (*RE*) calculated using

$$q_e = \frac{C_0 - C_e}{m} \times V \quad (2)$$

$$RE = \frac{C_0 - C_e}{C_0} \quad (3)$$

where C_0 and C_e (mg L^{-1}) are the concentration of IMD in the initial and equilibrium states, respectively, m (g) is the mass of the sorbent, and V (L) is the volume of the suspension.

In the second phase, the kinetic and equilibrium sorption analysis were performed at the optimal conditions of S/L and pH for the most effective materials for the sorption of imidacloprid: CD–HDA. Both NSs have shown as optimum S/L = 0.1 mg mL^{-1}, and pH 4.5 and 6.5, for α– and β–CD, respectively. It must be emphasized that βCD_2–HDA also shown remarkable removal efficiency at S/L = 10 mg mL^{-1} which was further investigated. Kinetic sorption was performed in an aqueous suspension of Confidor O–TEQ®, 150 mg L^{-1} of imidacloprid, for 30 h and kinetics was modelled using pseudo-first order (PFO) (4), and pseudo-second order (PSO) equations, respectively

$$q_t = q_e\left(1 - e^{-k_1 t}\right) \quad (4)$$

$$q_t = \frac{k_2 q_e^2 t}{1 + k_2 q_e t} \quad (5)$$

where q_t (mg g^{-1}) is the amount of sorbate at time, t (min). k_1 (min^{-1}) and k_2 (g mg^{-1} min^{-1}) are the rate constants for PFO and PSO, respectively [50]. The goodness of fit of the equations to the experimental data was evaluated using the adjusted coefficient of determination (Adj.-R^2) and the Akaike information criterion (AIC), which was

calculated as

$$AIC = Nln\left(\frac{RSS}{N}\right) + 2k + \frac{2k(k+1)}{N-k-1} for \frac{N}{k} < 40 \quad (6)$$

where N is the number of the experimental points, RSS is the residual sum of squares and k is the number of fitted parameters.

Isothermal sorption analysis was performed in an IMD concentration range of 2.5–150 mg L^{-1}. Fitting to the experimental data was performed using the equations of Langmuir and Brunauer-Emmet-Teller (BET), respectively

$$q_e = \frac{q_m K_L C_e}{1 + K_L C_e} \quad (7)$$

$$q_e = \frac{q_s C_{BET} C_e}{\left[C_s + (C_{BET} - 2)C_e - \left((C_{BET} - 1)C_e^2/C_s\right)\right]} \quad (8)$$

where q_m (mg g^{-1}) is the maximum sorption capacity per unit weight of sorbent and K_L (L mg^{-1}) is the Langmuir constant. q_s (mg g^{-1}), C_{BET} (L mg^{-1}) and C_s (mg L^{-1}) are the theoretical isothermal saturation capacity, BET constant for sorption isotherm and sorbate monolayer saturation concentration, respectively.

Since βCD_2–HDA is the best sorption material, its sorption capacity was tested at S/L = 0.1 mg mL^{-1} and 10 mg mL^{-1}, at pH 6.5 in the presence of NH_4NO_3 or urea (two of the most commonly used nitrogen fertilizers) as ionic and non-ionic interfering substances, respectively, at a molar ratio within 0.25–2 (mol/mol) with Confidor O–TEQ® (150 mg L^{-1} of imidacloprid).

The reusability of αCD_2–HDA and βCD_2–HDA was assessed. The analysis was performed considering the optimal experimental conditions in term of q_e, i.e. S/L = 0.1 mg mL^{-1} for both NSs, imidacloprid concentration of 150 mg L^{-1} as Confidor O–TEQ® at pH = 4.5 for αCD_2–HDA and 6.5 for βCD_2–HDA. The reusability was evaluated by performing 5 cycles of sorption/desorption (each one of 24 h), at 25 °C.

2.5. Molecular dynamics simulations

The specific recognition between αCD/βCD, αCD/βCD–HDA, αCD/βCD–DDA, and αCD/βCDNSs, represented as dimeric models, and imidacloprid was investigated by calculating the binding enthalpies associated with the formation of 1:1 complexes between these monomeric (αCD/βCD, αCD/βCD–HDA, αCD/βCD–DDA) and dimeric models ($\alpha CD_2/\beta CD_2$–HDA, $\alpha CD_2/\beta CD_2$–DDA) and imidacloprid, and by analyzing the topological features of the electronic charge densities of the –binding partners. Such an approach is described in detail in references [51] and [52].

The binding enthalpies are calculated from

$$\Delta H = \langle H \rangle_{complex} + \langle H \rangle_{purewater} - \langle H \rangle_{CD} - \langle H \rangle_{Imidacloprid} \quad (9)$$

where $\langle H \rangle_{complex}$, $\langle H \rangle_{purewater}$, $\langle H \rangle_{CD}$, and $\langle H \rangle_{Imidacloprid}$ correspond in each system to the Boltzmann averaged total potential energies for the complexes, pure water, solvated αCD/βCD, αCD/βCD–HDA, αCD/βCD–DDA, and $\alpha CD_2/\beta CD_2$–NSs and solvated imidacloprid simulations, respectively.

The nature and strength of intermolecular interactions from CD systems is decoupled and a complementary rationale to the influence of monomer chain length on αCD/βCDNS structure and sorption behavior is provided.

Single, solvated αCD/βCD, αCD/βCD–HDA, αCD/βCD–DDA, $\alpha CD_2/\beta CD_2$–HDA and $\alpha CD_2/\beta CD_2$–DDA, and imidacloprid molecules were considered as system references. For $\alpha CD_2/\beta CD_2$–HDA and $\alpha CD_2/\beta CD_2$–DDA backbones, two units of αCD/βCD–HDA and αCD/βCD–DDA were considered.

The starting geometries of CD-based and imidacloprid molecules were constructed in Avogadro and Pymol and optimized with the semi–empirical Antechamber/SQM method. Specifically, αCD/βCD–HDA and αCD/βCD–DDA, with a net charge of 12 (αCD) and 14 (βCD), were constructed from the initial coordinates of αCD/βCD extracted from the RCSB protein data bank (PDB codes: 4FEM and 1DMB, respectively), and by replacing the primary hydroxyl groups with HDA and DDA chains, to achieve the appropriate substitution degree of the αCD/ β CD used experimentally. The $\alpha CD_2/\beta CD_2$–HDA and $\alpha CD_2/\beta CD_2$–DDA dimers, with a net charge of 22 (αCD_2) and 26 (βCD_2), were constructed using, respectively, one HDA and one DDA chain as linker. The topologies for each binding partner were generated using the Automated Topology Builder server (version 3.0) and partial charges for each molecule were obtained from the semi-empirical (AM1) with bond charge correction (BCC) method. [53].

A cubic box of 7.5 nm edge-length was used for each system containing one single molecule or one molecule of each binding partner, solvated with explicit SPC216 water molecules.

MD simulations were performed with the GROMACS package (version 2019.1) using the all-atom gromos54a7 force field to describe both CD-based and imidacloprid molecules, under periodic boundary conditions, and with a NPT ensemble [47,54].

A constant temperature and pressure of 300 K and 1 bar, respectively, were imposed in all simulations, by the coupling constants of 0.1 ps and 2 ps, to v–rescale and Parrinello–Rahman external baths. Standard time steps of 1 (for dimers) and 2 fs (for monomers) were used for both equilibration and production runs. Nonbonded interactions were computed based on a neighbor list, updated every 10 steps. Lennard–Jones interactions and electrostatic interactions were computed using a cut-off of 1.2 nm and the particle mesh Ewald (PME) method, respectively. The constraints in the binding partners were imposed by the LINCS algorithm.

To obtain the starting configurations, each system was firstly subjected to energy minimization steps. Equilibrium properties, structure and dynamics of CD systems were calculated over the 200 ns simulation runs, after the systems were equilibrated for 50 ns. No pressure coupling was imposed during the production runs, allowing to keep the size of the simulation box constant. The simulated time was sufficient to provide robust statistics for the binding enthalpies, and the last 5 ns were subjected to the standard analysis. These include time-dependent RMSD for all αCD/ β CD, αCD/ β CD–HDA/DDA, and $\alpha CD_2/\beta CD_2$–HDA/DDA atoms free in solution and upon complexation, and geometric clustering performed to identify similar structures, sampled during the MD simulations. The algorithm for geometric cluster analysis is based on the hierarchical (top–down) approach, as described in [55], and allows evaluating the conformational prevalence of each CD structure, and selecting a representative complex conformation for further analysis by the Independent Gradient Method (IGM).

2.6. Analysis of noncovalent interactions

Evaluation of the noncovalent interactions (NCI) within αCD/ β CD: imidacloprid, αCD/βCD–HDA/DDA:imidacloprid and $\alpha CD_2/\beta CD_2$–HDA/DDA:imidacloprid complexes was performed based on IGM [28,36], and using the IGMPlot software (version 2.0). This method enables the analysis of the electronic charge density of the binding partners and the respective gradients, and the visualization and quantification of regions of stabilizing/destabilizing noncovalent interactions. It is based on the topological characteristics of the electronic charge density, ρ, of each system, and uses quantities corresponding to the first and second derivatives of the density. The computed δg^{inter} is the IGM descriptor estimated by the difference between the first derivatives of the charge densities for the final complexes and the respective free components,

$$\delta g^{inter} = \left|\nabla \rho^{IGM,inter}\right| - |\nabla \rho| \quad (10)$$

The nature and strength of NCI are detected when δg^{inter} takes positive values and is determined the size of the descriptor at a point in

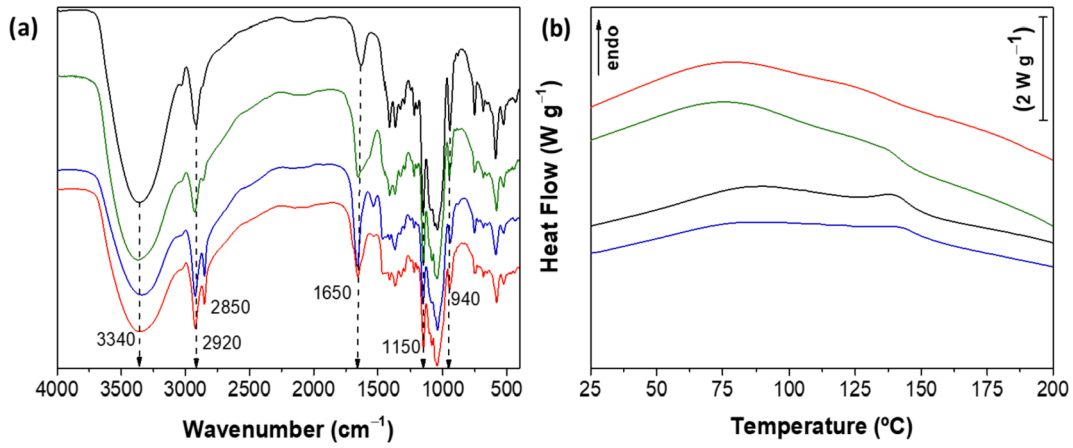

Fig. 1. FTIR spectra (a) and differential scanning calorimetry thermograms (b) of different NSs: βCD$_2$–HDA (black), αCD$_2$–HDA (green), βCD$_2$–DDA (blue) and αCD$_2$–DDA (red).

space. The term $\nabla\rho^{IGM,inter}$ is calculated from the sum of the N atoms in the two binding partners (A and B) along the x–direction,

$$\left(\frac{\delta_\rho}{\delta_x}\right)^{IGM,inter} = \left|\sum_{i=1}^{N_A}\frac{\delta_{\rho_i}}{\delta_x}\right| + \left|\sum_{i=1}^{N_B}\frac{\delta_{\rho_i}}{\delta_x}\right| \quad (11)$$

Visualization of NCI is enabled by IGMPlot by selecting the pre-computed atomic charge densities to estimate a pro-molecular density that has a minimal effect on the non–covalent interactions. While δg^{inter} allows identifying NCI regions, ∇^2_ρ, the second Laplacian derivative of the density, is used for discriminating stabilizing/destabilizing NCIs. The decomposition of ∇^2_ρ into the 3 eigenvalues (λ) of maximal variation, $\nabla^2_\rho = \lambda_1 + \lambda_2 + \lambda_3 (\lambda_1 \leq \lambda_2 \leq \lambda_3)$, provides information on the stabilizing ($\lambda_2 < 0$) or destabilizing ($\lambda_2 > 0$) interactions. Larger negative values of $sign(\lambda_2)\rho$ suggest stronger interactions (e.g., hydrogen bonds) while $sign(\lambda_2)\rho$ values close to zero indicate weak NCI (e.g., van der Waals forces). These values reflect both the extent and (de)stabilizing nature of the interactions.

The coordinates of the complexes were extracted from the ensemble of structures at the equilibrium state, sampled from the production runs using the clustering procedure detailed in [47] and the coordinates of the corresponding binding partners were isolated to perform the analysis. For each complex relevant NCI occurring between host and guest molecules are represented by isosurface volumes proportional to the δg^{inter} values and are colored according to the $sign(\lambda_2)\rho$ range. For details see [56].

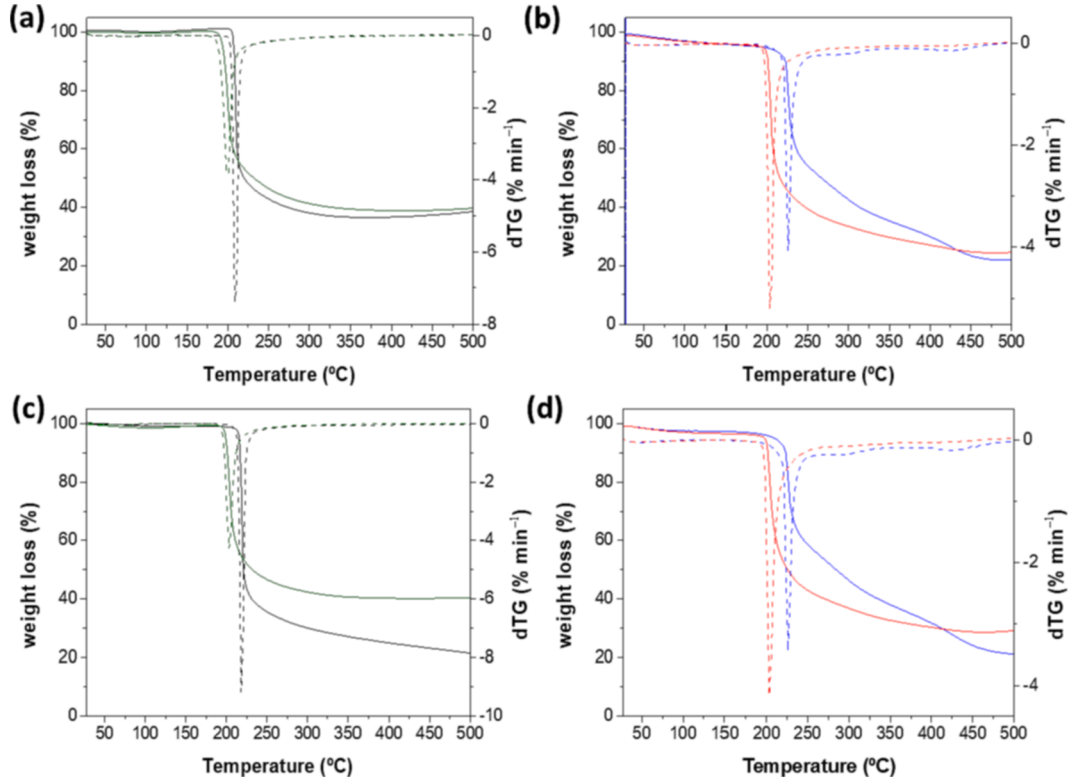

Fig. 2. TGA (solid curves), and dTG (dashed curves), of (a) pure βCD$_2$–HDA (black) and αCD$_2$–HDA (green) and, (c) in the presence of Confidor O–TEQ®; (b) pure βD$_2$–DDA (blue) and αCD$_2$–DDA (red) and, (d) in the presence of Confidor O–TEQ®.

Table 1
Elemental analysis, EDX and N_2 adsorption results for CDNSs.

Elemental and EDX analysis						
CDNSs	N% (w/w)	C% (w/w)	H% (w/w)	I% (w/w)[a]	CD% (w/w)[b]	DC[c]
αCD_2–HDA	1.04 ± 0.01	27.9 ± 0.2	3.4 ± 0.2	32 ± 1	0.69	1.5
αCD_2–DDA	1.69 ± 0.01	31.43 ± 0.02	4.1 ± 0.2	37 ± 1	0.59	2.9
βCD_2–HDA	0.51 ± 0.02	27.37 ± 0.06	2.95 ± 0.09	40 ± 2	0.62	0.8
βCD_2–DDA	3.25 ± 0.02	38.78 ± 0.07	5.7 ± 0.3	33 ± 3	0.46	7.0

N_2 adsorption			
	S_{BET} (m^2/g)	Porevolume ($cm^3\ g^{-1}$)	Porediameter (nm)
αCD_2–HDA	17.2	0.16	31.7
αCD_2–DDA	10.7	0.01	3.8
βCD_2–HDA	21.8	0.13	27.4
βCD_2–DDA	17.9	0.03	16.5

[a] I% (w/w) values are merely indicative because they are obtained by EDX analysis.
[b] CD% = (C% − C_{linker}%)/C_{CD}.
[c] DC (degree of crosslinking) is calculated as the amount of N per mole of cyclodextrin as obtained by elemental analysis.

3. Results and discussion

The rationale behind the development of CDNSs is becoming increasingly important, especially for the elimination of pesticides. Relying on supramolecular structures, which involve a degree of complexity related to, for example, the type and amount of CD, the type and size of the crosslinker, variations in conformational behavior must be supported by a deep understanding of the sorption mechanism. In this context, several questions arise: how can CDNSs with optimal sorption performance for imidacloprid be formed? Does the length of the monomer chain matter? What determines the sorption behavior at the molecular level? What are the most important interaction forces? These

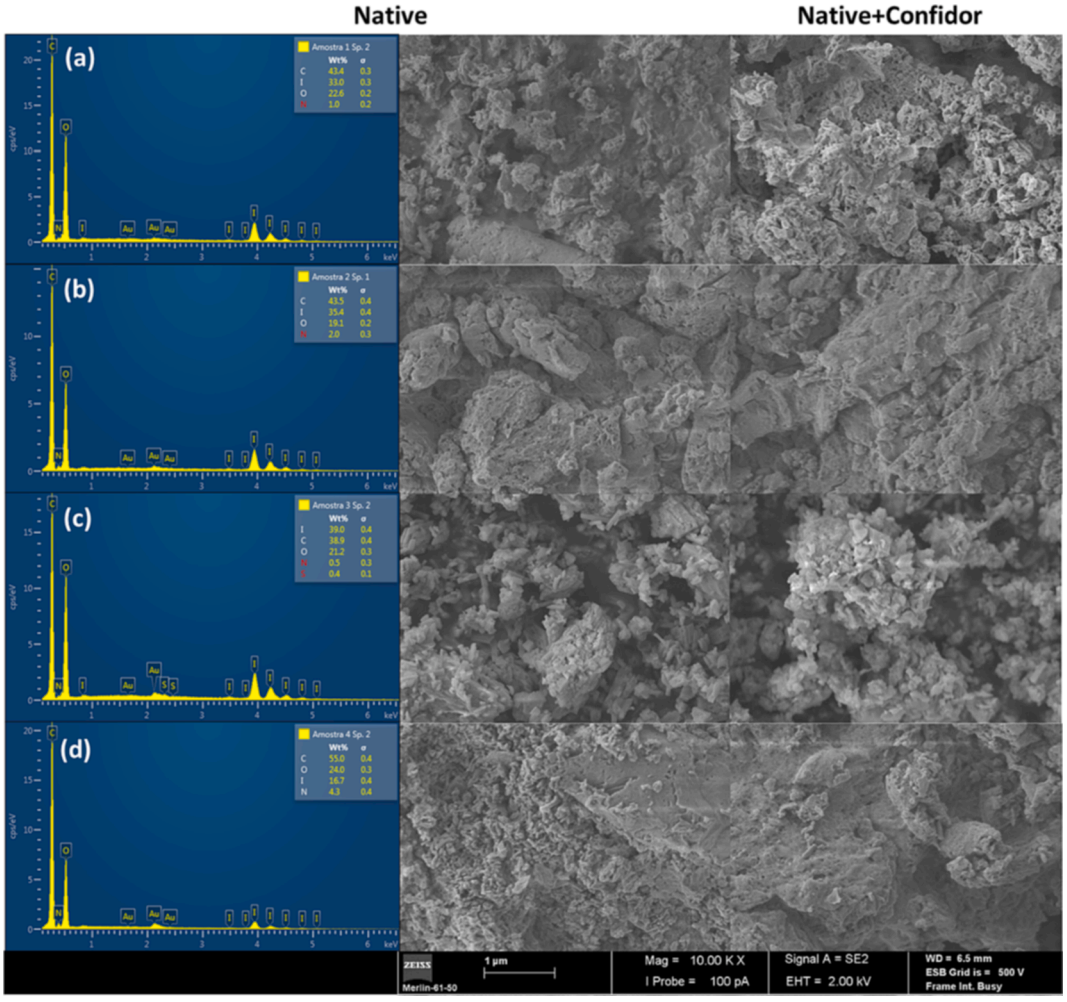

Fig. 3. SEM micrographs of CDNSs before and after contact for 24 h with a solution of Confidor O–TEQ® at imidacloprid concentration equal to 150 mg L^{-1} (magnification × 10000 and 2.0 kV). (a) αCD_2–HDA, (b) αCD_2–DDA, (c) βCD_2–HDA and (d) βCD_2–DDA.

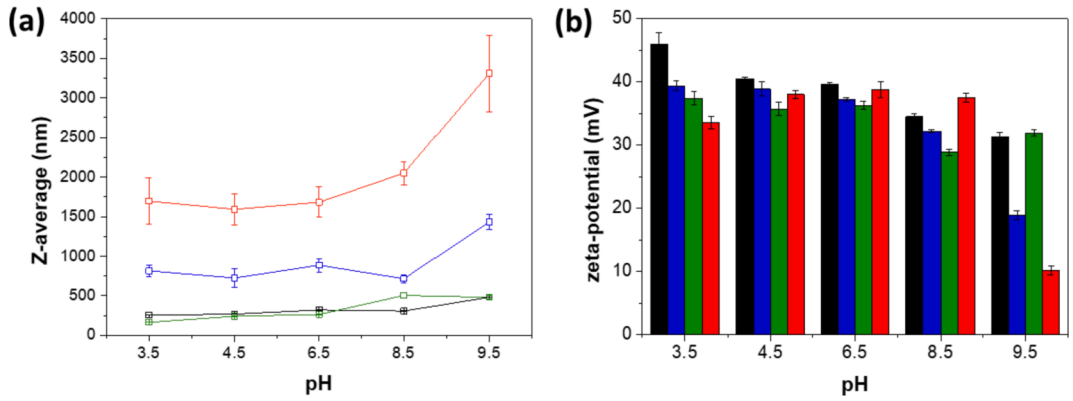

Fig. 4. Representation of particle size distribution (a) and ζ–potential (b) as a function of pH. Key: αCD$_2$–HDA (green), αCD$_2$–DDA (red), βCD$_2$–HDA (black) and βCD$_2$–DDA (blue).

challenging aspects are investigated below, combining insights from elemental analysis, N_2–sorption, surface tension, FTIR, TGA and DSC, SEM and EDS, DLS and ζ–potential and MD simulations.

3.1. Characterization of nanosponges

The FTIR spectra for α- and β–CD-based nanosponges are shown in Fig. 1a. It can be seen that the four polymers are characterized by similar vibrational modes at ca. 3340, 1650, 1150 and 1080 cm^{-1}, which are related to stretching and bending vibrations of the secondary –OH and –C—O—C– groups [57]. Even though, the band at ca. 3340 cm^{-1} of CDNSs is sharper than that normally observed in pristine cyclodextrin, which is due to the substitution of primary –OH groups in C6 position by primary and secondary –NH groups. The two bands at 2920 and 2850 cm^{-1} are associated with symmetric and asymmetric stretching vibrations of –CH_2– groups from the aliphatic chain of the monomers. These are better resolved for αCD$_2$–DDA and βCD$_2$–DDA with a longer aliphatic chain. Primary and secondary amine groups are also confirmed by the peaks at 1650, 1150 and 940 cm^{-1}, which are related to the –NH_2 and –NH– bending and wagging vibrations and the –C—N stretching vibration, respectively [18].

Looking at the effect of CDs and crosslinkers in the thermal analysis (Fig. 2), it can be seen that α CD$_2$–HDA, βCD$_2$–HDA and αCD$_2$–DDA have similar thermograms, with a single maximum of thermal degradation temperature (d^2(weight loss)/dT^2 = 0), $T_{max(2)}$, at about 200 °C for αCDNSs and 210 °C for βCD$_2$–HDA (Fig. 2-a and 2-b). The slightly higher stability of βCD$_2$–HDA can be justified by the high content of CD units per nitrogen unit, which prompts the formation of numerous inter- and intramolecular hydrogen bonds (see Table 1). The single degradation step may also indicate a more homogeneous supramolecular structure, as confirmed by SEM micrographs. In contrast, βCD$_2$–DDA exhibits three maximum of degradation temperatures; the first initial degradation temperatures (at 226 and 310 °C) may be related to the degradation of CDs in two different states (native and functionalized) [58], while the third degradation temperature ($T_{max(4)}$), which occurs at 415 °C, may be due to amine bond breaking [18]. No significant changes in the thermal profile of the αCDNSs were observed after 24 h of contact with Confidor O–TEQ® suspension. It should be noted that a slight shift to higher temperatures was observed for βCD$_2$–HDA ($T_{max(2)}$ = 220 °C), which can be related to the formation of inclusion complexes that increases the thermal stability of βCD$_2$–HDA by establishing inter– and intramolecular interactions. On the other hand, βCD$_2$–DDA shows a decrease of $T_{max(3)}$ to 280 °C, which is probably due to the highly compact structure of the materials. The diffusion of the pesticide into the porous network forces the structure to a more unstable conformation. A complete characterization of the thermograms is summarized in Table SI1.

Taking in mind the $T_{max(2)}$ values corresponding to the first thermal degradation, the DSC analysis were performed within 0 – 200 °C. No reversible transitions were observed during the cycles of heating/cooling (not shown). As it can be seen (Fig. 1b), all NSs show a very similar thermograms with two irreversible endothermic events. These are probably related with residual solvent loss such crystalline water, since the range of temperature is matching with that of TGA curves.

Table 2
DLS and zeta–potential parameters of CDNSs.

Nanosponges	Ph	Z–average ± std (d.nm)	PDI ± std	ζ ± std (mV)
βCD$_2$–HDA	3.5	253.7 ± 0.2	0.137 ± 0.006	46.0 ± 1.8
	4.5	267 ± 3	0.13 ± 0.02	40.5 ± 0.3
	6.5	320 ± 6	0.20 ± 0.03	39.6 ± 0.4
	8.5	306 ± 5	0.28 ± 0.01	34.5 ± 0.5
	9.5	481 ± 4	0.37 ± 0.01	31.3 ± 0.6
αCD$_2$–HDA	3.5	163 ± 2	0.16 ± 0.01	37.4 ± 1.0
	4.5	241 ± 4	0.18 ± 0.02	37.2 ± 1.0
	6.5	263 ± 3	0.19 ± 0.02	38.3 ± 0.4
	8.5	503 ± 36	0.46 ± 0.08	28.9 ± 0.5
	9.5	478 ± 24	0.41 ± 0.02	31.9 ± 0.5
βCD$_2$–DDA	3.5	814 ± 78 *	0.44 ± 0.04	39.4 ± 0.7
	4.5	7249 ± 122 *	0.6 ± 0.1	38.9 ± 1.1
	6.5	886 ± 84 *	0.6 ± 0.1	37.2 ± 0.3
	8.5	714 ± 52 *	0.51 ± 0.04	32.2 ± 0.2
	9.5	1432 ± 99 *	0.61 ± 0.08	18.9 ± 0.7
αCD$_2$–DDA	3.5	1696 ± 293 *	0.79 ± 0.08	33.5 ± 1.0
	4.5	1592 ± 193 *	0.8 ± 0.2	38.0 ± 0.68
	6.5	1682 ± 193 *	0.75 ± 0.06	32.0 ± 0.4
	8.5	2050 ± 145 *	0.747 ± 0.008	32.2 ± 0.2
	9.5	3311 ± 485 *	0.7 ± 0.2	18.8 ± 0.2

* Values obtained considering two nodal distributions.

The elemental composition of the NSs was evaluated by elemental analysis and EDX (Fig. 3) and data are reported in Table 1. From Table 1, it can be concluded that HDA–nanosponges are those with the lowest content of nitrogen and the highest values for CD%. Furthermore, degree of crosslinking increases in the order: βCD$_2$–HDA < αCD$_2$–HDA < αCD$_2$–DDA < βCD$_2$–DDA. Thus, there seems to be a strong correlation between the degree of freedom of crosslinkers, and consequently of NSs, and the ratio between N% and CD%. These outcomes agree with the results obtained by nitrogen adsorption (Table 1) and SEM (Fig. 3). It can also be concluded that in all NSs the amount of unreacted C-I groups is significant.

In general, it can be stated that S_{BET} depends on DC, i.e., lower DC leads to a higher S_{BET}. An exception is βCD$_2$–DDA, where both DC and S_{BET} are high. That can be justified by an entanglement of the longer monomer, which limits the CD content per unit of free –NH_2 and distorts the cyclodextrin structure. Thus, the higher degree of freedom of the aliphatic chain leads to a structural collapse and highly compact structures. It can also be observed that the pore volume and diameter depend essentially on the length of the alkyl chain of the anchor. In fact, the lowest pore volume for αCD$_2$–DDA and βCD$_2$–DDA is a possible

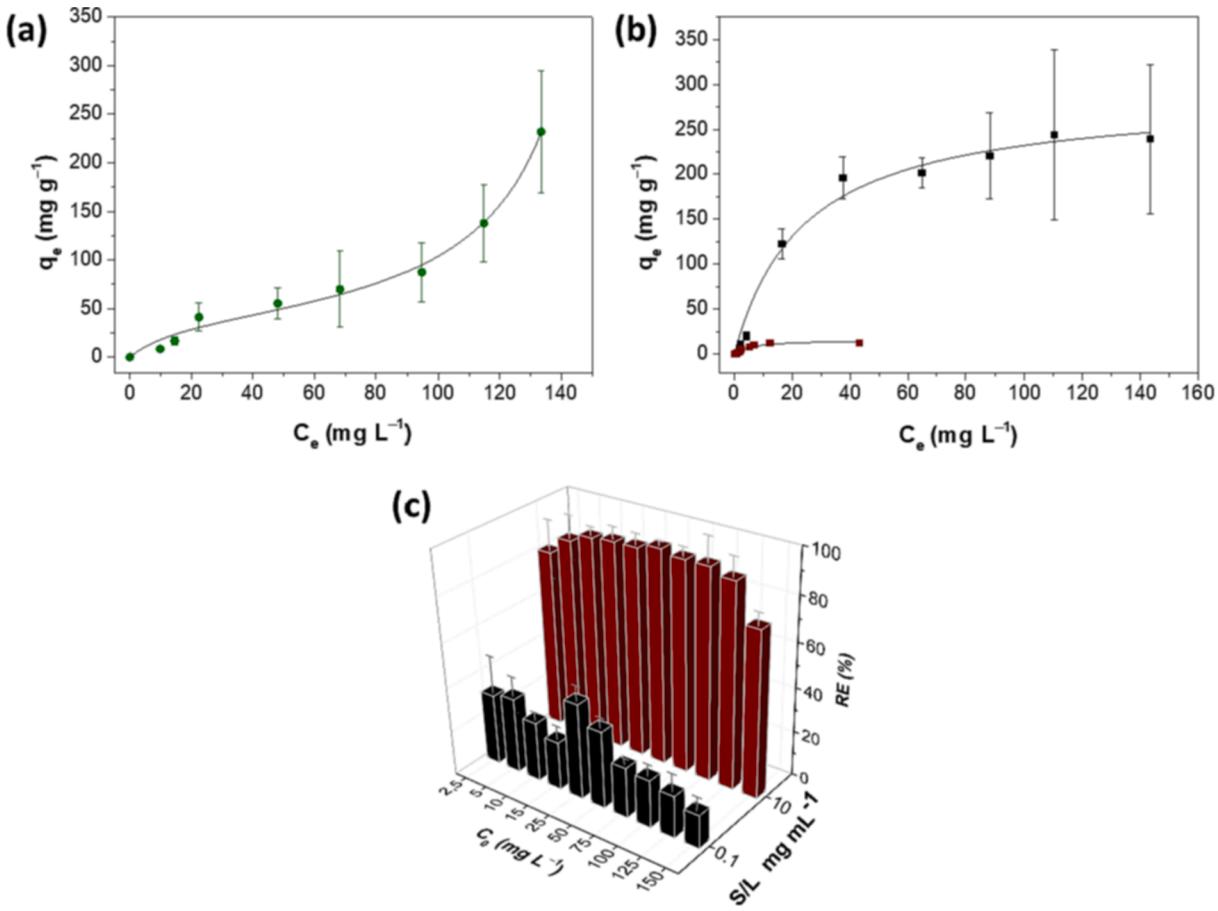

Fig. 5. Sorption analysis of Confidor O–TEQ® at 25 °C (a) into αCD$_2$–HDA at S/L = 0.1 mg mL^{-1} (green circles); (b) βCD$_2$–HDA at S/L = 0.1 mg mL^{-1} (black squares) and S/L = 10 mg mL^{-1} (purple squares); (c) removal efficiency of βCD$_2$–HDA at S/L = 0.1 mg mL^{-1} (black bars) and at S/L = 10 mg mL^{-1} (purple bars).

indication of a more compact structure, which is also confirmed by the surface morphology, as seen on SEM (see Fig. 3); indeed, HDA-containing NSs show a less smooth, rod-like structure than the DDA–NSs. Thus, the high S_{BET}, pore volume and diameter of αCD$_2$–HDA and βCD$_2$–HDA, combined with a less dense surface morphology, are key–factors for the interaction between NSs and Confidor O–TEQ®. Upon sorption of Confidor O–TEQ®, the surface morphology of αCD$_2$–HDA and βCD$_2$–HDA is altered, with increased aggregation and an apparent increase in pore size (for αCD$_2$–HDA). However, αCD$_2$–HDA and βCD$_2$–DDA exhibit a smoother surface, which may be due to interactions at the outer surface (see the section on MD) with formation of Confidor O–TEQ® layer.

To better characterize NSs, the effect of pH on the particle size and zeta potential (ζ) was investigated (Fig. 4 and Table 2). CD-based NSs show a positive ζ value in all pH ranges, and no noticeable effect of pH is observed – the exception being for αCD$_2$–DDA and βCD$_2$–DDA at pH 9.5, where the ζ values increase by ca. 50 and 100 %, respectively. Such positive ζ values indicate that no NS aggregation occurs. This is indeed true for αCD$_2$–HDA and βCD$_2$–HDA, which have smaller hydrodynamic diameters (approximately 163–480 nm and 250–480 nm, respectively). At pH ≤ 6.5, PDI less than 0.2 confirms the existence of monodisperse particles, suggesting that the HDA–NSs are characterized by a homogeneous network arrangement and size distribution. For DDA–NSs on the other hand, PDI ≥ 0.5 indicates a non–negligible polydispersity, which is also confirmed by the observation of a particle size at least twice as high as that found for αCD$_2$–HDA and βCD$_2$–HDA. In addition, the occurrence of two particle size populations for αCD$_2$–DDA and βCD$_2$–DDA is noteworthy. The higher particle size and aggregate formation is due to hydrophobic interactions and entanglements of the longer aliphatic chain of DDA. Thus, the balance between the surface charge displacement and the hydrophobic/hydrophilic interactions could play a crucial role in the dispersion and therefore in size distribution and, as we will see below, in the sorption efficiency.

3.2. Sorption analysis

Preliminary tests were conducted to investigate the effect of pH in the degradation of Confidor O–TEQ®, more specifically of its active ingredient, and the effect of CD–NSs dosages on Confidor O–TEQ® sorption. The stability of the aqueous suspension of Confidor O–TEQ® (150mg L^{-1}) at different pH values was initially evaluated [596061]. As can be seen in Figure S1, no significant degradation is observed up to 6 days (DR is always lower than 12% - Figure S1). Such behavior is a necessary condition for accurate quantification of imidacloprid in Confidor O–TEQ®. The dosage effect was evaluated by quantifying the maximum amount of adsorbate, q_e, and removal efficiency (*RE*) of imidacloprid, at different solid/liquid (S/L) ratios, from 0.1 to 10 mg mL^{-1}, at natural pH (6.5) – Figure S2. The maximum amount of imidacloprid adsorbed by α CD$_2$–HDA and β CD$_2$–HDA (131 mg g^{-1} and 112 mg g^{-1}, respectively) was determined for S/L = 0.1 mg mL^{-1}. These values are approximately 10-fold higher than the values obtained for α CD$_2$–DDA (8.5 mg g^{-1}) and β CD$_2$–DDA (12.3 mg g^{-1}) at their optimal S/L = 1.0 mg mL^{-1}.

These results clearly indicate that the linker plays the key role in the adsorption mechanism, either directly interacting with the adsorbate or by modifying the NS structures, thus equilibrating the hydrophilic/hydrophobic character. It is also worth noting that when the removal efficiency data (Fig S2-b) were analyzed, the best performance was

Table 3
Fitting parameters for Langmuir and BET models.

Model		βCD$_2$–HDA, S/L = 0.1 mg mL^{-1}	βCD$_2$–HDA, S/L = 10 mg mL^{-1}
Langmuir	$q_{e,\ exp}$ (mg g^{-1})	235 (±75)	11.6 (±0.8)
	q_m (mg g^{-1})	288 (±19)	15.8 (±1.8)
	K_L (10^{-2}) (L mg^{-1})	4.2 (±1.0)	17.2 (±5.0)
	R_L	0.9 – 0.1	0.9 – 0.1
	Adj.-R^2	0.9748	0.9181
Model	αCD$_2$–HDA, S/L = 0.1 mg mL^{-1}		
BET	q_s (mg g^{-1})	42.6 (±4.5)	
	C_{BET} (L mg^{-1})	10.0 (±5.0)	
	C_s (mg L^{-1})	162.7 (±4.0)	

obtained by βCD$_2$–HDA, with a 92 % removal of imidacloprid, followed by αCD$_2$–HDA and βCD$_2$–DDA, with 46 % and 45 %, respectively. However, the best *RE* was obtained by βCD$_2$–HDA at S/L = 10 mg mL^{-1}, indicating a *RE* improvement by increasing the adsorbent mass. These studies were complemented by the putative effect of pH (ranging from 3.5 to 9.5) on the physical parameters of adsorption: q_e and *RE* (Figure S3). This was done using the optimal S/L ratios 0.1 and 1.0 mg mL^{-1} for HDA- and DDA- based NSs, respectively. Although no significant effects were observed for *RE*s, pH strongly affects the maximum adsorption amount of imidacloprid on *α*CD$_2$–HDA and βCD$_2$–HDA, showing maximum q_e values for 4.5 (q_e = 151 mg g^{-1}) and 6.5 (q_e = 213 mg g^{-1}), respectively. In addition, the pH effect was also assessed for βCD$_2$–HDA, at S/L = 10 mg mL^{-1}, and the *RE*s are similar (ca. 95 %) in all pH ranges (Figure S4).

3.2.1. Sorption isotherms

Considering the previous discussion, the best materials, αCD$_2$–HDA (S/L = 0.1 mg mL^{-1}) and βCD$_2$–HDA (S/L = 0.1 and 10 mg mL^{-1}) were selected for further analysis. The sorption isotherm data are shown in Fig. 5. From Fig. 5 a) and b), the profile of q_e as a function of C_e changes significantly as a function of CD. While the sorption of imidacloprid (in Confidor dispersion) by the βCD–NS follows a Langmuir model, the sorption onto αCD–NS follows a BET isotherm. However, comparing the isotherms for the same S/L, the maximum sorbed concentration of imidacloprid is similar for both NSs: αCD$_2$–HDA and βCD$_2$–HDA. To gain further insight into the sorption mechanism, several sorption equations were fitted to the experimental data. Fig. 5 and Table 3 show the best fitting lines and corresponding fitting parameters for the equations of BET (eq. (8), αCD$_2$–HDA) and Langmuir (eq. (7), βCD$_2$–HDA). The sorption of imidacloprid by αCD$_2$–HDA is well described by the BET model (eq. (8)), which is usually associated with mesoporous materials with a heterogeneous sorption process through the formation of multilayers via cooperative sorbate–sorbate interactions, while the saturation of monolayers is indicated by the q_s value (43 ± 4 mg g^{-1}). Additionally, hydrophobic chain–π interactions with the pyridine and imidazole rings can also occur. On the other hand, the Langmuir equation (eq.7) for βCD$_2$–HDA at two different S/L best describes the sorption process, indicating a homogeneous distribution of active sites. This is complemented by a favorable sorption, as suggested by the separation factor, R_L, which is less than 1 [62]. From the experimental data Fig. 5a) and b), it can also be concluded that the maximum amounts of sorbed imidacloprid are 231.4 and 287.8 mg g^{-1} for αCD$_2$–HDA and βCD$_2$–HDA,

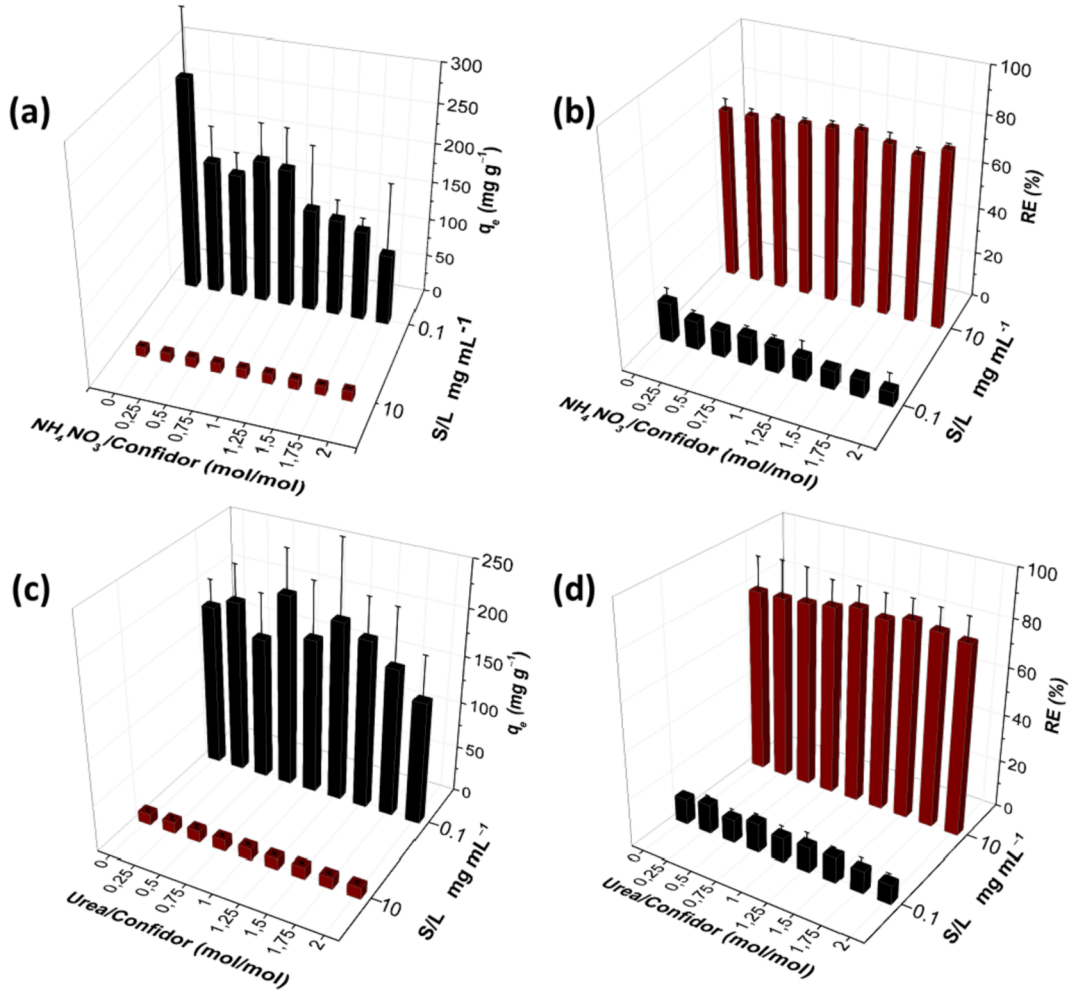

Fig. 6. Dependence of q_e and *RE* on the concentration of (a–b) NH_4NO_3 and (c–d) urea for two different S/L ratios, by using βCD$_2$–HDA.

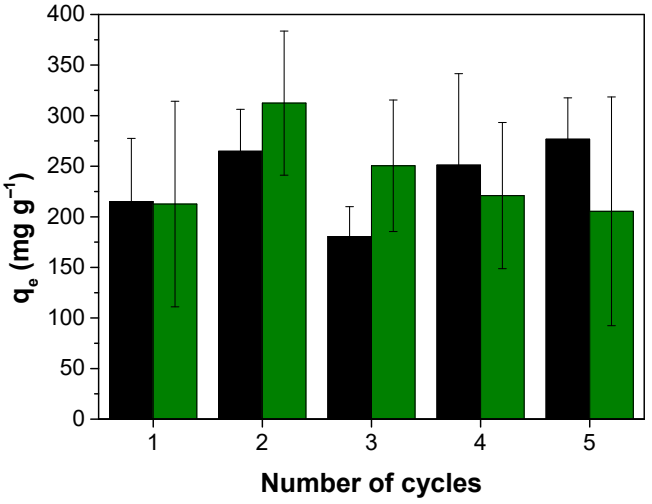

Fig. 7. Reusability of αCD$_2$–HDA (green bar) and βCD$_2$–HDA (black bar) for imidacloprid adsorption from Confidor O–TEQ®.

respectively, and again, increasing the mass of the latter leads to removal efficiencies greater than 95 % (Fig. 5c).

The above results are still surprising compared with those obtained, for the same NS-βCD$_2$–HDA, for the sorption of pure imidacloprid from an aqueous solution ($q_e = 27.4$ mg g^{-1} for a S/L = 5 mg mL^{-1} [18]). This clearly suggests that the Confidor O–TEQ® formulation plays a significant role in the sorption process, and dramatically increases the availability of active sites for sorption.

In the absence of information about the overall composition of Confidor, the possible effects of the two most commonly used fertilizers: ammonium nitrate and urea on the IMD sorption were evaluated [63]. From the analysis of Fig. 6, it can be concluded that the interactions between sorbate and sorbent are affected by both interfering factors. In particular, the salt affects the adsorption of imidacloprid at concentrations higher than 0.25 M. Indeed, at S/L = 0.1 mg mL^{-1}, a decrease up to 66 % and 30 % of q_e and *RE*, respectively, was observed. At S/L = 10 mg mL^{-1}, q_e is not affected, but *RE* decreases from 93 % to 75 %. This effect can be explained by the fact that NH_4^+ and NO_3^- ions act as counterions and reduce the active sites by electrostatic interaction between the positive and negative active sites of sorbate and sorbent. On the other hand, urea has a smaller effect on the sorbate–sorbent interactions, and no significant effect in terms of q_e. Concomitantly, a decrease in removal efficiency from 30 % to 11 % (S/L = 0.1 mg mL^{-1}) and from 93 % to 80 % (S/L = 10 mg mL^{-1}) is observed. This is likely due to a competitive sorption mechanism.

It is known that the sorption mechanism involves several steps, some of which depend on surface tension [64]. For this reason, we measured the surface tension of Confidor O–TEQ® and an aqueous solution of imidacloprid, at 25 °C. The following surface tension values were obtained: 29.1 (±0.2) mN m^{-1} and 67.6 (±0.4) mN m^{-1}. This suggests that the lowest surface tension obtained for Confidor could be responsible for a higher sorption capacity of the NS. This evidence remains to be confirmed.

The performance of αCD$_2$–HDA and βCD$_2$–HDA was tested in term of reusability (Fig. 7). As we can see, both NSs present similar sorbent capacity towards imidacloprid with an average value of q_e = 250 mg g^{-1}. Thus, the removal efficiency of the sorbent material is kept constant, taking into account the experimental error, along the 5 cycles. That is a noticeable result because it shows the potential of these mesoporous materials for real application in the removal of pesticides. It should also be stressed that just water is used in the regeneration step.

3.2.2. Sorption kinetics

The rate at which imidacloprid is sorbed by the HDA–based nanosponges was evaluated only for those that showed higher values of q_e and *RE*; i.e. βCD$_2$–HDA at S/L ratios of 0.1 and 10 mg mL^{-1} (Fig. S5b). At S/L = 0.1 mg mL^{-1} sorption is quite fast, reaching 82 % of cumulative removal in only 5 min. Such removal prevents a deeper kinetic analysis by using the models described in equations (4) and (5) once the fitting is

Table 4
Fitting parameters for the fitting of PFO, PSO kinetic models to sorption of imidacloprid, in Confidor O–TEQ® dispersions onto β CD$_2$–HDA at S/L = 10 mg mL^{-1}, and αCD$_2$–HDA* at S/L = 0.1 mg mL^{-1}.

	PFO		PSO	
βCD$_2$–HDA S/L = 10 mg mL^{-1}	$q_{e,\ exp}$ (mg g^{-1})	13.3 (±0.1)		
	q_e (mg g^{-1})	11.7 (±0.3)	q_e (mg g^{-1})	12.2 (±0.3)
	k_1 (10^{-2}) (min^{-1})	24.5 (±6.2)	k_2 (10^{-2}) (g mg^{-1} min^{-1})	3.0 (±0.7)
	Adj.-R²	0.9125	*Adj.-R²*	0.9621
	AIC	8.0	*AIC*	−2.0
αCD$_2$–HDA* S/L = 0.1 mg mL^{-1}	$q_{e,\ exp}$ (mg g^{-1})	226.7 (±5.3)		
	q_e (mg g^{-1})	172.2 (±83.3)	q_e (mg g^{-1})	191.1 (±64.2)
	q_o (mg g^{-1})	127.6 (±9.3)	q_o (mg g^{-1})	117.6 (±12.9)
	k_1 (10^{-2}) (min^{-1})	0.2 (±0.2)	k_2 (10^{-5}) (g mg^{-1} min^{-1})	1.9 (±2.2)
	Adj.-R²	0.9056	*Adj.-R²*	0.86
	AIC	63.7	*AIC*	67.6

*the parameter values for αCD$_2$–HDA were obtained by a modified PFO and PSO equations: $q_t = q_e\left(1 - e^{-k_1 t}\right) + q_0$ and $q_t = \frac{k_2 q_e^2 t}{1 + k_2 q_e t} + q_0$, respectively.

Table 5
Averaged total potential energies computed for the complexes between αCD/βCD, αCD/βCD–HDA, αCD/βCD–DDA, αCD$_2$/βCD$_2$–HDA and αCD$_2$/βCD$_2$–DDA and imidacloprid (Imd) in solution and the corresponding binding enthalpies (kJ.mol^{-1}).

		αCD	βCD
System	**Simulation**	**Potential Energy (kJ. mol^{-1})**	**Potential Energy (kJ. mol^{-1})**
CD:Imd	**Pure Water**	−551465	−46686
	Host	−551037	−45732
	Guest	−551584	−46689
	Complex	−551240	−45759
		Binding Enthalpy	**Binding Enthalpy**
	ΔH	−84	−25
CD–HDA: Imd	**Pure Water**	−548584	−125303
	Host	−553144	−129656
	Guest	−548753	−125311
	Complex	−553262	−129695
		Binding Enthalpy	**Binding Enthalpy**
	ΔH	51	−31
CD–DDA: Imd	**Pure Water**	−546785	−156829
	Host	−551140	−155392
	Guest	−546912	−156839
	Complex	−551263	−155434
		Binding Enthalpy	**Binding Enthalpy**
	ΔH	4	−32
CD$_2$–HDA: Imd	**Pure Water**	−541487	−253670
	Host	−548006	−252427
	Guest	−541568	−253624
	Complex	−548103	−252417
		Binding Enthalpy	**Binding Enthalpy**
	ΔH	−16	−36
CD$_2$–DDA: Imd	**Pure Water**	−544603	−392882
	Host	−552625	−389990
	Guest	−544736	−392845
	Complex	−552746	−389940
		Binding Enthalpy	**Binding Enthalpy**
	ΔH	12	13

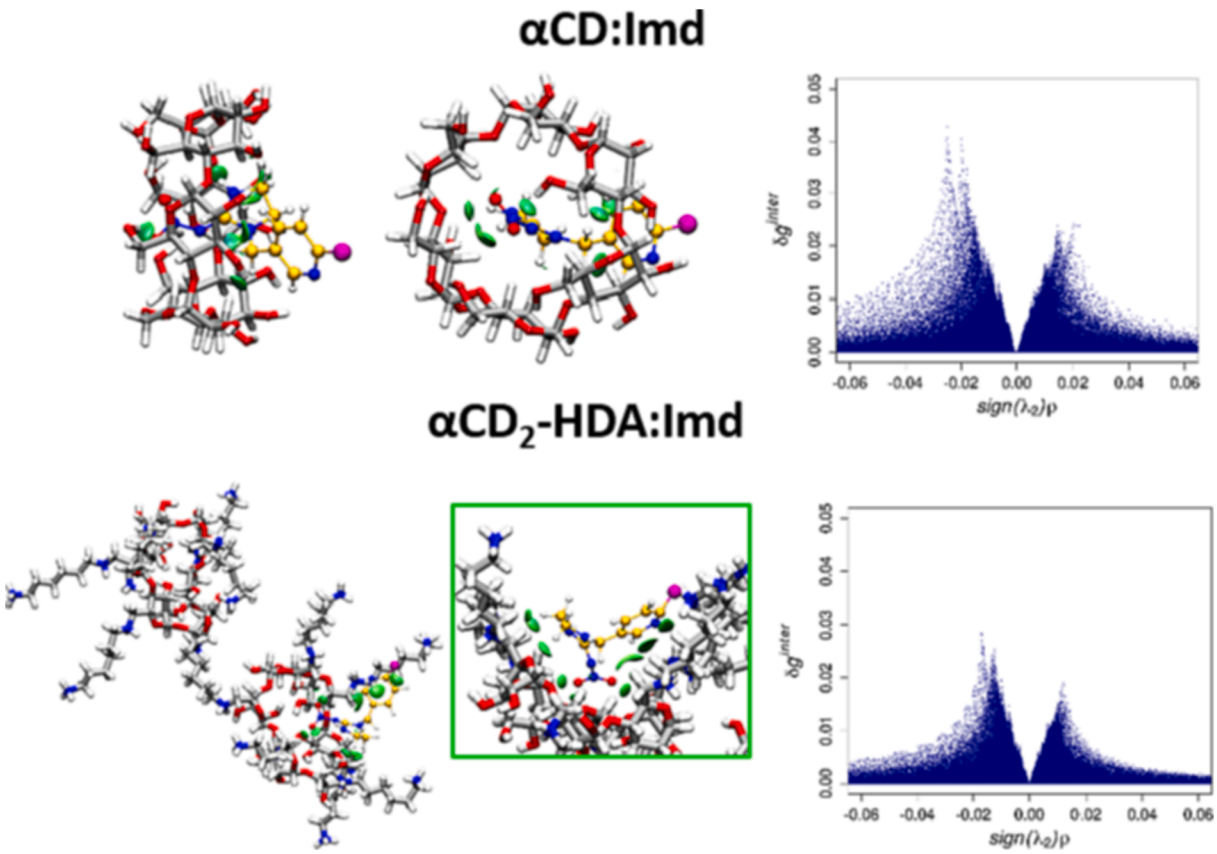

Fig. 8. Interaction patterns of the αCD:Imd and αCD_2-HDA:Imd complexes, corresponding to the most favorable binding enthapies (−82 and −16 kJ.mol^{-1}, respectively), illustrated by the 3D isosurfaces (right) and 2D scatter plots (left). Stabilizing/destabilizing NCI are represented in blue/red, and van der Waals forces are colored in green (volume cutoff of δginter = 0.05; color coding: $-0.1 \leq \text{sign}(\lambda_2)\rho \leq 0.1$). αCD and αCD_2–HDA backbones are featured in gray as licorice, while imidacloprid is represented in ball-and-stick and colored in yellow. Nitrogen, oxygen, chlorine, and hydrogen atoms are represented in blue, red, purple, and white, respectively.

controlled by the large number of data points in the sorption equilibrium. On the other hand, the sorption kinetic for βCD_2–HDA is slower at S/L = 10 mg mL^{-1}: after 5 min 67 % of the cumulative removal is achieved, and only after 90 min the cumulative removal (83 %) is similar to the one obtained at S/L = 0.1 mg mL^{-1}. At the S/L ratio of 0.1 mg mL^{-1}, αCD_2–HDA reaches the equilibrium after 5 h (Fig. S5a). These kinetic data may be indicative of the best performance of NS, at a lower S/L ratio. For the latter, the PFO and PSO equations (eq. (4) and (5)) were fitted to the experimental data, and the fitting parameters are summarized in Table 4. The PSO is the model that best fits the experimental data for βCD_2–HDA, which is consistent with the Langmuir equation for modelling sorption isotherms. The chemisorption process refers to the formation of hydrogen bonds between acceptor atoms, such as hydrogens in amine and hydroxyl groups, and donor atoms, such as nitrogen and oxygen in amine, hydroxyl, nitro groups and heterocycles. *Adj.-*R^2 and *AIC* values of PFO and PSO for αCD_2–HDA are lower for the PFO fitting. Furthermore, the sorption kinetics for αCD_2–HDA follows a diffusional behavior (i.e., q_t is linear as a function of $t^{1/2}$ – not shown).

3.3. *In silico rationale for describing CDNSs:imidacloprid interactions*

Results pertaining to MD simulations are discussed in what follows. Table 5 summarizes the total potential energies for the simulations of the complexes, single αCD/βCD, αCD/βCD–HDA, αCD/βCD–DDA, αCD_2/βCD_2–HDA, αCD_2/βCD_2–DDA, imidacloprid, and pure water, and the resulting binding enthalpies. It can be seen that the substitution of αCD and βCD primary hydroxyl groups by hexane–1,6–diamine and dodecane–1,12–diamine chains has a significant effect on the binding strength, as also found experimentally and in previous *in silico* studies. [52].

For αCD–based systems (Table 5) the binding enthalpies follow the order αCD:Imd < αCD_2–HDA:Imd < αCD–DDA:Imd < αCD_2–DDA:Imd < αCD–HDA:Imd. The formation of αCD:Imd and αCD_2–HDA:Imd are enthalpically favoured (−84 kJ.mol^{-1} and −16 kJ.mol^{-1}, respectively), while the formation of αCD–DDA:Imd, αCD_2–DDA:Imd and αCD–HDA:Imd are entalpically penalized as as evidenced by their positive values (4 kJ.mol^{-1}, 12 kJ.mol^{-1} and 51 kJ.mol^{-1}, respectively). The presence of HDA and DDA chains and the distortion of αCD structure (see Figure S6, top) percludes the inclusion of Imidacropid.

In βCD-based systems, the complexes that are more enthalpically favoured are βCD_2–HDA:Imd (−36 kJ.mol^{-1}), βCD–DDA:Imd (−32 kJ.mol^{-1}) and βCD–HDA:Imd (−31 kJ.mol^{-1}). This enthalpy contribution is smaller in the complex involving the natural βCD (−25 kJ.mol^{-1}). The ΔH values follow the order βCD_2–HDA:Imd < βCD–DDA:Imd < βCD–HDA:Imd < βCD:Imd < βCD_2–DDA:Imd, suggesting that the most stable complexes are those containing the βCD_2–HDA dimer with shorter chain length (−36 kJ.mol^{-1}) and the βCD functionalized monomer with longer chain length (−32 kJ.mol^{-1}). While αCD:Imd, αCD_2–DDA:Imd, βCD_2–HDA:Imd, βCD–DDA:Imd, βCD–HDA:Imd, and βCD:Imd complexes display binding enthalpies within typical range (see [52]), the αCD–DDA:Imd, αCD_2–HDA:Imd, αCD–HDA:Imd and βCD_2–DDA:Imd complexes display positive ΔH values, suggesting that the association between the two binding partners is unlikely (see Table 5). This can be explained by the higher degree of distortion/collapse observed for the βCD_2–DDA backbone (see Figures S6 and S7, top, in Supporting Information), either free in solution or in the presence of imidacloprid. This is due to the higher flexibility of the DDA chains and to the ability of some βCD glucopyranose units to rotate with respect to the cavity plane,

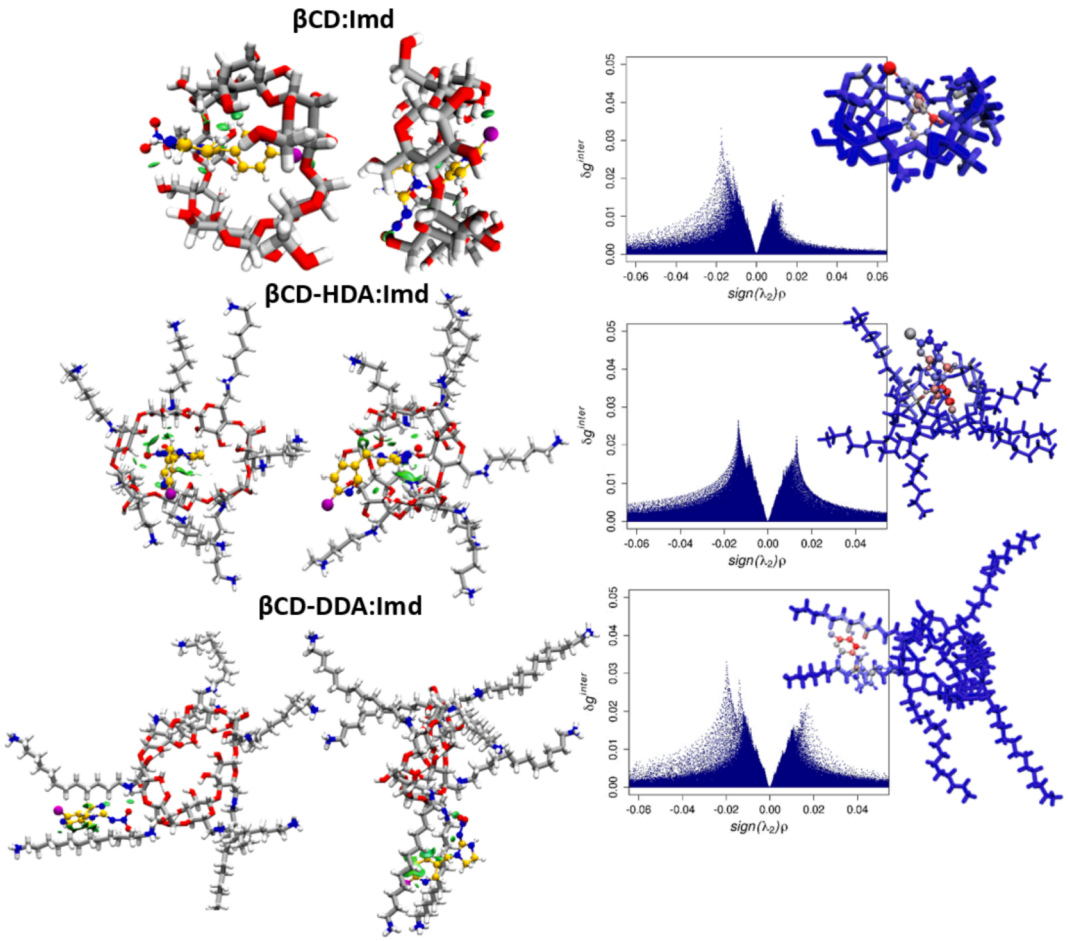

Fig. 9. An overview of the interaction patterns illustrated by the 3D isosurfaces (right) and 2D scatter plots (left) for each natural βCD, and monomeric βCD–HDA and βCD–DDA. Stabilizing/destabilizing NCI are represented in blue/red, and van der Waals forces are colored in green (volume cutoff of δginter = 0.05; color coding: $-0.1 \leq \text{sign}(\lambda_2)\rho \leq 0.1$). βCD, βCD–HDA, βCD–DDA, backbones are featured in gray as licorice, while imidacloprid is represented in ball-and-stick and colored in yellow. Nitrogen, oxygen, chlorine, and hydrogen atoms are represented in blue, red, purple, and white, respectively. Also included are the individual atomic contributions (left) to the complexation highlighted in the isosurfaces. A relative score (%) is attributed to each atom, which is colored using a gray–to–red color gradient, according to this percentage, with blue corresponding to no contribution to the noncovalent interaction, and red to a significant relative contribution to the CD–imidacloprid interaction.

which requires a high energy to fill the βCD cavities, preclude the interior vacuum states, and prevents the inclusion of imidacloprid. This behavior has been previously reported for other flexible hosts [55]. including other cyclodextrin derivatives [65]. In addition, electrostatic repulsion between the DDA chains is expected to overcome the stabilizing interactions that would favor complex formation.

In contrast, the presence of imidacloprid in the reference systems (αCD/βCD:Imd) and in αCD/βCD–HDA:Imd clearly prevents cyclodextrin distortion (as shown in Figures S6 and S7, top, of Supporting Information). This result is also confirmed by the smaller distances (Figure S6 and S7, bottom, in Supporting Information) between the centroids of the binding partners, indicating the formation of inclusion complexes. However, the distance profiles for αCD-DDA:Imd, αCD_2–HDA:Imd, αCD_2–DDA:Imd, βCD–DDA:Imd and βCD_2–HDA:Imd suggest that the interaction occurs mainly outside the CD cavity, with the aliphatic chains, suggesting a prevalence of weak interactions outside the CD cavity. The interaction of Imidacropid with HDA and DDA chains is also illustrated by the 3D isosurfaces in Figs. 8, 9 and 10 and Figures S8 and S9 (Supporting Information).

Further inspection of intermolecular signatures of the complexes allows evaluating the type and strength of the NCI interactions as a function of the respective electronic charge densities. Areas of low density, corresponding to stabilizing/destabilizing NCI within the different complexes are decoupled and represented by 3D IGM isosurfaces (Figs. 8, 9 and 10). These isosurfaces reflect the binding specificity by highlighting discrete regions of enhanced interactions, and are influenced by the nature of the αCD/βCD, αCD/βCD–HDA, αCD/βCD–DDA, $\alpha CD_2/\beta CD_2$–HDA and $\alpha CD_2/\beta CD_2$–DDA groups involved in the complexation. The volume of the interacting regions reflects the extent of the interactions. While stronger stabilizing (attractive) and destabilizing (repulsive) interactions are represented in blue and red, respectively, weak van der Waals forces are represented in green flat volumes.

A volume cutoff of $\delta g^{inter} = 0.05$ a.u. and a color range in $-0.1 \leq sign(\lambda_2)\rho \leq 0.1$ a.u. are used to represent the 3D convex surfaces. The corresponding 2D scatter plots depict the effective interactions between the binding partners as contact points, which represent the total interaction points for $\delta g^{inter} \leq 0.1$ in the range of $-0.2 \leq \text{sign}(\lambda 2)\rho \leq 0.2$. In each system, 35 Å spheres centered on the complexes were used, providing similar values for the lattice points and allowing relative comparison between complexes. The favorable nature of the interactions is reflected in the asymmetry of the peaks. In all cases, the peaks on the positive, destabilizing side of the 2D plot are smaller than the corresponding peaks on the negative, stabilizing side, indicating that the balance of NCI in the complex as a whole favors the complex formation.

The 3D isosurfaces represented in Fig. 8 and Figure S8 (Supporting Information) indicate that the favorable binding enthalpy of αCD:Imd is

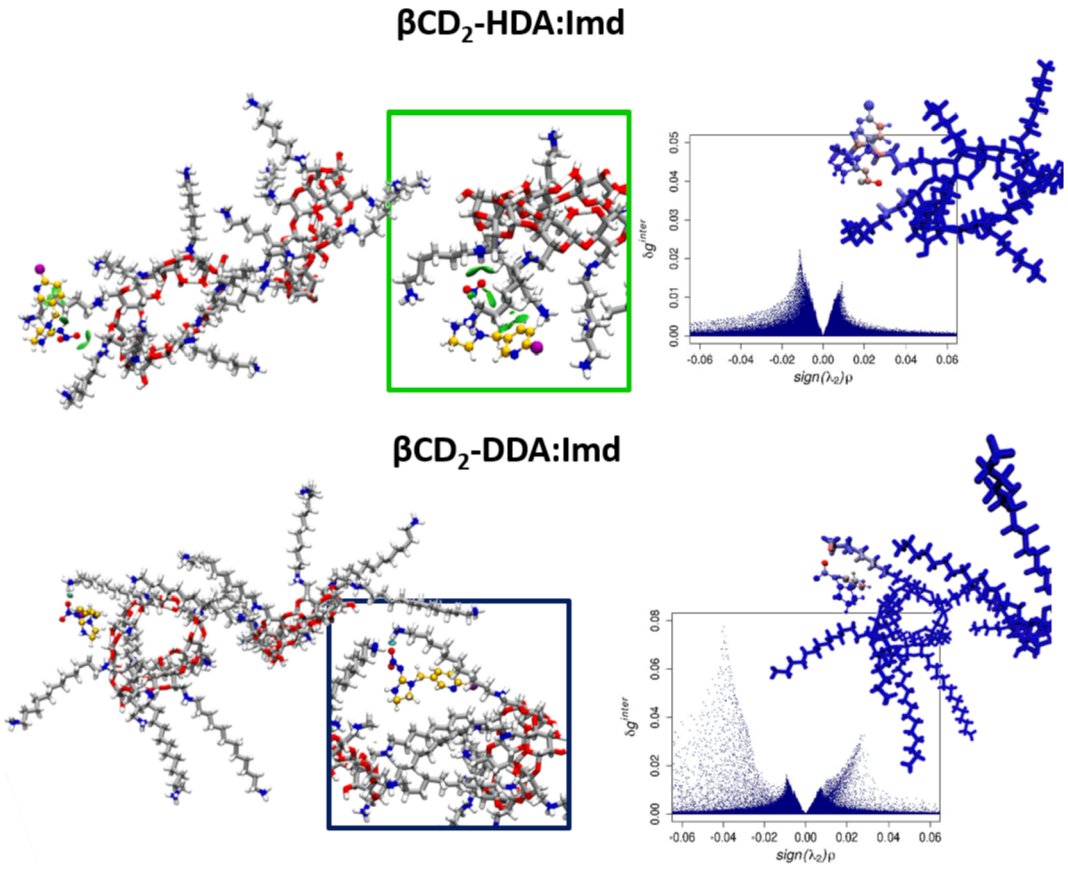

Fig. 10. IGMPlot isosurfaces (right), 2D scatter plots and individual atomic contributions (left) for the complex formation between βCD_2–HDA and βCD_2–DDA dimers and imidacloprid (Imd). For details see Fig. 9.

explained by the presence of mainly N—H···O, O—H···O and C—H···O interactions between the nitro group of imidacropid and the primary hydroxyl groups and the cavity C—H goups of αCD, as shown by large volumes in Fig. 8 (left) and intense peaks (Fig. 8, right) at $-0.01 < \text{sign}(\lambda_2)\rho < -0.03$. In the αCD_2–HDA:imd complex N—H···O and C—H—π interactions between the nitro group of imidacropid and the N—H group of HDA chains, as well as between the pyridine ring of imidacropid and the CH_2 groups of HDA chains, also favour the complex formation ($-0.01 < \text{sign}(\lambda_2)\rho < -0.02$, Fig. 8).

In βCD:Imd complex (Fig. 9), due to the polar nature of the βCD, stronger hydrogen-bonding interactions are also conceivable with imidacloprid. These include O—H···Cl, N—H···O and O—H···O interactions.

The stability of the monomeric βCD–HDA:Imd complex (Fig. 9) is largely determined by N—O···H and C—H···O type interactions, as shown by large volumes in Fig. 9 (left) and large peaks (Fig. 9, right), with respective maxima defined at $-0.01 < \text{sign}(\lambda_2)\rho < -0.02$. No interactions between the CD cavity and imidacloprid were detected in the presence of βCD–DDA. The interaction occurs outside the cavity and between two DDA chains and imidacloprid and is based on C—H···π dispersion interactions, C—H···C—H interactions and N—H···O interactions. The latter is shown as a large diffuse peak at $\text{sign}(\lambda_2)\rho \approx -0.02$ in Fig. 8 (left). This suggests a competitive effect between the two DDA chains and the CD cavity. The two chains promote a higher number of stabilizing interaction sites, as also indicated in Table 5. Similar behavior was found for the βCD_2–DDA dimer which binds to imidacloprid through C—H···π dispersion interactions and two distinct N—H···O interactions (Fig. 9, left), that are established between the DDA chain and the nitro group of imidacloprid.

These observations suggest that the introduction of the HDA chains into the dimeric CD structure prevents the formation of an inclusion complex, because the affinity between HDA chains and imidacloprid predominates. No stable complex is formed in the presence of longer alkyl chains (DDA), as suggested by the positive ΔH value (Table 5) and by the weak and diffuse N—H···O interaction (Fig. 9), and confirmed by sorption analysis.

Although βCD_2–HDA and βCD_2–DDA dimers have the possibility of forming hydrogen bond with the nitro group of imidacloprid, bonding involving HDA is more likely, based on the volumes of the isosurfaces and the corresponding peak densities. These interaction patterns confirm the previous results from the experimental studies and the corresponding estimated binding enthalpies.

4. Conclusions

Four different CD-based nanosponges were synthesized and characterized. Their performance as adsorbents for Confidor O–TEQ® were assessed. Of all the adsorbents evaluated βCD_2–HDA is the one that shows the best results both in absolute terms and when compared with the adsorption of the active ingredient imidacloprid. The maximum amount of sorbed Confidor O–TEQ® (288 mg g^{-1}) is ca. 4 times higher than that obtained for pure IMD (68 mg g^{-1}) per gram of sorbent. This might be justified by the decrease in surface tension of the oil formulation of Confidor O–TEQ® that leads to an improvement in wettability and the consequent increase of the amount of imidacloprid sorbed by β CD_2–HDA. In addition, the maximum sorption for Confidor O–TEQ® in β CD_2–HDA is observed at a pH of 6.5 while that for IMD it is found at pH of 3.5.

Although there are extensive experimental and theoretical studies on the complexation of organic pollutants in nanostructures based on CDs, a comprehensive description of the effects of the type and amount of CD, the type and size of the crosslinker, and the conformation on the sorption behavior of CDNSs, especially at the atomic level, is lacking.

Synthesis and sorption analysis of amine–cyclodextrin nanosponges and MD simulations were used in this work as tools to bridge this gap. MD simulation shed light on the relevant contacts between the interaction pairs and suggests that the αCD_2–HDA and βCD_2–HDA dimers with shorter chain lengths are potential materials for capturing imidacroprid from water. However, the βCD_2–HDA dimer outperforms αCD_2–HDA due to the possibility of forming stronger hydrogen bonds (N—H···O) between the nitro group of imidacloprid and the N—H group of HDA chains and C—H—π interactions between the pyridine ring of imidacropid and the CH_2 groups of HDA chains.

Modulation of the interaction between amine-CDNSs provides general rules for identifying the forces that govern binding with pesticides. The main driving forces are host–guest interactions, i.e., hydrogen bonding and van der Waals interactions. The present approach can be used to gain a detailed understanding of the mechanisms that determine the sorption behavior of nanosponges for environmental applications.

Declaration of Competing Interest

The authors declare that they have no known competing financial interests or personal relationships that could have appeared to influence the work reported in this paper.

Data availability

Data will be made available on request.

Acknowledgements

The authors acknowledge Fundação para a Ciência e a Tecnologia (FCT), the Portuguese Agency for Scientific Research for the financial support through projects UIDP/00313/2020. Gianluca Utzeri thanks FCT for the PhD grant SFR/BD/146358/2019. Tania Cova acknowledge the Junior Researcher Grant CEECIND/00915/2018 assigned by FCT.

Appendix A. Supplementary data

Supplementary data to this article can be found online at https://doi.org/10.1016/j.cej.2022.140882.

References

[1] A. Marican, E.F. Durán-Lara, A review on pesticide removal through different processes, Environ. Sci. Pollut. Res. 25 (2018) 2051–2064, https://doi.org/10.1007/s11356-017-0796-2.
[2] T.F.G.G. Cova, D. Murtinho, A.A.C.C. Pais, A.J.M. Valente, Cyclodextrin-based Materials for Removing Micropollutants From Wastewater, Curr. Org. Chem. 22 (2018) 2150–2181, https://doi.org/10.2174/1385272822666181019125315.
[3] S. Cosgrove, B. Jefferson, P. Jarvis, Pesticide removal from drinking water sources by adsorption: a review, Environ. Technol. Rev. 8 (2019) 1–24, https://doi.org/10.1080/21622515.2019.1593514.
[4] F. Guerra, M. Attia, D. Whitehead, F. Alexis, Nanotechnology for Environmental Remediation: Materials and Applications, Molecules. 23 (2018) 1760, https://doi.org/10.3390/molecules23071760.
[5] T.F. Cova, D. Murtinho, A.A.C.C. Pais, A.J.M. Valente, Combining Cellulose and Cyclodextrins: Fascinating Designs for Materials and Pharmaceutics, Front. Chem. 6 (2018) 271, https://doi.org/10.3389/fchem.2018.00271.
[6] T.F. Machado, M.E.S. Serra, D. Murtinho, A.J.M. Valente, M. Naushad, Covalent Organic Frameworks: Synthesis, Properties and Applications—An Overview, Polymers (Basel). 13 (2021) 970, https://doi.org/10.3390/polym13060970.
[7] P.N. Diagboya, B.I. Olu-Owolabi, F.M. Mtunzi, K.O. Adebowale, Clay-carbonaceous material composites: Towards a new class of functional adsorbents for water treatment, Surf. Interfaces. 19 (2020), 100506, https://doi.org/10.1016/j.surfin.2020.100506.
[8] A. Marocco, G. Dell'Agli, F. Sannino, S. Esposito, B. Bonelli, P. Allia, P. Tiberto, G. Barrera, M. Pansini, Removal of Agrochemicals from Waters by Adsorption: A Critical Comparison among Humic-Like Substances, Zeolites, Porous Oxides, and Magnetic Nanocomposites, Processes 8 (2020) 141, https://doi.org/10.3390/pr8020141.
[9] A. Jeyaseelan, I. Aswin Kumar, N. Viswanathan, M. Naushad, Development and characterization of hydroxyapatite layered lanthanum organic frameworks by template method for defluoridation of water, J. Colloid Interface Sci. 622 (2022) 228–238, https://doi.org/10.1016/j.jcis.2022.04.097.
[10] A. Jeyaseelan, N. Viswanathan, Investigation of Hydroxyapatite-Entrenched Cerium Organic Frameworks Incorporating Biopolymeric Beads for Efficient Fluoride Removal, Ind. Eng. Chem. Res. 61 (2022) 7911–7925, https://doi.org/10.1021/acs.iecr.2c00487.
[11] S. Sadjadi, M.M. Heravi, M. Daraie, Cyclodextrin nanosponges: a potential catalyst and catalyst support for synthesis of xanthenes, Res. Chem. Intermed. 43 (2017) 843–857, https://doi.org/10.1007/s11164-016-2668-7.
[12] S. Nazerdeylami, J.B. Ghasemi, G. Mohammadi Ziarani, A. Amiri, A. Badiei, Direct monitoring of diclofenac using a supramolecular fluorescent approach based on β-cyclodextrin nanosponge, J. Mol. Liq. 336 (2021), 116104, https://doi.org/10.1016/j.molliq.2021.116104.
[13] R.V. Pivato, F. Rossi, M. Ferro, F. Castiglione, F. Trotta, A. Mele, β-Cyclodextrin Nanosponge Hydrogels as Drug Delivery Nanoarchitectonics for Multistep Drug Release Kinetics, ACS Appl. Polym. Mater. 3 (2021) 6562–6571, https://doi.org/10.1021/acsapm.1c01262.
[14] S. Swaminathan, F. Trotta, Cyclodextrin Nanosponges, in: F. Trotta, A. Mele (Eds.), Nanosponges, Wiley-VCH Verlag GmbH & Co. KGaA, Weinheim, Germany, 2019: pp. 27–57. https://doi.org/10.1002/9783527341009.ch2.
[15] V. Rizzi, J. Gubitosa, R. Signorile, P. Fini, C. Cecone, A. Matencio, F. Trotta, P. Cosma, Cyclodextrin nanosponges as adsorbent material to remove hazardous pollutants from water: The case of ciprofloxacin, Chem. Eng. J. 411 (2021), 128514, https://doi.org/10.1016/j.cej.2021.128514.
[16] C. Varan, A. Anceschi, S. Sevli, N. Bruni, L. Giraudo, E. Bilgiç, P. Korkusuz, A. B. İskit, F. Trotta, E. Bilensoy, Preparation and characterization of cyclodextrin nanosponges for organic toxic molecule removal, Int. J. Pharm. 585 (2020), 119485, https://doi.org/10.1016/j.ijpharm.2020.119485.
[17] B. Tian, S. Hua, Y. Tian, J. Liu, Cyclodextrin-based adsorbents for the removal of pollutants from wastewater: a review, Environ. Sci. Pollut. Res. 28 (2021) 1317–1340, https://doi.org/10.1007/s11356-020-11168-2.
[18] G. Utzeri, D. Murtinho, T.M.R. Maria, A.A.C.C. Pais, F. Sannino, A.J.M. Valente, Amine-β-cyclodextrin-based nanosponges. The role of cyclodextrin amphiphilicity in the imidacloprid uptake, Colloids Surfaces A Physicochem. Eng. Asp. 635 (2022), 128044, https://doi.org/10.1016/j.colsurfa.2021.128044.
[19] G. Utzeri, P.M.C. Matias, D. Murtinho, A.J.M. Valente, Cyclodextrin-Based Nanosponges: Overview and Opportunities, Front. Chem. 10 (2022) 1–25, https://doi.org/10.3389/fchem.2022.859406.
[20] E. Martwong, S. Chuetor, J. Junthip, Adsorption of Cationic Contaminants by Cyclodextrin Nanosponges Cross-Linked with 1,2,3,4-Butanetetracarboxylic Acid and Poly(vinyl alcohol), Polymers (Basel). 14 (2022) 342, https://doi.org/10.3390/polym14020342.
[21] X. Liao, B. Wang, Q. Zhang, Synthesis of glycopolymer nanosponges with enhanced adsorption performances for boron removal and water treatment, J. Mater. Chem. A. 6 (2018) 21193–21206, https://doi.org/10.1039/C8TA06802J.
[22] T.F. Cova, D. Murtinho, R. Aguado, A.A.C.C. Pais, A.J.M. Valente, Cyclodextrin Polymers and Cyclodextrin-Containing Polysaccharides for Water Remediation, Cyclodextrin Polymers and Cyclodextrin-Containing Polysaccharides for Water Remediation 2 (1) (2021) 16–38.
[23] W. Xu, X. Liu, J. Cai, T. Xue, K. Tang, Synthesis of reusable cyclodextrin polymers for removal of naphthol and naphthylamine from water, Environ. Sci. Pollut. Res. 29 (2022) 22106–22121, https://doi.org/10.1007/s11356-021-17234-7.
[24] R. Romita, V. Rizzi, P. Semeraro, J. Gubitosa, J.A. Gabaldón, M.I.F. Gorbe, V.M. G. López, P. Cosma, P. Fini, Operational parameters affecting the atrazine removal from water by using cyclodextrin based polymers as efficient adsorbents for cleaner technologies, Environ. Technol. Innov. 16 (2019), 100454, https://doi.org/10.1016/J.ETI.2019.100454.
[25] M. Wang, G. Li, C. Xia, X. Jing, R. Wang, Q. Liu, X. Cai, Facile preparation of cyclodextrin polymer materials with rigid spherical structure and flexible network for sorption of organic contaminants in water, Chem. Eng. J. 411 (2021), 128489, https://doi.org/10.1016/j.cej.2021.128489.
[26] M. Raoov, S. Mohamad, M. Abas, Synthesis and Characterization of β-Cyclodextrin Functionalized Ionic Liquid Polymer as a Macroporous Material for the Removal of Phenols and As(V), Int. J. Mol. Sci. 15 (2014) 100–119, https://doi.org/10.3390/ijms15010100.
[27] Z. Wang, F. Cui, Y. Pan, L. Hou, B. Zhang, Y. Li, L. Zhu, Hierarchically micro-mesoporous β-cyclodextrin polymers used for ultrafast removal of micropollutants from water, Carbohydr. Polym. 213 (2019) 352–360, https://doi.org/10.1016/j.carbpol.2019.03.021.
[28] L. Zhou, Z. Xu, K. Yi, Q. Huang, K. Chai, Z. Tong, H. Ji, Efficient remediation of 2,4-dichlorophenol from aqueous solution using B-cyclodextrin-based submicron polymeric particles, Chem. Eng. J. 360 (2019) 531–541, https://doi.org/10.1016/j.cej.2018.11.196.
[29] A. Alsbaiee, B.J. Smith, L. Xiao, Y. Ling, D.E. Helbling, W.R. Dichtel, Rapid removal of organic micropollutants from water by a porous β-cyclodextrin polymer, Nature. 529 (2016) 190–194, https://doi.org/10.1038/nature16185.
[30] H. Liu, X. Cai, Y. Wang, J. Chen, Adsorption mechanism-based screening of cyclodextrin polymers for adsorption and separation of pesticides from water, Water Res. 45 (2011) 3499–3511, https://doi.org/10.1016/j.watres.2011.04.004.
[31] S. Salazar, D. Guerra, N. Yutronic, P. Jara, Removal of Aromatic Chlorinated Pesticides from Aqueous Solution Using β-Cyclodextrin Polymers Decorated with Fe3O4 nanoparticles, Polymers (Basel). 10 (2018) 1038, https://doi.org/10.3390/polym10091038.
[32] S. Salazar, N. Yutronic, P. Jara, Magnetic β-Cyclodextrin Nanosponges for Potential Application in the Removal of the Neonicotinoid Dinotefuran from Wastewater, Int. J. Mol. Sci. 21 (2020) 4079, https://doi.org/10.3390/ijms21114079.
[33] Q. Huang, K. Chai, L. Zhou, H. Ji, A phenyl-rich β-cyclodextrin porous crosslinked polymer for efficient removal of aromatic pollutants: Insight into adsorption

performance and mechanism, Chem. Eng. J. 387 (2020), 124020, https://doi.org/10.1016/j.cej.2020.124020.
[34] M. Anthe, B. Valles-Ebeling, J. Achtenhagen, M. Arenz-Leufen, J. Atkinson, M. Starp, C. Corsing, Development of an aquatic exposure assessment model for Imidacloprid in sewage treatment plant discharges arising from use of veterinary medicinal products, Environ. Sci. Eur. 32 (2020) 147, https://doi.org/10.1186/s12302-020-00424-4.
[35] D. Auteri, M. Arena, S. Barmaz, A. Ippolito, A. Linguadoca, T. Molnar, R. Sharp, C. Szentes, B. Vagenende, A. Verani, Neonicotinoids and bees: The case of the European regulatory risk assessment, Sci. Total Environ. 579 (2017) 966–971, https://doi.org/10.1016/j.scitotenv.2016.10.158.
[36] T. Parween, S. Jan, Pesticide consumption and threats to biodiversity, in: Ecophysiol. Pestic., first, Elsevier, 2019: pp. 39–73. https://doi.org/10.1016/B978-0-12-817614-6.00002-0.
[37] L.P. Sheets, Imidacloprid, in: P. Wexler (Ed.), Encycl. Toxicol., 3rd ed., Elsevier, 2014: pp. 1000–1003. https://doi.org/10.1016/B978-0-12-386454-3.00153-6.
[38] V. Silva, H.G.J. Mol, P. Zomer, M. Tienstra, C.J. Ritsema, V. Geissen, Pesticide residues in European agricultural soils – A hidden reality unfolded, Sci. Total Environ. 653 (2019) 1532–1545, https://doi.org/10.1016/j.scitotenv.2018.10.441.
[39] I. Krabicová, S.L. Appleton, M. Tannous, G. Hoti, F. Caldera, A. Rubin Pedrazzo, C. Cecone, R. Cavalli, F. Trotta, History of cyclodextrin nanosponges, Polymers (Basel). 12 (5) (2020) 1122.
[40] R.A. Osmani, P. Kulkarni, S. Manjunatha, R. Vaghela, R. Bhosale, Cyclodextrin nanosponge-based systems in drug delivery and nanotherapeutics, in: A.M. Grumezescu (Ed.), Org. Mater. as Smart Nanocarriers Drug Deliv., Elsevier, 2018: pp. 659–717. https://doi.org/10.1016/B978-0-12-813663-8.00016-6.
[41] M. Ma, D. Li, New Organic Nanoporous Polymers and Their Inclusion Complexes, Chem. Mater. 11 (1999) 872–874, https://doi.org/10.1021/cm981090y.
[42] A. Singireddy, S.R. Pedireddi, S. Subramanian, Optimization of reaction parameters for synthesis of Cyclodextrin nanosponges in controlled nanoscopic size dimensions, J Polym Res 26 (4) (2019).
[43] S. Iravani, R.S. Varma, Nanosponges for Water Treatment: Progress and Challenges, Appl. Sci. 12 (2022) 4182, https://doi.org/10.3390/app12094182.
[44] P. Jeschke, R. Nauen, M. Schindler, A. Elbert, Overview of the Status and Global Strategy for Neonicotinoids, J. Agric. Food Chem. 59 (2011) 2897–2908, https://doi.org/10.1021/jf101303g.
[45] M.J.L. Castro, C. Ojeda, A.F. Cirelli, Surfactants in Agriculture, in: E. Lichtfouse, J. Schwarzbauer, D. Robert (Eds.), Green Mater. Energy, Prod. Depollut, 1st ed.,, Springer, Dordrecht, 2013, pp. 287–334, https://doi.org/10.1007/978-94-007-6836-9_7.
[46] R. Vermeer, P. Baur, O-TEQ ®, a formulation concept that overcomes the incompatibil- ity between water and oil, Pflanzenschutz-Nachrichten Bayer. 60 (2007) 7–26.
[47] T.F. Cova, B.F. Milne, A.A.C.C. Pais, Host flexibility and space filling in supramolecular complexation of cyclodextrins: A free-energy-oriented approach, Carbohydr. Polym. 205 (2019) 42–54, https://doi.org/10.1016/j.carbpol.2018.10.009.
[48] P.R. Ashton, R. Königer, J.F. Stoddart, D. Alker, V.D. Harding, Amino Acid Derivatives of β-Cyclodextrin, J. Org. Chem. 61 (1996) 903–908, https://doi.org/10.1021/jo951396d.
[49] N.B. Vargaftik, B.N. Volkov, L.D. Voljak, International Tables of the Surface Tension of Water, J. Phys. Chem. Ref. Data. 12 (1983) 817–820, https://doi.org/10.1063/1.555688.
[50] G. William Kajjumba, S. Emik, A. Öngen, H. Kurtulus Özcan, S. Aydın, Modelling of Adsorption Kinetic Processes—Errors, Theory and Application, in: S. Edebali (Ed.), Adv. Sorption Process Appl., IntechOpen, 2019: pp. 116–124. https://doi.org/10.5772/intechopen.80495.
[51] A.T. Fenley, N.M. Henriksen, H.S. Muddana, M.K. Gilson, Bridging Calorimetry and Simulation through Precise Calculations of Cucurbituril-Guest Binding Enthalpies, J. Chem. Theory Comput. 10 (2014) 4069–4078, https://doi.org/10.1021/ct5004109.
[52] T.F.G.G. Cova, B.F. Milne, S.C.C. Nunes, A.A.C.C. Pais, Drastic Stabilization of Junction Nodes in Supramolecular Structures Based on Host-Guest Complexes, Macromolecules 51 (2018) 2732–2741, https://doi.org/10.1021/acs.macromol.8b00154.
[53] A. Jakalian, D.B. Jack, C.I. Bayly, Fast, efficient generation of high-quality atomic charges. AM1-BCC model: II. Parameterization and validation, J. Comput. Chem. 23 (2002) 1623–1641, https://doi.org/10.1002/jcc.10128.
[54] Z. Lin, W.F. van Gunsteren, Refinement of the application of the GROMOS 54A7 force field to β-peptides, J. Comput. Chem. 34 (2013) 2796–2805, https://doi.org/10.1002/jcc.23459.
[55] T.F.G.G. Cova, S.C.C. Nunes, T.M.V.D. Pinho e Melo, A.A.C.C. Pais, Bambusurils as effective ion caging agents: Does desolvation guide conformation? Chem. Phys. Lett. 672 (2017) 89–96.
[56] C. Lefebvre, G. Rubez, H. Khartabil, J.-C. Boisson, J. Contreras-García, E. Hénon, Accurately extracting the signature of intermolecular interactions present in the NCI plot of the reduced density gradient versus electron density, Phys. Chem. Chem. Phys. 19 (2017) 17928–17936, https://doi.org/10.1039/C7CP02110K.
[57] R.M. Silverstein, F.X. Webster, D.J. Kiemle, Infrared Spectrometry, in: D. Brennan, J. Yee, S. Wolfman-Robichaud (Eds.), Spectrom. Identif. Org. Compd., seventh ed, John Wiley & Sons, Inc., 2005: pp. 72–126.
[58] S. Kohata, K. Jyodoi, A. Ohyoshi, Thermal decomposition of cyclodextrins (α-, β-, γ-, and modified β-CyD) and of metal—(β-CyD) complexes in the solid phase, Thermochim. Acta. 217 (1993) 187–198, https://doi.org/10.1016/0040-6031(93)85107-K.
[59] W. Liu, W. Zheng, Y. Ma, K. Liu, Sorption and Degradation of Imidacloprid in Soil and Water, J. Environ. Sci. Heal. Part B Pestic. Food Contam. Agric. Wastes. 41 (2006) 623–634. https://doi.org/10.1080/03601230600701775.
[60] D.Q. Thuyet, H. Watanabe, J. Ok, Effect of pH on the degradation of imidacloprid and fipronil in paddy water, J. Pestic. Sci. 38 (2013) 223–227. https://doi.org/10.1584/jpestics.D12-080.
[61] W. Zheng, W. Liu, Kinetics and mechanism of the hydrolysis of imidacloprid, Pestic. Sci. 55 (1999) 482–485, https://doi.org/10.1002/(SICI)1096-9063(199904)55:4<482::AID-PS932>3.0.CO;2-3.
[62] J. Wang, X. Guo, Adsorption isotherm models: Classification, physical meaning, application and solving method, Chemosphere. 258 (2020), 127279, https://doi.org/10.1016/j.chemosphere.2020.127279.
[63] G. Utzeri, L. Verissimo, D. Murtinho, A.A.C.C. Pais, F.X. Perrin, F. Ziarelli, T.-V. Iordache, A. Sarbu, A.J.M. Valente, Poly(β-cyclodextrin)-Activated Carbon Gel Composites for Removal of Pesticides from Water, Molecules. 26 (2021) 1426, https://doi.org/10.3390/molecules26051426.
[64] T. Kairaliyeva, E.V. Aksenenko, N. Mucic, A.V. Makievski, V.B. Fainerman, R. Miller, Surface Tension and Adsorption Studies by Drop Profile Analysis Tensiometry, J. Surfactants Deterg. 20 (2017) 1225–1241, https://doi.org/10.1007/s11743-017-2016-y.
[65] F. Biedermann, W.M. Nau, H.-J. Schneider, The Hydrophobic Effect Revisited-Studies with Supramolecular Complexes Imply High-Energy Water as a Noncovalent Driving Force, Angew. Chemie Int. Ed. 53 (2014) 11158–11171, https://doi.org/10.1002/anie.201310958.

Click strategy for amine-cyclodextrin nanosponge synthesis for complete removal of bentazon and mecoprop

VIII

Gianluca Utzeri [a], Tânia F. Cova [a], Dina Murtinho [a], Alberto A.C.C. Pais [a], Artur J.M. Valente [a]

In preparation

Click strategy for the synthesis of amine-cyclodextrin nanosponges as promising materials for the complete removal of bentazon and mecoprop.

Gianluca Utzeri [a], Tânia F. Cova [a], Dina Murtinho [a], Alberto A.C.C. Pais [a], Artur J.M. Valente [a,*]

[a]CQC – IMS, Department of Chemistry, University of Coimbra, 3004-535 Coimbra, Portugal.

[*]Corresponding author: Prof. Artur J.M. Valente (avalente@ci.uc.pt)

Abstract

Bentazon (BTZ) and mecoprop (MCP) are two soluble and widely used post-emergence foliar herbicides. Various crops, such as soybeans, peanuts and corn, are sprayed with bentazon, which acts as a photosynthesis inhibitor. Mecoprop and bentazon present a half-life time (DT_{50}) in soil of *ca.* 25 and 75 days, respectively. Their solubility is a major concern due to their spread into surrounding soils and water-streams, where bentazon has a high persistence (DT_{50} = 200 – 7000 days). Herein, a click-imine synthesis reaction is proposed for the preparation of mesoporous, thermally stable and amine-rich *α*-, *β*-CD nanosponges with size *ca.* 500 nm, namely *α*CDGNH$_2$, *α*CDGAM$_6$, *α*CDGAM$_{12}$, *β*CDGNH$_2$, *β*CDGAM$_6$ and *β*CDGAM$_{12}$. The nanosponges were characterized by FTIR, TGA, CHNSO elemental analysis, phenolphthalein inclusion complexes, pH-titration, SEM, DLS and gas-sorption. The cyclodextrin-based nanosponges were applied as highly efficient sorbent materials towards bentazon and mecoprop. Both compounds were simultaneously quantified by HPLC-DAD through a novel analytically developed method with a LOD and a LOQ of 0.013 and 1 mg L^{-1}, respectively. As a first approach, *α*CDGNH$_2$, *β*CDGNH$_2$ and *α*CDGAM$_6$ have shown a superior performance for bentazon and mecoprop, both in individual batches and in mixtures, reaching a removal yield of ≈ 97% and ≥ 99% for BTZ and MCP, respectively. Molecular dynamic simulation have been used as complementary to tool for better understanding the sorbent-sorbate interactions at molecular level.

Keywords: Bentazon, Mecoprop, Cyclodextrin; Nanosponges; Sorption

1. Introduction

According to the European pesticides database, around 350 tons of pesticides were sold in 2021; fungicide-bactericide, herbicide and insecticide groups represent 43%, 33% and 15%, of the global sales, respectively. [1]. Their application is in line with the expanding of global population that is expected to reach *ca.* 10 billion by 2030 [2]. These pesticides have around 95 different modes of action [3–5], acting at the level of the nervous system and muscles, as inhibitor of photosynthesis, amino acids' or pigment syntheses, growth regulators or neurotransmitter inhibitors in the control of insects, weeds, bacteria or fungi [6,7]. However, only 0.1% reaches the target organisms, causing serious environmental concerns and human risks [8,9]. In Europe, there are 450 approved active substances and, once introduced into the environment, pesticides can follow different pathways depending on their physicochemical properties and the surrounding environment [10–15]. In fact, poorly soluble active ingredients are more persistent in soil than soluble compounds that show higher mobility [10,16–18]. Herein, two soluble active substances were taken into account: bentazon and mecoprop. The former is a benzothiazinone and the latter a phenoxypropionic compound; both are employed as post-emergence foliar-herbicides [19,20]. MCP is a systemic pesticide, with a half-life (DT_{50}) = 20 - 33 days in soil [21] that acts as a growth regulator at the neurological level and is associated with an increased risk of non-Hodgkin's lymphoma [22]. BTZ is used to control a wide range of weeds in various crops, such as soybeans, peanuts, and corn, acting as a photosynthesis inhibitor [23]. Moreover, BTZ is persistent in aqueous media with a DT_{50} = 200 – 7000 days [24], and is moderately toxic to birds and fish. Due to their persistence in the environment, these substances are of high environmental and health concern.

Hence, efficient strategies for water treatment are of utmost importance. In this work, six non-soluble cyclodextrin 3D-structures (α- and β-CDGNH$_2$, CDGAM$_6$ and CDGAM$_{12}$) have been synthesized for the first time via a *click* condensation reaction between the aldehyde groups of the glutaraldehyde and the amine groups at the C(6) position, of three different *heptakis*-amine-cyclodextrins ($_{NH2}$CD, $_{AM6}$CD and $_{AM12}$CD) obtained using both αCD and βCD. The nanosponges (NS) were characterized by means of different techniques, including scanning electron microscopy (SEM), dynamic light scattering (DLS) and ζ-potential, gas-adsorption, Fourier-transform infrared spectroscopy (FTIR) and elemental analysis. The cyclodextrin content was indirectly assessed by the formation of inclusion compounds, using probes, and potentiometric titration was performed for the determination of free amine (N_f). The nanosponges were employed as polymeric sorbent materials toward BTZ and MCP. An elution gradient HPLC-DAD method for the simultaneous quantification of BTZ and MCP, has been developed.

2. Materials and methods

2.1.Materials and methods

For the synthesis of cyclodextrin-based nanosponges (CDNS), *α*- and *β*-cyclodextrin (98% of purity), hexane-1,6-diamine (AM_6) and dodecane-1,12-diamine (AM_{12}) and a 25% aqueous solution of glutaraldehyde (GLT – d = 1.06 kg dm^{-3} at 25 °C) were supplied by Sigma-Aldrich. Triphenylphosphine (Ph_3P) was acquired from AlfaAesar and resublimed iodine (I_2) and sodium azide (NaN_3 – purity 99%) from Panreac. Bentazon and mecoprop, of analytical grade, were supplied by Sigma-Aldrich (purity > 99%).

2.2.Materials and methods

The three amine-cyclodextrin derivatives of *α*-CD and *β*-CD were obtained by substituting the iodine in the *heptakis*-(6-iodo)-(6-deoxy)-cyclodextrin (I-CD) with -NH_2, AM_6 and AM_{12}. Subsequently, the CDNS were obtained by polymerization with glutaraldehyde, according to the scheme depicted in Figure 1.

The I-CD (a white powder) was synthesized by a nucleophilic substitution (S_N2) through formation of a transition state via coordination with Ph_3P [25][26][27]. AM_6- and AM_{12}-modified cyclodextrin were synthesized by microwave-assisted procedure (MW) at fixed temperature (85 °C) for 30 min, in a CEM Discovery microwave [25,26,28].

The $_{NH2}$CD was obtained via formation of the *per*-6-azido-cyclodextrin ($_{N3}$CD). $_{N3}$CD was synthesized by reacting CD-I, in dried dimethylformamide (DMF), with NaN_3 (molar ratio 1:9 CD:NaN_3), at 60 °C for 20 hours, in N_2-atmosphere. The volume of DMF was reduced via rotary evaporator, and the product was precipitated in a large excess of water. $_{N3}$CD was filtered in vacuum and washed with water, resulting in a white powder. Then, the amine was prepared by reacting $_{N3}$CD with Ph_3P in DMF through the Staudinger reaction, which involves the formation of an iminophosphorane. Finally, the iminophosphorane intermediate was hydrolysed by adding an ammonia solution dropwise until a white suspension was formed. The mixture was then stirred overnight at room temperature. After volume reduction, the obtained product was precipitated in EtOH and collected through vacuum filtration [27].

The substitution yields for I-CD, $_{AM6}$CD and $_{AM12}$CD for both *α*-CD and *β*-CD have been reported in the previous scientific outcomes [25,26].$_{N3}$CD and $_{NH2}$CD were analyzed by ^{1}H-nuclear magnetic resonance (^{1}H-NMR) spectroscopy at 400 MHz, using 10 mg of each polymer dissolved

in DMSO-d_6 and D_2O, respectively, and 0.25% (m/v) of sodium trimethylsilylpropionic acid-d_4 (TSP, 98%, Euriso-Top).

The per-substitution with -N_3 in α-CD and β-CD, namely *hexakis*-(6-azido)-(6-deoxy)-α-cyclodextrin ($_{N3}\alpha$CD – yield 97%) and *heptakis*-(6-azido)-(6-deoxy)-β-cyclodextrin ($_{N3}\beta$CD – yield 94%), was confirmed by ^{1}H-NMR (400 MHz, DMSO-d_6):

^{1}H-NMR of $_{N3}$-αCD, δ (ppm): 3.30 – 3.35 (m, 6H), 3.41 – 3.43 (m, 6H), 3.62 (dd, J = 13.4, 6.9 Hz, 6H), 3.69 – 3.91 (m, 12H), 4.92 (d, J = 3.6 Hz, 6H), 5.58 (sl, 6H), 5.72 (sl, 6H)

^{1}H-NMR of $_{N3}$-βCD, δ (ppm): 3.33-3.38 (m, 7H), 3.40-3.46 (m, 7H), 3.62-3.67 (m, 14H), 3.76-3.84 (m, 14H), 4.95 (d, J = 3.5 Hz, 7H), 6.08 (sl, 7H), 6.19 (sl, 7H).

The structures of *hexakis*-(6-amino)-(6-deoxy)-α-cyclodextrin ($_{NH2}\alpha$CD – yield 40%) and *heptakis*-(6-amino)-(6-deoxy)-β-cyclodextrin ($_{NH2}\beta$CD – yield 86%), were confirmed by ^{1}H-NMR 400 MHz in D_2O):

^{1}H-NMR of $_{NH2}$-αCD, δ (ppm): 2.91-2.97 (m, 6H), 3.12-3.19 (m, 6H), 3.46-3.51 (m, 6H), 3.82-3.84 (m, 6H), 3.92-4.01 (m, 12H), 5.08 (sl, 6H).

^{1}H-NMR of $_{NH2}$-βCD, δ (ppm): 2.75-2.93 (m, 7H), 3.03 (approx. d, J = 13.7 Hz, 7H), 3.36 (t, J = 9.2 Hz, 14H), 3.68 – 3.83 (m, 14H), 4.96 (sl, 7H).

The last step of polymerization involved adding a 25% aqueous solution of GLT to the aminated intermediate in an agate mortar. The mixture was mechanically mixed to ensure a homogeneous and complete reaction. The *click*-imine reaction led to an instantaneous crosslinking with the immediate change of color from pale yellowish to red. The observed color change confirms the successful formation of the imine linkages (also known as Schiff bases) between the amine groups at C(6) of the cyclodextrin intermediate and the aldehyde groups of GLT. The click reaction drastically reduces the reaction time from 48 hours to some minutes, and increases the amount of polymer obtained, compared to other reported reactions [25,26]. However, imine groups are chemically unstable unless they are part of conjugated system; in acidic media, the reaction can be reversed with an optimum at pH = 4 [29]. Thus, the imine groups were reduced by reaction with $NaBH_4$ in methanol at molar ratio of 1:9 mol/mol amine-CD derivative/$NaBH_4$. When the formation of H_2 has ceased, the mixture was stirred and heated overnight, at 60 °C, under a N_2 atmosphere. The product was then filtered under vacuum, washed through 10 min sonication cycles with methanol, water and finally acetone, and then centrifuged to remove the supernatant. Prior to application, the nanosponges were ground by ball-milling at 30 Hz for 30 min.

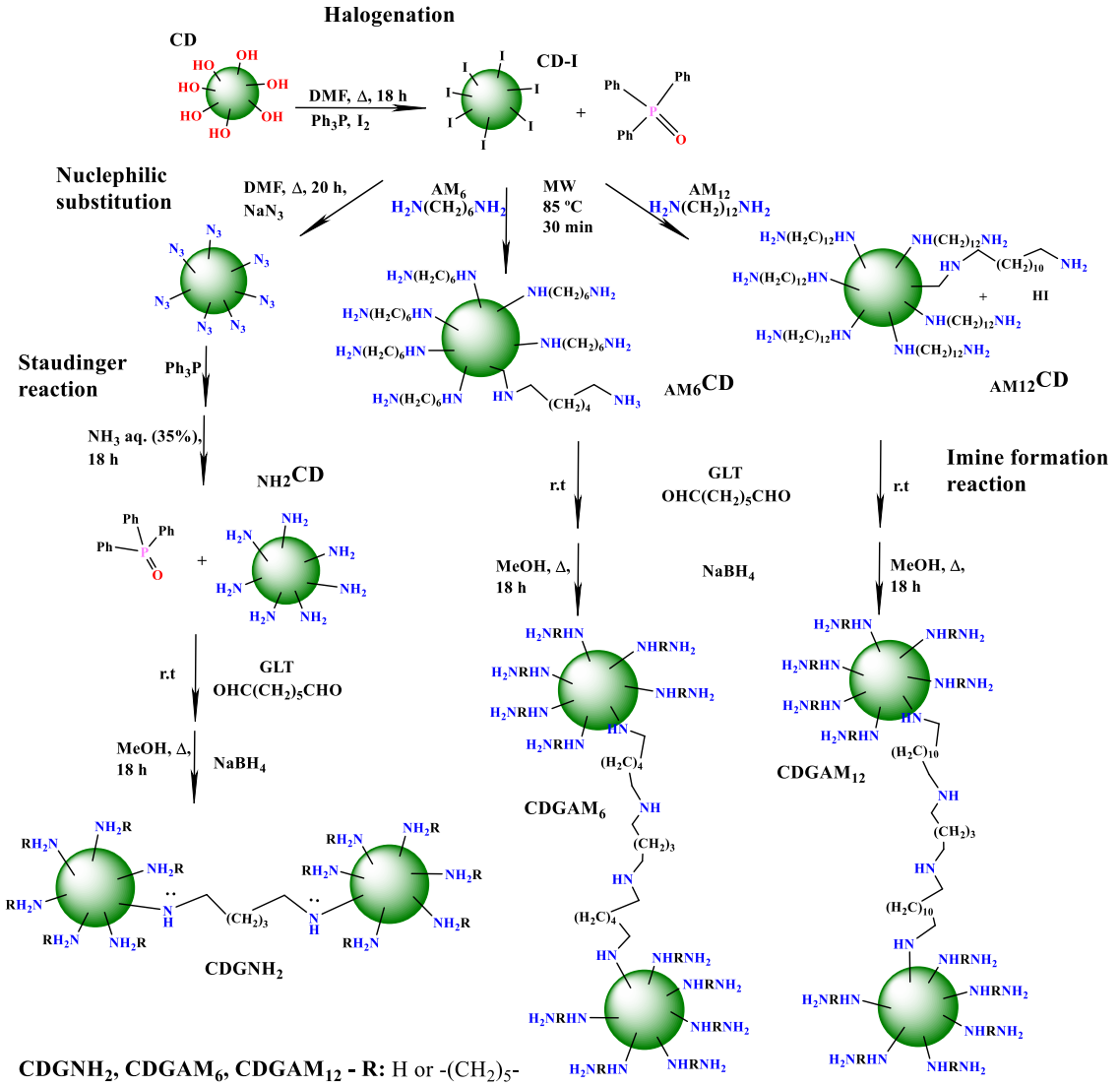

Figure 1. Schematic representation of the synthesis of the cyclodextrin-based nanosponges.

2.3.Physico-chemical characterization

The physical characterization was performed by means of several techniques. Morphology was evaluated by scanning SEM (*Gemini 2-Zeiss*) and the micrographs were obtained using an accelerating voltage of 1 kV and 4 kV for two magnifications ×1 and ×10k, respectively. Size particle was determined via dynamic light scattering (DLS) measurements using nanosponge dispersion of 1 mg mL^{-1} in water at 25 °C (*Malvern Zetasizer nanoZS*), with refractive index (RI) of 1.33 and a dynamic viscosity of 8×10^{-4} kg m^{-1} s^{-1}. The particle size was determined using a He-Ne laser at 663 nm, detector at 173° angle backscattering, and the *General Purpose* algorithm for the determination of the intensity scattering distribution.. Active surface area (SA – m^2 g^{-1}) and porosity were determined by N_2-adsorption analysis (*ASAP 2000*, Micrometrics); and the

average pore diameter (P_d – nm) was calculated by the single-point value of Brunauer-Emmett-Teller (BET) model:

$$P_d = \frac{4V_{pore}}{SA} \quad \text{(eq. 1)}$$

where V_{pore} (m^3) is the pore volume.

For the chemical characterization, FTIR spectroscopy (*Thermo Scientific,* model Nicolet 6700 FT-IR) allows to assess the presence of the main functional groups. The measurements were carried out using KBr pellets with CDNS at 1% (w/w). The CHNSO elemental analysis (EA 1108 CHNS-O, Fisons) was performed in order to determine the weight percentage (w/w) of C, N, H and O. Moreover, in order to better understand the polymer properties and their influence on the sorption process, the free amine groups (molN_{free}) of 10 mg CDNS were protonated in 0.02 mol dm^{-3} aqueous HCl solution and determined by pH titration via micro-addition of aqueous NaOH solution 0.1 mol L^{-1}. The content of free cyclodextrin (*CD-free*), which is likely capable to form inclusion complexes with bentazon [30] and mecoprop, was quantified using 1 mg of *β*CDNS in a constant concentration of phenolphthalein ([PP] = 4.2×10^{-5} mol dm^{-3}). Phenolphthalein was the guest probe of choice due to its high association constant ($K_{complex} = 2.4 \times 10^4$ or 1.05×10^4) [31,32]. The quantification of phenolphthalein was performed by UV-Vis (λ = 553 nm) using an aqueous solution of Na_2CO_3 0.02 mol L^{-1}, and the analytical range was determined ($0 – 4 \times 10^{-5}$ mol L^{-1}). The thermal stability of the CDNSs was measured via thermogravimetric analysis (TGA) (*Netzsch Instruments*, model TG209-F3 Tarsus). The analysis was performed using a temperature ramp within 25 – 600 °C, at a heating rate of 10 K min^{-1}, with a nitrogen flow of 50 mL min^{-1}.

2.4.High-Performance liquid chromatography

The quantification of bentazon and mecoprop was performed with a modular high-performance liquid chromatography (HPLC) Agilent-Technologies – 1260 Infinity II, equipped with a Agilent Manual FL-injection valve (up to 600 bar) coupled with 200 µL loop, quaternary pump G7111B (up to 600 bar), diode array detector (DAD) model G7115A set at 40 Hz (0.13 s response time), column and guard column Agilent, Poroshell 120 EC-C18 (2.1 × 150 mm × 4 µm) and Poroshell 120 EC-C18 (2.1 × 5 mm × 4 µm). The data were collected and treated with Agilent OpenLAB CDS ChemStation Edition *v.* A.01.10.128. The analysis was performed in an elution gradient, using acetonitrile and aqueous solution of phosphoric acid at 0.05 mol dm^{-3} 40:60 (v/v) as mobile phase, at a flow rate of 0.75 mL min^{-1}. The elution gradient was performed increasing the ACN percentage from 40% to 60% (v/v) in 6 min. For the detection of BTZ and MCP, the absorbances

at 225 nm and 230 nm were used, respectively. A stock solution of mixed BTZ/MCP at 50 mg L^{-1} was freshly prepared in Millipore water filtered via a 0.22 µm cellulose acetate syringe filter, and stored at 6 °C. The method was developed based on the literature [33–37] (Table 1).

Table 1. Parameter values of HPLC protocols for bentazon and mecoprop quantification.

High-performance liquid chromatography					
Bentazon	**Mobile phase**	**Flow rate (mL min^{-1})**	**Retention time (min)**	**LOD/LOQ (mg L^{-1})**	**Ref.**
λ = 230 nm, at 25 °C	MeOH:H_2O (60:40 v/v) pH 4.6	0.8	1.59	0.1×10^{-4} / 190×10^{-4}	[33]
λ = 215 nm, at 40 °C	ACN:FAc 0.1%	0.6	6	60 / 200	[34]
λ = 202 nm, at 25 °C	ACN:H_3PO_4 0.25% (64:36 v/v)	0.7	4.6	n.a.	[35]
λ = 225 nm, at 25 °C	ACN:H_3PO_4 0.05 mol L^{-1} (gradient)	0.75	4.3	0.004 / 0.013	this study
Mecoprop					
λ = 228 nm, at 25 °C	ACN:H_3PO_4 0.1% (50:50 v/v) pH 2.68	1.0	6	n.a.	[36]
λ = 230 nm, at 40 °C	ACN:H_3PO_4 0.05 mol L^{-1} pH 2.5	1.0	9.5	1.0×10^{-6} / 3.4×10^{-6}	[37]
λ = 230 nm, at 25 °C	ACN:H_3PO_4 0.05 mol L^{-1} (gradient)	0.75	5.3	0.004 / 0.013	this study

Notes: LOD: limit of detection; LOQ: limit of quantification; MeOH: methanol; ACN: acetonitrile; FAc: formic acid solution.

The linearity of the experimental data was statistically validated by one-tailed Grubb's and Mandel's tests to assess the data distribution and the presence of outliers, two-tailed F-test that confirm the homoscedasticity of the protocol. Thus, ordinary least square regression was used in the calibration with eight standard solutions in triplicate, to determine the analytical parameters, limit of determination (LOD) and limit of quantification (LOQ), through the residual standard deviation of the regression line.

The dead time (t_d) was determined by injecting a blank solution consisting of double-distilled water, filtered through a cellulose acetate syringe filter with a cut-off of 0.22 µm. Samples were injected after centrifugation at 4500 rpm for 30 min to ensure the removal of CDNS particles.

2.5.Sorption analysis

The sorption mechanism was studied through sorption kinetics and isothermal analysis, within the analytical range of BTZ and MCP, with a solid-liquid ratio (S/L) of 1 mg mL^{-1}, using 1 mg of CDNS in 1 mL of solution. The batches were shaken at 150 rpm, at 25 °C, in a LABWIT ZWY-100H incubator. The amount of pesticide sorbed per gram of sorbent (q_e – mg g^{-1}) and the removal efficiency (RE%) were calculated as follows:

$$q_e = (C_0 - C_e)\frac{V}{m} \quad \text{(eq. 2)}$$

$$RE\% = \frac{(C_0 - C_e)}{C_0} \times 100 \quad \text{(eq. 3)}$$

where C_0 and C_e (mg L^{-1}) are the concentrations at initial and equilibrium state, V (L) is volume of the solution and m (g) is the mass of sorbent.

2.6.Kinetic sorption

2.7.Equilibrium sorption

Equilibrium sorption analysis was performed using 1 mg of each nanosponge left in contact with 1 mL of pesticide aqueous solution, corresponding to a S/L = 1 mg mL^{-1}. In this way, the q_e values are only dependent on the initial and equilibrium concentrations and not on the volume of the solution or the mass of the sorbent. The batches are left 24 hours under shaking at 120 rpm, at 25 °C. In particular, the sorption analysis was performed on aqueous solution of BTZ, MCP and their mixture within the analytical range (0.13 – 1 mg L^{-1}), to understand the removal efficiency for each active ingredient and the influence caused by the presence of both compounds. The experimental data of q_e plotted as a function of C_e were fitted by the Sips model, with the following mathematical expression:

$$q_e = \frac{q_m K_S C_e^{1/n}}{1 + K_S C_e^{1/n}} \quad \text{(eq. 4.)}$$

where q_m (mg g^{-1}) is the maximum sorbed amount, K_s ($L^{1/n}$ $mg^{-1/n}$) is the Sips constant related to the sorption capacity, and n is a constant associated with the heterogeneity of the sorbent system.

2.8.Molecular dynamic simulations

3. Results and discussion

3.1. Characterization of cyclodextrin-based nanosponges.

The presence of functional groups resulting from the synthetic route was confirmed by FTIR analysis (Figure 2.). The band at 3400 cm^{-1}, in Figures 2-a and 2-b, is associated with stretching vibrations of -OH and -NH_x groups, provided by the cyclodextrin and crosslinker structures, respectively. The presence of primary and secondary amine groups is confirmed by the occurrence of a strong band at 1660 cm^{-1} and a weak band at 1550 cm^{-1}, assigned to the bending vibrations of the -NH-, and -NH_2 groups, respectively, or their protonated forms [25,38]. The change in intensity of these two bands associated to the primary and secondary amine groups in the nanosponge structure, can be justified by the total moles of nitrogen per gram of NS (molN_t g_{NS}^{-1}) indirectly assessed by CHNSO elemental analysis N% (w/w) values (Table 2), the free mole of nitrogen per gram of NS (molN_f g_{NS}^{-1}), measured by pH titration, and their ratio (molN_f g_{NS}^{-1}/molN_t g_{NS}^{-1}) (Figure 2-c/2-d and Table 3.). The higher molN_t g_{NS}^{-1} values for αCDGAM$_6$ and βCDGAM$_6$, reported in Table 3, can be due to their higher cyclodextrin content (*CD%*), directly related to the higher degree of crosslinking (*DC*) (Table 2). The two peaks around 2990 cm^{-1} are related to symmetrical and asymmetrical stretching vibrations of the -CH_2- groups, which intensity and separation increase from CDGNH$_2$ to CDGAM$_{12}$ probably related to the lengthening of the aliphatic chain. The methylene groups also present an intense peak at 1460 cm^{-1} associated with their scissoring vibration. The bands at 1150 cm^{-1}, 1080 cm^{-1} and 1040 cm^{-1} are related to stretching vibration of -C-C-N- and -C-O-C- groups (overlapped bands), -C-NH- group and -CH-OH group, respectively.

Table 2. CHNSO elemental analysis results of cyclodextrin-based nanosponges.

CDNSs	N% (w/w)	C% (w/w)	H% (w/w)	O% (w/w)	CD% (w/w)[a]	DC[b]
αCDGNH$_2$	3.84 ± 0.08	50.79 ± 0.02	7.58 ± 0.19	37.58 ± 0.08	0.32	1.4
αCDGAM$_6$	6.6 ±	61.05 ±	8.46 ±	23.67 ±	0.55	3.1
αCDGAM$_{12}$						
βCDGNH$_2$	4.7 ± 0.30	48.70 ± 0.23	8.04 ± 1.35	38.15 ± 2.35	0.32	2.3
βCDGAM$_6$	3.25 ± 0.02	38.78 ± 0.07	5.72 ± 0.31	19.14 ± 3.32	0.47	3.8
βCDGAM$_{12}$						

[a] CD% = C_{CDNS}% / $C_{CD;}$
[b] DC (degree of crosslinking) is calculated as the amount of N per mole of glutaraldehyde obtained as difference of C% − C_{CDNS}%.
–: values still not available.

Table 3. Molar nitrogen content in nanosponge structure.

Nanosponge	molN_t g$^{-1}_{NS}$	molN_f g$^{-1}_{NS}$	(molN_f g$^{-1}_{NS}$)/(molN_t g$^{-1}_{NS}$) %
αCDGNH$_2$	2.7×10^{-3}	7.4×10^{-6}	0.3
αCDGAM$_6$	4.7×10^{-3}	21.9×10^{-6}	0.5
βCDGNH$_2$	3.3×10^{-3}	2.7×10^{-6}	0.1
βCDGAM$_6$	4.7×10^{-3}	13.7×10^{-6}	0.3

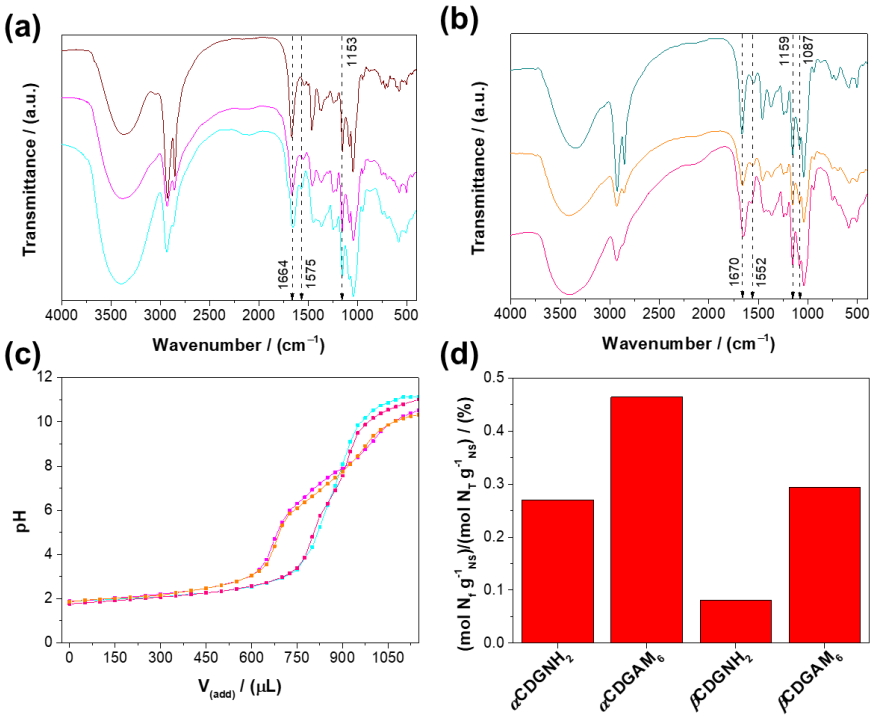

Figure 2. FT-IR spectra (a and b), potentiometric titration curves of amine groups in CDNS with NaOH 0.1 mol L^{-1} (c) and histogram of the ratio of molesN_f g$_{NS}^{-1}$/molesN_t g$_{NS}^{-1}$ (d). αCDGNH$_2$ (blue line), αCDGAM$_6$ (magenta line), αCDGAM$_{12}$ (brown line), βCDGNH$_2$ (pink line), βCDGAM$_6$ (orange line), βCDGAM$_{12}$ (dark-cyan line).

Exploiting the CDs host-guest formation capacity and considering that the CD% values in Table 2 are representative of the total amount of CD, the mol of free-CD per gram of NS was evaluated. Using the highest [PP] and considering a molar stoichiometry of 1:1, the $K_{complex}$ was computed using the equation 5 [39,40], by plotting the variation of the measured physical property (ΔAbs_{obs}) as a function of the [βCD].

$$\Delta Abs_{obs} = \frac{\Delta Abs_{CD-PP}}{2[CD]_T} \left\{\left([PP]_T + [CD]_T + \frac{1}{K_1}\right) - \left(\left([PP]_T + [CD]_T + \frac{1}{K_1}\right)^2 - 4([PP]_T[CD]_T)\right)^{\frac{1}{2}}\right\} \quad \text{(eq. 5)}$$

By fitting the eq.(2) to the experimental data, using a non-linear least-square method, the $K_{complex}$ = (2.2 ± 0.2) × 10^4 and $\Delta Abs_{CD\text{-}PP}$ = (1.17 ± 0.03) were obtained (Figure 3-a). The $K_{complex}$ value was used to determine the amount of free-CD in the *β*CDNS (Figure 3-b). As shown in Figure 3-c, the content of CD in *β*CDGAM$_6$ (4.9 × 10^{-5} mol_{CD} g_{NS}^{-1}) is 3.7 × 10^{12} times higher than in *β*CDGNH$_2$ (1.3 × 10^{-17} mol_{CD} g_{NS}^{-1}), suggesting a possible greater contribution to the sorption process. Moreover, the result confirms a strong influence of the aliphatic chain length on the *CD%* and *DC*. Once this arises, the longer linker achieves higher degree of freedom, being able to react with a greater number of amine active sites located on different CD units (Table 2.). The content of *β*CDGAM$_{12}$ was not determinable since $\Delta Abs_{CD\text{-}PP}$ values were in the range of the equipment sensitivity.

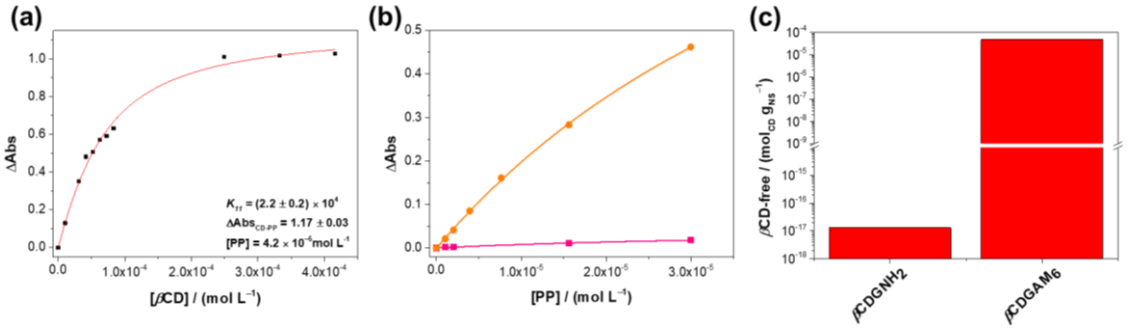

Figure 3. Host-guest complex analysis using [PP] = 4.2 × 10^{-5} mol L^{-1}, in a 0.02 mol L^{-1} Na_2CO_3 aqueous solution (a) plot of the measurable parameter of CD-PP as function of [*β*CD] for the determination of constant binding, $K_{complex}$, by titration; (b) plot of the measurable parameter of CD-PP as function of [PP], to determine [CD_T] in *β*CDGNH$_2$ (pink) and *β*CDGAM$_6$ (orange), by titration; (c) histogram of the *βCD-free* in terms of mol_{CD} g_{NS}^{-1}.

How do the type of CD and crosslinker as well as *CD%, DC*, primary and secondary amine groups affect the physical properties of the CDNSs? The SEM micrographs at ×1 k magnification, reported in Figure 4-a to Figure 4-f, show that the surface morphology of NSs is deeply affected by branch length rather than the type of CD. *α*CDGNH$_2$ (Figure 4-a), *β*CDGNH$_2$ (Figure 4-b), *α*CDGAM$_{12}$ (Figure 4-e) and *β*CDGAM$_{12}$ (Figure 4-f) have heterogeneous surfaces with aggregates of different sizes. The heterogeneity and the presence of aggregates is also confirmed by the polydispersity index (PDI) ≥ 0.8 (Table 4.). The Figure 4-a and 4-b show a similar morphology for *α*CDGNH$_2$ and *β*CDGNH$_2$, with monoliths surrounded by small particles with flatten globular-shape as it can be seen in Figure 4-a' and 4-b'. Such a characterization is confirmed by the N_2 adsorption; i.e., *α*CDGNH$_2$ and *β*CDGNH$_2$ have similar surface areas: 30.5 m^2 g^{-1} and 32.2 m^2 g^{-1}, respectively (Table 5.). More in detail, the morphological heterogeneity

strongly influences the size of NS particles, expressed by the average intensity values for αCDGNH$_2$ (489 ± 77) nm and βCDGNH$_2$ (600 ± 12) nm; the larger particles of βCDGNH$_2$ are also the result of a higher degree of crosslinking (Table 2). Considering αCDGAM$_{12}$ and βCDGAM$_{12}$, the presence of the smaller particles suggested by Figure 4-e and 4-f is actually an effect of an irregular surface as observed in Figure 4-e' and Figure 4-f', with the presence of pores of 39.6 and 38.2 nm, respectively (Table 5). The DLS and BET analysis also indicate that αCDGAM$_{12}$ and βCDGAM$_{12}$ have similar average sizes (584 ± 62) nm and (663 ± 33) nm (Table 4.), and surface area values of 12.6 m^2 g^{-1} and 14.1 m^2 g^{-1}, respectively (Table 5.). Interestingly, αCDGAM$_6$ and βCDGAM$_6$ have a completely different morphology with homotattic surfaces in smooth monoliths (Figure 4-c and 4-d). The compact structure of αCDGAM$_6$ and βCDGAM$_6$ can be explained by their higher values of *CD%* and DC (Table 2), which can influence the average intensity size value of (493 ± 5) nm and (545 ± 55) nm (Table 4.), respectively. The similar particle size can be explained by the content of cyclodextrin and *DC* values (Table 2). The Figure 4-c' and 4-d' at higher magnifications suggest the absence of pores or channels, in contradiction to the BET analysis results which show the highest P_d values of 54.8 nm and 42.9 nm, for αCDGAM$_6$ and βCDGAM$_6$, respectively (Table 5.). The influence of the type of cyclodextrin can be observed by comparing the particle size values between analogous CDNSs. Indeed, particle size values of the αCDNSs are smaller than the corresponding βCDNSs.

Table 4. Size particle parameters of the CDNSs measured by DLS analysis.

	Dynamic light scattering			
Nanosponges	**Intensity size (d. nm)**	**Volume size (d. nm)**	**Number size (d.nm)**	**PDI**
αCDGNH$_2$	489 ± 77	505 ± 96	467 ± 91	0.8 ± 0.1
αCDGAM$_6$	493 ± 5	507 ± 3	474 ± 9	0.8 ±0.1
αCDGAM$_{12}$	584 ± 62	619 ± 76	562 ± 62	0.9 ± 0.2
βCDGNH$_2$	600 ± 12	616 ± 14	596 ± 12	1.0 ± 0.1
βCDGAM$_6$	545 ± 55	558 ± 62	539 ± 52	1 ± 0
βCDGAM$_{12}$	663 ± 33	624 ± 33	569 ± 27	1 ± 0

Table 5. Parameters of N_2-sorption analysis of the cyclodextrin-based nanosponges.

N_2-sorption analysis			
Nanosponges	**Average pore diameter (nm)**	**Pore volume ($cm^3\ g^{-1}$)**	**Surface area ($m^2\ g^{-1}$)**
αCDGNH$_2$	30.5	0.16	20.6
αCDGAM$_6$	54.8	0.33	23.8
αCDGAM$_{12}$	39.6	0.12	12.6
βCDGNH$_2$	32.2	0.19	23.2
βCDGAM$_6$	42.9	0.10	9.3
βCDGAM$_{12}$	38.2	0.13	14.1

The thermal stability of the CDNS were evaluated by thermogravimetric analysis (Figure 5 and Table 6). All polymers show three degradation steps, except for αCDGAM$_6$. The first degradation ($T_{1,max}$) occurs at around 50 °C and represent the dehydration process, with a maximum weight loss of *ca.* 9%. The second degradation ($T_{2,max}$) occurring between 239 °C and 301 °C is associated with the thermolysis of αCD and βCD. It can also be seen that $T_{2,max}$ changes in the order: αCDGNH$_2$ < βCDGNH$_2$ < αCDGAM$_{12}$ < βCDGAM$_6$ < αCDGAM$_6$ < βCDGAM$_{12}$, which agrees with the *CD%* and *DC* values (see Table 2). From the thermogram shown in Figure 5-a, it can also be observed that the first degradation step for αCDGNH$_2$ and αCDGAM$_{12}$ is splitted, probably due to the heterogeneous morphology of the NS (Figure 4-a and 4-e). The $T_{3,max}$ can be associated with the breaking of the bond between cyclodextrin and amine group at C6 or between the amine group and glutaraldehyde. Moreover, αCDGAM$_6$ presents a fourth degradation temperature at $T_{4,max}$ = 559 °C, probably due to its compact structure and high number of molesN_f g_{NS}^{-1} (Table 3.) which can contribute to enhance thermal stability by forming inter- and intra-molecular electrostatic and hydrogen bonding interactions.

Table 6. Thermogravimetric analysis parameters of cyclodextrin-based nanosponges

Compounds	temperature range (°C)	temperature peak max (°C)	mass loss (%)
αCDGNH$_2$	T_1: 20-156 T_2: 156-330 T_3: 330-538	$T_{1,max}$: 55 $T_{2,max}$: 239 $T_{3,max}$: 424	T_1: 9.3 T_2: 40.1 T_3: 32.2
βCDGNH$_2$	T_1: 20-152 T_2: 152-354 T_3: 354-583	$T_{1,max}$: 49 $T_{2,max}$: 248 $T_{3,max}$: 417	T_1: 8.6 T_2: 39 T_3: 11.5
αCDGAM$_6$	T_1: 20-175 T_2: 175-361 T_3: 361-495 T_4: 495-586	$T_{1,max}$: n.a. $T_{2,max}$: 282 $T_{3,max}$: 444 $T_{4,max}$: 559	T_1: 0.1 T_2: 20.3 T_3: 27.8 T_4: 17.2
βCDGAM$_6$	T_1: 20-169 T_2: 169-338 T_3: 338-486	$T_{1,max}$: 55 $T_{2,max}$: 270 $T_{3,max}$: 418	T_1: 6.8 T_2: 26.4 T_3: 28.5
αCDGAM$_{12}$	T_1: 20-157 T_2: 157-374 T_3: 374-600	$T_{1,max}$: 45 $T_{2,max}$: 254 $T_{3,max}$: 446	T_1: 1.5 T_2: 28.2 T_3: 25.0
βCDGAM$_{12}$	T_1: 20-178 T_2: 178-379 T_3: 379-522	$T_{1,max}$: n.a. $T_{2,max}$: 301 $T_{3,max}$: 455	T_1: 2.7 T_2: 37.3 T_3: 47.9

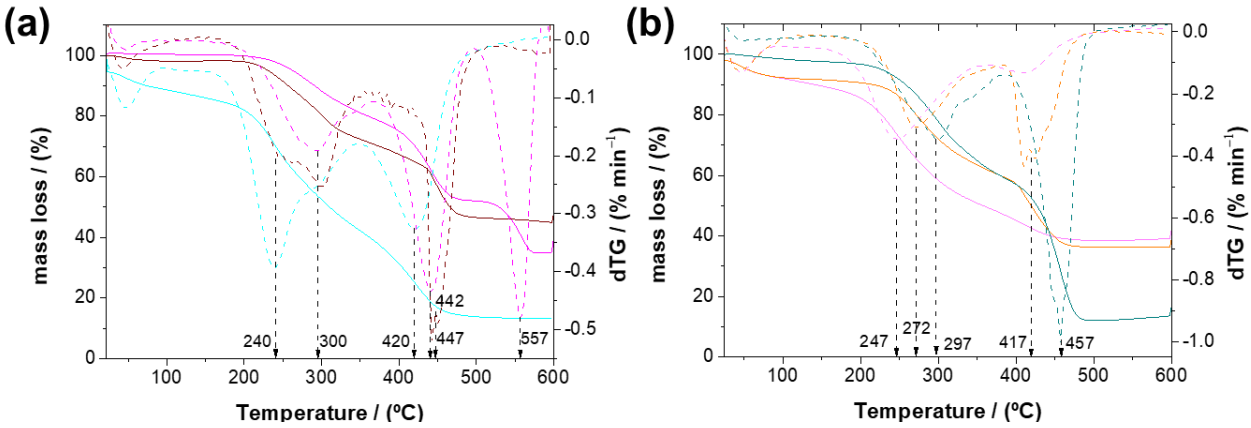

Figure. 5. TG (line) and DTG (dashed line) curves of: (a) αCDGNH$_2$ (blue line), αCDGAM$_6$ (magenta), αCDGAM$_{12}$ (brown); (b) βCDGNH$_2$ (pink), βCDGAM$_6$ (orange), βCDGAM$_{12}$ (cyan).

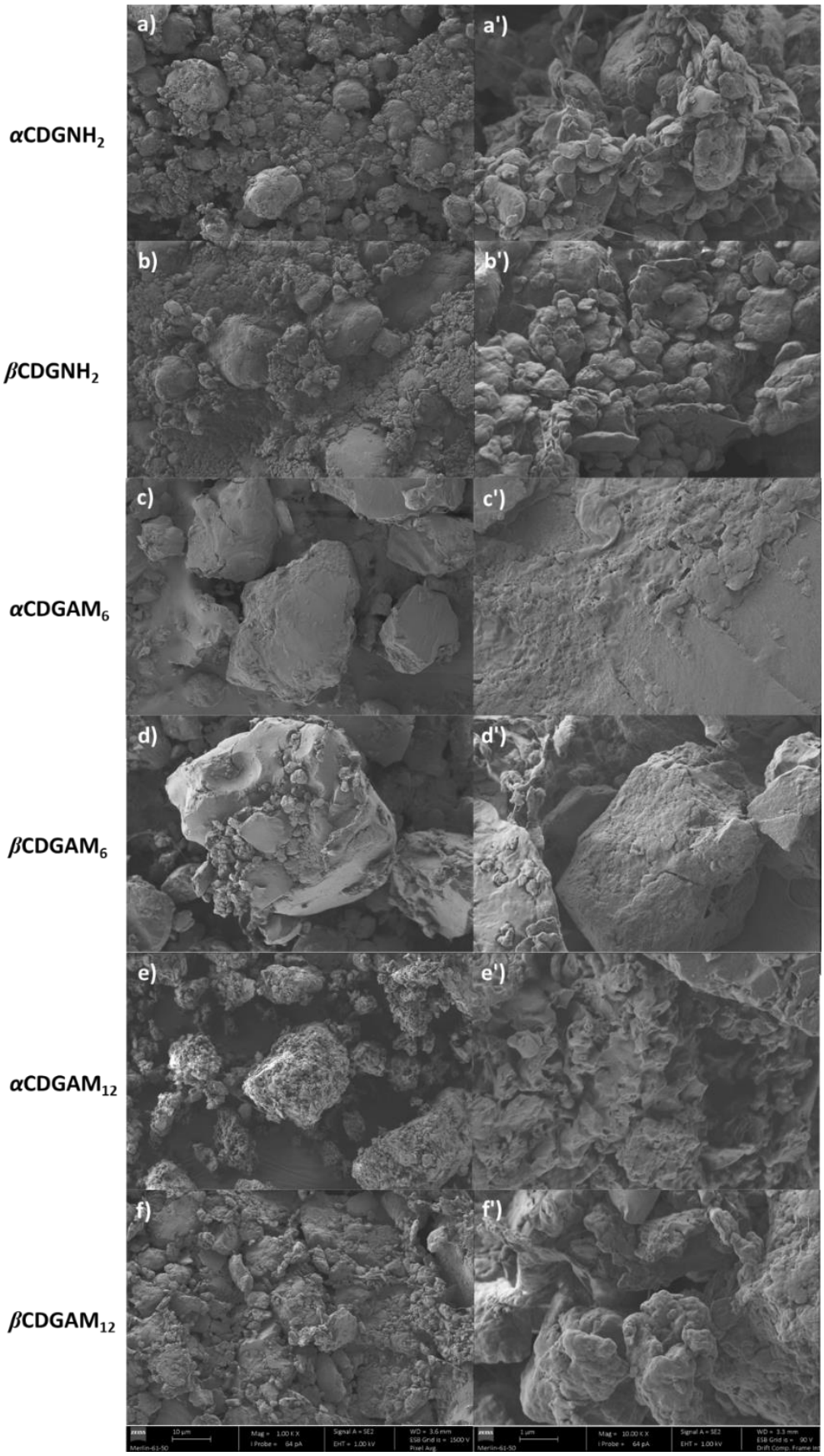

Figure 4. Micrographs of αCDGNH$_2$, βCDGNH$_2$, αCDGAM$_6$, βCDGAM$_6$, αCDGAM$_{12}$ and βCDGAM$_{12}$, taken with magnification ×1k and 1 kV (a-f) and ×10k and 4 kV (a' - f').

3.2.HPLC parameters for pesticide quantification

The analytical solutions for the calibration were measured in triplicate and the data was statistically validated. The presence of outliers was evaluated by one-tailed Grubbs test ($G_{(0.05,\ 8)}$ = 2.13) at 95% of confidence interval (CI); the variation of the deviation standard was tested by the two-tailed Fisher test ($F_{(0.005,7,7)}$ = 8.9) at 99% of CI indicating a homoscedastic system. The linearity was also confirmed by the one-tailed test-$F_{(0.01,1,5)}$ = 16.26, allowing the application of the ordinary least square method. The presence of the outliers in the model was tested by the Mandell test, one-tailed $F_{(0.01,1,5)}$ =16.26. The analytical parameters were determined by matrix treatment, the robustness was confirmed by the relative error (RE% < 30) and two-tailed t-student at 95% and 99% of CI ($t_{(0.05,8)}$ = 2.31 and $t_{(0.01,8)}$ = 3.36). The limit of detection and quantification were calculated by using, respectively:

$$LOD = \frac{2 \times t_{(0.05,5)} \times \sigma_{b_0}}{b_1} \qquad \text{(eq. 6)}$$

$$LOQ = \frac{6 \times t_{(0.05,5)} \times \sigma_{b_0}}{b_1} \qquad \text{(eq. 7)}$$

where $t_{(0.05,5)}$ is the one-tailed t value calculated at 99% of CI and 6 degree of freedom, σ_{b0} is the standard deviation of b_0 (intercept) and b_1 is the slope, obtained by plotting the peak areas as function of the concentration (Figure 6.).

In order to determine the accuracy of the method, the recovery test (RI%) was performed in triplicate, at three concentrations level low, medium and high (0.013, 0.0875 and 0.875 mg L^{-1}), using a 5.0 mg L^{-1} mix solution for spiking. The presence of outliers was assessed by the Grubbs test and the values of RI% were confirmed by two-tailed t-test at 95% and 99% of CI and p_value > 0.05 (Table 7.).

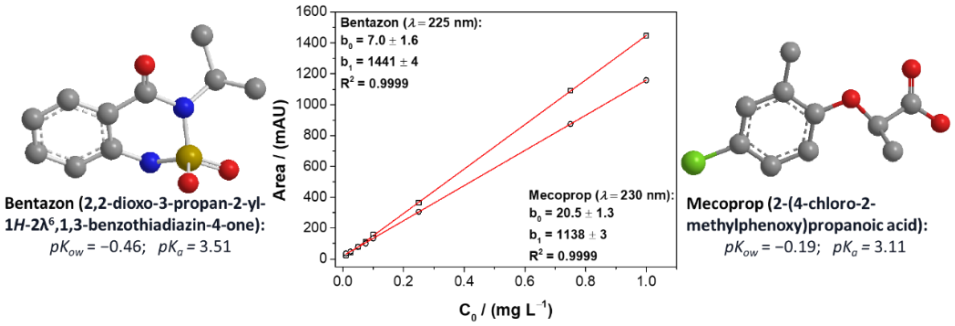

Figure 6. Representation of the calibration curve and molecular structures of bentazon and mecoprop.

Table 7. Recovery test of the HPLC analysis method.

Bentazon	**Level**	**RI%**	***p*_value**
Analytical range	low - I	94.2	0.131
(0.013 – 1.0) mg L^{-1}	medium - II	95.5	0.092
	high - III	103.0	0.656
Mecoprop	**Level**	**RI%**	***p*_value**
Analytical range	low - I	94.6	0.062
(0.013 – 1.0) mg L^{-1}	medium - II	94.2	0.064
	high - III	102.2	0.438

3.3.Sorption isotherm

In order to properly discuss the results, it is important to remember that BTZ and MCP have K_a = 3.51 and 3.11, respectively, which means that they are theoretically in a negatively charged state, at the pH of water, as reported in the literature (Figure 7) [41–44]. It must be noticed that only the isotherm sorption for BTZ individually and as a mixture (Figure 8-a and 8-b) are reported, for both αCDGNH$_2$ and βCDGNH$_2$. A RE% ≥ 99% of MCP, singularly or in mixture batches, was obtained by αCDGNH$_2$, βCDGNH$_2$ or αCDGAM$_6$ in the analytical range, as noticeable in Figure 8-c, 8-d and 8-e, so non-isotherm can be extrapolated.

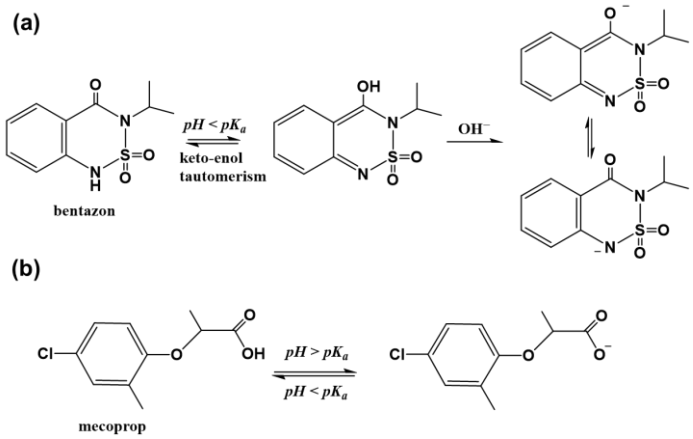

Figure 7. Scheme of BTZ (a) and MCP (b) speciation as function of pH.

The higher removal efficiency of the nanosponges towards MCP than BTZ, can be explained by the localized negative charge on the carboxylate group compared to the delocalized negative charge in BTZ species, at $pH > pK_a$. It can be suggested that MCP can form more stable electrostatic interactions with the positively charged amine groups in the CDNS surface. On the other hand, even if the RE of BTZ reaches up to ≈ 90%, at higher concentration, the delocalized charge can play an unfavourable role in the sorbate-sorbent interactions, especially at low concentrations. In fact, it can be observed in Figure 8-a and 8-b that the sorption capability of αCDGNH$_2$ and βCDGNH$_2$ towards BTZ increases with its concentration, as single specie or as mixture. This indicates that the presence of more moles of BTZ favours the formation of sorbent-sorbate interactions followed by cooperative sorbate-sorbate interactions, in agreement with the constant values $(1/n) > 1$ (Table 8), which indicates a homogeneous system characterized by multilayer formation involving cooperative processes. The Sips model was fitted to the experimental data of BTZ sorption, singularly and as a mixture (Figure 8-a and 8-b). The q_m values reported in Table 8 indicate that BTZ sorption increases in presence of MCP, *ca.*2-fold with βCDGNH$_2$, suggesting that BTZ establishes non-selective cooperative interactions, perhaps through hydrogen bonding or π- π stacking between the aromatic rings of both substances. αCDGAM$_6$ exhibited a different behaviour for BTZ alone or as a mixture, where the presence of mecoprop plays a key role in the sorption process. As shown in Figure 8-e, in the mixture batch, the removal efficiency for BTZ is ≥ 99% with a slight decrease to 97% at the higher [BTZ], probably caused by the active site saturation. For the single batch, the RE% reaches 97% only at the highest concentration, confirming the cooperative interactions.

Table 8. Fitting parameters for the application of the Sips isotherm model to the bentazon sorption.

model	bentazon		mix-bentazon	
Sips	αCDGNH$_2$	βCDGNH$_2$	αCDGNH$_2$	βCDGNH$_2$
q_m (mg g^{-1}) (× 10^{-2})	63 ± 5	66 ± 2	92 ± 4	109 ± 35
K_s (L$^{1/n}$ mg$^{-1/n}$) (× 10^6)	6 ± 36	214 ± 1055	0.002 ± 0.001	0.0003 ± 0.0006
$1/n$	5.0 ± 0.1	5.59 ± 0.04	2.78 ± 0.01	2.1 ± 0.1
R^2	0.9794	0.9930	0.9995	0.9784

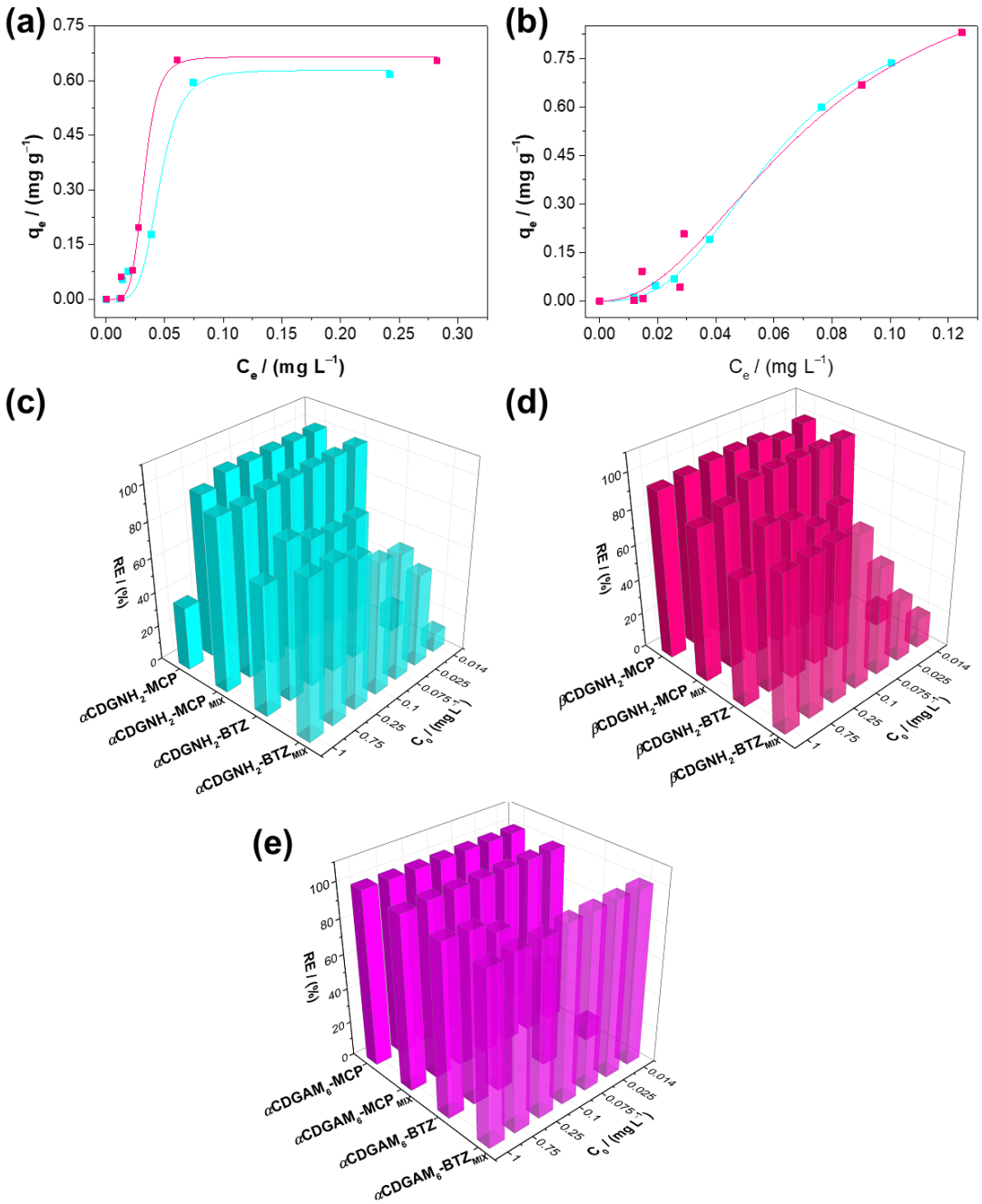

Figure 8. Performance of αCDGNH$_2$ (azure line) and βCDGNH$_2$ (pink line) in terms of sorption isotherm up-side (a) bentazon, (b) bentazon in mixture solution; and removal efficiency down-side of (c) αCDGNH$_2$, (d) βCDGNH$_2$, (e) αCDGAM$_6$.

4. Conclusions

Bentazon and mecoprop are two soluble foliar-pesticides widely applied and persistent in water. Hence, their application and spreading represent an environmental and social concern. A novel protocol for simultaneous quantification of bentazon and mecoprop via HPLC was developed with LOD and LOQ of 0.013 and 1 mg L^{-1}. Six mesoporous amine-cyclodextrin-based nanosponges, αCDGNH$_2$, αCDGAM$_6$, αCDGAM$_{12}$, βCDGNH$_2$, βCDGAM$_6$, and βCDGAM$_{12}$, were synthesized through a click-imine reaction resulting in a drastic reduction of the reaction time and an increase in the polymerization yield. The nanosponges present the size of *ca.* 500 nm, with a morphology strongly influenced by the length of the aliphatic chain, with heterogeneous surfaces for αCDGNH$_2$, βCDGNH$_2$, αCDGAM$_{12}$ and βCDGAM$_{12}$ and smooth homotattic surface for αCDGAM$_6$ and βCDGAM$_6$. The dense structure of the CDNS led to low active surface areas. Moreover, the length of the aliphatic chain also causes an increase in the number of moles of free cyclodextrin and amine groups per gram of material. The polymers were applied as sorbent material to remove bentazon and mecoprop from aqueous media, both individually and as a mixture. αCDGNH$_2$, βCDGNH$_2$, αCDGAM$_6$ have shown a superior performance reaching a RE% of *ca.* 97% and ≥ 99% for bentazon and mecoprop, respectively. In particular, it was observed that the nanosponges present higher efficiency at higher concentrations, as demonstrated by the sorption isotherms of bentazon which indicates the formation of multilayers via sorbent-sorbent, bentazon-bentazon or bentazon-mecoprop, interactions.

References

[1] A. Sharma, A. Shukla, K. Attri, M. Kumar, P. Kumar, A. Suttee, G. Singh, R.P. Barnwal, N. Singla, Global trends in pesticides: A looming threat and viable alternatives, Ecotoxicol. Environ. Saf. 201 (2020) 110812. https://doi.org/10.1016/j.ecoenv.2020.110812.

[2] U. Nations, World Population Prospects 2022, 2022. www.un.org/development/desa/pd/.

[3] A. Knowles, Recent developments of safer formulations of agrochemicals, Environmentalist. 28 (2008) 35–44. https://doi.org/10.1007/s10669-007-9045-4.

[4] A.B. de S. Cruz, P.R.R. Rocha, J.A.A. Albuquerque, J.M.A. Alves, D.L. de S. Cruz, E.L. Finoto, G.X.L. dos Santos, Selectivity of pre and post-emergency herbicides applied cowpea in the Amazon Savannah., Nativ. Pesqui. Agrárias e Ambient. 6 (2018) 625–630.

[5] A.T. Mohammed Amin, Management of Weeds in Maize (Zea mays L.) through Various Pre and Post Emergency Herbicides, Adv. Crop Sci. Technol. 02 (2014). https://doi.org/10.4172/2329-8863.1000151.

[6] J.E. Casida, Pest Toxicology: The Primary Mechanisms of Pesticide Action, Chem. Res. Toxicol. 22 (2009) 609–619. https://doi.org/10.1021/tx8004949.

[7] A. Mojiri, J.L. Zhou, B. Robinson, A. Ohashi, N. Ozaki, T. Kindaichi, H. Farraji, M. Vakili, Pesticides in aquatic environments and their removal by adsorption methods, Chemosphere. 253 (2020) 126646. https://doi.org/10.1016/j.chemosphere.2020.126646.

[8] D. Pimentel, Amounts of pesticides reaching target pests: Environmental impacts and ethics, J. Agric. Environ. Ethics. 8 (1995) 17–29. https://doi.org/10.1007/BF02286399.

[9] J. Cooper, H. Dobson, The benefits of pesticides to mankind and the environment, Crop Prot. 26 (2007) 1337–1348. https://doi.org/10.1016/j.cropro.2007.03.022.

[10] R. Schulz, Field Studies on Exposure, Effects, and Risk Mitigation of Aquatic Nonpoint-Source Insecticide Pollution: A Review, J. Environ. Qual. 33 (2004) 419–448. https://doi.org/10.2134/jeq2004.4190.

[11] J.S. Brown, K. Staňková, Game theory as a conceptual framework for managing insect pests, Curr. Opin. Insect Sci. 21 (2017) 26–32. https://doi.org/10.1016/j.cois.2017.05.007.

[12] T.W. Sappington, N.J. Miller, Editorial overview: Pests and resistance: Shedding the albatross of resistance starts by embracing the ecological complexities of its evolution, Curr. Opin. Insect Sci. 21 (2017) v–viii. https://doi.org/10.1016/j.cois.2017.07.003.

[13] T. Perry, P. Batterham, Harnessing model organisms to study insecticide resistance, Curr. Opin. Insect Sci. 27 (2018) 61–67. https://doi.org/10.1016/j.cois.2018.03.005.

[14] M. Zalucki, M. Furlong, Behavior as a mechanism of insecticide resistance: evaluation of the evidence, Curr. Opin. Insect Sci. 21 (2017) 19–25. https://doi.org/10.1016/j.cois.2017.05.006.

[15] A. Alyokhin, Y.H. Chen, Adaptation to toxic hosts as a factor in the evolution of insecticide resistance, Curr. Opin. Insect Sci. 21 (2017) 33–38. https://doi.org/10.1016/j.cois.2017.04.006.

[16] S. Rasool, T. Rasool, K.M. Gani, A review of interactions of pesticides within various interfaces of intrinsic and organic residue amended soil environment, Chem. Eng. J.

Adv. 11 (2022) 100301. https://doi.org/10.1016/j.ceja.2022.100301.

[17] P. Segurado, N. Caiola, D. Pont, J.M. Oliveira, O. Delaigue, M.T. Ferreira, Comparability of fish-based ecological quality assessments for geographically distinct Iberian regions, Sci. Total Environ. 476–477 (2014) 785–794. https://doi.org/10.1016/j.scitotenv.2013.09.004.

[18] I. Md Meftaul, K. Venkateswarlu, R. Dharmarajan, P. Annamalai, M. Megharaj, Pesticides in the urban environment: A potential threat that knocks at the door, Sci. Total Environ. 711 (2020) 134612. https://doi.org/10.1016/j.scitotenv.2019.134612.

[19] S.R. Buss, J. Thrasher, P. Morgan, J.W.N. Smith, A review of mecoprop attenuation in the subsurface, Q. J. Eng. Geol. Hydrogeol. 39 (2006) 283–292. https://doi.org/10.1144/1470-9236/04-081.

[20] R. Huber, S. Otto, Environmental behavior of bentazon herbicide., Rev. Environ. Contam. Toxicol. 137 (1994) 111–134. https://doi.org/10.1007/978-1-4612-2662-8_3/COVER.

[21] M. Arena, D. Auteri, S. Barmaz, G. Bellisai, A. Brancato, D. Brocca, L. Bura, H. Byers, A. Chiusolo, D. Court Marques, F. Crivellente, C. De Lentdecker, M. De Maglie, M. Egsmose, Z. Erdos, G. Fait, L. Ferreira, M. Goumenou, L. Greco, A. Ippolito, F. Istace, S. Jarrah, D. Kardassi, R. Leuschner, C. Lythgo, J.O. Magrans, P. Medina, I. Miron, T. Molnar, A. Nougadere, L. Padovani, J.M. Parra Morte, R. Pedersen, H. Reich, A. Sacchi, M. Santos, R. Serafimova, R. Sharp, A. Stanek, F. Streissl, J. Sturma, C. Szentes, J. Tarazona, A. Terron, A. Theobald, B. Vagenende, A. Verani, L. Villamar-Bouza, Peer review of the pesticide risk assessment of the active substance mecoprop-P, EFSA J. 15 (2017). https://doi.org/10.2903/j.efsa.2017.4832.

[22] H.H. McDuffie, P. Pahwa, J.R. McLaughlin, J.J. Spinelli, S. Fincham, J.A. Dosman, D. Robson, L.F. Skinnider, N.W. Choi, Non-Hodgkin's lymphoma and specific pesticide exposures in men: cross-Canada study of pesticides and health., Cancer Epidemiol. Biomarkers Prev. 10 (2001) 1155–63. http://www.ncbi.nlm.nih.gov/pubmed/11700263.

[23] Y. Fang, H. Lu, S. Chen, K. Zhu, H. Song, H. Qian, Leaf proteome analysis provides insights into the molecular mechanisms of bentazon detoxification in rice, Pestic. Biochem. Physiol. 125 (2015) 45–52. https://doi.org/10.1016/j.pestbp.2015.06.003.

[24] E. Kruisdijk, P.J. Stuyfzand, B.M. van Breukelen, Degradation of seven pesticides and two metabolites before and during aquifer storage transfer and recovery operation, J. Contam. Hydrol. 251 (2022) 104094. https://doi.org/10.1016/j.jconhyd.2022.104094.

[25] G. Utzeri, D. Murtinho, T.M.R. Maria, A.A.C.C. Pais, F. Sannino, A.J.M. Valente, Amine-β-cyclodextrin-based nanosponges. The role of cyclodextrin amphiphilicity in the imidacloprid uptake, Colloids Surfaces A Physicochem. Eng. Asp. 635 (2022) 128044. https://doi.org/10.1016/j.colsurfa.2021.128044.

[26] G. Utzeri, T.F. Cova, D. Murtinho, A.A.C.C. Pais, A.J.M. Valente, Insights on macro- and microscopic interactions between Confidor and cyclodextrin-based nanosponges, Chem. Eng. J. 455 (2023) 140882. https://doi.org/10.1016/j.cej.2022.140882.

[27] P.R. Ashton, R. Königer, J.F. Stoddart, D. Alker, V.D. Harding, Amino Acid Derivatives of β-Cyclodextrin, J. Org. Chem. 61 (1996) 903–908. https://doi.org/10.1021/jo951396d.

[28] A. Puglisi, J. Spencer, J. Clarke, J. Milton, Microwave-assisted synthesis of 6-amino-β-cyclodextrins, J. Incl. Phenom. Macrocycl. Chem. 73 (2012) 475–478. https://doi.org/10.1007/s10847-011-0054-z.

[29] W.H. Brown, B.L. Iverson, E. V. Anslyn, C.S. Foote, Organic chemistry, seventh, Mary Finch, 2014.

[30] C. Yañez, M. Araya, S. Bollo, Complexation of herbicide bentazon with native and modified β-cyclodextrin, J. Incl. Phenom. Macrocycl. Chem. 68 (2010) 237–241. https://doi.org/10.1007/s10847-010-9750-3.

[31] Á. Buvári, L. Barcza, M. Kajtár, Complex formation of phenolphthalein and some related compounds with β-cyclodextrin, J. Chem. Soc., Perkin Trans. 2. (1988) 1687–1690. https://doi.org/10.1039/P29880001687.

[32] P.K. Zarzycki, H. Lamparczyk, The equilibrium constant of β-cyclodextrin-phenolphtalein complex; Influence of temperature and tetrahydrofuran addition, J. Pharm. Biomed. Anal. 18 (1998) 165–170. https://doi.org/10.1016/S0731-7085(98)00150-2.

[33] G.M.F. Pinto, I.C.S.F. Jardim, Determination of bentazon residues in water by high-performance liquid chromatography, J. Chromatogr. A. 846 (1999) 369–374. https://doi.org/10.1016/S0021-9673(98)01031-0.

[34] M. V. Pergal, I.D. Kodranov, M.M. Pergal, V. V. Avdin, D.D. Manojlović, Oxidative degradation and mineralization of bentazone from water, J. Environ. Sci. Heal. Part B. 55 (2020) 1069–1079. https://doi.org/10.1080/03601234.2020.1816091.

[35] T. Paszko, P. Muszyński, Degradation rates of alachlor, atrazine and bentazone in the profiles of Polish Luvisols, Int. Agrophysics. 31 (2017) 401–410. https://doi.org/10.1515/intag-2016-0053.

[36] D. Šojić, V. Despotović, B. Abramović, N. Todorova, T. Giannakopoulou, C. Trapalis, Photocatalytic Degradation of Mecoprop and Clopyralid in Aqueous Suspensions of Nanostructured N-doped TiO2, Molecules. 15 (2010) 2994–3009. https://doi.org/10.3390/molecules15052994.

[37] F. Sánchez-Rasero, M.B. Matallo, E. Romero, G. Dios, A. Pena, Determination of Mecoprop and Dichlorprop in Aqueous Soil Solutions by HPLC with DAD, J. Liq. Chromatogr. Relat. Technol. 21 (1998) 2211–2218. https://doi.org/10.1080/10826079808006620.

[38] R.M. Silverstein, F.X. Webster, D.J. Kiemle, Infrared Spectrometry, in: D. Brennan, J. Yee, S. Wolfman-Robichaud (Eds.), Spectrom. Identif. Org. Compd., seventh ed, John Wiley & Sons, Inc., 2005: pp. 72–126.

[39] B.F.F. Medronho, S. Gonçalves, R. Rodríguez-Solana, A.J.M. Valente, A. Romano, Interactions between Bio-Based Compounds and Cyclodextrins, in: P. Arora, N. Dhingra (Eds.), Cyclodext. - A Versatile Ingred., IntechOpen, Rijeka, 2018: pp. 70–93. https://doi.org/10.5772/intechopen.73531.

[40] A.J.M. Valente, O. Söderman, The formation of host–guest complexes between surfactants and cyclodextrins, Adv. Colloid Interface Sci. 205 (2014) 156–176. https://doi.org/10.1016/j.cis.2013.08.001.

[41] J. Ali, E. Alhseinat, M. Abi Jaoude, I.M. Al Nashef, I.A. Adeyemi, T.M. Aminabhavi, H.A. Arafat, A mixed matrix polyimide ultrafiltration membrane for efficient removal of bentazon from water, Chem. Eng. J. 433 (2022) 134596. https://doi.org/10.1016/j.cej.2022.134596.

[42] A. Spaltro, S. Simonetti, S.A. Torrellas, J.G. Rodriguez, D. Ruiz, A. Juan, P. Allegretti, Adsorption of bentazon on CAT and CARBOPAL activated carbon: Experimental and computational study, Appl. Surf. Sci. 433 (2018) 487–501. https://doi.org/10.1016/j.apsusc.2017.10.011.

[43] Z. Liu, X. Yan, M. Drikas, D. Zhou, D. Wang, M. Yang, J. Qu, Removal of bentazone from micro-polluted water using MIEX resin: Kinetics, equilibrium, and mechanism, J.

Environ. Sci. 23 (2011) 381–387. https://doi.org/10.1016/S1001-0742(10)60441-X.

[44] A. Azzali, S. d'Agostino, F. Grepioni, Tuning the Solubility of the Herbicide Bentazon: From Salt to Neutral and to Inclusion Complexes, ACS Sustain. Chem. Eng. 9 (2021) 12530–12539. https://doi.org/10.1021/acssuschemeng.1c02749.

Conclusion and future perspectives

Several aims have been achieved throughout the thesis.

New routes for the synthesis of the cyclodextrin-based nanosponges have been developed and those include the use of greener route and lower energetic costs. The functionalization time using AM_6 and AM_{12} a novel linker was reduced from 48 hours to 40 minutes, from wet-chemistry to microwave-assisted procedure, with an energetic and solvent consume benefit, not affecting the reaction yield (≥ 80%). The synthesis route was valid not only for *β*-CD but also for *α*-CD. In the synthesis of the second class of nanosponges, *α*$CDGNH_2$, *α*$CDGAM_6$, *α*$CDGAM_{12}$, *β*$CDGNH_2$, *β*$CDGAM_6$ and *β*$CDGAM_{12}$, the polymerization step was upgraded from nucleophilic substitution reaction (48 hours) to click-condensation reaction (some minutes) using the highly reactive glutaraldehyde as crosslinker, used for the first time in nanosponge synthesis.

As results, a batch of 10 CDAM-NSs was developed and the effect of *α*-CD or *β*-CD as substrates and -NH_2, AM_6, AM_{12} and GLT as linkers was assessed both in the physico-chemical properties of the polymeric 3D-structures and in sorbent performance. The aliphatic chain length of the crosslinker plays a key role in defining the characteristics of the sorbents due to growing hydrophobic character, their entanglement and steric hindrance. Generally, longer linkers are less affected by steric hindrance allowing higher *DC* in both classes of CDAM-NS. In the first class of CDAM-NS, higher *N%* (w/w) led to higher *DC*, larger particle size and thermal stability, with a decrease of *CD%* and *free-CD*. The higher surface area, *CD%* and *free-N* per gram of *β*$CDGAM_6$ can justified its superior performance towards pure-imidacloprid and its commercial formulation, with a constant efficiency after 5 cycles of reuse. In the second class of CDAM-NS, longer linker led to higher *DC* directly related to *CD%* and *free-CD*, *free-N* and its ratio with *total-N* per gram of NS. The second class of CDAM-NS also shown a higher thermal stability than the first class. Moreover, considering the data available *α*CDGNH2, *β*$CDGNH_2$ and *β*$CDGAM_6$ reach a complete removal of mecoprop (≥ 99%) from aqueous solution without or with presence of bentazon. *β*$CDGAM_6$ presents the highest removal efficiency for bentazon with a maximum of 97% at higher concentration, in individual batch, probably due to its higher amount of molN_f per gram of NS. In presence of mecoprop the uptake capability rises to ≥ 99%, at lower concentrations.

Molecular dynamic simulation was used as powerful and complementary tool for better understanding the effects of pure or modified cyclodextrins used as substrate and of the different crosslinkers. Thermodynamic assessment of the sorbent-sorbate non-covalent interactions is obtained. It also makes possible to quantify and visualize the point of interaction.

The major drawback of these systems is their powder-state which form suspensions in water, making difficult the recovery and reuse, at expense of possible industrial application; even considering the high removal efficiency towards several pesticides.

At this regard, it could be of great interest the development of polymeric carrier matrix such as membranes. A first method, it could be the homogeneous dispersion of the CDAM-NS in a neutral membrane matrix such as cellulose acetate. A second method, it can consider the grafting of the amine-cyclodextrin derivatives or CDAM-NS at the surface of the membrane containing available and reactive functional groups. In this way, the recovery and the reuse of the materials would be facilitate paving the way for their application as sorbent materials and/or pesticide carriers.